NASA Technical Memorandum 4511

C. D. Andrews
NASA-MSFC
ED31
Huntsville, AL 35812

Terrestrial Environment (Climatic) Criteria Guidelines for Use in Aerospace Vehicle Development, 1993 Revision

AUGUST 1993

NASA

NASA Technical Memorandum 4511

Terrestrial Environment (Climatic) Criteria Guidelines for Use in Aerospace Vehicle Development, 1993 Revision

D. L. Johnson, *Editor*
George C. Marshall Space Flight Center
Marshall Space Flight Center, Alabama

National Aeronautics and
Space Administration
Office of Management
Scientific and Technical
Information Program
1993

ACKNOWLEDGMENTS

A large number of aerospace engineers and personnel in varying scientific fields have contributed and assisted in the preparation of this document. The following personnel were responsible for the sections identified below.

SECTION		RESPONSIBLE PERSONS
I.	Introduction	C. Kelly Hill* and B. Jeffrey Anderson
II.	Winds	O.E. Smith, Robert E. Smith, and Steven A. Smith*
III.	Atmospheric Models and Thermodynamic Properties	Dale L. Johnson*
IV.	Thermal Radiation	Glenn E. Daniels and Dale L. Johnson*
V.	U.S. and World Surface Extremes	DeAnna Skow, Susanna McSwain, and Gwenevere Jasper*
VI.	Humidity	William R. Jeffries, Gwenevere Jasper,* and Susanna McSwain
VII.	Precipitation, Fog, and Icing	Gwenevere Jasper,* William R. Jeffries, and Susanna McSwain
VIII.	Cloud Phenomena and Cloud Cover Models	W. R. Jeffries, S. Clark Brown, and Dale L. Johnson*
IX.	Atmospheric Electricity	Charles D. Weidman, Richard J. Blakeslee, and William J. Koshak*
X.	Atmospheric Constituents	Susanna McSwain, Glenn E. Daniels, and Dale L. Johnson*
XI.	Aerospace Vehicle Exhaust and Toxic Chemical Release	Harry V. Geary, Jeff Record, B. Jeffrey Anderson, and John W. Kaufman*
XII.	Occurrences of Tornadoes and Hurricanes	Gwenevere Jasper,* Susanna McSwain, and Dale L. Johnson
XIII.	Geologic Hazards	C.J. Shin, Nicholas C. Costes, and Dale L. Johnson*
XIV.	Sea State	S. Clark Brown and Dale L. Johnson*
XV.	Conversion Units	Lisa W. Tyree (Dale L. Johnson*)
	Index	Dale L. Johnson

*NASA person to contact regarding further information.

Other members of the Earth Science and Applications Division or Space Science Laboratory who contributed to this document were Margaret B. Alexander, Michael Susko, and George H. Fichtl.

Special acknowledgments are given to Greg S. Wilson (Chief) and Ronald J. Koczor (Deputy Chief) of the Earth Science and Applications Division (ES41); to C. Kelly Hill and B. Jeffery Anderson of the Environmental Analysis Branch (ES44); and to Dr. David Bowdle of the University of Alabama in Huntsville for their guidance and support which led to the completion of the revision of this report.

Also, thanks go to Ms. Tauna Moorehead (ES01), Ms. Joyce Turner (CN22), Ms. Diane Stephanouk (MSI) for coordinating and proofing, and Judy Maples (DPTI) for final computer typing, assembly, and printing of this document. Finally, special thanks to Ms. Lisa Tyree and Ms. Susanna McSwain for their needed assistance, and in the initial proofreading of the document.

The authors wish to thank the following people, outside NASA, for their review or assistance which offered valuable suggestions used to enhance this document.

Dr. S.T. Algermissen, U.S. Geological Survey–Denver, CO
Dr. William L. Chameides, Georgia Institute of Technology, GA
Dr. Patrick F. Dunn, University of Notre Dame, IN
Dr. John Hallett, University of Nevada–Reno, NV
Dr. James K. Luers, University of Dayton, OH
Mr. Paul Tattelman, Phillips Laboratory, MA
Dr. William W. Vaughan, University of Alabama–Huntsville, AL
Dr. Gerald F. Wieczorek, U.S. Geological Survey–Reston, VA

FOREWORD

This document provides information relative to the natural environment for altitudes between 90 km and the surface of the Earth for the principal space vehicle development, operational, and launch locations and associated local and worldwide geographical areas.

There is no intent to automatically change any references to previous documents in aerospace vehicle development contract scopes of work currently in effect by the issuance of the 1993 revision of this document.

This document, which supersedes all editions of TM 82473, entitled "Terrestrial Environment (Climatic) Criteria Guidelines for Use in Aerospace Vehicle Development, 1982 Revision," is recommended for use in the development of design requirements/specifications for aerospace vehicles and associated equipment.

The information presented in this document is based on data and models considered to be accurate. However, in those design applications which indicate a critical environment interface, the user should consult an environmental specialist to insure application of the most current information and scientific-engineering interpretation.

Various NASA programs have provided resources required for the preparation of this document. Major support came from NASA Headquarters Office of Safety and Mission Quality (Code Q) and Office of Space Flight (Code M).

A companion document, entitled "Natural Orbital Enviroment Guidelines for Use in Aerospace Vehicle Development" by Dr. B. Jeffrey Anderson and Dr. Robert E. Smith, is being prepared for 1993 publication as a NASA TM at MSFC. It will cover all natural environmental guidelines at orbital altitudes within the Earth's thermosphere and exosphere.

TABLE OF CONTENTS

TABLE OF CONTENTS (Continued)

TABLE OF CONTENTS (Continued)

TABLE OF CONTENTS (Continued)

TABLE OF CONTENTS (Continued)

TABLE OF CONTENTS (Continued)

TABLE OF CONTENTS (Continued)

TABLE OF CONTENTS (Continued)

TABLE OF CONTENTS (Continued)

TECHNICAL MEMORANDUM

TERRESTRIAL ENVIRONMENT (CLIMATIC) CRITERIA GUIDELINES FOR USE IN AEROSPACE VEHICLE DEVELOPMENT 1993 REVISION

SUMMARY

Atmospheric phenomena play a significant role in the design and flight of aerospace vehicles and in the integrity of the associated aerospace systems and structures. Environmental design criteria guidelines in this report are based on statistics of atmospheric and climatic phenomena relative to various aerospace development, operational, and vehicle launch locations. This revision contains new and updated material in most sections.

Specifically, aerospace vehicle design guidelines are established for the following environmental phenomena and presented by sections: Winds; Atmospheric Models and Thermodynamic Properties; Thermal Radiation; U.S. and World Surface Extremes; Humidity; Precipitation, Fog, and Icing; Cloud Phenomena and Cloud Cover Models; Atmospheric Electricity; Atmospheric Constituents; Aerospace Vehicle Exhaust and Toxic Chemical Release; Occurrences of Tornadoes and Hurricanes; Geologic Hazards; and Sea State. The last section in this document includes conversion constants.

Atmospheric data are presented for application to aerospace vehicle design studies and the development of design requirements/specifications. The atmospheric parameters are scaled to show the probability of reaching or exceeding certain limits to assist in establishing design and operating criteria. Additional information cited in the text on the different parameters may be found in the numerous references following each section.

I. INTRODUCTION

1.1 General

For climatic extremes, there is no known physical upper or lower bound except for certain conditions; for example, wind speed does have a strict physical lower bound of zero. Therefore, for any observed extreme condition, there is a finite probability of it being exceeded. Consequently, climatic extremes for design must be accepted with the knowledge that there is some risk of the values being exceeded. The measurement of many environmental parameters is not as accurate as desired. In some cases, theoretical estimates of extreme values are believed to be more representative than those indicated by empirical distributions from short periods of record. Therefore, theoretical values are given considerable weight in selecting extreme values for some parameters, i.e., the peak surface winds. Criteria guidelines are presented for various percentiles based on available data samples. Caution should be exercised in the interpretation of these percentiles in vehicle studies to ensure consistency with physical reality and the specific design and operational problems of concern.

Aerospace vehicles are not normally designed for launch and flight in severe weather conditions such as hurricanes, thunderstorms, and squalls. Atmospheric parameters associated with severe weather which may be hazardous to aerospace vehicles are strong ground and inflight winds, strong wind shears, turbulence, icing conditions, and electrical activity. The guidelines given usually provide information relative to severe weather characteristics, which may be included in design requirements/specifications if required.

Environmental data in this report are primarily limited to information below 90 km. Specific aerospace vehicle natural environmental design criteria are normally specified in the appropriate organizational aerospace vehicle design ground rules and design criteria data documentation. The information in this document is recommended for use in the development of aerospace vehicles and associated equipment design criteria (requirements/specifications) unless otherwise stated in contract work specifications.

The data in all sections are based on conditions which have actually occurred, or are statistically probable in nature over a longer reference period than the available data based on established theoretical models.

Assessment of the natural environment in the early stages of an aerospace vehicle development program will be advantageous in developing a vehicle with a minimum operational sensitivity to the environment. For those areas of the environment that need to be monitored prior to and during tests and operations, this early planning will permit development of the required measuring and communication systems for accurate and timely monitoring of the environment.

A knowledge of the Earth's atmospheric environment parameters is necessary for the establishment of design requirements for aerospace vehicles and associated equipment. Such data are required to define the fabrication, storage, transportation, test, preflight, and inflight design conditions and should be considered for both the whole system and the components which make up the system. One of the purposes of this document is to provide guideline data on natural environmental conditions, for the various major geographic locations which are applicable to the design of aerospace vehicle and associated equipment.

Good engineering judgment must be exercised in the application of the Earth's atmospheric data to aerospace vehicle design analysis. Consideration must be given to the overall vehicle mission and performance requirements. Knowledge is still lacking on the relationships between some of the atmospheric variates which are required as inputs to the design of aerospace vehicles. Also, interrelationships between aerospace vehicle parameters and atmospheric variables cannot always be clearly defined. Therefore, a close working relationship and team philosophy must exist between the design/operational engineer and the respective organization's aerospace environmentalists. Although, ideally, an aerospace vehicle design should accommodate all expected operational atmospheric conditions, it is neither economically nor technically feasible to design aerospace vehicles to withstand all atmospheric extremes. For this reason, consideration should be given to protection of aerospace vehicles from some extremes by use of support equipment and by using specialized forecast personnel to advise on the expected occurrence of critical environmental conditions. The services of specialized forecast personnel may be very economical in comparison with more expensive designing which would be necessary to cope with all environmental possibilities.

In general this document does not specify how the designer should use the data in regard to a specific aerospace vehicle design. Such specifications may be established only through analysis and study of a particular design problem. Although of operational significance, descriptions of some atmospheric conditions have been omitted since they are not of direct concern for structural and control system design, the primary emphasis of this document. Induced environments (vehicle caused) may be more critical than natural environments for certain vehicle operational situations. In some cases the combination of natural and induced environments will be more severe than either environment alone. Induced environments are considered in other space vehicle criteria documents, which should be consulted for such data.

The natural environment criteria guidelines data presented in this document were formulated based on discussions with and requests from engineers involved in space vehicle development and operations; therefore, they represent responses to actual engineering problems and are not just a general compilation of environmental data. This report is used extensively by the Marshall Space Flight Center (MSFC), other NASA Centers, various other government agencies, and their associated contractors in design and operational studies. Considerably more information is available on topics covered in this report than is presented here. Users of this document who have questions or require further information on the data provided may direct their requests to the Earth Science and Applications Division (ES41), Space Science Laboratory, NASA Marshall Space Flight Center, Alabama 35812.

1.2 Main Geographical Areas Covered in Document:

a. Kennedy Space Center, Florida

b. Vandenberg Air Force Base, California

c. Edwards Air Force Base, California

d. Johnson Space Center, Houston, Texas

e. White Sands Missile Range, New Mexico

f. Michoud Assembly Facility, New Orleans, Louisiana

g. Stennis Space Center, Mississippi.

Some other geographical areas are also presented.

This document does not include the subject of environmental test procedures. Reference should be made to Department of Defense MIL-STD-810E Environmental Test Methods and Engineering Guidelines, 14 July, 1989, available from the National Technical Information Service, Springfield, Virginia 22161. This MIL-STD covers procedures for: Low Pressure (Altitude), High and Low Temperature, Temperature Shock, Temperature Altitude and Temperature-Humidity Altitude, Solar Radiation, Rain, Humidity, Fungus, Salt Fog, Dust (Fine Sand), and Space Simulations (Unmanned Test). An excellent comparison of the various international environmental testing standards may be found in the Journal of Environmental Sciences, vol. XXIV, No. 2, March/April 1981. The *Glossary of Meteorology* published by the American Meteorological Society, 45 Beacon Street, Boston, MA 02108, may be consulted for the definition of terms not otherwise defined in this document.

SECTION II. WINDS

2.1 Introduction

An aerospace vehicle's response to atmospheric disturbances, especially wind, must be carefully evaluated to ensure that its design will allow it to meet its operational requirements. The choice of criteria depends upon the specific launch location(s), vehicle configuration, and mission. The vehicle's design, operation, and flight procedures must be separated into phases for proper assessment of environmental influences and impacts upon its life history. These phases include (1) the initial purpose and concept of the vehicle, (2) its preliminary engineering design for flight, (3) its structural design, (4) its guidance and flight control design, (5) optimizations of its design limits, and (6) the final assessment of its capability for launch and operations.

Because the wind environment significantly affects the design and operation of aerospace vehicles, and it is necessary to use good technical judgment and to apply sound engineering principles in preparing wind criteria that are descriptive and representative. Although wind criteria guidelines contained in this document were especially prepared for application to aerospace vehicle programs, they are applicable to other areas such as aeronautical engineering, architecture, atmospheric diffusion, wind and solar energy conversion research, and many others. The proper selection, analysis, and interpretation of wind information are responsibilities of the atmospheric scientists working in collaboration with the design engineers.

The information given in this document covers wind models and criteria guidelines applicable to various design problems. The risk level selected for the design depends upon the design philosophy used by management for the aerospace vehicle development effort. To maximize vehicle performance flexibility, it is considered best to utilize those wind data associated with the minimum acceptable risk levels. In addition, the critical mission-related parameters, such as exposure time of the vehicle being affected by the natural environment quantities, launch windows, reentry periods, launch turnaround periods, etc., should be considered carefully. Initial design work using unbiased (with respect to wind) trajectories based on nondirectional ground or in-flight winds may be used unless the vehicle and its mission are well known and the exact launch azimuth and time(s) are established and adhered to throughout the program. In designs that use wind-biased trajectories and directional (vector) wind criteria, rather severe wind constraints can result if the vehicle is used for other missions, different flight azimuths, or if other vehicle configurations are developed. Therefore, caution must be exercised in using wind criteria models to ensure consistency with the physical interpretation of each specific vehicle design problem relative to the overall design philosophy for the vehicle. Several references are cited throughout this document which discuss special and specific problems related to the development and specification of wind environments for aerospace vehicle programs.

2.2 Ground Wind (1 to 150 m)

2.2.1 Introduction

Ground winds for aerospace vehicle development applications are defined in this document to be those winds in the lowest 150 m of the atmosphere. The winds in this layer of the atmosphere are characterized by very complicated three-dimensional flow patterns with rapid variations in magnitude and direction in space and time. An engineering requirement exists for models which define the structure of wind in this layer because of the complicated and possibly critical manner in which a vehicle might respond to certain aspects of the flow, both when the vehicle is stationary on the launch pad and during the first few seconds after the launch. The forces generated by von Karman vortex shedding are an example of the effect of wind on aerospace vehicles. These forces can result in base bending moments while the vehicle is on the launch pad and pitch and yaw plane angular accelerations and vehicle drift during lift-off. Other equally important examples can be cited. The basic treatment of the ground wind problem relative to vertically oriented vehicles on-pad and during lift-off has been to estimate the risk of encountering crucial aspects of wind along the vertical. It should be noted that, in addition to the engineering requirements for on-pad and launch winds for vertically ascending vehicles, a requirement for ground wind models also exists for horizontally flying vehicles

for take-off and landing. This aspect of the natural wind environment is discussed in sections 2.3.13 through 2.3.16.

Because ground wind data are applied by aerospace vehicle engineers in numerous ways, dependent upon the specific problem, various viewpoints and kinds of analytical techniques were used to obtain the environmental models presented here. Program planning, for instance, requires considerable climatological insight to determine the frequency and persistence distributions for wind speeds and wind directions. However, for design purposes, the aerospace vehicle must withstand certain unique predetermined structural loads that are generated from exposure to known peak ground wind conditions. Ground wind profiles and the ground wind turbulence spectra contribute to the development of the design ground wind models. Surface roughness, launch site structures, thermal environment, and various transient local and large-scale meteorological systems influence the ground wind environment for each launch site.

2.2.2 Considerations in Ground Wind Design Criteria

To establish the ground wind design criteria for aerospace vehicles, several important factors must be considered.

a. Where is the vehicle to operate?

b. What is the launch location?

c. What are the proposed vehicle missions?

d. How many hours, days, or months will the vehicle be exposed to ground winds?

e. What are the consequences of operational constraints that may be imposed upon the vehicle because of wind constraints?

f. What are the consequences if the vehicle is destroyed or damaged by ground winds?

g. What are the cost and engineering practicalities for designing a functional vehicle to meet the desired mission requirements?

h. What is the risk that the vehicle will be destroyed or damaged by excessive wind loading?

In view of this list of questions or any similar list that a design group may enumerate, it becomes obvious that the establishment of ground wind environment design criteria for a aerospace vehicle requires an interdisciplinary approach involving several engineering and scientific disciplines. Furthermore, the process is an iterative one. To begin the iterative process, specific information on ground winds is required.

2.2.3 Introduction to Exposure Periods Analysis

Valid, quantitative answers to such questions as the following are of primary concern in the design, mission planning, and operation of aerospace vehicles:

a. What is the probability that the peak ground wind at some specified reference height will exceed (or not exceed) a given magnitude in some specified time period?

b. Given a design wind profile in terms of peak wind speed versus height from 10 to 150 m, what is the probability that the design wind profile will be exceeded in some specified time period?

Given a statistical sample of peak wind measurements for a specific location, the first question can be answered in as much detail as a statistical analyst finds necessary and sufficient. This first question has been

thoroughly analyzed for Kennedy Space Center (KSC), partially for Vandenberg Air Force Base (VAFB), and to a lesser degree for other locations of interest.

The analysis becomes considerably more complex in answering the second question. A wind profile is required, and, to develop the model, measurements of the wind profiles by properly instrumented ground wind towers are required as well as a program for scheduling the measurements and data reduction. Every instantaneous wind profile is unique; similarity is a matter of degree. Given the peak wind speed at one height, there is a whole family of possible profiles extending from the specified wind at that height. Thus for each specified wind speed at a given height, there is a statistical distribution of wind profiles. Recommended profile shapes for KSC and other locations are given in this document. The analysis needed to answer the second question is not complete, but we can assume that, given a period of time, the design wind profile shape will occur for a specified wind speed at a given height. For example, in the event that a thunderstorm passes over the vehicle, it is logical to assume that the design wind profile shape will occur and that the chance of the design wind profile being exceeded is the same as the probability that the peak wind (gust) during the passage of the thunderstorm will strike the vehicle or point of interest (ref. 2-1).

2.2.4 Development of Extreme Value Concept

It has been estimated from wind tunnel tests that only a few seconds are required for the wind to produce near steady-state drag loads on a vehicle such as the space shuttle in an exposed condition on the launch pad. For this and other reasons, we have adopted the peak wind speed as our fundamental measurement of wind for use in design studies. Equally important, when the engineering applications of winds can be made in terms of peak wind speeds, it is possible to obtain an appropriate statistical sample that conforms to the fundamental principles of extreme value theory. One hour is a convenient and physically meaningful minimum time interval from which to select the peak wind. An hourly peak wind speed sample has been established for KSC from wind information on continuous recording charts. Representative peak wind samples for VAFB have been derived from hourly steady-state wind measurements using statistical and physical principles. From the hourly peak wind records, the daily peak, and monthly peak wind records can be computed. An extreme value probability function is used to summarize these statistics.

2.2.4.1 Envelope of Distributions

In the development of the statistics for peak winds, it was recognized that the probability of hourly, daily, and monthly peak winds exceeding (or not exceeding) specified values varied with time of day and from month to month. The Gumbel extreme value probability distribution (ref. 2.56) was an excellent fit to the samples of hourly, daily, monthly, bimonthly (in two combinations), and trimonthly (in three combinations) periods taken over the complete period of record, thereby justifying the use of this distribution. However, in establishing vehicle wind design criteria for the peak winds versus exposure time, it is desired to present a simple set of wind statistics in such a manner that every reference period and exposure time would not have to be examined to determine the probability that the largest peak wind during the exposure time would exceed some specified magnitude. To accomplish this objective, envelopes of the distributions of the largest peak winds for various time increments for the various reference periods were constructed. For example, to obtain the envelope distribution of hourly peak winds for the month of March, the largest peak wind was selected at each percentage point from the 24 peak wind distributions (one for each hour). For a 365-day exposure, the distribution for the extreme largest yearly peak wind data sample is used.

Selected wind profile envelopes of distributions are given in subsection 2.2.5.5. It is recommended that these envelopes of distributions be used for vehicle wind design considerations. This recommendation is made under the assumption that it is not known what time of day or season of year critical vehicle operations are to be conducted. Furthermore, it is not desirable to design a vehicle to operate only during selected hours or months. Should all other design alternatives fail to lead to a functionally engineered vehicle with an acceptable risk of not being compromised by wind loads, then distributions for peak winds by time of day for monthly reference periods may be considered for limited missions. For vehicle operations, detailed statistics of peak winds for specific missions are meaningful for management decisions, in planning missions, and in establishing mission rules and alternatives for the operational procedures. To present the wind statistics for

these purposes is beyond the scope of this document. Each space mission has many facets that make it difficult to generalize and to present all the available statistics in brief form.

2.2.5 Design Wind Profiles for Aerospace Vehicles

Specific information about the wind profile is required to calculate ground wind loads on aerospace vehicles. The Earth's surface is a rigid boundary that exerts a frictional force on the lower layers of the atmosphere, causing the wind to approach zero velocity at the ground. In addition, the characteristic length and velocity scales of the mean (steady-state) flow in the first 150 m (boundary layer) of the atmosphere combine to yield extremely high Reynolds numbers with values that range between approximately 10^6 and 10^8, so that for most conditions (wind speeds >1 m/s) the flow is fully turbulent. The lower boundary condition, the thermal and dynamic stability properties of the boundary layer, the distributions of the large-scale pressure, the Coriolis force, and the structure of the turbulence combine to yield an infinite number of wind profiles.

Data on basic wind speed profiles given in this section are for use in vehicle design studies. With respect to design practices, the application of peak winds and the associated turbulence spectra and discrete gusts should be considered. The maximum response obtained for the selected risk levels for each physically realistic combination of conditions should be employed in the design. Care should be exercised so that wind inputs are not taken into account more than once. For example, the discrete gust and spectrum (a discrete bandwidth of energy in the turbulent spectrum) of turbulence are representations of the same thing, namely atmospheric turbulence. Thus, one should not calculate the responses of a vehicle due to the discrete gust and spectrum and then combine the results by addition, root-sum-square, or any other procedure since these inputs represent the same thing. Rather, the responses should be calculated with each input and then enveloped.

2.2.5.1 Philosophy

An example of a peak wind speed is given in figure 2-1. Peak wind statistics have three advantages over mean wind statistics. First, peak wind statistics do not depend upon an averaging operation as do mean

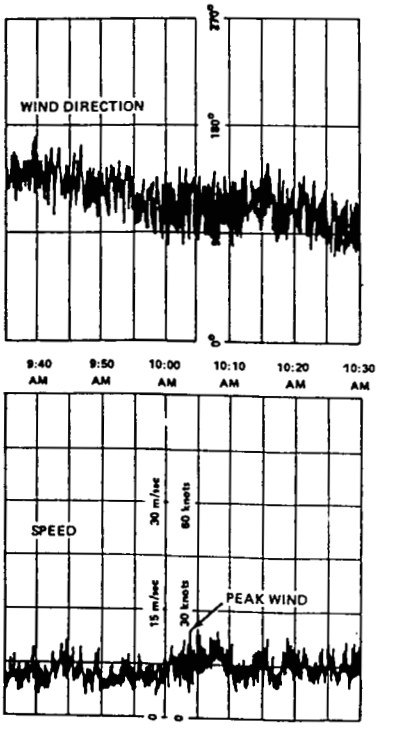

Figure 2-1. Example of peak wind speed and direction records.

wind statistics. Second, to construct a mean wind sample, a chart reader or weather observer must perform an "eyeball" average of the wind data, causing the averaging process to vary from day to day according to the mood of the observer, and from observer to observer. Hourly peak wind speed readings avoid this subjective averaging process. Third, to monitor winds during the countdown phase of an aerospace vehicle launch, it is easier to monitor peak wind speed than the mean wind speed. With today's modern electronic computational techniques available, monitoring a mean wind speed over any given time interval is not as serious a problem.

Smith et al. (ref. 2-2) have performed extensive statistical analyses with peak wind speed samples measured at the 10-m level. In the course of the work, he and his collaborators introduced the concept of exposure period probabilities into the design and operation of aerospace vehicles. By determining the distribution functions of peak wind speeds for various periods of exposure (hour, day, month, year, etc.), it is possible to determine the probability of a certain peak wind speed magnitude occurring during a prescribed period of exposure. Thus, if an operation requires, for example, 1 hour to complete, and if the critical wind loads on the aerospace vehicle can be defined in terms of the peak wind speed, then it is the probability of occurrence of the peak wind speed during a 1-hour period that gives a measure of the risk of the occurrence of structural failure. Similarly, if an operation requires 1 day to complete, then it is the probability of occurrence of the peak wind speed during a 1-day period that gives a measure of the risk of structural failure.

These peak wind statistics are usually transformed to the 18.3-m (60-ft) reference level for design purposes (or sometimes to higher levels for operational applications). However, to perform loading and response calculations resulting from steady-state and random turbulence drag loads and von Karman vortex shedding loads, the engineer requires information about the vertical variation of the mean wind and the structure and turbulence in the atmospheric boundary layer. The philosophy is to extrapolate the peak wind statistics up in height via a peak wind profile, and the associated steady-state or mean wind profile is obtained by applying a gust factor that is a function of wind speed and height.

2.2.5.2 Peak Wind Profile Shapes

To develop a peak wind profile model, approximately 6,000 hourly peak wind speed profiles measured at NASA's ground wind tower facility at KSC have been analyzed. The sample, composed of profiles of hourly peak wind speeds measured at the 18-, 30-, 60-, 90-, 120-, and 150-m levels, showed that the variation of the peak wind speed in the vertical, below 150 m, for engineering purposes, could be described with a power law relationship given by

$$u(z) = u_{18.3}\left(\frac{z}{18.3}\right)^{k}, \tag{2.1}$$

where $u(z)$ is the peak wind speed at height z in meters above the natural grade and $u_{18.3}$ is a known peak wind speed at z = 18.3 m. The peak wind is referenced to the 18.3-m level because this level has been selected as the standard reference for the KSC launch area. A reference level should always be stated when discussing ground winds to avoid confusion in interpretation of risk statements and structural load calculations.

A statistical analysis of the peak wind speed profile data revealed that, for engineering purposes, k is distributed normally for any particular value of the peak wind speed at the 18.3-m level. Thus, for a given percentile level of occurrence, k is approximately equal to a constant for $u_{18.3} \leq 2$ m/s. For $u_{18.3} > 2$ m/s,

$$k = c(u_{18.3})^{-3/4}, \qquad c = 1.6 \tag{2.2}$$

where $u_{18.3}$ has the units of meters per second. The parameter c, for engineering purposes, is distributed normally with mean value 0.52 and standard deviation 0.36 and has units of $(\text{m/s})^{3/4}$. The distribution of k as a function of $u_{18.3}$ is depicted in figure 2-2. The $\bar{k}+3\sigma$ values are used in design studies.

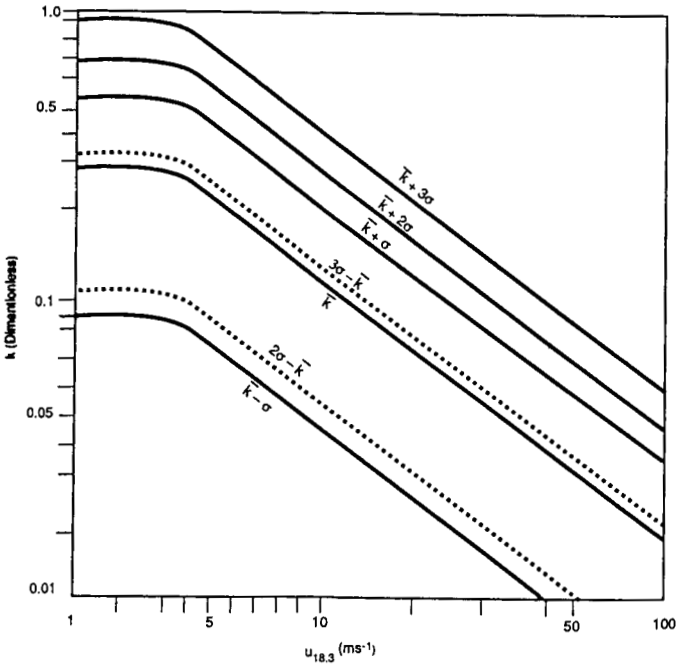

Figure 2-2. Distribution of the peak wind profile parameter k for various peak wind speeds at the 18.3-m level for KSC.

2.2.5.3 Instantaneous Extreme Wind Profiles

The probability that the hourly peak wind speeds will occur at all levels simultaneously is small. Accordingly, the practice of using peak wind profiles introduces some conservatism into the design criteria; however, the probability is relatively large that when the hourly peak wind occurs at the 18.3-m level, the winds at the other levels almost take on the hourly peak values.

To gain some insight into this question, approximately 35 hours of digitized magnetic tape data were analyzed. The data were digitized at 0.2-s intervals in real time and partitioned into 0.5-, 2-, 5-, and 10-min samples. The vertical average peak wind speed u_P and the 18-m mean wind $\bar{u}_{18}$ were calculated for each sample. In addition, the instantaneous vertical average wind speed time history at 0.2-s intervals was calculated for each sample, and the peak instantaneous vertical average wind speed u_I was selected for each sample. The quantity u_I/u_P was then interpreted to be a measure of how well the peak wind profile approximated the instantaneous extreme wind profile.

Figure 2-2A is a plot of $\bar{u}_I / \bar{u}_P$ as a function of $\bar{u}_{18}$. The data points tend to scatter about a mean value of $\bar{u}_I / \bar{u}_P$ 0.93; however, some of the data points have values equal to 0.98. These results justify the use of peak wind profiles for engineering design purposes.

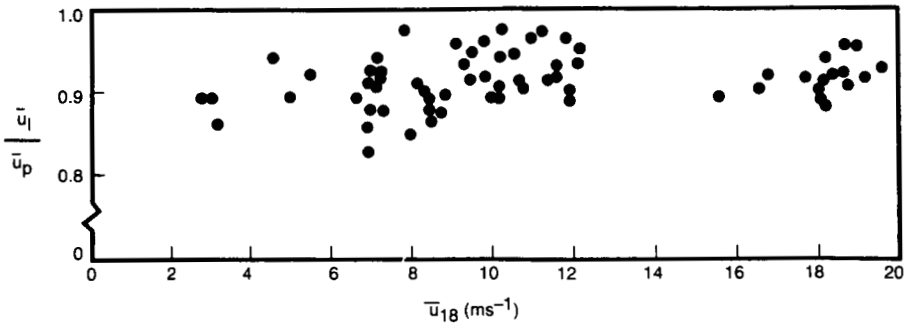

Figure 2-2A. The ratio $\bar{u}_I / \bar{u}_P$ as a function of the 18.3-m level mean wind speed ($\bar{u}_{18}$) for a 10-min sampling period.

2.2.5.4 Peak Wind Profile Shapes for Other Test Ranges and Sites

Detailed analyses of wind profile statistics are not available for test ranges and sites other than KSC. The exponent k in equation (2.1) is a function of wind speed, surface roughness, etc. For moderate surface roughness conditions, the extreme value of k is usually equal to 0.2 or less during high winds (=>15 m/s). For design and planning purposes for test ranges and sites other than KSC, it is recommended that the values of k given in table 2-1 be used. These values of k are the only values specified in this document for sites other than KSC and represent estimates for 99.87 percentile, or $+3\sigma$ (0.13-percent risk), values for the peak wind speed profile shape. A recent study resulted in $k = 0.085$ for EAFB, with associated peak wind speeds corresponding to an altitude of 4 m (13 ft).

Table 2-1. Values of k to use for test ranges other than KSC.

k Value	18.3-m Level Peak Wind Speed (m/s)
$k = 0.2$	$7 \leq u_{18.3} < 22$
$k = 0.14$	$22 \leq u_{18.3}$

2.2.5.5 Aerospace Vehicle Design Wind Profiles

The data presented in this section provide basic peak wind speed profile (envelope) information for test, free-standing, launch, and lift-off conditions to ensure satisfactory performance of an aerospace vehicle. To establish vehicle responses, the peak design surface winds are assumed to act normal to the longitudinal axis of the vehicle on the launch pad and to be from the most critical direction.

2.2.5.5.1 Design Wind Profiles for Kennedy Space Center

Peak wind profiles are characterized by two parameters, the peak wind speed at the 18.3-m level and the shape parameter k. Once these two quantities are defined, the peak wind speed profile envelope is completely specified. Accordingly, to construct a peak wind profile for KSC, in the context of launch vehicle loading and response calculations, two pieces of information are required. First, the risk of exceeding the design wind peak speed at the reference level for a given period must be specified. Once this quantity is given, the design peak wind speed at the reference level is automatically specified (fig. 2-3). Second, the risk associated with compromising the structural integrity of the vehicle, once the reference level design wind occurs, must be specified. This second quantity and the reference level peak wind speed will determine the value of k that is to be used in equation (2.1).

It is recommended that the $\bar{k}+3\sigma$ value of k be used for the design of aerospace vehicles. Thus, if an aerospace vehicle designed to withstand a particular value of peak wind speed at the 18.3-m reference level is exposed to that peak wind speed, the vehicle has at least a 99.865-percent chance of withstanding possible peak wind profile conditions.

Operational ground wind constraints for established vehicles should be determined for a reference level (above natural grade) near the top of the vehicle while on the launch pad. The profile may be calculated using equations (2.1) and (2.2) with a value of $k = \bar{k}+3\sigma$. This will produce a peak wind profile envelope associated with an upper reference level ground wind constraint.

Table 2-2 contains peak wind speed profiles for various envelope values of peak wind speed at the 10-m level for fixed values of risk for the worst monthly-hourly reference periods of the year for a 1-hour exposure. To construct these profiles, the 1-hour exposure period statistics for each hour in each month were constructed. This exercise yielded 288 distribution functions (12 months times 24 hours), which were enveloped to yield the largest or "worst" 10-m level peak wind speed associated with a given level of risk for all monthly-hourly reference periods. Thus, for example, according to table 2-2 there is at most a 10-percent

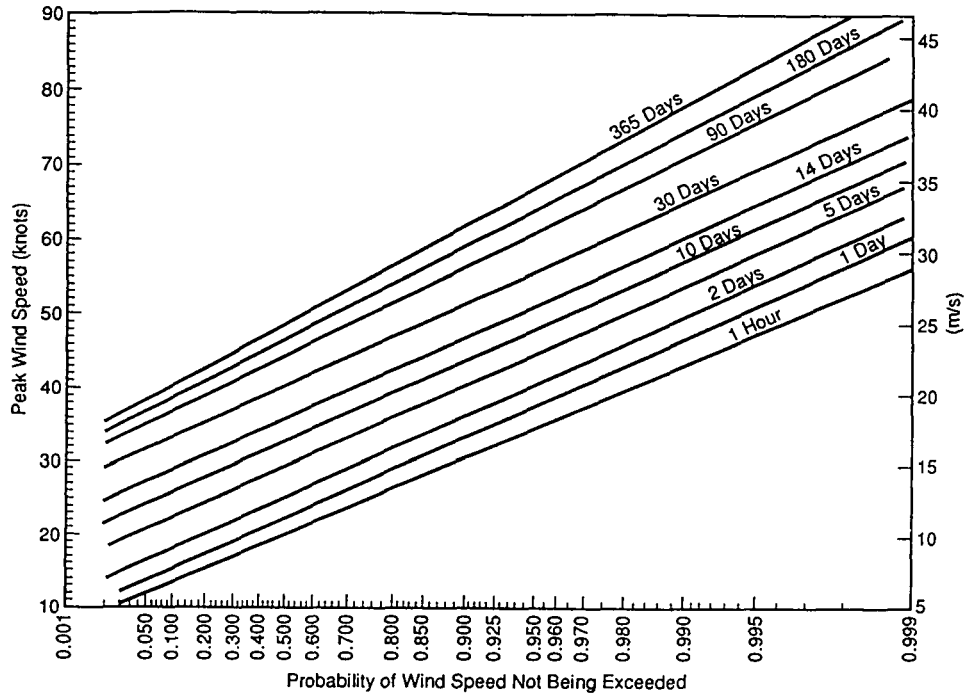

Figure 2-3. 18.3-m reference level; KSC peak wind speed for windiest reference period versus probability for several exposure periods applicable to vehicle design criteria development.

Table 2-2. Peak wind speed profile envelopes for various values of risk of exceeding the 10-m level peak wind speed for 1-h exposure (hourly-monthly reference period) for KSC.

Height		Risk (%)									
		20		10		5		1		0.1	
(m)	(ft)	knots	ms^{-1}	knots	ms^{-1}	knots	ms^{-1}	knots	ms^{-1}	knots	ms^{-1}
10.0	33	22.9	11.8	27.0	13.9	30.8	15.8	39.5	20.3	51.9	26.7
18.3	60	26.3	13.5	30.5	15.7	34.4	17.7	43.4	22.3	56.0	28.8
30.5	100	29.5	15.2	33.8	17.4	37.9	19.5	47.0	24.2	59.8	30.8
61.0	200	34.5	17.8	38.9	20.0	43.0	22.1	52.3	26.9	65.5	33.6
91.4	300	37.8	19.5	42.2	21.7	46.4	23.9	55.7	28.7	68.9	35.4
121.9	400	40.4	20.8	44.7	23.0	48.9	25.2	58.3	30.0	71.5	36.8
152.4	500	42.5	21.9	46.8	24.1	51.0	26.2	60.3	31.0	73.6	37.8

risk that the peak wind speed will exceed 13.9 m/s (27.0 knots) during any particular hour in any particular month at the 10-m level; and if a peak wind speed equal to 13.9 m/s (27.0 knots) should occur at the 10-m level, then there is only a 0.135-percent chance that the peak wind speed will exceed 24.1 m/s (46.8 knots) at the 152.4-m level or the corresponding values given at the other heights.

Tables 2-3 through 2-5 contain peak wind speed profile envelopes for various values of peak wind speed at the 10-m level and fixed values of risk for various exposure periods, The 1-day exposure values of peak wind speed were obtained by constructing the daily peak wind statistics for each month and then enveloping these distributions to yield the worst 1-day exposure, 10-m level peak wind speed for a specified value of risk (daily-monthly reference period). The 30-day exposure envelope peak wind speeds were

Table 2-3. Peak wind speed envelopes for a 10-percent risk, value of exceeding the 10-m level peak wind speed for various reference periods of exposure for KSC.

Height		Exposure (Days)									
		1		10		30		90		365	
(m)	(ft)	knots	ms^{-1}	knots	ms^{-1}	knots	ms^{-1}	knots	ms^{-1}	knots	ms^{-1}
10.0	33	29.6	15.2	39.8	20.5	47.1	24.3	52.0	26.8	57.4	29.5
18.3	60	33.2	17.1	43.7	22.5	51.2	26.4	56.2	28.9	61.7	31.8
30.5	100	36.6	18.8	47.3	24.3	54.9	28.3	60.0	30.9	65.6	33.8
61.0	200	41.8	21.5	52.7	27.1	60.4	31.1	65.6	33.8	71.3	36.7
91.4	300	45.1	23.2	56.1	28.9	63.9	32.9	69.1	35.6	74.8	38.5
121.9	400	47.6	24.5	58.6	30.2	66.5	34.2	71.7	36.9	77.4	39.8
152.4	500	49.7	25.6	60.7	31.2	68.5	35.3	73.8	38.0	79.5	40.9

Table 2-4. Peak wind speed profile envelopes for a 5-percent risk value of exceeding the 10-m level peak wind speed for various reference periods of exposure for KSC.

Height		Exposure (Days)									
		1		10		30		90		365	
(m)	(ft)	knots	ms^{-1}	knots	ms^{-1}	knots	ms^{-1}	knots	ms^{-1}	knots	ms^{-1}
10.0	33	33.7	17.3	43.9	22.6	51.2	26.4	56.4	29.0	62.3	32.1
18.3	60	37.4	19.3	47.9	24.7	55.4	28.5	60.7	31.2	66.7	34.3
30.5	100	40.9	21.0	51.6	26.5	59.2	30.5	64.6	33.2	70.7	36.4
61.0	200	46.1	23.7	57.0	29.3	64.8	33.3	70.2	36.2	76.4	39.3
91.4	300	49.5	25.5	60.4	31.1	68.2	35.1	73.7	38.0	80.0	41.2
121.9	400	52.0	26.8	63.0	32.4	70.8	36.5	76.4	39.3	82.6	42.5
152.4	500	54.1	27.8	65.1	33.5	72.9	37.5	78.5	40.4	84.7	43.6

Table 2-5. Peak wind speed profile envelopes for a 1-percent risk value of exceeding the 10-m level peak wind speed for various reference periods of exposure for KSC.

Height		Exposure (Days)									
		1		10		30		90		365	
(m)	(ft)	knots	ms^{-1}	knots	ms^{-1}	knots	ms^{-1}	knots	ms^{-1}	knots	ms^{-1}
10.0	33	43.0	22.1	53.3	27.4	60.6	31.2	66.5	34.2	73.4	37.8
18.3	60	47.0	24.2	57.5	29.6	65.0	33.5	71.0	36.6	78.0	40.2
30.5	100	50.7	26.1	61.3	31.6	68.9	35.5	75.0	38.6	82.1	42.3
61.0	200	56.1	28.9	66.9	34.5	74.7	38.4	80.8	41.6	88.0	45.3
91.4	300	59.5	30.6	70.4	36.3	78.2	40.3	84.4	43.5	91.7	47.2
121.9	400	62.1	32.0	73.0	37.6	80.8	41.6	87.1	44.8	94.3	48.6
152.4	500	64.1	33.0	75.1	38.7	82.9	42.7	89.2	45.9	96.5	49.7

obtained by constructing the monthly peak wind statistics for each month and then constructing the envelope of the distributions (monthly-annual reference period). The 10-day exposure statistics were obtained by interpolating between the 1- and 30-day exposure period results. The envelopes of the 90-day exposure period statistics are the 90-day exposure statistics associated with the 12 trimonthly periods

(January-February-March, February-March-April, March-April-May, and so forth) (90-day-annual reference period). Finally, the 365-day exposure period statistics were calculated with the annual peak wind sample (17 data points) to yield one distribution. Tables 2-3 through 2-5 contain the largest or "worst" 10-m level peak wind speed associated with a given level of risk for the stated exposure periods.

It is recommended that the data in tables 2-2 through 2-5 be used as the basis for aerospace vehicle design for KSC operations. Wind profile statistics for the design of permanent ground support equipment are discussed in subsection 2.2.10.

Mean wind profiles or steady-state wind profiles can be obtained from the peak wind profiles by dividing the peak wind by the appropriate gust factor (subsection 2.2.7). It is recommended that the 10-min gust factors be used for structural design purposes. Application of the 10-min gust factors to the peak wind profile corresponds to averaging the wind speed over a 10-min period. This averaging period appears to result in a stable mean value of the wind speed. Within the range of variation of the data, the 1-h and 10-min gust factors are approximately equal for sufficiently high wind speed. This occurs because the spectrum of the horizontal wind speed near the ground is characterized by a broad energy gap centered at a frequency approximately equal to 0.000278 Hz (1 cycle/h) and typically extends over the frequency domain 0.000139 Hz (0.5 cycles/h) $< \omega <$ 0.0014 Hz (5 cycles/h). The Fourier spectral components associated with frequencies less than 0.000278 Hz (1 cycle/h) correspond to the meso- and synoptic-scale atmospheric motions, while the remaining high-frequency spectral components correspond to mechanically and thermally produced turbulence. Thus, a statistically stable estimate of the mean or steady-state wind speed can be obtained by averaging over a period in the range from 10 min to an hour. Since this period is far longer than any natural period of structural vibration, it assures that effects caused by the mean wind properly represent steady-state, nontransient effects. The steady-state wind profiles, calculated with the 10-min gust factors, that correspond to those in tables 2-2 through 2-5, are given in tables 2-6 through 2-9.

Table 2-6. 10-min mean wind speed profile envelopes for various values of risk of exceeding the 10-m level mean wind speed for a 1-h exposure (hourly-monthly reference period) for KSC.

Height		Risk (%)									
		20		10		5		1		0.1	
(m)	(ft)	knots	ms^{-1}	knots	ms^{-1}	knots	ms^{-1}	knots	ms^{-1}	knots	ms^{-1}
10.0	33	14.1	7.2	16.6	8.6	19.1	9.8	24.6	12.7	32.4	16.7
18.3	60	17.1	8.8	19.9	10.3	22.6	11.7	28.7	14.8	37.2	19.1
30.5	100	20.0	10.3	23.1	11.9	26.0	13.4	32.6	16.8	41.6	21.4
61.0	200	24.7	12.7	28.1	14.5	31.3	16.1	38.3	19.7	48.1	24.7
91.4	300	27.8	14.3	31.3	16.1	34.7	17.9	42.0	21.6	52.1	26.8
121.9	400	30.3	15.6	33.9	17.4	37.3	19.2	44.8	23.0	55.1	28.3
152.4	500	32.3	16.6	35.9	18.5	39.4	20.3	47.0	24.2	57.5	29.6

Table 2-7. 10-min mean wind speed profile envelopes for a 10-percent risk value of exceeding the 10-m level mean wind speed for various reference periods of exposure for KSC.

Height		Exposure (Days)									
		1		10		30		90		365	
(m)	(ft)	knots	ms^{-1}	knots	ms^{-1}	knots	ms^{-1}	knots	ms^{-1}	knots	ms^{-1}
10.0	33	18.3	9.4	24.8	12.8	29.4	15.1	32.5	16.7	35.9	18.5
18.3	60	21.8	11.2	28.9	14.9	34.0	17.5	37.3	19.2	41.0	21.1
30.5	100	25.2	12.9	32.8	16.9	38.1	19.6	41.7	21.5	45.6	23.5
61.0	200	30.3	15.6	38.6	19.9	44.3	22.8	48.2	24.8	52.4	27.0
91.4	300	33.7	17.3	42.3	21.8	48.3	24.8	52.2	26.9	56.6	29.1
121.9	400	36.3	18.7	45.0	23.2	51.2	26.3	55.2	28.4	59.7	30.7
152.4	500	38.4	19.7	47.3	24.3	53.5	27.6	57.6	29.7	62.2	32.0

Table 2-8. 10-min mean wind speed profile envelopes for a 5-percent risk of exceeding the 10-m level mean wind speed for various reference periods of exposure for KSC.

Height		Exposure (Days)									
		1		10		30		90		365	
(m)	(ft)	knots	ms^{-1}	knots	ms^{-1}	knots	ms^{-1}	knots	ms^{-1}	knots	ms^{-1}
10.0	33	20.9	10.8	27.4	14.1	32.0	16.5	35.3	18.2	39.0	20.1
18.3	60	24.7	12.7	31.8	16.3	36.8	18.9	40.3	20.7	44.3	22.8
30.5	100	28.2	14.5	35.8	18.4	41.1	21.2	44.9	23.1	49.1	25.3
61.0	200	33.6	17.3	41.8	21.5	47.6	24.5	51.6	26.6	56.2	28.9
91.4	300	37.1	19.1	45.6	23.5	51.6	26.6	55.8	28.7	60.5	31.2
121.9	400	39.8	20.5	48.5	25.0	54.6	28.1	58.9	30.3	63.7	32.8
152.4	500	42.0	21.6	50.8	26.1	57.0	29.3	61.4	31.6	66.3	34.1

Table 2-9. 10-min mean wind speed profile envelopes for a 1-percent risk value of exceeding the 10-m level mean wind speed for various reference periods of exposure for KSC.

Height		Exposure (Days)									
		1		10		30		90		365	
(m)	(ft)	knots	ms^{-1}	knots	ms^{-1}	knots	ms^{-1}	knots	ms^{-1}	knots	ms^{-1}
10.0	33	26.8	13.8	33.3	17.1	37.9	19.5	41.6	21.4	45.9	23.6
18.3	60	31.1	16.0	38.2	19.7	43.2	22.2	47.2	24.3	51.8	26.7
30.5	100	35.1	18.1	42.6	21.9	47.9	24.7	52.2	26.9	57.1	29.4
61.0	200	41.1	21.2	49.2	25.3	54.9	28.3	59.4	30.6	64.7	33.2
91.4	300	44.9	23.1	53.3	27.4	59.2	30.5	63.9	32.9	69.4	35.7
121.9	400	47.7	24.6	56.3	29.0	62.4	32.1	67.2	34.6	72.8	37.5
152.4	500	50.0	25.8	58.7	30.2	64.9	33.4	69.8	35.9	75.5	38.9

2.2.5.5.2 Design Ground Wind Profiles for Other Locations

Tables 2-10 through 2-17 contain recommended design ground wind profiles for several different risks of exceeding the 10-m level peak wind speed and 10-min mean wind speed for a 1-h exposure period. These tables are based on the same philosophy as table 2-2 and table 2-6 for KSC. The locations for which data are provided include Stennis Space Center, MS; VAFB, CA; White Sands Missile Range, NM; and Edwards Air Force Base (EAFB), CA.

Table 2-10. Surface peak wind speed profile envelopes for various values of risk of exceeding the 10-m level peak wind speed for 1-h exposure (hourly-monthly reference period) for the Stennis Space Center area.

Height		Risk (%)									
		20		10		5		1		0.1	
(m)	(ft)	knots	ms^{-1}	knots	ms^{-1}	knots	ms^{-1}	knots	ms^{-1}	knots	ms^{-1}
10.0	33	19.8	10.2	23.9	12.3	27.6	14.2	37.2	19.1	53.0	27.3
18.3	60	22.4	11.5	27.0	13.9	31.2	16.0	42.0	21.5	57.7	29.7
30.5	100	24.8	12.8	29.9	15.4	34.5	17.8	46.5	23.9	61.9	31.8
61.0	200	28.4	14.6	34.3	17.7	39.6	20.4	53.4	27.4	68.1	35.1
91.4	300	30.8	15.9	37.2	19.2	43.0	22.1	57.9	29.8	72.2	37.2
121.9	400	32.7	16.8	39.4	20.3	45.5	23.4	61.4	31.5	75.2	38.7
152.4	500	34.2	17.6	41.3	21.3	47.7	24.5	64.3	33.0	77.5	39.9

Table 2-11. Surface mean wind speed profile envelopes for various values of risk of exceeding the 10-m level 10-min mean wind speed for 1-h exposure (hourly-monthly reference period) for Stennis Space Center area.

Height		Risk (%)									
		20		10		5		1		0.1	
(m)	(ft)	knots	ms^{-1}	knots	ms^{-1}	knots	ms^{-1}	knots	ms^{-1}	knots	ms^{-1}
10.0	33	14.1	7.3	17.1	8.8	19.7	10.1	26.6	13.7	37.9	19.5
18.3	60	16.0	8.2	19.3	9.9	22.3	11.4	30.0	15.4	41.2	21.2
30.5	100	17.7	9.1	21.4	11.0	24.7	12.7	33.2	17.1	44.2	22.8
61.0	200	20.3	10.5	24.5	12.6	28.3	14.6	38.2	19.6	48.6	25.0
91.4	300	22.0	11.3	26.6	13.7	30.7	15.8	41.4	21.3	51.0	26.6
121.9	400	23.3	12.0	28.2	14.5	32.5	16.7	43.8	22.5	53.7	27.7
152.4	500	24.4	12.6	29.5	15.2	34.1	17.5	45.9	23.6	55.4	28.5

Table 2-12. Surface peak wind speed profile envelopes for various values of risk of exceeding the 10-m level peak wind speed for 1-h exposure (hourly-monthly reference period) for VAFB, CA.

Height		Risk (%)									
		20		10		5		1		0.1	
(m)	(ft)	knots	ms^{-1}	knots	ms^{-1}	knots	ms^{-1}	knots	ms^{-1}	knots	ms^{-1}
10.0	33	20.0	10.3	23.8	12.3	27.5	14.2	35.8	18.4	47.3	24.3
18.3	60	22.5	11.6	26.8	13.8	31.0	16.0	40.3	20.8	51.4	26.5
30.5	100	25.0	12.9	29.7	15.3	34.3	17.7	44.7	23.0	55.2	28.5
61.0	200	28.7	14.8	34.1	17.6	39.4	20.3	51.3	26.4	60.9	31.3
91.4	300	31.1	16.0	37.0	19.0	42.8	22.0	56.7	28.7	64.4	33.2
121.9	400	32.9	16.9	39.2	20.2	45.3	23.3	59.0	30.4	67.1	34.5
152.4	500	34.4	17.7	41.0	21.1	47.4	24.4	61.7	31.7	69.2	35.6

Table 2-13. Surface mean wind speed profile envelopes for various values of risk of exceeding the 10-m level 10-min mean wind speed for 1-h exposure (hourly-monthly reference period) for VAFB, CA.

Height		Risk (%)									
		20		10		5		1		0.1	
(m)	(ft)	knots	ms^{-1}	knots	ms^{-1}	knots	ms^{-1}	knots	ms^{-1}	knots	ms^{-1}
10.0	33	14.3	7.4	17.0	8.9	19.6	10.1	25.6	13.1	33.8	17.4
18.3	60	16.1	8.3	19.2	9.9	22.1	11.4	28.8	14.8	36.7	18.9
30.5	100	17.8	9.2	21.2	10.9	24.5	12.6	31.9	16.4	39.5	20.3
61.0	200	20.5	10.5	24.4	12.6	28.1	14.5	36.7	18.9	43.5	22.4
91.4	300	22.2	11.4	26.4	13.6	30.5	15.7	39.8	20.5	46.0	23.7
121.9	400	23.5	12.1	28.0	14.4	32.3	16.7	42.1	21.7	17.9	24.7
152.4	500	24.6	12.7	29.3	15.1	33.8	17.4	44.0	22.7	49.4	25.5

Table 2-14. Surface peak wind speed profile envelopes for various values of risk of exceeding the 10-m level peak wind speed for 1-h exposure (hourly-monthly reference period) for White Sands Missile Range, NM.

Height		Risk (%)									
		20		10		5		1		0.1	
(m)	(ft)	knots	ms^{-1}	knots	ms^{-1}	knots	ms^{-1}	knots	ms^{-1}	knots	ms^{-1}
10.0	33	15.3	7.9	20.9	10.7	24.7	12.7	34.3	17.7	52.1	26.8
18.3	60	17.3	8.9	23.6	12.1	27.9	14.3	38.8	20.0	56.7	29.2
30.5	100	19.1	9.9	26.1	13.4	30.9	15.9	42.9	22.1	60.9	31.3
61.0	200	22.0	11.3	30.0	15.4	35.5	18.2	49.3	25.4	66.9	34.4
91.4	300	23.8	12.3	32.6	16.7	38.5	19.8	53.4	27.6	71.0	36.5
121.9	400	25.2	13.0	34.5	17.7	40.8	21.0	56.6	29.2	73.9	38.0
152.4	500	26.4	13.7	36.1	18.5	42.7	22.0	59.3	30.6	76.2	39.2

Table 2-15. Surface mean wind speed profile envelopes for various values of risk of exceeding the 10-m level 10-min mean wind speed for 1-h exposure (hourly-monthly reference period) for White Sands Missile Range, NM.

Height		Risk (%)									
		20		10		5		1		0.1	
(m)	(ft)	knots	ms^{-1}	knots	ms^{-1}	knots	ms^{-1}	knots	ms^{-1}	knots	ms^{-1}
10.0	33	10.9	5.6	14.9	7.7	17.6	9.1	24.5	12.6	37.2	19.2
18.3	60	12.3	6.4	16.9	8.6	19.9	10.2	27.7	14.3	40.5	20.8
30.5	100	13.7	7.1	18.7	9.6	22.1	11.3	30.7	15.8	43.4	22.4
61.0	200	15.7	8.1	21.4	11.0	25.3	13.0	35.2	18.2	47.8	24.6
91.4	300	17.0	8.8	23.3	11.9	27.5	14.1	38.2	19.7	50.7	26.1
121.9	400	18.0	9.3	24.6	12.6	29.1	15.0	40.4	20.9	52.8	27.1
152.4	500	18.9	9.8	25.8	13.2	30.5	15.7	42.3	21.9	54.4	28.0

Table 2-16. Surface peak wind speed profile envelopes for various values of risk of exceeding the 10-m level peak wind speed for 1-h exposure (hourly-monthly reference period) for EAFB, CA.

Height		Risk (%)									
		20		10		5		1		0.1	
(m)	(ft)	knots	ms^{-1}	knots	ms^{-1}	knots	ms^{-1}	knots	ms^{-1}	knots	ms^{-1}
10.0	33	27.7	14.3	32.7	16.8	37.9	19.5	48.5	24.9	63.9	32.9
18.3	60	29.2	15.0	34.4	17.7	39.9	20.5	51.0	26.2	67.2	34.6
30.5	100	30.4	15.7	35.9	18.5	41.6	21.4	53.3	27.4	70.2	36.1
61.0	200	32.3	16.6	38.1	19.6	44.2	22.7	56.5	29.1	74.4	38.3
91.4	300	33.4	17.2	39.4	20.3	45.7	23.5	58.5	30.1	77.0	39.6
121.9	400	34.3	17.6	40.4	20.8	46.8	24.1	59.9	30.8	78.9	40.6
152.4	500	34.9	18.0	41.2	21.2	47.7	24.6	61.1	31.4	80.5	41.4

Table 2-17. Surface mean wind speed profile envelopes for various values of risk of exceeding the 10-m level 10-min mean wind speed for 1-h exposure (hourly-monthly reference period) for EAFB, CA.

Height		Risk (%)									
		20		10		5		1		0.1	
(m)	(ft)	knots	ms^{-1}	knots	ms^{-1}	knots	ms^{-1}	knots	ms^{-1}	knots	ms^{-1}
10.0	33	19.6	10.1	24.6	12.7	30.0	15.4	41.4	21.3	57.9	29.8
18.3	60	21.1	10.8	26.4	13.6	32.1	16.5	44.1	22.7	61.5	31.6
30.5	100	22.4	11.5	28.0	14.4	34.0	17.5	46.5	23.9	64.7	33.3
61.0	200	24.2	12.5	30.3	15.6	36.7	18.9	50.0	25.7	69.2	35.6
91.4	300	25.4	13.1	31.7	16.3	38.4	19.7	52.2	26.8	72.0	37.0
121.9	400	26.2	13.5	32.7	16.8	39.6	20.4	53.7	27.6	74.0	38.1
152.4	500	26.9	13.8	33.5	17.2	40.5	20.9	55.0	28.3	75.6	38.9

The peak/mean wind profiles were constructed with a 1.4 gust factor and mean $+3\sigma$ value of k, as given in subsection 2.2.5.4. Some additional general ground wind data are given in references 2-3 and 2-4 for several other locations.

2.2.5.5.3 Frequency of Reported Calm Winds

Generally, aerospace vehicle design criteria wind problems are concerned with high wind speeds, but a condition of calm or very low speeds (generally < 1 kt) may also be important. For example, with no wind to disperse venting vapors such as LOX, a poor visibility situation could develop around the vehicle. Calm wind conditions can also have significant implications relative to the atmospheric diffusion of vehicle exhaust clouds. In addition, calm wind in conjunction with high solar heating can result in significantly high vehicle compartment temperatures. Table 2-18 shows the frequency of calm winds at the 10-m level for KSC as a function of time of day and month. The maximum percentage of calms appears in the summer and during the early morning hours, with the minimum percentage appearing throughout the year during the afternoon. Similar tables for other locations are available upon request.

Table 2-18. Frequency (percent) of reported calm wind at the 10-m level for KSC.

Hour EST	Month												
	Jan	Feb	Mar	Apr	May	June	July	Aug	Sep	Oct	Nov	Dec	Ann.
00	4.8	4.0	3.6	1.3	7.3	9.2	11.7	13.7	6.3	6.9	6.3	6.0	6.8
01	2.8	1.3	2.4	1.7	8.9	8.3	10.9	14.1	7.1	4.8	6.3	6.5	6.3
02	4.8	2.2	3.6	2.9	7.7	10.0	11.7	13.7	10.4	7.3	5.4	4.0	7.0
03	5.2	3.1	2.0	3.8	8.5	12.1	11.3	17.3	12.1	5.2	2.9	3.2	7.3
04	2.8	4.4	2.4	3.8	5.2	13.8	14.5	13.7	10.8	5.2	4.6	2.8	7.0
05	4.4	4.0	3.2	2.9	9.7	16.3	15.3	18.5	13.3	3.6	4.6	4.4	8.4
06	4.4	4.0	4.4	2.9	8.9	16.3	19.8	19.0	13.3	3.2	5.0	5.2	8.9
07	3.6	4.4	4.8	6.3	10.5	16.7	18.1	19.4	15.8	4.4	5.4	5.6	9.6
08	3.6	6.6	6.5	2.9	2.4	5.4	6.0	6.9	4.6	4.0	8.8	4.4	5.2
09	3.6	1.8	2.0	2.1	2.8	3.8	4.8	1.6	4.2	0.8	4.6	5.6	3.1
10	0.4	1.8	1.6	1.7	0.4	3.8	4.0	2.8	2.1	*	1.3	2.4	1.8
11	0.4	1.3	1.2	1.7	0.8	1.3	2.4	0.8	2.9	0.8	1.7	0.8	1.3
12	1.6	0.4	*	*	*	0.8	0.8	0.4	1.3	0.4	2.1	1.2	0.8
13	2.0	0.4	*	*	0.4	1.3	0.4	1.6	0.8	0.4	1.7	0.4	0.8
14	0.8	4.0	0.8	0.4	0.4	0.8	1.2	1.6	1.3	0.8	*	0.4	0.7
15	0.4	1.3	*	*	*	0.8	0.4	1.6	2.5	0.4	0.4	0.4	0.7
16	0.4	0.4	0.4	*	0.8	0.4	0.8	0.4	1.3	0.8	*	0.8	0.5
17	1.6	0.4	*	0.4	0.4	2.1	0.8	3.2	2.1	1.6	1.7	2.0	1.4
18	4.0	1.8	0.8	0.4	1.6	2.5	3.2	4.0	2.9	1.2	5.0	7.7	2.9
19	2.8	3.5	2.0	*	1.6	5.0	2.8	5.2	4.6	1.2	7.1	6.5	3.5
20	4.4	3.5	2.8	1.7	3.2	6.7	5.6	8.5	7.5	1.6	6.3	6.0	4.8
21	5.2	4.0	3.2	1.3	4.8	7.5	10.5	8.9	8.3	4.4	5.0	6.0	5.8
22	3.6	2.2	2.4	1.7	6.0	7.5	7.7	12.9	7.9	4.8	6.3	5.2	5.7
23	5.6	3.5	4.8	0.8	6.5	8.3	10.5	15.3	10.0	5.6	4.6	5.2	6.8
All Hours	3.1	2.5	2.3	1.7	4.1	6.7	7.3	8.6	6.4	2.9	4.0	3.9	4.5

2.2.6 Spectral Ground Wind Turbulence Model

Under most conditions, ground winds are fully developed turbulent flows. This is particularly true when the wind speed is greater than a few meters per second or the atmosphere is unstable, and especially when both conditions exist. During nighttime conditions when the wind speed is typically low and the stratification is stable, the intensity of turbulence is small if not nil. Spectral methods are a particularly useful way of representing the turbulent portion of the ground wind environment for launch vehicle design purposes, as well as for use in diffusion calculations of toxic fuels and atmospheric pollutants.

2.2.6.1 Introduction

At a fixed point in the atmospheric boundary layer, the instantaneous wind vector from the quasi-steady wind vector is the horizontal vector component of turbulence. This vector departure can be represented by two components, the longitudinal and the lateral components of turbulence which are parallel and perpendicular to the steady-state wind vector in the horizontal plane (fig. 2-4). The model contained herein is a spectral representation of the characteristics of the longitudinal and lateral components of turbulence. The model analytically defines the spectra of these components of turbulence for the first 200 m of the boundary layer. In addition, it defines the longitudinal and lateral cospectra, quadrature spectra, and corresponding coherence functions associated with any pair of levels in the boundary space. Details concerning the model can be found in references 2-5 through 2-8.

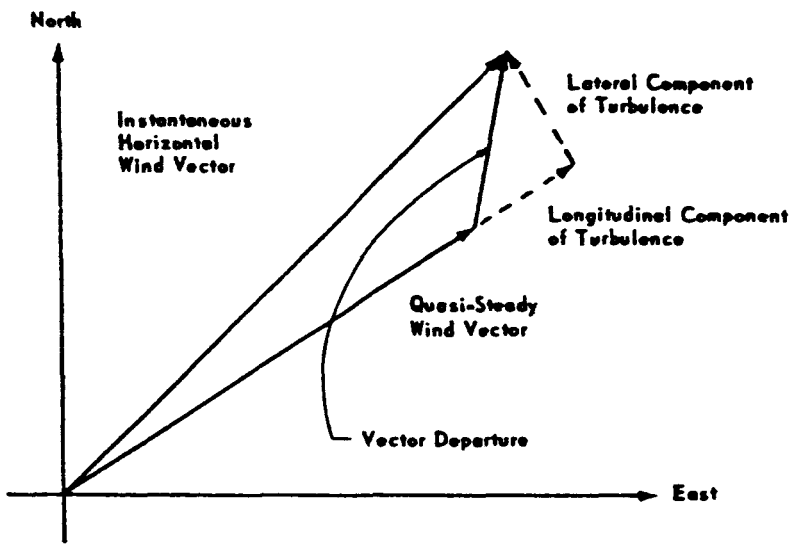

Figure 2-4. The relationship between the quasi-steady state and the horizontal instantaneous wind vectors and the longitudinal and lateral components of turbulence.

2.2.6.2 Turbulence Spectra

The longitudinal and lateral spectra of turbulence at frequency ω, and height z can be represented by a dimensionless function of the form

$$\frac{\omega S(\omega)}{\beta u_*^2} = \frac{C_1 f/f_m}{\left[1+1.5\,(f/f_m)^{C_2}\right]^{(5/3)C_2}}, \tag{2.3}$$

where

$$f = \frac{\omega z}{u(z)} , \tag{2.4}$$

$$f_m = C_3 \left(\frac{z}{z_r}\right)^{C_4} , \tag{2.5}$$

$$\beta = \left(\frac{z}{z_r}\right)^{C_5} , \tag{2.6}$$

$$u_* = c_6 \bar{u}(z_r) . \tag{2.7}$$

In these equations z_r is a reference height equal to 18.3 m (60 ft); $u(z_r)$ is the quasi-steady wind speed at height z; and the quantities c_i (i = 1,2,3,4,5) are dimensionless constants that depend upon the site and the atmospheric stability. The frequency, ω, in units of cycles per unit time, is defined with respect to a structure or vehicle at rest relative to the Earth. The reader is referred to sections 2.3.13 and 2.3.14 for the definition of turbulence spectral inputs for application to the takeoff and landing of conventional aeronautical systems and the landing of the space shuttle orbiter vehicle. The spectrum $S(\omega)$ is defined so that integration over the domain $0 \leq \omega \leq \infty$ yields the variance of the turbulence. Engineering values of c_i are given in table 2-19 for the longitudinal spectrum and in table 2-20 for the lateral spectrum. The constant c_6 to input into equation (2.7) can be estimated with the equation

$$c_6 = \frac{0.4}{\ln\left(\frac{z_r}{z_0}\right) - \psi} , \tag{2.8}$$

where z_0 is the surface roughness length of the site and Ψ is a parameter that depends upon the stability. If z_0 is not available for a particular site, then an estimate of z_0 can be obtained by taking 10 percent of the typical height of the surface obstructions (grass, shrubs, trees, rocks, etc.). The typical height is determined over a fetch (the distance the wind blows over a surface) equal to approximately 1,500 m. The parameter Ψ vanishes for strong wind conditions and is of order unity for light wind, unstable daytime conditions at KSC. Typical values of z_0 for various surfaces are given in table 2-21.

Table 2-19. Dimensionless constants (C_i) for the longitudinal spectrum of turbulence for KSC.

Conditions	c_1	c_2	c_3	c_4	c_5
Light Wind Daytime Conditions	2.905	1.235	0.04	0.87	–0.14
Strong Winds	6.198	0.845	0.03	1.0	–0.63

Table 2-20. Dimensionless constants (C_i) for the lateral spectrum of turbulence for KSC.

Conditions	c_1	c_2	c_3	c_4	c_5
Light Wind Daytime Conditions	4.599	1.144	0.033	0.72	–0.04
Strong Winds	3.954	0.781	0.1	0.58	–0.35

Table 2-21. Typical values of surface roughness length (z_0) for various types of surfaces.

Type of Surface	z_0 (m)	z_0 (ft)
Mud flats, ice	10^{-5}–3×10^{-5}	3×10^{-5}–10^{-4}
Smooth sea	2×10^{-4}–3×10^{-4}	7×10^{-4}–10^{-3}
Sand	10^{-4}–10^{-3}	3×10^{-4}–3×10^{-3}
Snow surface	10^{-3}–6×10^{-3}	3×10^{-4}–2×10^{-2}
Mown grass (~0.01 m)	10^{-3}–10^{-2}	3×10^{-3}–3×10^{-2}
Low grass, steppe	10^{-2}–4×10^{-2}	3×10^{-2}–10^{-1}
Fallow field	2×10^{-2}–3×10^{-2}	6×10^{-2}–10^{-1}
High grass	4×10^{-2}–10^{-1}	10^{-1}–3×10^{-1}
Palmetto	10^{-1}–3×10^{-1}	3×10^{-1}–1
Suburbia	1–2	3–6
City	1–4	3–13

The function given by equation (2.3) is depicted in figures 2-5 and 2-6. Upon prescribing the steady-state wind profile $u(z)$ and the site (z_0), the longitudinal and lateral spectra are completely specified functions of height, z, and frequency, ω. A discussion of the units of the various parameters mentioned previously is given in subsection 2.2.6.4.

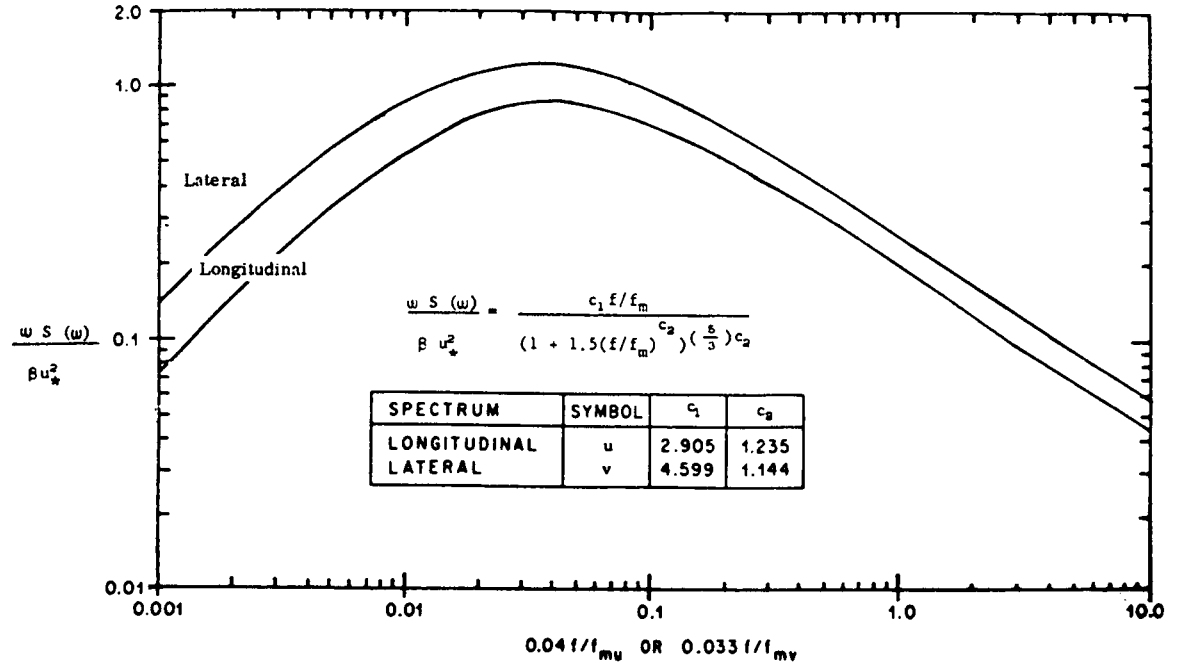

Figure 2-5. $\omega S(\omega)/\beta u_*^2$ versus $0.04f/f_m$ (longitudinal) and $0.033f/f_m$ (lateral) for light wind daytime conditions.

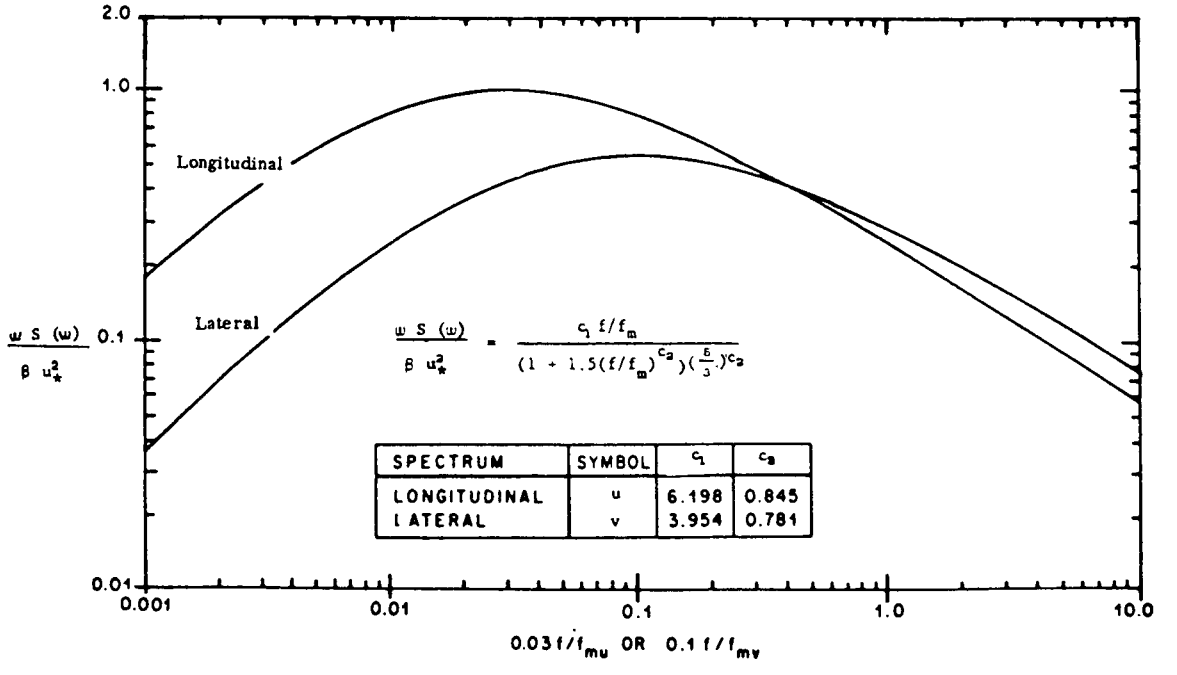

Figure 2-6. $\omega S(\omega)/\beta u_*^2$ versus $0.03f/f_m$ (longitudinal) and $0.1f/f_m$ (lateral) for strong wind conditions.

2.2.6.3 The Cospectrum and Quadrature Spectrum

The cospectrum (C) and the quadrature (Q) spectrum associated with either the longitudinal or lateral components of turbulence at levels z_1 and z_2 can be represented by the following:

$$C(\omega,z_1,z_2) = \sqrt{S_1 S_2}\, exp\left(-0.3465 \frac{\Delta f}{\Delta f_{0.5}}\right) \cos(2\pi\gamma \Delta f) , \tag{2.9}$$

$$Q(\omega,z_1,z_2) = \sqrt{S_1 S_2}\, exp\left(-0.3465 \frac{\Delta f}{\Delta f_{0.5}}\right) \sin(2\pi\gamma \Delta f) , \tag{2.10}$$

where

$$\Delta f = \frac{\omega z_2}{\bar{u}(z_2)} - \frac{\omega z_1}{\bar{u}(z_1)} . \tag{2.11}$$

The quantities S_1 and S_2 are the longitudinal or lateral spectra at levels z_1 and z_2, respectively, and $u(z_1)$ and $u(z_2)$ are the steady-state wind speeds at levels z_1 and z_2. The quantity $\Delta f_{0.5}$ is a nondimensional function of stability, where $\Delta f_{0.5}$ is that value for which the coherence (coh) is equal to 0.5, and values of this parameter for KSC are given in table 2-22. The nondimensional quantity, τ, should depend upon height and stability. However, it has only been possible to detect a dependence on height at KSC. Based upon analysis of turbulence data measured at the NASA 150-m Ground Wind Tower Facility at KSC, the values of γ in table 2-23 are suggested for KSC. The quantity $\Delta f_{0.5}$, can be interpreted by constructing the coherence function, which is defined to be

$$\text{coh}(\omega,z_1,z_2) = \frac{C^2+Q^2}{S_1 S_2} . \tag{2.12}$$

Table 2-22. Values of $\Delta f_{0.5}$ for KSC.

Turbulence Component	Light Wind Daytime Conditions	Strong Winds
Longitudinal	0.04	0.036
Lateral	0.06	0.045

Table 2-23. Values of γ for KSC.

Turbulence Component	$(z_1+z_2)/2 \leq 100$ m	$(z_1+z_2)/2 > 100$ m
Longitudinal	0.7	0.3
Lateral	1.4	0.5

Substituting equations (2.9) and (2.10) into equation (2.12) yields

$$\text{coh}(\omega,z_1,z_2) = \exp\left(-0.693 \frac{\Delta f}{\Delta f_{0.5}}\right) . \tag{2.13}$$

2.2.6.4 Units

The spectral model of turbulence presented in subsections 2.2.6.2 and 2.2.6.3 is a dimensionless model. Accordingly, the user is free to select the system of units he desires, except that ω must have the units of cycles per unit time. Table 2-24 gives the appropriate metric and U.S. customary units for the various quantities in the model.

Table 2-24. Metric and U.S. customary units of various quantities in the turbulence model.

Quantity	Metric Units	U.S. Customary Units
ω	Hz	Hz
$S(\omega), Q(\omega), C(\omega)$	$m^2\ s^{-2}/z$	$ft^2\ s^{-2}/Hz$
$f, f_m, \Delta f, \Delta f_{0.5}$	Dimensionless	Dimensionless
z, s_r, z_0	m	ft
u, u_*	ms^{-1}	$ft\ s^{-1}$
β	Dimensionless	Dimensionless
Coh	Dimensionless	Dimensionless
γ	Dimensionless	Dimensionless
Ψ	Dimensionless	Dimensionless

2.2.7 Ground Wind Gust Factors

The gust factor G is defined to be

$$G=\frac{u}{\bar{u}}\ , \tag{2.14}$$

where

u = maximum wind speed at height z within an average period of length τ in time

$\bar{u}$ = mean wind speed associated with the average period τ, given by

$$\bar{u}=\frac{1}{\tau}\int_0^{\tau} u_i\,(t)\,dt\ , \tag{2.15}$$

$u_i(t)$ = instantaneous wind speed at time t

t = time reckoned from the beginning of the averaging period.

If $\tau = 0$, then $\bar{u} = u$ according to equation (2.15), and it follows from equation (2.14) that $G = 1.0$. As τ increases, $\bar{u}$ departs from u, and $\bar{u} \leq u$ and $G > 1.0$. Also, as τ increases, the probability of finding a maximum wind of a given magnitude increases. In other words, the maximum wind speed increases as τ increases. In the case of $\bar{u} \rightarrow 0$ and $u \geq 0$ ($\bar{u} = 0$ might correspond to windless free convection), $G \rightarrow \infty$. As $\bar{u}$ or u increases, G tends to decrease for fixed $\tau > 0$; while for very high wind speeds, G tends to approach a constant value for given values of z and τ. Finally, as z increases, G decreases. Thus, the gust factor is a function of the averaging time, τ, over which the mean wind speed is calculated, the height, z, and wind speed (mean or maximum).

2.2.7.1 Gust Factor as a Function of Peak Wind Speed ($u_{18.3}$) at Reference Height for KSC

Investigations (ref. 2-8) of gust factor data have revealed that the vertical variation of the gust factor can be described with the following relationship:

$$G = 1 + \frac{1}{g_0}\left(\frac{18.3}{z}\right)^p , \tag{2.16}$$

where z is the height in meters above natural grade. The parameter, p, a function of the 18.3-m peak wind speed in meters per second, is given by

$$p = 0.283 - 0.435 e^{-0.2 u_{18.3}} . \tag{2.17}$$

The parameter g_0 depends on the averaging time and the 18.3-m peak wind speed and is given by

$$g_0 = 0.085\left(\ln\frac{\tau}{10}\right)^2 - 0.329\left(\ln\frac{\tau}{10}\right) + 1.98 - 1.887 e^{-0.2 u_{18.3}} , \tag{2.18}$$

where τ is given in minutes and $u_{18.3}$ in meters per second.

These relationships are valid for $u_{18.3} \geq 4$ m/s and $\tau \leq 10$ min. In the interval 10 min $\leq \tau \leq 60$ min, G is a slowly increasing monotonic function of τ, and for all engineering purposes the 10-min gust factor ($\tau = 10$ min) can be used as an estimate of the gust factors associated with averaging times greater than 10 min and less than 60 min (10 min $\leq \tau \leq 60$ min).

The calculated mean gust factors for 10 min for values of $u_{18.3}$ in the interval 4.63 m/s $\leq u_{18.3} \leq \infty$ are presented in table 2-25 in both the U.S. customary and metric units for $u_{18.3}$ and z. As an example, the gust factor profile for $\tau = 10$ min and $u_{18.3} = 9.27$ m/s (18 knots) is given in table 2-26. Since the basic wind statistics are given in terms of hourly peak wind, use the $\tau = 10$ min gust factors to convert the peak winds to mean winds by dividing by G. All gust factors in these sections are expected values for any particular set of values for u, τ, and z.

2.2.7.2 Gust Factors for Other Locations

For design purposes, the gust factor value of 1.4 should be used over all heights of the ground wind profile at other test ranges. This gust factor should correspond to approximately a 10-min averaging period.

Table 2-25. 10-min gust factors for KSC.

Reference Height 60-ft (18.3 m) Peak Wind knots (ms^{-1})	Height Above Natural Grade in Feet (meters)						
	33 (10.0)	60 (18.3)	100 (30.5)	200 (61.0)	300 (91.4)	400 (121.9)	500 (152.4)
9.0 (4.63)	1.868	1.812	1.767	1.710	1.679	1.658	1.642
10.0 (5.15)	1.828	1.766	1.718	1.657	1.624	1.602	1.585
11.0 (5.66)	1.795	1.729	1.678	1.614	1.580	1.556	1.539
12.0 (6.18)	1.768	1.699	1.645	1.579	1.544	1.520	1.502
13.0 (6.69)	1.746	1.674	1.618	1.552	1.514	1.489	1.471
14.0 (7.21)	1.727	1.652	1.595	1.525	1.488	1.464	1.446
15.0 (7.72)	1.712	1.634	1.576	1.505	1.467	1.442	1.424
16.0 (8.24)	1.698	1.619	1.559	1.487	1.449	1.424	1.409
17.0 (8.75)	1.686	1.606	1.545	1.472	1.424	1.409	1.390
18.0 (9.27)	1.676	1.594	1.532	1.459	1.421	1.395	1.377
19.0 (9.78)	1.668	1.584	1.522	1.447	1.409	1.384	1.365
20.0 (10.3)	1.660	1.575	1.512	1.437	1.399	1.374	1.355
25.0 (12.9)	1.634	1.545	1.480	1.403	1.365	1.339	1.321
30.0 (15.4)	1.619	1.528	1.462	1.385	1.346	1.321	1.302
∞ (∞)	1.599	1.505	1.437	1.359	1.320	1.295	1.277

Table 2-26. Gust factor profile for $\tau = 10$ min and $u_{18.3} = 9.27$ m/s (18 knots).

Height		Gust Factors (G)
(ft)	(m)	
33	10.0	1.676
60	18.3	1.594
100	30.5	1.532
200	61.0	1.459
300	91.4	1.421
400	121.9	1.395
500	152.4	1.377

2.2.8 Ground Wind Shear

Wind shear near the surface, for design purposes, is a shear that acts upon an aerospace vehicle, freestanding on the pad, or at time of lift-off. For overturning moment calculations, the wind shear shall be computed by first subtracting the 10-min mean wind speed at the height corresponding to the base of the vehicle from the peak wind speed at the height corresponding to the top of the vehicle (see sections 2.3.5.5 for mean and peak wind profiles) and then dividing the difference by the height of the vehicle. The reader should consult references 2-9 through 2-17 for a detailed discussion of the statistical properties of wind shear near the ground for engineering applications.

2.2.9 Ground Wind Direction Characteristics

Figure 2-1 (subsection 2.2.5.1) shows a time trace of wind direction (section of a wind direction recording chart). This wind direction trace may be visualized as being composed of a mean wind direction plus fluctuations about the mean. An accurate measure of ambient wind direction near the ground is difficult to obtain sometimes because of the interference of the structure that supports the instrumentation and other obstacles in the vicinity of the measurement location (ref. 2-18). This is particularly true for launch pads; therefore, care must be exercised in locating wind sensors in order to obtain representative measurements of the ambient wind direction.

General information, such as that which follows, is available and may be used to specify conditions for particular engineering studies. For instance, the variation of wind direction as a function of mean wind speed and height from analysis of NASA's 150-m Ground Winds Tower Facility data at KSC is discussed in reference 2-2. A graph is shown in reference 2-2 that gives values of the standard deviation of the wind direction σ_θ as a function of height for a sampling time of approximately 5 min.

2.2.10 Design Winds for Facilities and Ground Support Equipment

2.2.10.1 Introduction

In this section, the important relationships between desired lifetime, N (years); calculated risk, U(%÷100); design return period, T_D (years); and design wind, W_D (m/s or knots) will be described for use in facilities design for several locations.

The desired lifetime N is expressed in years, and preliminary estimates must be made as to how many years the proposed facility is to be used.

The calculated risk U is a probability expressed either as a percentage or as a decimal fraction. Calculated risk, sometimes referred to as design risk, is a probability measure of the risk the designer is willing to accept that the facility will be destroyed by wind loading in less time than the desired lifetime.

The design return period T_D is expressed in years and is a function of desired lifetime and calculated risk.

The design wind W_D is a function of the desired lifetime and calculated risk and is derived from the design return period and a probability distribution function of yearly peak winds.

2.2.10.2 Development of Relationships

From the theory of repeated trial probability the following expression can be derived:

$$N = \frac{ln\,(1-U)}{ln\left(1-\frac{1}{T_D}\right)} . \tag{2.19}$$

Equation (2.19) gives the important relationships for the three variables, calculated risk, U(%÷100); design return period, T_D (years); and desired lifetime, N (years). If estimates for any two variables are available, the third can be determined from this equation.

Design return period, T_D, calculated with equation (2.19), for various values of desired lifetime, N, and design risk are given in table 2-27. The table presents the exact and adopted values for design return period versus desired lifetime for various design risks. The adopted values for T_D are in some cases greatly oversized to facilitate a convenient use of the tabulated probabilities for distributions of yearly peak winds.

Table 2-27. Exact (Ex) and adopted values for design return period (T_D, years) versus desired lifetime (N, years) for various design risks (U).

N (years)	Design Return Period (years)									
	$U = 0.5$ (50%)		$U = 0.2$ (20%)		$U = 0.1$ (10%)		$U = 0.05$(5%)		$U = 0.01$ (1%)	
	Ex	Adopt	Ex	Adopt	Ex	Adopt	Ex	Adopt	Ex	Adopt
1	2	2	15	5	10	10	20	20	100	100
10	15	15	45	50	95	100	196	200	996	1,000
20	29	30	90	100	190	200	390	400	1,991	2,000
25	37	40	113	125	238	250	488	500		
30	44	50	135	150	285	300	585	600		
50	73	100	225	250	475	500	975	1,000		
100	145	150	449	500	950	1,000	1,950	2,000		

2.2.10.3 Design Winds for Facilities

To obtain the design wind, the wind speed corresponding to the design return period must be determined. Since the design return period is a function of risk, either of two procedures can be used to determine the design wind: One is through a graphical or numerical interpolation procedure; the second is based on an analytical function. A knowledge of the distribution of yearly peak winds is required for both procedures. For the greatest statistical efficiency in arriving at the probability that the peak winds will be less than or equal to some specified value of yearly peak winds, an appropriate probability distribution function must be selected, and the parameters for the function estimated from the sample of yearly peak winds. The Gumbel distribution (ref. 2.56) is an excellent fit for the yearly peak ground wind speed at the 10-m level for KSC. The distribution of yearly peak wind speed (10-m level), as obtained by the Gumbel distribution, is tabulated for various percentiles together with the corresponding return periods in table 2-28. The values for the parameters α and μ for this distribution are also given in this table.

The design wind speed can now be determined by choosing a desired lifetime, design risk, by taking the design return period from table 2-27 and looking up the wind speed corresponding to the return periods in table 2-28. For combinations not tabulated in tables 2-27 and 2-28, the design return period can be interpolated.

2.2.10.4 Procedure to Determine Design Winds for Facilities

The design wind, W_D, as a function of desired lifetime, N, and calculated risk, U, for the Gumbel distribution of peak winds at the 10-m reference level, can be derived as

$$W_D = \frac{1}{\alpha}[-ln[-ln(1-U)] + ln\, N] + \mu \ , \qquad (2.20)$$

where α and μ are estimated from the sample of yearly peak wind.

Taking the values for α^{-1} = 5.59 m/s (10.87 knots) and for μ = 23.4 m/s (45.49 knots) from table 2-28 and evaluating equation (2.20) for selected values of N and U yields the data in table 2-29.

Design wind speed versus desired lifetime is plotted in figure 2-7 where the slopes of the lines are equal.

Table 2-28. Gumbel distribution for yearly peak wind speed, 10-m reference level, including hurricane winds, KSC.

Return Period (years)	Probability	y	m/s	knots
2	0.50	0.36651	25.45	49.47
5	0.80	1.49994	31.79	61.79
10	0.90	2.25037	35.98	69.95
15	0.933	2.66859	38.33	74.50
20	0.95	2.97020	40.01	77.77
30	0.967	3.39452	42.38	82.39
45	0.978	3.80561	44.68	86.86
50	0.98	3.90191	45.22	87.90
90	0.9889	4.49523	48.54	94.35
100	0.99	4.60015	49.12	95.49
150	0.9933	5.00229	51.37	99.86
200	0.995	5.29581	53.01	103.05
250	0.996	5.51946	54.26	105.48
300	0.9967	5.71218	55.34	107.58
400	0.9975	5.99021	56.90	110.60
500	0.9980	6.21361	58.14	113.02
600	0.9983	6.37628	58.75	114.20
1,000	0.9990	6.90726	62.02	120.56
10,000	0.9999	9.21029	74.90	145.60

α^{-1} = 5.5917 m/s (10.87 knots) μ = 23.4 m/s (45.49 knots)

$\Phi = \exp(-\exp(-y))$, where $y = \alpha(x-\mu)$

Φ is the probability distribution function of the reduced variate, y.

Table 2-29. Facility design wind, $W_{D\,10}$, with respect to the 10-m reference level peak wind speed for various lifetimes (N), KSC.*

Design Risk U	$1-U$	$-\ln(-\ln(1-U))$	Design Wind (W_{D10}) for Various Lifetimes (N)*							
			$N=1$		$N=10$		$N=30$		$N=100$	
			(m/s)	(knots)	(m/s)	(knots)	(m/s)	(knots)	(m/s)	(knots)
0.63212	0.36788	0	23.40	45.49	36.28	70.52	42.42	82.46	49.15	95.55
0.50	0.50	0.37	25.45	49.47	38.33	74.50	44.47	86.44	51.20	99.53
0.4296	0.5704	0.58	26.62	51.76	39.50	76.79	45.65	88.73	52.38	101.82
0.40	0.60	0.67	27.16	52.79	40.03	77.82	46.18	89.76	52.92	102.85
0.30	0.70	1.03	29.17	56.70	42.04	81.72	48.19	93.67	54.92	106.75
0.20	0.80	1.50	31.79	61.79	44.66	86.82	50.81	98.76	57.54	111.85
0.10	0.90	2.25	35.99	69.95	48.86	94.98	55.00	106.92	61.74	120.01
0.05	0.95	2.97	40.01	77.77	52.88	102.80	59.03	114.74	65.76	127.83
0.01	0.99	4.60	49.12	95.49	62.00	120.52	68.14	132.46	74.88	145.55

*Values of N are given in years.

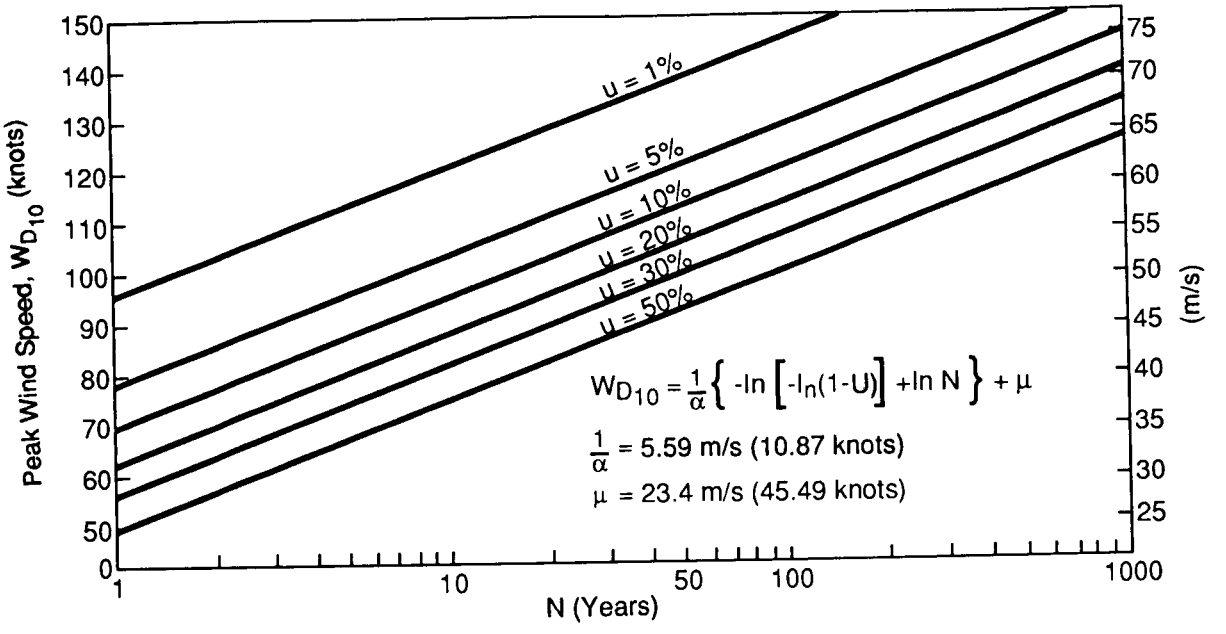

Figure 2-7. Facility design wind, $W_{D\,10}$, with respect to the 10-m reference level peak wind speed for various lifetimes (N), KSC.

2.2.10.5 Wind Load Calculations

The design wind for a structure cannot be determined solely by wind statistics at a particular height. The design engineer is most interested in designing a structure which satisfies the user's requirements for utility, which will have a small risk of failure within the desired lifetime of the structure, and which can carry a sufficiently large wind load and be constructed at a sufficiently low cost. The total wind loading on a structure is composed of two interrelated components, steady-state drag wind loads and dynamic wind loads (time-dependent drag loads, vortex shedding forces, etc.). The time required for a structure to respond to the drag wind loads dictates the averaging time for the design wind profile. In general, the structure response time depends upon the shape of the structure. The natural frequency of the structure and its components are important in estimating the dynamic wind load. It is conceivable that a structure could be designed to withstand very high wind speeds without structural failure and still oscillate in moderate wind speeds. If such a structure, for example, is to be used to support a precision tracking radar, then there may be little danger of overloading the structure by high winds; but the structure might be useless for its intended purpose if it were to oscillate in a moderate wind. Also, a building may have panels or small members that could respond to dynamic loading in such a way that long-term vibrations could cause failure, without any structural failure of the main supporting members. Since dynamic wind loading requires an intricate knowledge of the particular facility and its components, no attempt is made here to state generalized design criteria for dynamic wind loading. The emphasis in this section is upon winds for estimating drag wind loads in establishing design wind criteria for structures. Reference is made to subsection 2.2.5.5 and 2.2.6 for information appropriate to dynamic wind loads.

2.2.10.6 Wind Profile Construction

Given the peak wind at the 10-m level, the peak wind profile can be constructed with the peak wind profile law from subsection 2.2.5.5. Steady-state wind profiles can be obtained by using appropriate gust factors which are discussed in subsection 2.2.7.

To illustrate the procedures and operations in deriving the wind profile and the application of the gust factor, three examples are worked out for KSC. Peak wind speeds at the 10-m level of 36, 49, and 62 m/s (70, 95, and 120 knots) have been selected for these examples. These three wind speeds were selected because they correspond to a return period of 10, 100, and 1,000 years for a peak wind at the 10-m level at KSC. Table 2-30 contains the risks of exceeding these peak winds for various values of desired lifetime. Table 2-31 gives the peak design wind profiles corresponding to the desired lifetimes and calculated risks presented in table 2-30. These profiles were calculated with equation (2.22).

Table 2-30. Calculated risk (U) versus desired lifetime (N, years) for assigned design winds related to peak winds at the 10-m reference level, KSC.

N (years)	W_{D10} = 36 m/s (70 knots) T_D = 10 years U%	W_{D10} = 49 m/s (95 knots) T_D = 100 years U%	W_{D10} = 62 m/s (120 knots) T_D = 1,000 years U%
1	10	1.0	0.1
10	65	10	1
20	88	18	2
25	93	22	2.5
30	95.8	26	3
50	99.5	39.5	5
100	99.997	63.397	10
T_D = Design return period			

Table 2-31. Design peak wind profiles for design wind relative to the 10-m reference level, KSC.

Height		W_{D10} = 36 m/s (70 knots)		W_{D10} = 49 m/s (95 knots)		W_{D10} = 62 m/s (120 knots)	
(ft)	(m)	(knots)	(ms^{-1})	(knots)	(ms^{-1})	(knots)	(ms^{-1})
33	10.0	70.0	36.0	95.0	48.9	120.0	61.8
60	18.3	74.5	38.4	99.9	51.4	125.2	64.5
100	30.5	78.6	40.0	104.2	53.7	129.8	66.8
200	61.0	84.4	43.4	110.4	56.8	136.2	70.1
300	91.4	88.0	45.3	114.2	58.8	140.2	72.2
400	121.9	90.7	46.7	117.0	60.2	143.0	73.6
500	152.4	92.8	47.8	119.1	61.3	145.3	74.8

Table 2-32. Gust factors for various averaging times (τ) for peak winds > 15 m/s (29 knots) at the 10-m reference level versus height, KSC.

Height		Various Averaging Times (τ, min)				
(ft)	(m)	$\tau = 0.5$	$\tau = 1$	$\tau = 2$	$\tau = 5$	$\tau = 10$
33	10.0	1.318	1.372	1.528	1.599	1.599
60	18.3	1.268	1.314	1.445	1.505	1.505
100	30.5	1.232	1.271	1.385	1.437	1.437
200	61.0	1.191	1.223	1.316	1.359	1.359
300	91.4	1.170	1.199	1.282	1.320	1.320
400	121.9	1.157	1.183	1.260	1.295	1.295
500	152.4	1.147	1.172	1.244	1.277	1.277

2.2.10.7 Use of Gust Factors Versus Height

In estimating the drag load on a particular structure, it may be determined that wind force of a given magnitude must act on the structure for some period (for example, 1 min) to produce a critical drag load. To obtain the wind profile corresponding to a time-averaged wind, the peak wind profile values are divided by the required gust factors. The gust factors for winds greater than 15 m/s (29 knots) versus height given in table 2-32 are taken from section 2.2.7. This operation may seem strange to someone who is accustomed to multiplying the given wind by a gust factor in establishing the design wind. This is because most literature on this subject gives the reference wind as averaged over some time increment (for example, 1, 2, or 5 min) or in terms of the "fastest mile" of wind that has a variable averaging time depending upon the wind speed. The design wind profiles for the three examples, peak winds of 36, 49, and 62 m/s (70, 95, and 120 knots) at the 10-m level for various averaging times τ given in minutes, are illustrated in tables 2-33, 2-34, and 2-35. Following the procedures presented herein, the design engineer can objectively derive several important design parameters that can be used in designing a facility that will (1) meet the requirements for utility and desired lifetime, (2) withstand a sufficiently large wind loading with a known calculated risk of failure due to wind loads, and (3) allow him to proceed with trade-off studies between the design parameters and to estimate the cost of building the structure to best meet these design objectives.

Table 2-33. Design wind profiles for various averaging times (τ) for peak design wind of 36.0 m/s (70.0 knots) relative to the 10-m reference level, KSC.

Height		Design Wind Profiles for Various Averaging Times (τ) in Minutes											
(ft)	(m)	$\tau = 0$		$\tau = 0.5$		$\tau = 1$		$\tau = 2$		$\tau = 5$		$\tau = 10$	
		(m/s)	(knots)	(m/s)	(knots)	(m/s)	(knots)	(m/s)	(knots)	(m/s)	(knots)	(m/s)	(knots)
33	10.0	36.0	70.0	27.3	53.1	26.2	51.0	25.1	48.8	23.6	45.8	22.5	43.8
60	18.3	38.3	74.5	30.2	58.8	29.2	56.7	28.0	54.5	26.5	51.6	25.5	49.5
100	30.5	40.4	78.6	32.8	63.8	31.8	61.8	30.7	59.7	29.2	56.8	28.1	54.7
200	61.0	43.4	84.4	36.5	70.9	35.5	69.0	34.4	66.9	33.0	64.1	31.9	62.1
300	91.4	45.3	88.0	38.7	75.2	37.8	73.4	36.7	71.4	35.3	68.6	34.3	66.7
400	121.9	46.7	90.7	40.3	78.4	39.5	76.7	38.4	74.7	37.0	72.0	36.0	70.0
500	152.4	47.7	92.8	41.6	80.9	40.7	79.2	39.8	77.3	38.4	74.6	37.4	72.7

Table 2-34. Design wind profiles for various averaging times (τ) for peak design wind of 49.0 m/s (95 knots) relative to the 10-m reference level, KSC.

Height		Design Wind Profiles for Various Averaging Times (τ) in Minutes											
(ft)	(m)	$\tau = 0$		$\tau = 0.5$		$\tau = 1$		$\tau = 2$		$\tau = 5$		$\tau = 10$	
		(m/s)	(knots)	(m/s)	(knots)	(m/s)	(knots)	(m/s)	(knots)	(m/s)	(knots)	(m/s)	(knots)
33	10.0	48.9	95.0	37.1	72.1	35.6	69.2	34.1	66.2	32.0	62.2	30.6	59.4
60	18.3	51.4	99.9	40.5	78.8	39.1	76.0	37.6	73.1	35.5	69.1	34.2	66.4
100	30.5	53.6	104.2	43.5	84.6	42.2	82.0	40.7	79.1	38.7	75.2	37.3	72.5
200	61.0	56.8	110.4	47.7	92.7	46.5	90.3	45.0	87.5	43.2	83.9	41.8	81.2
300	91.4	58.7	114.2	50.2	97.6	49.0	95.2	47.7	92.7	45.8	89.1	44.5	86.5
400	121.9	60.2	117.0	52.0	101.1	50.9	98.9	49.6	96.4	47.8	92.9	46.5	90.3
500	152.4	61.3	119.1	53.4	103.8	52.3	101.6	51.0	99.2	49.2	95.7	48.0	93.3

Table 2-35. Design wind profiles for various averaging times (τ) for peak design wind of 62.0 m/s (120 knots) relative to the 10-m reference level, KSC.

Height		Design Wind Profiles for Various Averaging Times (τ) in Minutes											
(ft)	(m)	$\tau = 0$		$\tau = 0.5$		$\tau = 1$		$\tau = 2$		$\tau = 5$		$\tau = 10$	
		(m/s)	(knots)	(m/s)	(knots)	(m/s)	(knots)	(m/s)	(knots)	(m/s)	(knots)	(m/s)	(knots)
33	10.0	61.7	120.0	46.8	91.0	45.0	87.5	43.0	83.6	40.4	78.5	38.6	75.0
60	18.3	64.4	125.2	50.8	98.7	49.0	95.3	47.2	91.7	44.6	86.6	42.8	83.2
100	30.5	66.8	129.8	54.2	105.4	52.5	102.1	50.7	98.6	48.2	93.7	46.5	90.3
200	61.0	70.1	136.2	58.9	114.4	57.3	111.4	55.6	108.0	53.2	103.5	51.5	100.2
300	91.4	72.1	140.2	61.6	119.8	60.1	116.9	58.5	113.8	56.3	109.4	54.6	106.2
400	121.9	73.6	143.0	63.6	123.6	62.2	120.9	60.6	117.8	58.4	113.5	56.8	110.4
500	152.4	74.7	145.3	65.2	126.7	63.8	124.0	62.2	121.0	60.1	116.8	58.5	113.8

2.2.10.8 Recommended Design Risk Versus Desired Lifetime

Unfortunately, there is not a clear-cut precedent from building codes to follow in recommending design risk for a given desired lifetime of a structure. Conceivably, a value analysis in terms of original investment cost, replacement cost, safety of property and human life, loss of national prestige, and many other factors should be made to give a measure of the consequences of the loss of a particular structure in arriving at a decision as to what risk management is willing to accept for the loss within the desired lifetime of the structure. If the structure is an isolated shed, then obviously its loss is not as great as a structure that would house many people or a structure that is critical to the mission of a large organization; nor is it as potentially unsafe as the loss of a nuclear power plant or storage facility for explosives or highly radioactive materials.

To give a starting point for design studies aimed at meeting the design objectives, it is recommended that a design risk of 10 percent for the desired lifetime be used in determining the wind loading on structures that have a high replacement cost. Should the loss of the structure be extremely hazardous to life or property, or critical to the mission of a large organization, then a design risk of 5 percent or less for the desired lifetime is recommended. These are subjective recommendations involving arbitrary assumptions about the design objectives. Note that the longer the desired lifetime, the greater the design risk is for a given wind speed (or wind loading). Therefore, realistic appraisals should be made for desired lifetimes.

2.2.10.9 Design Winds for Facilities at VAFB, White Sands Missile Range, Edwards AFB, and Stennis Space Center

2.2.10.9.1 Wind Statistics

The basic wind statistics for these four locations are taken from reference 2-19, which presents isotach maps for the United States for the 50-, 98-, and 99-percentile values for the yearly maximum "fastest mile" of wind at the ~10-m (30-ft) reference height above natural grade. By definition, the fastest mile is the fastest wind speed in miles per hour of any mile of windflow past an anemometer during a specified period (usually taken as the 24-h observational day), and the largest of these in a year for the period of record constitutes the statistical sample of yearly fastest mile. From this definition, it is noted that the fastest mile as a measure of wind speed has a variable averaging time; for example, if the wind speed is 60 miles per hour (mi/h), the averaging time for the fastest mile of wind is 1 min. For a wind speed of 120 mi/h, the averaging time for the fastest mile of wind is 0.5 min. Thom (ref. 2-19) reports that the Frechet probability distribution function fits his samples of fastest mile very well. The Frechet probability distribution function is given as

$$F(x) = e^{-\left(\frac{x}{\beta}\right)^{-\gamma}}, \tag{2.21}$$

where the two parameters β and γ are estimated from the sample by the maximum likelihood method. From Thom's maps of the 50, 98, and 99 percentiles of fastest mile of wind for yearly extremals, we have estimated (interpolated) for these percentiles for the four locations and calculated the values for the parameters β and γ for the Frechet distribution function and computed several additional percentiles, as shown in table 2-36. To have units consistent with the other sections of this document, the percentiles and the parameters β and γ have been converted from miles per hour to knots and m/s. Thus table 2-36 gives the Frechet distribution for the fastest mile of winds at the ~10-m (30-ft) level for the four locations with the units in knots and m/s.

The discussion in section 2.2.10.2, devoted to desired lifetime, calculated risk, and design wind relationships with respect to the wind statistics at a particular height (10-m level) is applicable here, except that the reference statistics are with respect to the fastest mile converted to knots and m/s. (Also see reference 2-20.)

2.2.10.9.2 Conversion of the Fastest Mile to Peak Winds

The Frechet distributions for the fastest mile were obtained from Thom's analysis for KSC. From these two distributions (the Frechet for the peak winds as well as for the fastest mile), the ratio of the percentiles of the fastest mile to the peak winds were taken. This ratio varied from 1.12 to 1.09 over the range of probabilities from 30 to 99 percent. Thus, we adopted 1.10 as a factor to multiply the statistics of the fastest mile of wind to obtain peak (instantaneous) wind statistics. This procedure is based on the evidence of only one station. A gust factor of 1.10 is often applied to the fastest mile statistics in facility design work to account for gust loads.

Table 2-36. Frechet distribution of fastest mile wind at the 10-m height of yearly extremes for the indicated locations.

P Probability	T_D Return Period (years)	Fastest Mile Wind					
		Stennis Space Center		Vandenberg AFB		Edwards AFB	
		(m/s)	(knots)	(m/s)	(knots)	(m/s)	(knots)
0.50	2	22.1	42.9	18.0	34.9	11.3	22.0
0.80	5	26.6	51.8	21.6	42.0	15.0	29.1
0.90	10	30.1	58.6	24.4	47.4	18.1	35.2
0.95	20	33.9	65.9	27.4	53.3	21.6	42.0
0.98	50	39.6	76.9	31.8	61.9	27.3	53.0
0.99	100	44.4	86.4	35.7	69.4	32.4	63.1
0.9933	150	47.4	92.2	38.0	73.9	35.1	68.3
0.995	200	49.7	96.7	39.9	77.6	38.6	75.0
0.996	250	51.6	100.4	41.4	80.4	40.8	79.3
0.99667	300	53.2	103.5	42.6	82.9	42.7	83.1
0.9975	400	55.8	108.4	44.6	86.7	45.8	89.1
0.998	500	57.9	112.5	46.2	89.9	48.5	94.2
0.99833	600	59.4	115.5	47.5	92.3	50.5	98.1
0.99875	800	62.6	121.6	50.3	97.7	54.0	105.0
0.999	1,000	64.9	126.1	51.8	100.6	57.6	111.9
γ	Unitless	6.08075		6.19591		4.02093	
$1/\gamma$	Unitless	0.16445		0.16140		0.24870	
$\ln \beta$	Unitless	3.70093		3.49620		2.99989	
β	m/s	20.829		16.968		10.322	
	(knots)	(40.488)		(32.983)		(20.065)	

2.2.10.9.3 The Peak Wind Profile

The peak wind profile law adopted for the four locations for peak winds at the 10-m level greater than 22.6 m/s (44 knots) is

$$u = u_{10}\left(\frac{z}{10}\right)^{1/7} , \tag{2.22}$$

where u_{10} is the peak wind at the 10-m height and u is the peak wind at height z in meters.

2.2.10.9.4 The Mean Wind Profile

To obtain the mean wind profile for various averaging times, the gust factors (table 2-32) are applied to the peak wind profile as determined by equation (2.22).

2.2.10.9.5 Design Wind Profiles for Station Locations

The design peak wind profiles for the peak winds in table 2-37 are obtained from the peak wind power law given by equation (2.22), and the mean wind profiles for various averaging times are obtained by dividing by the gust factors for the various averaging times. (The gust factors versus height and averaging times are presented in table 2-32.) The resulting selected design wind profiles for design return periods of 10, 100, and 1,000 years for the four locations are given in tables 2-38 through 2-46, in which values of τ are given in minutes. The design risk versus desired lifetime for the design return periods of 10, 100, and 1,000 years is presented in table 2-30.

Table 2-37. Peak winds (fastest mile values times 1.10) for the 10-m reference level for 10-, 100-, and 1,000-year return periods.

T_D (years)	Peak Winds (U_{10})					
	Stennis Space Center		Vandenberg AFB		Edwards AFB	
	(m/s)	(knots)	(m/s)	(knots)	(m/s)	(knots)
10	33.2	64.5	26.8	52.1	19.9	38.7
100	48.9	95.0	39.3	76.3	35.7	69.4
1,000	71.4	138.7	56.9	110.7	63.4	123.2

Table 2-38. Facilities design wind as a function of averaging time (τ) for a peak wind of 33.2 m/s (64.5 knots) (10-year return period) for Stennis Space Center.

Height		Facilities Design Wind as a Function of Averaging Times (τ) in Minutes											
(ft)	(m)	$\tau = 0$ (peak)		$\tau = 0.5$		$\tau = 1$		$\tau = 2$		$\tau = 5$		$\tau = 10$	
		(m/s)	(knots)	(m/s)	(knots)	(m/s)	(knots)	(m/s)	(knots)	(m/s)	(knots)	(m/s)	(knots)
33	10.0	33.2	64.5	25.2	48.9	24.2	47.0	23.1	44.9	21.7	42.2	20.7	40.3
60	18.3	36.2	70.3	28.5	55.4	27.5	53.5	26.5	51.5	25.1	48.7	24.0	46.7
100	30.5	38.9	75.6	31.6	61.4	30.6	59.5	29.5	57.4	28.1	54.6	27.1	52.6
200	61.0	43.0	83.5	36.1	70.1	35.1	68.3	34.1	66.2	32.6	63.4	31.6	61.4
300	91.4	45.5	88.5	38.9	75.6	38.0	73.8	36.9	71.8	35.5	69.0	34.5	67.0
400	121.9	47.4	92.2	41.0	79.7	40.1	77.9	39.0	75.9	37.7	73.2	36.6	71.2
500	152.4	48.5	94.3	42.3	82.2	41.4	80.5	40.4	78.5	39.0	75.8	38.0	73.8

Table 2-39. Facilities design wind as a function of averaging time (τ) for a peak wind of 48.9 m/s (95.0 knots) (100-year return period) for Stennis Space Center

Height		Facilities Design Wind as a Function of Averaging Times (τ) in Minutes											
(ft)	(m)	$\tau = 0$ (peak)		$\tau = 0.5$		$\tau = 1$		$\tau = 2$		$\tau = 5$		$\tau = 10$	
		(m/s)	(knots)	(m/s)	(knots)	(m/s)	(knots)	(m/s)	(knots)	(m/s)	(knots)	(m/s)	(knots)
33	10.0	48.9	95.0	37.1	72.1	35.6	69.2	34.1	66.2	32.0	62.2	30.6	59.4
60	18.3	53.3	103.6	42.0	81.7	40.5	78.8	39.0	75.8	36.9	71.7	35.4	68.8
100	30.5	57.3	111.4	46.5	90.4	45.1	87.6	43.5	84.6	41.4	80.4	40.8	79.3
200	61.0	63.3	123.0	53.1	103.3	51.8	100.6	50.2	97.5	48.1	93.5	46.6	90.5
300	91.4	67.0	130.3	57.3	111.4	55.9	108.7	54.4	105.8	52.3	101.6	50.8	98.7
400	121.9	69.9	135.8	60.4	117.4	59.1	114.8	57.6	111.9	55.5	107.8	54.0	104.9
500	152.4	71.4	138.8	62.2	121.0	60.9	118.4	59.5	115.6	57.4	111.6	55.9	108.7

Table 2-40. Facilities design wind as a function of averaging time (τ) for a peak wind of 71.4 m/s (138.7 knots) (1,000-year return period) for Stennis Space Center.

Height		Facilities Design Wind as a Function of Averaging Times (τ) in Minutes											
(ft)	(m)	$\tau = 0$ (peak)		$\tau = 0.5$		$\tau = 1$		$\tau = 2$		$\tau = 5$		$\tau = 10$	
		(m/s)	(knots)	(m/s)	(knots)	(m/s)	(knots)	(m/s)	(knots)	(m/s)	(knots)	(m/s)	(knots)
33	10.0	26.8	52.1	20.3	39.5	19.5	38.0	18.7	36.3	17.5	34.1	16.8	32.6
60	18.3	29.2	56.8	23.0	44.8	22.2	43.2	21.4	41.6	20.2	39.3	19.4	37.7
100	30.5	31.4	61.1	25.5	49.6	24.7	48.1	23.9	46.4	22.7	44.1	21.9	42.5
200	61.0	34.7	67.5	29.2	56.7	28.4	55.2	27.5	53.5	26.4	51.3	25.6	49.7
300	91.4	36.8	71.5	31.4	61.1	30.7	59.6	29.8	58.0	28.7	55.8	27.9	54.2
400	121.9	38.3	74.5	33.1	64.4	32.4	63.0	31.6	61.4	30.4	59.1	29.6	57.5
500	152.4	39.1	76.1	34.1	66.3	33.4	64.9	32.6	63.3	31.5	61.2	30.7	59.6

Table 2-41. Facilities design wind as a function of averaging time (τ) for a peak wind of 26.8 m/s (52.1 knots) (10-year return period) for VAFB and White Sands Missile Range.

Height		Facilities Design Wind as a Function of Averaging Times (τ) in Minutes											
(ft)	(m)	$\tau = 0$ (peak)		$\tau = 0.5$		$\tau = 1$		$\tau = 2$		$\tau = 5$		$\tau = 10$	
		(m/s)	(knots)	(m/s)	(knots)	(m/s)	(knots)	(m/s)	(knots)	(m/s)	(knots)	(m/s)	(knots)
33	10.0	71.4	138.7	54.1	105.2	52.0	101.1	49.7	96.7	46.7	90.8	44.6	86.7
60	18.3	77.8	151.2	61.3	119.2	59.2	115.1	56.9	110.7	53.8	104.6	51.7	100.5
100	30.5	83.7	162.7	68.0	132.1	65.8	128.0	63.5	123.5	60.4	117.5	58.2	113.2
200	61.0	92.4	179.6	77.6	150.8	75.6	146.9	73.3	142.4	70.2	136.5	68.0	132.2
300	91.4	97.9	190.3	83.6	162.6	81.6	158.7	79.5	154.5	76.3	148.4	74.2	144.2
400	121.9	102.0	198.2	88.1	171.3	86.2	167.5	84.0	163.3	80.9	157.3	78.8	153.1
500	152.4	104.3	202.7	90.9	176.7	89.0	173.0	86.8	168.8	83.8	162.9	81.6	158.7

Table 2-42. Facilities design wind as a function of averaging time (τ) for a peak wind of 39.3 m/s (76.3 knots) (100-year return period) for VAFB and White Sands Missile Range.

Height		Facilities Design Wind as a Function of Averaging Times (τ) in Minutes											
(ft)	(m)	$\tau = 0$ (peak)		$\tau = 0.5$		$\tau = 1$		$\tau = 2$		$\tau = 5$		$\tau = 10$	
		(m/s)	(knots)	(m/s)	(knots)	(m/s)	(knots)	(m/s)	(knots)	(m/s)	(knots)	(m/s)	(knots)
33	10.0	39.3	76.3	29.8	57.9	28.6	55.6	27.4	53.2	25.7	49.9	24.5	47.7
60	18.3	42.8	83.2	33.7	65.6	32.6	63.3	31.3	60.9	29.6	57.6	28.4	55.3
100	30.5	46.0	89.5	37.3	72.6	36.2	70.4	35.0	68.0	33.2	64.6	32.0	62.3
200	61.0	50.8	98.8	42.7	83.0	41.6	80.8	40.3	78.4	38.6	75.1	37.4	72.7
300	91.4	53.9	104.7	46.0	89.5	44.9	87.3	43.7	85.0	42.0	81.7	40.8	79.3
400	121.9	56.1	109.1	48.5	94.3	47.4	92.2	46.2	89.9	44.6	86.6	43.3	84.2
500	152.4	57.4	111.5	50.0	97.2	48.9	95.1	47.7	92.8	46.1	89.6	44.9	87.3

Table 2-43. Facilities design wind as a function of averaging time (τ) for a peak wind of 56.9 m/s (110.7 knots) (1,000-year return period) for VAFB and White Sands Missile Range.

Height		Facilities Design Wind as a Function of Averaging Times (τ) in Minutes											
(ft)	(m)	$\tau = 0$ (peak)		$\tau = 0.5$		$\tau = 1$		$\tau = 2$		$\tau = 5$		$\tau = 10$	
		(m/s)	(knots)	(m/s)	(knots)	(m/s)	(knots)	(m/s)	(knots)	(m/s)	(knots)	(m/s)	(knots)
33	10.0	56.9	110.7	43.2	84.0	41.5	80.7	39.7	77.1	37.2	72.4	35.6	69.2
60	18.3	62.1	120.7	49.0	95.2	47.3	91.9	45.5	88.4	43.0	83.5	41.3	80.2
100	30.5	66.8	129.8	54.2	105.4	52.5	102.1	50.7	98.6	48.2	93.7	46.5	90.3
200	61.0	73.7	143.3	61.9	120.3	60.3	117.2	58.4	113.6	56.0	108.9	54.2	105.4
300	91.4	78.1	151.9	66.8	129.8	65.2	126.7	63.4	123.3	61.0	118.5	59.2	115.1
400	121.9	81.4	158.2	70.3	136.7	68.8	133.7	67.0	130.3	64.6	125.6	62.9	122.2
500	152.4	83.2	161.8	72.6	141.1	71.0	138.1	69.3	134.7	66.9	130.1	65.2	126.7

Table 2-44. Facilities design wind as a function of averaging time (τ) for a peak wind of 19.9 m/s (38.7 knots) (10-year return period) for EAFB.

Height		Facilities Design Wind as a Function of Averaging Times (τ) in Minutes											
(ft)	(m)	$\tau = 0$ (peak)		$\tau = 0.5$		$\tau = 1$		$\tau = 2$		$\tau = 5$		$\tau = 10$	
		(m/s)	(knots)	(m/s)	(knots)	(m/s)	(knots)	(m/s)	(knots)	(m/s)	(knots)	(m/s)	(knots)
33	10.0	38.7	19.9	29.4	15.1	28.2	14.5	27.0	13.9	25.3	13.0	24.2	12.4
60	18.3	42.1	21.7	33.2	17.1	32.0	16.5	30.8	15.8	29.1	15.0	28.0	14.4
100	30.5	45.1	23.2	36.6	18.8	35.5	18.3	34.2	17.6	32.6	16.8	31.4	16.2
200	61.0	50.1	25.8	42.1	21.7	41.0	21.1	39.7	20.4	38.1	19.6	36.9	19.0
300	91.4	53.1	27.3	45.4	23.4	44.3	22.8	43.1	22.2	41.4	21.3	40.2	20.7
400	121.9	55.3	28.4	47.8	24.6	46.7	24.0	45.6	23.5	43.9	22.6	42.7	22.0
500	152.4	57.1	29.4	49.8	25.6	48.7	25.1	47.5	24.4	45.9	23.6	44.7	23.0

Table 2-45. Facilities design wind as a function of averaging time (τ) for a peak wind of 35.7 m/s (69.4 knots) (100-year return period) for EAFB.

Height		Facilities Design Wind as a Function of Averaging Times (τ) in Minutes											
(ft)	(m)	τ = 0 (peak)		τ = 0.5		τ = 1		τ = 2		τ = 5		τ = 10	
		(m/s)	(knots)	(m/s)	(knots)	(m/s)	(knots)	(m/s)	(knots)	(m/s)	(knots)	(m/s)	(knots)
33	10.0	69.4	35.7	52.7	27.1	50.6	26.0	48.4	24.9	45.4	23.4	43.4	22.3
60	18.3	75.5	38.8	59.5	30.6	57.5	29.6	55.3	28.4	52.2	26.9	50.2	25.8
100	30.5	80.9	41.6	65.7	33.8	63.7	32.8	61.4	31.6	58.4	30.0	56.3	29.0
200	61.0	89.9	46.2	75.5	38.8	73.5	37.8	71.3	36.7	68.3	35.1	66.2	34.1
300	91.4	95.2	49.0	81.4	41.9	79.4	40.8	77.3	39.8	74.3	38.2	72.1	37.1
400	121.9	99.2	51.0	85.7	44.1	83.9	43.2	81.7	42.0	78.7	40.5	76.6	39.4
500	152.4	102.4	52.7	89.3	45.9	87.4	45.0	85.3	43.9	82.3	42.3	80.2	41.3

Table 2-46. Facilities design wind as a function of averaging time (τ) for a peak wind of 63.3 m/s (123.0 knots) (1,000-year return period) for EAFB.

Height		Facilities Design Wind as a Function of Averaging Times (τ) in Minutes											
(ft)	(m)	τ = 0 (peak)		τ = 0.5		τ = 1		τ = 2		τ = 5		τ = 10	
		(m/s)	(knots)	(m/s)	(knots)	(m/s)	(knots)	(m/s)	(knots)	(m/s)	(knots)	(m/s)	(knots)
33	10.0	123.0	63.3	93.3	48.0	89.7	46.1	85.7	44.1	80.5	41.4	76.9	39.6
60	18.3	133.8	68.8	105.5	54.3	101.8	52.4	98.0	50.4	92.6	47.6	88.9	45.7
100	30.5	143.2	73.7	116.2	59.8	112.7	58.0	108.7	55.9	103.4	53.2	99.7	51.3
200	61.0	159.3	82.0	133.8	68.8	130.3	67.0	126.3	65.0	121.0	62.2	117.2	60.3
300	91.4	168.7	86.8	144.2	74.2	140.7	72.4	136.9	70.4	131.6	67.7	127.8	65.7
400	121.9	175.8	90.4	151.9	78.1	148.6	76.4	144.8	74.5	139.5	71.8	135.8	69.9
500	152.4	181.5	93.4	158.2	81.4	154.9	79.7	151.1	77.7	145.9	75.1	142.1	73.1

2.2.11 Ground Winds for Runway Orientation Optimization

Runway orientation is influenced by a number of factors; for example, winds, terrain features, population interference, etc. In some cases, the frequency of occurrence of crosswind components of some significant speed has received insufficient consideration. Aligning the runway with the prevailing wind will not insure that crosswinds will be minimized. In fact, two common synoptic situations (one producing light easterly winds, and the other causing strong northerly winds) might exist in such a relationship that a runway oriented with the prevailing wind might be the least useful to an aircraft constrained by crosswind components. Two methods, one empirical and the other theoretical, based on the bivariate normal distribution for wind vectors, of determining the optimum runway orientation to minimize critical crosswind component speeds are available (ref. 2-21).

In the empirical method, the runway crosswind components are computed for all azimuth and wind speed categories in the wind rose (ref. 2-21). From these values, the optimum runway orientation can be selected that will minimize the risk of occurrence of any specified crosswind speed.

The theoretical method requires that the wind components are bivariate normally distributed; i.e., a vector wind data sample is resolved into wind components in a rectangular coordinate system, and the bivariate normal elliptical distribution is applied to the data sample of component winds. For example, let x_1 and x_2 be normally distributed variables with parameters (ξ_1, σ_1) and (ξ_2, σ_2). ξ_1 and ξ_2 are the respective means, while σ_1 and σ_2 are the respective standard deviations. Let ρ be the correlation coefficient, which is a measure of the dependence between x_1 and x_2. Now, the bivariate normal density function is

$$p(x_1,x_2) = [2\pi\sigma_1\sigma_2(1-\rho^2)^{1/2}]^{-1} * \exp\left[-[2(1-\rho^2)]^{-1}\left[\left(\frac{x_1-\xi_1}{\sigma_1}\right)^2 - 2\rho\left(\frac{x_1-\xi_1}{\sigma_1}\right)\left(\frac{x_2-\xi_2}{\sigma_2}\right)+\left(\frac{x_2-\xi_2}{\sigma_2}\right)^2\right]\right]. \quad (2.23)$$

Let α be an arbitrary angle in the rectangular coordinate system. From the statistics in the (x_1,x_2) space, the statistics for any rotation of the axes of the bivariate normal distribution through any arbitrary angle α may be computed (ref. 2-22). Let α denote the desired increments for which runway orientation accuracy is required; e.g., one may wish to minimize the probability of crosswinds with a runway orientation accuracy down to $\alpha = 10°$. This means we must rotate the bivariate normal axes through every 10°. It is only necessary to rotate the bivariate normal surface through 180° since the distribution is symmetric in the other two quadrants. Let (y_1,y_2) denote the bivariate normal space after rotation.

This rotation process will result in 18 sets of statistics in the (y_1,y_2) space. The quantity y_1 is the head wind component, while y_2 is the crosswind component. Since we are concerned with minimizing the probability of cross winds (y_2) only, we now examine the marginal distribution $p(y_2)$ for the 18 orientations (α). Since $p(y_1,y_2)$ is bivariate normal, the 18 marginal distributions $p(y_2)$ must be univariate normal:

$$p(y_2) = [\sigma_2\,(2\pi)^{1/2}]^{-1} \exp\left[-\frac{1}{2}\left[\frac{(y_2-\xi_2)}{\sigma_2}\right]^2\right]. \quad (2.24)$$

ξ_2 and σ_2 are replaced by their sample estimates Y_2 and S_{y2}. Now, let

$$z = \frac{Y_2-\bar{Y}_2}{S_{y_2}}, \quad (2.25)$$

where y_2 is the critical crosswind of interest and S_{y_2} is the standard deviation of the y_2 with respect to its mean $\bar{y}_2$. The quantity z is a normal variable, and the probability of its exceedence is easily calculated from the tables of the standard normal integral. Since a right or left crosswind (y_2) is a constraint to an aircraft, the critical region (exceedence region) for the normal distribution is two-tailed; i.e., we are interested in twice the probability of exceeding $|y_2|$. Let this probability of exceedence or risk equal R. Now, the orientation for which R is a minimum is the desired optimum runway orientation. The procedure described may be used for any station. Only parameters estimated from the data are required as input. Consequently, many runways and locations may be examined rapidly.

Either the empirical or theoretical method may be used to determine an aircraft runway orientation that minimizes the probability of critical crosswinds. Again, it is emphasized that the wind components must be bivariate normally distributed to use the theoretical method. In practical applications, the following steps are suggested.

1. Test the component wind samples for bivariate normality if these samples are available.

2. If the component winds are available and cannot be rejected as bivariate normal using the bivariate normal goodness-of-fit test, use the theoretical method since it is more expedient and easily programmed.

3. If the component wind data samples are not available and there is doubt concerning the assumption of bivariate normality of the wind components, use the empirical method.

2.3 In-flight Winds

2.3.1 Introduction

In-flight wind speed profiles are used in vehicle design studies primarily to establish structural and control system capabilities and to compute performance requirements. The in-flight wind speeds selected for vehicle design may not represent the same percentile value as the design surface wind speed. The selected wind speeds (in-flight and surface) are determined by the desired on-pad stay time and vehicle launch capabilities and can differ in the percentile level since the in-flight and surface wind speeds differ in degree of persistence for a given reference time period, they can be treated as being statistically independent for engineering design purposes.

Wind profile information for in-flight design studies is presented in two basic forms: discrete or synthetic profiles and measured profile samples. There are certain limitations to each of these wind input forms, and their utility in design studies depends upon a number of considerations such as (1) accuracy of basic measurements, (2) complexity of input to vehicle design, (3) economy and practicality for design use, (4) ability to represent significant features of the wind profile, (5) statistical assumption versus physical representation of the wind profile, (6) ability of input to ensure control system and structural integrity of the vehicle, and (7) flexibility for use in design trade-off studies.

An accurate and adequate number of measured wind profiles are necessary for developing a valid statistical description of the wind profile. Fortunately, current records of data from some locations (KSC in particular) fulfill these requirements, although a continuing program of data acquisition is vital to further enhance the confidence of the statistical information generated. Various methods and sensors for obtaining in-flight profiles include the rawinsonde, radar wind profiler, the FPS-16 radar/jimsphere, and the rocketsonde. The statistical analyses performed on the in-flight wind profiles provide detailed descriptions of the upper winds and an understanding of the profile characteristics, such as temporal and height variations, as well as indications of the frequency and the persistence of transient meteorological systems.

The synthetic type of wind profile is the oldest method used to present in-flight design wind data. The synthetic wind profile data are presented in this document because this method of presentation provides a reasonable approach for most design studies when properly used, especially during the early design periods. Also, the concept of synthetic wind profiles is generally understood and employed in most aerospace organizations for design computations. The synthetic wind profile includes the wind speed, wind speed change, maximum wind layer thickness, and gusts that are required to establish vehicle design structural and control system values.

Currently, launch vehicles for use at various launch sites and in comprehensive space research mission and payload configurations are designed by use of synthetic vector wind and wind shear models with regard to specific wind direction. However, if a vehicle is not restricted to a given launch site, and flight azimuths, and a specific configuration and mission, wind components (head, tail, left cross, or right cross) are often used. Component wind profiles are sometimes used, and, for a given percentile, the magnitudes of component winds are equal to or less than those of the scalar winds. Component or directionally dependent winds should not be employed in initial design studies unless specifically authorized by the cognizant design organization. Vector wind and vector wind shear models may be more applicable and were used for the space shuttle vehicle.

Selection of a set of detailed wind profiles for final design verification and launch delay risk calculations requires the matching of vehicle simulation resolution and technique to frequency or information content of the profile. Detailed wind profile data sets for design verification use are available for KSC, FL, and VAFB, CA (see section 2.3.12.1). Selected samples of detailed wind profiles are available for other locations.

The synthetic wind profile provides a conditionalized wind shear/gust state with respect to the given design wind speed. Therefore, in concept, the synthetic wind profile should produce a vehicle design which has

a launch delay risk not greater than a specified value which is generally the value associated with the design wind speed. This statement, although generally correct, depends on the control system response characteristics, the vehicle structural integrity, etc. A joint condition of wind shear, gust, and speeds is given in selection of detailed wind profiles for design verification. Therefore, the resulting launch delay risk for a given vehicle design is the specified value of risk computed from the vehicle responses associated with the various profiles. For the synthetic profile, a vehicle in-flight wind speed capability and maximum launch delay risk may be stated which is conditional upon the wind/gust design values. However, for the selection of detailed wind profiles, only a vehicle launch risk value may be given since the wind characteristics are treated as a joint event. These two differences in philosophy should be understood to avoid misinterpretation of vehicle response calculation comparisons. In both cases, allowance for dispersions in vehicle characteristics should be made prior to flight simulation through the wind profiles and establishment of vehicle design response or operational launch delay risk values. The objective is to ensure that an aerospace vehicle will accommodate the desired percentage of wind profiles or conditions in its non-nominal flight mode (i.e., engine out, etc.).

2.3.2 Wind Aloft Climatology

The development of design wind speed profiles and associated shears and gusts requires use of the measured wind speed and wind direction data collected at the area of interest for some reasonably long period of time, i.e., 10 years or longer. The subject of wind climatology for an area, if treated in detail, would make up a voluminous document. The intent here is to give a brief treatment of selected topics that are frequently considered in aerospace vehicle development and operation problems and provide references to more extensive information.

Considerable data summaries (monthly and seasonal) exist on wind aloft statistics for the world. However, it is necessary to interpret these data in terms of the engineering design problem and design philosophy. For example, wind requirements for performance calculations relative to aircraft fuel consumption requirements must be derived for the specific routes and design reference period. Such data are available on request.

2.3.3 Wind Component Statistics

Wind component statistics are used in mission planning to provide information on the probability of exceeding a given wind speed in the pitch or yaw planes and to bias the tilt program at a selected launch time. The vector wind and vector wind shear model discussed in section 2.3.10 is directly applicable to the description of these input data.

The wind component statistics can be computed for various launch azimuths (15° intervals were selected by MSFC) for each month for the pitch plane (range) and yaw plane (cross range) at KSC and VAFB, CA. References 2-23 through 2-25 contain information on the statistical distributions of wind speeds and vector wind components for the various vehicle flight centers and test ranges.

2.3.3.1 Upper Wind Correlations

Coefficients of correlations of wind components between altitude levels with means and standard deviations at altitude levels may be used in a statistical model to derive representative wind profiles. A method of preparing synthetic wind profiles by use of correlation coefficients between wind components is described in reference 2-26. In addition, these correlation data are applicable to certain statistical studies of vehicle responses (ref. 2-27).

Data on correlations of wind between altitude levels for various geographical locations are presented in references 2-28, 2-29, and 2-30. The reports give values of the interlevel and intralevel coefficients of linear correlations between wind components. The linear correlation coefficients between altitudes within the 10- to 15-km altitude region are very high, but decrease with greater altitude separation.

Correlations between wind components separated by a horizontal distance are now available. The reader is referred to the work of Buell (refs. 2-31 and 2-32) for a detailed discussion of the subject.

2.3.3.2 Thickness of Strong Wind Layers

Wind speeds in the middle latitudes generally increase with altitude to a maximum between 10- and 14-km. Above 14 km, the wind speeds decrease with altitude, then increase at higher altitude, depending upon season and location. Frequently, these winds exceed 50 m/s in the jet stream, a core of maximum winds over the midlatitudes in the 10- to 14-km altitudes. The vertical extent of the core of maximum winds, or the sharpness of the extent of peak winds on the wind profile, is important in some vehicle design studies. For information concerning the thickness of strong wind layers, the reader is referred to reference 2-33.

Table 2-47 shows design values of vertical thickness (based on maximum thickness) of the wind layers for wind speeds for KSC. Similar data for VAFB are given in table 2-48. At both ranges, the thickness of the layer decreases with increase of wind speed; that is, the sharpness of the wind profile in the vicinity of the jet core becomes more pronounced as wind speed increases.

Table 2-47. Design thickness for strong wind layers at KSC.

Quasi-Steady-State Wind Speed (± 5 ms^{-1})	Maximum Thickness (km)	Altitude Range (km)
50	4	8.5 to 16.5
75	2	10.5 to 15.5
92	1	10.0 to 14.0

Table 2-48. Design thickness for strong wind layers at VAFB, CA.

Quasi-Steady-State Wind Speed (± 5 ms^{-1})	Maximum Thickness (km)	Altitude Range (km)
50	4	8.0 to 16
75	2	9.5 to 14

2.3.3.3 Exceedance Probabilities

The probability of in-flight winds exceeding or not exceeding some critical wind speed for a specified time duration may be of considerable importance in mission planning, and, in many cases, more information than just the occurrence of critical winds is desired. If a dual launch, with the second vehicle being launched 1 to 3 days after the first, is planned and if the launch opportunity extends over a 10-day period, what is the probability that winds below (or above) critical levels will last for the entire 10 days? What is the probability of 2 or 3 consecutive days of favorable winds in the 10-day period? Suppose the winds are favorable on the scheduled launch day, but the mission is delayed for other reasons. Now, what is the probability that the winds will remain favorable for 3 or 4 more days? Answers to these questions could also be used for certain design considerations involving specific vehicles prepared for a given mission and launch window. A body of statistics is available from the NASA-MSFC's Earth Science and Applications Division which can be used to answer these and possibly other related questions. An example of the kind of wind persistence statistics that are available is given in figure 2-9. This figure gives the probability of the maximum wind speed in the 10- to 15-km region being less than, equal to, or greater than 50 and 75 ms^{-1}, for various multiples of 12 hours for the month of January. Thus, for example, there is approximately an 18-percent chance that the wind speed

will be greater than or equal to 50 m/s for 10 consecutive 12-h periods in January. The random series is plotted as p^k, for k = 1,2,..., 12-h periods.

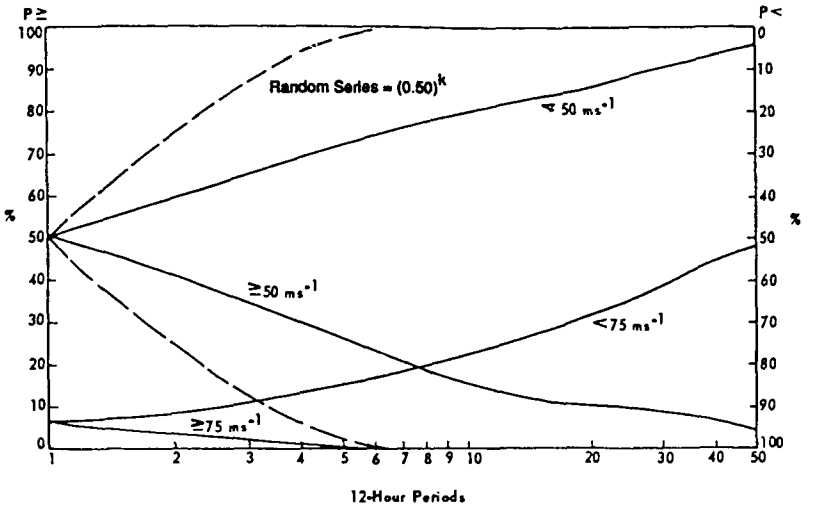

Figure 2-9. Probability of the maximum wind speed in the 10- to 15-km layer being less than, equal to, or greater than specified values for k-consecutive 12-h periods during January at KSC.

2.3.3.4 Design Scalar Wind Speeds (10- to 15-km Altitude Layer)

The distributions of design scalar wind speed in the 10- to 15-km altitude layer over the United States are shown in figure 2-10 for the 95-percentile value and figure 2-11 for the 99-percentile values. The location of local maximum in the isopleths (maximum wind speeds) is shown by heavy lines with arrows. These winds occur at approximately the level of maximum dynamic pressure for most aerospace vehicles.

2.3.3.5 Temporal Wind Changes

Atmospheric wind fields change with time. Significant wind direction and speed changes can occur over time scales as short as a few minutes or less. There is no upper bound limit on the time scale over which the wind field can change. To develop real time wind biasing programs for aerospace vehicle control purposes, which involve the use of wind profiles observed a number of hours prior to launch, it is necessary that consideration be given to the changes in wind speed and direction that can occur during the time elapsed from entering the biasing profile into the vehicle control system logic to the time of launch. If the observed wind profile 8 h prior to launch is to be used as a wind biasing profile, then consideration should be given to the dispersions in wind direction and speed that could occur over this period of time. Wind speed and direction change data are also useful for mission operation purposes. Results of studies conducted by the NASA-MSFC's Earth Science and Applications Division to define these dispersions in a statistical context are presented herein. Specialized data bases containing pairs of FPS-16 Jimsphere measured detail wind profiles over time periods of 2 to 12 h are available upon request to the Earth Science and Applications Division, Marshall Space Flight Center, AL 35812.

To account for the differences between the dynamics of the flow in the atmospheric boundary layer and the free atmosphere, the atmosphere over KSC is usually partitioned at the 2-km level in studies of the temporal changes in the wind field. Below the 2-km level, the flow is significantly influenced by the surface of the Earth and is predominantly a turbulent flow. In the free atmosphere above the 2-km level for terrain similar to KSC, the flow is, for all practical purposes, free of the effects of the surface boundary layer of the Earth. In mountainous areas this level can vary considerably.

Figures 2-12 and 2-13 contain idealized 99-percent wind direction and speed changes as a function of elapsed time and observed or referenced wind speed for altitudes between 150 m and 2 km for KSC. The wind

speed may increase or decrease from the reference profile value; thus, envelopes of each category are presented in figure 2-13. Figures 2-14 and 2-15 are the idealized 99-percent wind direction and speed changes as a function of elapsed time and observed or reference wind speed for altitudes between 2 and 16 km.

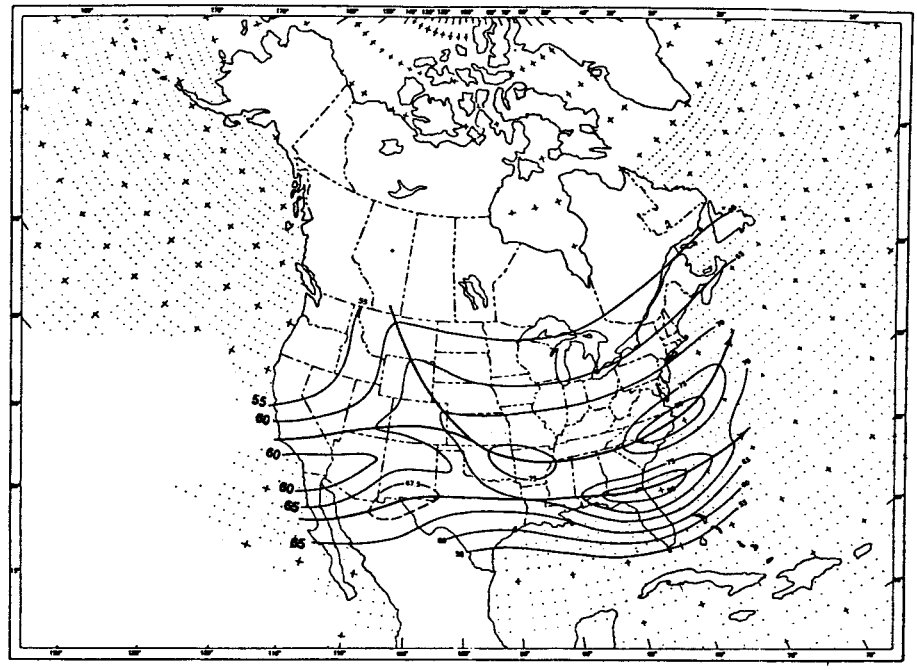

Figure 2-10. Design scalar wind speeds (m/s) 95-percentile envelope analysis prepared from windiest month and maximum winds in the 10- to 15-km layer.

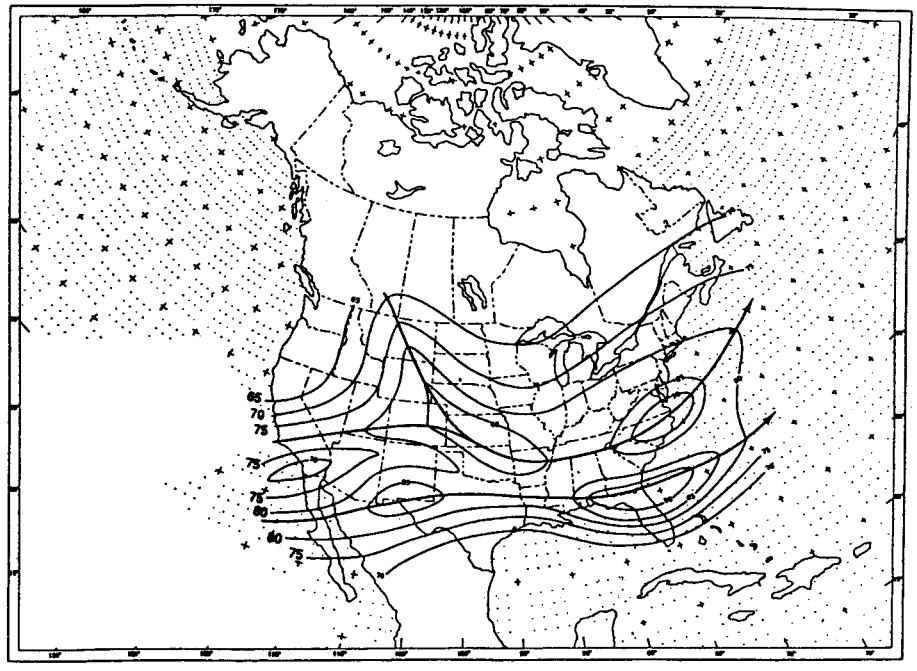

Figure 2-11. Design scalar wind speeds (m/s) 99-percentile envelope analysis prepared from windiest month and maximum winds in the 10- to 15-km layer.

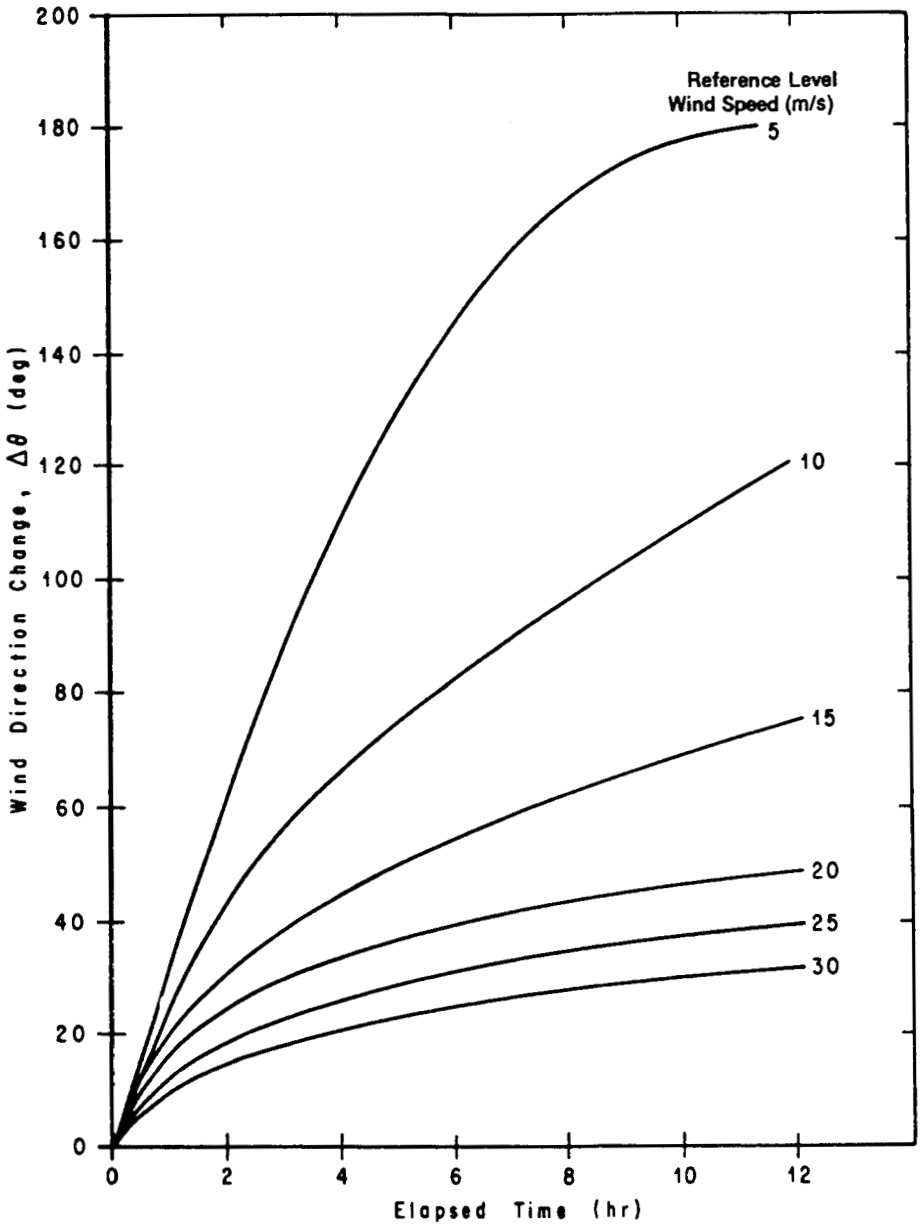

Figure 2-12. Idealized 99-percent wind direction change as a function of time and wind speed in the 150-m to 2-km altitude region of KSC.

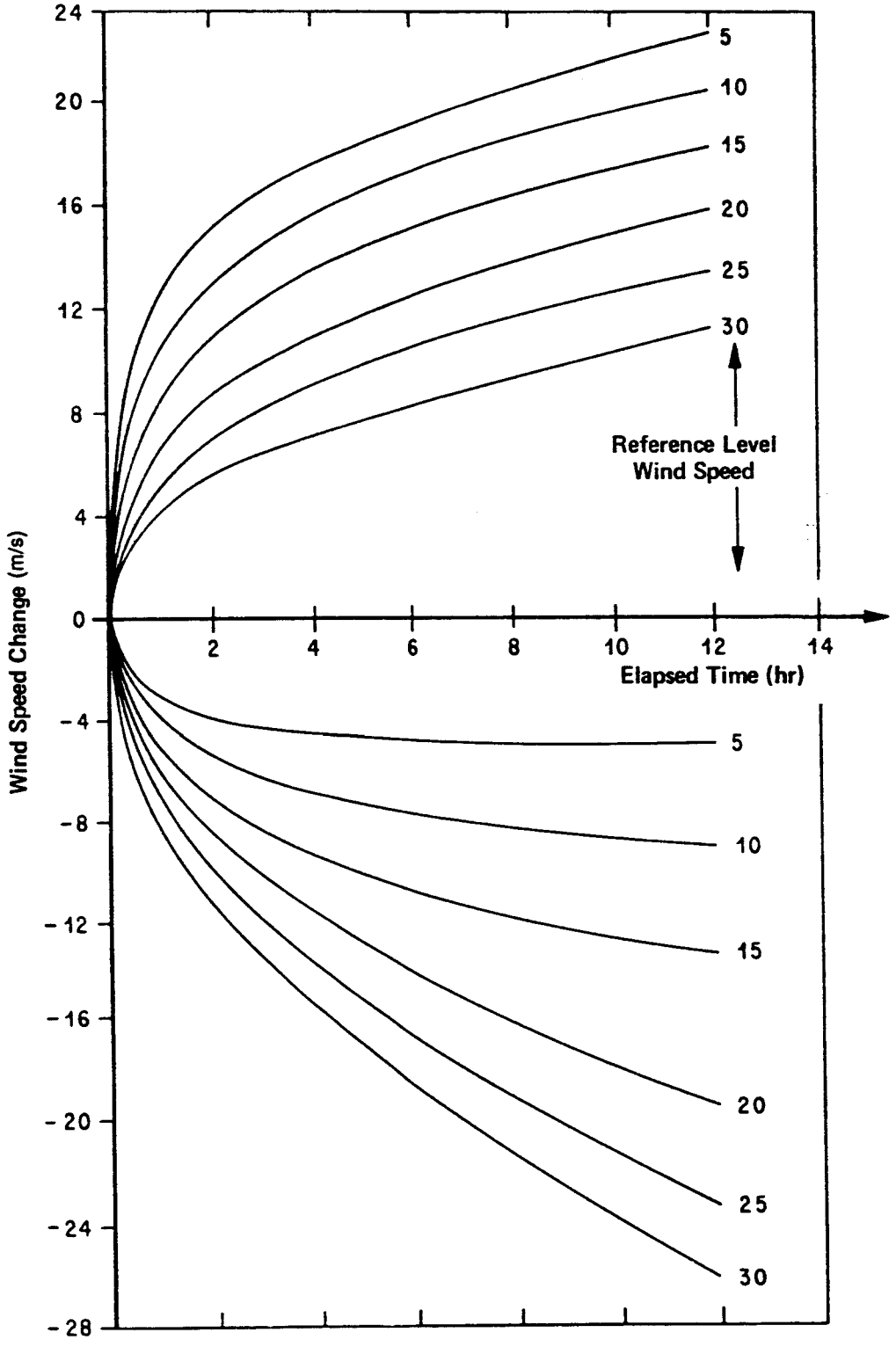

Figure 2-13. Idealized 99-percent wind speed change as a function of time and wind speed in the 150-m to 2-km altitude region of KSC.

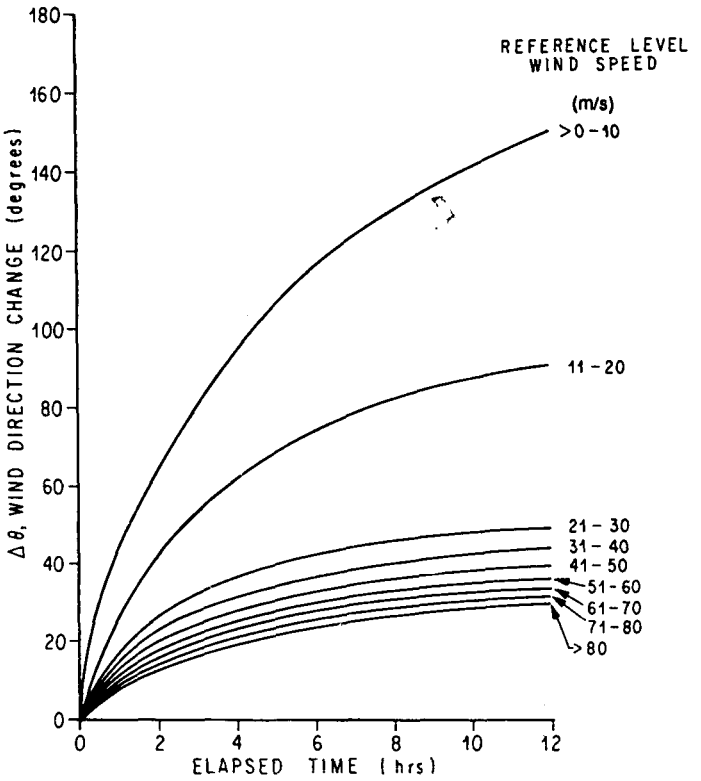

Figure 2-14. Idealized 99-percent wind direction change as a function of time and wind speed in the 2- to 16-km region of KSC.

The preceding data are applicable only to the KSC launch area because differences are known to exist in the data for other geographical locations. Conclusions should not be drawn relative to frequency content and phase relationships of the wind profile since the data given herein provide only envelope conditions for ranges of speed and direction changes. Direction correlations have not been developed between the changes of wind direction and wind speed.

Additional information concerning wind speed and direction changes can be found in reports by Camp and Susko (ref. 2-34) and Camp and Fox (ref. 2-35).

Temporal vector wind change at KSC and VAFB has been studied by Adelfang (refs. 2-36 and 2-37). The joint distribution of the four variables represented by the u and v components of the wind vector at an initial time and after a specified elapsed time is hypothesized to be quadravariate normal. The 14 statistics of this distribution are presented according to monthly reference period for altitudes from 0 to 27 km. These statistics are used to calculate percentiles of the theoretical distribution of wind component change with respect to time (univariate normal distribution), the joint distribution of wind component change (bivariate normal), the modulus of vector wind change (Rayleigh), and the vector wind at a future time given the vector wind at an initial time (conditional bivariate normal); the large body of statistics contained in these references are not repeated herein. For the purpose of illustrating the application of these statistics, the 95-percentile vector wind change ellipses for time intervals of 12, 24, 36, 48, 60, and 72 h at 6, 12, and 18 km during April at KSC and during January at VAFB have been calculated. Each ellipse illustrated in figure 2-16 was calculated from the bivariate normal statistics of vector wind change given in the referenced reports; each ellipse encompasses 95 percent of the wind change expected for the indicated time interval. The methodology for calculation of wind or wind change ellipses for any percentile is described by Smith (ref. 2-38). The wind change ellipses illustrated in figure 2-16 clearly indicate the strong variation of wind change for time intervals less than 48 hours, and the relatively large wind change for VAFB.

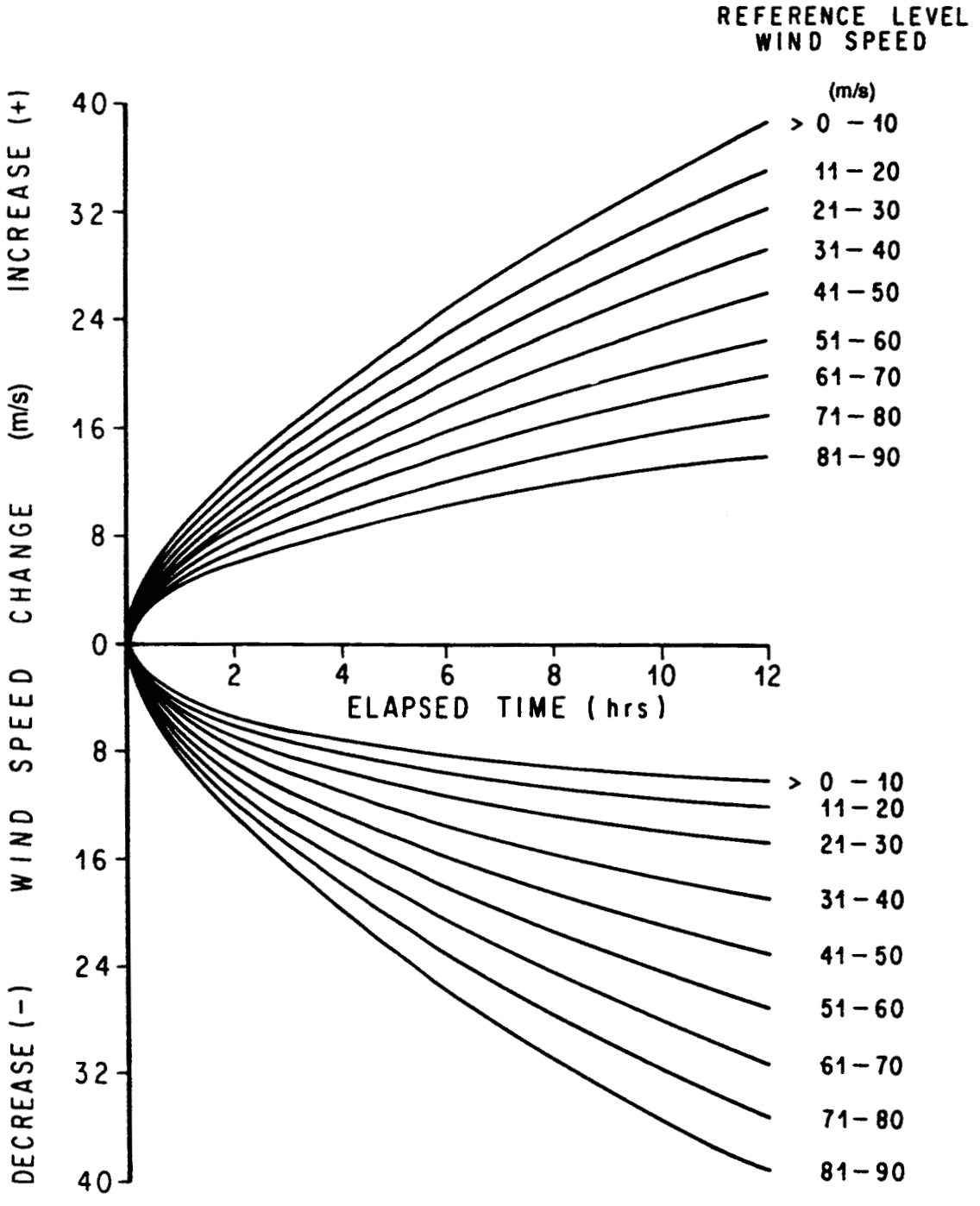

Figure 2-15. Idealized 99-percent wind speed change as a function of time and wind speed in the 2- to 16-km region of KSC.

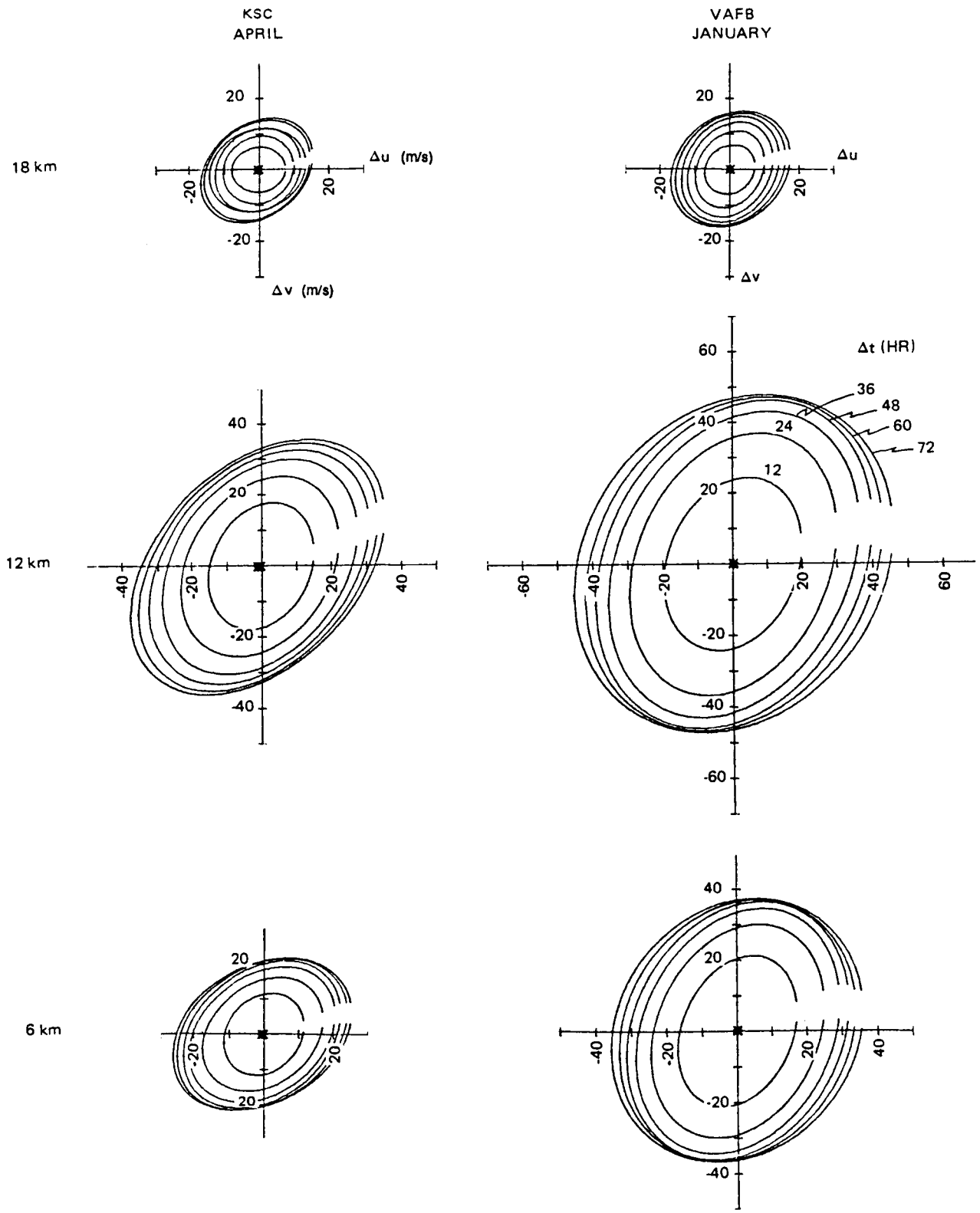

Figure 2-16. April KSC and January VAFB 95-percentile wind change (Δu and Δv) ellipses at 6, 12, and 18 km altitude for time intervals of 12, 24, 36, 48, 60, and 72 h.

2.3.4 Wind Speed Profiles for Biasing Tilt Program

In attempting to maintain a desired flight path for an aerospace vehicle through a strong wind region, the vehicle control system could introduce excessive bending moments and orbit anomalies. To reduce this problem, it is sometimes desirable to wind bias the pitch program; that is, to tilt the vehicle sufficiently to produce the desired flight path and minimize dynamic pressure level loads with the expected wind profile. Since most in-flight strong winds over KSC are winter westerlies, it is sometimes expedient to use the monthly or seasonal pitch plane median wind speed profile for bias analyses.

Head and tail wind components and right and left crosswind components from 0- to 70-km altitudes can be computed for any flight azimuth used at KSC or VAFB. For applications where both pitch and yaw biasing are used, monthly vector mean winds may be more efficient for wind biasing. Such statistics can be made available upon request, or see reference 2-38 and section 2.3.10 and reference 2-55 for a new wind biasing technique.

2.3.5 Design Wind Speed Envelopes

The wind data given in section 2.3.5.1 are not expected to be exceeded by the given percentages of time (time as related to the observational interval of the data sample) based upon the windiest monthly reference period. To obtain the profiles, monthly frequency distributions are combined for each percentile level to give the envelope over all months. The profiles represent horizontal wind flow referenced to the Earth's surface. Vertical wind flow is negligible except for that associated with gusts or turbulence. The scalar wind speed envelopes are normally applied without regard to flight directions to establish the initial design requirements. Directional wind criteria for use with the synthetic wind profile techniques should be applied with care and specific knowledge of the vehicle mission and flight path, since severe wind constraints could result for other flight paths and missions.

2.3.5.1 Scalar Wind Speed Envelopes

Scalar wind speed profile envelopes are presented in tables 2-49 through 2-53. These are idealized steady-state scalar wind speed profiles for four active or potential operational aerospace vehicle launch or landing sites; i.e., KSC, FL, VAFB, CA; White Sands Missile Range, NM; and Edwards AFB, CA. Table 2-53 provides data which envelopes the 95- and 99-percentile steady-state scalar wind speed profile for the same four locations. They are applicable to design criteria when initial design or operational capability has not been restricted to specific launch and landing sites or may involve several geographical locations. However, if the specific geographical location for application has been determined as being near one of the four referenced sites then the relevant data should be applied.

These tables provide design nondirectional wind data for various percentiles; therefore, the specific percentile wind speed envelope applicable to design should be specified in the appropriate space vehicle specification documentation. For engineering convenience, the design wind speed profile envelopes are given as linear segments between altitude levels; therefore, the tabular values can be linearly interpolated.

2.3.5.2 Vector Wind Models

Wind is a vector quantity having a magnitude and direction. A coordinate system and a statistical model are required. The bivariate normal probability distribution is used to model the wind at discrete altitudes. Wind measurements are recorded in terms of wind direction and magnitude. The wind direction is measured in degrees clockwise from true north and is the direction from which the wind is blowing. The wind magnitude (the modulus of the vector) is the scalar quantity and is referred to as wind speed or scalar wind. The standard meteorological coordinate system (fig. 2-17) has been chosen for the wind statistics and tables of statistical parameters.

Table 2-49. Scalar wind speed W (m/s) steady-state envelopes as functions of altitude H (km) for various probabilities P (%) for KSC.

Altitude (km)	Percentile				
	50	75	90	95	99
1	8	13	16	19	24
6	23	31	39	44	52
11	43	55	66	73	88
12	45	57	68	75	92
13	43	56	67	74	86
20	7	12	17	20	25
23	7	12	17	20	25
40	43	57	70	78	88
50	75	83	91	95	104
58	85	96	106	112	123
60	85	96	106	112	123
75	15	22	28	30	37
80	15	22	28	30	37

Table 2-50. Scalar wind speed W (m/s) steady-state envelopes as functions of altitude H (km) for various probabilities P (%) for VAFB, CA.

Altitude (km)	Percentile				
	50	75	90	95	99
1	7	10	13	15	19
6	20	29	36	41	50
11	31	43	53	60	73
12	32	44	55	62	79
13	32	44	55	62	79
20	6	10	14	17	26
23	6	10	14	17	26
40	55	67	82	90	105
50	79	96	111	120	132
58	83	107	128	140	164
60	83	107	128	140	164
75	50	65	87	98	118
80	50	65	87	98	118

Table 2-51. Scalar wind speed W (m/s) steady-state envelopes as functions of altitude H (km) for various probabilities P (%) for White Sands Missile Range, NM.

$P = 50$		$P = 75$		$P = 90$		$P = 95$		$P = 99$	
H	W	H	W	H	W	H	W	H	W
1	4	1	7	1	11	1	13	1	22
2	5	2	8	2	12	2	15	2	22
						7	50	7	68
		9	45	8	49	9	67	9	88
11	42	10	53	11	71	11	76		
13	42	12	55	13	63	12	78	14	88
				15	45	15	52	15	69
20	10	20	14	20	20	20	24	20	41
23	10	23	14	23	20	23	24	23	41
50	85	50	104	50	120	50	130	50	150
60	85	60	104	60	120	60	130	60	150
75	60	75	77	75	93	75	102	75	120
80	60	80	77	80	93	80	102	80	120

Table 2-52. Scalar wind speed W (m/s) steady-state envelopes as functions of altitude H (km) for various probabilities P (%) for EAFB, CA.

$P = 50$		$P = 75$		$P = 90$		$P = 95$		$P = 99$	
H	W	H	W	H	W	H	W	H	W
1	8	1	11	1	16	1	17	1	25
2	8	2	12	2	16	2	18	2	28
				5	30	5	36	5	56
10	29			10	51	10	61	10	77
12	32	11	44	11	56			12	77
15	25	13	39	12	56	12	61	14	65
18	13	17	21	17	28	16	38	16	43
20	9	20	13	20	19	20	23	20	30
23	9	23	13	23	19	23	23	23	30
50	85	50	104	50	120	50	130	50	150
60	85	60	104	60	120	60	130	60	150
75	60	75	77	75	93	75	102	75	120
80	60	80	77	80	93	80	102	80	120

Table 2-53. Scalar wind speed W (m/s) steady-state envelopes as functions of altitude H (km) for various probabilities P (%) for all four locations.

$P = 95$				$P = 99$			
H	W	H	W	H	W	H	W
1	22	17	44	1	28	15	70
3	31	20	29	3	38	20	41
		23	29	5	56	23	41
6	54	50	150	6	60	50	170
		60	150	7	68	60	170
10	75	75	120	9	88	75	135
11	76	80	120	11	88	80	135
12	78			12	92		
13	74			13	88		
				14	88		

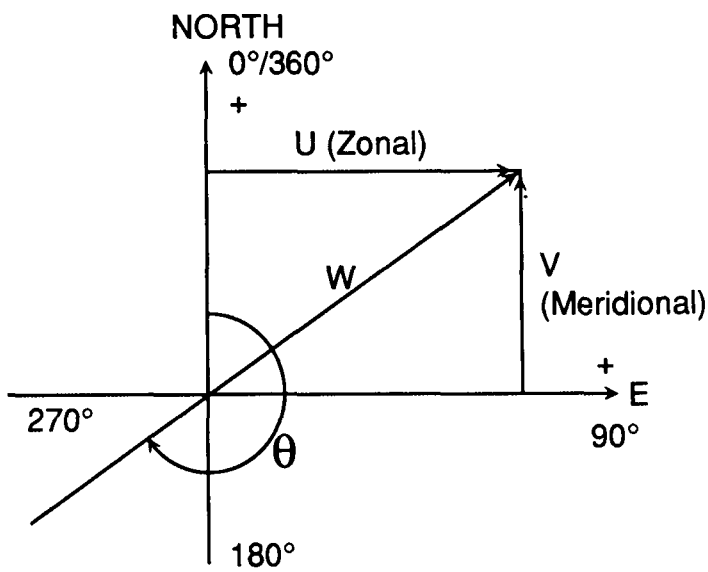

Definitions:

U is the zonal wind component, positive west to east in units, m/s.

V is the meridional wind component, positive south to north in units, m/s.

W is the wind speed in units, m/s.

θ is the wind direction measured in degrees clockwise from true north and is the direction from which the wind is blowing.

$U = -W \cos \theta$,

$V = -W \sin \theta$,

where $0° \leq \theta \leq 360°$.

Figure 2-17. Meteorological coordinate system.

The bivariate normal probability density function (BNpdf) can be expressed in cartesian and polar coordinates. Using population notations for the required five statistical parameters, the BNpdf in the usual mathematical cartesian coordinates is:

$$f(\bar{x},\bar{y}) = \frac{1}{2\pi\sigma_x\sigma_y\sqrt{1-\rho^2}} \exp\left[\frac{1}{2(1-\rho^2)}\left[\frac{(X-\bar{X})^2}{\sigma_x^2} - \frac{2\rho\,(X-\bar{X})\,(Y-\bar{Y})}{\sigma_x\sigma_y} + \frac{(Y-\bar{Y})^2}{\sigma_y^2}\right]\right], \tag{2.26}$$

where $-\infty \leq X \leq \infty$ and $-\infty \leq Y \leq \infty$. This function is completely described by the five parameters: the means X and Y, the standard deviations σ_x and σ_y, and the linear correlation coefficient, ρ, between the variables x and y.

The contours of equal probability density form a family of concentric ellipses with respect to the centroid located at the point $\{\bar{x},\bar{y}\}$. The probability contained within a contour of equal probability density is obtained by integrating the probability density function over the region defined by the contour.

This integration is obtained in closed form. The result is called a probability ellipse for the assigned probability area.

Using the properties of the bivariate normal probability distribution to model the wind as a vector quantity at discrete altitudes, many other probability functions can be derived. All that is required are the five bivariate normal statistical parameters with respect to an orthogonal coordinate system. The practical system of equations are given by Smith (ref. 2-38) and repeated in the range reference atmosphere publications (ref. 2-23) with illustrations. In terms of wind statistics, some of these properties are:

1. The five statistical parameters that have been computed with respect to a meteorological zonal and meridional coordinate system can be rotated to any other orthogonal coordinate system and the properties of the bivariate normal distribution still holds.

2. The wind components are univariate normally distributed. Percentile values and interpercentile values can be computed.

3. The conditional distribution of one wind component given the other is univariate normally distributed.

4. The sum and difference of bivariate normally distributed variates are univariate normally distributed.

5. The probability ellipse that contains p-percent of the wind vectors can be computed.

6. The probability density function for wind direction can be derived, and, by numerical integration, the probability for wind direction within any assigned limits can be computed.

7. The conditional probability density function for wind speed given a wind direction can be obtained.

8. The conditional probability distribution function for wind speed given a wind direction can be obtained.

9. The probability density function for wind speed can be derived as a generalized Rayleigh distribution (ref. 2-38). It is expressed as a series of the sum of products of the modified Bessel function.

The equations for the above functions are given in the most general form for all five statistical parameters for the bivariate normal distribution. For assumptions such as independent variates, zero means and equal variances are treated as special cases. With the advent of modern computers, these functions can be readily evaluated and graphic illustrations made. Some of these probability functions are presented in this subsection because of their important role in wind vector modeling.

2.3.5.2.1 Bivariate Normal Wind Parameters

There are several publications (refs. 2-23, 2-24, 2-25, and 2-51) that contain the bivariate normal wind statistical parameters versus altitude. All of these reports give tabulations for the five bivariate normal parameters with respect to the meteorological coordinate system.

The five statistical parameters are:

$\overline{U}$ = the monthly mean zonal wind component (m/s)

$\overline{V}$ = the monthly mean meridional wind component (m/s)

S_u = the standard deviation with respect to the monthly mean for the zonal wind component (m/s)

S_v = the standard deviation with respect to the monthly mean for the meridional wind component (m/s)

$R(U,V)$ = the correlation coefficient between the two components.

Tables 2-54 through 2-57 are taken from reference 2-51. These statistical parameters are for KSC, February and July; and for VAFB, December and July. For the altitude region 0 to 27 km, these parameters are from twice daily, serially complete rawinsonde wind measurements. The altitudes from 28 to 86 km are from rocketsonde wind measurements. For KSC, the period of record is 19 years, and, for VAFB, the period of record is 10 years. These months for the respective sites are chosen for illustration because they reasonably envelop the winds for both sites for all months.

For aerospace vehicle applications, it is often desired to express the wind statistics with respect to the vehicle flight azimuth.

By using coordinate rotation equations, these five statistical parameters can be calculated with respect to any orthogonal coordinates. Let the vehicle flight azimuth, α, be measured in degrees clockwise from true north, then the five statistical parameters with respect to the flight axes are given by the following equations:

(a) The means

$$\overline{X}_\alpha = \overline{U}\sin\alpha + \overline{V}\cos\alpha, \tag{2.27}$$

$$\overline{Y}_\alpha = \overline{V}\sin\alpha - \overline{U}\cos\alpha. \tag{2.28}$$

(b) The variances

$$S^2_{x\alpha} = S^2_u \sin^2\alpha + S^2_v \cos^2\cos^2\alpha + 2R(U,V)S_U S_V \sin\alpha\cos\alpha, \tag{2.29}$$

$$S^2_{y\alpha} = S^2_v \sin^2\alpha + S^2_u \cos^2\cos^2\alpha - 2R(U,V)S_U S_V \sin\alpha\cos\alpha. \tag{2.30}$$

(c) The correlation coefficients

$$R(x,y)_\alpha = \frac{COV(x,y)_\alpha}{S_{x\alpha}S_{y\alpha}}, \tag{2.31}$$

where $\mathrm{cov}(X,Y)_\alpha$ is the rotated covariance

$$COV(x,y)_\alpha = R(U,V)S_u S_v\,(\sin^2\alpha - \cos^2\alpha) + \sin\alpha\cos\alpha(S^2_v - S^2_u). \tag{2.32}$$

Table 2-54. KSC bivariate normal wind statistics, 90° flight azimuth.

February

Alt (km)	$\bar{u}$	$\bar{v}$	$S(u)$	$S(v)$	$R(uv)$	N
0	0.65	-0.21	3.28	3.68	-0.2615	1,074
1	3.70	1.62	7.17	6.80	-0.0277	1,074
2	7.88	1.48	7.74	6.82	0.0083	1,074
3	11.70	1.68	8.20	7.40	0.0437	1,074
4	15.21	2.10	9.11	8.10	0.0338	1,074
5	18.97	2.49	10.16	8.98	0.0501	1,074
6	22.95	2.98	11.14	9.62	0.1124	1,074
7	26.58	3.31	12.43	10.48	0.1653	1,074
8	30.23	3.40	13.80	11.54	0.1991	1,074
9	34.26	3.50	15.38	12.64	0.2148	1,074
10	38.18	3.39	16.45	13.89	0.2159	1,074
11	42.13	3.32	17.08	14.91	0.2281	1,074
12	44.84	3.49	16.53	14.56	0.2267	1,074
13	44.76	3.52	15.06	12.85	0.2863	1,074
14	41.65	3.33	13.08	11.05	0.2759	1,074
15	36.73	2.90	11.45	9.28	0.2060	1,074
16	31.59	2.60	10.27	8.25	0.1485	1,074
17	25.36	1.94	9.20	7.04	0.1429	1,074
18	18.78	1.41	8.49	5.67	0.2378	1,074
19	12.77	0.99	7.84	4.52	0.2280	1,074
20	7.85	0.63	7.40	3.89	0.2540	1,074
21	5.21	0.18	7.26	4.23	0.2321	1,074
22	4.04	-0.14	7.66	4.11	0.2344	1,074
23	3.47	-0.02	7.87	4.10	0.2736	1,074
24	3.65	0.09	8.27	3.89	0.2797	1,074
25	3.88	-0.02	9.15	3.85	0.3470	1,074
26	4.48	0.11	9.82	4.09	0.3075	1,074
27	5.14	0.35	10.57	4.13	0.2299	1,074
28	9.08	3.22	9.48	4.85	0.2951	79
29	10.78	3.67	9.42	5.67	0.2540	79
30	12.53	4.18	9.91	6.03	0.3252	77
31	14.63	4.15	10.65	6.80	0.3548	81
32	16.83	3.73	11.72	6.39	0.3957	81
33	18.41	2.85	12.90	6.36	0.3947	81
34	18.41	1.51	13.55	6.31	0.3675	81
35	17.61	0.38	14.31	6.10	0.3274	85
36	16.64	-0.96	14.59	6.74	0.2480	85
37	15.13	-0.45	15.13	7.87	0.2802	87
38	14.47	0.23	15.83	7.59	0.2648	87
39	13.94	0.18	16.79	8.00	0.1863	88
40	12.71	0.94	18.33	8.39	0.1776	87
41	11.60	2.74	18.69	7.60	0.0952	88
42	11.82	3.63	18.82	7.55	0.0531	89
43	13.25	5.08	18.76	8.96	0.1419	89
44	13.86	5.74	18.75	9.34	0.1513	86
45	14.87	6.27	19.63	10.11	0.1188	88
46	16.49	7.30	20.52	10.88	0.1161	90
47	18.46	8.75	20.73	10.76	0.0906	89
48	18.87	8.83	21.28	11.22	0.0649	89
49	19.98	9.23	21.02	11.23	0.0061	88
50	21.35	8.57	21.48	12.30	0.0203	88
51	22.91	9.72	21.19	12.61	0.1194	85
52	25.42	9.51	21.33	12.36	0.0854	84
53	28.18	9.16	20.59	12.27	0.1107	82
54	30.62	8.99	19.63	13.02	0.1702	82
55	34.27	11.12	18.00	13.33	0.1582	82
56	38.00	12.25	18.41	13.41	0.1751	80
57	41.51	13.97	18.57	12.58	0.1623	79
58	45.58	15.42	17.90	11.80	0.2153	66
59	48.06	16.24	18.17	12.11	0.2007	63
60	49.71	15.19	18.69	12.01	0.0992	59
61	54.11	14.82	18.05	11.80	0.2973	44
62	57.30	13.09	19.38	11.85	0.2644	33
63	58.44	10.28	18.68	11.33	-0.0387	32
64	60.36	6.82	15.37	10.89	-0.0402	28
65	59.89	3.50	15.01	11.49	0.0436	28
66	60.07	-0.26	15.83	12.08	-0.0695	27
67	60.64	-5.68	15.12	13.12	-0.2037	25
68	59.52	-5.70	16.42	9.90	-0.0087	23
69	56.48	-8.22	16.75	11.44	0.1063	23
70	50.52	-12.81	18.49	13.25	0.0056	21
71	42.76	-14.81	19.21	13.63	0.1244	21
72	37.11	-15.58	20.49	13.01	0.3917	19
73	30.11	-11.11	21.77	12.79	0.4381	19
74	24.20	-8.55	23.75	13.37	0.1233	20
75	19.25	-5.70	22.79	16.99	-0.0194	20
76	13.78	-0.28	21.72	19.80	0.1905	18
77	11.94	5.87	20.09	22.48	0.2601	16
78	8.31	10.81	20.44	23.17	0.3862	16
79	6.75	15.69	20.60	22.81	0.4347	16
80	6.37	18.87	20.72	22.49	0.4223	16
81	5.81	21.56	21.39	22.65	0.3534	16
82	5.37	23.12	22.95	23.44	0.2424	16
83	6.53	26.47	25.31	22.52	0.0293	15
84	4.93	25.43	29.40	25.08	-0.0659	14
85	5.27	30.00	38.65	27.99	-0.1226	11
86	8.20	25.20	12.45	27.20	0.8446	5

Table 2-55. KSC bivariate normal wind statistics, 90° flight azimuth.

July

Alt (km)	$\bar{u}$	$\bar{v}$	$S(u)$	$S(v)$	$R(uv)$	N
0	-0.54	1.53	2.29	1.96	-0.1370	1,178
1	0.63	2.74	4.34	3.35	-0.0144	1,178
2	0.95	1.94	4.43	3.54	0.0654	1,178
3	1.12	1.63	4.61	3.54	0.0995	1,178
4	1.11	1.42	4.81	3.79	0.0843	1,178
5	0.88	1.08	4.92	3.95	0.0510	1,178
6	0.52	0.77	4.95	4.17	0.0431	1,178
7	0.02	0.39	5.02	4.35	0.0935	1,178
8	-0.34	-0.13	5.50	4.74	0.1759	1,178
9	-0.82	-0.71	6.38	5.46	0.2705	1,178
10	-1.19	-1.31	7.35	6.28	0.3098	1,178
11	-1.70	-2.01	8.66	7.05	0.3235	1,178
12	-2.30	-2.95	9.77	7.64	0.3190	1,178
13	-3.01	-4.08	10.30	7.92	0.2831	1,178
14	-3.55	-4.57	9.09	7.21	0.2509	1,178
15	-4.26	-3.86	6.75	5.63	0.2748	1,178
16	-4.86	-2.63	4.93	4.16	0.3044	1,178
17	-6.00	-1.76	3.73	3.35	0.2364	1,178
18	-8.10	-1.21	3.16	2.97	0.0879	1,178
19	-10.44	-0.99	3.05	2.71	0.1215	1,178
20	-12.88	-0.89	3.50	2.59	0.0010	1,178
21	-14.97	-0.54	3.50	2.90	-0.2085	1,178
22	-16.50	-0.24	3.32	3.35	-0.1356	1,178
23	-17.60	-0.08	3.38	3.24	-0.0129	1,178
24	-18.62	-0.14	3.56	2.98	-0.0581	1,178
25	-19.34	-0.44	3.91	2.94	-0.0430	1,178
26	-20.00	-0.49	4.41	3.21	-0.1577	1,178
27	-20.41	-0.61	4.64	3.54	-0.1129	1,178
28	-22.01	-1.11	3.21	2.62	0.1234	97
29	-23.34	-0.83	3.35	2.80	0.0700	95
30	-24.78	-0.07	3.75	3.06	0.2547	96
31	-25.64	1.09	4.46	3.13	0.0244	99
32	-26.25	1.56	4.63	3.56	-0.0625	99
33	-26.40	1.13	5.10	3.71	-0.0094	100
34	-27.03	0.61	5.16	3.34	-0.0764	99
35	-28.10	0.48	4.86	3.77	-0.1564	99
36	-29.21	0.19	4.61	3.74	-0.0919	101
37	-30.91	0.24	5.24	4.29	-0.0018	100
38	-32.28	0.35	5.46	4.70	0.0628	102
39	-34.15	0.14	5.24	4.78	-0.0275	104
40	-35.96	0.04	5.23	4.90	-0.0682	103
41	-37.69	-0.82	5.82	5.08	-0.0481	104
42	-39.93	-1.75	6.07	5.81	-0.1918	106
43	-43.22	-1.40	6.20	6.16	-0.1917	104
44	-46.58	-0.18	5.80	6.99	-0.0695	106
45	-48.60	1.66	6.34	7.60	0.1183	107
46	-49.14	3.22	7.69	7.65	0.2902	106
47	-50.39	3.88	7.85	6.69	0.2375	106
48	-51.40	4.10	8.54	6.59	0.2990	105
49	-51.35	4.54	8.57	6.30	0.0453	105
50	-52.11	4.93	8.52	7.40	-0.0417	104
51	-52.91	4.97	8.58	7.71	-0.0531	103
52	-54.59	5.62	8.19	7.92	-0.0735	101
53	-54.51	5.67	9.09	9.44	-0.1176	100
54	-54.17	6.33	9.78	10.84	0.0299	101
55	-53.70	6.03	10.47	11.50	0.2275	94
56	-51.89	5.62	11.76	11.45	0.2552	93
57	-51.29	4.13	12.65	11.21	0.2054	87
58	-49.30	3.92	14.23	12.04	0.1667	79
59	-47.97	3.76	15.15	12.32	0.0217	71
60	-46.13	4.98	16.16	13.47	0.0904	62
61	-45.33	4.16	20.90	16.18	0.2517	43
62	-42.28	5.19	24.50	17.57	0.3672	36
63	-37.80	4.30	29.76	17.32	0.3026	30
64	-35.70	5.09	32.20	18.25	0.2689	23
65	-35.62	6.04	31.20	18.07	0.2073	26
66	-35.35	6.57	30.59	20.24	0.2556	23
67	-38.45	13.15	33.24	21.67	0.0476	20
68	-32.53	14.26	27.37	21.18	-0.0163	19
69	-28.16	6.16	26.24	22.93	-0.0761	19
70	-20.50	-1.28	23.73	20.55	-0.1924	18
71	-22.65	-5.71	21.02	18.05	-0.2565	17
72	-21.44	-12.37	21.69	21.78	-0.3460	16
73	-22.20	-20.33	23.45	24.42	-0.4228	15
74	-29.58	-18.17	17.93	25.34	-0.2819	12
75	-25.73	-22.73	20.10	29.03	-0.3982	11
76	-22.60	-24.40	21.90	29.47	-0.4009	10
77	-20.00	-24.00	23.75	30.51	-0.4689	9
78	-12.30	-20.70	27.19	29.59	-0.3069	10
79	-12.10	-23.90	24.32	27.73	-0.6421	10
80	-8.20	-24.40	24.75	27.89	-0.7128	10
81	-5.40	-24.90	24.34	28.76	-0.7349	10
82	-1.60	-24.40	23.39	28.79	-0.7536	10
83	0.89	-21.22	23.13	29.65	-0.7295	9
84	4.44	-18.67	20.62	29.10	-0.6736	9
85	8.11	-15.67	17.69	28.62	-0.5784	9
86	11.17	-17.67	13.99	27.32	0.0452	6
87	13.25	-23.25	14.10	19.49	0.0066	4
88	12.50	-7.75	10.92	20.35	-0.5731	4
89	11.25	1.00	11.01	22.05	-0.6428	4
90	8.67	17.33	14.61	25.10	-0.5821	3

Table 2-56. VAFB bivariate normal wind statistics, 90° flight azimuth.

December

Alt (km)	$\bar{u}$	$\bar{v}$	$S(u)$	$S(v)$	$R(uv)$	N
0	0.42	-1.10	2.83	3.19	-0.4912	620
1	1.26	-2.66	4.47	7.29	-0.0611	620
2	3.84	-3.63	5.80	8.50	0.0404	620
3	6.77	-4.34	7.54	9.85	0.0973	620
4	9.62	-4.95	9.38	11.60	0.1032	620
5	12.03	-5.36	10.96	13.02	0.1663	620
6	14.15	-5.89	12.39	14.87	0.2362	620
7	16.21	-6.43	14.05	16.83	0.3037	620
8	18.23	-6.67	15.60	18.32	0.3539	620
9	20.20	-7.09	16.77	19.84	0.3781	620
10	22.04	-7.14	17.47	20.94	0.4048	620
11	23.47	-6.98	17.02	20.60	0.3873	620
12	24.04	-6.00	15.52	18.85	0.3938	620
13	23.41	-4.83	13.90	16.23	0.3869	620
14	21.68	-3.76	11.78	13.94	0.3941	620
15	19.36	-3.13	10.00	11.72	0.4016	620
16	16.25	-2.72	8.84	9.77	0.4085	620
17	13.07	-2.31	7.83	8.26	0.4364	620
18	9.49	-2.23	6.71	6.35	0.4716	620
19	6.20	-2.34	6.07	4.95	0.4525	620
20	3.93	-2.50	5.97	4.26	0.3638	620
21	1.91	-2.66	5.99	3.95	0.2496	620
22	0.37	-2.53	6.41	3.80	0.2832	620
23	-0.40	-2.48	7.23	3.59	0.2116	620
24	-0.57	-2.73	7.77	3.50	0.1918	620
25	-0.84	-2.52	8.63	3.53	0.2330	620
26	-0.56	-2.49	9.99	3.96	0.2718	620
27	0.38	-2.67	11.78	4.53	0.3282	620
28	0.17	-3.03	13.65	4.04	0.3967	106
29	2.03	-3.18	15.22	4.78	0.5140	108
30	4.52	-3.20	17.05	5.48	0.5903	113
31	6.86	-3.19	18.71	6.40	0.6286	111
32	9.51	-2.79	20.17	7.01	0.6830	110
33	14.00	-2.26	22.75	7.86	0.7448	112
34	18.29	-1.53	24.38	8.75	0.7516	113
35	22.04	-0.89	25.28	9.45	0.7375	112
36	26.55	-0.22	26.22	10.17	0.7641	113
37	31.68	0.12	27.04	10.67	0.7702	112
38	36.19	0.03	27.37	11.06	0.7547	114
39	39.77	-0.34	27.19	11.28	0.7617	111
40	42.83	0.17	27.23	11.77	0.7349	114
41	45.87	1.35	27.99	13.06	0.6655	110
42	48.88	3.02	28.51	14.11	0.5957	110
43	53.18	4.46	29.04	14.46	0.5164	111
44	57.08	6.14	28.86	14.90	0.4416	112
45	60.79	7.65	28.65	15.63	0.3723	110
46	63.97	9.41	28.87	16.39	0.3035	111
47	67.35	11.59	28.74	16.41	0.3110	113
48	70.04	13.00	28.86	16.97	0.2797	112
49	72.05	14.28	28.58	17.59	0.2734	109
50	73.92	14.67	29.24	18.60	0.2191	106
51	75.08	14.23	29.00	17.95	0.1898	108
52	76.38	15.02	29.36	18.01	0.1559	108
53	77.19	14.67	29.87	17.75	0.1501	106
54	77.14	14.57	29.66	17.38	0.1622	106
55	78.67	13.91	29.99	16.80	0.0698	103
56	78.75	11.93	30.38	18.05	0.0278	99
57	78.57	10.00	29.99	19.05	0.0012	93
58	78.51	12.06	30.49	21.88	0.1326	89
59	79.89	12.51	31.18	23.15	0.1744	75
60	76.98	10.59	34.74	23.43	0.2544	54
61	75.62	5.53	34.24	24.43	0.1737	32
62	66.76	-3.38	33.96	22.77	0.0731	21
63	69.73	6.53	33.16	18.59	0.2412	15
64	69.94	7.00	29.87	15.68	0.4678	16
65	66.13	8.40	28.03	17.35	0.7231	15
66	64.20	7.73	28.53	18.78	0.5116	15
67	63.17	5.75	31.69	15.96	0.7011	12
68	60.85	4.92	32.18	18.40	0.3654	13
69	61.93	0.00	32.28	17.72	0.3567	14
70	60.92	2.00	34.46	13.97	0.6552	12
71	57.08	-1.38	32.15	20.62	0.5138	13
72	53.92	0.46	30.98	22.33	0.4664	13
73	56.09	4.91	28.16	23.85	0.2784	11
74	54.73	7.09	24.92	24.54	0.2137	11
75	54.20	9.80	22.30	26.00	0.2352	10
76	51.80	10.10	18.37	25.87	0.3741	10
77	49.60	9.20	15.42	25.25	0.5487	10
78	47.00	7.50	14.23	24.24	0.6515	10
79	44.10	5.90	15.29	22.78	0.5755	10
80	41.30	2.70	18.23	21.28	0.3401	10
81	38.30	-0.20	21.45	20.40	0.0525	10
82	34.90	-3.50	24.28	20.59	-0.2082	10
83	33.56	-4.00	27.43	22.22	-0.5057	9
84	29.89	-7.78	28.92	26.07	-0.5441	9
85	26.67	-11.44	28.56	29.41	-0.5107	9
86	15.33	-26.67	33.48	36.75	-0.5011	3

Table 2-57. VAFB bivariate normal wind statistics, 90° flight azimuth.

July

Alt (km)	$\bar{u}$	$\bar{v}$	$S(u)$	$S(v)$	$R(uv)$	N
0	2.03	-1.61	1.93	1.82	-0.4607	620
1	0.25	-1.90	2.54	3.87	-0.2064	620
2	-0.25	-0.16	3.04	3.92	-0.1869	620
3	0.88	1.60	4.03	4.32	-0.1257	620
4	1.76	2.82	4.86	4.66	0.0035	620
5	2.26	3.40	5.46	4.83	0.0642	620
6	2.90	3.94	6.24	5.29	0.0861	620
7	3.83	4.72	6.98	6.08	0.0503	620
8	5.03	5.86	7.90	6.95	0.0402	620
9	6.17	7.29	8.72	7.80	0.0001	620
10	7.28	9.00	9.47	8.60	-0.0109	620
11	8.53	10.92	9.98	9.35	-0.0191	620
12	9.46	12.23	9.98	9.69	-0.0163	620
13	9.65	12.21	9.54	9.29	0.0354	620
14	8.59	11.05	8.47	8.28	0.1050	620
15	6.15	8.55	7.07	6.18	0.1610	620
16	2.64	5.89	5.19	4.63	0.1318	620
17	-0.71	3.89	3.93	3.57	0.2216	620
18	-3.43	2.26	3.29	2.78	0.2395	620
19	-5.61	1.43	2.71	2.13	0.1653	620
20	-7.34	0.85	2.49	1.99	0.1657	620
21	-9.10	0.44	2.49	1.99	0.0821	620
22	-10.66	0.10	2.43	1.99	0.0760	620
23	-11.96	-0.12	2.54	2.00	0.0085	620
24	-13.25	-0.17	2.61	2.12	0.0240	620
25	-14.36	0.06	2.76	2.09	0.0014	620
26	-15.11	0.25	2.88	2.11	0.0669	620
27	-15.58	0.15	3.03	2.17	0.0456	620
28	-19.11	0.11	3.38	2.25	-0.0097	94
29	-20.29	0.04	3.38	2.48	-0.0823	97
30	-21.55	0.18	3.43	2.39	-0.0422	101
31	-22.25	0.64	3.55	2.47	-0.0375	104
32	-22.84	1.23	3.68	2.70	-0.2192	106
33	-23.46	1.57	3.26	2.90	-0.0749	106
34	-24.06	1.33	3.48	3.09	-0.0253	107
35	-24.90	0.79	4.18	3.30	0.0198	107
36	-26.35	1.13	4.43	3.44	-0.0830	110
37	-27.69	1.11	4.88	3.53	-0.1381	108
38	-29.02	1.17	5.07	4.25	-0.1775	109
39	-30.62	0.49	4.59	3.99	-0.0286	107
40	-33.05	0.04	4.21	4.44	-0.0276	108
41	-35.54	-0.23	4.34	5.07	0.0997	109
42	-37.88	-0.19	4.99	5.29	0.1510	107
43	-40.41	0.31	5.39	5.54	0.1417	109
44	-41.96	2.01	5.52	5.87	0.0613	109
45	-43.64	3.27	5.60	5.44	0.0489	107
46	-44.57	4.10	6.07	5.20	0.1344	108
47	-46.00	4.44	6.75	5.71	0.1801	105
48	-47.52	4.45	6.90	6.29	0.2254	106
49	-49.40	4.80	6.92	5.90	0.1944	107
50	-51.39	5.17	7.59	5.63	0.2488	105
51	-53.31	5.58	8.49	6.16	0.2050	106
52	-54.01	6.71	8.81	6.67	0.2925	100
53	-54.54	7.59	8.93	6.89	0.1842	98
54	-54.53	7.49	9.41	7.36	0.1331	97
55	-55.53	6.77	9.92	9.20	0.2014	91
56	-58.55	4.79	11.25	9.96	0.1319	91
57	-60.73	2.68	11.63	11.46	0.1282	82
58	-61.06	0.53	12.14	12.78	0.2108	72
59	-61.69	0.70	14.06	13.00	0.1816	61
60	-62.30	2.51	16.77	14.48	0.0693	47
61	-63.34	4.29	17.03	18.07	0.0136	38
62	-64.82	9.15	19.55	11.57	0.1036	33
63	-61.93	8.34	20.59	11.08	0.0527	29
64	-63.50	7.08	23.47	10.66	0.1710	26
65	-61.59	6.41	21.56	13.39	0.0952	27
66	-52.89	8.96	20.48	13.47	0.1283	27
67	-46.48	10.48	20.58	14.90	0.1038	25
68	-40.27	11.82	19.36	15.72	0.0554	22
69	-32.54	11.50	19.87	18.69	0.2531	24
70	-29.90	12.35	23.40	16.05	0.2602	20
71	-28.60	11.05	23.10	16.57	0.0236	20
72	-26.47	11.00	23.99	17.53	-0.2058	19
73	-24.11	8.89	24.28	20.22	-0.4865	18
74	-22.94	7.59	24.42	25.17	-0.5938	17
75	-20.00	2.50	23.17	26.61	-0.5001	16
76	-20.06	-0.13	23.21	28.44	-0.4357	16
77	-20.20	-2.33	24.18	29.82	-0.3646	15
78	-19.73	-4.47	24.27	29.18	-0.2964	15
79	-19.13	-6.13	23.86	28.03	-0.2276	15
80	-17.93	-7.20	22.73	26.61	-0.1851	15
81	-16.33	-7.80	21.10	24.87	-0.1278	15
82	-13.93	-8.13	19.00	23.38	-0.0680	15
83	-10.47	-7.87	16.97	22.18	0.0175	15
84	-5.80	-7.27	15.04	21.31	0.1098	15
85	-0.07	-6.20	14.07	20.86	0.2286	15
86	6.71	7.00	12.58	23.11	0.5795	7
87	16.83	14.83	12.35	20.36	0.3009	6
88	20.50	22.00	13.61	14.54	0.3903	4
89	21.67	25.00	9.98	15.77	0.7796	3
90	27.33	25.33	7.41	13.57	0.6983	3

2.3.5.2.2 The Wind Vector Probability Ellipse

Using the meteorological cartesian notation, the probability ellipse that contains p-percent of the wind vectors is expressed in the most general form by the conic equation defined by:

$$AX^2+BXY+CY^2+DX+EY+F=0 \ . \tag{2.33}$$

where

$$A = S_v^2$$

$$B = -2R(U,V)\, S_u S_v$$

$$C = S_u^2$$

$$D = -(B\ \overline{V} + 2A\ \overline{U})$$

$$E = -(B\ \overline{U} + 2C\ \overline{V})$$

$$F = A(\overline{U})^2 + C(\overline{V})^2 + B\,\overline{U}\ \overline{V} - AC\ \{1-[R(U,V)]^2\}\ \lambda_e^2$$

and

$$\lambda_e = \sqrt{-2\ln(1-P)} \ ,$$

where P is probability.

For convenient usage, values for the lambda parameter to the bivariate normal probability ellipse, λ_e, and for the bivariate circular normal distribution for selected probabilities are given in table 2-58. Circular distributions arise when the component standard deviations are equal.

Equation (2.33) is used to derive other functional relationships that describe the properties of the bivariate normal probability ellipse and for graphical displays. The largest and smallest values for x and y of a given probability ellipse are given by:

$$X_{(w,s)} = \overline{u} \pm S_u \lambda_e \ , \tag{2.34}$$

$$Y_{(w,s)} = \overline{v} \pm S_v \lambda_e \ . \tag{2.35}$$

Using the quadratic equation, solutions for Y in equation (2.33) are made by incrementing X from X_S to X_L and plotting on a scale that has the same range for X and Y, as shown in figure 2-18. Such illustrations are helpful in comparing the wind statistics from month to month and between sites. For example, assume that a vehicle trajectory has been wind biased to the monthly mean wind and the flight azimuth is 180° (south) for VAFB, then at 12-km altitude the head and tail quartering wind relative to the monthly mean to the 99-percent probability ellipse would be larger than that for an east launch from KSC, wind biased to the monthly mean.

2.3.5.2.3 The Bivariate Normal Distribution in Polar Coordinates

The bivariate normal probability density function expressed in polar coordinates is used to derive the probability distribution for wind speed given the wind direction, and to express the special relationship for wind vectors relative to the monthly mean wind to an assigned probability ellipse. These relationships are used in the selection of wind vectors to the probability ellipse in subsection 2.3.10 for the synthetic vector wind profile model.

Table 2-58. Values of λ for bivariate normal distribution ellipses and circles.

P (Percent)	λ_e (ellipse)	λ_c (circle)	P (Percent)	λ_e (ellipse)	λ_c (circle)
0.000	0.0000	0.0000	65.000	1.4490	1.0246
5.000	0.3203	0.2265	68.268	1.5151	1.0713
10.000	0.4590	0.3246	70.000	1.5518	1.0973
15.000	0.5701	0.4031	75.000	1.6651	1.1774
20.000	0.6680	0.4723	80.000	1.7941	1.2686
25.000	0.7585	0.5363	85.000	1.9479	1.3774
30.000	0.8446	0.5972	86.466	2.0000	1.4142
35.000	0.9282	0.6563	90.000	2.1460	1.5175
39.347	1.0000	0.7071	95.000	2.4477	1.7308
40.000	1.0108	0.7147	95.450	2.4860	1.7579
45.000	1.0935	0.7732	98.000	2.7971	1.9778
50.000	1.1774	0.8325	98.168	2.8284	2.0000
54.406	1.2533	0.8862	98.889	3.0000	2.1213
55.000	1.2637	0.8936	99.000	3.0348	2.1460
60.000	1.3537	0.9572	99.730	3.4393	2.4320
63.212	1.4142	1.0000	99.9877	4.2426	3.0000

$$\lambda_e = \sqrt{2}\sqrt{-\ln(1-P)}$$

$$\lambda_c = \sqrt{-\ln(1-P)}$$

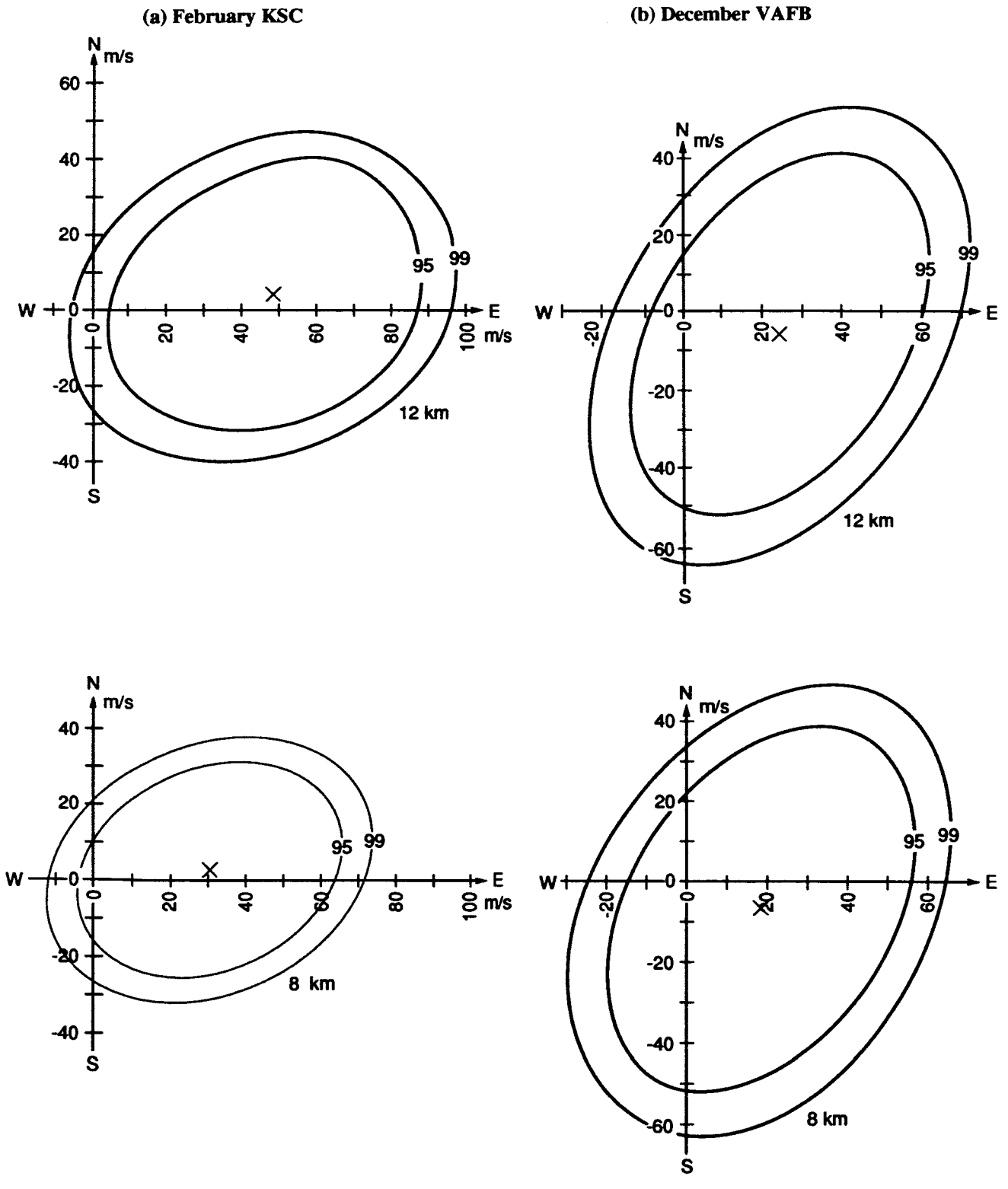

Figure 2-18. Comparison of wind vector probability ellipses (a) February KSC and (b) December VAFB.

The bivariate normal probability density function in the meteorological polar coordinate system is:*

$$g(r,\theta) = rd_1\, e^{-1/2\,(a^2r^2-2br+c^2)}\,, \tag{2.36}$$

where

$$a^2 = \frac{1}{(1-\rho^2)}\left[\frac{\sin^2\theta}{\sigma_x^2} - \frac{2\rho\cos\theta\sin\theta}{\sigma_x\sigma_y} + \frac{\cos^2\theta}{\sigma_y^2}\right],$$

$$b = \frac{1}{(1-\rho^2)}\left[\frac{\bar{x}\sin\theta}{\sigma_x^2} - \frac{\rho(\bar{x}\cos\theta + \bar{y}\sin\theta)}{\sigma_x\sigma_y} + \frac{\bar{y}\cos\theta}{\sigma_y^2}\right],$$

$$c^2 = \frac{1}{(1-\rho^2)}\left[\frac{\bar{x}\sin\theta}{\sigma_x^2} - \frac{2\rho xy}{\sigma_x\sigma_y} + \frac{\bar{y}_2}{\sigma_y^2}\right],$$

$$d_1 = \frac{1}{2\pi\sigma_x\sigma_y\sqrt{1-\rho^2}}\,.$$

$r = \sqrt{x^2+y^2}$ is the modulus of the vector or speed, and θ is the direction of the vector. After integrating $g(r,\theta)$ over $r = 0$ to ∞, the probability density function of θ is

$$g(\theta) = \frac{d_1}{a^2}\, e^{1/2c^2}\left[1 + \sqrt{2\pi}\left(\frac{b}{a}\right) e^{1/2\left(\frac{b}{a}\right)^2}\, \Phi\left(\frac{b}{a}\right)\right], \tag{2.37}$$

where a^2, b, c^2, and d_1 are as previously defined in equation (2.36) and

$$\Phi\left(\frac{b}{a}\right) = \Phi(x) = \frac{1}{\sqrt{2\pi}}\int_{-\infty}^{x} e^{-1/2t^2}\, dt\,,$$

is taken from tables of normal distributions or made available through computer subroutines.

If desired, equation (2.37) can be integrated numerically over a chosen range of θ to obtain the probability that the vector direction will lie within the chosen range; i.e.,

$$F(\theta) = \int_{\theta_2}^{\theta_1} g(\theta)\, d\theta\,. \tag{2.38}$$

One application may be to obtain the probability that the wind flow will be from a given quadrant or sector as, for example, onshore.

* This expression, equation (2.36) (in Smith 1976), is given with respect to the mathematical convention for a vector direction. Not the meteorological convention.

2.3.5.2.4 The Derived Conditional Distribution of Wind Speed Given the Wind Direction (Wind Rose)

The conditional probability density function for wind speed, r, given a specified value for the wind direction, θ, can be expressed as

$$f(r|\theta) = \frac{a^2 r e^{-\frac{1}{2}(a^2r^2 - br)}}{1 + \sqrt{2\pi}\left(\frac{b}{a}\right) e^{\frac{1}{2}\left(\frac{b}{a}\right)^2} \Phi\left(\frac{b}{a}\right)}, \tag{2.39}$$

where the coefficients, a and b and the function $\Phi\{b/a\}$ are as previously defined in equations (2.33) and (2.37).

From equation (2.39), the mode (most frequent value) of the conditional wind speed given a specified value of the wind direction is the positive solution of the quadratic equation,

$$a^2b^2 - br - 1 = 0, \tag{2.40}$$

which is

$$(f|\theta) = \frac{1}{2a}\left[\left(\frac{b}{a}\right) + \sqrt{4 + \left(\frac{b}{a}\right)^2}\right]. \tag{2.41}$$

The locus of the conditional modal values of wind speed when plotted in polar coordinates versus the given wind directions forms an ellipse.

The noncentral moment for equation (2.39) is expressed as

$$\mu_n' = \int_0^\infty r^n f(r|\theta)\, dr. \tag{2.42}$$

Now the first noncentral moment is identical to the first central moment or the expected value, $E(r|\theta)$. The integration of equation (2.42) for the first moment is sufficiently simple to yield practical computations and can be expressed as

$$E(r|\theta) = \frac{\left(\frac{b}{a}\right) + \left[1 + \left(\frac{b}{a}\right)^2\right]\sqrt{2\pi}\, e^{\frac{1}{2}\left(\frac{b}{a}\right)^2} \Phi\left(\frac{b}{a}\right)}{a\left[1 + \left(\frac{b}{a}\right)\sqrt{2\pi}\, e^{\frac{1}{2}\left(\frac{b}{a}\right)^2} \Phi\left(\frac{b}{a}\right)\right]}. \tag{2.43}$$

Hence, equation (2.43) gives the conditional mean value of the wind speed given a specified value for the wind direction.

The integration of equation (2.39) for the limits $r = 0$ to $r = r^*$ gives the probability that the conditional wind speed is $\leq r^*$ given a value for the wind direction, θ. This conditional probability distribution function can be written as

$$Pr\{r \leq r^* | \theta = \theta_0\} = 1 - \left[\frac{e^{-\frac{1}{2}r_s^2} + \sqrt{2\pi}\left(\frac{b}{a}\right)\{1 - \Phi(r_s)\}}{e^{-\frac{1}{2}\left(\frac{b}{a}\right)^2} + \sqrt{2\pi}\left(\frac{b}{a}\right)\Phi\left(\frac{b}{a}\right)}\right], \tag{2.44}$$

where

$$r_s = \left[a r^* - \left(\frac{b}{a} \right) \right] .$$

By definition, equation (2.44) is an expression for a "wind rose." Empirical wind rose statistics are often tabulated or graphically illustrated giving the frequency that the wind speed is not exceeded for those wind speed values that lie within assigned class intervals of the wind direction. After evaluation of equation (2.41) for various values of wind speed, r^*, and the given wind directions, θ, interpolations can be performed to obtain various percentile values of the conditional wind speed.

For the special case when $\underline{b}$ in equation (2.36) equals zero (i.e., for $\bar{x} = \bar{y} = 0$), the conditional modal values of wind speeds (equation (2.41)), the conditional mean values of wind speeds (equation (2.43)), and the fixed conditional percentile values of wind speeds (interpolated from evaluations of equation (2.44)), when plotted in polar form versus the given wind directions, produce a family of ellipses.

For the special case when $\bar{x} = \bar{y} = 0$, equation (2.39) reduces to the following simple case:

$$Pr\{r_s = r^* | \theta = \theta_0\} = 1 - e^{\frac{(-a^2 r^{*2})}{2}} . \tag{2.45}$$

There is a special significance of equation (2.45) when related to the bivariate normal probability distribution. If r^* and θ are measured from the centroid of the probability ellipse, then the probability that $r \leq r^*$ is the same as the given probability ellipse. Further, solving equation (2.45) for r^*, gives

$$r^* = \frac{1}{a} \sqrt{-2 ln(1-P)} . \tag{2.46}$$

If a probability ellipse P is chosen, equation (2.45) gives the distance of r along any θ from the centroid of the ellipse to the intercept of the probability ellipse. When computing the wind speed probability for a given θ relative to the monthly means, equation (2.46) is applicable.

2.3.5.2.5 Wind Component Statistics

The univariate normal (Gaussian) probability distribution function is used to obtain wind component statistics. In generalized notations, this probability density function is

$$f(t) = \frac{e^{\left(-\frac{1}{2} t^2\right)}}{\sqrt{2\pi}} , \tag{2.47}$$

where $t = (X - \xi)/\sigma_x$ is the standard variate, with ξ defining the mean and σ_x the standard deviation. The cumulative probability distribution function is

$$F(X) = \int_{-\infty}^{X} f(t)\, dt . \tag{2.48}$$

Because this integral cannot be obtained in closed form, it is widely tabulated for zero mean and unit standard deviation. For a convenient reference, selected values of $F(X)$ are given in table 2-59. To emphasize the connotation of probability, $F(X)$ is shown in table 2-59 as $P\{X\}$.

Table 2–59. Values of t for standardized normal (univariate) distribution for percentiles and interpercentile ranges.

t	$P(X)$	X	$P(X_1 \leq X \leq X_2)$ (%)
–3.0000	0.00135	$\xi - 3.0000\,\sigma$	
–2.5758	0.00500	$\xi - 2.5758\,\sigma$	
–2.3263	0.01000	$\xi - 2.3263\,\sigma$	
–2.2410	0.0125	$\xi - 2.2410\,\sigma$	
–2.0000	0.02275	$\xi - 2.0000\,\sigma$	
–1.9600	0.02500	$\xi - 1.9600\,\sigma$	
–1.6449	0.05000	$\xi - 1.6449\,\sigma$	
–1.2816	0.10000	$\xi - 1.2816\,\sigma$	
–1.0000	0.15866	$\xi - 1.0000\,\sigma$	
–0.8416	00.2000	$\xi - 0.8416\,\sigma$	
–0.6745	0.25000	$\xi - 0.6745\,\sigma$	
–0.2533	0.40000	$\xi - 0.2533\,\sigma$	
0.0000	0.50000	ξ	
0.2533	0.60000	$\xi + 0.2533\,\sigma$	
0.6745	0.75000	$\xi + 0.6745\,\sigma$	
0.8416	0.80000	$\xi + 0.8614\,\sigma$	
1.0000	0.84134	$\xi + 1.0000\,\sigma$	
1.2816	0.90000	$\xi + 1.2816\,\sigma$	
1.6449	0.95000	$\xi + 1.6449\,\sigma$	
1.9600	0.97500	$\xi + 1.9600\,\sigma$	
2.0000	0.97725	$\xi + 2.0000\,\sigma$	
2.2410	0.9875	$\xi + 2.2410\,\sigma$	
2.3263	0.99000	$\xi + 2.3263\,\sigma$	
2.5758	0.99500	$\xi + 2.5758\,\sigma$	
3.0000	0.99865	$\xi + 3.0000\,\sigma$	
		where $X_1 = \xi - t\sigma$ and $X_2 = \xi + t\sigma$	

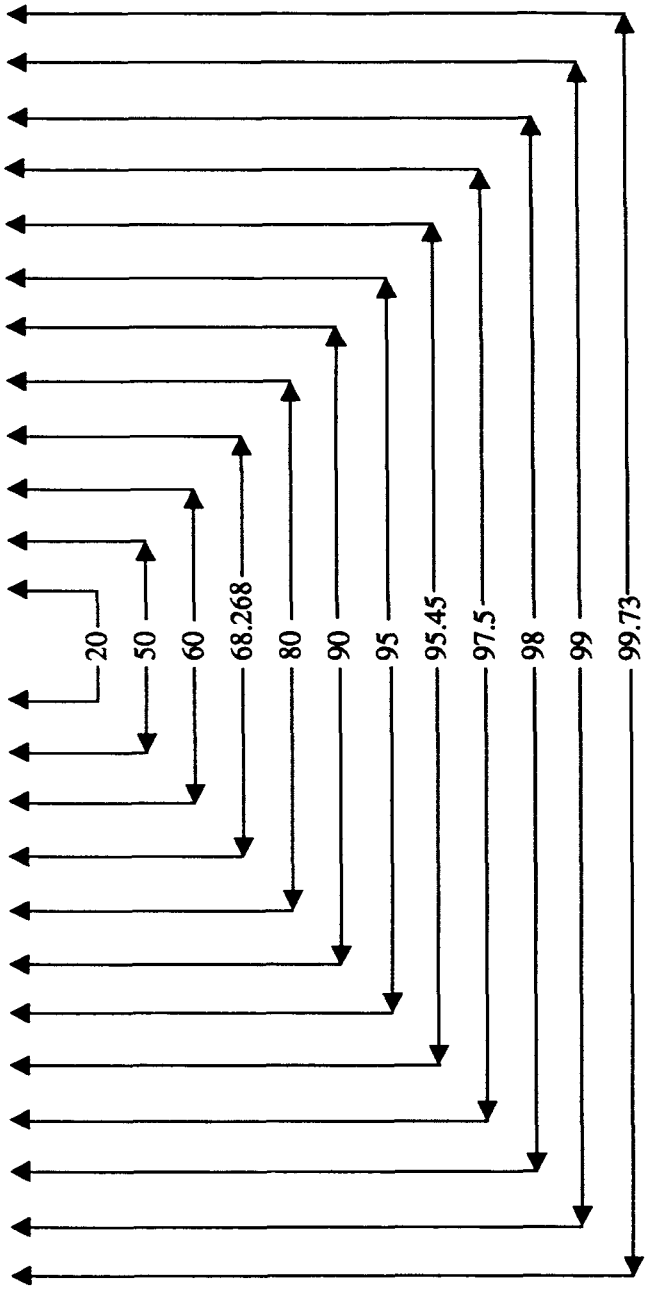

The t values in table 2-59 are used as multiplier factors to the standard deviation to express the probability that a normally distributed variable, X, is less than or equal to a given value as

$$P\{X \leq \text{mean} + t\sigma_x\} = \text{probability, } p \ . \tag{2.49}$$

For example, when $t = 1.6449$, the probability that X is less than or equal to the mean plus 1.6449 standard deviations is called the 95th percentile value of X. Also given in table 2-59 are the numerical values to express the probability that X falls in the interval X_1 to X_2; i.e.,

$$P\{X_1 \leq X \leq X_2\} = \text{Interpercentile Range} \ , \tag{2.50}$$

where

$$X_1 = \overline{X} - t\sigma_x$$

$$X_2 = \overline{X} + t\sigma_x \ .$$

For $t = 1.9602$ the probability that X lies in the interval X_1 to X_2 is 0.95. The values of X_1 and X_2 in this example comprise the 95th interpercentile range.

For a normally distributed variable, the mode (most frequent value) and the median (50th percentile) are the same as the mean value. The means and standard deviations of wind components are used in equations (2.49) and (2.50) to compute the percentile values and interpercentile ranges of the U and V wind components. Equation (2.49) is a straight line on a normal probability graph.

To obtain the wind component statistics with respect to orthogonal coordinate axes other than zonal and meridional, one should use the coordinate rotation equations (2.27) through (2.32).

2.3.5.2.6 Envelope of Wind Profiles Versus an Envelope of Percentiles

It is a usual practice to plot the points versus altitude for the interpercentile range for wind components (e.g., $u \pm ts_u$) at discrete altitudes and to connect these points. This convenient display can be misinterpreted. Since the winds are not perfectly correlated between all altitude levels, then the envelope of percentile values, for example the 95th interpercentile range ($u \pm 1.96 s_u$), the percentage of wind profiles would lie on the interpercentile bounds over all altitudes. The interlevel wind correlations decrease as the altitude interval increases. Suppose that there are five independent wind altitude levels between 0- and 12-km altitude. Then the percentage of wind profiles that lie within the bounds of the 95-interpercentile range is only 77.4 percent. This is obtained by $(0.95)^5 = 0.7737$. For five independent wind levels, the required interpercentile range taken at discrete altitudes to envelop 95 percent of the wind profiles is 98.98th interpercentile range, $(0.95)^{1/5} = 0.9898$. The percentage of wind profiles that lie within the 95-percent probability ellipses at 1-km intervals from 3- to 16-km altitude from a 12-year period of wind records for KSC approximates this example. The percentage of wind profiles for KSC, April, that lie within the 95th percent wind ellipses taken at 1-km intervals versus altitude is illustrated in figure 2-19. An aerospace vehicle should be designed to fly through a certain percent of the wind profiles by monthly reference periods, not just an assigned percent of the wind vectors at discrete altitudes. This raises the issue: What size should the wind vector probability ellipses at discrete altitudes be for aerospace vehicle design? This analysis suggests that the monthly 99-percent probability ellipses at discrete altitudes should be used to envelop 95 percent of the wind profiles over the altitudes of primary interest. This subject is further addressed in section 2.3.10 for synthetic vector wind profile models.

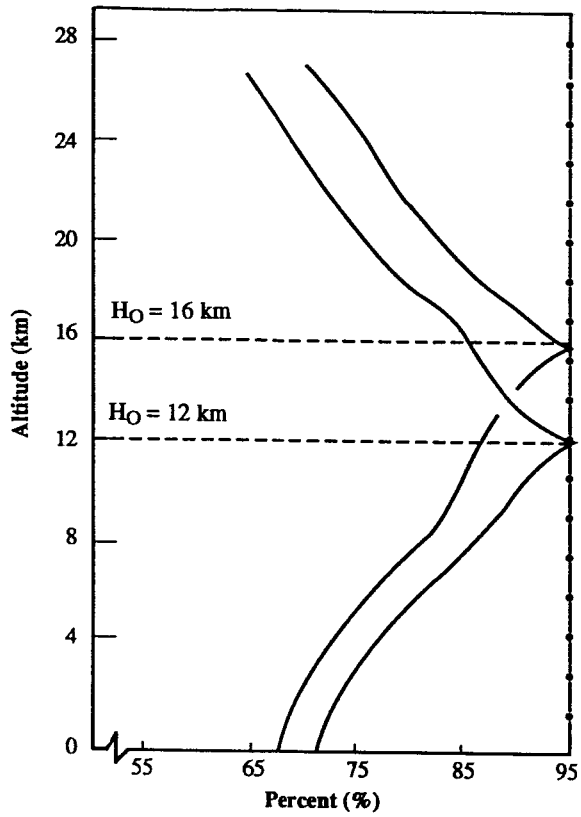

Figure 2-19. Percentage of wind profiles (wind vectors at 1-km intervals) that are within the 95-percent ellipses versus altitude, April, KSC.

2.3.5.3 Wind Shear

This subsection presents two wind shear models. They are based on different concepts and methodologies. In section 2.3.5.3.1 a review and presentation of the classical wind speed shear model is presented to contrast with a new wind shear modeling technique given in section 2.3.5.3.2.

2.3.5.3.1 Empirical Wind Shear Model

This is the classical wind speed shear model that has been used with minor modifications for aerospace vehicle design since the early 1960's. It is based on empirical conditional percentile values for wind speed shear for given values for wind speed. Here, wind speed shear is by definition the difference in wind speed between two altitudes divided by the altitude interval. If the altitude interval is specified, then the wind speed change between the two altitudes can be called wind shear for the specified shear interval. Refer to subsection 2.3.6. Historically, two-way empirical frequency distributions for wind speed change for various shear intervals versus wind speed were established by monthly reference periods using rawinsonde data bases for the 99th conditional speed change (or wind speed shear for the specified shear intervals) for given wind speed values. These were established and then enveloped "over" all months to give a "worst" case condition. With the availability of jimsphere wind profile data bases, refinements were made for shear intervals less than 1,000 m. The results are given in tables 2-64 to 2-73 as wind buildup and back-off wind speed change versus scales of distance (shear interval) and further discussed in section 2.3.6. When applied to the synthetic scalar wind profile model for aerospace vehicle design, the term wind buildup refers to the change in wind speed up to the reference altitude of the given wind speed and wind back-off refers to the change in wind speed for altitudes above the reference altitude. In statistical terms, tables 2-64 to 2-73 give the 99th conditional wind speed shear for various shear intervals for given wind speed values that envelop all months for each respective site.

2.3.5.3.2 Extreme Value Wind Shear Model

The wind shear model in this subsection has several advantages over the classical empirical wind shear model presented in section 2.3.5.3.1. The technique used to derive this new wind shear model is based on an analytically defined probability function. The procedure is objective. The analytical equations permit generalizations to give consistent comparative results. The empirical wind shear tabulations (tables 2-64 to 2-73) are for only the 99th conditional percentile value for given wind speeds whereas this new model permits computations for any conditional percentile for wind speed shear given any wind speed.

The extreme, largest wind speed shears for various altitude shear intervals that occurred in the 3- to 16-km altitude layer, for each of 150 per month jimsphere wind profiles, described in subsection 2.3.12.1, were computed. The associated wind speeds for the extreme wind shears were obtained. These data samples were fit by the univariate Gumbel (ref. 2-56) extreme value probability distribution function. A bivariate extreme value distribution function was used to model the extreme value conditional distribution for wind shear given the wind speed. This wind shear model is used to establish a synthetic wind profile model in section 2.3.10. The bivariate extreme value probability distribution has proven to be a powerful modeling tool for wind shear and for aerospace vehicle ascent structural loads (ref. 2-52).

There are two forms for the bivariate extreme value probability distribution (ref. 2-58). They are called the a-case and the m-case. Since the m-case is more general than the a-case; it is used to model the relationship between the extreme largest wind shear and the wind speed. The probability distribution function for the m-case is:

$$\Phi(X,Y,m) = \exp\left[-\left(e^{-mX}+e^{-mY}\right)^{\frac{1}{m}}\right], \tag{2.51}$$

where

$$-\infty \le X \le \infty$$
$$-\infty \le Y \le \infty$$
$$m \ge 1$$

is a measure of association (correlation) between the two variables.

X and Y are called the reduced variates; which are defined by:

$$X = \frac{\left(x-\mu_x\right)}{\alpha_x}, \tag{2.52}$$

and x and y are the extreme largest values for the original variates.

$$Y = \frac{\left(y-\mu_y\right)}{\alpha_y}, \tag{2.53}$$

Where μ_x, μ_y is the location parameter or modal value and α_x, α_y is the shape parameter. They are estimated from the sample extremes, means, $\bar{x}, \bar{y}$, and standard deviations s_x, s_y using Gumbel's (ref. 2-56) modified method of moments.

$$\hat{\alpha}_x = \frac{s_x}{\sigma_n} \quad \text{and} \quad \hat{\mu}_x = \bar{x} - \hat{\alpha}\bar{y}_n ,$$

where σ_n and $\bar{y}_n$ are the population parameters. They are a function of sample size, n. For $n = 150$, σ_n = 1.22534, and $\bar{y}_n = 0.56461$. For large n -> ∞, $\sigma_n = \pi/\sqrt{6}$ and $\bar{y}_n$ is Euler's constant, 0.57722.

$$\hat{m} = \frac{1}{\sqrt{1-r(x,y)}} , \tag{2.54}$$

where for the condition that m is >1, equation (2.51) becomes the product of two independent extreme value distributions which are univariate extreme value probability distribution functions. Some further notations are useful (refs. 2-57 and 2-58).

$$\Phi(X,Y;m) = P\{X = X_1, Y \le Y_2; m\} = \int_{-\infty}^{Y}\int_{-\infty}^{X} \varphi(X,Y;m)\, dX\, dY ,$$

where $\varphi(X,Y;m)$ is the probability density function defined by

$$\varphi(x,Y;m) = \Phi(X,Y;m) * \left| \left(e^{-mX}+e^{-mY}\right)^{\frac{1}{m}-2} e^{(-mX-mY)} \left\{ \left(e^{-mX}+e^{-mY}\right)^{\frac{1}{m}} + (m-1) \right\} \right| . \tag{2.55}$$

It is important to note that:

$$\Phi(X_\infty,Y;m) = \exp(e^{-Y}) .$$

These functions are used in deriving the conditional probability distribution function. The interest is to present tables for the conditional percentile values for wind speed shear given class intervals for wind speed. Let X stand for the reduced variate for wind shear and Y stand for the reduced variate for wind speed. The conditional probability distribution function for assigned values for X for given class intervals for Y is:

$$Pr\{X \le X^* | Y_1 \le Y \le Y_2\} = \frac{\Phi(X,Y_2;m) - \Phi(X^*,Y_1;m)}{\Phi(Y_2) - \Phi(Y_1)} , \tag{2.56}$$

where the denominator, the univariate extreme value probability distribution function for wind speed, is

$$\Phi(Y) = \exp(-e^{-Y}) , \tag{2.57}$$

is evaluated for assigned values for Y_1 and Y_2. The conditional probability distribution function in terms of the reduced variates is then interpolated for assigned conditional percentile values and then converted into the original extreme value variables using equations (2.52) and (2.53). This is the general method used to establish the conditional percentile shears (table 2-60) for the assigned class intervals for wind speed. An alternate conditional probability distribution function is:

$$\Pr\{X \le X^* | Y = Y_1\} = Z^{\left(\frac{1}{m}-1\right)} e^{\left[-Z^{\frac{1}{m}}-(m-1)Y_1+e^{-Y_1}\right]} , \tag{2.58}$$

where

$$Z = \left(e^{-mX^*}+e^{-mY}\right) .$$

This conditional probability distribution function is for the given value for Y equal to exactly the assigned value for Y_1 instead of an assigned class interval as presented in equation (2.56). An explicit inverse solution cannot be obtained to find the conditional percentile values for X^* as a function of probability, P. If interactive techniques are used such as Newton's method to do this, care must be taken for the computational precision for small values of Y_1. The usual practical range for the reduced variates is from –3.5 to +5.0. The extreme wind speed shear and associated wind speed data computed from the 150 per month jimsphere samples for KSC revealed that the data for February would encompass the other months. Hence, February is used to

Table 2-60. Conditional percentiles of wind speed shear (m/s) given wind speed (m/s) applicable over the 3- to 16-km altitude range, KSC, February.*

h = 100 meters Wind Speed Range (W1 to W2 m/s)

PROB	20 25	25 30	30 35	35 40	40 45	45 50	50 55	55 60	60 65	65 70	70 75	75 80	80 85	85 90
0.36788	3.83	3.91	3.99	4.07	4.16	4.26	4.36	4.47	4.58	4.71	4.84	4.99	5.16	5.35
0.50	4.04	4.12	4.21	4.30	4.41	4.52	4.63	4.77	4.91	5.07	5.24	5.44	5.65	5.88
0.60	4.22	4.30	4.39	4.49	4.60	4.72	4.86	5.00	5.17	5.35	5.56	5.78	6.02	6.27
0.70	4.42	4.51	4.60	4.71	4.82	4.96	5.10	5.27	5.46	5.66	5.89	6.13	6.39	6.67
0.80	4.68	4.77	4.87	4.98	5.11	5.25	5.41	5.60	5.80	6.03	6.27	6.53	6.81	7.09
0.85	4.86	4.95	5.05	5.16	5.29	5.44	5.61	5.80	6.02	6.25	6.51	6.77	7.05	7.34
0.90	5.10	5.19	5.29	5.41	5.54	5.70	5.87	6.07	6.30	6.54	6.80	7.08	7.36	7.65
0.95	5.50	5.59	5.69	5.81	5.95	6.11	6.29	6.50	6.73	6.98	7.25	7.53	7.82	8.11
0.98	6.01	6.11	6.21	6.33	6.47	6.63	6.82	7.03	7.27	7.53	7.80	8.08	8.37	8.66
0.99	6.40	6.49	6.60	6.72	6.86	7.02	7.21	7.43	7.66	7.92	8.19	8.47	8.77	9.06
0.995	6.78	6.87	6.98	7.10	7.24	7.41	7.60	7.81	8.05	8.31	8.58	8.86	9.15	9.45

h = 200 meters (W1 to W2 m/s)

PROB	20 25	25 30	30 35	35 40	40 45	45 50	50 55	55 60	60 65	65 70	70 75	75 80	80 85	85 90
0.36788	5.11	5.26	5.42	5.59	5.77	5.95	6.15	6.37	6.60	6.85	7.13	7.43	7.76	8.13
0.50	5.50	5.66	5.83	6.01	6.21	6.43	6.66	6.92	7.20	7.52	7.86	8.24	8.66	9.11
0.60	5.81	5.98	6.16	6.35	6.57	6.81	7.07	7.36	7.68	8.04	8.43	8.86	9.32	9.81
0.70	6.18	6.35	6.54	6.75	6.98	7.23	7.52	7.85	8.20	8.60	9.03	9.50	9.99	10.51
0.80	6.67	6.84	7.03	7.25	7.49	7.77	8.08	8.44	8.83	9.26	9.73	10.22	10.74	11.28
0.85	6.99	7.17	7.36	7.58	7.83	8.12	8.45	8.82	9.22	9.67	10.15	10.66	11.18	11.72
0.90	7.43	7.61	7.81	8.03	8.29	8.59	8.93	9.31	9.73	10.19	10.68	11.20	11.73	12.28
0.95	8.16	8.34	8.54	8.77	9.04	9.34	9.70	10.09	10.53	11.00	11.50	12.03	12.57	13.12
0.98	9.10	9.28	9.49	9.72	9.99	10.30	10.66	11.06	11.51	11.99	12.50	13.03	13.57	14.12
0.99	9.81	9.99	10.19	10.43	10.70	11.01	11.37	11.78	12.23	12.71	13.22	13.75	14.29	14.85
0.995	10.51	10.69	10.89	11.13	11.40	11.72	12.08	12.49	12.93	13.42	13.93	14.46	15.00	15.56

h = 300 meters (W1 to W2 m/s)

PROB	20 25	25 30	30 35	35 40	40 45	45 50	50 55	55 60	60 65	65 70	70 75	75 80	80 85	85 90
0.36788	5.98	6.21	6.45	6.69	6.96	7.24	7.53	7.85	8.20	8.57	8.99	9.44	9.94	10.49
0.50	6.52	6.75	7.01	7.28	7.57	7.89	8.24	8.62	9.04	9.50	10.01	10.56	11.17	11.82
0.60	6.96	7.20	7.46	7.75	8.07	8.41	8.80	9.22	9.69	10.21	10.78	11.40	12.07	12.77
0.70	7.47	7.72	7.99	8.29	8.63	9.00	9.42	9.89	10.41	10.98	11.60	12.27	12.98	13.71
0.80	8.13	8.39	8.67	8.99	9.34	9.74	10.20	10.71	11.27	11.89	12.55	13.25	13.99	14.74
0.85	8.58	8.84	9.12	9.45	9.81	10.23	10.70	11.22	11.81	12.44	13.13	13.84	14.59	15.35
0.90	9.19	9.45	9.74	10.07	10.44	10.87	11.36	11.90	12.51	13.16	13.86	14.59	15.34	16.11
0.95	10.19	10.46	10.75	11.09	11.47	11.91	12.41	12.98	13.60	14.27	14.98	15.72	16.48	17.26
0.98	11.49	11.76	12.05	12.39	12.78	13.23	13.74	14.32	14.95	15.63	16.35	17.09	17.86	18.64
0.99	12.46	12.73	13.03	13.37	13.76	14.21	14.73	15.30	15.94	16.62	17.34	18.09	18.86	19.64
0.995	13.43	13.70	14.00	14.34	14.73	15.18	15.70	16.28	16.91	17.60	18.32	19.07	19.84	20.62

h = 400 meters (W1 to W2 m/s)

PROB	20 25	25 30	30 35	35 40	40 45	45 50	50 55	55 60	60 65	65 70	70 75	75 80	80 85	85 90
0.36788	6.65	6.94	7.25	7.58	7.93	8.30	8.69	9.11	9.57	10.06	10.61	11.21	11.87	12.59
0.50	7.30	7.61	7.95	8.30	8.68	9.10	9.56	10.05	10.60	11.21	11.87	12.59	13.37	14.21
0.60	7.84	8.16	8.51	8.88	9.29	9.75	10.24	10.80	11.41	12.08	12.81	13.61	14.46	15.35
0.70	8.48	8.80	9.16	9.55	9.99	10.47	11.01	11.62	12.29	13.02	13.81	14.66	15.56	16.48
0.80	9.29	9.63	9.99	10.40	10.86	11.38	11.96	12.62	13.33	14.12	14.96	15.85	16.78	17.73
0.85	9.84	10.18	10.55	10.97	11.44	11.97	12.58	13.25	14.00	14.80	15.66	16.57	17.51	18.47
0.90	10.59	10.93	11.31	11.73	12.22	12.77	13.39	14.08	14.85	15.68	16.56	17.48	18.43	19.40
0.95	11.83	12.17	12.56	12.99	13.48	14.05	14.69	15.40	16.19	17.04	17.93	18.87	19.82	20.80
0.98	13.43	13.77	14.16	14.60	15.10	15.67	16.32	17.05	17.85	18.71	19.61	20.55	21.51	22.49
0.99	14.62	14.97	15.36	15.80	16.30	16.88	17.53	18.26	19.07	19.93	20.83	21.77	22.74	23.72
0.995	15.82	16.16	16.55	16.99	17.49	18.07	18.73	19.46	20.27	21.13	22.04	22.98	23.95	24.93

* h = height interval (m)

Table 2-60. Conditional percentiles of wind speed shear (m/s) given wind speed (m/s) applicable over the 3- to 16-km altitude range, KSC, February (continued).*

h = 500 meters (W1 to W2 m/s)

PROB	20 25	25 30	30 35	35 40	40 45	45 50	50 55	55 60	60 65	65 70	70 75	75 80	80 85	85 90
0.36788	7.18	7.54	7.92	8.33	8.75	9.20	9.69	10.21	10.77	11.39	12.07	12.81	13.62	14.50
0.50	7.94	8.32	8.72	9.16	9.63	10.14	10.70	11.30	11.97	12.71	13.51	14.39	15.34	16.34
0.60	8.56	8.95	9.37	9.83	10.33	10.88	11.49	12.16	12.90	13.72	14.60	15.56	16.58	17.64
0.70	9.29	9.69	10.13	10.61	11.14	11.72	12.38	13.11	13.92	14.80	15.75	16.76	17.82	18.93
0.80	10.24	10.65	11.10	11.59	12.15	12.78	13.48	14.26	15.12	16.06	17.06	18.12	19.22	20.35
0.85	10.88	11.29	11.74	12.25	12.82	13.46	14.19	14.99	15.88	16.84	17.87	18.94	20.06	21.20
0.90	11.74	12.16	12.62	13.13	13.72	14.38	15.12	15.96	16.87	17.85	18.90	19.99	21.11	22.26
0.95	13.18	13.60	14.06	14.59	15.18	15.86	16.63	17.48	18.42	19.42	20.49	21.59	22.72	23.88
0.98	15.03	15.45	15.92	16.45	17.05	17.74	18.52	19.39	20.34	21.35	22.43	23.54	24.67	25.83
0.99	16.42	16.84	17.31	17.84	18.45	19.14	19.92	20.79	21.75	22.77	23.84	24.95	26.09	27.25
0.995	17.80	18.22	18.69	19.22	19.83	20.52	21.31	22.18	23.14	24.16	25.24	26.35	27.49	28.65

h = 600 meters (W1 to W2 m/s)

PROB	20 25	25 30	30 35	35 40	40 45	45 50	50 55	55 60	60 65	65 70	70 75	75 80	80 85	85 90
0.36788	7.60	8.03	8.49	8.96	9.47	10.00	10.57	11.19	11.86	12.59	13.39	14.26	15.22	16.25
0.50	8.45	8.90	9.38	9.89	10.44	11.04	11.70	12.41	13.20	14.06	15.00	16.02	17.12	18.28
0.60	9.15	9.61	10.11	10.64	11.23	11.87	12.58	13.37	14.23	15.17	16.20	17.30	18.47	19.69
0.70	9.97	10.44	10.95	11.51	12.13	12.81	13.57	14.42	15.35	16.37	17.46	18.62	19.84	21.10
0.80	11.02	11.50	12.03	12.61	13.26	13.98	14.79	15.70	16.69	17.77	18.91	20.12	21.38	22.66
0.85	11.73	12.22	12.75	13.34	14.00	14.75	15.58	16.51	17.53	18.63	19.81	21.03	22.30	23.60
0.90	12.70	13.19	13.73	14.33	15.00	15.77	16.63	17.58	18.63	19.76	20.95	22.19	23.47	24.78
0.95	14.30	14.80	15.34	15.95	16.64	17.42	18.30	19.28	20.35	21.50	22.71	23.97	25.26	26.57
0.98	16.37	16.87	17.41	18.03	18.73	19.52	20.41	21.41	22.49	23.65	24.87	26.14	27.43	28.75
0.99	17.92	18.41	18.96	19.58	20.28	21.08	21.98	22.97	24.06	25.23	26.45	27.72	29.02	30.33
0.995	19.46	19.96	20.51	21.12	21.83	22.62	23.52	24.52	25.62	26.78	28.01	29.28	30.57	31.89

h = 700 meters (W1 to W2 m/s)

PROB	20 25	25 30	30 35	35 40	40 45	45 50	50 55	55 60	60 65	65 70	70 75	75 80	80 85	85 90
0.36788	7.92	8.41	8.93	9.47	10.04	10.66	11.31	12.01	12.77	13.60	14.52	15.51	16.60	17.76
0.50	8.84	9.35	9.90	10.48	11.11	11.79	12.52	13.33	14.22	15.19	16.25	17.39	18.62	19.92
0.60	9.60	10.12	10.69	11.29	11.96	12.68	13.48	14.36	15.33	16.39	17.53	18.77	20.07	21.43
0.70	10.49	11.02	11.60	12.23	12.93	13.70	14.55	15.49	16.54	17.67	18.89	20.18	21.54	22.94
0.80	11.64	12.18	12.77	13.43	14.15	14.96	15.87	16.87	17.98	19.17	20.45	21.79	23.18	24.61
0.85	12.41	12.96	13.56	14.22	14.96	15.79	16.72	17.75	18.89	20.11	21.41	22.77	24.18	25.62
0.90	13.46	14.02	14.62	15.29	16.05	16.90	17.85	18.91	20.08	21.32	22.64	24.02	25.44	26.89
0.95	15.21	15.76	16.38	17.06	17.83	18.70	19.67	20.76	21.94	23.22	24.56	25.95	27.38	28.83
0.98	17.46	18.02	18.63	19.32	20.10	20.98	21.97	23.07	24.27	25.55	26.90	28.30	29.74	31.20
0.99	19.14	19.70	20.32	21.01	21.79	22.67	23.67	24.77	25.98	27.27	28.62	30.02	31.46	32.92
0.995	20.82	21.38	22.00	22.69	23.47	24.36	25.35	26.46	27.67	28.96	30.31	31.72	33.16	34.62

h = 800 meters (W1 to W2 m/s)

PROB	20 25	25 30	30 35	35 40	40 45	45 50	50 55	55 60	60 65	65 70	70 75	75 80	80 85	85 90
0.36788	8.27	8.83	9.41	10.02	10.67	11.37	12.10	12.90	13.77	14.71	15.74	16.86	18.08	19.40
0.50	9.26	9.84	10.45	11.11	11.82	12.58	13.41	14.32	15.32	16.41	17.60	18.88	20.24	21.68
0.60	10.07	10.66	11.30	11.98	12.73	13.54	14.44	15.43	16.51	17.70	18.97	20.33	21.77	23.27
0.70	11.02	11.63	12.28	12.99	13.77	14.63	15.59	16.64	17.81	19.06	20.41	21.84	23.33	24.86
0.80	12.25	12.87	13.53	14.27	15.08	15.99	17.00	18.12	19.35	20.67	22.07	23.54	25.07	26.63
0.85	13.08	13.70	14.37	15.12	15.95	16.88	17.92	19.06	20.32	21.67	23.10	24.59	26.13	27.70
0.90	14.21	14.83	15.51	16.27	17.11	18.06	19.13	20.30	21.59	22.96	24.41	25.92	27.47	29.05
0.95	16.07	16.70	17.39	18.15	19.02	19.99	21.07	22.28	23.58	24.98	26.45	27.97	29.53	31.12
0.98	18.48	19.11	19.80	20.57	21.44	22.43	23.53	24.75	26.07	27.48	28.96	30.49	32.06	33.65
0.99	20.28	20.91	21.60	22.38	23.25	24.24	25.35	26.57	27.90	29.31	30.79	32.33	33.90	35.49
0.995	22.07	22.70	23.40	24.18	25.05	26.04	27.15	28.37	29.70	31.12	32.60	34.14	35.71	37.30

* h = height interval (m)

Table 2-60. Conditional percentiles of wind speed shear (m/s)given wind speed (m/s) applicable over the 3- to 16-km altitude range, KSC, February (continued).*

h = 900 meters (W1 to W2 m/s)

PROB	20 25	25 30	30 35	35 40	40 45	45 50	50 55	55 60	60 65	65 70	70 75	75 80	80 85	85 90
0.36788	8.59	9.21	9.85	10.54	11.26	12.03	12.85	13.74	14.71	15.76	16.90	18.16	19.50	20.95
0.50	9.63	10.27	10.96	11.69	12.47	13.32	14.25	15.25	16.36	17.56	18.87	20.27	21.76	23.33
0.60	10.49	11.15	11.85	12.61	13.44	14.34	15.33	16.43	17.62	18.92	20.31	21.80	23.36	24.98
0.70	11.50	12.16	12.89	13.67	14.54	15.49	16.55	17.71	18.98	20.36	21.82	23.37	24.98	26.64
0.80	12.80	13.48	14.21	15.03	15.93	16.93	18.04	19.27	20.61	22.05	23.57	25.16	26.81	28.49
0.85	13.67	14.35	15.10	15.93	16.84	17.87	19.01	20.26	21.63	23.10	24.65	26.26	27.92	29.62
0.90	14.86	15.55	16.30	17.14	18.08	19.12	20.29	21.57	22.97	24.46	26.03	27.66	29.33	31.03
0.95	16.83	17.52	18.28	19.13	20.08	21.15	22.34	23.65	25.07	26.59	28.18	29.82	31.50	33.21
0.98	19.37	20.06	20.83	21.69	22.65	23.73	24.93	26.26	27.70	29.22	30.82	32.47	34.16	35.87
0.99	21.27	21.97	22.74	23.59	24.56	25.64	26.85	28.18	29.62	31.15	32.76	34.41	36.10	37.81
0.995	23.16	23.86	24.63	25.49	26.45	27.54	28.75	30.08	31.53	33.06	34.67	36.32	38.01	39.72

h = 1,000 meters (W1 to W2 m/s)

PROB	20 25	25 30	30 35	35 40	40 45	45 50	50 55	55 60	60 65	65 70	70 75	75 80	80 85	85 90
0.36788	8.88	9.55	10.27	11.02	11.81	12.65	13.56	14.54	15.60	16.75	18.01	19.38	20.86	22.42
0.50	9.97	10.67	11.42	12.22	13.08	14.01	15.02	16.13	17.34	18.65	20.07	21.59	23.20	24.88
0.60	10.87	11.59	12.36	13.19	14.10	15.08	16.17	17.36	18.65	20.07	21.57	23.17	24.85	26.58
0.70	11.92	12.65	13.44	14.30	15.25	16.29	17.44	18.70	20.08	21.56	23.14	24.80	26.53	28.30
0.80	13.28	14.02	14.83	15.72	16.70	17.79	19.00	20.33	21.78	23.32	24.96	26.66	28.42	30.22
0.85	14.19	14.94	15.76	16.66	17.66	18.77	20.01	21.37	22.84	24.42	26.08	27.80	29.58	31.38
0.90	15.43	16.19	17.02	17.93	18.95	20.08	21.35	22.73	24.24	25.84	27.52	29.25	31.04	32.85
0.95	17.49	18.25	19.09	20.01	21.05	22.20	23.49	24.91	26.44	28.06	29.76	31.51	33.30	35.12
0.98	20.14	20.91	21.75	22.68	23.73	24.90	26.20	27.63	29.17	30.81	32.52	34.28	36.07	37.90
0.99	22.13	22.89	23.74	24.67	25.72	26.90	28.20	29.64	31.19	32.83	34.54	36.30	38.10	39.92
0.995	24.11	24.87	25.72	26.65	27.70	28.88	30.19	31.63	33.18	34.82	36.53	38.30	40.10	41.92

h = 1,500 meters (W1 to W2 m/s)

PROB	20 25	25 30	30 35	35 40	40 45	45 50	50 55	55 60	60 65	65 70	70 75	75 80	80 85	85 90
0.36788	10.03	10.98	11.98	13.04	14.16	15.35	16.64	18.02	19.51	21.14	22.88	24.74	26.72	28.79
0.50	11.29	12.27	13.32	14.44	15.64	16.94	18.34	19.87	21.52	23.30	25.19	27.19	29.28	31.43
0.60	12.31	13.32	14.40	15.55	16.81	18.17	19.66	21.28	23.02	24.88	26.86	28.93	31.07	33.26
0.70	13.51	14.54	15.64	16.83	18.13	19.56	21.12	22.80	24.63	26.57	28.61	30.73	32.90	35.12
0.80	15.06	16.10	17.22	18.45	19.80	21.28	22.90	24.65	26.55	28.54	30.62	32.78	34.98	37.22
0.85	16.10	17.14	18.28	19.52	20.89	22.40	24.04	25.83	27.75	29.77	31.88	34.05	36.26	38.50
0.90	17.51	18.57	19.71	20.97	22.36	23.89	25.57	27.38	29.32	31.36	33.49	35.67	37.89	40.14
0.95	19.85	20.91	22.07	23.34	24.75	26.30	28.00	29.85	31.81	33.87	36.01	38.21	40.44	42.69
0.98	22.86	23.93	25.09	26.37	27.79	29.36	31.08	32.94	34.91	36.99	39.13	41.33	43.57	45.83
0.99	25.12	26.19	27.35	28.63	30.06	31.63	33.35	35.22	37.20	39.28	41.43	43.63	45.86	48.13
0.995	27.37	28.43	29.60	30.88	32.31	33.88	35.61	37.47	39.46	41.54	43.69	45.89	48.13	50.39

h = 2,000 meters (W1 to W2 m/s)

PROB	20 25	25 30	30 35	35 40	40 45	45 50	50 55	55 60	60 65	65 70	70 75	75 80	80 85	85 90
0.36788	10.91	12.10	13.35	14.67	16.07	17.56	19.16	20.88	22.73	24.72	26.84	29.09	31.44	33.86
0.50	12.24	13.47	14.77	16.16	17.64	19.25	20.98	22.85	24.84	26.98	29.23	31.58	34.01	36.49
0.60	13.32	14.58	15.91	17.34	18.89	20.57	22.37	24.33	26.42	28.63	30.94	33.35	35.81	38.33
0.70	14.59	15.86	17.22	18.69	20.29	22.03	23.91	25.93	28.09	30.37	32.74	35.18	37.68	40.21
0.80	16.21	17.50	18.89	20.40	22.05	23.84	25.78	27.87	30.09	32.41	34.82	37.29	39.81	42.36
0.85	17.30	18.60	20.01	21.53	23.20	25.02	26.99	29.10	31.35	33.69	36.12	38.60	41.13	43.68
0.90	18.79	20.10	21.51	23.05	24.74	26.59	28.58	30.72	32.99	35.35	37.79	40.29	42.82	45.38
0.95	21.24	22.56	23.98	25.54	27.25	29.12	31.14	33.30	35.59	37.97	40.43	42.93	45.47	48.04
0.98	24.41	25.73	27.16	28.73	30.45	32.33	34.36	36.54	38.84	41.23	43.70	46.21	48.75	51.32
0.99	26.77	28.10	29.53	31.10	32.82	34.71	36.75	38.94	41.24	43.63	46.10	48.61	51.15	53.72
0.995	29.13	30.45	31.89	33.46	35.19	37.07	39.12	41.30	43.61	46.01	48.47	50.98	53.53	56.10

* h = height interval (m)

Table 2-60. Conditional percentiles of wind speed shear (m/s) given wind speed (m/s) applicable over the 3- to 16-km altitude range, KSC, February (continued).*

h = 2,500 meters (W1 to W2 m/s)

PROB	20 25	25 30	30 35	35 40	40 45	45 50	50 55	55 60	60 65	65 70	70 75	75 80	80 85	85 90
0.36788	11.64	13.04	14.51	16.06	17.69	19.43	21.31	23.30	25.45	27.73	30.14	32.66	35.27	37.95
0.50	13.00	14.43	15.96	17.58	19.30	21.17	23.16	25.31	27.58	29.98	32.50	35.11	37.79	40.52
0.60	14.10	15.56	17.12	18.79	20.58	22.51	24.58	26.80	29.16	31.64	34.21	36.87	39.58	42.34
0.70	15.38	16.87	18.45	20.16	22.00	24.00	26.13	28.42	30.84	33.38	36.00	38.68	41.41	44.18
0.80	17.04	18.54	20.16	21.90	23.79	25.83	28.04	30.38	32.85	35.42	38.07	40.78	43.54	46.32
0.85	18.14	19.66	21.28	23.05	24.96	27.03	29.26	31.62	34.12	36.71	39.37	42.09	44.85	47.64
0.90	19.65	21.17	22.81	24.59	26.52	28.62	30.87	33.26	35.78	38.38	41.06	43.79	46.56	49.34
0.95	22.13	23.66	25.32	27.11	29.06	31.18	33.46	35.87	38.40	41.03	43.72	46.45	49.22	52.02
0.98	25.34	26.87	28.53	30.34	32.30	34.43	36.72	39.15	41.69	44.32	47.02	49.76	52.53	55.33
0.99	27.73	29.27	30.93	32.74	34.71	36.84	39.14	41.57	44.11	46.75	49.45	52.19	54.96	57.76
0.995	30.12	31.66	33.32	35.13	37.10	39.24	41.53	43.96	46.51	49.15	51.85	54.59	57.37	60.16

h = 3,000 meters (W1 to W2 m/s)

PROB	20 25	25 30	30 35	35 40	40 45	45 50	50 55	55 60	60 65	65 70	70 75	75 80	80 85	85 90
0.36788	12.29	13.86	15.51	17.25	19.10	21.05	23.16	25.38	27.76	30.28	32.93	35.67	38.49	41.37
0.50	13.64	15.26	16.96	18.78	20.72	22.79	25.01	27.38	29.87	32.50	35.23	38.04	40.91	43.83
0.60	14.75	16.39	18.13	20.00	22.00	24.13	26.42	28.87	31.44	34.12	36.90	39.75	42.65	45.58
0.70	16.02	17.69	19.46	21.37	23.42	25.62	27.97	30.47	33.10	35.83	38.65	41.52	44.43	47.38
0.80	17.67	19.35	21.16	23.11	25.20	27.45	29.86	32.40	35.07	37.84	40.68	43.58	46.51	49.47
0.85	18.77	20.47	22.28	24.25	26.36	28.64	31.07	33.64	36.33	39.11	41.97	44.87	47.81	50.77
0.90	20.26	21.97	23.80	25.78	27.92	30.22	32.67	35.26	37.97	40.77	43.63	46.54	49.49	52.45
0.95	22.73	24.45	26.29	28.29	30.44	32.77	35.24	37.86	40.58	43.39	46.26	49.18	52.13	55.10
0.98	25.91	27.64	29.49	31.49	33.66	35.99	38.48	41.11	43.84	46.66	49.54	52.46	55.41	58.38
0.99	28.29	30.02	31.87	33.88	36.05	38.39	40.88	43.51	46.25	49.07	51.95	54.87	57.82	60.79
0.995	30.66	32.39	34.24	36.25	38.43	40.77	43.26	45.89	48.63	51.45	54.33	57.26	60.21	63.18

h = 3,500 meters (W1 to W2 m/s)

PROB	20 25	25 30	30 35	35 40	40 45	45 50	50 55	55 60	60 65	65 70	70 75	75 80	80 85	85 90
0.36788	12.87	14.61	16.41	18.32	20.35	22.49	24.78	27.19	29.76	32.47	35.30	38.21	41.19	44.22
0.50	14.21	15.98	17.85	19.84	21.96	24.20	26.61	29.16	31.83	34.63	37.53	40.50	43.53	46.60
0.60	15.30	17.10	19.01	21.04	23.21	25.53	28.00	30.62	33.36	36.21	39.15	42.15	45.20	48.28
0.70	16.56	18.38	20.32	22.40	24.62	26.99	29.52	32.20	34.99	37.88	40.85	43.87	46.93	50.02
0.80	18.18	20.02	22.00	24.10	26.38	28.80	31.37	34.09	36.92	39.85	42.84	45.87	48.95	52.05
0.85	19.26	21.12	23.10	25.23	27.52	29.96	32.57	35.31	38.16	41.09	44.09	47.14	50.22	53.32
0.90	20.73	22.60	24.60	26.74	29.05	31.52	34.14	36.90	39.76	42.71	45.72	48.77	51.86	54.96
0.95	23.16	25.04	27.05	29.21	31.53	34.03	36.67	39.44	42.32	45.29	48.30	51.36	54.45	57.56
0.98	26.29	28.17	30.19	32.36	34.70	37.20	39.85	42.64	45.53	48.49	51.52	54.58	57.67	60.78
0.99	28.63	30.51	32.53	34.71	37.05	39.55	42.21	45.00	47.89	50.86	53.89	56.95	60.04	63.15
0.995	30.96	32.84	34.86	37.04	39.38	41.89	44.55	47.34	50.23	53.20	56.23	59.29	62.38	65.49

h = 4,000 meters (W1 to W2 m/s)

PROB	20 25	25 30	30 35	35 40	40 45	45 50	50 55	55 60	60 65	65 70	70 75	75 80	80 85	85 90
0.36788	13.41	15.27	17.23	19.29	21.46	23.76	26.21	28.79	31.52	34.38	37.35	40.40	43.51	46.66
0.50	14.72	16.63	18.65	20.78	23.04	25.45	28.01	30.71	33.53	36.47	39.50	42.61	45.76	48.95
0.60	15.79	17.73	19.78	21.96	24.28	26.75	29.38	32.13	35.01	38.00	41.06	44.19	47.36	50.57
0.70	17.03	18.99	21.07	23.29	25.66	28.18	30.86	33.67	36.60	39.62	42.71	45.86	49.05	52.24
0.80	18.61	20.60	22.71	24.97	27.37	29.95	32.67	35.53	38.49	41.54	44.65	47.81	50.99	54.20
0.85	19.67	21.67	23.79	26.06	28.50	31.09	33.83	36.70	39.68	42.74	45.87	49.04	52.23	55.44
0.90	21.11	23.12	25.25	27.54	29.99	32.61	35.37	38.26	41.25	44.33	47.46	50.63	53.83	57.04
0.95	23.48	25.50	27.65	29.95	32.43	35.06	37.84	40.74	43.75	46.83	49.97	53.15	56.35	59.57
0.98	26.54	28.56	30.72	33.03	35.51	38.16	40.95	43.86	46.08	49.97	53.11	56.29	59.49	62.71
0.99	28.82	30.85	33.01	35.33	37.81	40.46	43.25	46.17	49.19	52.28	55.42	58.60	61.81	65.03
0.995	31.10	33.12	35.28	37.60	40.09	42.74	45.53	48.45	51.47	54.57	57.71	60.89	64.09	67.32

* h = height interval (m)

Table 2-60. Conditional percentiles of wind speed shear (m/s) given wind speed (m/s) applicable over the 3- to 16-km altitude range, KSC, February (continued).*

h = 5,000 meters (W1 to W2 m/s)

PROB	20 25	25 30	30 35	35 40	40 45	45 50	50 55	55 60	60 65	65 70	70 75	75 80	80 85	85 90
0.36788	14.39	16.49	18.66	20.97	23.38	25.96	28.65	31.49	34.46	37.56	40.74	43.99	47.30	50.65
0.50	15.64	17.78	20.02	22.39	24.90	27.57	30.35	33.28	36.34	39.50	42.73	46.03	49.37	52.74
0.60	16.66	18.82	21.11	23.52	26.09	28.79	31.64	34.62	37.73	40.92	44.18	47.49	50.85	54.22
0.70	17.83	20.02	22.33	24.79	27.40	30.15	33.05	36.08	39.21	42.43	45.72	49.04	52.40	55.79
0.80	19.33	21.55	23.89	26.38	29.02	31.82	34.76	37.82	40.99	44.23	47.53	50.87	54.24	57.64
0.85	20.34	22.56	24.91	27.42	30.08	32.90	35.86	38.95	42.12	45.38	48.68	52.02	55.39	58.78
0.90	21.70	23.93	26.30	28.82	31.50	34.34	37.32	40.41	43.61	46.87	50.18	53.53	56.90	60.29
0.95	23.94	26.19	28.57	31.10	33.80	36.65	39.65	42.76	45.96	49.23	52.55	55.91	59.28	62.67
0.98	26.83	29.08	31.47	34.02	36.72	39.59	42.59	45.71	48.92	52.19	55.51	58.87	62.25	65.64
0.99	28.99	31.25	33.64	36.18	38.89	41.76	44.77	47.89	51.10	54.38	57.70	61.06	64.43	67.83
0.995	31.15	33.40	35.79	38.34	41.05	43.92	46.93	50.05	53.26	56.54	59.86	63.22	66.60	69.99

h = 6,000 meters (W1 to W2 m/s)

PROB	20 25	25 30	30 35	35 40	40 45	45 50	50 55	55 60	60 65	65 70	70 75	75 80	80 85	85 90
0.36788	15.27	17.53	19.91	22.38	25.02	27.75	30.64	33.68	36.84	40.10	43.44	46.84	50.28	53.76
0.50	16.45	18.77	21.19	23.75	26.45	29.27	32.25	35.36	38.59	41.90	45.28	48.71	52.18	55.68
0.60	17.41	19.76	22.22	24.82	27.55	30.44	33.47	36.63	39.89	43.23	46.63	50.08	53.55	57.05
0.70	18.52	20.89	23.39	26.01	28.79	31.73	34.81	37.99	41.28	44.65	48.07	51.53	55.01	58.51
0.80	19.94	22.33	24.85	27.51	30.33	33.31	36.41	39.63	42.95	46.33	49.77	53.23	56.72	60.23
0.85	20.88	23.29	25.82	28.50	31.34	34.32	37.44	40.67	44.00	47.39	50.83	54.31	57.81	61.32
0.90	22.16	24.58	27.12	29.82	32.67	35.67	38.81	42.06	45.39	48.79	52.23	55.71	59.22	62.74
0.95	24.28	26.70	29.26	31.97	34.84	37.85	41.00	44.26	47.61	51.02	54.47	57.95	61.45	64.97
0.98	27.00	29.43	31.99	34.71	37.58	40.61	43.77	47.04	50.39	53.80	57.25	60.74	64.24	67.76
0.99	29.03	31.46	34.03	36.75	39.63	42.66	45.82	49.09	52.44	55.85	59.31	62.79	66.30	69.81
0.995	31.05	33.48	36.05	38.77	41.65	44.69	47.85	51.12	54.47	57.89	61.34	64.83	68.33	71.85

h = 7,000 meters (W1 to W2 m/s)

PROB	20 25	25 30	30 35	35 40	40 45	45 50	50 55	55 60	60 65	65 70	70 75	75 80	80 85	85 90
0.36788	16.06	18.48	20.98	23.63	26.38	29.28	32.34	35.52	38.81	42.20	45.65	49.16	52.70	56.27
0.50	17.18	19.64	22.21	24.90	27.74	30.73	33.85	37.10	40.44	43.87	47.36	50.89	54.45	58.04
0.60	18.08	20.58	23.18	25.91	28.81	31.82	34.98	38.26	41.63	45.09	48.60	52.16	55.75	59.34
0.70	19.13	21.65	24.27	27.06	29.97	33.03	36.22	39.53	42.94	46.41	49.93	53.50	57.09	60.70
0.80	20.47	23.00	25.66	28.46	31.41	34.51	37.74	41.08	44.50	47.99	51.53	55.10	58.69	62.31
0.85	21.35	23.90	26.57	29.39	32.36	35.48	38.72	42.07	45.51	49.01	52.54	56.11	59.70	63.31
0.90	22.56	25.12	27.80	30.64	33.62	36.75	40.00	43.36	46.81	50.31	53.86	57.44	61.03	64.64
0.95	24.55	27.12	29.81	32.66	35.66	38.80	42.07	45.44	48.90	52.41	55.96	59.53	63.13	66.74
0.98	27.10	29.68	32.38	35.23	38.24	41.39	44.67	48.05	51.50	55.02	58.57	62.15	65.75	69.37
0.99	29.01	31.59	34.29	37.15	40.16	43.31	46.59	49.98	53.43	56.95	60.50	64.08	67.68	71.30
0.995	30.91	33.49	36.20	39.05	42.07	45.22	48.50	51.88	55.34	58.86	62.41	66.00	69.60	73.21

h = 8,000 meters (W1 to W2 m/s)

PROB	20 25	25 30	30 35	35 40	40 45	45 50	50 55	55 60	60 65	65 70	70 75	75 80	80 85	85 90
0.36788	16.79	19.31	21.96	24.69	27.58	30.62	33.76	37.04	40.42	43.91	47.46	51.07	54.72	58.36
0.50	17.84	20.43	23.10	25.92	28.88	31.96	35.17	38.51	41.95	45.47	49.05	52.68	56.34	60.01
0.60	18.70	21.30	24.03	26.87	29.86	32.99	36.25	39.63	43.10	46.64	50.23	53.86	57.51	61.19
0.70	19.68	22.32	25.06	27.94	30.97	34.15	37.44	40.84	44.34	47.90	51.50	55.13	58.79	62.46
0.80	20.94	23.60	26.36	29.28	32.34	35.54	38.86	42.29	45.80	49.38	53.00	56.64	60.30	63.90
0.85	21.75	24.44	27.23	30.15	33.22	36.44	39.78	43.22	46.73	50.31	53.93	57.58	61.25	64.94
0.90	22.91	25.59	28.38	31.32	34.41	37.64	41.00	44.45	47.97	51.55	55.18	58.83	62.50	66.18
0.95	24.78	27.47	30.28	33.23	36.33	39.57	42.93	46.39	49.93	53.52	57.15	60.80	64.47	68.16
0.98	27.19	29.88	32.69	35.65	38.76	42.01	45.38	46.85	52.39	55.98	59.61	63.27	66.94	70.63
0.99	28.98	31.68	34.50	37.46	40.57	43.82	47.19	50.66	54.20	57.80	61.43	65.09	68.76	72.45
0.995	30.77	33.47	36.29	39.25	42.36	45.61	48.99	52.46	56.00	59.59	63.23	66.88	70.56	74.24

* h = height interval (m)

Table 2-60. Conditional percentiles of wind speed shear (m/s) given wind speed (m/s) applicable over the 3- to 16-km altitude range, KSC, February (continued).*

h = 9,000 meters (W1 to W2 m/s)

PROB	20 25	25 30	30 35	35 40	40 45	45 50	50 55	55 60	60 65	65 70	70 75	75 80	80 85	85 90
0.36788	17.54	20.17	22.86	25.69	28.64	31.72	34.95	38.30	41.76	45.31	48.92	52.58	56.27	60.00
0.50	18.57	21.22	23.98	26.86	29.87	33.03	36.33	39.74	43.24	46.82	50.46	54.13	57.84	61.57
0.60	19.38	22.08	24.86	27.78	30.85	34.04	37.36	40.80	44.33	47.94	51.61	55.30	59.00	62.72
0.70	20.34	23.05	25.86	28.82	31.90	35.13	38.49	41.95	45.51	49.12	52.79	56.49	60.22	63.97
0.80	21.54	24.28	27.13	30.10	33.22	36.48	39.87	43.36	46.93	50.56	54.23	57.94	61.67	65.41
0.85	22.35	25.10	27.95	30.95	34.08	37.36	40.75	44.25	47.83	51.48	55.16	58.87	62.59	66.33
0.90	23.45	26.20	29.07	32.07	35.22	38.51	41.92	45.43	49.02	52.66	56.35	60.06	63.79	67.54
0.95	25.25	28.01	30.89	33.91	37.07	40.37	43.79	47.31	50.91	54.56	58.25	61.96	65.70	69.44
0.98	27.56	30.34	33.22	36.24	39.41	42.72	46.15	49.68	53.28	56.93	60.62	64.34	68.07	71.81
0.99	29.29	32.07	34.95	37.98	41.15	44.47	47.90	51.43	55.03	58.68	62.37	66.09	69.82	73.56
0.995	31.02	33.79	36.68	39.70	42.88	46.19	49.63	53.16	56.76	60.41	64.10	67.82	71.55	75.30

h = 10,000 meters (W1 to W2 m/s)

PROB	20 25	25 30	30 35	35 40	40 45	45 50	50 55	55 60	60 65	65 70	70 75	75 80	80 85	85 90
0.36788	18.05	20.77	23.59	26.49	29.54	32.74	36.08	39.52	43.06	46.67	50.34	54.05	57.79	61.56
0.50	18.99	21.78	24.62	27.59	30.72	33.96	37.33	40.81	44.39	48.05	51.76	55.50	59.25	63.02
0.60	19.76	22.56	25.45	28.45	31.59	34.88	38.29	41.80	45.40	49.06	52.77	56.52	60.30	64.09
0.70	20.64	23.47	26.37	29.41	32.60	35.92	39.35	42.89	46.52	50.19	53.91	57.65	61.42	65.21
0.80	21.76	24.60	27.55	30.62	33.82	37.16	40.62	44.18	47.81	51.51	55.24	59.01	62.78	66.56
0.85	22.50	25.37	28.31	31.39	34.62	37.97	41.45	45.02	48.66	52.35	56.08	59.84	63.62	67.41
0.90	23.52	26.39	29.35	32.45	35.68	39.04	42.52	46.10	49.75	53.46	57.20	60.96	64.74	68.53
0.95	25.18	28.06	31.04	34.14	37.39	40.77	44.26	47.85	51.50	55.21	58.96	62.72	66.50	70.29
0.98	27.33	30.21	33.19	36.30	39.56	42.94	46.44	50.04	53.70	57.40	61.15	64.91	68.70	72.49
0.99	28.93	31.81	34.79	37.91	41.17	44.55	48.06	51.65	55.31	59.02	62.77	66.53	70.32	74.11
0.995	30.52	33.40	36.39	39.50	42.76	46.15	49.66	53.25	56.91	60.62	64.37	68.14	71.92	75.71

* h = height interval (m)

typify these wind shear statistics. For computational conveniences, the five required parameters for the bivariate extreme value distribution were fit by empirical equations as a function of altitude shear interval, h, valid for $100 \leq h \leq 10{,}000$ m. For the extreme largest wind speed shear parameters:

$$\mu_s(h) = 0.4747\, h^{0.47}\ ,\ (100 \leq h \leq 10{,}000\, m) \tag{2.59}$$

and

$$\alpha_s(h) = \frac{10h}{1{,}300 + h}\ ,\ (100 \leq h \leq 10{,}000\, m)\ . \tag{2.60}$$

For the associated wind speed with the extreme largest wind speed shear parameters:

$$\mu_w(h) = 34.71 + 0.0071\, h\ ;\ \ (100 \leq h \leq 600\, m) \tag{2.61}$$

$$\mu_w(h) = 39.2936 + 0.001127\, h\ ;\ \ (600 < h \leq 10{,}000\, m)\ .$$

and

$$\alpha_w(h) = 11.60 \text{ for all } h \geq 100\,m \ . \tag{2.62}$$

The units for these parameters are m/s.

The empirical equation for the m-parameter is:

$$m(h) = 1.27 + 0.00026\,h \ , \ (100 \leq h \leq 10{,}000\,m) \ . \tag{2.63}$$

Evaluating this equation for h = 100 m and h = 10,000 m yields the values of 1.296 and 3.870. From equation (2.54), this gives the correlation coefficients between the extreme largest shear and associated wind speed for h = 100 m as 0.4046 and for h = 10,000 m as 0.9332. Hence, as the altitude shear interval increases, this correlation coefficient between the wind shear and wind speed increases.

The above empirical equations for the five bivariate extreme value distribution functions were used in equation (2.56) to establish the conditional percentile values for wind speed shear for the given wind speed class intervals shown in table 2-60. The 99th conditional extreme value wind shear at various shear intervals, h, gives the associated wind speed. As shown, for the given wind speed, the conditional wind shear over large shear intervals exceeds the given wind speed. This indicates that this wind shear model is invalid in this domain.

2.3.5.3.3 Percentile Values for Extreme Largest Wind Speed Shear

The univariate extreme value distribution for wind speed shear can be computed using the $u_s(h)$ and $\alpha_s(h)$ parameters from equations (2.59) and (2.60) in the univariate extreme value probability distribution function. The percentile values for wind speed shear versus shear intervals, $S(h;P)$, in table 2-61, are computed from:

$$S(h;P) = u_s(h) + \alpha_s(h)\,Y \ , \tag{2.64}$$

where

$$Y = -ln(-ln\,P) \text{ and } P \text{ is probability.}$$

Using the same procedure, the empirical equations for $u_s(h)$ and $\alpha_s(h)$ for the extreme largest wind speed shear in the 3- to 16-km altitude for KSC, July, are:

$$u_s(h) = 0.5822\,h^{0.36} \ , \tag{2.65}$$

and

$$\alpha_s(h) = 0.0507\,h^{0.57} \ . \tag{2.66}$$

The KSC February and July percentile values for the extreme largest wind speed shear are given in tables 2-61 and 2-62, respectively. Comparing the wind shears (tables 2-61 and 2-62) it is seen that the wind shears are greater during February than July for shear intervals, h, greater than 100 m. This is because the extreme largest wind profile shears are correlated with the wind speed, and as the shear interval increases the correlation increases.

Table 2-61. Percentile values (m/s) versus shear intervals for extreme largest shear (3- to 16-km altitude) February, KSC, FL.

Shear Interval (m)	36.79	50.00	60.00	70.00	80.00	85.00	90.00	95.00	98.00	99.00	99.50
100.0	4.13	4.40	4.61	4.87	5.21	5.43	5.74	6.26	6.92	7.42	7.92
200.0	5.73	6.22	6.62	7.10	7.73	8.15	8.73	9.69	10.93	11.86	12.79
300.0	6.93	7.62	8.19	8.86	9.74	10.34	11.15	12.50	14.25	15.55	16.86
400.0	7.93	8.79	9.51	10.36	11.46	12.21	13.23	14.92	17.11	18.76	20.39
500.0	8.81	9.83	10.68	11.67	12.98	13.86	15.06	17.06	19.65	21.59	23.52
600.0	9.60	10.75	11.72	12.85	14.33	15.34	16.70	18.98	21.92	24.12	26.32
700.0	10.32	11.60	12.67	13.93	15.57	16.68	18.19	20.71	23.98	26.42	28.85
800.0	10.99	12.38	13.55	14.91	16.70	17.91	19.56	22.30	25.85	28.51	31.16
900.0	11.61	13.11	14.36	15.83	17.75	19.05	20.82	23.76	27.57	30.43	33.28
1,000.0	12.20	13.80	15.12	16.68	18.72	20.10	21.99	25.12	29.17	32.20	35.23
1,500.0	14.76	16.73	18.36	20.29	22.80	24.50	26.82	30.68	35.67	39.41	43.13
2,000.0	16.90	19.12	20.97	23.15	25.99	27.91	30.54	34.90	40.55	44.78	49.00
2,500.0	18.77	21.18	23.19	25.55	28.64	30.72	33.57	38.31	44.44	49.03	53.61
3,000.0	20.45	23.01	25.14	27.64	30.91	33.13	36.15	41.17	47.67	52.54	57.40
3,500.0	21.99	24.66	26.88	29.50	32.92	35.23	38.39	43.64	50.44	55.53	60.60
4,000.0	23.41	26.18	28.48	31.19	34.73	37.12	40.39	45.83	52.86	58.13	63.38
5,000.0	26.00	28.91	31.33	34.18	37.90	40.42	43.86	49.57	56.97	62.51	68.03
6,000.0	28.32	31.34	33.84	36.80	40.65	43.26	46.82	52.74	60.39	66.13	71.85
7,000.0	30.45	33.54	36.12	39.15	43.10	45.78	49.43	55.50	63.36	69.25	75.12
8,000.0	32.42	35.58	38.20	41.29	45.33	48.05	51.78	57.97	65.99	72.00	77.98
9,000.0	34.27	37.47	40.14	43.28	47.38	50.15	53.93	60.22	68.36	74.47	80.54
10,000.0	36.01	39.25	41.95	45.13	49.28	52.09	55.92	62.29	70.54	76.72	82.88

Table 2-62. Percentile values (m/s) versus shear intervals for extreme largest wind shear (3- to 16-km altitude) July, KSC, FL.

Shear Interval (m)	36.79	50.00	60.00	70.00	80.00	85.00	90.00	95.00	98.00	99.00	99.50
100.0	3.06	3.31	3.53	3.78	4.11	4.33	4.63	5.13	5.79	6.27	6.76
200.0	3.92	4.30	4.62	4.99	5.48	5.81	6.26	7.01	7.98	8.70	9.42
300.0	4.54	5.02	5.42	5.89	6.50	6.92	7.48	8.43	9.65	10.56	11.47
400.0	5.03	5.60	6.07	6.62	7.35	7.84	8.50	9.61	11.05	12.13	13.20
500.0	5.45	6.10	6.63	7.26	8.08	8.64	9.40	10.66	12.29	13.51	14.73
600.0	5.82	6.54	7.13	7.83	8.74	9.35	10.20	11.60	13.41	14.76	16.12
700.0	6.16	6.93	7.58	8.34	9.34	10.01	10.93	12.46	14.44	15.92	17.39
800.0	6.46	7.30	8.00	8.82	9.89	10.62	11.61	13.26	15.39	16.99	18.58
900.0	6.74	7.64	8.38	9.26	10.41	11.19	12.25	14.01	16.29	18.00	19.71
1,000.0	7.00	7.95	8.75	9.68	10.90	11.72	12.85	14.72	17.15	18.96	20.77
1,500.0	7.50	8.61	9.54	10.63	12.05	13.02	14.33	16.52	19.35	21.47	23.58
2,000.0	7.88	9.12	10.15	11.37	12.96	14.03	15.50	17.94	21.09	23.46	25.82
2,500.0	8.18	9.53	10.66	11.98	13.71	14.88	16.48	19.13	22.57	25.14	27.71
3,000.0	8.44	9.89	11.09	12.51	14.37	15.62	17.33	20.18	23.86	26.62	29.37
3,500.0	8.66	10.20	11.48	12.98	14.95	16.28	18.09	21.11	25.01	27.94	30.85
4,000.0	8.86	10.48	11.82	13.41	15.47	16.87	18.78	21.96	26.06	29.14	32.21
5,000.0	9.20	10.96	12.43	14.15	16.40	17.92	20.00	23.46	27.93	31.28	34.62
6,000.0	9.49	11.38	12.95	14.79	17.21	18.84	21.07	24.77	29.56	33.15	36.73
7,000.0	9.74	11.74	13.41	15.37	17.92	19.65	22.02	25.94	31.02	34.83	38.63
8,000.0	9.97	12.07	13.82	15.88	18.57	20.39	22.88	27.01	32.36	36.36	40.35
9,000.0	10.17	12.37	14.20	16.36	19.17	21.07	23.67	27.99	33.58	37.77	41.94
10,000.0	10.35	12.64	14.55	16.79	19.72	21.70	24.41	28.90	34.72	39.08	43.43

2.3.5.3.4 Percentile Values for Extreme Largest Wind Speed

An estimate for the extreme value pdf for the extreme largest wind speed in the 3- to 16-km layer can be obtained by evaluating equations (2.49) and (2.50) at the shear interval h = 10,000 m for the parameters μ_w and α_w. For KSC February, this gives μ_w = 50.56 m/s and α_w = 11.60 m/s. The percentile values for the extreme largest wind speed is then estimated by:

$$W(P) = 50.56+11.60Y \ , \tag{2.67}$$

where

$$Y = -ln(-ln\ P) \ , \text{ and } P \text{ is probability.}$$

Table 2-63. Comparison of some wind speed percentile values, KSC.

Probability (Percent)	Scalar Wind Speed (a) (m/s)	Extreme Wind Speed (b) (m/s)	Largest u-Component (c) (m/s)
50	45	54.8	49.8
75	57	65.0	68.1
80	68	68.0	71.0
95	75	85.0	85.8
99	92	103.9	99.1

(a) From table 2-49, empirical monthly envelope for percentile values at 12-km altitude.

(b) Estimated from equation (2.67), February.

(c) The largest zonal wind component to probability ellipses using monthly enveloping bivariate normal parameters at 12-km altitude presented later in table 2-74. At 12-km altitude, u_A = 30.34 m/s and s_{Au} = 22.67 m/s, $u_L = u_A + s_{Au}\ \lambda e$, where $\lambda e = \sqrt{-2\ ln(1-p)}$.

Considering that the wind speed percentile values in table 2-63 are derived from three different methods and three different data bases, the agreement is remarkably close.

2.3.6 Wind Speed Change Envelopes

This section provides representative information on wind speed change (shear) for scales of distance $\Delta H \leq$ 5,000 m. Wind speed change is defined as the total magnitude (speed) change between the wind vector at the top and bottom of a specified layer, regardless of wind direction. Wind shear is defined as the wind speed change divided by the altitude interval. When applied to aerospace vehicle synthetic profile criteria, it is frequently referred to as a wind buildup or back-off rate depending upon whether it occurs below (buildup) or above (back-off) the reference height of concern. Thus, a buildup wind value is the change in wind speed which a vehicle may experience while ascending vertically through a specified layer to the known altitude. Back-off magnitudes describe the speed change which may be experienced above the chosen level. Both buildup and back-off wind speed change data are presented in this section as a function of reference level wind vector magnitude and geographical location. Wind buildup or back-off may be determined for a vehicle with other than a vertical flight path by multiplying the wind speed change by the cosine of the angle between the vertical axis and the vertical trajectory. Wind shears for scales of distance $\Delta H \geq$ 1,000 m thickness are computed from rawinsonde and rocketsonde observations, while the small-scale shears associated with scales of distance $\Delta H \leq$ 1,000 m are computed from a relationship developed by Fichtl (ref. 2-39) based on experimental results from FPS-16 radar/jimsphere balloon wind sensor measurements of the detail wind

profile structure. This relationship states that the back-off or buildup wind shear Δu for $\Delta H < 1{,}000$ m for a given risk of exceedance is related to the $\Delta H = 1{,}000$ m shear, $(\Delta u)_{1,000}$, at the same risk of exceedance, through the expression

$$\Delta u = (\Delta u)_{1,000}\left(\frac{\Delta H}{1{,}000}\right)^{0.7}, \tag{2.68}$$

where ΔH has the units of meters. Equation (2.68) was used to construct tables 2-64 to 2-73 for scales of distance ≤1,000 m.

An envelope of the 99-percentile wind speed buildup is used currently in constructing synthetic wind profiles. For most design studies, the use of this 99-percent scalar buildup wind shear data is warranted. The envelopes for back-off shears have application to certain design studies and should be considered where appropriate. These envelopes are not meant to imply perfect correlation between shears for the various scales of distance; however, certain correlations do exist, depending upon the scale of distance and the wind speed magnitude considered. This method of describing the wind shear for vehicle design has proven to be especially acceptable in preliminary design studies since the dynamic response of the structure or control system of a vehicle is essentially influenced by specific wavelengths as represented by a given wind shear. Construction of synthetic profiles for vehicle design applications is described in section 2.3.9.

Wind speed change (shear) statistics for various locations differ primarily because of prevailing meteorological conditions, orographic features, and data sample size. Significant differences, especially from an engineering standpoint, are known to exist in the shear profiles for different locations. Therefore, consistent vehicle design shear data (99-percentile) representing four active or potentially operational space vehicle launch or landing sites are presented in tables 2-64 through 2-71; i.e., for KSC, VAFB, White Sands Missile Range, and EAFB. Tables 2-72 and 2-73 envelope the 99-percentile shears from these four locations. They are applicable for design criteria when initial design or operational capability has not been restricted to a specific launch site or may involve several geographical locations. However, if the specific geographic location for application has been determined as being near one of the four referenced sites, then the relevant data should be applied.

2.3.7 Wind Direction Change Envelopes

This section provides representative information on wind direction change $\Delta\theta$ for scales of distance $\Delta H \leq 4$ km. Wind direction change is defined as the total change in direction of wind vectors at the top and bottom of a specified layer. Wind direction changes can occur above or below a reference point in the atmosphere. As in the case of the wind speed changes in section 2.3.6, we will call changes below the reference level buildup wind changes and those above the reference level back-off wind direction changes. These changes can be significantly different. For example, if the reference point is at the 4-km level, the buildup changes between the 1- and 4-km levels will be distinctly different from the back-off changes between the 5- to 7-km levels. This results from the fact that variations of wind direction tend to be larger in the atmospheric boundary layer. In this light, the following model is recommended as an integrated wind direction change criterion for design studies. The model consists of the 8- to 16-km 99-percent direction changes in figure 2-20 and a set of functions $R(\Delta H, H_r, u_r)$ to transfer these changes to any reference level H_r above the 1-km level, where u_r is the reference level wind speed.

Table 2-64. Buildup design envelopes of 99-percentile wind speed change (m/s), 1- to 80-km reference altitude region, KSC.

Wind Speed (m/s) at Reference Altitude	Altitude Interval (m)									
	5,000	4,000	3,000	2,000	1,000	800	600	400	200	100
≥ 90	65.6	59.5	52.3	43.5	34.0	29.0	23.8	17.9	11.2	6.8
= 80	60.4	55.5	49.7	42.0	32.7	27.7	22.7	17.0	10.6	6.5
= 70	56.0	51.7	47.0	40.4	31.2	26.6	21.8	16.4	10.1	6.2
= 60	51.3	48.5	44.5	38.6	30.0	25.6	21.1	15.8	9.8	6.0
= 50	46.5	45.0	41.2	36.5	28.5	24.4	20.0	15.0	9.2	5.7
= 40	38.5	37.7	36.8	34.9	26.5	22.6	18.5	13.8	8.6	5.3
= 30	28.0	27.5	26.5	24.5	20.8	17.8	14.5	10.8	6.7	4.1
= 20	17.6	17.3	16.6	15.8	14.6	12.5	10.2	7.2	4.7	2.9

Table 2-65. Back-off design envelopes of 99-percentile wind speed change (m/s), 1- to 80-km reference altitude region, KSC.

Wind Speed (m/s) at Reference Altitude	Altitude Interval (m)									
	5,000	4,000	3,000	2,000	1,000	800	600	400	200	100
≥ 90	77.5	74.4	68.0	59.3	42.6	36.4	29.7	22.4	13.8	8.5
= 80	71.0	68.0	63.8	56.0	40.5	34.7	28.5	21.4	13.2	8.1
= 70	63.5	61.0	57.9	52.0	38.8	33.1	27.0	20.3	12.5	7.7
= 60	56.0	54.7	52.3	47.4	36.0	31.0	25.3	18.9	11.7	7.2
= 50	47.5	47.0	46.2	43.8	33.0	28.3	23.2	17.5	10.7	6.6
= 40	39.0	38.0	37.0	35.3	29.5	25.3	20.6	15.5	9.6	5.9
= 30	30.0	30.0	29.4	26.9	22.6	19.4	15.8	11.9	7.3	4.5
= 20	18.0	17.5	16.7	15.7	14.2	12.2	9.9	7.5	4.6	2.8

Table 2-66. Buildup design envelopes of 99-percentile wind speed change (m/s), 1- to 80-km reference altitude region, VAFB.

Wind Speed (m/s) at Reference Altitude	Altitude Interval (m)									
	5,000	4,000	3,000	2,000	1,000	800	600	400	200	100
≥ 90	62.1	59.9	57.8	51.5	35.2	30.1	24.6	18.4	11.5	7.0
= 80	58.7	57.7	55.6	48.8	33.5	29.0	23.6	17.8	11.0	6.7
= 70	55.0	54.5	53.4	48.1	33.0	28.8	23.0	16.8	10.5	6.5
= 60	50.4	49.9	49.0	44.0	32.7	27.9	22.8	16.2	9.7	5.3
= 50	45.4	44.8	43.7	40.0	29.9	25.4	21.8	15.6	9.2	5.0
= 40	38.9	38.7	37.2	34.9	25.1	22.4	19.1	14.9	8.8	4.7
= 30	30.0	29.4	28.3	25.4	19.9	17.8	14.8	11.5	7.1	4.2
= 20	20.0	19.8	19.5	18.4	15.0	13.1	10.9	8.0	4.7	2.6

Table 2-67. Back-off design envelopes of 99-percentile wind speed change (m/s), 1- to 80-km reference altitude region, VAFB.

Wind Speed (m/s) at Reference Altitude	Altitude Interval (m)									
	5,000	4,000	3,000	2,000	1,000	800	600	400	200	100
≥ 90	66.9	62.5	57.7	49.9	37.5	32.1	26.1	19.7	12.0	7.4
= 80	64.1	60.8	56.6	48.3	36.9	31.5	25.6	19.1	11.6	6.8
= 70	62.0	59.2	54.8	47.1	36.0	31.0	25.0	18.6	11.2	6.5
= 60	57.1	54.5	51.3	45.4	32.6	28.5	23.0	17.1	10.2	5.3
= 50	49.6	47.8	45.7	42.1	30.1	25.9	20.8	15.5	9.2	5.0
= 40	39.4	38.8	37.9	35.5	25.9	23.5	19.6	14.0	8.2	4.8
= 30	29.9	29.3	28.3	26.3	20.5	18.6	15.8	12.2	8.0	4.6
= 20	19.8	19.5	19.0	17.7	13.4	12.2	10.7	9.0	6.3	4.3

Table 2-68. Buildup design envelopes of 99-percentile wind speed change (m/s), 1- to 80-km reference altitude region, White Sands Missile Range.

Wind Speed (m/s) at Reference Altitude	Altitude Interval (m)									
	5,000	4,000	3,000	2,000	1,000	800	600	400	200	100
≥ 90	70.7	67.0	61.2	52.4	42.0	36.0	29.4	22.1	13.6	8.4
= 80	66.0	63.0	57.7	50.0	40.2	34.5	28.1	21.2	13.0	8.0
= 70	60.2	57.0	53.0	46.5	38.0	32.6	26.6	20.0	12.3	7.6
= 60	52.4	50.0	46.5	42.3	35.5	30.5	24.9	18.7	11.5	7.1
= 50	44.8	43.0	40.2	36.5	32.0	28.3	23.1	17.4	10.7	6.6
= 40	36.4	35.3	33.8	31.0	27.5	23.6	19.3	14.5	8.9	5.5
= 30	27.4	26.5	25.6	24.3	20.6	17.7	14.4	10.8	6.7	4.1
= 20	18.4	17.7	17.3	16.5	15.0	12.9	10.5	7.9	4.9	3.0

Table 2-69. Back-off design envelopes of 99-percentile wind speed change (m/s), 1- to 80-km reference altitude region, White Sands Missile Range.

Wind Speed (m/s) at Reference Altitude	Altitude Interval (m)									
	5,000	4,000	3,000	2,000	1,000	800	600	400	200	100
≥ 90	66.2	62.0	57.0	50.0	37.0	31.7	25.9	19.5	12.0	7.4
= 80	62.0	58.5	54.0	48.0	35.8	30.7	25.1	18.9	11.6	7.1
= 70	57.5	54.5	50.7	44.3	34.2	29.3	23.9	18.0	11.1	6.8
= 60	52.6	49.2	45.5	40.5	32.8	28.1	23.0	17.3	10.6	6.5
= 50	45.0	42.8	40.1	37.0	31.0	26.6	21.7	16.3	10.0	6.2
= 40	36.5	35.5	34.8	33.5	29.3	25.1	20.5	15.4	9.5	5.8
= 30	27.4	27.0	26.4	24.8	22.0	19.3	15.8	11.8	7.3	4.5
= 20	17.7	17.3	16.7	15.8	14.1	12.1	9.9	7.4	4.6	2.8

Table 2-70. Buildup design envelopes of 99-percentile wind speed change (m/s), 1- to 80-km reference altitude region, EAFB.

Wind Speed (m/s) at Reference Altitude	Altitude Interval (m)									
	5,000	4,000	3,000	2,000	1,000	800	600	400	200	100
≥ 90	69.0	65.0	59.5	52.0	39.5	33.9	27.7	20.8	12.8	7.9
= 80	64.9	61.8	56.9	50.0	38.2	32.8	26.7	20.1	12.4	7.6
= 70	59.0	57.0	53.0	46.8	37.0	31.7	25.9	19.5	12.0	7.4
= 60	51.8	50.4	47.8	43.6	35.5	30.5	24.9	18.7	11.5	7.1
= 50	44.8	43.6	41.3	38.2	31.8	27.5	22.4	16.9	10.4	6.4
= 40	36.5	35.5	34.3	32.0	26.5	23.0	18.8	14.1	8.7	5.3
= 30	28.0	27.3	26.3	24.5	20.8	17.8	14.6	11.0	6.7	4.2
= 20	18.0	17.7	17.4	16.7	15.2	13.0	10.6	8.0	4.9	3.0

Table 2-71. Back-off design envelopes of 99-percentile wind speed change (m/s), 1- to 80-km reference altitude region, EAFB.

Wind Speed (m/s) at Reference Altitude	Altitude Interval (m)									
	5,000	4,000	3,000	2,000	1,000	800	600	400	200	100
≥ 90	75.2	72.0	67.3	59.0	42.8	36.7	30.2	22.5	13.9	8.5
= 80	68.0	66.3	62.5	55.5	40.8	35.0	28.6	21.5	13.2	8.1
= 70	60.4	59.0	56.8	51.4	38.7	33.2	27.0	20.4	12.5	7.7
= 60	53.0	51.8	49.3	45.0	36.0	30.9	25.2	19.0	11.7	7.2
= 50	44.5	43.3	41.5	38.4	32.0	27.5	22.4	16.9	10.4	6.4
= 40	35.7	35.3	34.5	33.0	27.0	23.2	18.9	14.2	8.8	5.4
= 30	27.1	27.0	26.9	26.3	21.4	18.4	15.0	11.3	6.9	4.3
= 20	18.0	17.0	16.6	15.7	14.2	12.2	9.9	7.5	4.6	2.8

Table 2-72. Buildup design envelopes of 99-percentile wind speed change (m/s), 1- to 80-km reference altitude region, for all four locations.

Wind Speed (m/s) at Reference Altitude	Altitude Interval (m)									
	5,000	4,000.	3,000	2,000	1,000	800	600	400	200	100
≥ 90	71.0	67.0	61.2	52.4	42.0	36.0	29.4	22.1	13.6	8.4
= 80	66.5	63.0	57.7	50.0	40.2	34.5	28.1	21.2	13.0	8.0
= 70	61.2	58.5	53.8	48.1	38.0	32.6	26.6	20.0	12.3	7.6
= 60	54.4	52.5	50.0	44.2	35.5	30.5	24.9	18.7	11.5	7.1
= 50	46.5	45.0	43.7	40.0	33.0	28.3	23.2	17.4	10.7	6.6
= 40	38.9	38.7	37.2	34.9	27.6	23.7	19.3	14.9	8.9	5.5
= 30	30.0	29.4	28.3	25.4	20.8	17.8	14.8	11.5	7.1	4.2
= 20	20.0	19.8	19.5	18.4	15.2	13.1	10.9	8.0	4.9	3.0

Table 2-73. Back-off design envelopes of 99-percentile wind speed change (m/s), 1- to 80-km reference altitude region, for all four locations.

Wind Speed (m/s) at Reference Altitude	Altitude Interval (m)									
	5,000	4,000	3,000	2,000	1,000	800	600	400	200	100
≥ 90	77.5	74.4	68.0	59.3	42.8	36.7	30.2	22.5	13.9	8.5
= 80	71.0	68.0	63.8	56.0	40.8	35.0	28.6	21.5	13.2	8.1
= 70	63.5	61.0	57.9	52.0	38.8	33.2	27.0	20.4	12.5	7.7
= 60	57.1	54.7	52.3	47.4	36.0	31.0	25.3	19.0	11.7	7.2
= 50	49.6	47.8	46.2	43.8	33.0	28.3	23.2	17.5	10.7	6.6
= 40	39.4	38.8	37.9	35.5	29.5	25.3	20.6	15.5	9.6	5.9
= 30	30.0	30.0	29.4	26.9	22.6	19.4	15.8	12.2	7.3	4.6
= 20	19.8	19.5	19.0	17.7	14.2	12.2	10.7	9.0	6.3	4.3

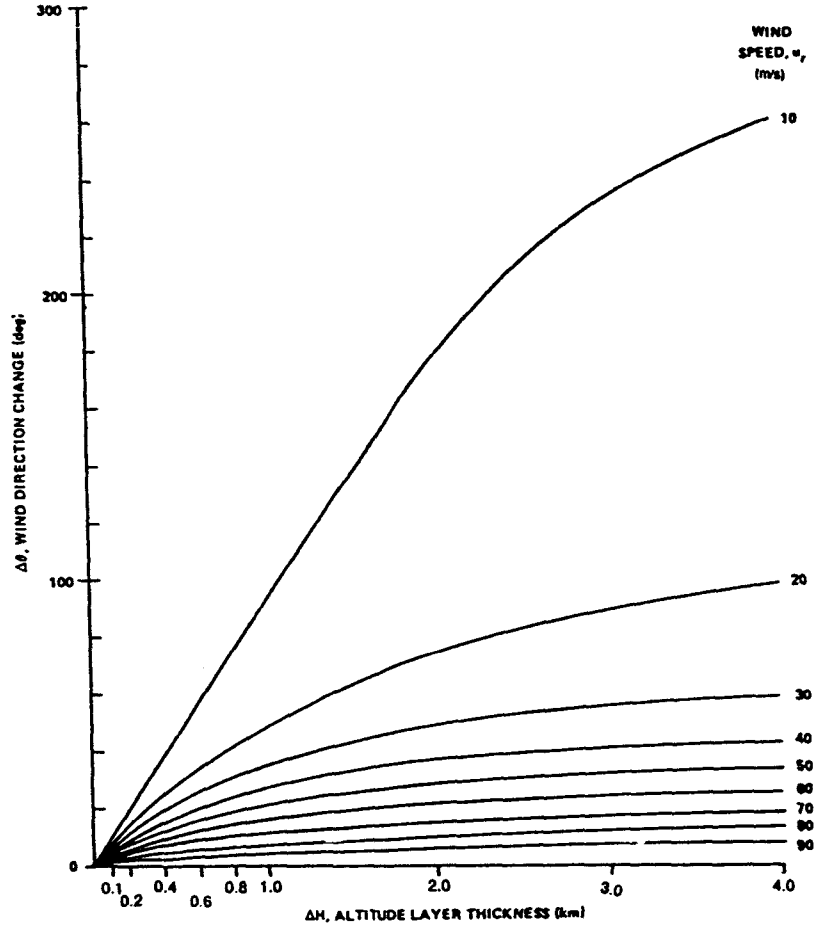

Figure 2-20 Idealized 99-percent wind direction change as a function of wind speed for varying layers in the 8- to 16-km altitude region of KSC.

The quantity R is defined such that multiplication of the 8- to 16-km wind direction changes by $R(\Delta H, H_r, u_r)$ will yield the changes in wind direction over a layer of thickness ΔH with top or bottom of the reference level located at height H_r above sea level and reference level wind speed equal to u_r. The functions $R(\Delta H, H_r, u_r)$ for back-off and buildup wind direction changes are defined as

Back-off:

$$R = R^* , \qquad 1 \le H_r < 1.5 \text{ km}$$

$$R = 2(1-R^*)\,(H_r-1.5)+R^* , \qquad 1.5 \le H_r < 2 \text{ km}$$

$$R = 1 \qquad 2 \text{ km} \le H_r .$$

Buildup:

$$R = R^* , \qquad 0 < H_r \le 2 \text{ km}$$

$$\left.\begin{aligned} R &= \left[\frac{R^*-1}{2}\right][1-\cos\pi(\Delta H - H_r+3)]+1 \ , \ 1 < \Delta H \le H_r-2 \\ R &= R^* \ , H_r-2 < \Delta H \le H_r \end{aligned}\right\} , \qquad 2 < H_r \le 3 \text{ km}$$

$$\left.\begin{aligned} R &= 1 \ , \ 0 < \Delta H \le H_r-3 \text{ km} \\ R &= \left[\frac{R^*-1}{2}\right][1-\cos\pi(\Delta H - H_r+3)]+1 \ , \ H_r-3 < \Delta H \le H_r-2 \\ R &= R^* \ , H_r-2 < \Delta H \le 4 \text{ km} \end{aligned}\right\} , \qquad 3 < H_r \le 6 \text{ km}$$

$$R = 1 , \qquad 6 \text{ km} \le H_r ,$$

where ΔH and H_r have units of kilometers and R is a nondimensional quantity. The quantity R^* is a function of ΔH and u_r and is given in figure 2-21.

To apply these wind direction change data, one first constructs a synthetic wind profile (see subsection 2.3.9), wind profile envelopes, and wind speed envelopes, with or without gust (see subsection 2.3.8), as the case may be. A reference point is selected at height H_r above sea level on this synthetic wind profile. One then turns the wind direction above or below this point according to the schedule of wind direction changes given by the preceding model. Thus, for example, if the 12-km reference point wind speed and direction are 20 m s^{-1} and 90° (east wind, i.e., a wind blowing from the east), then according to the wind direction change model discussed previously the wind directions at 0.2, 0.6, 1.0, 2.0, 3.0, and 4.0 km below or above the 12-km reference point, as the case may be, are 107°, 123°, 140°, 165°, 180°, and 190° for clockwise turning of the wind vector starting with the reference point wind vector at 12 km and looking toward the Earth. Counterclockwise turning is also permissible. The direction of rotation of the wind vector should be selected to produce the most adverse wind situation from a vehicle response point of view.

In view of the unavailability of wind direction change statistics above the 16-km level, at this time, it is recommended that the preceding procedure be used for $H_r > 16$ km.

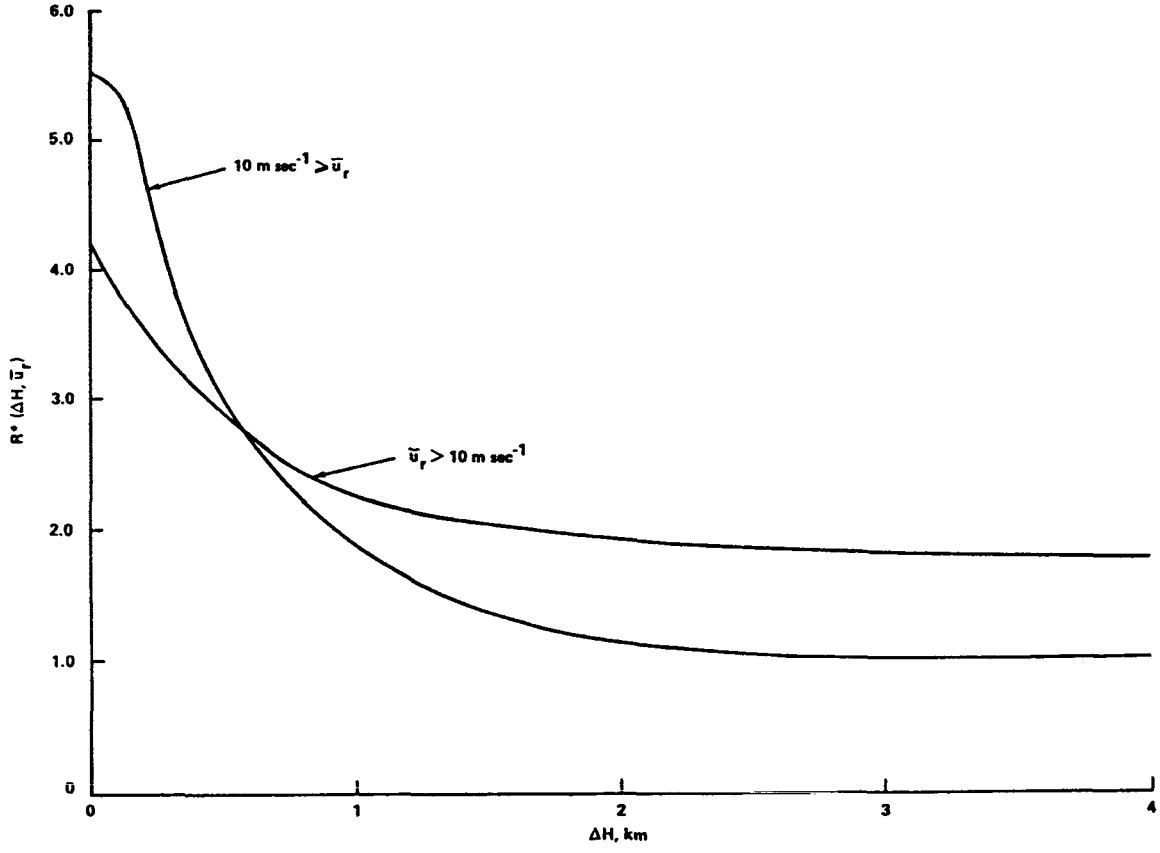

Figure 2-21. The function R^* versus ΔH for various categories of wind speed $\bar{u}_r$ at the reference level.

2.3.8 Gusts—Vertically Flying Vehicles

The steady-state in-flight wind speed envelopes presented in section 2.3.5 do not contain the gust (high frequency content) portion of the wind profile. The steady-state wind profile measurements have been defined as those obtained by the rawinsonde system. These measurements represent wind speeds averaged over approximately 1,000 m in the vertical and, therefore, eliminate features with smaller scales. These smaller scale features are contained in the detailed profiles measured by the FPS-16 radar/jimsphere system.

A number of attempts have been made to represent the high frequency content of vertical profiles of wind in a suitable form for use in vehicle design studies. Most of the attempts resulted in gust information that could be used for specific applications, but, to date, no universal gust representation has been formulated. Information on discrete and continuous gust representations is given below relative to vertically ascending aerospace vehicles.

2.3.8.1 Discrete Gusts

Discrete gusts are specified in an attempt to represent, in a physically reasonable manner, characteristics of small-scale motions associated with vertical profiles of wind velocity. Gust structure usually is quite complex and it is not always understood. For vehicle design studies, discrete gusts are usually idealized because of their complexity and to enhance their utilization.

Well-defined, sharp-edged, and repeated sinusoidal gusts are important types in terms of their influence upon space vehicles. Quasi-square-wave gusts with amplitudes of approximately 9 m/s have been estimated as extreme gusts, and have been used in various NASA aerospace vehicle design studies. These gusts are frequently referred to as embedded jets or singularities in the vertical profile wind.

By definition, a gust is a wind speed in excess of the defined steady-state value; therefore, these gusts are employed on top of the steady-state wind profile values.

If a design wind speed profile envelope without a wind shear envelope is to be used in a design study, it is recommended that the associated discrete gust vary in length from 60 to 300 m. The leading and trailing edge should conform to a 1-cosine buildup of 30 m and corresponding decay also over 30 m, as shown in figure 2-22. The plateau region of the gust can vary in thickness from zero to 240 m. An analytical expression for the value of this gust of height H above natural grade is given by

$$
\begin{aligned}
u_g &= \frac{A}{2}\left\{1-\cos\left[\frac{\pi}{30}(H-H_b)\right]\right\}, \quad H_b \le H \le H_b+30\,\text{m}, \\
u_g &= A, \quad H_b+30\,\text{m} \le H \le H_b+\lambda-30\,\text{m}, \\
u_g &= \frac{A}{2}\left\{1-\cos\left[\frac{\pi}{30}(H-H_b-\lambda)\right]\right\}, \quad H_b+\lambda-30\,\text{m} \le H \le H_b+\lambda,
\end{aligned}
\tag{2.69}
$$

where H_b is the height of the base of the gust above natural grade, λ is the gust thickness ($60 \le \lambda \le 300$ m), A is the gust amplitude, and *MKS* units are understood.

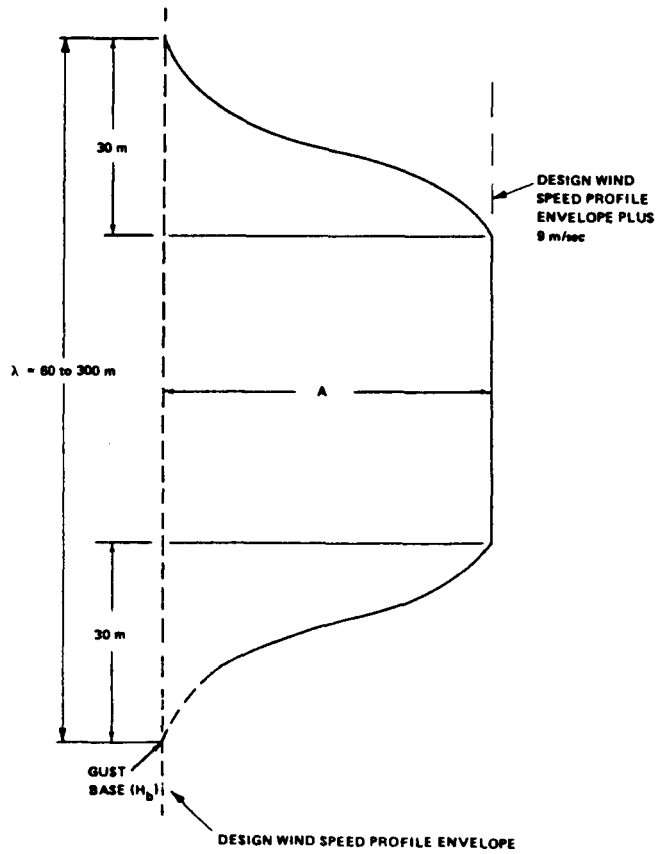

Figure 2-22. Relationship between discrete gust and/or embedded jet characteristics (quasi-square-wave shape) and the design wind speed profile envelope.

The gust amplitude is a function of H_b, and, for design purposes, the 1-percent risk gust amplitude is given by

$$A = 6 \text{ m/s} \ , \ H_b < 300 \text{ m}$$

$$A = \frac{3}{700}(H_b - 300) + 6 \ , \ 300 \text{ m} \le H_b \le 1{,}000 \text{ m} \tag{2.70}$$

$$A = 9 \text{ m/s}^{-1} \ , \ 1{,}000 \text{ m} < H_b \ .$$

If a wind speed profile envelope with a buildup wind shear envelope (section 2.3.6) is to be used in a design study, it is recommended that the previously mentioned discrete gust be modified by replacing the leading edge 1-cosine shape with the following formula

$$u_g = 10A\left\{\left(\frac{H-H_b}{30}\right)^{0.9} - 0.9\left(\frac{H-H_b}{30}\right)\right\} \ , \ H_b \le H \le H_b + 30 \text{ m} \ . \tag{2.71}$$

The height of the gust base H_b corresponds to the point where the design wind speed profile envelope intersects the design buildup shear envelope. If a discrete gust is to be used with a back-off wind shear envelope, then the 1-cosine trailing edge shall be given by

$$u_g = 10A\left\{\left(\frac{H_b+\lambda-H}{30}\right)^{0.9} - 0.9\left(\frac{H_b+\lambda-H}{30}\right)\right\} \ , \ H_b+\lambda-30 \text{ m} \le h \le H_b+\lambda \ , \tag{2.72}$$

and the leading edge shall conform to a 1-cosine shape. In this case, the height, $H_b+\lambda$, of the end of the gust corresponds to the point where the design wind speed profile envelope intersects the design back-off shear envelope. This modification of the 1-cosine shape at the leading and trailing edges, as the case may be, results in a continuous merger of the shear envelope and the discrete gust and shear should be reduced to 0.85 of the original value to account for the nonperfect correlation between wind shears and gusts (section 2.3.9.2 gives details).

2.3.8.1.1 Sinusoidal Gust

Another form of discrete gust that has been observed is approximately sinusoidal in nature, where gusts occur in succession. Figure 2-23 illustrates the estimated number of consecutive approximately sinusoidal type gusts that may occur and their respective amplitudes for design purposes. It is extremely important when applying these gusts in vehicle studies to realize that these are pure, mathematical sinusoidal representations that are an over-simplification of what has been observed in nature. These gusts should be superimposed symmetrically upon the steady-state profile. The data presented here on sinusoidal gusts are at best initial representations and should be treated as such in design studies.

2.3.8.1.2 An Undamped-Damped Sinusoidal Gust Model

The sinusoidal gust profile model presented in this section is an extension of the one presented in section 2.3.8.1.1. This model is recommended for idealized analysis to determine to what wind profile perturbations (wavelengths) and amplitudes a vehicle's guidance and control systems and structures responds. The gust model is for wind components (u' and v'). It is completely defined by a simple undamped-damped sine function in terms of gust length, L (2 times L equals wavelength), and phase angle, ϕ, by:

$$u' = v' = a_1 e^{[b(H-\theta)H]} \sin\left[\left[\frac{\pi H}{L}\right] + \phi\right] \ , \tag{2.73}$$

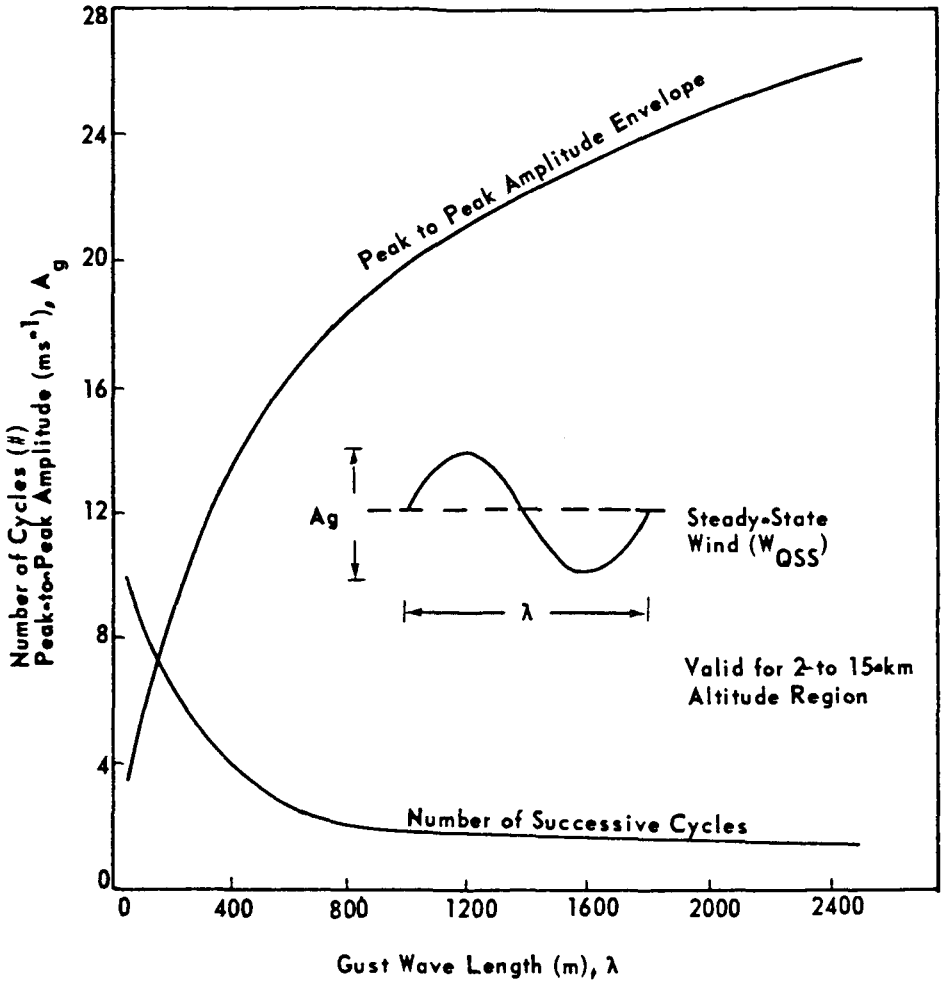

Figure 2-23. Best estimate of expected (≥99 percentile) gust amplitude and number of cycles as a function of gust wavelength.

where

H = altitude, km

L = gust length, km

ϕ = phase angle in radians, $-\pi/2 \leq \phi \leq \pi/2$

u' and v' = components, ms^{-1}

and

$b = 0.0110\ km^{-2}$ for $(0 \leq H \leq 12)$ for all L's

$b = -0.0025\ km^{-2}$ for $(12 < H \leq 24)$ for all L's

and a_1 is a function of L for the altitude intervals given in the following table.

Gust Length (L) versus Coefficient a_1 for Two Altitude Regimes (H)

L	a_1 (ms^{-1})	
(m)	$0 \leq H \leq 12$ (km)	$12 < H \leq 24$ (km)
400	2.95	5.6375
800	5.00	9.5600
1,600	7.00	13.3834

Three gust lengths are given in this model. The gust amplitude depends on the gust length. For only three phase angles between the components there are nine possible combinations for each of the three gust lengths. Figures 2-24 to 2-26 illustrate the u-component gust model for the three phases and the three gust lengths. It is recommended that the first engineering analysis be performed using the gust component in-phase and then out-of-phase for each of the three gust lengths added to the profiles of the monthly mean wind components as shown in figures 2-27 and 2-28 for a zero-phase angle and a gust length, L, of 800 m.

The gust profile model may also be applied to any other wind component percentile profile or the envelope of the profile of wind vector ellipses. The most unrealistic characteristic of this model is the number of idealized perturbations versus altitude. The amplitudes are in good agreement with the wind shear statistics for corresponding shear intervals and gust lengths. It is no more severe than that given by the previous sinusoidal gust model.

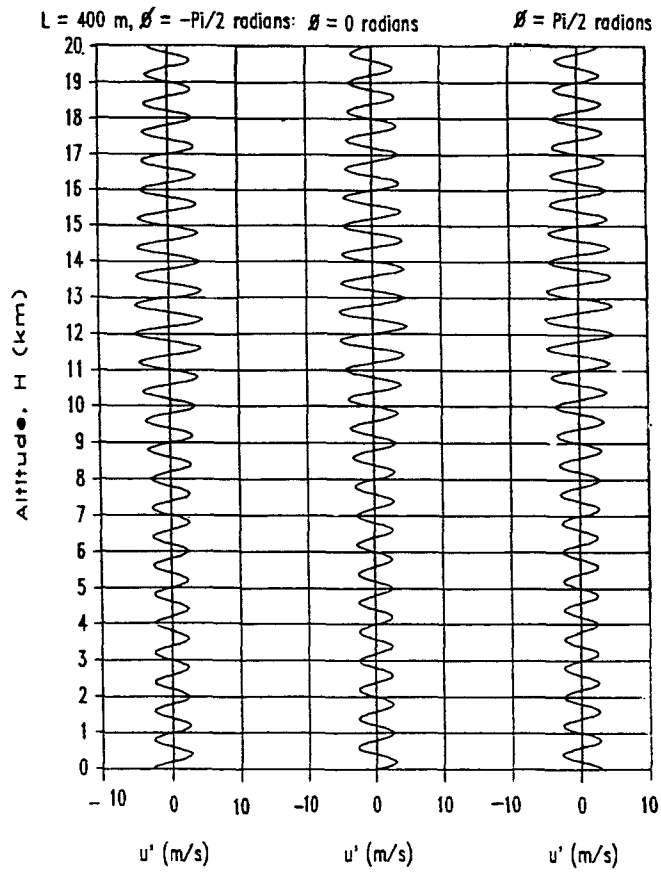

Figure 2-24. Undamped-damped sine gust model.

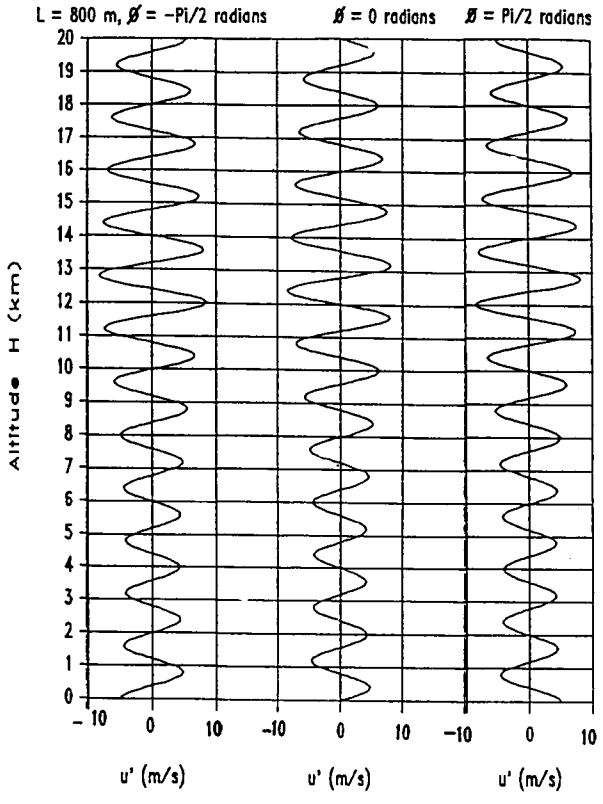

Figure 2-25. Undamped-damped sine gust model.

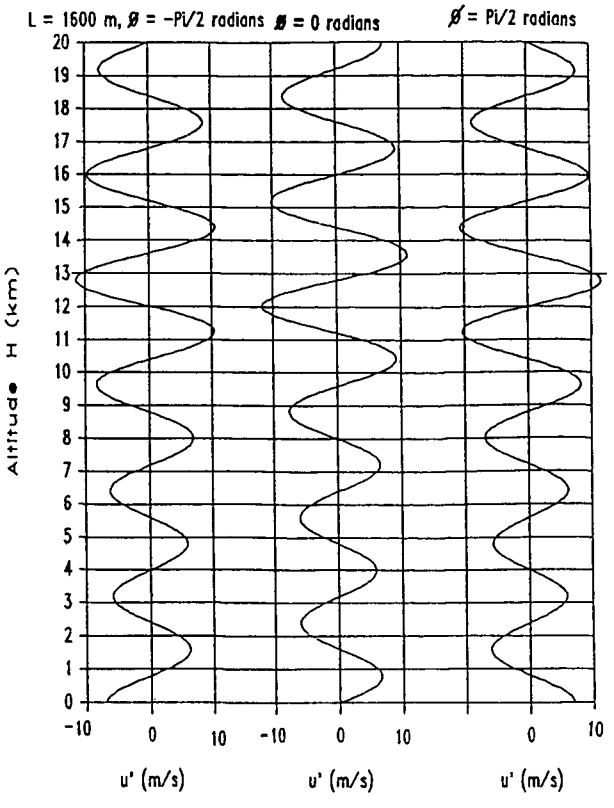

Figure 2-26. Undamped-damped sine gust model.

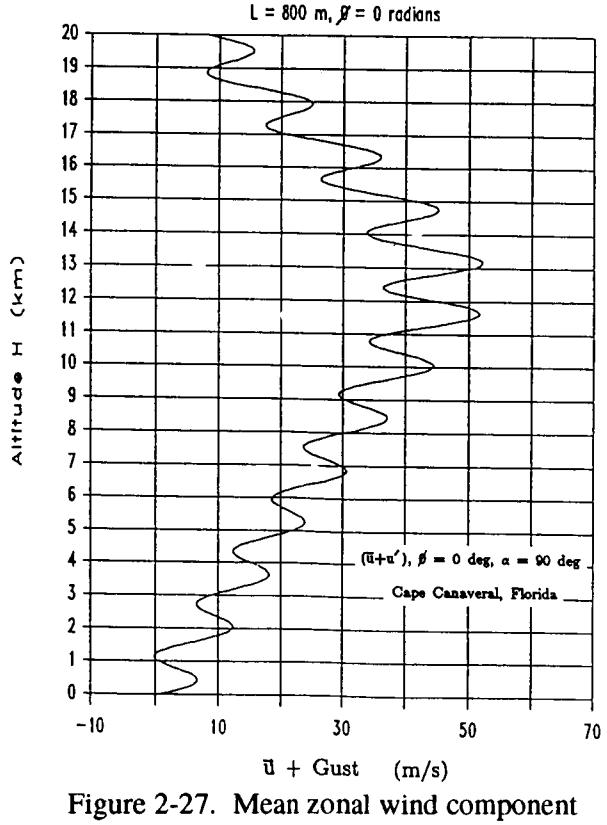

Figure 2-27. Mean zonal wind component combined with gust.

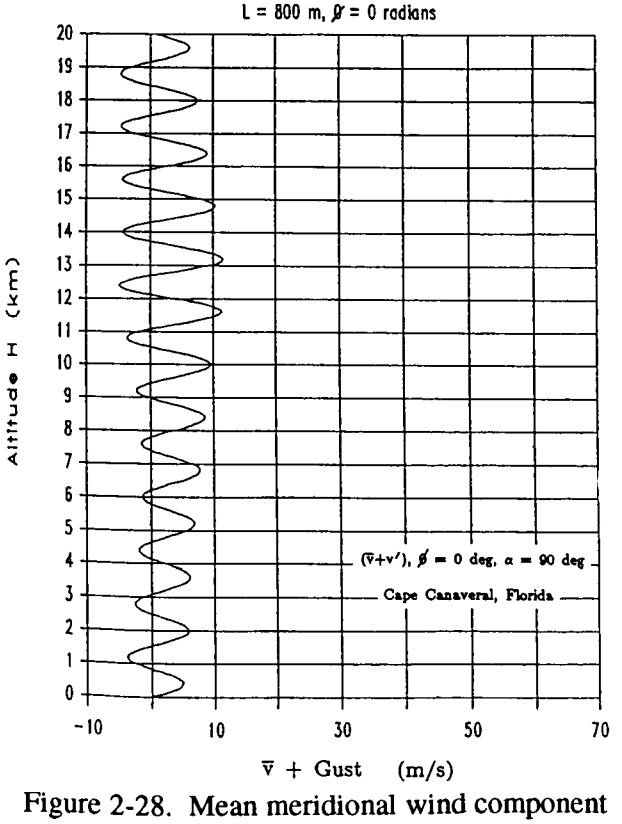

Figure 2-28. Mean meridional wind component combined with gust.

2.3.8.2 Gust Spectra

In general, the small-scale motions associated with vertical detailed profiles of wind are characterized by a superposition of discrete gusts and many random components. Spectral methods have been employed to specify the characteristics of this superposition of small-scale motions.

A digital filter was developed to separate small-scale motions from the steady-state wind profile. The steady-state wind profile defined by the separation process approximates those obtained by the rawinsonde system.* Thus, a spectrum of small-scale motions is representative of the motions included in the FPS-16 radar/jimsphere measurements, which are not included in the rawinsonde measurements. Therefore, a spectrum of those motions should be considered in addition to the steady-state wind profiles to obtain an equivalent representation of the detailed wind profile. Spectra of the small-scale motions for various probability levels have been determined and are presented in figure 2-29. The spectra were computed from approximately 1,200 detailed wind profile measurements by computing the spectra associated with each profile and then determining the probabilities of occurrence of spectral density as a function of vertical wave numbers (cycles/4,000 m). Thus, the spectra represent envelopes of spectral density for the given probability

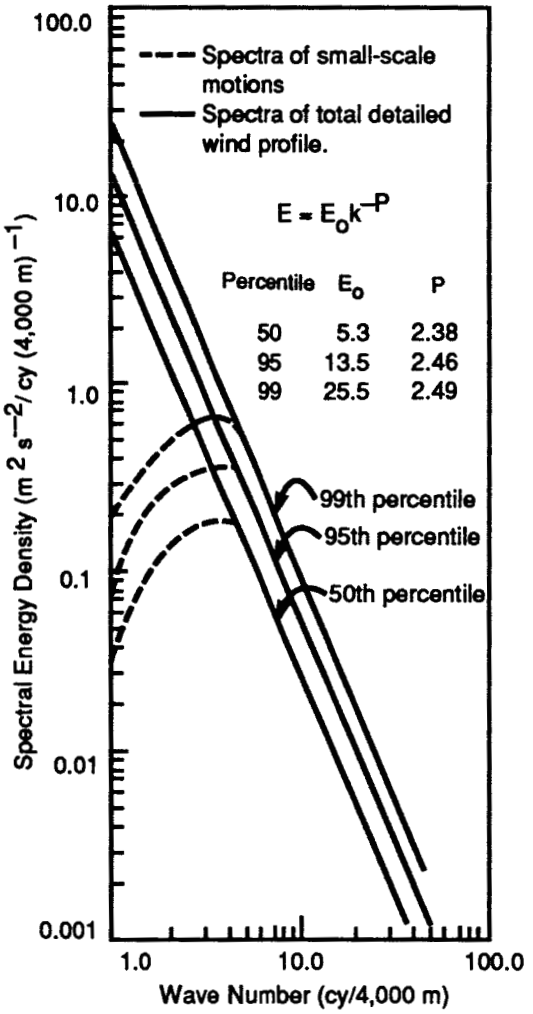

Figure 2-29. Spectra of detailed wind profiles.

*This definition was selected to enable use of the much larger rawinsonde data sample in association with a continuous-type gust representation.

levels. Spectra associated with each profile were computed over the altitude range between approximately 4 and 16 km. It has been shown that energy (variance) of the small-scale motions is not vertically homogeneous, that is, it is not constant with altitude. The energy content over limited altitude intervals and for limited wavenumber bands may be much larger than that represented by the spectra in figure 2-29. This should be kept in mind when interpreting the significance of vehicle responses when employing the spectra of small-scale motions. Additional details on this subject are available upon request. Envelopes of spectra for detailed profiles without filtering (solid lines) are also shown in figure 2-29.

These spectra are well represented for wavenumbers ≥5 cycles per 4,000 m by the equation

$$E(k) = E_0 k^{-P} \ , \tag{2.74}$$

where E is the spectral density at any wave number k (cycles/4,000 m) between 1 and 20, $E_0 = E(1)$, and p is a constant for any particular percentile level of occurrence of the power spectrum.

Spectra of the total wind speed profiles may be useful in control systems and other slow response parametric studies for which the spectra of small-scale motions may not be adequate.

The power spectrum recommended for use in elastic body studies is given by the following expression:

$$E(k) = \frac{683.4\,(4{,}000\,k)^{1.62}}{1+0.0067\,(4{,}000\,k)^{4.05}} \ , \tag{2.75}$$

where the spectrum $E(k)$ is defined so that integration over the domain $0 \le k \le \infty$ yields the variance of the turbulence. In this equation $E(k)$ is now the power spectral density ($m^2\ s^{-2}$/(cycles per meter)) at wave number k (cycles per meter). This function represents the 99-percentile scalar wind spectra for small-scale motions given by the dashed curve and its solid line extension into the high wave number region in figure 2-29. The associated design turbulence loads are obtained by multiplying the load standard deviations by a factor greater than one to reflect an acceptable level of risk. For example, a factor of 3 will correspond to a risk of 0.99865, assuming the small scale motions constitute a Gaussian process. (Spectra for meridional and zonal components are available upon request.)

An alternate power spectrum specification has been developed (ref. 2-59) by combining an analysis of jimsphere wind measurements and knowledge of the spectrum of clear-air turbulence (CAT) at scales smaller than those reliably measured by jimsphere. The spectrum covering wavelengths from 1,000 m to 200 m was determined by finding the spectrum that only one spectrum computed from a random sample of 100 jimsphere profiles would have a power spectral density greater than somewhere in the 1,000-m to 200-m range. The part of the spectrum with the $k^{-2.4}$ shape is the result. Then to cover wavelengths smaller than 200 m, an isotropic type spectrum corresponding to moderate CAT was added, the $k^{-5/3}$ part. The spectra are specified as:

$$E(k_z) = 5.3(10^{-4})\ k_z^{-2.4} + 1(10^{-2}) k_z^{-5/3} \ , \text{ for } z \ge 10 \text{ km} \ ,$$

and

$$E(k_z) = 2.4(10^{-4})\ k_z^{-2.4} + 1(10^{-2}) k_z^{-5/3} \ , \text{ for } z < 10 \text{ km} \ ,$$

where

k_z = vertical wavenumber (cycles/meter)

z = altitude above mean sea level (km).

These spectra are based on KSC measurements but are expected to be applicable at other locations since research suggests that small-scale motions are nearly universal in amplitude. However, the 99-percent

spectral envelope level and moderate CAT do not apply near thunderstorms or other locations where turbulence is categorized as severe.

Vehicle responses obtained from application of these turbulence spectra should be added to rigid vehicle responses resulting from use of the synthetic wind speed and wind profile (with the 0.85 factor on shears) but without a discrete gust. One method of application is to inverse Fourier transform from wavenumber space to height space with random, uniformly distributed phase spectra and add the transformed small-scale winds to synthetic profiles in a Monte Carlo analysis.

2.3.9 Synthetic Wind Speed Profiles

Methods of constructing synthetic wind speed profiles are described herein. One method uses design wind speed profile envelopes (section 2.3.5) and discrete gusts or spectra (section 2.3.8) without considering the correlation between the shears and gusts. Another method (section 2.3.9.2) takes into account the relationships between the wind shear and gust characteristics.

2.3.9.1 Synthetic Wind Speed Profiles for Vertical Flight Path Considering Only Speeds and Shears

In the method that follows, correlation between the design wind speed profile envelope and wind shear envelope is considered. The method is illustrated with the 95-percentile design nondirectional (scalar) wind speed profile and the 99-percentile scalar wind speed buildup for KSC (fig. 2-30) and is stated as follows:

a. Start with a speed on the design wind speed profile envelope at a selected (reference) altitude.

b. Subtract the amount of the shear (wind speed change) for each required altitude layer from the value of the wind speed profile envelope at the selected altitude. Figure 2-30 presents an example of a 99-percentile shear buildup envelope starting from a reference altitude of 11 km on the KSC 95-percentile wind speed profile envelope (table 2-49). The 10-km wind speed of 41.3 m/s is determined by subtracting 31.7 m/s (i.e., a linearly interpolated shear value for 73 m/s from the 1,000-m column of table 2-64), from 73 m/s.

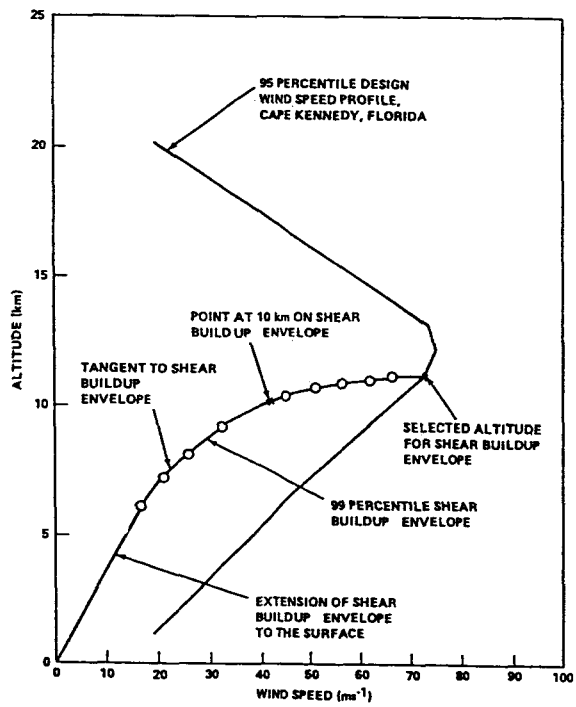

Figure 2-30. Example of synthetic wind speed profile construction without addition of gust.

c. Plot values obtained for each altitude layer at the corresponding altitudes. (The value of 41.3 m/s, obtained in the example in b, would be plotted at 10 km.) Continue plotting values until a 5,000-m layer is reached (5,000-m below the selected altitude).

d. Draw a smooth curve through the plotted points starting at the selected altitude on the wind speed profile envelope. The lowest point is extended from the origin with a straight line tangent to the plotted shear buildup curve. This curve then becomes the shear build-up envelope.

2.3.9.2 Synthetic Wind Speed Profiles for Vertical Flight Path Considering Relationships Between Speeds, Shears, and Gusts

In the construction of a synthetic wind speed profile, the lack of perfect correlation between the wind shear and gust can be taken into account by multiplying the shears (wind speed changes) (section 2.3.6) and the recommended design discrete gusts (section 2.3.8) by a factor of 0.85 before constructing the synthetic wind profile. This is equivalent, as an engineering approximation, to taking the combined 99-percentile values for the gusts and shears in a perfectly correlated manner. This approach was used successfully in both the Apollo/Saturn and space shuttle vehicle development programs.

Thus, to construct the synthetic wind speed profile (considering relationships between shears, speeds, and gusts, using the design wind speed envelopes given in section 2.3.5), the procedure that follows is used.

a. Construct the shear buildup envelope in the way described in section 2.3.9.1, except multiply the values of wind speed change used for each scale-of-distance by 0.85. (In the example for the selected altitude of 11 km, the point at 10 km will be found by using the wind speed change of 31.2×0.85, or 25.5 m/s.) This value subtracted from 73 m/s then gives a value of 46.5 m/s for the point plotted at 10 km instead of the value of 41.8 m/s used when shear and gust relationships were not considered.

b. The discrete gust is superimposed on the buildup wind shear envelope/wind speed profile envelope by adding the gust given by equation (2.69) with leading edge in the region $H_b \leq H \leq H_b + 30$ m replaced with equation (2.71). The base of the discrete gust is located at the intersection of the buildup wind shear envelope and the wind speed profile envelope (fig. 2-32). The gust amplitude, A, shall be multiplied by a factor of 0.85 to account for the nonperfect correlation between shears and gusts. Figure 2-32 gives an example of a synthetic profile with shears and gust in combination.

c. When the gust ends at the design wind envelope, the synthetic wind profile may follow the design wind speed envelope or shear back-off profile. If the synthetic wind profile follows the design wind speed envelope, then the trailing edge of the discrete gust will be a 1-cosine shape as given by equation (2.69). If the synthetic wind profile follows the shear back-off profile, then the trailing edge of the discrete gust will be that given by equation (2.72). This modified gust shape will guarantee a continuous transition from the gust to the back-off shear envelope. Vehicle response through both the wind profile envelope with gusts and the synthetic wind profile with shears and gusts in combination should be examined.

d. If a power spectrum representation (section 2.3.8.2) is used, then disregard all previous references to discrete gusts. Use the 0.85 factor on shears and apply the spectrum as given in section 2.3.8.2.

Figures 2-31 and 2-32 show an example using the 95-percentile design wind speed profile envelope, the 99-percentile wind speed buildup envelope, and the modified 1-cosine discrete gust shape.

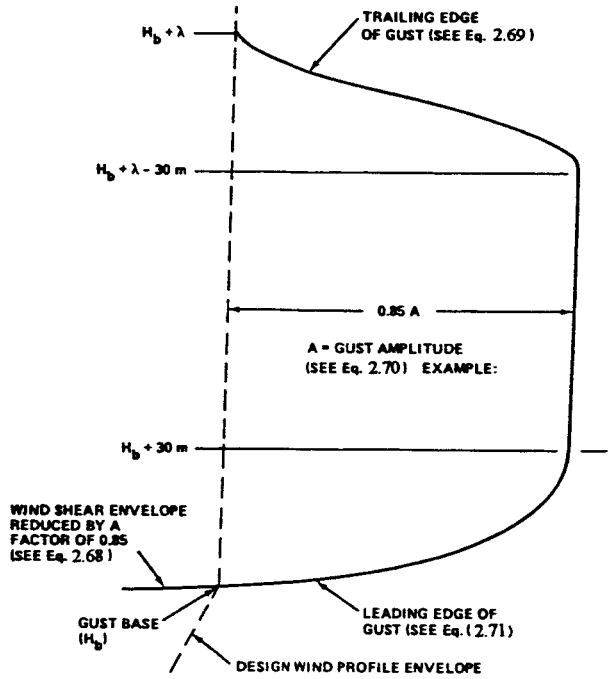

Figure 2-31. Relationship between revised gust shape, design wind profile envelope, and speed buildup (shear) envelope.

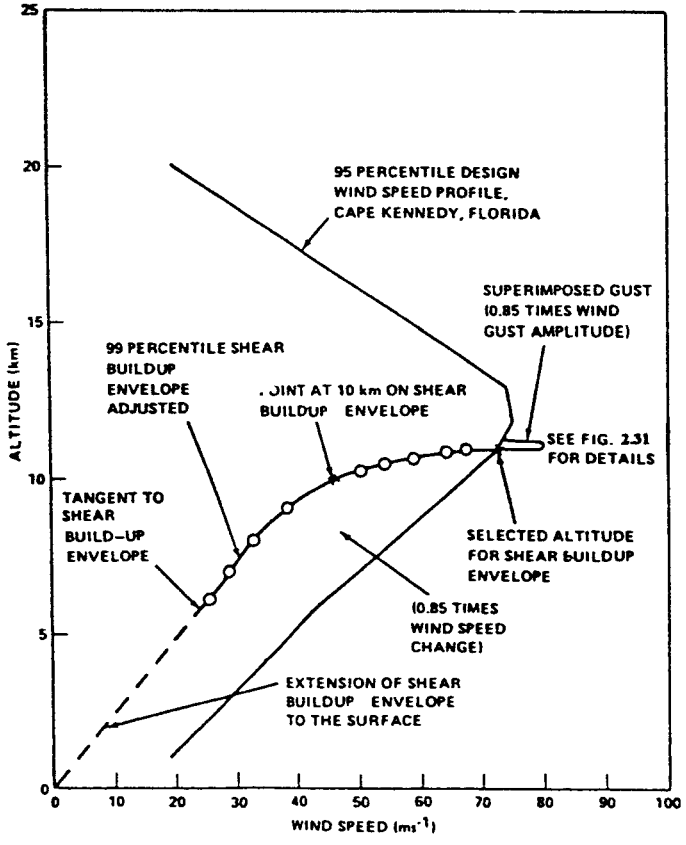

Figure 2-32. Example of synthetic wind profile construction, with relationship of wind shears and gusts assumed.

2.3.9.3 Synthetic Wind Profile Merged to the Ground Wind Profile

Up to this point we have considered only those wind shear envelopes which are linearly extrapolated to a zero wind condition at the ground. This procedure does not allow for the possibility of the vehicle to enter a wind shear envelope/gust above the H = 1,000-m altitude in a perturbed state resulting from excitations of the control system by the ground wind profile and the associated ground wind shears and gusts. To allow for these possibilities, it is recommended that the wind shear envelopes which begin above the 3,000-m level be combined with the wind profile envelope and discrete gust as stated in section 2.3.9.2; however, a linear extrapolation shall be used to merge the wind defined by the shear envelope at the 3,000-m level with the 1,000-m wind on the wind profile envelope.

The steady-state ground wind profile up to the 150-m level is defined by the peak wind profile (section 2.2.5.2) reduced to a steady-state wind profile by division with a 10-min average gust factor profile (section 2.2.7.1). To merge, this steady-state wind speed in the layer between 150 to 300 m shall take on a constant value equal to the steady-state wind at the 150-m level defined by the peak wind profile and gust factor profile between the surface of the Earth and the 150-m level. The flow between the 300-m level and the 1,000-m level shall be obtained by linear interpolation. If the discontinuities in slope of the wind profile at the 150-, 300-, and 1,000-m levels resulting from this merging procedure introduce significant false vehicle responses, it is recommended that this interpolation procedure be replaced with a procedure involving a smooth continuous function which closely approximates the piece-wise linear segment interpolation function between the 150- and 1,000-m levels with continuous values of wind speed and slope at the 150- and 1,000-m levels.

2.3.9.4 Synthetic Wind Speed Profiles for Nonvertical Flight Path

To apply the synthetic wind profile for other than vertical flight, multiply the wind shear buildup and back-off values by the cosine of the angle between the vertical axis (Earth-fixed coordinate system) and the vehicle's flight path. The gust (or turbulence spectra) is applied directly to the vehicle without respect to the flight path angle. The synthetic wind profile is otherwise developed according to procedures given in section 2.3.9.2.

2.3.10 Vector Wind and Vector Wind Shear Models

2.3.10.1 Vector Wind Profile Models

This subsection presents the concepts for a vector wind profile model, an outline of procedures to compute synthetic vector wind profiles (SVWP) followed by examples, and some suggestions for alternate approaches. Applications of the theoretical relationships between the variables and the parameters of the multivariate probability distribution function are made. The vector wind profile models presented in this section have potential applications for aerospace vehicle ascent and reentry analysis for the altitude range from 1 to 27 km for KSC, FL, and VAFB, CA (ref. 2-38).

2.3.10.2 Vector Wind Profile Model Concepts

Purpose of a Model. What is a model? One definition is that a model is a representation of one or more attributes or characteristics to make the real wind profiles more understandable and less complicated for certain engineering applications.

The modeling tools are those of mathematical probability theory and statistical analysis of wind data samples. Hopefully, through these methods, a wind model can be derived that will be a cost saving device for use in aerospace vehicle programs and still be sufficiently representative of the real wind profiles to answer engineering questions that arise in the aerospace vehicle analysis. However, the most realistic test of aerospace vehicle performance is an evaluation by flight simulations through detailed wind profiles. A sample of 150 detailed wind profiles (jimsphere wind profiles) for each month for KSC has been made available (see subsection 2.3.12.1). A sample of 150 detailed wind profiles for each month which have all the power spectra

characteristics that measured jimsphere profiles have for VAFB has been made available for flight simulations for aerospace vehicle flights from VAFB. These two detailed wind profile data samples have the same moment statistical parameters at 1-km intervals (within statistical confidences) as the 14 parameters presented in the referenced report (ref. 2-38). This was the basis for the selection of the 150 detailed wind profiles for each month.

Synthetic Vector Wind Model. In this discussion, it is assumed that the reader is familiar with the synthetic scalar wind profile model presented in this document. By definition, the synthetic scalar wind profile model is the locus of wind speeds versus altitude obtained from conditional wind shears given a specified wind speed at a reference altitude. The profile is constructed by subtracting the conditional wind shears from the specified wind speed. The scalar wind shears are a function of wind speed only. The SVWP extends this concept to the vector wind representation. For the SVWP, the vector wind shears are a function of: (a) the reference altitude; (b) the given wind vector at the reference altitude, which makes the conditional vector wind shears wind-azimuth dependent; (c) the conditional wind shears; and (d) the monthly reference period. References 2-53 and 2-54 give some engineering results using the SVWP model.

For a given wind vector, the SVWP has three dimensions, whereas the synthetic scalar wind profile has two dimensions. A wind vector is selected at the reference altitude H_o, and the conditional vector wind shears are computed for altitudes H below and above H_o. The conditional wind shears are then subtracted from the given wind vector at H_o. For two-point separation in altitude (H_o–H), the cone formed by this procedure contains a specified percentage of the wind vectors at altitude H for the given wind vector at H_o. The base is an ellipse in which a specified percentage (usually taken as 99 percent) of the wind vectors will lie given the wind vector at H_o. The interest in modeling the wind profile is to make some logical or orderly choice to arrive at the conditional wind vectors versus altitude. It is illustrated in reference 2-38 that there are an infinite number of paths along the surface of the conditional cone from reference altitude H_o down to level H. Hence, a choice of an orderly path along the surface of the conditional cone of wind vectors should be dictated by the desired scientific or engineering application. A step-by-step procedure is given to compute the SVWP that is in-plane with the given wind vector. This in-plane profile has two branches: one is the smallest conditional vector wind and has the largest shears, and the other is the outer branch, which has the largest in-plane conditional wind vector but not necessarily the largest shear. Also presented is the SVWP derived from the tangent intercepts to the conditional vector winds. These out-of-plane synthetic vector wind profiles have two branches: a right-turning wind direction and a left-turning wind direction with respect to altitude. The two-part, in-plane SVWP and the two-part, out-of-plane SVWP give a total of four synthetic vector wind profiles.

An actual example of the conditional vector winds are shown in reference 2-38 (fig. 15). The example was derived from the December wind parameters for VAFB. The reference altitude H_o is 10 km; the given wind vector at H_o is from 330° at 57.8 m/s or, in terms of the components, u^* = 28 m/s and v^* = –50 m/s. Instead of conditional ellipses, 99-percent conditional circles have been computed for each altitude at 1-km intervals from 0- to 27-km altitude. As presented, the dashed line connecting the center of the conditional circles versus altitude is the conditional mean vector. The smooth curve connecting the intercepts of the conditional circles is the in-plane SVWP that has the largest conditional shears.

2.3.10.3 Computation of the Synthetic Vector Wind Profile

Discussion in reference 2-38 is sufficiently detailed for a computer program development to code the procedures to compute the SVWP. Digressions are made in the procedures to clarify some points. The primary objectives, however, are to illustrate some applications of the probability theory of vector winds and to show the use of the tabulated wind statistical parameters to compute synthetic vector wind profiles.

2.3.10.4 Monthly Enveloping Wind Probability Ellipse (MEWPE)

The five adjusted parameters, given in table 2-74 for KSC and table 2-75 for VAFB, are used to obtain the 99-percent probability ellipse at each altitude that envelops the monthly 99-percent ellipses. This procedure is more desirable than using the annual bivariate normal statistical parameters because the annual parameters

Table 2-74. KSC Adjusted Bivariate Normal Statistics*

Alt. (km)	UA (m/s)	SAU (m/s)	R(U,V)	VA (m/s)	SAV (m/s)
0	–0.296	3.587	–0.120	–0.168	3.691
1	2.482	7.568	0.084	1.620	6.793
2	6.107	8.325	0.115	1.484	6.821
3	9.184	9.025	0.118	1.684	7.399
4	12.432	10.025	0.132	2.105	8.095
5	15.807	11.200	0.165	2.487	8.978
6	19.229	12.357	0.203	2.979	9.612
7	22.465	13.785	0.232	3.369	10.498
8	25.653	15.299	0.250	3.397	11.538
9	29.370	16.976	0.260	3.389	12.666
10	31.872	18.523	0.265	2.462	14.187
11	32.983	20.080	0.261	1.266	15.577
12	31.529	20.909	0.278	–0.766	15.955
13	28.098	20.540	0.309	–1.494	14.967
14	25.102	18.523	0.339	–1.833	12.772
15	23.029	15.954	0.344	0.010	10.811
16	21.111	13.717	0.323	0.329	9.391
17	17.574	11.766	0.291	0.705	7.957
18	13.431	10.248	0.268	0.794	6.303
19	8.172	9.354	0.253	0.583	4.901
20	3.374	8.869	0.214	–0.141	4.141
21	0.941	8.740	0.141	0.179	4.230
22	0.651	8.974	0.097	–0.140	4.103
23	0.562	9.363	0.097	–0.023	4.098
24	1.611	10.273	0.109	0.329	3.969
25	2.835	11.219	0.137	0.486	4.256
26	3.830	12.266	0.156	0.661	4.632
27	5.083	13.040	0.172	1.109	5.315
28	6.866	13.407	0.261	2.210	5.130
29	8.141	14.685	0.296	2.384	5.564
30	11.355	15.594	0.321	3.360	5.950
32	9.482	16.544	0.256	5.610	7.629
34	14.036	18.595	0.224	4.604	8.649
36	16.852	20.164	0.126	1.602	8.601
38	16.271	21.514	0.150	4.108	9.798
40	15.123	22.758	0.244	7.786	10.470
42	14.753	24.487	0.334	8.480	11.850
44	16.079	26.769	0.358	8.950	12.340
46	14.703	28.956	0.255	10.840	13.710
48	15.617	30.658	0.243	10.065	13.223
50	14.219	31.726	0.217	9.170	13.932
52	16.943	32.413	0.169	9.223	15.504
54	17.726	33.891	0.185	9.810	14.900
56	15.871	34.430	0.237	11.900	15.700
58	14.117	35.760	0.271	11.366	15.594
60	14.518	36.407	0.298	13.270	16.570
62	4.837	41.488	0.266	6.471	17.965
64	5.219	45.358	0.197	6.311	18.154
66	17.022	46.408	0.100	1.558	20.768
68	19.604	45.477	–0.028	7.418	23.605
70	31.883	46.583	–0.075	2.556	26.806

Table 2-75. VAFB Adjusted Bivariate Normal Statistics*

Alt. (km)	UA (m/s)	SAU (m/s)	R(U,V)	VA (m/s)	SAV (m/s)
0	1.192	3.103	–0.582	–1.486	3.653
1	0.750	4.320	–0.157	–1.577	7.412
2	3.070	5.640	–0.159	–2.172	8.476
3	5.790	7.290	–0.122	–2.852	9.606
4	8.280	9.080	–0.083	–4.385	11.172
5	10.385	10.561	–0.021	–4.570	12.420
6	12.214	12.058	0.030	–4.860	14.100
7	14.317	13.481	0.076	–5.320	15.810
8	16.031	15.029	0.110	–5.550	17.130
9	17.520	16.180	0.157	–5.307	18.149
10	19.660	17.210	0.174	–5.299	18.934
11	21.600	17.300	0.170	–4.504	18.486
12	23.082	16.336	0.154	–3.472	17.415
13	21.535	14.229	0.128	–2.698	15.190
14	19.891	12.588	0.098	–2.160	13.162
15	16.982	10.876	0.047	–2.243	10.786
16	14.570	9.355	0.008	–2.349	9.099
17	11.340	7.968	–0.019	–2.395	7.608
18	8.467	7.247	–0.039	–1.880	6.198
19	5.527	6.491	–0.053	–1.939	5.111
20	4.021	6.184	–0.065	–1.835	4.225
21	2.340	6.480	–0.094	–2.422	3.790
22	0.730	7.100	–0.066	–2.660	3.790
23	–0.170	7.700	–0.016	–2.633	3.694
24	–0.830	8.970	0.027	–2.860	3.940
25	–1.060	10.350	0.069	–2.590	4.130
26	–0.840	11.790	0.121	–2.424	4.548
27	–0.330	13.280	0.163	–2.530	5.080
28	1.285	14.752	0.205	–2.700	5.940
29	2.537	16.515	0.228	–2.690	6.740
30	4.141	18.307	0.248	–2.480	7.580
32	12.870	21.230	0.205	–1.174	7.804
34	20.660	24.500	0.286	–0.756	8.907
36	24.996	26.947	0.344	–0.130	9.800
38	28.187	29.450	0.310	0.070	10.530
40	31.206	30.569	0.259	–0.564	11.581
42	36.167	31.664	0.255	1.905	13.792
44	40.478	33.152	0.243	2.916	15.365
46	42.923	35.135	0.252	6.740	18.450
48	44.999	36.966	0.285	8.720	19.030
50	45.371	39.033	0.276	11.150	19.204
52	45.250	40.967	0.279	14.396	18.804
54	45.666	42.131	0.286	14.040	18.922
56	41.941	43.665	0.264	12.030	18.450
58	37.535	45.109	0.286	11.210	21.120
60	33.377	47.988	0.256	8.850	24.060
62	22.936	48.100	0.186	3.570	28.780
64	27.992	49.300	0.153	7.421	23.010
66	31.660	49.006	0.045	–2.518	26.311
68	32.805	45.888	–0.008	4.050	25.520
70	29.956	46.262	–0.070	2.260	26.056

*Adjusted bivariate normal statistics for ellipse at each altitude that envelops the monthly ellipses for P = 0.99. The monthly KSC statistical parameters for 0- to 27-km altitude are from the 19-year (1956 to 1974) twice daily, serially complete KSC rawinsonde data base, and for 28- to 70-km altitude they are from the KSC Range Reference Atmosphere (RCC/RRA DOC 361-83) (ref. 2-23). VAFB 0- to 70-km altitude parameters are from VAFB RCC/RRA DOC 362-83 (ref. 2-23).

are from a mixture of the monthly bivariate normal distributions, and this does not insure that all monthly reference periods will contain the assigned percentage of wind vectors. The 99-percent probability ellipses at discrete altitudes are required to assure that 95-percent of the wind vector profiles will lie within the 99-percent ellipses at discrete altitudes. An application for the 99-percent MEWPE may be for range safety.

An example wind vector profile model based on MEWPE for KSC follows. The theoretical basis for the model is that the wind components of a vector at a reference altitude, H_0, and the wind components at any other altitude, H, above or below H_0 have a probability distribution that is quadravariate normal, where H and H_0 range from 0 to 27 km. The wind components of the model profiles are derived from the conditional bivariate normal distribution of wind components at H, given the components of a wind vector at H_0. The given wind vectors at each reference altitude, H_0, are the wind vectors to the 99-percent MEWPE for clocking angles at 30° increments (0 to 330°) as measured counterclockwise from the centroid of MEWPE. The 14 quadravariate normal parameters, which include the inter- and intra-level correlation coefficients, are used to compute the 99-percent bivariate normal conditional ellipses at each altitude, H. The wind vector to the 99-percent conditional wind ellipse, as measured from the centroid of the conditional ellipse that is 180° from the given clocking angle at H_0, is selected. These wind vectors versus altitude H form the wind vector profile model. For this model there are 12 wind profiles (one each for the clocking angles) for each reference altitude H_0 = 0,1,2,...,27 km. Hence, there are 336 wind model profiles. These profiles will be made available on electronic data transfer (only) upon request to NASA/MSFC Earth Science and Applications Division. (This wind model has not been established for VAFB.)

The advantages of the MEWPE model are:

1. It is more realistic than the synthetic scalar wind profile model.

2. It is less complicated than the monthly synthetic vector wind profile used for STS design.

3. The mathematical formulation permits generalizations.

4. The wind vectors can be computed for any conditional probability ellipse.

5. A single model envelops all months.

This wind vector profile model has been used in ascent design studies for the National Launch System (NLS).

2.3.11 Characteristic Wind Profiles to a Height of 18 km

A significant problem in aerospace vehicle design is to provide assurance of an adequate design for flight through wind profiles of various configurations. During the major design phase of an aerospace vehicle, the descriptions of various characteristics of the wind profile are employed in determining the applicable vehicle response requirement. Since much of the vehicle is in a preliminary status of design and the desired detail data on structural dynamic modes and other characteristics are not known at this time, the use of statistical and synthetic representations of the wind profile is desirable. However, after the vehicle design has been finalized and tests have been conducted to establish certain dynamic capabilities and parameters, it is desirable to evaluate the total system by simulated dynamic flight through wind profiles containing adequate frequency resolution (ref. 2-40). The profiles shown in figures 2-33 through 2-38 are profiles of a scalar wind measured by the FPS-16 radar/jimsphere wind measuring system, and they illustrate the following: (1) jet stream winds, (2) sinusoidal variation in wind with height, (3) high winds over a broad altitude band, (4) light wind speeds, and (5) discrete gusts.

These profiles show only a few of the possible wind profiles that can occur. Jet stream winds (fig. 2-33) are quite common over the various test ranges during the winter months and can reach magnitudes in excess of 100 m/s. These winds occur over a limited altitude range, making the wind shears very large.

Figure 2-34 depicts winds having sinusoidal behavior in the 10- to 14-km region. These types of winds can create excessive loads upon a vertically rising vehicle, particularly if the reduced forcing frequencies couple with the vehicle control frequencies and result in additive leads. Periodic variations in the vertical wind profile are not uncommon. Some variations are of more concern than others, depending upon wavelength and, of course, amplitude.

Figure 2-35 is an interesting example of high wind speeds that occurred over 6 km in depth. Such flow is not uncommon for the winter months. Figure 2-36 shows scalar winds of very low values. These winds were generally associated with easterly flow over the entire altitude interval (surface to 16 km) at KSC, FL. The last examples (figs. 2-37 and 2-38) illustrate two samples of discrete gusts.

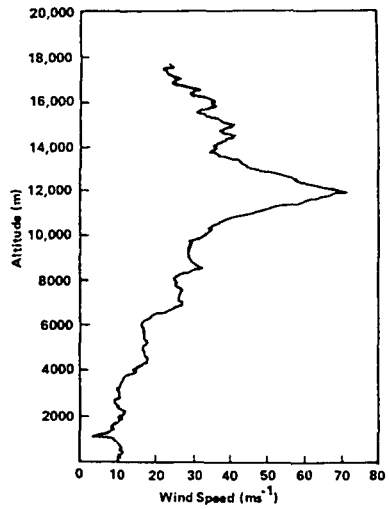

Figure 2-33. Example of jet stream winds.

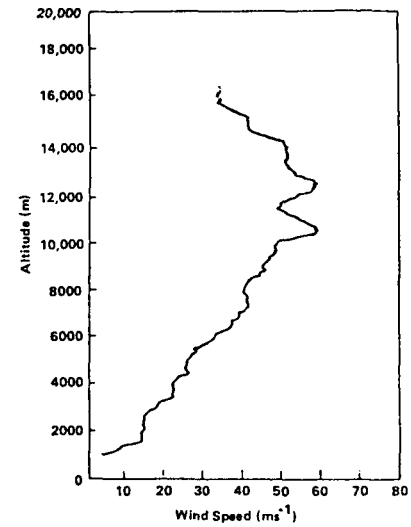

Figure 2-34. Example of sine wave flow in the 10- to 14-km altitude region.

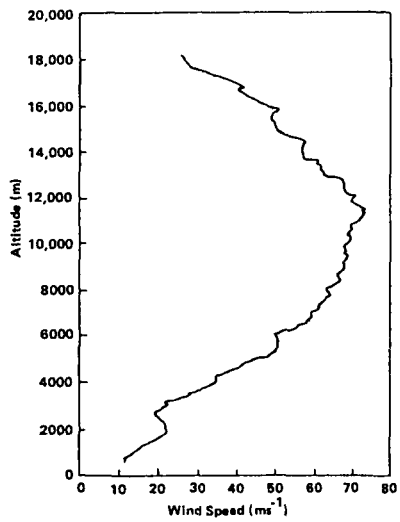

Figure 2-35. Example of high wind speeds over a deep altitude layer.

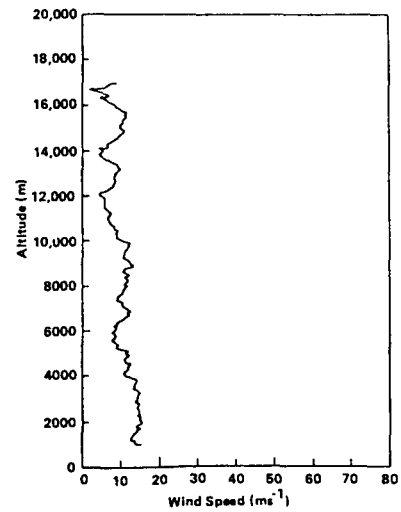

Figure 2-36. Example of low wind speeds.

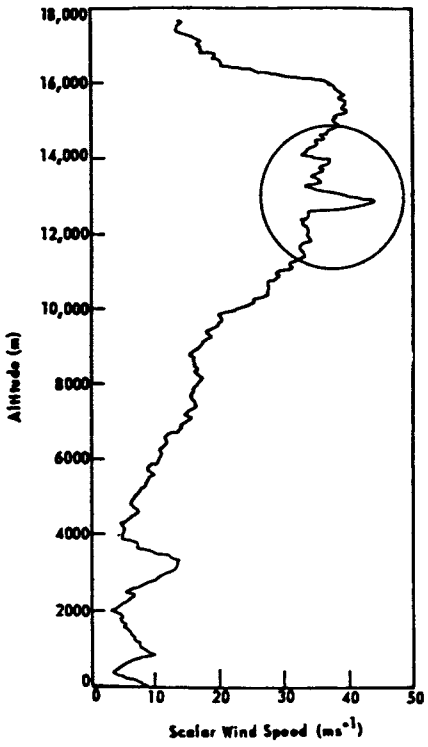

Figure 2-37. Example of a discrete gust observed at at 1300Z on January 21, 1968, at KSC.

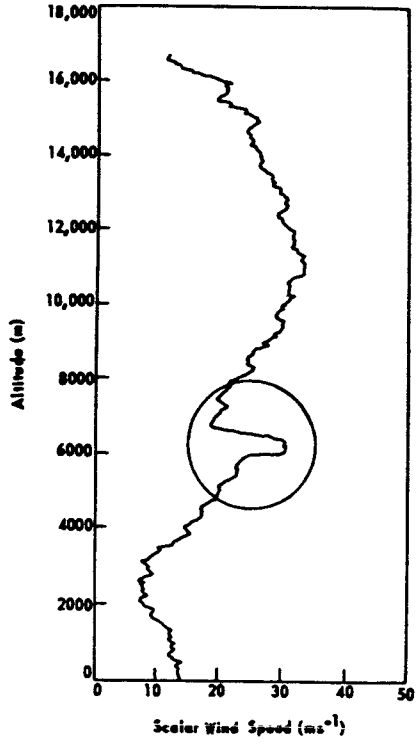

Figure 2-38. Example of a discrete gust observed by a Jimsphere released at 2103Z on November 8, 1967 at KSC.

2.3.12 Wind Profile Data Availability

2.3.12.1 KSC, FL, and VAFB, CA, Jimsphere Wind Design Assessment and Verification Data Base

The jimsphere wind design assessment and verification data tapes serve as a very special data set for wind aloft vehicle response and other analytical studies. When properly integrated into a flight-simulation program (space shuttle, for example), vehicle operational risks can be more accurately assessed relative to the true representation of wind velocity profile characteristics. The wind velocity profiles contain wind vectors for each 25 m in altitude from near surface to an altitude of approximately 18 km. The high frequency resolution is one cycle per 100 m with an rms error of approximately 0.5 m/s for velocities averaged over a 50-m height interval. Launch probability statements may be specified from flight simulations and related analyses. Through in-depth mathematical and statistical interpretations of these data, specific criteria can be generated on details of vector winds, gusts, shears, and the wind flow field interrelationships.

Two special jimsphere wind profile data sets of 150 profiles per month are available for KSC, FL, and VAFB, CA. In addition, a set of jimsphere wind profiles for 2, 3.5-, 7-, and 10.5-h pairs grouped according to summer, winter, and transition seasonal months has been prepared for KSC. A similar set of 3.5-h wind profile pairs has also been assembled for VAFB. These data sets were selected based on an extensive statistical and physical analysis of the vector wind profile characteristics and their representativeness. They have been specified for use in the space shuttle program for system design assessment, performance analysis, and prelaunch wind-loads calculations.

These data sets are available upon request to the Earth Science and Applications Division, Space Science Laboratory, NASA/George C. Marshall Space Flight Center, Marshall Space Flight Center, Alabama 35812. There are also a large number of jimsphere wind velocity profile data available for KSC, Point Mugu, White Sands Missile Range, Green River, Wallops Island, and VAFB.

2.3.12.2 Availability of Rawinsonde Wind Velocity Profiles

A very unique serially complete, edited, and corrected rawinsonde wind profile data at 1-km intervals to approximately 30 km are available for 19 years (two observations per day) for KSC, for 9 years (four observations per day) for Santa Monica, and for 14 years (two observations per day) for VAFB. A representative serial complete rawinsonde wind profile data set is available for the Wallops Flight Center (12 years, two observations per day). Qualified requestors may obtain these data upon request to the Chief, Earth Science and Applications Division, NASA/George C. Marshall Space Flight Center, Marshall Space Flight Center, Alabama 35812. They are also available as card deck 600 from the National Climatic Data Center, Asheville, North Carolina 28801.

2.3.12.3 Availability of Rocketsonde Wind Velocity Profiles

Rocketsonde wind profile data at 1-km intervals from approximately 20 to 75 km have been collected from various launch sites around the world. These data can be obtained from the World Data Center A, Asheville, North Carolina 28801.

2.3.12.4 Utility of Data

All wind profile data records should be checked carefully by the user before employing them in any vehicle response calculations. Wherever practical, the user should become familiar with the representativeness of the data and frequency content of the profile used, as well as the measuring system and reduction schemes employed in handling the data. For those organizations that have aerospace meteorology oriented groups or individuals on their staffs, consultations should be held with them. Otherwise, various government groups concerned with aerospace vehicle design and operation can be of assistance. Such action by the user can prevent expensive misuse and error in interpretation of the data relative to the intended application.

2.3.13 Atmospheric Turbulence Criteria for Horizontally Flying Vehicles

This section presents the continuous random turbulence model for the design of aerospace vehicles capable of flying horizontally, or nearly so, through the atmosphere. In general, both the continuous random model (sections 2.3.13 and 2.3.14) and the discrete model (section 2.3.15) are used to calculate vehicle responses, with the procedure producing the larger response being used for design.

The lateral and vertical components of turbulence are perpendicular to the relative mean wind vector and act in the lateral and vertical directions relative to the vehicle flight path. To a reasonable degree of approximation, in-flight atmospheric turbulence experienced by horizontally flying vehicles can be assumed to be homogeneous, stationary, Gaussian, and isotropic. Under some conditions, these assumptions might appear to be drastic, but for engineering purposes they seem to be appropriate, except for low-level flight in approximately the first 300 m of the atmosphere. It has been found that the spectrum of turbulence first suggested by von Karman appears to be a good analytical representation of atmospheric turbulence. The longitudinal spectrum is given by

$$\Phi_u(\Omega,L) = \sigma^2 \frac{2L}{\pi} \frac{1}{\left[1+(1.339\,L\Omega)^2\right]^{\frac{5}{6}}}, \tag{2.76}$$

where σ^2 is the variance of the turbulence, L is the scale of turbulence, and Ω is the wave number in units of radians per unit length. The spectrum is defined so that

$$\sigma^2 = \int_0^\infty \Phi_u(\Omega,L)\, d\Omega\ . \tag{2.77}$$

The theory of isotropic turbulence predicts that the spectra Φ_w of the lateral components of turbulence are related to the longitudinal spectrum through the differential equation

$$\Phi_w = \frac{1}{2}\left(\Phi_u - \Omega \frac{d\Phi_u}{d\Omega}\right). \tag{2.78}$$

Substitution of equation (2.76) into equation (2.78) yields

$$\Phi_w = \sigma^2 \frac{L}{\pi} \frac{1+\frac{8}{3}(1.339\,L\Omega)^2}{\left[1+(1.339\,L\Omega)^2\right]^{\frac{11}{6}}}. \tag{2.79}$$

The nondimensional spectra $2\pi\Phi_u/\sigma^2 L$ are depicted in figure 2-39 as functions of ΩL. As $L\Omega > \infty$, Φ_u and Φ_w asymptotically behave like

$$\Phi_u \sim \sigma^2 \frac{2L}{\pi} \frac{(L\Omega)^{-\frac{5}{3}}}{(1.339)^{\frac{5}{3}}} (L\Omega \to \infty) \ , \tag{2.80}$$

$$\Phi_w \sim \sigma^2 \frac{8L}{3\pi} \frac{(L\Omega)^{-\frac{5}{3}}}{(1.339)^{\frac{5}{3}}} (L\Omega \to \infty) \ , \tag{2.81}$$

consistent with the concept of the Kolmogorov inertial subrange. In addition, $\Phi_w/\Phi_u \to 4/3$ as $\Omega L \to \infty$. Design values of the scale of turbulence L are given in table 2-76. Experience indicates that the scale of turbulence increases as height increases in the first 762 m (2,500 ft) of the atmosphere, and typical values of L range from 10 m (~30 ft) near the surface to 610 m (2,000 ft) at approximately a 762-m (2,500-ft) level, typical values of L are in the order of 762 to 1,829 m (2,500 to 6,000 ft). The scales of turbulence in table 2-76 above the 300-m level are probably low, and they would be expected to give a somewhat conservative or high number of load or stress exceedances per unit length of flight. The scale of turbulence indicated for the first 304.8 m of the atmosphere in table 2-76 is a typical value. The use of this average scale of turbulence may be appropriate for load studies; however, it is inappropriate for control system and flight simulation purposes, in which event the vertical variation of the first 304.8 m of the atmosphere in table 2-76 is a typical value. The use of this average scale of turbulence may be appropriate for load studies; however, it is inappropriate for control system and flight simulation purposes, in which event the vertical variation of the scale of turbulence in the first 300 m of the atmosphere should be taken into account.

The power spectrum analysis approach is applicable only to stationary Gaussian continuous turbulence, but atmospheric turbulence is neither statistically stationary nor Gaussian over long distances. The statistical quantities used to describe turbulence vary with altitude, wind direction, terrain roughness, atmospheric stability, and a host of other variables. Nevertheless, it is valid to a sufficient degree of engineering approximation to recommend that atmospheric turbulence be considered locally Gaussian and stationary and that the total flight history of a horizontally flying vehicle be considered to be composed of an ensemble of exposures to turbulence of various intensities, all using the same power spectrum shape. Furthermore, it is recommended that the following statistical distribution of rms gust intensities be used:

$$p(\sigma) = \frac{P_1}{b_1}\sqrt{\frac{2}{\pi}} \exp\left(-\frac{\sigma^2}{2b_1^2}\right) + \frac{P_2}{b_2}\sqrt{\frac{2}{\pi}} \exp\left(-\frac{\sigma^2}{2b_2^2}\right), \tag{2.82}$$

where b_1 and b_2 are the standard deviations of σ in nonstorm turbulence. The quantities P_1 and P_2 denote the fractions of flight time or distance flown in nonstorm and storm turbulence. It should be noted that if P_o is the fraction of flight time or distance in smooth air, then

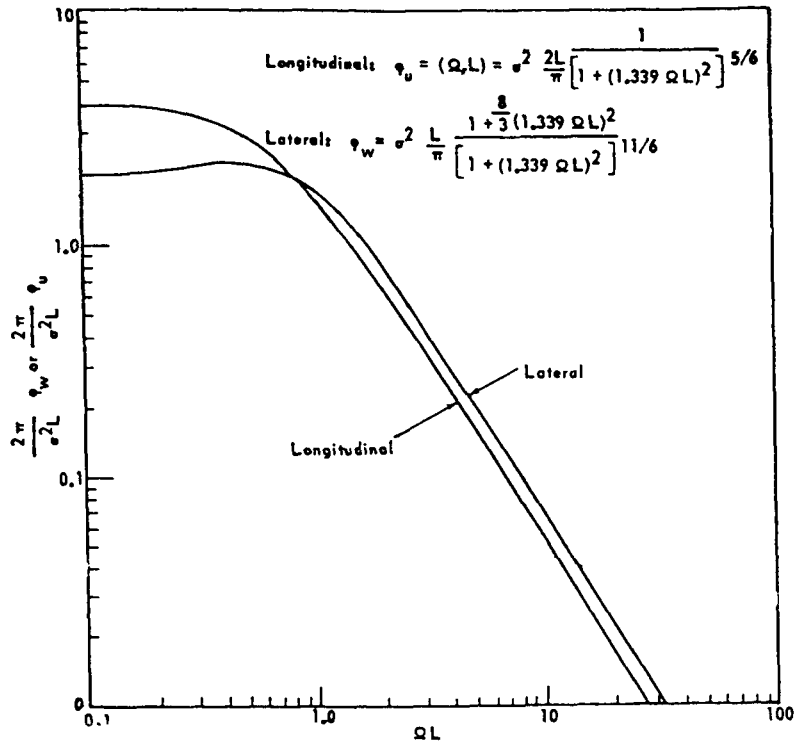

Figure 2-39. The nondimensional longitudinal and lateral, $2\pi\Phi_u/\sigma^2 L$ and $2\pi\Phi_w/\sigma^2 L$, spectra as functions of the dimensionless frequency $L\Omega$.

Table 2-76. Parameters for the turbulence model for horizontally flying vehicles.

Altitude		Mission	Turbulence	P_1	b_1		P_2	b_2		L	
(m)	(ft)	Segment*	Component**	(unitless)	(m/s)	(ft/s)	(unitless)	(m/s)	(ft/s)	(m)	(ft)
0–304.8	0–1,000	Low Level Contour (rough terrain)	V	1.00	0.82	2.7	10^{-5}	3.25	10.65	152.4	500
0–304.8	0–1,000	Low Level Contour (rough terrain)	L, L	1.00	0.94	3.1	10^{-5}	4.29	14.06	152.4	500
0–304.8	0–1,000	C, C, D	V, L, L	1.00	0.77	2.51	0.005	1.54	5.04	152.4	500
304.8–672	1,000–2,500	C, C, D	V, L, L	0.42	0.92	3.02	0.0033	1.81	5.94	533.4	1,750
672–1,524	2,500–5,000	C, C, D	V, L, L	0.30	1.04	3.42	0.0020	2.49	8.17	762	2,500
1,524–3,048	5,000–10,000	C, C, D	V, L, L	0.15	1.09	3.59	0.00095	2.81	9.22	762	2,500
3,048–6,096	10,000–20,000	C, C, D	V, L, L	0.062	1.00	3.27	0.00028	3.21	10.52	762	2,500
6,096–9,144	20,000–30,000	C, C, D	V, L, L	0.025	0.96	3.15	0.00011	3.62	11.88	762	2,500
9,144–12,192	30,000–40,000	C, C, D	V, L, L	0.011	0.89	2.93	0.000095	3.00	9.84	762	2,500
12,192–15,240	40,000–50,000	C, C, D	V, L, L	0.0046	1.00	3.28	0.000115	2.69	8.81	762	2,500
15,240–18,288	50,000–60,000	C, C, D	V, L, L	0.0020	1.16	3.82	0.000078	2.15	7.04	762	2,500
18,288–21,336	60,000–70,000	C, C, D	V, L, L	0.00088	0.89	2.93	0.000057	1.32	4.33	762	2,500
21,336–24,384	70,000–80,000	C, C, D	V, L, L	0.00038	0.85	2.80	0.000044	0.55	1.80	762	2,500
above 24,384	above 80,000	C, C, D	V, L, L	0.00025	0.76	2.50	0	0	0	762	2,500

*Climb, cruise, and descent (C, C, D).
**Vertical, Lateral, and longitudinal (V, L, L).

$$P_0+P_1+P_2=1 \tag{2.83}$$

The recommended design values of P_1, P_2, b_1, and b_2 are given in table 2-76. Note that over rough terrain b_2 can be extremely large in the first 304 m (1,000 ft) above the terrain and the b's for the vertical, the lateral, and the longitudinal standard deviations of the turbulence are not equal. Thus, in the first 304 m (1,000 ft) of the atmosphere above rough terrain, turbulence is significantly anisotropic, and this anisotropy must be taken into account in engineering calculations.

An exceedance model of gust loads and stresses can be developed with the preceding information. Let y denote any load quantity that is a dependent variable in a linear system of response equations (for example, bending moment at a particular wind station). This system is forced by the longitudinal, lateral, and vertical components of turbulence and, upon producing the Fourier transform of the system, it is possible to obtain the spectrum of y. This spectrum will be proportional to the input turbulence spectra, the function of proportionality being the system transfer function. Upon integrating the spectrum of y over the domain $0 < \Omega < \infty$, we obtain the relationship

$$\sigma_y = A\sigma \ , \tag{2.84}$$

where A is a positive constant that depends upon the system parameters and the scale of turbulence, and σ_y is the standard deviation of y.

If the output y is considered to be Gaussian for a particular value of σ, then the expected number of fluctuations of y that exceed y^* with positive slope per unit distance with reference to a zero mean is

$$N(y^*) = N_0 \exp\left(\frac{y^{*2}}{2\sigma_y^2}\right), \tag{2.85}$$

where N_0 is the expected number of zero crossings of y units distance with h positive slope and is given by

$$N_0 = \frac{1}{2\pi\sigma_y}\left[\int_0^\infty \Omega^2 \Phi_y(\Omega)\, d\Omega\right]^{\frac{1}{2}} \tag{2.86}$$

In this equation, Φ_y is the spectrum of y and

$$\sigma_y = \left[\int_0^\infty \Phi_y(\Omega)\, d\Omega\right]^{\frac{1}{2}} \tag{2.87}$$

The standard deviation of σ_y is related to standard deviation of turbulence through equation (2.84) and σ is distributed according to equation (2.82). Accordingly, the number of fluctuations of y that exceed y^* for standard deviations of turbulence in the interval σ to $\sigma+d\sigma$ is $N(y^*)p(\sigma)d\sigma$, so that integration over the domain $0 < \sigma < \infty$ yields

$$\frac{M(y^*)}{N_0} = P_1 \exp\left(-\frac{|y^*|}{b_1 A}\right) + P_2 \exp\left(-\frac{|y^*|}{b_2 A}\right), \tag{2.88}$$

where $M(y^*)$ is the overall expected number of fluctuations of y that exceed y^* with positive slope. To apply this equation, the engineer needs only to calculate A and N_0 and specify the risk of failure he wishes to accept. The appropriate values of P_1, P_2, b_1, and b_2.are given in table 2-76. Figures 2-40 and 2-41 give plots of $M(y^*)/N_0$ as a function of $|y^*|/A$ for the various altitudes for the design data given in table 2-76. Table 2-77 provides a summary of the units of the various quantities in this model.

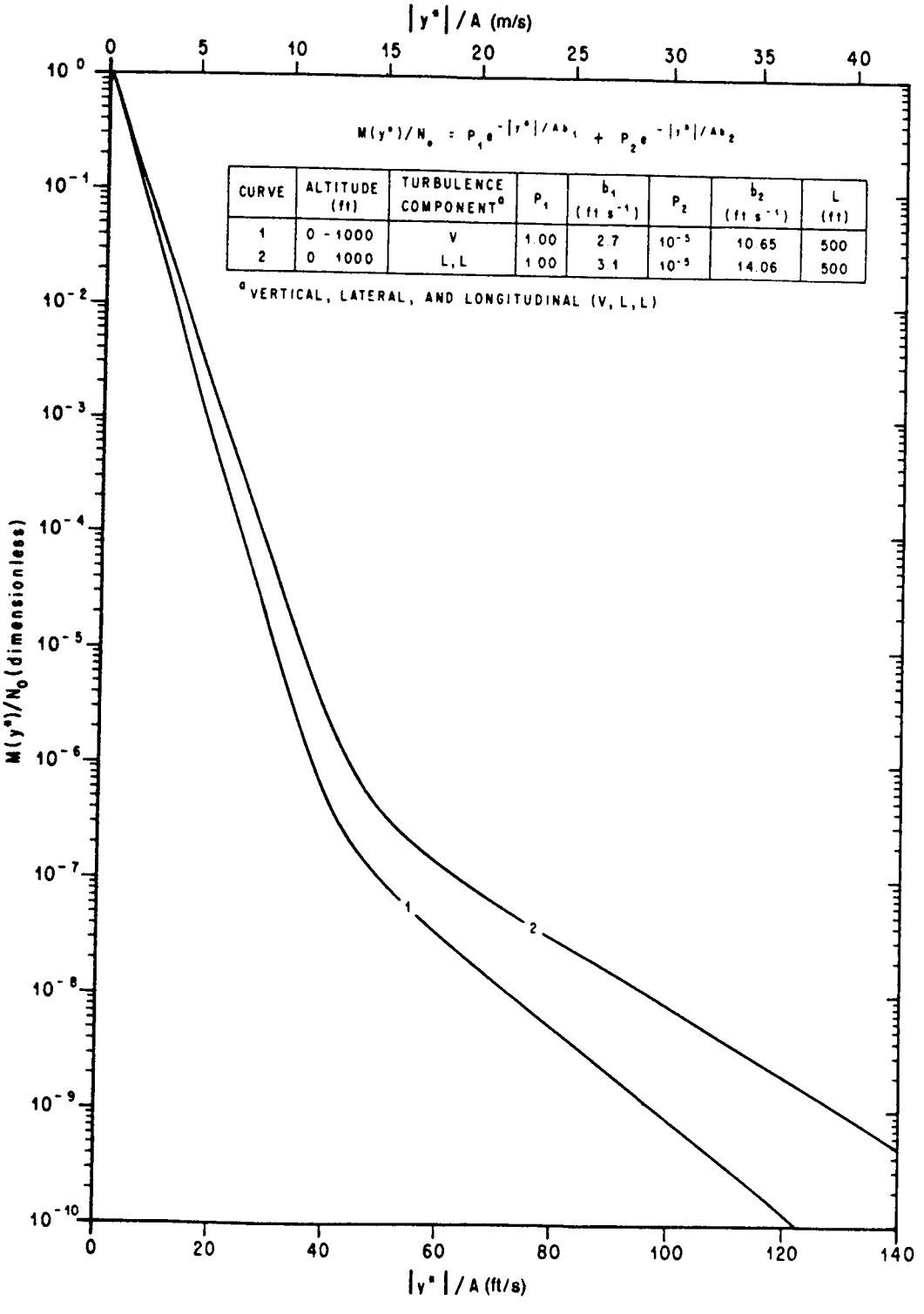

Figure 2-40. Exceedance curves for the vertical, lateral, and longitudinal components of turbulence for the 0- to 1,000-ft altitude range.

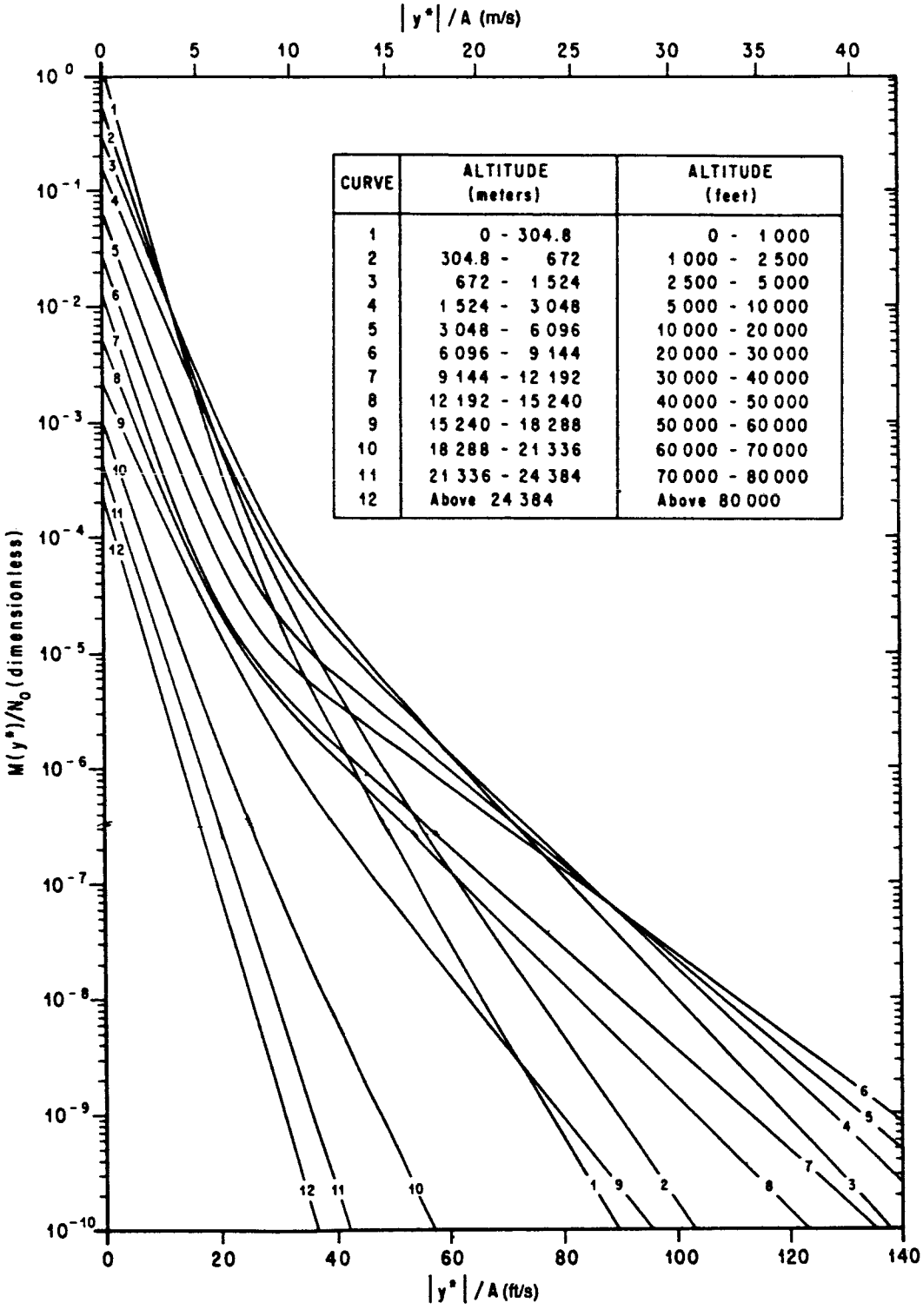

CURVE	ALTITUDE (meters)	ALTITUDE (feet)
1	0 - 304.8	0 - 1 000
2	304.8 - 672	1 000 - 2 500
3	672 - 1 524	2 500 - 5 000
4	1 524 - 3 048	5 000 - 10 000
5	3 048 - 6 096	10 000 - 20 000
6	6 096 - 9 144	20 000 - 30 000
7	9 144 - 12 192	30 000 - 40 000
8	12 192 - 15 240	40 000 - 50 000
9	15 240 - 18 288	50 000 - 60 000
10	18 288 - 21 336	60 000 - 70 000
11	21 336 - 24 384	70 000 - 80 000
12	Above 24 384	Above 80 000

Figure 2-41. Exceedance curves for the vertical, lateral, and longitudinal components of turbulence for various altitude ranges.

Table 2-77. Metric and U.S. customary units of various quantities in the turbulence model for horizontally flying vehicles.

Quantity	Metric Units	U.S. Customary Units
Ω	rad/m	rad/ft
Φ_u, Φ_w	m^2/s^2/rad/m	ft^2/s^2/rad/ft
σ^2	m^2/s^2	ft^2/s^2
L	m	ft
b_1, b_2	m/s	ft/s
P_1, P_2	dimensionless	dimensionless
σ_y/A	m/s	ft/s
$\lvert y^* \rvert/A$	m/s	ft/s
N_0, N, M	rad/s	rad/s

2.3.13.1 Application of Power Spectral Model

To apply equation (2.88), the engineer can either calculate A and N_0 and then calculate the load quantity y^* for a specified value of $M(y^*)$, or calculate A and calculate the load quantity y^* for a specified value of $M(y^*)/N_0$. These design criteria are consistent with the limit load capability of present day commercial aircraft. The criterion in which $M(y^*)$ is specified is suitable for a mission analysis approach to the design problem. The criterion in which $M(y^*)/N_0$ is specified is suitable for a design envelope approach to aircraft design.

In the design envelope approach, it is assumed that the airplane operates 100 percent of the time at its critical design envelope point. The philosophy is that if the vehicle can operate 100 percent of the time at any point on the envelope, it can surely operate adequately in any combination of operating points in the envelope. A new vehicle is designed on a limit load basis for a specified value of M/N_0. Accordingly, $M/N_0 = 6 \times 10^{-9}$ is suitable for the design of commercial aircraft. To apply this criterion, all critical altitudes, weights, and weight distributions are specified configurations with equation (2.88) for $M/N_0 = 6 \times 10^{-9}$.

In the mission analysis approach, a new aircraft is designed on a limit load basis for $M = 2 \times 10^{-5}$ load exceedances per hour. To apply this criterion, the engineer must construct an ensemble of flight profiles which define the expected range of payloads and the variation with time of speed, altitude, gross weight, and center of gravity position. These profiles are divided into mission segments, or blocks, for analysis; and average or effective values of the pertinent parameters are defined for each segment. For each mission segment, values of A and N_0 are determined by dynamic analysis. A sufficient number of load and stress quantities are included in the dynamic analysis to assure that stress distributions throughout the structure are realistically or conservatively defined. Now the contribution of $M(y^*)$ from the ith flight segment is $t_i M_i(y^*/T)$, where t_i is the amount of time spent in the ith flight regime (mission segment), T is the total time flown by the vehicle over all mission segments, and $M_i(y^*)$ is the exceedance rate associated with the ith segment. The total exceedance rate for all mission segments, k, is

$$M(y^*) = \sum_{i=1}^{k} \frac{t_i}{T} N_{0_i} \left(P_1 e^{-\frac{|y^*|}{b_1 A}} + P_2 e^{-\frac{|y^*|}{b_2 A}} \right), \tag{2.89}$$

where subscript i denotes the ith mission segment. The limit gust load quantity $|y^*|$ can be calculated with this formula upon setting $M(y^*) = 2 \times 10^{-5}$ exceedances per hour.

The previously mentioned limit load criteria were derived for commercial aircraft which are normally designed for 50,000-h lifetimes. Therefore, to apply these criteria to horizontally flying aerospace vehicles which will have relatively short lifetimes would be too conservative. However, it is possible to modify these criteria so that they will reflect a shorter vehicle lifetime. The probability F_p that a load will be exceeded in a given number of flight hours T is

$$F_p = 1 - e^{-TM} . \tag{2.90}$$

If it is assumed that the limit load criterion $M = 2 \times 10^{-5}$ exceedances per hour is associated with an aircraft with a lifetime T equal to 50,000 h, this means that $F_p = 0.63$; i.e., there is a 63-percent chance that an aircraft design for a 50,000-h operating lifetime will exceed its limit load capability at least once during its operating lifetime. This high failure probability, based on limit loads, is not excessive in view of the fact that an aircraft will receive many inspections on a routine basis during its operating lifetime. In addition, after safety factors are applied to the design limit loads, the ultimate load exceedance rate will be on the order of 10^{-8} exceedances per hour. Substitution of this load exceedance rate into equation (2.90) for $T = 50{,}000$ h yields a failure probability, on an ultimate load basis, of $F_p = 0.0005$. This means that there will be only a 0.05-percent chance that an aircraft will exceed its ultimate load capability during its operating lifetime of 50,000 h. Thus, a failure probability of $F_p = 0.63$ in the limit load basis is reasonable for design. Let us now assume that $F_p = 0.63$ is the limit load design failure probability so that equation (2.90) can be used to calculate design values of M associated with a specified vehicle lifetime. Thus, for example, if we expect a vehicle to fly only 100 h, then according to equation (2.90), we have $M = 10^{-2}$ exceedances per hour. Similarly, if we expect a vehicle to be exposed to the atmosphere for 1,000 h of flight, then $M = 10^{-3}$ exceedances per hour.

The corresponding design envelope criterion can be obtained by dividing the preceding calculated values of M by an appropriate value of N_0. In the case of the 50,000-h criterion, we have $M/N_0 = 6 \times 10^{-9}$ and $M = 2 \times 10^{-5}$ exceedances per hour, so that an estimate of N_0 for purposes of obtaining a design criterion is $N_0 = 0.333 \times 10^4$ h^{-1}. Thus, upon solving equation (2.90) for M and dividing by $N_0 = 0.333 \times 10^4$ h^{-1}, the design envelope criterion takes the form

$$\frac{M}{N_0} = \frac{3 \times 10^{-4}}{T} , \tag{2.91}$$

where we have used $F_p = 0.63$. Thus, for a 100-h aircraft, the design envelope criterion is $M/N_0 = 3 \times 10^{-6}$ and for a 1,000-h aircraft $M/N_0 = 3 \times 10^{-7}$.

It is recommended that the power spectral approach be used in place of the standard discrete gust methods. Reasonably discrete gusts undoubtedly occur in the atmosphere; however, there is accumulating evidence that the preponderance of gusts are better described in terms of continuous turbulence models. It has been accepted that clear air turbulence at moderate intensity levels is generally continuous in nature. Thunderstorm gust velocity profiles are now available in considerable quantity, and they almost invariably display the characteristics of continuous turbulence. Also, low-level turbulence is best described with power spectral methods. A power spectral method of load analysis is not necessarily more difficult to apply than a discrete gust method. The present static load "plunge-only discrete gust methods" can, in fact, be converted to a power spectral basis by making a few simple modifications in the definitions of gust alleviation factor and the design discrete gust. To be sure, this simple rigid-airplane analysis does not exploit the full potentiality of the power spectral approach, but it does account more realistically for the actual mix of gust gradient distances in the atmosphere and the variation of gust intensity with gradient distance.

2.3.14 Turbulence Model for Flight Simulation*

The lateral and vertical components of turbulence are perpendicular to the relative mean wind vector and act in the lateral and vertical directions relative to the vehicle flight path. For simulation of turbulence in either an analog or digital fashion, the turbulence realizations are to be generated by passing a white noise process through a passive filter. The model of turbulence as given in section 2.3.13 is not particularly suited for the simulation of turbulence with white noise because the von Karman spectra given by equations (2.76) and (2.79) are irrational. Thus, for engineering purposes, the Dryden spectra may be used for simulation of continuous random turbulence. They are given by

$$\text{Longitudinal: } \Phi_u(\Omega) = \sigma^2 \frac{2L}{\pi} \frac{1}{1+(L\Omega)^2}, \tag{2.92}$$

$$\text{Lateral and Vertical: } \Phi_w(\Omega) = \sigma^2 \frac{L}{\pi} \frac{1+3(L\Omega)^2}{\left[1+(L\Omega)^2\right]^2}. \tag{2.93}$$

Since these spectra are rational, a passive filter may be generated. It should be noted that the Dryden spectra are somewhat similar to the von Karman spectra. As $\Omega L \rightarrow 0$, the Dryden spectra asymptotically approach the von Karman spectra. As $\Omega L \rightarrow \infty$, the Dryden spectra behave like $(\Omega L)^{-2}$, while the von Karman spectra behave like $(\Omega L)^{-5/3}$. Thus, the Dryden spectra depart from the von Karman spectra by a factor proportional to $(\Omega L)^{-1/3}$ as $\Omega L \rightarrow \infty$, so that at sufficiently large values of ΩL the Dryden spectra will fall below the von Karman spectra. However, this deficiency in spectral energy of the Dryden spectra with respect to the von Karman spectra is not serious from an engineering point of view. If the capability to use the von Karman spectra is already available, the user should use it in flight simulation rather than the Dryden spectra.

The spectra as given by equations (2.92) and (2.93) can be transformed from the wave number (Ω) domain to the frequency domain (ω, rad/s) with a Jacobian transformation by noting that $\Omega = \omega/V$, so that

$$\Phi_u(\omega) = \frac{L}{V} \frac{2\sigma^2}{\pi} \frac{1}{1+\left(\frac{L\omega}{V}\right)^2}, \tag{2.94}$$

$$\Phi_w(\omega) = \frac{L}{V} \frac{\sigma^2}{\pi} \frac{1+3\left(\frac{L\omega}{V}\right)^2}{\left[1+\left(\frac{L\omega}{V}\right)^2\right]^2}. \tag{2.95}$$

The quantity V is the magnitude of the mean wind vector relative to the aerospace vehicle, u–e. The quantities u and e denote the velocity vectors of the mean flow of the atmosphere and the aerospace vehicle relative to the Earth. In the region above the 300-m level of the longitudinal component of turbulence is defined to be the component of turbulence parallel to the mean wind vector relative to the aerospace vehicle (u–e).

*Details on simulations should be requested from Earth Science and Applications Division, Space Science Laboratory, Marshall Space Flight Center, AL 35812.

2.3.14.1 Transfer Functions

Atmospheric turbulence can be simulated by passing white noise through filters with the following frequency response functions:

$$\text{Longitudinal: } F_u(j\omega) = \frac{(2k)^{\frac{1}{2}}}{a+j\omega}, \tag{2.96}$$

$$\text{Lateral and Vertical: } F_w(j\omega) = \frac{(3k)^{\frac{1}{2}}\left(\frac{a}{\sqrt{3}}+j\omega\right)}{(a+j\omega)^2}, \tag{2.97}$$

where

$$a = \frac{V}{L}, \tag{2.98}$$

$$k = \frac{a\sigma^2}{\pi}. \tag{2.99}$$

To generate the three components of turbulence, three distinct uncorrelated Gaussian white noise sources should be used.

To define the rate of change of gust velocities about the pitch, yaw, and roll axes for simulation purposes, a procedure consistent with the preceding formulation can be found in reference 2-41, section 3.7.5, "Application of Turbulence Models and Analyses." This should be checked for applicability.

2.3.14.2 Boundary Layer Turbulence Simulation

The turbulence in the atmospheric boundary layer, defined here for engineering purposes to be approximately the first 300 m of the atmosphere, is inherently anisotropic. To simulate this turbulence as realistically as possible, the differences between the various scales and intensities of turbulence should be taken into account. There are various problems associated with developing an engineering model of turbulence for simulation purposes. The most outstanding one concerns how one should combine the landing or takeoff steady-state wind and turbulence conditions near the ground (18.3-m level, for example) with the steady-state wind and turbulence conditions at approximately the 300-m level. The wind conditions near the ground are controlled by local conditions and are usually derived from considerations of the risks associated with exceeding the design takeoff or landing wind condition during any particular mission. The turbulence environments at and above the 300-m level are controlled by relatively large-scale conditions rather than local landing or takeoff wind conditions, and these turbulence environments are usually derived from considerations of the risks associated with exceeding the design turbulence environment during the total life or total exposure time of the vehicle to the natural environment. The use of the risk associated with exceeding the design turbulence environment during the total life of the vehicle is justified on the basis that, if the landing conditions are not acceptable, the pilot has the option to land at an alternate airfield and thus avoid the adverse landing wind conditions at the primary landing site. Similarly, in the takeoff problem, the pilot can wait until the adverse low-level wind and turbulence conditions have subsided before taking off. The use of the risk associated with exceeding the design turbulence environment during the total life of the vehicle above the atmospheric boundary layer to develop design turbulence environments for vehicle design studies is justified because the pilot does not have the option of avoiding adverse flight turbulence conditions directly ahead of the vehicle. In addition, the art of forecasting in-flight turbulence has not progressed to the point where a flight plan can be established which avoids in-flight turbulence with a reasonably small risk so that design environments can be established on a per flight basis rather than on a total lifetime basis.

How does one then establish a set of values for L and σ for each component of turbulence which merges together these two distinctly different philosophies? It is recommended that design values for each component of turbulence be established at the 18.3-m and 304.8-m levels based on the previously stated philosophies. Once these values of σ and L are established, the corresponding values between 18.3-m and 304.8-m levels can be obtained with the following interpolation formulas

$$\sigma(H) = \sigma_{18.3}\left(\frac{H}{18.3}\right)^p , \tag{2.100}$$

$$L(H) = L_{18.3}\left(\frac{H}{18.3}\right)^q , \tag{2.101}$$

where $\sigma(H)$ and $L(H)$ are the values of σ and L at height H above natural grade, $\sigma_{18.3}$ and $L_{18.3}$ are the values of σ and L at the 18.3-m level, and p and q are constants selected such that the appropriate values of σ and L occur at the 304.8-m level. Representative values of $L_{18.3}$ for the Dryden spectrum are given by

$$L_{u_{18.3}} = 31.5\,m \;;\; L_{v_{18.3}} = 18.4\,m \;;\; L_{w_{18.3}} = 10.0\,m , \tag{2.102}$$

where subscripts u, v, and w denote the longitudinal, lateral, and vertical components of turbulence. The corresponding design values of $\sigma_{18.3}$ are given by

$$\sigma_{u_{18.3}} = 2.5_{u_{*_o}} , \tag{2.103}$$

$$\sigma_{v_{18.3}} = 1.91_{u_{*_o}} , \tag{2.104}$$

$$\sigma_{w_{18.3}} = 1.41_{u_{*_o}} , \tag{2.105}$$

where u_{*0} is the surface friction velocity which is given by

$$u_{*_0} = 0.4\frac{\bar{u}_{18.3}}{ln\left(\frac{18.3}{z_0}\right)} . \tag{2.106}$$

The quantity $\bar{u}_{18.3}$ is the mean wind or steady-state wind at the 18.3-m level, z_0 is the surface roughness length (section 2.2.6.2), and SI units are understood. The quantity $\bar{u}_{18.3}$ is related to the 18.3-m level peak wind speed $u_{18.3}$ (section 2.2.4) through the equation

$$\bar{u}_{18.3} = \frac{u_{18.3}}{G_{18.3}} , \tag{2.107}$$

where $G_{18.3}$ is the 18.3-m level gust factor (section 2.2.7.1) associated with a 1-h average wind. This gust factor is a function of the 18.3-m level peak wind speed so that, upon specifying $u_{18.3}$ and the surface roughness length, the quantity u_{*0} is defined by equation (2.106).

The values of L and σ must satisfy the Dryden isotropy conditions demanded by the equation of mass continuity for incompressible flow. These isotropy conditions are given by

$$\frac{\sigma_u^2}{L_u} = \frac{\sigma_v^2}{L_v} = \frac{\sigma_w^2}{L_w} , \tag{2.108}$$

and must be satisfied at all altitudes. The length scales given by equation (2.102) and the standard deviations of turbulence given by equations (2.103) through (2.105) were selected so that they satisfy the isotropy condition given by equation (2.108); i.e.,

$$\frac{\sigma_{u_{18.3}}^2}{L_{u_{18.3}}} = \frac{\sigma_{v_{18.3}}^2}{L_{v_{18.3}}} = \frac{\sigma_{w_{18.3}}^2}{L_{w_{18.3}}} \tag{2.109}$$

At the 304.8-m level, equation (2.108) is automatically satisfied because $\sigma_u = \sigma_v = \sigma_w$ and $L_u = L_v = L_w$.

To calculate the value of $\sigma_{304.8}$ appropriate for performing a simulation, the following procedure is used to calculate the design instantaneous gust from which the design value of $\sigma_{304.8}$ shall be obtained. The procedure consists of specifying the vehicle lifetime T; calculating the limit load design value of M/N_0 with equation (2.76) to (2.80); and then calculating the limit load instantaneous gust velocity, w^*, say, with equation (2.88) for $A = 1$ with the values of P_1, P_2, b_1, and b_2 associated with the 0–304.8-m height interval for climb, cruise, and descent in table 2-76. The instantaneous gust velocity w^* should be associated with the 99.98-percent value of gust velocity for a given realization of turbulence. In addition, the turbulence shall be assumed to be Gaussian, so that the value of $\sigma_{304.8}$ and the values of σ at the 18.3-m level (equations (2.103) through (2.105)) shall be used to determine the values of p for each component of turbulence with equation (2.100); i.e.,

$$p = 0.356\, ln\left(\frac{\sigma_{304.8}}{\sigma_{18.3}}\right). \tag{2.110}$$

The integral scale of turbulence at the 304.8-m level appropriate for simulation of turbulence with the Dryden turbulence model is $L_{304.8} = 190$ m. This scale of turbulence and the 18.3-m level scales of turbulence given by equation (2.102) yield the following values of q appropriate for the simulation of turbulence with the Dryden turbulence model in the atmospheric boundary layer:

$$q_u = 0.64 \;;\; q_v = 0.83 \;;\; q_w = 1.05 \;. \tag{2.111}$$

The vertical distributions of σ and L given by equations (2.100) and (2.101) satisfy the isotropy condition given by equation (2.108).

Below the 18.3-m level, σ and L shall take on constant values equal to corresponding 18.3-m level values.

The steady-state wind profile to be used with this model shall be obtained by the procedure given in section 2.3.9.3 for merging ground wind and in-flight wind profile envelopes.

To determine the steady-state wind direction, $\theta(z)$ at any level H between the surface and the 1,000-m level, use the following formula

$$\theta(H) = \theta_{1,000} + \left[2\left(\frac{H-1{,}000}{1{,}000}\right) + \left(\frac{H-1{,}000}{1{,}000}\right)^2\right]\Delta \,,$$

where $\theta_{1,000}$ is the selected 1,000-m level wind direction and H is altitude above the surface of the Earth in meters. The quantity Δ is the angle between the wind vectors at the 10-, and 1,000-m levels. This quantity for engineering purposes is distributed according to a Gaussian distribution with mean value and standard deviation given by

$$\bar{\Delta} = 31° \,,\; \bar{u}_{1,000} \le 4 \text{ m s}^{-1} \,,$$

$$\bar{\Delta} = 31 - 2.183\, ln\left(\frac{\bar{u}_{1,000}}{4}\right) \,,\; \bar{u}_{1,000} > 4 \text{ m s}^{-1} \,,$$

$$\sigma_\Delta = 64° \,,\; \bar{u}_{1,000} \le 4 \text{ m s}^{-1} \,,$$

$$\sigma_\Delta = 63\, e^{-0.0531\,(\bar{u}_{1,000} - 4)} \,,\; \bar{u}_{1,000} > 4 \text{ m s}^{-1} \,,$$

where $\bar{u}_{1,000}$ is the 1,000-m level steady-state wind speed. To avoid unrealistic wind direction changes, Δ, between the surface and the 1,000-m level, only those values of Δ that occur in the interval $-180° \leq 0 \leq 180°$ should be used. It is recommended that ±1-percent risk wind direction changes be used for vehicle design studies.

To apply this model, the longitudinal component of turbulence shall be assigned to be that component of turbulence parallel to the horizontal component of the relative wind vector. The lateral component of turbulence is perpendicular to the longitudinal component and lies in the horizontal plane. The vertical component of turbulence is orthogonal to the horizontal plane.

The following procedure shall be used to calculate profiles of σ and L in the first 304.8 m of the atmosphere for simulation of turbulence with the Dryden turbulence model:

a. Specify the peak wind speed at the 18.3-m level consistent with the accepted risk of exceeding the design 18.3-m level peak wind speed.

b. Calculate the steady-state wind speed at the 18.3-m level with equation (2.107).

c. Calculate the surface friction velocity with equation (2.106).

d. Calculate the 18.3-m level standard deviations of turbulence with equations (2.103) through (2.105).

e. Calculate the 304.8-m level standard deviation of turbulence consistent with the accepted risks of encountering the design instantaneous gust during the total exposure of the vehicle to the natural environments (remembering $\sigma_u = \sigma_v = \sigma_w$ at the 304.8-m level).

f. Calculate p_u, p_v, and p_w with equation (2.110).

g. Calculate the distribution of σ and L with equations (2.110) and (2.111) for the altitudes at and between the 18.3- and 304.8-m levels.

h. Below the 18.3-m level, σ and L shall take on constant values equal to the 18.3-m level values of σ and L.

The reader should consult reference 2-42 for a detailed discussion concerning the philosophy and problem associated with the simulation of turbulence for engineering purposes.

2.3.14.3 Turbulence Simulation in the Free Atmosphere (Above 304.8 m)

To simulate turbulence in the free atmosphere (above 304.8 m), it is recommended that equations (2.88) and (2.91) and the supporting data in table 2-76 be used to specify the appropriate values of σ. The turbulence at these altitudes can be considered to be isotropic for engineering purposes so that the integral scales and intensities of turbulence are independent of direction. Past studies have shown that when the Dryden turbulence model is being used, the scales of turbulence $L = 533.4$ m in the 304.8- to 672-m altitude band and $L = 762$ m above the 672-m level in table 2-76 should be replaced with the values $L = 300$ m and $L = 533$ m, respectively (ref. 2-41). This reduction in scales tends to bring the Dryden spectra in line with the von Karman spectra over the band of wave numbers of the turbulence which are of primary importance in the design of aerospace vehicles. Accordingly, it is recommended that these reduced scales be used in the simulation of turbulence above the 304.8-m level when the Dryden model is being used.

To calculate the values of σ above the 304.8-m level appropriate for performing a simulation of turbulence, it is recommended that the procedure used to calculate the 304.8-m level of σ be used. The appropriate values of P_1, P_2, b_1, and b_2 for the various altitude bands above the 304.8-m level are given in table 2-76.

Section 2.3.14.5.1 and table 2-79b give recently updated values of sigma, scale-length, and probability for light, moderate, and severe turbulence, from 1 to 200 km altitude (ref. 2-60).

2.3.14.4 Design Floor on Gust Environments

If the design lifetime, T, is sufficiently small, it is possible that the turbulence models described herein for horizontally and nearly horizontally flying vehicles will result in a vehicle design gust environment which is characterized by discrete gusts with amplitudes less than 9 m s^{-1} for $dm/L > 10$ in figure 2-42 above the 1-km level. This is especially true for altitudes above the 18-km level. In view of the widespread acceptance of the 9 m s^{-1} gust as a minimum gust amplitude for design studies in the aerospace community and in view of the increased uncertainty in gust data as altitude increases, it is recommended that a floor be established on gust environments for altitudes above the 1-km level so that the least permissible values of σ shall be 3.4 m s^{-1}. Applications concerning figure 2-42 are described in subsection 2.3.15.

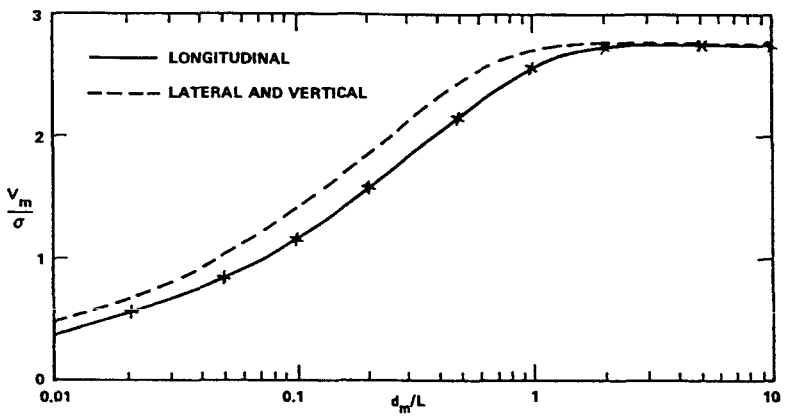

Figure 2-42. Nondimensional discrete gust magnitude, V_m/σ, as a function of nondimensional gust half-width.

2.3.14.5 Multimission Turbulence Simulation

The effects of atmospheric turbulence in both horizontal and near-horizontal flight, during reentry, or atmospheric flight of aerospace vehicles, are important for determining design, control, and "pilot-in-the-loop" effects. A nonrecursive model (based on realistic von Karman spectra) is described. Aerospace vehicles will respond not only to turbulent gusts, but also to spatial gradients of instantaneous gusts (roll, pitch, and yaw). The model described (ref. 2-43) simulates the vertical and horizontal instantaneous gusts, and three of the nine instantaneous gust gradients, as shown in table 2-78.

Simulation of turbulence is achieved by passing a white noise process through a filter whose transfer function yields a von Karman power spectrum. The von Karman spectral functions are:

$$\Phi_{ii} = \frac{55\sigma^2}{36a\pi^2} \frac{\left[(aLK)^2 - (aLK_i)^2\right]}{\left[1+(aLK)^2\right]^{\frac{17}{6}}}, \tag{2.112}$$

$$\Phi_{\substack{ii \\ jj}} = \frac{55\sigma^2}{36\pi^2 a^3 L^2} \frac{(aLK_i)^2\left[(aLK)^2 - (aLK_j)^2\right]}{\left[1+(aLK)^2\right]^{\frac{17}{6}}}, \tag{2.113}$$

Table 2-78. Simulated quantities.

Variable	Spectrum	Comments
U_1	Φ_{11}	Longitudinal gust
U_2	Φ_{22}	Lateral gust
U_3	Φ_{33}	Vertical gust
$\partial U_2/\partial X_1$	$\Phi_{22/33}$	Yaw*
$\partial U_3/\partial X_1$	$\Phi_{33/11}$	Pitch
$\partial U_3/\partial X_2$	$\Phi_{33/22}$	Roll

*X_1, X_2, X_3 are aircraft fixed coordinates with X_1 along the flight path, X_2 the lateral direction and X_3 vertically upward.

where

a = von Karman constant (1.339)

σ^2 = variance of turbulence

k = magnitude of wave number vector

k_i = ith component of wave number

L = length scale of turbulence

Φ_{ii} = three-dimensional gust spectrum

$\Phi_{ii/jj}$ = three-dimensional gust gradient spectrum.

Simulating turbulence with a von Karman spectrum is not a simple process, and generating von Karman turbulence fast enough for real-time simulations is difficult. One procedure for real-time simulations involves generating a large number of data sets for each new mission profile. An alternate approach was suggested by Fichtl (ref. 2-44). In this approach, the turbulent spectra are represented in nondimensional form using the length scale of turbulence, the standard deviation of turbulence, and vehicle true air speed. One set of nondimensional turbulence is generated based on the von Karman spectrum. These data bases can be Fourier analyzed to assure the spectra conform to von Karman's model. To run any mission profile, an efficient real-time routine reads the tapes and transforms them to dimensional format giving the desired output.

The conversion to dimensional values is accomplished as follows:

$$u_i^* = \sigma_i U_i \,, \tag{2.114}$$

where

u_i* = dimensional gust

σ_i = standard deviation of ith gust component

$$\frac{\partial u_i^*}{\partial x_j^*} = \frac{\sigma_i}{L_j} \frac{\partial u_i}{\partial x_j} \,, \tag{2.115}$$

where

$\frac{\partial u_i^*}{\partial x_j^*}$ = dimensional gust gradient

L_j = jth length scale of turbulence

$$\Delta t^* = \frac{aL_1 T}{V}, \tag{2.116}$$

where

Δt^* = dimensional time step

T = dimensionless time step.

Note that Δt^* is not a constant because L_1 and V vary with altitude. To obtain dimensional time, t_N^*, a summation process is involved,

$$t_N^* = \sum_{n=0}^{N} \Delta t_N^* = aT \sum_{n=0}^{N} \frac{L_{in}}{V_n}. \tag{2.117}$$

For digital simulations, turbulence generated with uneven time steps is undesirable. A simple interpolation routine is used to obtain values of turbulence at equal time steps. Specific values of σ_i must be determined for specific applications. Sections 2.3.14.2 through 2.3.14.4 prescribe the techniques for specifying the standard deviation. Values of the turbulent length scales and standard deviations are given in table 2-79*a* up to 1-km altitudes. Table 2-79*b* specifies light, moderate, and severe turbulence sigmas, length scales, and probabilities versus altitude, from 1 to 200 km. The following paragraph discusses these newer, updated values.

2.3.14.5.1 New Turbulence Statistics/Model

At altitude levels greater than 1,000 m, new turbulence velocity component magnitudes (σ_u and σ_w), and scale lengths (L_x and L_z), and their associated probabilities for light, moderate, and severe turbulence have been assembled and modeled (ref. 2-60). These results are presented in table 2-79b. This turbulence modeling update was done in order to provide the space shuttle reentry engineering simulation area with a more realistic/less conservative turbulence model when involved with control system fuel expenditures upon reentry/landing.

2.3.15 Discrete Gust Model—Horizontally Flying Vehicles

Often it is useful for the engineer to use discrete gusts in load and flight control system calculations of horizontally flying vehicles. The discrete gust is defined as follows:

$$V_d = 0, \quad x < 0$$

$$V_d = \frac{V_m}{2}\left(1 - \cos\frac{\pi x}{d_m}\right), \quad 0 \le x \le 2d_m$$

$$V_d = 0, \quad x > 2d_m$$

where x is distance and V_m is maximum velocity of the gust which occurs at position $x = d_m$ in the gust.

To apply the model, the engineer specifies several values of the gust half-width, d_m, so as to cover the range of frequencies of the system to be analyzed. To calculate the gust parameter, V_m, one enters figure 2-42 with d_m/L and reads out V_m/σ. Figure 2-42 is based on the Dryden spectrum of turbulence. Accordingly, the procedures outlined in sections 2.3.14.2 and 2.3.14.3 can be used for the specification of the σ's and L's to determine the gust magnitude V_m from figure 2-42. In the boundary layer, three values of V_m will occur at each altitude, one for each component of turbulence. In the free atmosphere, the lateral and vertical values of V_m are equal at each altitude. In general, both the continuous random gust model (section 2.3.13 and 2.3.14) and the discrete gust models are often used to calculate vehicle responses, with the procedure producing the larger response being used for design.

Table 2-79*a*. Variation of standard deviation and length scale of turbulence with height within the boundary layer.*

	Standard Deviation of Turbulence (Severe)			Integral Scales of Turbulence (All)		
Height (m)	Longitudinal σ_1 (m/s)	Lateral σ_2 (m/s)	Vertical σ_3 (m/s)	Longitudinal L_1 (m)	Lateral L_2 (m)	Vertical L_3 (m)
10	2.31	1.67	1.15	21	11	5
20	2.58	1.98	1.46	33	19	11
30	2.75	2.20	1.71	43	28	17
40	2.88	2.36	1.89	52	35	23
50	2.98	2.49	2.05	61	42	29
60	3.07	2.61	2.19	68	49	35
70	3.15	2.71	2.32	75	56	41
80	3.22	2.81	2.43	82	63	47
90	3.28	2.89	2.54	89	69	53
100	3.33	2.97	2.64	95	75	59
200	3.72	3.53	3.38	149	134	123
304.8	3.95/4.37	3.95/4.37	3.95/4.39	196/300	190/300	192/300
400	4.39	4.39	4.39	300	300	300
500	4.39	4.39	4.39	300	300	300
600	4.39	4.39	4.39	300	300	300
700	4.39	4.39	4.39	300	300	300
762	4.39/5.70	4.39/5.70	4.39/5.70	300/533	300/533	300/533
800	5.70	5.70	5.70	533	533	533
900	5.70	5.70	5.70	533	533	533
1000	5.70	5.70	4.67	832	832	624

*Double entries for a tabulated height indicate a step change in standard deviation or integral scale at that height.

Table 2-79*b*. Mean horizontal and vertical turbulence (light, moderate, and severe) magnitudes (σ_h, σ_w), wind scale (L_h, L_w), and probability for encountering turbulence, versus altitude (MSL)

	Light Turbulence			Moderate Turbulence			Severe Turbulence			Turbulence Length Scales	
Altitude (MSL) km	Horizontal σ_h m/s	Vertical σ_w m/s	Probability of Light Turbulence	Horizontal σ_h m/s	Vertical σ_w m/s	Probability of Moderate Turbulence	Horizontal σ_h m/s	Vertical σ_w m/s	Probability of Severe Turbulence	Horizontal L_h km	Vertical L_w km
1	0.17	0.14	0.776	1.65	1.36	0.199	5.70	4.67	0.025	0.832	0.624
2	0.17	0.14	0.8910	1.65	1.43	0.0979	5.80	4.75	0.0111	0.902	0.831
4	0.20	0.17	0.9199	2.04	1.68	0.0738	6.24	5.13	0.0063	1.04	0.972
6	0.21	0.17	0.9294	2.13	1.69	0.0650	7.16	5.69	0.0056	1.04	1.01
8	0.22	0.17	0.9247	2.15	1.69	0.0704	7.59	5.98	0.0049	1.04	0.98
10	0.22	0.17	0.9280	2.23	1.73	0.0677	7.72	6.00	0.0043	1.23	1.10
12	0.25	0.18	0.9464	2.47	1.79	0.0502	7.89	5.71	0.0034	1.80	1.54
14	0.26	0.19	0.9605	2.62	1.91	0.0368	6.93	5.05	0.0027	2.82	2.12
16	0.24	0.21	0.9639	2.44	2.10	0.0337	5.00	4.31	0.0024	3.40	2.60
18	0.22	0.21	0.9703	2.21	2.07	0.0277	4.07	3.81	0.0020	5.00	3.34
20	0.23	0.20	0.9804	2.26	1.99	0.0180	3.85	3.38	0.0016	8.64	4.41
25	0.27	0.21	0.9839	2.71	2.09	0.0146	4.34	3.34	0.0015	12.0	6.56
30	0.37	0.24	0.9797	3.73	2.39	0.0185	5.60	3.59	0.0018	28.6	8.88
35	0.46	0.26	0.9726	4.59	2.58	0.0249	6.89	3.87	0.0025	35.4	8.33
40	0.53	0.29	0.9650	5.26	2.87	0.0318	7.89	4.30	0.0032	42.6	6.2
45	0.62	0.33	0.9575	6.22	3.25	0.0386	9.33	4.88	0.0039	50.1	5.2
50	0.73	0.42	0.9500	7.27	4.21	0.0455	10.90	6.31	0.0045	57.9	5.3
55	0.87	0.44	0.9250	8.70	4.40	0.0682	13.06	6.60	0.0068	66.0	6.0
60	1.01	0.44	0.9000	10.1	4.42	0.0917	15.1	6.63	0.0083	74.4	6.8
65	1.13	0.41	0.8250	11.3	4.05	0.1620	16.9	6.0	0.0130	83.2	7.5
70	1.59	0.50	0.7500	15.9	5.04	0.2336	23.8	7.5	0.0164	92.3	8.2
75	1.92	0.63	0.6750	19.2	6.3	0.3066	28.7	9.5	0.0184	102	9.0
80	2.26	0.83	0.6000	22.6	8.3	0.3810	33.8	12.4	0.0190	111	9.7
85	2.73	1.03	0.4000	27.3	10.3	0.5769	40.9	15.4	0.0231	121	10.4
90	3.32	1.18	0.2000	33.2	11.8	0.7767	49.8	17.7	0.0233	132	11.2
100	3.56	1.14	0.0000	35.6	11.4	0.9804	53.3	17.1	0.0196	153	12.7
120	4.23	1.07	0.0000	42.3	10.7	0.9901	63.4	16.0	0.0099	200	15.8
140	4.43	1.08	0.0000	44.3	10.8	0.9901	66.4	16.1	0.0099	232	17.6
160	4.82	1.17	0.0000	48.2	11.7	0.9901	72.2	17.6	0.0099	270	20.0
180	4.89	1.18	0.0000	48.9	11.8	0.9901	73.3	17.8	0.0099	300	22.2
200	4.95	1.20	0.0000	49.5	12.0	0.9901	74.2	18.1	0.0099	300	24.3

2.3.16 Flight Regimes for Use of Horizontal and Vertical Turbulence Models (Spectra and Discrete Gusts)

Sections 2.3.8, 2.3.13, and 2.3.15 contain turbulence (spectra and discrete gusts) models for response calculations of vertically ascending and horizontally flying aerospace vehicles.

The turbulence model for the horizontally flying vehicles was derived from wind profile measurements made with vertically ascending jimsphere balloons and smoke trails. In many instances, aerospace vehicles neither fly in a pure horizontal flight mode nor ascend or descend in a strictly vertical flight path. At this time, there does not appear to be a consistent way of combining the turbulence models for horizontal and vertical flight paths without being unduly complicated or overly conservative. In addition, the unavailability of a sufficiently large data sample of turbulence measurements in three dimensions precludes the development of such a combined model.

Accordingly, in lieu of the availability of a combined turbulence model and for the sake of engineering simplicity, the turbulence model in section 2.3.8 should be applied to ascending and descending aerospace vehicles when the angle between the flight path and the local vertical is less than or equal to 30°. Similarly, the turbulence model in sections 2.3.13 and 2.3.15 should be applied to aerospace vehicles when the angle between the flight path and the local horizontal is less than or equal to 30°. In the remaining flight path region between 30° from the local vertical and 30° from the local horizontal, both turbulence models should be independently applied and the most adverse responses used in the design.

2.4 Mission Analysis, Prelaunch Monitoring, and Flight Evaluation

Wind information is useful in the following three general cases of mission analysis:

a. Mission Planning. Since this activity will normally take place well in advance of the mission, the statistical attributes of the wind are used.

b. Prelaunch Operations. Although wind statistics are useful at the beginning of this period, the emphasis is placed upon forecasting and especially wind monitoring.

c. Postflight Evaluation. The effect of the observed winds on the flight is analyzed.

2.4.1 Mission Planning

From wind climatology, the optimum time (month and time of day) and place to conduct the operation can be identified. Missions with severe wind constraints may have such a low probability of success that the risk is unacceptable. Feasibility studies based upon wind statistics can identify these problem areas and answer questions such as: "Is the mission feasible as planned?" and "If the probable risk of mission delay or failure is unacceptably high, can it be reduced by rescheduling to a lighter wind period?"

The following examples are given to illustrate the use of the many wind statistics available to the mission planner.

If it is necessary to remove the ground wind loads damper from a large launch vehicle for a number of hours and this operation must be scheduled some days in advance, the well-known diurnal ground wind variation should be considered for this problem. If, for example, 10.3 m/s (20 knots) were the critical wind speed, there is a 1-percent risk at 0600 e.s.t, but a 13-percent risk at 1500 e.s.t. in July. Obviously, the midday period in the summer should be avoided for this operation. Since these probability values apply to 1-h exposure periods, it is important to recognize that the wind risk depends not only upon wind speed but also upon exposure time. From figure 2-43, the risk in percentage associated with a 15.4 m/s (30-knot) wind at 10 m in February at KSC can be obtained for various exposure times. The upper curve shows the risk increasing from 1 percent for 1-h exposure starting at 0400 e.s.t. to 9.3 percent for 12-h exposure starting at 0400 e.s.t. In this case, the exposure period extends through the high risk part of the day. The lower curve illustrates the minimum risk associated with each exposure period. The lowest risk, of course, can be realized if the starting

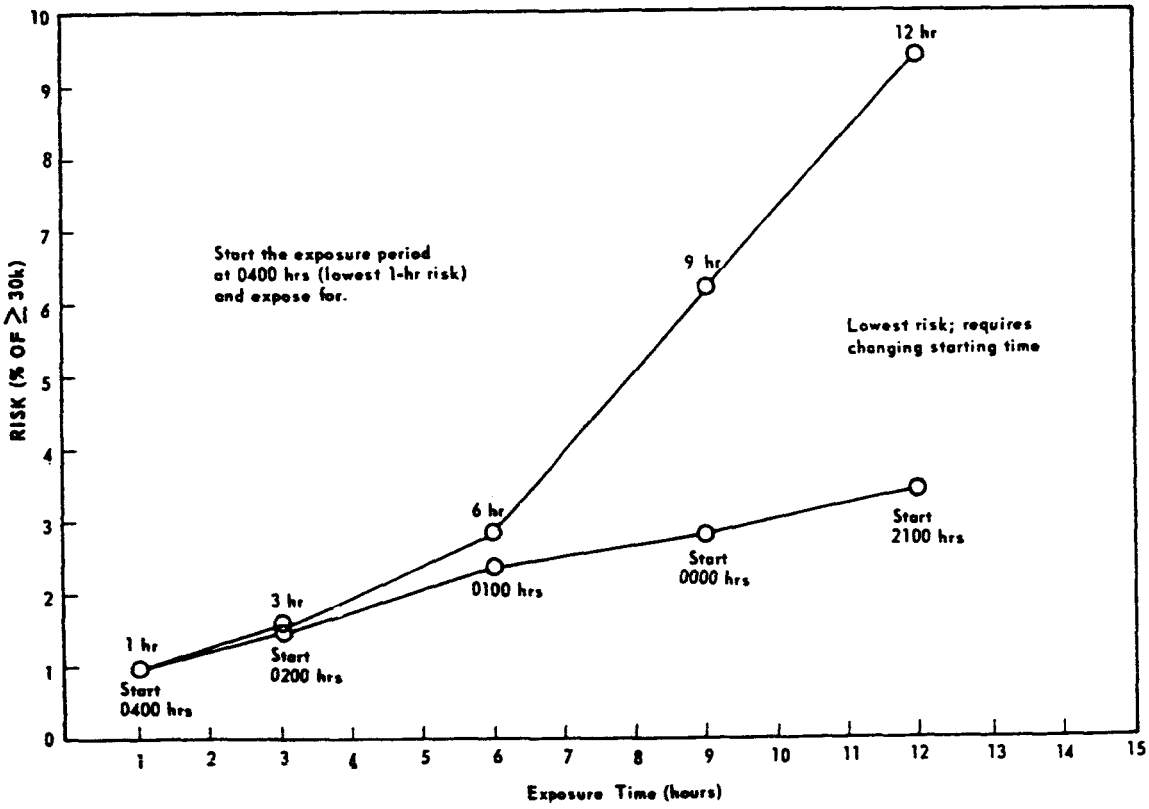

Figure 2-43. Example of wind risk for various exposure times.

times are changed to avoid the windy portion of the day. Although there is no space here for the tabulation, wind risk probabilities by month and starting hour for exposure periods from 1 h to 365 days are available upon request.

When winds aloft are considered for mission planning purposes, again the first step might be to acquire general climatological information on the area of concern. From figure 2-44, it is readily apparent that for KSC most strong winds occur during winter in the 10- to 15-km altitude region (this applies also to nearly all midlatitude locations). It is also true that these strong winds are usually westerly.

Next, the mission analyst might ask if a particular mission is feasible. If, for example, the flight is to take place in January and 10- to 15-km altitude winds ≥50 m/s are critical, the probability of favorable winds on any given day in January is 0.496. With such a low probability of success, this mission may not be feasible. But, to continue the example, if it is necessary that continuously favorable winds exist for 3 days (perhaps for a dual launch), the probability of success will decrease to 0.256. Obviously an alternate mission schedule must be planned or else the scheduled space vehicle must be provided additional capability through redesign.

Perhaps the vehicle can remain on the pad in a state of near readiness awaiting launch for several days. In this case, it would be desirable to know that the probability of occurrence of at least one favorable wind speed, for example in a 4-day period, is 0.813. If greater flexibility of operation is desired, one might require four favorable opportunities in 4 days. This probability is 0.550. Now, if consecutive favorable opportunities are required, for example, four consecutive in eight periods, the probability of success will be somewhat lower (0.431).

The mission planner might also gain some useful information from the persistence of the wind aloft within the 10- to 15-km altitude region. The probability of winds <50 m/s on any day in January is 0.496. But if a wind speed <50 m/s does occur, then the probability that the next observed wind 12 h later would be <50 m/s is 0.82, a rather dramatic change. Furthermore, if the wind continues below 50 m/s for five observations, the probability that it will remain there for one more 12-h period is 0.92.

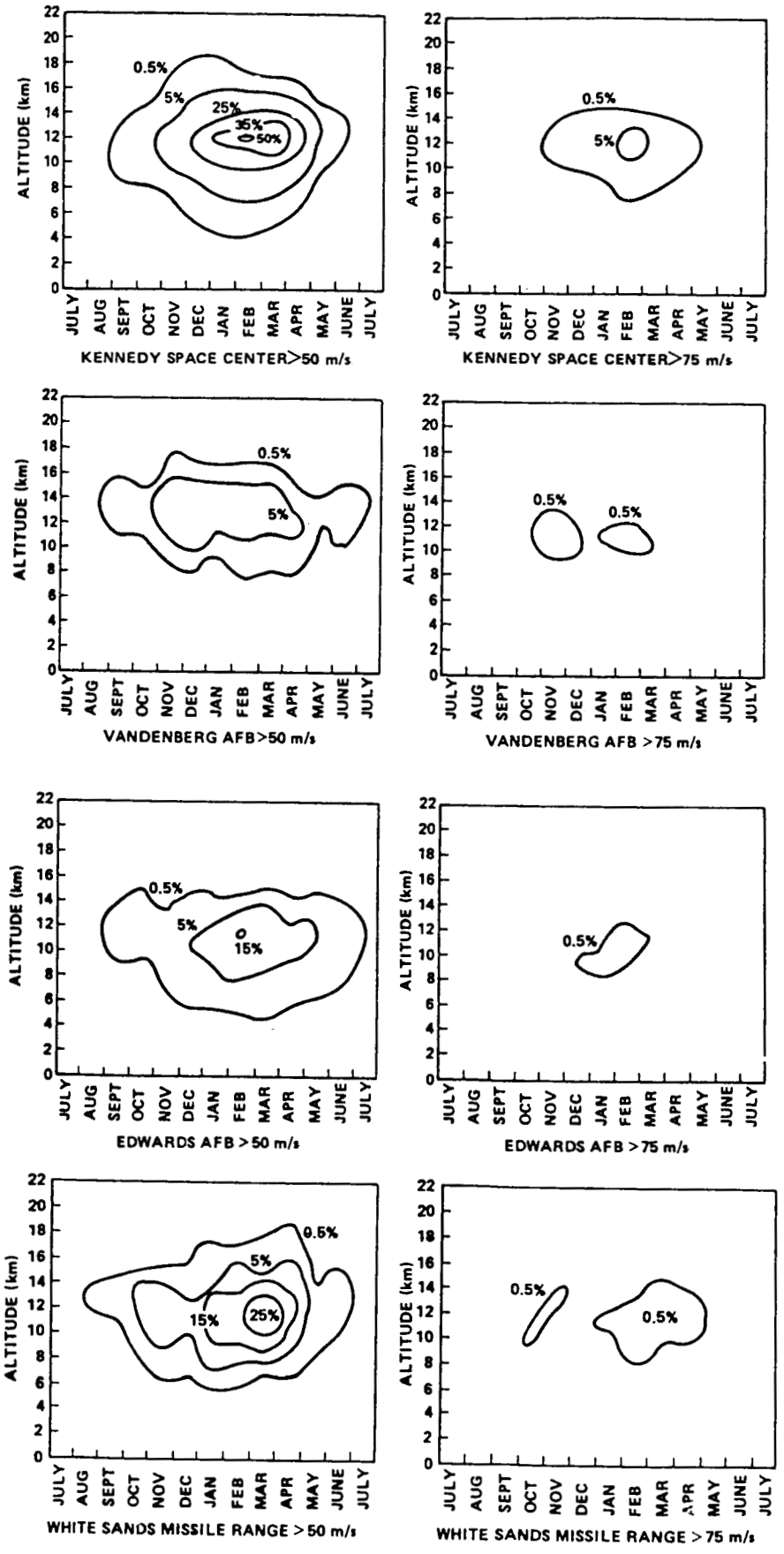

Figure 2-44. Frequency of scalar wind speed exceeding given wind speed as a function of altitude for stations indicated.

As the time of the operation approaches T-4 to T-1 days, the conditional probability statements assume a more significant role. At this point, as the winds will usually be monitored, the appropriate conditional probability value can be identified and used to greater advantage.

The preceding examples are intended to illustrate the type of analysis that can be accomplished to provide objective data for program decisions. This may best be accomplished by a close working relationship between the analyst and those concerned with the decision.

2.4.2 Prelaunch Wind Monitoring

In-flight winds constitute the major atmospheric parameter in aerospace vehicle and missile design and operations. A frequency content of the wind profile near the bending mode frequencies or wind shear with the characteristics of a step input may exceed the vehicle's structural capabilities (especially on forward stations for the small-scale variations of the wind profile). Wind profiles with high speeds and shears exert high structural loads at all stations on a large space vehicle, and when the influences of bending dynamics are high, even a profile with low speeds and high shears can create large loads (ref. 2-45).

Because of the possibility of launch into unknown winds, operational missile systems must accept some in-flight loss risk in exchange for a rapid-launch capability. But research and development missiles, and space vehicles in particular, cost so much that the overall success of a flight outweighs the consideration of launch delays caused by excessive in-flight wind loads. If the exact wind profile could be known in advance, it would be a relatively simple task to decide upon the launch date and time. However, there is little hope of accurately forecasting the detailed wind profile far into the future.

Over the years, these situations have increasingly put emphasis on prelaunch monitoring of in-flight winds. Today, prelaunch and profile determination techniques essentially preclude the risk of launching a space vehicle or research and development missile into an in-flight wind condition that would cause it to fail.

The development and operational deployment of the FPS-16 radar/jimsphere system (ref. 2-46) significantly minimizes vehicle failure risks when properly integrated into a flight simulation program. The jimsphere sensor, when tracked with the FPS-16 or other radar with equal tracking capability, provides a very accurate "all weather" detailed wind profile measurement. FPS-16 radars are available at all national test ranges.

In general, the system provides a wind profile measurement from the surface to an altitude of 17 km in slightly less than 1 h, a vertical spatial frequency resolution of 1 cycle per 200 m, and an rms error of about 0.5 m/s or less for wind velocities averaged over 50-m intervals. The resolution of these data permits calculating the structural loads associated with the first bending mode and generally the second mode of missiles and space vehicles during the critical, high dynamic pressure phase of flight. This provides better than an order-of-magnitude accuracy improvement over the conventional rawinsonde wind profile measurement system.

By employing the appropriate data transmission resources, a detailed wind profile from the FPS-16 radar can be ready for input to the vehicle's flight simulation program within a few minutes after tracking of the jimsphere. The flight simulation program provides flexibility relative to vehicle dynamics and other parameters in order to make maximum use of detailed wind profiles.

If very critical wind conditions exist and the mission requirement dictates a maximum effort to launch with provision for last-minute termination of the operation, then a contingency plan that will provide essentially real-time wind profile and flight simulation data may be employed. This is done while the jimsphere balloon is still in flight.

An example of the FPS-16 radar/jimsphere system data appears in figure 2-45 — the November 8 and 9, 1967, sequence observed during prelaunch activities for the first Apollo/Saturn-V test flight, AS-501.

Reference 2-47 contains additional sequential jimsphere wind profile sets for KSC and Point Mugu, CA, respectively. The persistence over a period of 1 h of some small-scale features in the wind profile structure, as well as the rather distinct changes that developed in the profiles over a period of a few hours, is evident.

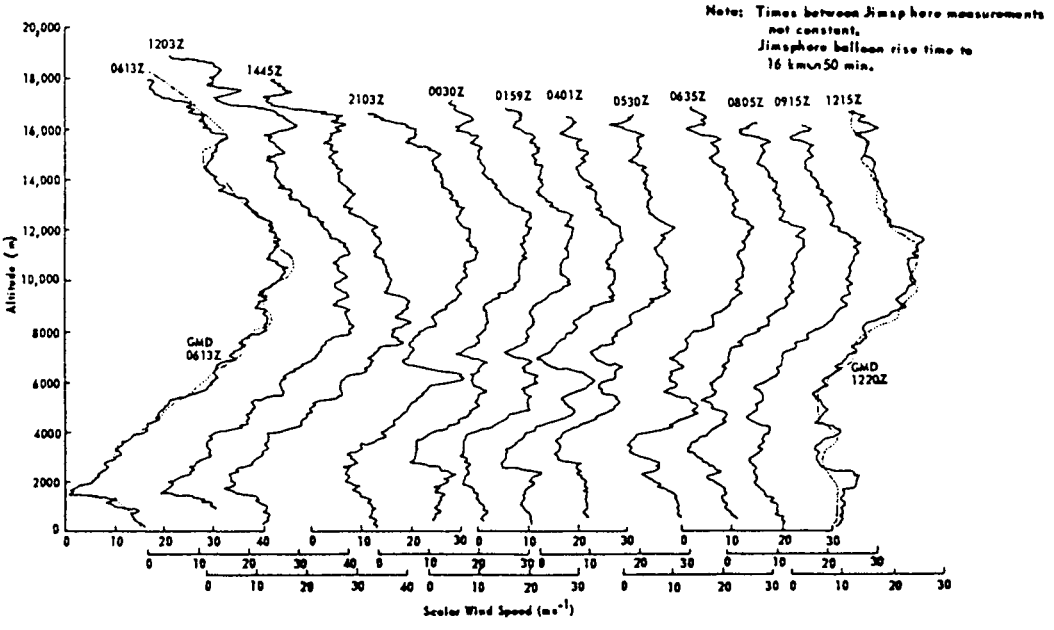

Figure 2-45. Examples of the FPS-16 radar/jimsphere system data, November 8–9, 1967.

The FPS-16 radar/jimsphere system (fig. 2-46) was routinely used in the prelaunch monitoring of NASA's Apollo/Saturn and the space shuttle flights. The wind profile data were transmitted to the Johnson Space Center and Marshall Space Flight Center, and the flight simulation results were sent to the launch complex at KSC.

An FPS-16 radar/jimsphere operational measurement program capability exists at all the national test ranges to obtain detailed wind profile data for use in space vehicle and missile response studies, airplane turbulence analysis, atmospheric turbulence investigations, and mesometeorological studies. Sequential measurements similar to those made in support of a Saturn-V launch shown here—of 8 to 10 jimsphere wind profiles approximately 1 h apart—were made on at least 1 day per month for each location. Single profile measurements were also made daily at KSC.

A radar wind profiler is currently operating at KSC and measures wind profiles between 2- and 19-km altitude. The profiler gives better temporal resolution than balloons. Various profiler data bases are available upon request.

2.4.3 Post-Flight Evaluation

2.4.3.1 Introduction

Because of the variable effects of the atmosphere upon a large aerospace vehicle at launch and during flight, various meteorological parameters were measured at the time of each vehicle launch, including wind and thermodynamic data at the Earth's surface and up to an altitude of at least 36 km. To make the data available, meteorological tapes were prepared, presentations were made at flight evaluation meetings, memoranda of data tabulations were prepared and distributed, and a summary was written. Reference 2-48 for space shuttle STS-1 is an example of one of the reports with an atmospheric section.

2.4.3.2 Meteorological Data Profiles

Shortly after the launch of each aerospace vehicle under the cognizance of MSFC, a meteorological ascent data profile was prepared by combining the FPS-16 radar/jimsphere wind profile data and the rawinsonde wind profile and thermodynamic data (temperature, pressure, and humidity) observed as near the vehicle launch time as feasible. This was done under the supervision of the MSFC's Earth Science and Applications Division. The meteorological data was normally available within 3 days after launch time and provided data to approximately 36 km. In the meteorological data profile, thermodynamic and wind data above the measured data are given by the Range Reference Atmosphere (ref. 2-23) and the Global Reference Atmosphere (ref. 2-49) values. To prevent unnatural jumps in the data when the two types are merged, the data were carefully examined to pick the best altitude for the merging, and a ramping procedure was employed. The meteorological data profiles were made available to all government and contractor groups for their use in the space vehicle launch and flight evaluation. This provides a consistent set of data for all evaluation studies and ensures the best available information of the state of the atmosphere during launch. For space shuttle launches, an SRB descent meteorological data tape was constructed using rawinsonde data taken from a ship stationed near the SRB impact site. Twenty parameters of data were included in the meteorological data tape at 100-ft increments of altitude.* Table 2-80 presents the parametric format of the L–0 atmospheric data profile that is assembled after each NASA-MSFC associated vehicle launch.

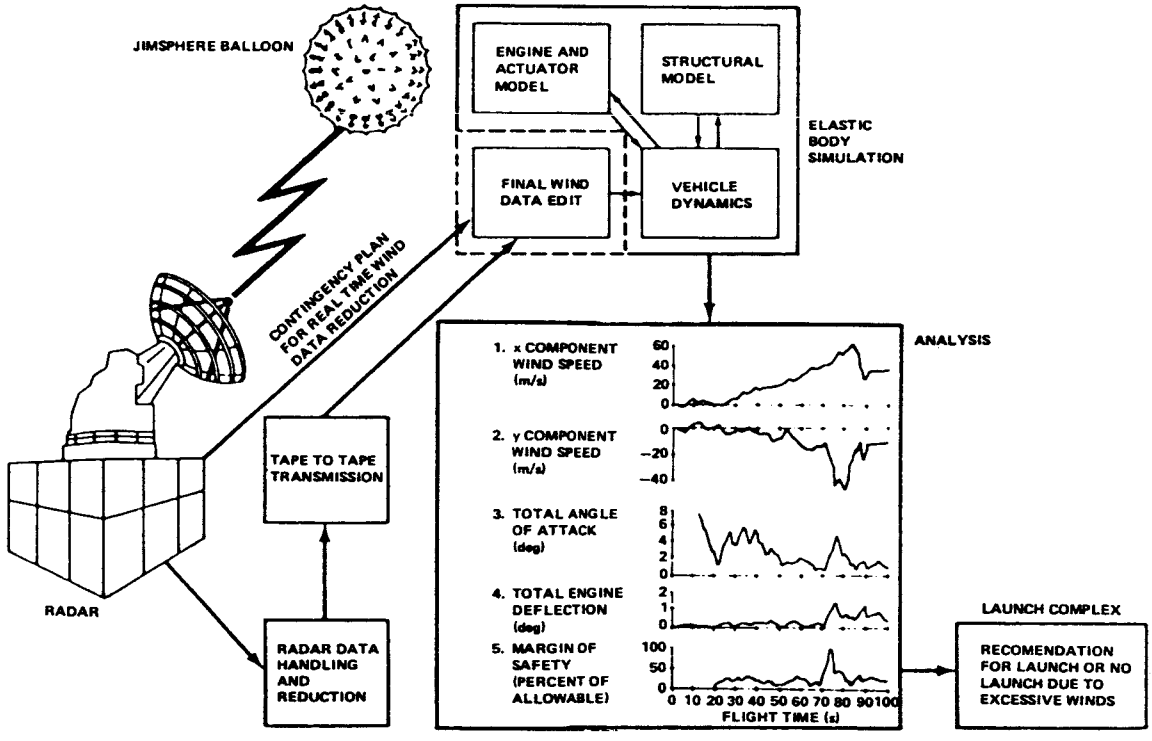

Figure 2-46. Operation of the FPS-16 radar/jimsphere system.

Pad winds and thermodynamic data were measured and recorded at different heights above the launch pad starting several hours before launch time. Reference 2-50 summarizes atmospheric data observations for 155 flights of NASA/MSFC-related launches. Records and summary reports are maintained on the atmospheric parameters for MSFC-sponsored vehicle test flights conducted at KSC, FL. Requests for summaries of these atmospheric data, or related questions on specific topics, should be directed to the Earth Science and Applications Division, Space Science Laboratory, NASA Marshall Space Flight Center, Alabama 35812.

*Altitude increments of 100 ft were chosen to provide for maximum engineering value and for use of the available atmospheric data and do not necessarily represent the attainable response frequency of the measurements.

Table 2-80. Format of meteorological data profile.

Word	Symbol	Description	Units
1	LAT	Latitude	degrees, +N
2	LON	Longitude	degrees, +E to 360
3	FLAG	0 = measured data, 1 = modeled data, 2 = combined measured and modeled data	
4	—	Spare	
5	ALT	Geometric altitude	ft
6	WS	Horizontal wind speed	ft/s
7	WD	Directional horizontal wind is coming from relative to true north, North being 0°, increasing positively clockwise	deg
8	TE	Ambient temperature	°C
9	PR	Ambient pressure	millibars
10	D	Ambient density	gram/m^3
11	DW	Dew point	°C
12	TEU	Ambient temperature systematic uncertainty	°C
13	PRU	Ambient pressure systematic uncertainty	millibars
14	DU	Ambient density systematic uncertainty	gram/m^3
15	HWSUS	Horizontal wind speed systematic uncertainty	ft/s
16	HWSUN	Horizontal wind speed noise or fluctuation uncertainty	ft/s
17	VWSUN	Vertical wind speed noise or fluctuation uncertainty	ft/s
18	HWDUS	Horizontal wind direction systematic uncertainty	deg
19	HWDUN	Horizontal wind direction noise or fluctuation uncertainty	deg
20		Spare	

REFERENCES

2-1 Carter, E.A., and Schuknecht, L.A.: "Peak Wind Statistics Associated With Thunderstorms at Cape Kennedy, Florida." NASA CR-61304, NASA-MSFC, Marshall Space Flight Center, Alabama, August 1969.

2-2 Smith, O.E., Falls, L.W., and Brown, S.C.: "Research Achievements Review." vol. II, report No. 10, "Terrestrial and Space Environment Research at MSFC," NASA TM X-53706, NASA-MSFC, Marshall Space Flight Center, Alabama, 1967.

2-3 Lee, R.F., Goodge G.W., and Crutcher, H.L.: "Surface Climatological Information for Twelve Selected Stations for Reentry Vehicles." NASA CR-61319, Marshall Space Flight Center, Alabama, 1970.

2-4 Goodge, G.W., Bilton, T.H., and Quinlin, F.T.: "Surface Climatological Information for Twelve Selected Stations for Reentry Vehicles." NASA CR-61342, Marshall Space Flight Center, Alabama, 1971.

2-5 Fichtl, G.H., and McVehil, G.E.: "Longitudinal and Lateral Spectra of Turbulence in the Atmospheric Boundary Layer at the Kennedy Space Center." Journal of Applied Meteorology, vol. 9, No. 1, February 1970, pp. 51–63.

2-6 Blackadar, A.K., et al.: "Investigation of the Turbulent Wind Field Below 150-M Altitude at the Eastern Test Range." NASA CR-1410, NASA-MSFC, Marshall Space Flight Center, Alabama, August 1969.

2-7 McVehil, G.E., and Camnitz, H.G.: "Ground Wind Characteristics at Kennedy Space Center." NASA CR-1418, NASA-MSFC, Marshall Space Flight Center, Alabama, September 1969.

2-8 Fichtl, G.H., Kaufman, J.W., and Vaughn, W.W.: "Characteristics of Atmospheric Turbulence as Related to Wind Loads on Tall Structures." Journal of Spacecraft and Rockets, vol. 6, No. 12, December 1969, pp. 1396–1403.

2-9 Fichtl, G.H.: "Problems in the Simulation of Atmospheric Boundary Layer Flows." AGARD-DP-140 (1973) 2-1. (Paper presented at AGARD Flight Mechanics Panel Symposium on "Flight in Turbulence," England, May 1973.)

2-10 Fichtl, G.H.: "Wind Shear Near the Ground and Aircraft Operations." Journal of Spacecraft and Rockets, vol. 9, No. 11, November 1972, pp. 765–770.

2-11 Fichtl, G.H.: "Probability Distribution of Vertical Longitudinal Shear Fluctuations." Journal of Applied Meteorology, vol. 11, No. 6, September 1972, pp. 918–925.

2-12 Fichtl, G.H.: "Standard Deviation of Vertical Two-Point Longitudinal Velocity Differences in the Boundary Layer." Boundary-Layer Meteorology, vol. 2, 1971, pp. 137–151.

2-13 Luers, J.K., and Reese, J.B.: "Effects of Shear on Aircraft Landing." NASA CR-2287, NASA-MSFC, Marshall Space Flight Center, Alabama, July 1973.

2-14 Luers, J.K.: "A Model of Wind Shear and Turbulence in the Surface Boundary Layer." NASA CR-2288, NASA-MSFC, Marshall Space Flight Center, Alabama, July 1973.

2-15 Sowa, D.: "Low-Level Wind Shear." D.C. Flight Approach, No. 20, Douglas Aircraft Co., Long Beach, California, 1974.

2-16 Barr, N.M., Gangaas, D.; and Schaeffer, D.R.: "Wind Models for Flight Simulator Certification of Landing and Approach Guidance and Control Systems." Report No. FAA-RD-74-206, U.S. Department of Transportation, Federal Aviation Administration, Washington, DC 20590, December 1974.

2-17 Lewell, W.S., and Williamson, G.G.: "Wind Shear and Turbulence Around Airports." NASA CR-2752, NASA-MSFC, Marshall Space Flight Center, Alabama, October 1976.

2-18 Camp, D.W., and Kaufman, J.W.: "Comparison of Tower Influence on Wind Velocity for NASA's 150-Meter Meteorological Tower and a Wind Tunnel Model of the Tower." Journal of Geophysical Research, vol. 75, No. 6, February 20, 1970.

2-19 Thom, H.C.S.: "New Distributions of Extreme Winds in the United States." Journal of the Structural Division Proceedings of the American Society of Civil Engineers, ST-7, July 1968, pp. 1787–1801.

2-20 Thom, H.C.S.: "Distribution of Extreme Winds Over Oceans." J. Waterways, Harbors, and Coastal Engr. Div., Proc. Am. Soc. Civ. Engr., February 1973, pp. 1–17.

2-21 Falls, L.W., and Brown, S.C.: "Optimum Runway Orientation Relative to Crosswinds." NASA TN D-6930, September 1972.

2-22 Falls, L.W., and Crutcher, H.L.: "Determination of Statistics for Any Rotation of Axes of a Bivariate Normal Elliptical Distribution." NASA TM X-64595, May 1971.

2-23 IRIG Document No. 104-63, Range Reference Atmosphere Documents published by Secretariat, Range Commander's Council, White Sands Missile Range, New Mexico. The following reference atmospheres have been published:

Kwajalein Missile Range, Kwajalein, Marshall Islands, Range Reference Atmosphere, 0- to 70-km Altitude, Document 360-82, December 1982. (AD123424)

Cape Canaveral, Florida, Range Reference Atmosphere, 0- to 70-km Altitude, Document 361-83, February 1983. (ADA125553)

Vandenberg Air Force Base, California, Range Reference Atmosphere, 0- to 70-km Altitude, Document 362-83, April 1983.

Dugway, Utah, Range Reference Atmosphere, 0- to 30-km Altitude, Document 363-83, June 1983.

Wallops Island, Virginia, Range Reference Atmosphere, 0- to 70-km Altitude, Document 364-83, July 1983.

White Sands Missile Range, New Mexico, Range Reference Atmosphere, 0- to 70-km Altitude, Document 365-83, August 1983.

Edwards Air Force Base, California, Range Reference Atmosphere, 0- to 70-km Altitude, Document 366-83, August 1983.

Eglin Air Force Base, Florida, Range Reference Atmosphere, 0- to 30-km Altitude, Document 367-83, September 1983.

Taquac, Guam Island, Range Reference Atmosphere, 0- to 30-km Altitude, Document 368-83, September 1983.

Point Mugu, California, Range Reference Atmosphere, 0- to 70-km Altitude, Document 369-83, September 1983.

Barking Sands, Hawaii, Range Reference Atmosphere, 0- to 70-km Altitude, Document 370-83, December 1983.

Ascension Island, South Atlantic, Range Reference Atmosphere, 0- to 70-km Altitude, Document 371-84, January 1984.

2-24 Falls, L.W.: "Normal Probabilities for Cape Kennedy Wind Components—Monthly Reference Periods for All Flight Azimuths, Altitudes 0 to 70 km." NASA TM X-64771, NASA-MSFC, Marshall Space Flight Center, Alabama, April 16, 1973.

2-25 Falls, L.W.: "Normal Probabilities for Vandenberg AFB Wind Components—Monthly Reference Periods for All Flight Azimuths, 0- to 70-km Altitudes." NASA TM X-64897, NASA-MSFC, Marshall Space Flight Center, Alabama, January 1975.

2-26 Henry. R.M.: "A Statistical Model for Synthetic Wind Profiles for Aerospace Vehicle Design and Launching Criteria." NASA TN D-1813, 1963.

2-27 Bieber, R.E.: "Missile Structural Loads by Nonstationary Statistical Methods." Technical Report No. LMSD 49703, Lockheed Missile and Space Division, Huntsville, Alabama, April 1959. (Also available as DDC AD220595 or NTIS PB157733.)

2-28 Vaughan, W.W.: "Interlevel and Intralevel Correlations of Wind Components for Six Geographical Locations." NASA TN D-561, December 1960.

2-29 Daniels, G.E., and Smith, O.E.: "Scalar and Component Wind Correlations Between Altitude Levels for Cape Kennedy, Florida, and Santa Monica, California." NASA TN D-3815, April 1968.

2-30 Cochrane, J.A., Henry, R.M., and Weaver, W.L.: "Revised Upper Air Wind Data for Wallops Island Based on Serially Complete Data for the Years 1956 to 1964." NASA TN D-4570, NASA-Langley Station, Hampton, Virginia, May 1968.

2-31 Buell, C.E.: "Correlation Functions for Wind and Geographical on Isobaric Surfaces." Journal of Applied Meteorology, vol. II, No. 1, February 1972, pp. 51–59.

2-32 Buell, C.E.: "Variability of Wind With Distance and Time on an Isobaric Surface." Journal of Applied Meteorology, vol. II, No. 7, October 1972, pp. 1085–1091.

2-33 Truppi, L.E.: "Probabilities of Zero Wind Shear Phenomena Based on Rawinsonde Data Records." NASA TM X-53452, NASA-MSFC, Marshall Space Flight Center, Alabama, April 27, 1966.

2-34 Camp, D.W., and Susko, M.: "Percentage Levels of Wind Speed Differences Computed by Using Rawinsonde Wind Profile Data From Cape Kennedy, Florida." NASA TM X-53461, NASA-MSFC, Marshall Space Flight Center, Alabama, May 12, 1966.

2-35 Camp, D.W., and Fox, P.A.: "Percentage Levels of Wind Speed Differences Computed by Using Rawinsonde Wind Profile Data From Santa Monica, California." NASA TM X-53428, NASA-MSFC, Marshall Space Flight Center, Alabama, October 21, 1966.

2-36 Adelfang, S.I.: "Analysis of Vector Wind Change With Respect to Time for Cape Kennedy, Florida." NASA CR-15077, NASA-MSFC, Marshall Space Flight Center, Alabama, August 1978.

2-37 Adelfang, S.I.: "Analysis of Vector Wind Change With Respect to Time for Vandenberg Air Force Base, California." NASA CR-150776, NASA-MSFC, Marshall Space Flight Center, Alabama, August 1978.

2-38 Smith. O.E.: "Vector Wind and Vector Wind Shear Models 0- to 27-km Altitude for Cape Kennedy, Florida, and Vandenberg AFB, California." NASA-MSFC, Marshall Space Flight Center, Alabama, July 1976.

2-39 Fichtl, G.H.: "Small-Scale Wind Shear Definition for Aerospace Vehicle Design." Journal of Spacecraft and Rockets, vol. 9, No. 2, February 1972, pp. 79–83.

2-40 Fichtl, G.H., Camp, D.W., and Vaughan, W.W.: "Detailed Wind and Temperature Profiles." Clear Air Turbulence and It's Detection, Edited by Yih-Hc Pao and Arnold Goldburg, Plenum Press, New York, 1969, pp. 308–333.

2-41 Chalk, C.R., et al.: "Background Information and User Guide for MIL-F-8758B (ASG), 'Military Specification—Flying Qualities for Piloted Airplanes.' " AFFDL-TR-69-72, Air Force Flight Dynamics Laboratory, Air Force Systems Command, 1969.

2-42 Dutton, J.A.: "Broadening Horizons in Prediction of the Effects of Atmospheric Turbulence on Aeronautical Systems." AIAA Selected Reprints Series, vol. XIII, The Earth's Atmosphere, W.W. Vaughan and L.L. DeVries Editors, Published by the American Institute of Aeronautics and Astronautics, New York, 1972.

2-43 Tatom, F.B., and Smith, S.R.: "Advanced Shuttle Simulation Turbulence Tapes (SSTT) User's Guide." Engineering Analysis, Incorporated, contract NAS8-33818, September 29, 1981.

2-44 Fichtl, G.H.: "A Technique for Simulating Turbulence for Aerospace Vehicle Flight Simulation Studies." NASA TM-78141, November 1977.

2-45 Ryan, R.S., Scoggins, J.R., and King, A.W.: "Use of Wind Shears in the Design of Aerospace Vehicles." Journal of Spacecraft and Rockets, vol. 4, No. 11, November 1967, pp. 1526–1532.

2-46 Vaughan, W.W.: "New Wind Monitoring System Protects R and D Launches." Journal of Astronautics and Aeronautics, December 1968, pp. 41–43.

2-47 Johnson, D.L., and Vaughan, W.W.: "Sequential High Resolution Wind Profile Measurements." NASA TP-1354, December 1978.

2-48 Johnson, D.L., Jasper, G., and Brown, S.C.: "Atmospheric Environment for Space Shuttle (STS-1) Launch." NASA TM-82436, July 1981.

2-49 Justus, C.G., Alyea, F.N., Cunnold, D.M., Jeffries, W.R. III, and Johnson, D.L.: "The NASA/MSFC Global Reference Atmospheric Model—1990 Version (GRAM-90); Part I Technical/Users Manual." NASA TM-4268, April 1991.

2-50 Johnson, D.L.: "Summary of Atmospheric Data Observations for 155 Flights of MSFC/ABMA Related Aerospace Vehicles." NASA TM X-64796, NASA-MSFC, Marshall Space Flight Center, Alabama, December 5, 1973.

2-51 Johnson, D.L., and Brown, S.C.: "Surface to 90-km Winds for Kennedy Space Center, Florida, and Vandenberg AFB, California." NASA TM-78233, July 1979.

2-52 Smith, O.E., Adelfang, S.I., and Brown, R.P.: "Ascent Structural Wind Loads for the National Space Transportation System (NSTS)." Proceedings paper AIAA-88-0293, AIAA 26th Aerospace Sciences Meeting, January 11–14, 1988, Reno, Nevada.

2-53 Smith. O.E., and Austin, L.D., Jr.: "Space Shuttle Response to Ascent Wind Profiles." AIAA Journal of Guidance Control and Dynamics, vol. 6, No. 5, September–October 1983, pp. 355–360.

2-54 Smith, O.E., and Austin, L.D., Jr.: "Sensitivity Analysis of the Space Shuttle to Ascent Wind Profiles." NASA TP-1988, March 1982.

2-55 Smith, O.E., Adelfang, S.I., Batts, G.W., and Hill, C.K.: "Wind Models for the NSTS Ascent Trajectory Biasing for Wind Load Alleviation." NASA TM-100375, August 1989.

2-56 Gumbel, E.J.: "Statistics of Extremes." Columbia University Press, New York, New York, 1958, 57-10160.

2-57 Gumbel, E.J., Mustafi, C.K., and Smith, O.E.: "Tables of the Probability and Density Functions for the Bivariate Extremal Distributions." Department of Industrial Engineering, Columbia University, New York, New York, April 1968.

2-58 Gumbel, E.J., and Mustafi, C.K.: "Some Analytical Properties of the Bivariate Extremal Distributions." American Statistical Association Journal, June 1967, pp. 569–588.

2-59 Smith, S.A.: "Revised Gust Model." Memo ES44-(147-89), NASA Marshall Space Flight Center, Earth Science and Applications Division, Environmental Analysis Branch, October 24, 1989.

2-60. Justus, C.G., Campbell, C.W., Doubleday, M.K., and Johnson, D.L.: "New Atmospheric Turbulence Model for Shuttle Applications." NASA TM-4168, January 1990.

SECTION III. THERMODYNAMIC PROPERTIES AND ATMOSPHERIC MODELS

3.1 Introduction

This section presents the surface and inflight thermodynamic parameters (temperature, pressure, and density) of the atmosphere in a statistical and a modeling mode. Mean and extreme values of these thermodynamic parameters can be used in application to many aerospace problems, such as: (1) research planning and engineering design of remote Earth sensing systems; (2) vehicle design and development; and (3) vehicle trajectory analysis, dealing with vehicle thrust, dynamic pressure, aerodynamic drag, aerodynamic heating, vibration, structural and guidance limitations, and reentry analysis. The first part of this section gives median and extreme values of these thermodynamic variables at sea level and surface level. The thermodynamic variables are then presented as a function of altitude in terms of median and extreme values. An approach is also presented for relating temperature, pressure, and density as independent variables, with a method to obtain simultaneous values of these variables at discrete altitude levels. A subsection on reentry is presented, giving atmospheric models for use in reentry heating, trajectory, etc., analyses. Sites presented in this section include Kennedy Space Center (KSC), Florida, Vandenberg Air Force Base (VAFB), California, Edwards AFB (EAFB), California, and White Sands Missile Range (WSMR), New Mexico. If other United States or world site surface extreme thermodynamic parameter values are needed, consult section V. Many of the atmospheric models described in this section are available as a computer program or subroutine, from NASA/MSFC Earth Science and Applications Division.

3.2 U.S. Standard Atmosphere 1976 Sea Level Values

Standard sea level values of temperature, pressure, and density (ref. 3.1), which are representative of annual conditions at 45° latitude in the U.S., are given below.

	Metric Units	U.S. Customary Units
Temperature	15.0 °C or 288.15 K	59 °F or 518.67 °R
Pressure	1.013250×10^5 Newton m^{-2} [Newton m^{-2} is equivalent to a Pascal (Pa) in SI units; a Pascal is equivalent to 100 millibars (mb)]	2,116.22 lb ft^{-2} or 14.696 lb in^{-2}
Density	1.2250 kg m^{-3}	0.076474 lb ft^{-3}

3.3 Surface Atmospheric Thermodynamic Parameters

3.3.1 Atmospheric Temperature

3.3.1.1 Definition

The normal thermodynamic definition of temperature, the derivative of energy with respect to entropy, applies to the atmospheric environment.

There is also a virtual temperature, T_V, of a sample of moist air is defined as the temperature at which dry air of the same total pressure would have the same density as the sample.

$$T_V = T\,(1+0.61\,w)\,, \tag{3.1}$$

where w = mixing ratio of water vapor to dry air (g/kg).

By substituting T_V into the ideal gas law in place of T, the variations of temperature and humidity are accounted for (to within the limits of ideal gas approximation).

$$PV = (R/M)\ T_V\ , \tag{3.2}$$

where

P = pressure

V = volume

M = molecular weight, where $M_{\text{dry air}} = 28.966$ and $M_{\text{water vapor}} = 18.016$

R = universal gas constant = 8.31436×10^7 erg $\cdot$ K^{-1} $\cdot$ g mol^{-1}

3.3.1.2 Surface Temperature

Median and extreme values of surface atmospheric temperature for various NASA sites of interest are presented in subsection 3.4.1. Temperature aloft statistics are also presented in section 3.4.1. Other U.S. and world surface temperature extremes are given in section V. Extreme and 95th percentile values of surface temperature for selected areas are given in table 4.2.

3.3.2 Atmospheric Pressure

3.3.2.1 Definition

Atmospheric pressure (also called barometric pressure) is the force exerted, as a consequence of gravitational attraction, by the mass of the column of air of unit cross section lying directly above the area in question. It is expressed as force per unit area (Newtons per square meter or Newtons per square centimeter or millibars).

3.3.2.2 Surface Pressure

The total variation of pressure from day to day is relatively small. Diurnal, semidiurnal, and terdiurnal tidal variations can all affect the normal surface atmospheric pressure pattern. Rapid and slightly greater variations of pressure occur as the result of the passage of frontal systems, while the passage of a hurricane can cause somewhat larger, but still not significant, changes for pressure environment design of space vehicles. The pressure drop in a tornado is significant and can exceed 20 percent of ambient during the few seconds of its passage. Surface pressure extremes for various locations and their extreme ranges are given in table 3.1. The data at these locations were mostly taken from their respective surface weather observation summaries (see ref. 3.2 for example). Section V gives extreme pressures across the United States and around the world.

3.3.2.3 Surface Pressure Change

a. A gradual rise or fall in pressure of 3 mb (0.04 lb in^{-2}) and then a return to original pressure can be expected within a 24-h period.

b. A maximum pressure change (frontal passage change) of 6 mb (0.09 lb in^{-2}) (rise or fall) can be expected within a 1-h period at all localities.

Table 3.1 Surface pressure extremes (values apply to station altitude above mean sea level (m.s.l.)).

Location	Units	Pressure			Station Elevation	
		Maximum	Mean	Minimum†	ft	m
Huntsville, AL	$N\ m^{-2}$	102,080.0	99,540.0	97,210.0		
	mb	1,020.8	995.4	972.1	644	196
	$lb\ in^{-2}$	14.8	14.4	14.1		
Kennedy Space Center, FL		103,600.0	101,670.0	99,970.0	16	5
		1,036.0	1,016.7*	999.7		
		15.0	14.7	14.5	9‡	2.7‡
Vandenberg AFB, CA		102,000.0	100,250	99,010.0	371	113
		1,020.0	1,002.5*	990.1		
		14.8	14.5	14.4	368‡	112.2‡
Edwards AFB, CA		95,560.0	93,410.0	92,030.0	2,316	706
		955.6	934.1*	920.3		
		13.9	13.5	13.3	2,302‡	701.7‡
New Orleans, LA		104,160.0	101,780.0	99,900.0		
		1,041.6	1,017.8	999.0	6	2
		15.1	14.8	14.5		
Stennis Space Center, MS		104,410.0	101,640.0	99,150.0		
		1,044.1	1,016.4	991.5	31	9
		15.1	14.7	14.4		
Johnson Space Center, TX		103,960.0	101,530.0	99,530.0		
		1,039.6	1,015.3	995.3	50	15
		15.1	14.7	14.4		
White Sands Missile Range, NM		89,010.0	87,130.0	85,200.0		
		890.1	871.3*	852.0	4,239	1,292
		12.9	12.6	12.4		

* The mean values given here will differ from the median surface values as given in tables 3.10, 3.11, 3.12, and ref. 3.5.

† Hurricane-influenced low pressures are not given here.

‡ Runway elevations above m.s.l..

3.3.2.4 Pressure Decrease With Altitude

a. Pressure decrease is approximately logarithmic with height. Materials transported in mountainous terrain or in cargo compartments of aircraft must be packaged to stand the pressure differential without damage. Near sea level (i.e., <3 km) the pressure will vary about 1 mb for each 10-m change in altitude. Figure 3.1 shows the standard atmospheric pressure decrease up to 5-km altitude (ref. 3.1).

b. More detailed data on pressure distribution with altitude are given in subsection 3.4.2.1.

3.3.3 Atmospheric Mass Density

3.3.3.1 Definition

Mass density (ρ) is the ratio of the mass of a substance to its volume. (It also is defined as the reciprocal of specific volume.) Density is usually expressed in grams per cubic centimeter or kilograms per cubic meter.

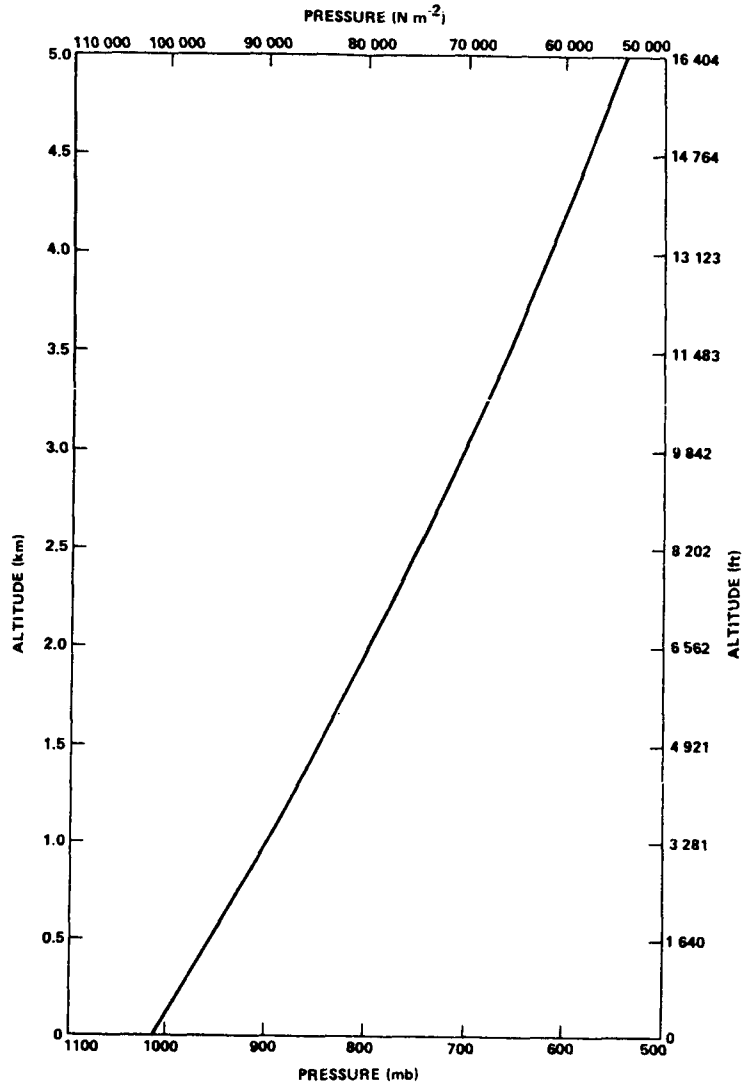

Figure 3.1 Pressure change with altitude for packaging materials (ref. 3.1).

3.3.3.2 Surface Density

Generally the variation of atmospheric density at the Earth's surface between the measured station average and the area of interest (i.e., launch pad, runway, etc.) is small and should have no significant effect on preflight planning and operations. Table 3.2 gives annual median density values at the surface for the four main test ranges.

Atmospheric density, especially low density, is important to aircraft takeoff and landing operations and should therefore be considered when designing runway lengths or planning space shuttle orbiter ferry flights. Table 3.3 gives low density values that are equaled or exceeded approximately 5 percent of the time during the hottest part of the day in summer. Typical associated temperatures needed for engine power calculations are also listed. Since low density is found at high elevation and high temperatures, only the highest enroute airfield and the ferry flight terminals were considered. Since KSC and VAFB density extremes are given in section 3.4.3, only EAFB and Biggs AFB are listed here.

Table 3.2 Annual median surface densities.

Area	Surface Altitude (m*)	Source of Data	Atmospheric Density	
			kg m^{-3}	lb ft^{-3}
Kennedy Space Center, FL	5	(Ref. 3.3)	1.1830	7.385×10^{-2}
Vandenberg AFB, CA	113	(Ref. 3.4)	1.2190	7.610×10^{-2}
White Sands Missile Range, NM	1,292	(Ref. 3.5 Item 5)	1.0580	6.661×10^{-2}
Edwards AFB, CA	706	(Ref. 3.13)	1.1210	6.998×10^{-2}

*Station elevation above m.s.l.

Table 3.3 Low surface density (5 percentile worst day of year reference) and accompanying temperatures for orbiter ferry operations.

Location	Low Density		Temperature	
	kg m^{-3}	Percent Departure* from US 76	°C	°F
Edwards AFB California	1.0246	–10.5	39.4	103
Biggs AFB Texas	0.97555	–10.5	37.8	100

*Departure from U.S. Standard Atmosphere/1976 (3.1).

3.3.3.3 Surface Density Variability and Altitude Variations

Data on the variation of surface density and density aloft about its median annual values can be found in section 3.4. The Global Reference Atmosphere (ref. 3.6) will also provide monthly mean density values versus altitude together with variability for any point on the globe.

3.4 Inflight Atmospheric Thermodynamic Parameters

Median and extreme values of atmospheric temperature, pressure, and density are presented in this subsection for various sites of interest to NASA. References 3.8 and 3.9 give worldwide extremes of the thermodynamic parameters aloft.

3.4.1 Atmospheric Temperature

3.4.1.1 Air Temperature at Altitude

Median and extreme air temperatures for the following list of test ranges were compiled from frequency distributions of radiosonde measured temperature data from 0- through 30-km altitude. Above 30-km altitude, mean and extreme temperatures for the different test ranges were obtained from meteorological rocketsonde observations.

a. KSC air temperature values with altitude are given in table 3.4 (ref. 3.3).

b. VAFB air temperature values with altitude are given in table 3.5 (ref. 3.4).

c. EAFB air temperature values with altitude are given in table 3.6 (ref. 3.5, item 6).

d. WSMR air temperature values with altitude are given in table 3.7 (ref. 3.5, item 5).

Reference 3.10 presents a classic description of the vertical temperature profile characteristics (and the variability of the tropopause level) by altitude, month, and latitude. A comprehensive listing of the extremes of surface temperature for different locations of interest to NASA can be obtained from section IV, table 4.2 of this document.

3.4.1.2 Extreme Cold Temperature

Extreme cold temperatures for nonheated compartments during aircraft flight for KSC, VAFB, WSMR, and EAFB, are given in table 3.8. Hot compartment temperatures are given in section IV, paragraph 4.6.4.

3.4.2 Atmospheric Pressure

3.4.2.1 Atmospheric Pressure at Altitude

Atmospheric pressure extremes which envelope all four locations (KSC, VAFB, WSMR, and EAFB) are given in table 3.9. These values were taken from pressure frequency distributions of radiosonde observations from the four test ranges. Pressure means and extremes were computed above 25-km altitude using meteorological rocketsonde measurements.

Mean and extreme values of station pressure for many locations of interest are given in table 3.1, whereas median pressure values up to 90 km altitude for the four key sites are given in tables 3.10, 3.11, 3.12, and in reference 3.5. The U.S. standard atmosphere pressure decrease with altitude is illustrated in figure 3.1.

3.4.3 Atmospheric Density

3.4.3.1 Atmospheric Density at Altitude

The density of the atmosphere decreases rapidly with height, decreasing to one-half of the surface value at approximately 7-km altitude. Density is also variable at a fixed altitude, with the greatest relative variability occurring at approximately 70-km altitude in the high northern latitudes (60° N.). Other altitudes of maximum density variability occur around 16 km and 0 km. Altitudes of minimum variability occur around 8-, 24-, and 90-km altitude.

Density varies with latitude in each hemisphere, with the mean annual density near the surface increasing toward the poles. In the region around 8-km altitude in the northern hemisphere, for example,

Table 3.4 KSC air temperatures at various altitudes.

Geometric Altitude (km)	Minimum		Median*†		Maximum	
	(°C)	(°F)	(°C)	(°F)	(°C)	(°F)
SFC (0.005 m.s.l.)	-7.2	19	23.5	74	37.2	99
1	-8.9	16	17.4	63	27.8	82
2	-10.0	14	12.2	54	21.1	70
3	-11.1	12	7.1	45	16.1	61
4	-13.9	7	1.8	35	11.1	52
5	-20.0	-4	-4.1	25	5.0	41
6	-26.1	-15	-10.5	13	-1.1	30
7	-33.9	-29	-17.4	1	-7.2	19
8	-41.1	-42	-24.8	-13	-13.9	7
9	-50.0	-58	-32.4	-26	-21.1	-6
10	-56.1	-69	-40.0	-40	-30.0	-22
16.2	-80.0	-112	-70.3	-95	-57.8	-72
20	-76.1	-105	-62.8	-81	-47.8	-54
25	-67.5	-90	-51.4	-61	-38.9	-38
30	-58.9	-74	-42.4	-44	-30.0	-22
35	-47.4	-53	-30.6	-23	-14.6	6
40	-36.7	-34	-17.8	0	1.9	35
45	-23.0	-9	-6.3	21	12.8	55
50	-18.2	-1	-2.5	27	22.0	72
55	-34.4	-30	-12.4	10	18.9	66
60	-28.5	-19	-26.1	-15	17.0	63

* For higher altitudes, see ref. 3.3 and table 3.10 of this report.
† Median values aloft are annual values taken from ref. 3.3.

Table 3.5 VAFB air temperatures at various altitudes.

Geometric Altitude (km)	Minimum		Median*†		Maximum	
	(°C)	(°F)	(°C)	(°F)	(°C)	(°F)
SFC (0.1 m.s.l.)	-3.9	25	12.7	55	37.8	100
1	-3.6	26	13.3	56	33.4	92
2	-7.0	19	10.1	50	28.0	82
3	-15.2	5	5.1	41	17.6	64
4	-22.6	-9	-1.0	30	12.1	54
5	-29.7	-22	-7.5	18	3.3	38
6	-35.6	-32	-14.4	6	-2.7	27
7	-43.3	-46	-21.8	-7	-9.9	14
8	-47.4	-53	-29.5	-21	-15.9	3
9	-51.3	-60	-37.3	-35	-26.8	-16
10	-57.0	-71	-44.6	-48	-31.2	-24
16.3	-76.0	-105	-64.0	-83	-51.0	-60
20	-74.9	-103	-59.8	-76	-49.0	-56
25	-69.3	-93	-51.2	-60	-39.2	-39
30	-63.7	-83	-42.7	-45	-29.4	-21
35	-53.0	-63	-32.1	-26	-5.8	22
40	-42.2	-44	-19.3	-3	17.8	64
45	-30.5	-23	-5.8	21	27.6	82
50	-18.2	-1	-2.0	28	28.0	82
55	-21.8	-7	-6.8	20	31.6	89
60	-25.1	-13	-20.5	-5	35.7	96

* For higher altitudes, see ref. 3.4 and table 3.11.
† Median values aloft are annual values taken from ref. 3.4.

Table 3.6 EAFB air temperatures at various altitudes

Geometric Altitude (km)	Minimum		Median*†		Maximum	
	(°C)	(°F)	(°C)	(°F)	(°C)	(°F)
SFC (0.7 m.s.l.)	-15.6	4	16.1	61	45.0	113
1	-6.0	21	16.2	61	35.3	96
2	-12.9	9	11.2	53	26.2	79
3	-16.9	2	5.1	42	19.0	66
4	-23.4	-10	-1.0	30	10.7	51
5	-29.7	-21	-7.5	17	5.2	41
6	-35.2	-31	-14.4	4	-2.9	27
7	-42.0	-44	-21.8	-9	-12.1	10
8	-48.9	-56	-29.5	-23	-17.4	1
9	-55.0	-67	-37.3	-37	-24.2	-12
10	-58.8	-74	-44.7	-50	-30.8	-23
17.8	-78.0	-108	-64.3	-82	-53.0	-63
20	-73.5	-100	-59.8	-76	-49.6	-57
25	-73.2	-100	-51.2	-62	-40.4	-41
30	-66.1	-87	-42.7	-49	-29.1	-20
35	-54.2	-66	-32.1	-26	-5.7	22
40	-42.2	-44	-19.3	-3	17.8	64
45	-30.5	-23	-5.8	21	27.6	82
50	-18.2	-1	-2.0	28	28.0	82
55	-21.8	-7	-6.8	20	31.6	89
60	-25.1	-13	-20.5	-5	35.7	96

* For higher altitudes, see ref. 3.13 and table 3.12.

† Median values aloft are annual values taken from ref. 3.5, Item 6.

Table 3.7 WSMR air temperatures at various altitudes

Geometric Altitude (km)	Minimum		Median*		Maximum	
	(°C)	(°F)	(°C)	(°F)	(°C)	(°F)
SFC (1.3 m.s.l.)	-25.6	-14	14.6	58	44.4	112
2	-11.7	11	12.7	55	31.1	88
3	-18.9	-2	6.0	43	22.2	72
4	-23.9	-11	-0.8	31	12.8	55
5	-31.1	-24	-7.5	19	6.1	43
6	-36.1	-33	-14.2	6	0.0	32
7	-42.2	-44	-21.1	-6	-7.2	19
8	-48.9	-56	-28.3	-19	-13.9	7
9	-55.0	-67	-35.6	-32	-21.1	-6
10	-60.0	-76	-42.7	-45	-27.2	-17
16.5	-80.0	-112	-66.3	-87	-47.8	-54
20	-77.8	-108	-61.0	-78	-52.2	-62
25	-68.4	-91	-52.2	-62	-39.2	-39
30	-58.9	-74	-44.3	-48	-26.1	-15
35	-52.2	-62	-33.2	-28	-7.8	18
40	-41.8	-43	-19.7	-3	5.0	41
45	-30.5	-23	-7.9	18	19.6	67
50	-29.1	-20	-5.8	22	25.9	79
55	-28.7	-20	-11.7	11	30.2	86
60	-35.8	-32	-19.9	-4	28.0	82
65	-36.5	-34	-30.2	-22	31.3	88

* Median values aloft are annual values taken from ref. 3.5, Item 5.

Table 3.8 Low atmospheric temperature extremes applicable for all locations (KSC, VAFB, WSMR, and EAFB).

Maximum Flight Altitude (Geometric) of Aircraft Used for Transport		Compartment Cold Temperature Extreme	
(m)	(ft)	(°C)	(°F)
3,048	10,000	–25.0	–13
4,572	15,000	–35.0	–31
6,096	20,000	–45.0	–49
7,620	25,000	–50.0	–58
9,144	30,000	–57.0	–71
10,668	35,000	–65.0	–85
12,192	40,000	–70.0	–94
13,716	45,000	–75.0	–103

Table 3.9 Atmospheric pressure-height extremes applicable for all locations (KSC, VAFB, WSMR, and EAFB).

Geometric Altitude (above m.s.l.)		Atmospheric Pressure			
		Maximum		Minimum	
(km)	(ft)	(mb)	(lb in^{-2})	(mb)	(lb in^{-2})
0	0	(Use values in table 3.1 for surface pressure for each station)			
3	9,800	730	10.6	680	9.86
6	19,700	510	7.40	457	6.63
10	32,800	295	4.28	251	3.64
15	49,200	135	1.96	116	1.68
20	65,600	60	8.7×10^{-1}	51	7.4×10^{-1}
25	82,000	30	4.4×10^{-1}	22	3.2×10^{-1}
30	98,400	14.5	2.1×10^{-1}	10.4	1.5×10^{-1}
35	114,800	7.4	1.1×10^{-1}	4.9	7.1×10^{-2}
40	131,200	3.8	5.5×10^{-2}	2.4	3.5×10^{-2}
45	147,600	2.0	2.9×10^{-2}	1.2	1.7×10^{-2}
50	164,000	1.2	1.7×10^{-2}	6.1×10^{-1}	8.8×10^{-3}
55	180,400	6.0×10^{-1}	8.7×10^{-3}	3.1×10^{-1}	4.5×10^{-3}
60	196,800	3.2×10^{-1}	4.6×10^{-3}	1.6×10^{-1}	2.3×10^{-3}
65	213,300	1.7×10^{-1}	2.5×10^{-3}	8.3×10^{-2}	1.2×10^{-3}
70	229,700	8.5×10^{-2}	1.2×10^{-3}	4.1×10^{-2}	5.9×10^{-4}
75	246,100	3.1×10^{-2}	4.5×10^{-4}	2.1×10^{-2}	3.0×10^{-4}
80	262,500	1.4×10^{-2}	2.0×10^{-4}	8.9×10^{-3}	1.3×10^{-4}
85	278,900	5.9×10^{-3}	8.6×10^{-5}	3.7×10^{-3}	5.4×10^{-5}
90	295,300	2.6×10^{-3}	3.8×10^{-5}	1.4×10^{-3}	2.0×10^{-5}

Table 3.10 KSC (Patrick) reference atmosphere (PRA-63) (ref. 3.3).

Geometric Altitude (MSL) Z (km)	Kinetic Temperature T (K)	Virtual Temperature T* (K)	Atmospheric Pressure P (Newtons cm^{-2})	Atmospheric Density D (kg m^{-3})
0	296.68	299.37	1.01701+1	1.18355+0
2	285.33	286.53	8.05212+0	9.79028–1
4	274.92	275.31	6.31517+0	7.99157–1
6	262.68	262.74	4.90089+0	6.49834–1
8	248.34	248.33	3.75320+0	5.26518–1
10	233.14	233.15	2.82776+0	4.22555–1
12	218.82	218.82	2.09093+0	3.33021–1
14	208.16	208.16	1.51990+0	2.54326–1
16	203.04	203.04	1.09118+0	1.87177–1
18	205.30	205.30	7.80974–1	1.32392–1
20	210.35	210.35	5.63157–1	9.31938–2
22	215.37	215.37	4.08992–1	6.61933–2
24	219.81	219.81	2.99188–1	4.74789–2
26	223.45	223.45	2.20382–1	3.43825–2
28	226.44	226.44	1.63274–1	2.51190–2
30	230.79	230.79	1.21463–1	1.83341–2
32	235.32	235.32	9.09051–2	1.34578–2
34	240.07	240.07	6.84299–2	9.93010–3
36	245.04	245.04	5.18072–2	7.36542–3
38	250.16	250.16	3.94480–2	5.49342–3
40	255.31	255.31	3.02092–2	4.12202–3
42	260.28	260.28	2.32624–2	3.11347–3
44	264.82	264.82	1.80045–2	2.36846–3
46	268.59	268.59	1.39948–2	1.81515–3
48	271.19	271.19	1.09106–2	1.40158–3
50	270.61	270.61	8.51802–3	1.09655–3
52	267.31	267.31	6.63932–3	8.65267–4
54	263.13	263.13	5.15531–3	6.82532–4
56	258.26	258.26	3.58521–3	5.37567–4
58	252.87	252.87	3.06511–3	4.22275–4
60	247.10	247.10	2.34420–3	3.30489–4
62	241.11	241.11	1.78185–3	2.57452–4
64	235.00	235.00	1.34542–3	1.99444–4
66	228.89	228.89	1.00864–3	1.53525–4
68	222.84	222.84	7.50591–4	1.17342–4
70	216.91	216.91	5.54143–4	8.89980–5
72	211.14	211.14	4.05760–4	6.69493–5
74	205.51	205.51	2.94587–4	4.99355–5
76	200.02	200.02	2.12002–4	3.69234–5
78	194.60	194.60	1.51198–4	2.70674–5
80	189.15	189.15	1.06843–4	1.96775–5
82	183.56	183.56	7.47938–5	1.41944–5
84	180.65	180.65	5.18782–5	1.00043–5
86	180.65	180.65	3.59147–5	6.92584–6
88	180.65	180.65	2.48690–5	4.79578–6
90	180.65	180.65	1.72244–5	3.32158–6

Table 3.11 VAFB reference atmosphere (VRA-71) (ref. 3.4).

Geometric Altitude (MSL) Z (km)	Kinetic Temperature T (K)	Virtual Temperature T* (K)	Atmospheric Pressure P (Newtons cm^{-2})	Atmospheric Density D (kg m^{-3})
0	285.88	287.15	1.01899+1	1.23618+0
2	283.30	283.59	8.02435+0	9.85756–1
4	272.17	272.35	6.27618+0	8.02762–1
6	258.71	258.79	4.85388+0	6.53426–1
8	243.68	243.70	3.69780+0	5.28600–1
10	228.50	228.50	2.77068+0	4.22426–1
12	217.79	217.79	2.03786+0	3.25934–1
14	212.89	212.89	1.48392+0	2.42845–1
16	209.46	209.46	1.07403+0	1.78628–1
18	210.39	210.39	7.76046–1	1.28512–1
20	213.39	213.39	5.63983–1	9.20191–2
22	217.34	217.34	4.10463–1	6.58104–2
24	220.68	220.68	3.00775–1	4.74989–2
26	223.11	223.11	2.22059–1	3.46574–2
28	226.09	226.09	1.64058–1	2.52891–2
30	230.43	230.43	1.22067–1	1.84539–2
32	234.66	234.66	9.12335–2	1.35440–2
34	238.84	238.84	6.85327–2	9.99594–3
36	243.35	243.35	5.17707–2	7.41121–3
38	248.38	248.38	3.93437–2	5.51828–3
40	253.89	253.89	3.00832–2	4.12777–3
42	259.62	259.62	2.31396–2	3.10498–3
44	265.00	265.00	1.78959–2	2.35255–3
46	269.19	269.19	1.39041–2	1.79938–3
48	270.97	270.97	1.08385–2	1.39342–3
50	271.16	271.16	8.45501–3	1.08625–3
52	270.79	270.79	6.60657–3	8.49939–4
54	268.26	268.26	5.14789–3	6.68511–4
56	264.09	264.09	3.99676–3	5.27219–4
58	258.74	258.74	3.08929–3	4.15944–4
60	252.61	252.61	2.37542–3	3.27585–4
62	246.07	246.07	1.81566–3	2.57051–4
64	239.38	239.38	1.37858–3	2.00620–4
66	232.78	232.78	1.03911–3	1.55505–4
68	226.40	226.40	7.77072–4	1.19570–4
70	220.28	220.28	5.76248–4	9.11308–5
72	214.39	214.39	4.23554–4	6.88241–5
74	208.58	208.58	3.08459–4	5.15182–5
76	202.61	202.61	2.22508–4	3.82588–5
78	196.11	196.11	1.58952–4	2.82366–5
80	188.60	188.60	1.12437–4	2.07684–5
82	180.65	180.65	7.86738–5	1.51716–5
84	180.65	180.65	5.44290–5	1.04962–5
86	180.65	180.65	3.76643–5	7.26323–6
88	180.65	180.65	2.60693–5	5.02723–6
90	180.65	180.65	1.80492–5	3.48063–6

Table 3.12 EAFB reference atmosphere (ERA-75) (ref. 3.13).

Geometric Altitude (MSL) Z (km)	Kinetic Temperature T (K)	Virtual Temperature T* (K)	Atmospheric Pressure P (Newtons cm^{-2})	Atmospheric Density D (kg m^{-3})
0.706	289.27	290.27	9.34079+0	1.12105+0
2	284.35	284.70	8.00722+0	9.79796–1
4	272.17	272.35	6.27618+0	8.02762–1
6	258.71	258.79	4.85388+0	6.53426–1
8	243.68	243.70	3.69780+0	5.28600–1
10	228.50	228.50	2.77068+0	4.22426–1
12	217.79	217.79	2.03786+0	3.25934–1
14	212.89	212.89	1.48392+0	2.42845–1
16	209.46	209.46	1.07403+0	1.78628–1
18	210.39	210.39	7.76046–1	1.28512–1
20	213.39	213.39	5.63983–1	9.20191–2
22	217.34	217.34	4.10463–1	6.58104–2
24	220.68	220.68	3.00775–1	4.74989–2
26	223.11	223.11	2.22059–1	3.46574–2
28	226.09	226.09	1.64058–1	2.52891–2
30	230.43	230.43	1.22067–1	1.84539–2
32	234.66	234.66	9.12335–2	1.35440–2
34	238.84	238.84	6.85327–2	9.99594–3
36	243.35	243.35	5.17785–2	7.41121–3
38	248.38	248.38	3.93437–2	5.51828–3
40	253.89	253.89	3.00832–2	4.12777–3
42	259.62	259.62	2.31396–2	3.10498–3
44	265.00	265.00	1.78959–2	2.35255–3
46	269.19	269.19	1.39041–2	1.79938–3
48	270.97	270.97	1.08385–2	1.39342–3
50	271.16	271.16	8.45501–3	1.08625–3
52	270.79	270.79	6.60657–3	8.49939–4
54	268.26	268.26	5.14789–3	6.68511–4
56	264.09	264.09	3.99676–3	5.27219–4
58	258.74	258.74	3.08929–3	4.15944–4
60	252.61	252.61	2.37542–3	3.27585–4
62	246.07	246.07	1.81565–3	2.57051–4
64	239.38	239.38	1.37858–3	2.00620–4
66	232.78	232.78	1.03911–3	1.55505–4
68	226.40	226.40	7.77072–4	1.19570–4
70	220.28	220.28	5.76248–4	9.11308–5
72	214.39	214.39	4.23554–4	6.88241–5
74	208.58	208.58	3.08459–4	5.15182–5
76	202.61	202.61	2.22508–4	3.82588–5
78	196.11	196.11	1.58952–4	2.82366–5
80	188.60	188.60	1.12437–4	2.07684–5
82	180.65	180.65	7.86738–5	1.51716–5
84	180.65	180.65	5.44290–5	1.04962–5
86	180.65	180.65	3.76643–5	7.26323–6
88	180.65	180.65	2.60693–5	5.02723–6
90	180.65	180.65	1.80492–5	3.48063–6

the density variation with latitude and season is small. Above 8 km to approximately 28 km, the mean annual density decreases toward the north. Mean monthly densities between 30- and 90-km increase toward the north in July and toward the equator in January.

Considerable data are now available on the mean density and its variability below 30 km at the various test ranges from the data collected for preparation of the Range Commanders Council (RCC) Range Reference Atmospheres (ref. 3.5). Additional information on the seasonal variability of density below 30 km is presented in reference 3.14. Above 30 km, the data are less plentiful and the accuracy of the temperature measurements (used to compute some densities) decreases with altitude.

Extreme minimum and maximum values of density for the KSC and VAFB are given in table 3.13. These extreme density values approximate the $\pm 3\sigma$ (corresponding to the normal distribution) density values. The relative deviations of density for KSC and VAFB as given in table 3.13, are, respectively, defined as percentage departures from the Patrick Reference Atmosphere (ref 3.3) and the Vandenberg Reference Atmosphere (ref. 3.4).

Median values of surface density for different locations of interest are given in table 3.2 of this section, and mean values with altitude are given in table 3.10 through 3.12 and in reference 3.5.

3.5 Simultaneous Values of KSC Temperature, Pressure, and Density at Discrete Altitude Levels

3.5.1 Introduction

This subsection presents simultaneous values for temperature, pressure, and density as guidelines for aerospace vehicle design considerations. The necessary assumptions and the lack of sufficient statistical data samples restrict the precision with which these data can currently be presented. The analysis is limited to KSC.

3.5.2 Method of Determining Simultaneous Value

An aerospace vehicle design problem that often arises in considering natural environmental data is stated by the following question: "How should the extremes (maxima and minima) of temperature, pressure, and density be combined (a) at discrete altitude levels? (b) versus altitude?" As an example, suppose one desires to know what temperature and pressure should be used simultaneously with a maximum density at a discrete altitude. From statistical principles set forth by Dr. C.E. Buell in reference 3.15, the solution results by allowing mean density plus three standard deviations to represent maximum density and using the coefficients of variations, correlations, and mean values as expressed in equation (3.1).

$$\text{Maximum } \rho = (\bar{\rho} + 3\sigma_\rho) = \bar{\rho}\left(1+3\frac{\sigma_\rho}{\bar{\rho}}\right) = \bar{\rho}\left\{1+3\left[\underbrace{\left(\frac{\sigma_P}{\bar{P}}\right)r(P\rho)}_{(A)} - \underbrace{\left(\frac{\sigma_T}{\bar{T}}\right)r(\rho T)}_{(B)}\right]\right\}. \tag{3.3}$$

The associated values for pressure and temperature are the last two terms of equation (3.3), (A) and (B), multiplied by $\bar{P}$ and $\bar{T}$, respectively, and then this result is added to $\bar{P}$ and $\bar{T}$, respectively. Appropriate values of correlation coefficients (r) and coefficients of variation (CV) are obtained from table 3.14.

In general, the three extreme ρ, P, and T equations of interest are:

$$\text{extreme } \rho = (\bar{\rho} \pm M\sigma_\rho) = \bar{\rho}\left[1 \pm M\left(\frac{\sigma_\rho}{\bar{\rho}}\right)\right] = \bar{\rho}\left\{1 \pm M\left[\left(\frac{\sigma_P}{\bar{P}}\right)r(P\rho) - \left(\frac{\sigma_T}{\bar{T}}\right)r(\rho T)\right]\right\}, \tag{3.4}$$

Table 3.13 Density height maximum (≈ +3 sigma) and minimum (≈ –3 sigma) for KSC and VAFB.

Altitude*		Kennedy Space Center Density				Vandenberg AFB Density			
		Maximum		Minimum		Maximum		Minimum	
(km)	(ft)	(kg m^{-3})	% Deviation From PRA-63	(kg m^{-3})	% Deviation From PRA-63	(kg m^{-3})	% Deviation From VRA-71	(kg m^{-3})	% Deviation From VRA-71
0	0	1.326	12.0	1.141	–3.6	1.302	5.3	1.140	–7.8
2	6,600	1.047	6.1	9.497×10^{-1}	–3.0	1.046	6.1	9.518×10^{-1}	–3.5
4	13,100	8.287×10^{-1}	3.7	7.824×10^{-1}	–2.1	8.484×10^{-1}	5.7	7.766×10^{-1}	–3.3
6	19,700	6.706×10^{-1}	3.2	6.355×10^{-1}	–2.2	6.906×10^{-1}	5.7	6.299×10^{-1}	–3.6
8	26,200	5.428×10^{-1}	3.1	5.055×10^{-1}	–4.0	5.601×10^{-1}	6.0	4.971×10^{-1}	–6.0
10	32,800	4.352×10^{-1}	3.0	3.938×10^{-1}	–6.8	4.624×10^{-1}	9.5	3.835×10^{-1}	–9.2
15	49,200	2.345×10^{-1}	7.0	1.979×10^{-1}	–9.7	2.337×10^{-1}	12.0	1.851×10^{-1}	–11.3
20	65,600	1.002×10^{-1}	7.5	8.751×10^{-2}	–6.1	1.001×10^{-1}	8.8	8.420×10^{-2}	–8.5
25	82,000	4.274×10^{-2}	5.9	3.790×10^{-2}	–6.1	4.460×10^{-2}	10.0	3.634×10^{-2}	–10.4
30	98,400	1.976×10^{-2}	7.8	1.700×10^{-2}	–7.3	2.085×10^{-2}	13.0	1.634×10^{-2}	–11.5
35	114,800	9.427×10^{-3}	10.3	7.640×10^{-3}	–10.6	9.786×10^{-3}	13.8	7.505×10^{-3}	–12.8
40	131,200	4.637×10^{-3}	12.5	3.512×10^{-3}	–14.8	4.747×10^{-3}	15.0	3.424×10^{-3}	–17.0
50	164,000	1.275×10^{-3}	16.3	8.630×10^{-4}	–21.3	1.325×10^{-3}	22.0	8.473×10^{-4}	–22.0
60	196,800	3.946×10^{-4}	19.4	2.465×10^{-4}	–25.4	4.422×10^{-4}	35.0	2.359×10^{-4}	–28.0
70	229,700	1.100×10^{-4}	23.6	6.666×10^{-5}	–25.1	1.203×10^{-4}	32.0	6.197×10^{-5}	–32.0
80	262,500	2.342×10^{-5}	19.0	1.596×10^{-5}	–18.9	2.617×10^{-5}	26.0	1.433×10^{-5}	–31.0
90	295,300	3.684×10^{-6}	10.9	2.930×10^{-6}	–11.8	4.177×10^{-6}	20.0	2.785×10^{-6}	–20.0

* Geometric altitude above mean sea level.

Table 3.14 Coefficients of variation and discrete altitude level correlation coefficients between pressure-density $r(P\rho)$; pressure-temperature $r(PT)$; and density-temperature $r(\rho T)$, KSC, annual.

Altiitude	Coefficients of Variation (CV)			Correlation Coefficients (r)		
(km)	$\sigma(\rho)/\bar{\rho}$ (percent)	$\sigma(P)/\bar{P}$ (percent)	$\sigma(T)/\bar{T}$ (percent	$r(P\rho)$ (unitless)	$r(PT)$ (unitless)	$r(\rho T)$ (unitless)
0	1.8000	0.6000	1.5000	0.6250	0.3500	–0.9500
1	1.7000	0.5500	1.6000	0.3382	–0.0156	–0.9462
2	1.5000	0.8000	1.5900	0.1508	0.3609	–0.8675
3	1.1800	0.9800	1.5700	–0.0485	0.6606	–0.7818
4	0.9700	0.8500	1.4000	–0.1799	0.7318	–0.8021
5	0.8000	0.8700	1.3400	–0.2864	0.8203	–0.7830
6	0.7400	0.8400	1.2600	–0.2690	0.8246	–0.7666
7	0.8800	0.9800	1.4200	–0.1633	0.7913	–0.7324
8	0.9000	1.1300	1.4700	–0.0364	0.7910	–0.6402
9	1.1800	1.4700	1.6200	0.2678	0.7124	–0.4854
10	1.6300	1.7500	1.7200	0.4840	0.5588	–0.4553
11	1.8800	1.8000	1.7800	0.5328	0.4485	–0.5174
12	2.1500	1.8700	1.8500	0.5841	0.3320	–0.5717
13	2.3800	1.9000	1.8500	0.6470	0.1946	–0.6220
14	2.6200	1.9200	1.7700	0.7373	–0.0066	–0.6804
15	2.7800	1.8800	1.6700	0.8107	–0.2238	–0.7520
16	2.8800	1.8400	1.7100	0.8262	–0.3154	–0.7953
17	2.8800	1.8000	1.7000	0.8338	–0.3537	–0.8113
18	2.7500	1.7500	1.7000	0.8036	–0.2706	–0.7904
19	2.5000	1.7800	1.6700	0.7449	–0.0492	–0.7031
20	2.2700	1.8500	1.6500	0.6969	0.1625	–0.5944
21	2.0800	1.9500	1.6200	0.6786	0.3325	–0.4672
22	1.9800	2.1200	1.5700	0.7087	0.4565	–0.3041
23	1.9200	2.3200	1.4800	0.7721	0.5659	–0.0870
24	1.9500	2.4000	1.4300	0.8032	0.5831	–0.0157
25	2.0000	2.4300	1.4200	0.8116	0.5682	–0.0196
26	2.0800	2.5000	1.5000	0.8006	0.5565	–0.0523
27	2.1500	2.6000	1.5800	0.7948	0.5640	–0.0528
28	2.2300	2.6700	1.7500	0.7591	0.5584	–0.1161
29	2.3700	2.6300	1.8700	0.7249	0.4877	–0.2479
30	2.5200	2.6300	1.9200	0.7228	0.4211	–0.3224
31	2.7000	2.7000	2.0000	0.7257	0.3704	–0.3704
32	2.8800	2.7500	2.0800	0.7279	0.3142	–0.4222
33	3.0700	2.7300	2.1700	0.7260	0.2310	–0.5014
34	3.2700	2.6800	2.2300	0.7361	0.1223	–0.5817
35	3.4800	2.6000	2.3200	0.7454	0.0027	–0.6647
36	3.7000	2.5000	2.4300	0.7587	–0.1263	–0.7421
37	3.9200	2.3700	2.5500	0.7793	–0.2686	–0.8129
38	4.1200	2.4600	2.6300	0.7947	–0.3096	–0.8232
39	4.3300	2.6400	2.6900	0.8084	–0.3199	–0.8163
40	4.5500	2.7900	2.7680	0.8220	–0.3442	–0.8176
41	4.7500	2.8600	3.0200	0.7958	–0.3046	–0.8192
42	4.9300	2.9200	3.2600	0.7712	–0.2706	–0.8215
43	5.1300	3.0000	3.3400	0.7850	–0.3075	–0.8309
44	5.3200	3.1800	3.3500	0.8037	–0.3270	–0.8252
45	5.5000	3.2400	3.6000	0.7797	–0.2912	–0.8261
46	5.6700	3.3200	3.8300	0.7571	–0.2539	–0.8242
47	5.8300	3.4100	3.9800	0.7489	–0.2402	–0.8232
48	5.9800	3.4800	4.1900	0.7284	–0.2090	–0.8223
49	6.1300	3.5900	4.1400	0.7572	–0.2540	–0.8241
50	6.2700	3.6900	4.1900	0.7644	–0.2633	–0.8232
51	6.4200	3.8200	4.0800	0.7984	–0.3201	–0.8260
52	6.5500	3.9100	4.1800	0.7950	–0.3103	–0.8234
53	6.7000	4.0100	4.2700	0.7953	–0.3089	–0.8222
54	6.8000	4.0700	4.3100	0.7990	–0.3164	–0.8232
55	6.9200	4.1400	4.3700	0.8016	–0.3220	–0.8241
56	7.0300	4.2100	4.4200	0.8043	–0.3267	–0.8244
57	7.1500	4.2800	4.4700	0.8081	–0.3351	–0.8258
58	7.2700	4.3600	4.5100	0.8127	–0.3434	–0.8263
59	7.3700	4.4200	4.5400	0.8172	–0.3530	–0.8277
60	7.4700	4.4800	4.5900	0.8188	–0.3565	–0.8283

Table 3.14 Coefficients of variation and discrete altitude level correlation coefficients between pressure-density $r(P\rho)$; pressure-temperature $r(PT)$; and density-temperature $r(\rho T)$, KSC, annual (continued).

Altiitude	Coefficients of Variation (CV)			Correlation Coefficients (r)		
(km)	$\sigma(\rho)/\bar{\rho}$ (percent)	$\sigma(P)/\bar{P}$ (percent)	$\sigma(T)/\bar{T}$ (percent	$r(P\rho)$ (unitless)	$r(PT)$ (unitless)	$r(\rho T)$ (unitless)
61	7.5700	4.5400	4.6300	0.8217	–0.3629	–0.8293
62	7.6500	4.7000	4.8600	0.7926	–0.2805	–0.8076
63	7.7500	4.9000	5.0000	0.7778	–0.2256	–0.7878
64	7.8300	5.1500	5.1500	0.7602	–0.1558	–0.7602
65	7.9000	5.3800	5.3800	0.7342	–0.0781	–0.7342
66	7.9800	5.5700	5.4400	0.7324	–0.0505	–0.7170
67	8.0300	5.6600	5.4700	0.7326	–0.0408	–0.7099
68	8.0700	5.7700	5.4000	0.7437	–0.0429	–0.6998
69	8.1000	5.8200	5.5100	0.7331	–0.0215	–0.6957
70	8.1200	5.8700	5.4900	0.7369	–0.0208	–0.6911
71	8.1200	5.8900	5.4700	0.7392	–0.0205	–0.6885
72	8.0700	5.7900	5.3800	0.7459	–0.0426	–0.6973
73	8.1200	5.6500	5.2900	0.7615	–0.1008	–0.7216
74	8.0700	5.5000	5.1700	0.7733	–0.1432	–0.7383
75	7.9000	5.2900	5.4100	0.7313	–0.0901	–0.7452
76	7.6800	4.9900	5.6500	0.6779	–0.0383	–0.7606
77	7.3800	5.0100	6.1600	0.5628	0.1390	–0.7403
78	7.0500	5.0400	6.5200	0.4587	0.2771	–0.7267
79	6.6800	5.1100	6.8400	0.3508	0.4045	–0.7145
80	6.3200	5.2700	6.7800	0.3265	0.4730	–0.6784
81	5.9500	5.3600	6.7200	0.2975	0.5342	–0.6482
82	5.5800	5.5200	6.6600	0.2800	0.5942	–0.6057
83	5.2500	5.1300	6.6100	0.1891	0.6259	–0.6475
84	4.9200	4.7800	6.5600	0.0855	0.6645	–0.6877
85	4.6300	4.4700	6.5100	–0.0232	0.7032	–0.7272
86	4.4000	4.1900	6.4500	–0.1271	0.7363	–0.7647
87	4.2000	3.9600	6.4000	–0.2296	0.7694	–0.7983
88	4.0200	4.0500	6.3400	–0.2344	0.7874	–0.7838
89	3.8800	4.1400	6.2800	–0.2255	0.7986	–0.7665
90	3.7800	4.0400	5.9600	–0.1608	0.7798	–0.7432

$$\text{extreme } P = (\bar{P} \pm M\sigma_P) = \bar{P}\left[1 \pm M\left(\frac{\sigma_P}{\bar{P}}\right)\right] = \bar{P}\left\{1 \pm M\left[\left(\frac{\sigma_\rho}{\bar{\rho}}\right) r(P\rho) + \left(\frac{\sigma_T}{\bar{T}}\right) r(PT)\right]\right\}, \tag{3.5}$$

$$\text{extreme } T = (\bar{T} \pm M\sigma_T) = \bar{T}\left[1 \pm M\left(\frac{\sigma_T}{\bar{T}}\right)\right] = \bar{T}\left\{1 \pm M\left[\left(\frac{\sigma_P}{\bar{P}}\right) r(PT) - \left(\frac{\sigma_\rho}{\bar{\rho}}\right) r(\rho T)\right]\right\}, \tag{3.6}$$

where M denotes the multiplication factor to give the desired deviation. The values of M for the normal distribution and the associated percentile levels are as follows:

	M		Percentile
Mean	–3	standard deviations	0.135
Mean	–2	standard deviations	2.275
Mean	–1	standard deviations	15.866
Mean	±0	standard deviations = median	50.000
Mean	+1	standard deviations	84.134
Mean	+2	standard deviations	97.725
Mean	+3	standard deviations	99.865

The two associated atmospheric parameters that deal with a third extreme parameter are listed, in more detail, in the following chart.

	For Extreme Density	For Extreme Temperature	For Extreme Pressure
$P_{assoc.} =$	$\bar{P}\left[1 \pm \left\{M\left(\frac{\sigma_P}{\bar{P}}\right) r(P\rho)\right\}\right]$	$\bar{P}\left[1 \pm \left\{M\left(\frac{\sigma_P}{\bar{P}}\right) r(PT)\right\}\right]$	
$T_{assoc.} =$	$\bar{T}\left[1 \pm \left\{M\left(\frac{\sigma_T}{\bar{T}}\right) r(\rho T)\right\}\right]$		$\bar{T}\left[1 \pm \left\{M\left(\frac{\sigma_T}{\bar{T}}\right) r(PT)\right\}\right]$
$\rho_{assoc.} =$		$\bar{\rho}\left[1 \pm \left\{M\left(\frac{\sigma_\rho}{\bar{\rho}}\right) r(\rho T)\right\}\right]$	$\bar{\rho}\left[1 \pm \left\{M\left(\frac{\sigma_\rho}{\bar{\rho}}\right) r(P\rho)\right\}\right]$

Use + sign when extreme parameter is maximum
Use – sign when extreme parameter is minimum.

It must be emphasized that this procedure is to be used at discrete altitudes only. Whenever extreme profiles of pressure, temperature, and density are required for engineering application, the use of these correlated variables at discrete altitudes is not satisfactory. Subsection 3.6 deals directly with this problem, since profiles of only extreme values of pressure, temperature, or density from 0 to 90 km altitude is unrealistic in the real atmosphere.

3.6 Extreme Hot and Cold Atmospheric Profiles for KSC, VAFB, and EAFB

Given in this section are the two extreme density profiles that correspond to the summer (hot) and winter (cold) extreme atmospheres for KSC (tables 3.15A and 3.15B); VAFB (tables 3.16A and 3.16B); and EAFB (tables 3.17A and 3.17B)(see refs. 3.12 and 3.13 for detailed information pertaining to the VAFB and EAFB extreme atmospheres, respectively). Associated values of extreme temperature and pressure versus altitude are also tabulated. These extreme atmospheric profiles should be used in ascent design analyses at all altitudes. For reentry studies they are to apply only from 30 km to the surface for vehicles to be used at KSC, VAFB, or EAFB. For those aerospace vehicles with ferrying capability, design calculations should use these extreme profiles in conjunction with the hot or cold day design ambient air temperatures over runways from paragraph 5.1.3.1 of section V. The extreme atmosphere producing the maximum vehicle design requirement should be utilized to determine the design.

The envelopes of density deviations given in table 3.13 imply that a typical individual extreme density profile may be represented by a similarly shaped profile; that is, deviations of density are either all negative or all positive from sea level to 90-km altitude. However, examination of many individual density profiles shows that when large positive deviations of density occur at the surface, correspondingly large negative deviations will occur near 15-km altitude and above. Such a situation occurs during the winter season (cold atmosphere). The reverse is also true—density profiles with large negative deviations at lower levels will have correspondingly large positive deviations at higher levels. This situation occurs in the summer season (hot atmosphere) (figs. 3.2, 3.3, and 3.4).

The two extreme KSC density profiles of figure 3.2 are shown as percent deviations from the Patrick Reference Atmosphere, 1963 density profile (ref. 3.3). The two profiles obey the hydrostatic equation and the ideal gas law. The extreme density profiles shown up to 30-km altitude were observed in the atmosphere. The results shown above 30-km altitude are somewhat speculative because of the limited data from this region of the atmosphere. Quasi-isopycnic levels (levels of minimum density variation) are noted at approximately 8 and 86 km. Another level of minimum density variability is seen at 24 km, and levels of maximum variability occur at 0-, 15-, and 68-km altitude. The associated extreme virtual temperature profiles for KSC are given in figure 3.5.

Table 3.15A KSC summer (hot) atmosphere (KHA-71).

Geometric Altitude (MSL) km	Kinetic Temperature T (K)	Virtual Temperature T* (K)	Atmospheric Pressure P (N cm^{-2})	Atmospheric Density D (kg m^{-3})	Rel. Dev. (T*) Percent From PRA-63 RD (T*) %	Rel. Dev. (P) Percent From PRA-63 RD (P) %	Rel. Dev. (D) Percent From PRA-63 RD (D) %
0	307.40	309.90	1.01000+1	1.13537+0	3.5	–0.7	–4.1
2	294.70	296.37	8.06143+0	9.47571–1	3.4	0.1	–3.2
4	282.00	282.85	6.36690+0	7.84181–1	2.7	0.8	–1.9
6	269.32	269.32	4.97073+0	6.42972–1	2.5	1.4	–1.1
8	255.79	255.79	3.83152+0	5.21824–1	3.0	2.1	–0.9
10	242.26	242.26	2.91191+0	4.18724–1	3.9	3.0	–0.9
12	228.20	228.20	2.17801+0	3.32493–1	4.3	4.2	–0.2
14	213.60	213.60	1.59836+0	2.60682–1	2.6	5.2	2.5
16	199.00	199.00	1.14755+0	2.00889–1	–2.0	5.2	7.3
18	200.00	200.00	8.13695–1	1.41732–1	–2.6	4.2	7.1
20	208.33	208.33	5.82229–1	9.73585–2	–1.0	3.4	4.5
22	215.67	215.67	4.22016–1	6.81728–2	0.1	3.2	3.0
24	222.00	222.00	3.08751–1	4.84476–2	1.0	3.2	2.1
26	228.33	228.33	2.27940–1	3.47755–2	2.2	3.4	1.2
28	234.67	234.67	1.69726–1	2.51992–2	3.8	3.9	0.3
30	241.00	241.00	1.27321–1	1.84051–2	4.4	4.8	0.4
32	247.33	247.33	9.61987–2	1.35465–2	5.1	5.9	0.7
34	253.67	253.67	7.32790–2	1.00657–2	5.7	7.1	1.3
36	260.00	260.00	5.61455–2	7.52274–3	6.1	8.4	2.1
38	265.77	265.77	4.32945–2	5.67493–3	6.2	9.8	3.3
40	271.54	271.54	3.35705–2	4.30688–3	6.4	11.1	4.5
42	277.31	277.31	2.61721–2	3.28794–3	6.5	12.5	5.8
44	283.08	283.08	2.05077–2	2.52378–3	6.9	13.9	6.6
46	288.85	288.85	1.61481–2	1.94746–3	7.5	15.4	7.3
48	294.62	294.62	1.27777–2	1.51091–3	8.6	17.1	7.8
50	297.50	297.50	1.01482–2	1.18840–3	9.9	19.2	8.4
52	289.00	289.00	8.03999–3	9.69103–4	8.1	21.1	12.0
54	280.50	280.50	6.32437–3	7.85430–4	6.6	22.9	15.1
56	272.00	272.00	4.93788–3	6.32455–4	5.3	23.9	17.7
58	263.50	263.50	3.82537–3	5.05788–4	4.2	24.8	19.8
60	255.00	255.00	2.93909–3	4.01549–4	3.2	25.4	21.5
62	246.50	246.50	2.23836–3	3.16317–4	2.2	25.8	22.9
64	238.00	238.00	1.68846–3	2.47098–4	1.3	25.5	23 9
66	229.50	229.50	1.26059–3	1.91294–4	0.3	24.9	24.6
68	221.00	221.00	9.30524–4	1.46662–4	–0.8	24.0	25.0
70	212.50	212.50	6.78561–4	1.11268–4	–2.0	22.5	25.0
72	204.00	204.00	4.88448–4	8.34696–5	–3.4	20.5	24.7
74	195.50	195.50	3.47004–4	6.18641–5	–4.9	17.9	23.9
76	187.00	187.00	2.43192–4	4.52595–5	–6.5	14.6	22.6
78	178.50	178.50	1.67780–4	3.26383–5	–8.3	10.5	20.5
80	170.00	170.00	1.12901–4	2.31514–5	–10.1	5.7	17.6
82	170.00	170.00	7.55119–5	1.55048–5	–7.4	1.0	9.1
84	170.00	170.00	5.06592–5	1.03855–5	–5.9	–2.6	3.5
86	170.00	170.00	3.39222–5	6.97136–6	–5.9	–5.9	0.0
88	170.00	170.00	2.27356–5	4.67110–6	–5.9	–9.1	–3.4
90	170.00	170.00	1.51348–5	3.10707–6	–5.9	–12.2	–6.6

Table 3.15B KSC winter (cold) atmosphere (KCA-71).

Geometric Altitude (MSL) km	Kinetic Temperature T (K)	Virtual Temperature T* (K)	Atmospheric Pressure P (N cm^{-2})	Atmospheric Density D (kg m^{-3})	Rel. Dev. (T*) Percent From PRA-63 RD (T*) %	Rel. Dev. (P) Percent From PRA-63 RD (P) %	Rel. Dev. (D) Percent From PRA-63 RD (D) %
0	274.50	275.00	1.02700+1	1.30099+0	–8.1	1.0	9.9
2	264.70	265.00	7.97353+0	1.04820+0	–7.5	–1.0	7.1
4	254.90	255.00	6.13058+0	8.37528–1	–7.4	–2.8	4.8
6	245.24	245.24	4.66465+0	6.62784–1	–6.7	–4.8	2.0
8	235.87	235.87	3.51072+0	5.18423–1	–5.0	–6.5	–1.6
10	227.67	227.67	2.61414+0	4.00022–1	–2.4	–7.6	–5.3
12	220.59	220.59	1.92692+0	3.04362–1	0.8	–7.9	–8.6
14	214.29	214.29	1.40710+0	2.28093–1	3.0	–7.4	–10.1
16	209.49	209.49	1.01913+0	1.69535–1	3.1	–6.6	–9.5
18	208.28	208.28	7.34536–1	1.22832–1	1.4	–6.0	–7.2
20	209.00	209.00	5.29299–1	8.82292–2	–0.6	–6.0	–5.3
22	210.91	210.91	3.82184–1	6.31426–2	–2.1	–6.5	–4.6
24	213.63	213.63	2.77005–1	4.51690–2	–2.8	–7.4	–4.9
26	216.78	216.78	2.01682–1	3.23964–2	–3.0	–8.5	–5.8
28	220.08	220.08	1.47487–1	2.33454–2	–2.3	–9.7	–7.0
30	223.31	223.31	1.08321–1	1.69107–2	–3.2	–10.8	–7.9
32	226.44	226.44	7.99577–2	1.23019–2	–3.8	–12.0	–8.6
34	229.60	229.60	5.93149–2	8.98540–3	–4.3	–13.4	–9.5
36	233.84	233.84	4.41165–2	6.57245–3	–4.6	–14.9	–10.8
38	239.02	239.02	3.30396–2	4.81532–3	–4.5	–16.2	–12.3
40	244.20	244.20	2.49012–2	3.55236–3	–4.4	–17.6	–13.8
42	249.38	249.38	1.88809–2	2.63764–3	–4.2	–18.8	–15.3
44	254.55	254.55	1.43942–2	1.96985–3	–3.9	–20.1	–16.8
46	259.73	259.73	1.10347–2	1.47978–3	–3.3	–21.2	–18.5
48	264.91	264.91	8.50858–3	1.11871–3	–2.3	–22.1	–20.2
50	267.50	267.50	6.58344–3	8.57370–4	–1.2	–22.7	–21.8
52	267.50	267.50	5.09811–3	6.63959–4	0.1	–23.2	–23.3
54	264.64	264.64	3.94567–3	5.19359–4	0.6	–23.5	–23.9
56	261.79	261.79	3.04283–3	4.04911–4	1.4	–23.7	–24.7
58	258.93	258.93	2.33950–3	3.14785–4	2.4	–23.7	–25.4
60	256.07	256.07	1.79403–3	2.44083–4	3.6	–23.4	–26.1
62	253.21	253.21	1.37225–3	1.88792–4	5.0	–23.0	–26.7
64	250.36	250.36	1.04675–3	1.45631–4	6.5	–22.2	–27.0
66	247.50	247.50	7.95920–4	1.11993–4	8.1	–21.2	–27.1
68	244.64	244.64	6.02732–4	8.58059–5	9.8	–19.8	–26.9
70	241.79	241.79	4.54550–4	6.54950–5	11.5	–17.9	–26.4
72	238.93	238.93	3.41463–4	4.98157–5	13.2	–15.7	–25.5
74	236.07	236.07	2.56128–4	3.78041–5	14.9	–12.9	–24.2
76	233.21	233.21	1.92122–4	2.86884–5	16.6	–9.5	–22.4
78	230.36	230.36	1.43852–4	2.17018–5	18.4	–5.5	–20.2
80	227.50	227.50	1.05991–4	1.62312–5	20.3	–0.8	–17.5
82	221.00	221.00	7.81453–5	1.23199–5	20.4	4.5	–13.2
84	214.50	214.50	5.71060–5	9.27639–6	18.7	10.1	–7.3
86	208.00	208.00	4.13394–5	6.92224–6	15.1	15.1	–0.1
88	201.50	201.50	2.96044–5	5.11897–6	11.5	19.0	6.7
90	195.00	195.00	2.09474–5	3.74532–6	7.9	21.7	12.8

Table 3.16A VAFB summer (hot) atmosphere (VHA-73) (ref. 3.12).

Geometric Altitude (MSL) km	Kinetic Temperature T (K)	Virtual Temperature T* (K)	Atmospheric Pressure P (N cm^{-2})	Atmospheric Density D (kg m^{-3})	Rel. Dev. (T*) Percent From VRA-71 RD (T*) %	Rel. Dev. (P) Percent From VRA-71 RD (P) %	Rel. Dev. (D) Percent From VRA-71 RD (D) %
0	310.40	312.70	1.01000+1	1.12520+0	8.9	–0.9	–9.0
2	296.80	298.59	8.07642+0	9.42286–1	5.3	0.7	–4.4
4	283.20	284.48	6.38872+0	7.82355–1	4.5	1.8	–2.5
6	269.60	270.37	4.99378+0	6.43448–1	4.5	2.9	–1.5
8	256.00	256.26	3.85219+0	5.23688–1	5.2	4.2	–0.9
10	240.53	240.53	2.92684+0	4.23899–1	5.3	5.6	0.4
12	223.20	223.20	2.17953+0	3.40178–1	2.5	7.0	4.4
14	205.87	205.87	1.58478+0	2.68177–1	–3.3	6.8	10.4
16	195.70	195.70	1.12412+0	2.00106–1	–6.6	4.7	12.0
18	200.74	200.74	7.95730–1	1.38101–1	–4.6	2.5	7.4
20	207.82	207.82	5.69371–1	9.54397–2	–2.6	1.0	3.7
22	214.89	214.89	4.12139–1	6.68144–2	–1.1	0.4	1.5
24	221.97	221.97	3.01463–1	4.73175–2	0.6	0.2	–0.4
26	229.05	229.05	2.22578–1	3.38482–2	2.7	0.3	–2.3
28	236.12	236.12	1.65959–1	2.44859–2	4.4	1.2	–3.2
30	243.20	243.20	1.24774–1	1.78725–2	5.5	2.2	–3.1
32	249.44	249.44	9.45606–2	1.32071–2	6.3	3.6	–2.5
34	255.67	255.67	7.21309–2	9.82767–3	7.1	5.3	–1.7
36	261.91	261.91	5.53982–2	7.36860–3	7.6	7.0	–0.6
38	268.14	268.14	4.28172–2	5.56344–3	8.0	8.8	0.8
40	274.38	274.38	3.32792–2	4.22565–3	8.1	10.6	2.4
42	280.61	280.61	2.60056–2	3.22793–3	8.1	12.4	4.0
44	286.85	286.85	2.04445–2	2.48289–3	8.2	14.3	5.6
46	293.08	293.08	1.61641–2	1.92235–3	8.9	16.2	6.7
48	296.20	296.20	1.28182–2	1.50758–3	9.3	18.3	8.2
50	296.20	296.20	1.01776–2	1.19701–3	9.2	20.4	10.2
52	296.20	296.20	8.08051–3	9.50404–4	9.4	22.3	11.8
54	287.91	287.91	6.39556–3	7.73812–4	7.3	24.2	15.8
56	279.63	279.63	5.02673–3	6.26232–4	5.9	25.8	18.8
58	271.34	271.34	3.92216–3	5.03576–4	4.9	27.0	21.1
60	263.06	263.06	3.03703–3	4.02224–4	4.1	27.9	22.8
62	254.77	254.77	2.33271–3	3.18976–4	3.5	28.5	24.1
64	246.49	246.49	1.77625–3	2.51029–4	3.0	28.8	25.1
66	238.20	238.20	1.34000–3	1.95943–4	2.3	28.9	26.0
68	229.91	229.91	1.00067–3	1.51604–4	1.6	28.8	26.8
70	221.63	221.63	7.39117–4	1.16191–4	0.6	28.3	27.5
72	213.34	213.34	5.39672–4	8.81491–5	–0.5	27.5	28.1
74	205.06	205.06	3.89199–4	6.61538–5	–1.7	26.3	28.4
76	196.77	196.77	2.77271–4	4.90758–5	–2.9	24.6	28.3
78	188.49	188.49	1.94712–4	3.59435–5	–3.9	22.3	27.2
80	180.20	180.20	1.34206–4	2.59447–5	–4.5	19.3	24.9
82	180.20	180.20	9.18913–5	1.77441–5	–0.3	16.7	17.0
84	180.20	180.20	6.29807–5	1.21765–5	–0.3	15.5	15.8
86	180.20	180.20	4.31919–5	8.33893–6	–0.3	14.2	14.5
88	180.20	180.20	2.96783–5	5.71060–6	–0.3	12.9	13.2
90	180.20	180.20	2.01511–5	3.90816–6	–0.3	11.7	11.9

Table 3.16B VAFB winter (cold) atmosphere (VCA-73) (ref. 3.12).

Geometric Altitude (MSL) km	Kinetic Temperature T (K)	Virtual Temperature T* (K)	Atmospheric Pressure P (N cm^{-2})	Atmospheric Density D (kg m^{-3})	Rel. Dev. (T*) Percent From VRA-71 RD (T*) %	Rel. Dev. (P) Percent From VRA-71 RD (P) %	Rel. Dev. (D) Percent From VRA-71 RD (D) %
0	272.10	272.70	1.01800+1	1.30047+0	-5.0	-0.1	5.2
2	260.86	261.22	7.88092+0	1.05101+0	-7.9	-1.8	6.6
4	249.62	249.74	6.03127+0	8.41315-1	-8.3	-3.9	4.8
6	238.30	238.30	4.55804+0	6.66334-1	-7.9	-6.1	2.0
8	226.90	226.90	3.39765+0	5.21654-1	-6.9	-8.1	-1.3
10	220.87	220.87	2.49937+0	3.94219-1	-3.3	-9.8	-6.7
12	220.20	220.20	1.83347+0	2.90065-1	1.1	-10.0	-11.0
14	219.53	219.53	1.34374+0	2.13232-1	3.1	-9.5	-12.2
16	218.87	218.87	9.83871-1	1.56602-1	4.5	-8.4	-12.3
18	218.20	218.20	7.19692-1	1.14902-1	3.7	-7.3	-10.6
20	219.20	219.20	5.26594-1	8.36900-2	2.7	-6.6	-9.1
22	220.20	220.20	3.85822-1	6.10388-2	1.3	-6.0	-7.3
24	221.20	221.20	2.83123-1	4.45893-2	0.2	-5.9	-6.1
26	222.20	222.20	2.08033-1	3.26157-2	-0.4	-6.3	-5.9
28	223.20	223.20	1.53042-1	2.38865-2	-1.3	-6.7	-5.5
30	224.20	224.20	1.12781-1	1.75244-2	-2.7	-7.6	-5.0
32	225.20	225.20	8.32025-2	1.28706-2	-4.0	-8.8	-5.0
34	229.60	229.60	6.16129-2	9.34844-3	-3.9	-10.1	-6.5
36	234.00	234.00	4.58777-2	6.82981-3	-3.8	-11.4	-7.8
38	238.40	238.40	3.43580-2	5.02066-3	-4.0	-12.7	-9.0
40	242.80	242.80	2.58661-2	3.71133-3	-4.4	-14.0	-10.1
42	247.20	247.20	1.95663-2	2.75710-3	-4.8	-15.4	-11.2
44	251.60	251.60	1.48762-2	2.05959-3	-5.1	-16.9	-12.4
46	256.00	256.00	1.13715-2	1.54768-3	-4.9	-18.3	-14.0
48	258.20	258.20	8.71913-3	1.17640-3	-4.7	-19.6	-15.6
50	258.20	258.20	6.69192-3	9.02894-4	-4.8	-20.9	-16.9
52	258.20	258.20	5.13323-3	6.92657-4	-4.7	-22.3	-18.5
54	255.43	255.43	3.93843-3	5.37093-4	-4.8	-23.5	-19.7
56	252.65	252.65	3.00886-3	4.14851-4	-4.3	-24.7	-21.3
58	249.88	249.88	2.29069-3	3.19393-4	-3.4	-25.8	-23.2
60	247.10	247.10	1.73914-3	2.45237-4	-2.2	-26.7	-25.1
62	244.33	244.33	1.31731-3	1.87851-4	-0.7	-27.4	-26.9
64	241.55	241.55	9.95395-4	1.43540-4	0.9	-27.8	-28.5
66	238.78	238.78	7.50022-4	1.09377-4	2.6	-28.0	-29.8
68	236.01	236.01	5.62873-4	8.30355-5	4.2	-27.8	-30.7
70	233.23	233.23	4.20198-4	6.27451-5	5.9	-27.2	-31.2
72	230.46	230.46	3.11980-4	4.71759-5	7.5	-26.2	-31.4
74	227.68	227.68	2.30470-4	3.53189-5	9.2	-24.8	-31.1
76	224.91	224.91	1.70264-4	2.64292-5	11.0	-22.9	-30.6
78	222.14	222.14	1.26467-4	1.98240-5	13.3	-20.5	-29.9
80	219.36	219.36	9.43661-5	1.49002-5	16.3	-17.6	-29.1
82	216.59	216.59	6.84452-5	1.09730-5	19.9	-13.9	-28.2
84	215.20	215.20	4.93374-5	7.98684-6	19.1	-9.4	-23.9
86	215.20	215.20	3.59130-5	5.81396-6	19.1	-4.6	-20.0
88	215.20	215.20	2.61438-5	4.23253-6	19.1	0.3	-15.8
90	215.20	215.20	1.90330-5	3.08138-6	19.1	5.5	-11.5

Table 3.17A EAFB summer (hot) atmosphere (EHA-75) (ref. 3.13).

Geometric Altitude (MSL) km	Kinetic Temperature T (K)	Virtual Temperature T* (K)	Atmospheric Pressure P (N cm^{-2})	Atmospheric Density D (kg m^{-3})	Rel. Dev. (T*) Percent From ERA-75 RD (T*) %	Rel. Dev. (P) Percent From ERA-75 RD (P) %	Rel. Dev. (D) Percent From ERA-75 RD (D) %
0.7	316.45	318.05	9.29000+0	1.01756+0	9.6	-0.5	-9.2
2	300.67	301.46	8.04214+0	9.29341-1	5.9	0.4	-5.2
4	284.48	285.00	6.37015+0	7.78659-1	4.7	1.5	-3.0
6	268.92	269.16	4.97668+0	6.44131-1	4.0	2.5	-1.4
8	254.92	254.92	3.83393+0	5.23930-1	4.6	3.7	-0.9
10	241.23	241.23	2.91079+0	4.20355-1	5.6	5.1	-0.5
12	227.04	227.04	2.17387+0	3.33561-1	4.3	6.7	2.3
14	212.84	212.84	1.59320+0	2.60764-1	-0.0	7.4	7.4
16	198.65	198.65	1.14285+0	2.00419-1	-5.2	6.4	12.2
18	207.65	207.65	8.16392-1	1.36963-1	-1.3	5.2	6.6
20	214.23	214.23	5.91070-1	9.61192-2	0.4	4.8	4.5
22	218.38	218.38	4.30924-1	6.87411-2	0.5	5.0	4.5
24	222.53	222.53	3.16101-1	4.94846-2	0.8	5.1	4.2
26	226.69	226.69	2.33206-1	3.58394-2	1.6	5.0	3.4
28	230.84	230.84	1.72959-1	2.61005-2	2.1	5.4	3.2
30	235.00	235.00	1.29000-1	1.91239-2	2.0	5.7	3.6
32	239.15	239.15	9.66936-2	1.40849-2	1.9	6.0	4.0
34	246.76	246.76	7.29929-2	1.03052-2	3.3	6.5	3.1
36	254.36	254.36	5.55635-2	7.60930-3	4.5	7.3	2.7
38	261.97	261.97	4.26481-2	5.67157-3	5.5	8.4	2.8
40	269.58	269.58	3.29812-2	4.26250-3	6.2	9.6	3.2
42	277.18	277.18	2.56820-2	3.22755-3	6.8	11.0	4.0
44	284.79	284.79	2.01373-2	2.46297-3	7.5	12.5	4.7
46	292.40	292.40	1.58997-2	1.89494-3	8.6	14.3	5.2
48	296.20	296.20	1.26103-2	1.48314-3	9.3	16.4	6.4
50	296.20	296.20	1.00125-2	1.17761-3	9.2	18.4	8.4
52	296.20	296.20	7.94989-3	9.35009-4	9.4	20.3	10.0
54	287.91	287.91	6.29186-3	7.61269-4	7.3	22.2	13.9
56	279.63	279.63	4.94523-3	6.16080-4	5.9	23.7	16.9
58	271.34	271.34	3.85861-3	4.95412-4	4.9	24.9	19.1
60	263.06	263.06	2.98778-3	3.95703-4	4.1	25.8	20.8
62	254.77	254.77	2.29489-3	3.13804-4	3.5	26.4	22.1
64	246.49	246.49	1.74742-3	2.46960-4	3.0	26.8	23.1
66	238.20	238.20	1.31829-3	1.92767-4	2.3	26.8	24.0
68	229.91	229.91	9.84449-4	1.49145-4	1.6	26.7	24.7
70	221.63	221.63	7.27181-4	1.14307-4	0.6	26.2	25.4
72	213.34	213.34	5.30913-4	8.67226-5	-0.5	25.4	26.0
74	205.06	205.06	3.82895-4	6.50828-5	-1.7	24.2	26.3
76	196.77	196.77	2.72746-4	4.82824-5	-2.9	22.5	26.2
78	188.49	188.49	1.91569-4	3.53618-5	-3.9	20.3	25.2
80	180.20	180.20	1.32041-4	2.55060-5	-4.5	17.4	22.9
82	180.20	180.20	9.02891-5	1.74789-5	-0.3	14.8	15.1
84	180.20	180.20	6.19698-5	1.19743-5	-0.3	13.6	13.9
86	180.20	180.20	4.23431-5	8.20160-6	-0.3	12.4	12.6
88	180.20	180.20	2.90775-5	5.62477-6	-0.3	11.1	11.4
90	180.20	180.20	1.98078-5	3.84521-6	-0.3	9.8	10.1

Table 3.17B EAFB winter (cold) atmosphere (ECA-75) (ref. 3.13).

Geometric Altitude (MSL) km	Kinetic Temperature T (K)	Virtual Temperature T* (K)	Atmospheric Pressure P (N cm^{-2})	Atmospheric Density D (kg m^{-3})	Rel. Dev. (T*) Percent From ERA-75 RD (T*) %	Rel. Dev. (P) Percent From ERA-75 RD (P) %	Rel. Dev. (D) Percent From ERA-75 RD (D) %
0.7	273.15	273.65	9.39000+0	1.19539+0	-5.7	0.5	6.6
2	264.71	265.06	7.96264+0	1.04652+0	-6.9	-0.6	6.8
4	251.67	251.79	6.11233+0	8.45689-1	-7.6	-2.6	5.4
6	239.65	239.65	4.62679+0	6.72573-1	-7.4	-4.7	2.9
8	228.65	228.65	3.45563+0	5.26494-1	-6.2	-6.6	-0.4
10	222.48	222.48	2.54834+0	3.99023-1	-2.6	-8.0	-5.5
12	221.15	221.15	1.87275+0	2.95006-1	1.5	-8.1	-9.5
14	219.82	219.82	1.37372+0	2.17708-1	3.3	-7.4	-10.4
16	218.48	218.48	1.00575+0	1.60365-1	4.3	-6.4	-10.2
18	217.15	217.15	7.34954-1	1.17907-1	3.2	-5.3	-8.3
20	217.48	217.48	5.36679-1	8.59659-2	1.9	-4.8	-6.6
22	217.82	217.82	3.92083-1	6.27082-2	0.2	-4.5	-4.7
24	218.15	218.15	2.86583-1	4.57648-2	-1.2	-4.7	-3.7
26	219.91	219.91	2.09783-1	3.32322-2	-1.4	-5.5	-4.1
28	221.68	221.68	1.53949-1	2.41935-2	-2.0	-6.2	-4.3
30	223.44	223.44	1.13252-1	1.76572-2	-3.0	-7.2	-4.3
32	225.20	225.20	8.35144-2	1.29190-2	-4.0	-8.5	-4.6
34	229.60	229.60	6.18410-2	9.38307-3	-3.9	-9.8	-6.1
36	234.00	234.00	4.60475-2	6.85513-3	-3.8	-11.1	-7.5
38	238.40	238.40	3.44851-2	5.03925-3	-4.0	-12.4	-8.7
40	242.80	242.80	2.59613-2	3.72509-3	-4.4	-13.7	-9.8
42	247.20	247.20	1.96382-2	2.76744-3	-4.8	-15.1	-10.9
44	251.60	251.60	1.49321-2	2.06726-3	-5.1	-16.6	-12.1
46	256.00	256.00	1.14139-2	1.55352-3	-4.9	-17.9	-13.7
48	258.20	258.20	8.75152-3	1.18076-3	-4.7	-19.3	-15.3
50	258.20	258.20	6.71674-3	9.06220-4	-4.8	-20.6	-16.6
52	258.20	258.20	5.15508-3	6.95519-4	-4.7	-22.0	-18.2
54	255.43	255.43	3.95301-3	5.39081-4	-4.8	-23.3	-19.4
56	252.65	252.65	3.01997-3	4.16381-4	-4.3	-24.5	-21.0
58	249.88	249.88	2.29916-3	3.20568-4	-3.4	-25.5	-22.9
60	247.10	247.10	1.74555-3	2.46135-4	-2.2	-26.4	-24.8
62	244.33	244.33	1.32215-3	1.88541-4	-0.7	-27.1	-26.6
64	241.55	241.55	9.99067-4	1.44072-4	0.9	-27.6	-28.2
66	238.78	238.78	7.52785-4	1.09777-4	2.6	-27.7	-29.5
68	236.01	236.01	5.64923-4	8.33397-5	4.2	-27.5	-30.4
70	233.23	233.23	4.21743-4	6.29730-5	5.9	-26.9	-31.0
72	230.46	230.46	3.13067-4	4.73404-5	7.5	-26.0	-31.1
74	227.68	227.68	2.31276-4	3.54486-5	9.2	-24.6	-30.9
76	224.91	224.91	1.70860-4	2.65102-5	11.0	-22.7	-30.3
78	222.14	222.14	1.26944-4	1.98898-5	13.3	-20.3	-29.6
80	219.36	219.36	9.46903-5	1.49574-5	16.3	-17.3	-28.9
82	216.59	216.59	6.87218-5	1.10025-5	19.9	-13.6	-27.9
84	215.20	215.20	4.95183-5	8.01647-6	19.1	-9.0	-23.6
86	215.20	215.20	3.60456-5	5.83524-6	19.1	-4.3	-19.7
88	215.20	215.20	2.62412-5	4.24784-6	19.1	0.7	-15.5
90	215.20	215.20	1.91021-5	3.09271-6	19.1	5.8	-11.2

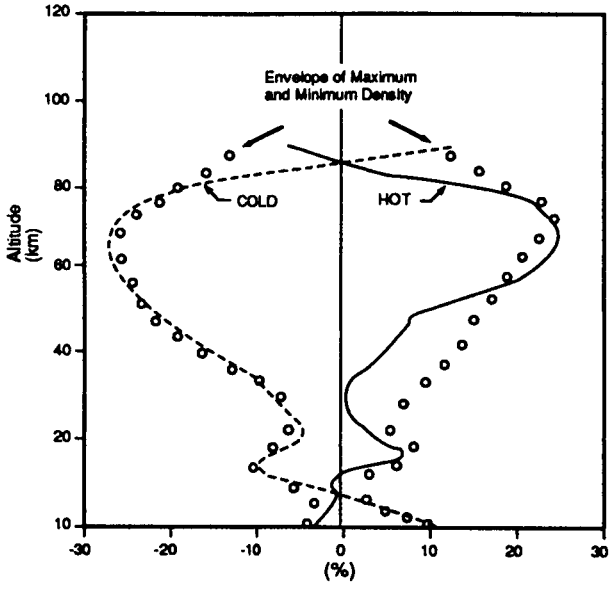

Figure 3.2 Relative deviations (%) of extreme KSC density profiles with respect to PRA-63.

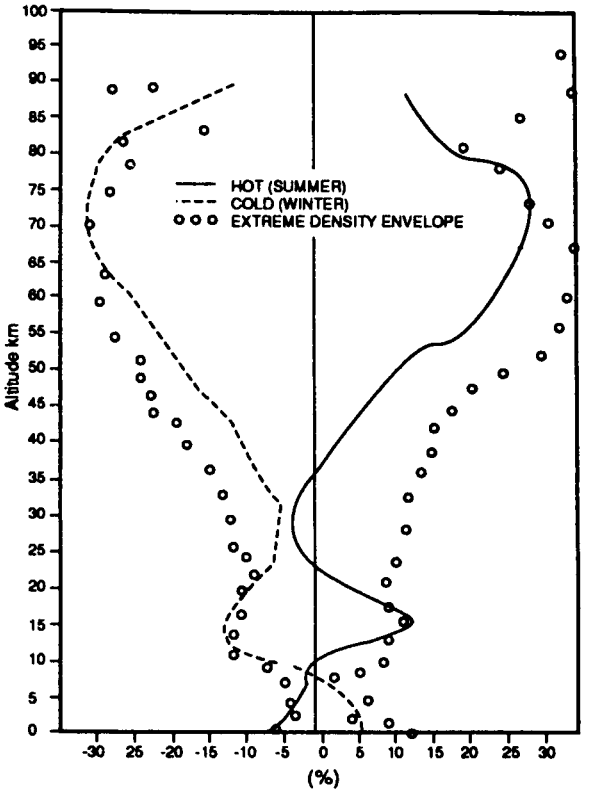

Figure 3.3 Relative deviations (%) of extreme VAFB density profiles with respect to VRA-71.

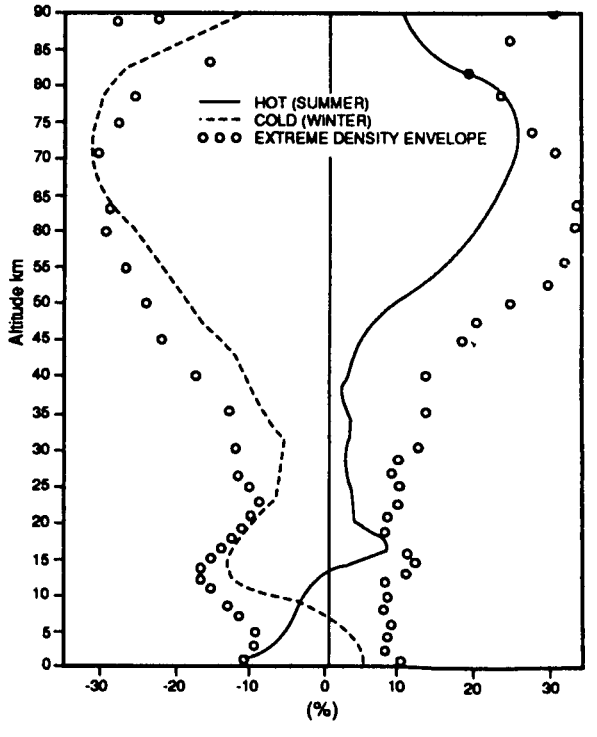

Figure 3.4 Relative deviations (%) of extreme EAFB density profiles with respect to ERA-75.

The two VAFB extreme density profiles are shown in figure 3.3 as percent deviations from the Vandenberg Reference Atmosphere, 1971. Levels of minimum density variation are located at ~8, 30, and 90-km altitude. Levels of maximum variability occur at 0, 15 and 73 km. The hot and cold VAFB virtual temperature profiles are shown in figure 3.6.

The two EAFB extreme density profiles are shown in figure 3.4 as percent deviations from the Edwards Reference Atmosphere, 1975. The hot and cold EAFB virtual temperature profiles are shown in figure 3.7. These extreme density and temperature profiles again have structures similar to the KSC and VAFB models. Temperatures below approximately 10-km altitude are virtual temperatures. Virtual temperature includes moisture to avoid computation of specific gas constant for moist air (see section 3.3.1.1).

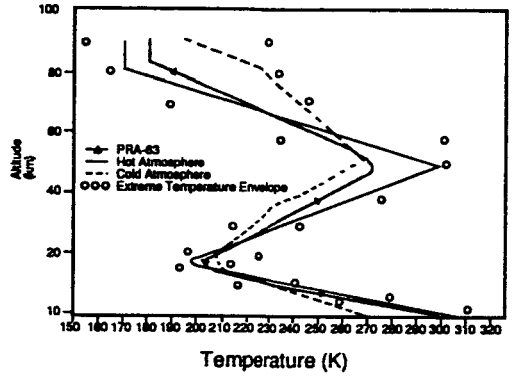

Figure 3.5 Virtual temperature profiles of the KSC hot, cold, and PRA-63.

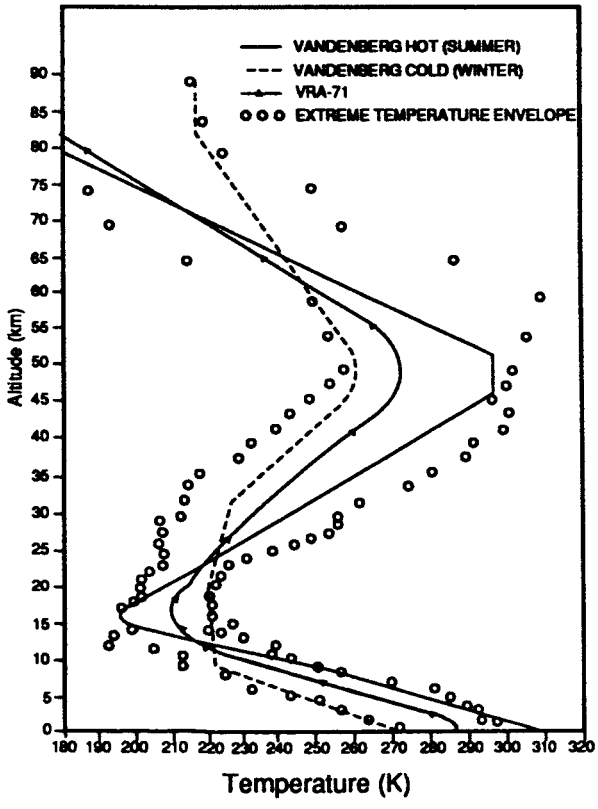

Figure 3.6 Virtual temperture profiles of the VAFB hot, cold, and VRA-71.

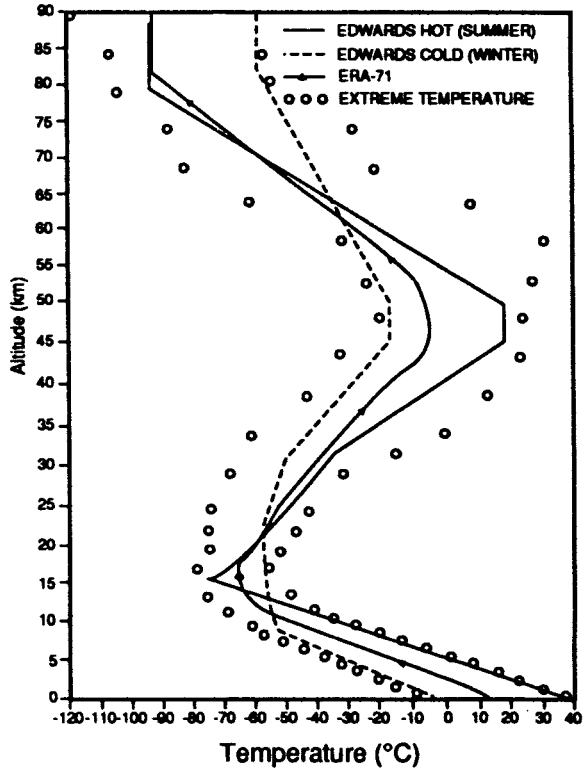

Figure 3.7 Virtual temperature profiles of the EAFB hot, cold, and ERA-75.

Tables 3.15A and B, 3.16A and B, and 3.17A and B give the numerical data used to prepare figures 3.2 through 3.7.

3.7 Reference Atmospheres

In design and preflight analysis of aerospace vehicles, special average atmospheric models are used to represent the mean or median thermodynamic conditions with respect to altitude. For general worldwide design, the U.S. Standard Atmosphere, 1976 (US 76) (ref. 3.1), is used, but site specific atmosphere models are needed at each launch area. A group of Range Reference Atmospheres (ref. 3.5) have been prepared to represent the thermodynamic medians in the first 70-km altitude at various ranges and launch areas. References 3.16 and 3.17 (supplemental atmospheres) together with references 3.6 and 3.7, which describes the Global Reference Atmosphere Model (GRAM), are also useful in this regard.

The Patrick Reference Atmosphere (PRA-63) is a more extensive reference atmosphere presenting data to 700-km altitude for KSC. Because of the utility of this atmosphere, a simplified version is given as Table 3.10 from Reference 3.3. Criteria for orbital studies are given in reference 3.11.

Reference atmospheres are also available for VAFB (ref. 3.4 and table 3.11) and EAFB (ref. 3.13 and table 3.12). These provide an annual reference atmosphere model to 700 km and have been designated as computer subroutines VRA-71 and ERA-75, respectively.

In tables 3.10, 3.11, and 3.12 the reference atmosphere values are given in standard computer printout, where the two-digit numbers that are at the end of the tabular value (number preceded by E) indicate the power of 10 by which the respective principal value must be multiplied. For example, a tabular value indicated as 2.9937265E 02 is 299.37265 or 0.15464054E-04 is 0.000015464054.

A detailed listing and description of many world-wide reference and standard atmospheric models is given in reference 3.18.

3.8 Reentry—Global Reference Atmosphere Model

3.8.1 Reentry Atmospheric Model

The atmospheric model recommended for all reentry analyses, except lower altitudes specified in subsection 3.6, is the NASA-MSFC Global Reference Atmosphere Model (GRAM)(ref. 3.6). This model generates monthly profiles of atmospheric variables—wind, pressure, temperature, and density—along any vehicle trajectory from orbital altitudes to sea level on a worldwide basis. GRAM can also generate many different realistic, simulated atmospheric profiles. A Monte Carlo procedure utilizing correlative techniques with the daily variability of the atmospheric parameters has been used to accomplish the construction of individual, atmospheric profiles.

The GRAM model has been computerized and is available to give these variables and their structure as a function of the three spatial coordinates—latitude, longitude, and altitude—and of the time domain (monthly). The GRAM model is a composite of other atmospheric models melded together with new techniques to join models and simulate perturbations. The GRAM-90 computer program (MFS-28577) is available from COSMIC, The University of Georgia, 382 E. Broad St., Athens, GA 30602

3.8.2 Atmospheric Model for Simulation

A National Aero-Space Plane (NASP) Integrated Atmospheric Model (NIAM) (ref. 3.7) has been developed at NASA/Ames-Dryden under guidance from NASA/MSFC, for NASP engineering design and flight simulation studies. The NIAM is based on the GRAM-90 (ref. 3.6), but has been expanded to incorporate other specific, realistic atmospheric thermodynamic and wind (turbulence) perturbations. NIAM is specific to NASP and was developed for real-time simulations; but is also appropriate for use in NASP off-line control, structure, and propulsion subsystem design activities, and in batch simulations. It simulates ascent, cruise, and descent of the X-30.

3.9 Atmospheric Orbital Model

General environmental criteria for NASA orbital studies are given in reference 3.11. The atmospheric model baselined to be used in all space station design studies (ref. 3.19) is the NASA-Marshall Engineering Thermosphere Model (NASA-MET) (ref. 3.20 and 3.21). A good description of the upper atmospheric variations that have been programmed into the MSFC orbital atmospheric model can be obtained from References 3.22 and 3.11. The above mentioned GRAM-90 model also has the NASA-MET within its upper structure above 120-km altitude.

SECTION IV. THERMAL RADIATION

4.1 Introduction

The natural thermal environments, such as solar and sky radiation (thermal radiation) and temperature, can produce undesirable effects on aerospace vehicles while being fabricated, transported, tested, on the pad, or in flight. The ground support system may also be affected. Effects on the vehicles and ground support system include:

a. Unequal heating resulting in stresses of various types.

b. Temperature extremes (high or low) occurring inside or on the vehicle surface which may cause equipment malfunctions or uncomfortable/undesirable conditions for manned missions.

c. Difficulties in alignment of the vehicle parts at interfaces, and calibration of R&D instruments on the vehicle because of variations in size, thermal effects, and/or shape with temperature.

Because of these and other effects, information on the radiation/thermal environment at the Earth's surface and up to 90-km altitude is presented in the following order:

a. Thermal definitions.

b. Extraterrestrial solar radiation over small wavelength intervals that irradiate the atmosphere from approximately 20-km to 90-km altitude.

c. Solar radiation transmitted, absorped, and scattered through a reference atmosphere in small wavelength interval irradiances (direct solar). Data are valid at the Earth's surface on a very clear day.

d. Diffuse (sky) radiation.

e. Extreme values of total horizontal, diffuse, total normal incident, and total 45° surface solar radiation at various times of day at the Earth's surface for various geographic locations.

f. Application of solar radiation in design using solar radiation design curves.

g. Methods of using surface emittance and the effect of wind speed to determine temperatures on surfaces exposed to solar radiation and sky radiation, and the application of solar radiation in design with solar radiation design curves.

h. Extreme and mean values of monthly air temperature at the Earth's surface at various times of day.

i. Extreme temperature changes, surface skin temperatures, and compartment temperature values.

4.2 Definitions

The thermal and radiation terms used in this section are defined as follows:

Absorption bands are those portions of the solar spectrum or other continuous spectra which have lesser intensity because of absorption by gaseous elements or molecules. In general, elements give sharp lines, but molecules, such as water vapor or carbon dioxide, give broad diffuse bands.

Absorptivity for any object is the fraction of the radiant energy falling on an object that is absorbed or transferred into heat. It is the ratio of the radiation absorbed by any substance to that absorbed under the same conditions by a blackbody.

Air mass (atmosphere) is the amount of atmosphere that the solar radiation passes through, considering the vertical path at sea level as unity (i.e., when the Sun is at the zenith, directly overhead). The air mass (atmosphere) will always be greater than 1.0 when the path deviates from the vertical.

Air temperature (surface) is the free or ambient air temperature measured under standard conditions of height, ventilation, and radiation shielding. The air temperature is normally measured with liquid-in-glass thermometers in a louvered wooden shelter, painted white inside and outside, with the base of the shelter normally 1.22 m (4 ft) above a close-cropped grass surface (ref. 4.1). Unless an exception is stated, surface air temperatures given in this report are temperatures measured under these standard conditions.

Atmospheric transmittance is the ratio between the intensity of the extraterrestrial solar radiation and intensity of the solar radiation after passing through the atmosphere.

Astronomical unit (au) is the mean distance of Earth from the Sun (1.496×10^8 km).

Blackbody is an ideal emitter which radiates energy at the maximum possible rate per unit area at each wavelength for any given temperature and which absorbs all incident radiation at all wavelengths. Its absorptivity is always 1.0.

Diffuse (sky) radiation (I_{dH}) is the solar radiation reaching the Earth's surface after having been scattered from the direct solar beam by molecules and particles in the atmosphere. It is measured at the Earth's surface by subtracting the direct solar radiation from the total horizontal radiation.

Direct normal incident radiation (I_{DN}): see normal incident.

Direct solar radiation is the solar radiation received by an object from on a line directly to the Sun. It does not include diffuse radiation.

Emittance is the ratio of the energy emitted by a body at a specific temperature to the energy which would be emitted by a blackbody at the same temperature. All real bodies will emit energy in different amounts from a blackbody at various wavelengths; i.e., low-temperature bodies emit in the IR not visible spectrum. They are colored because they reflect the colored part of the visible spectrum. In this document, the assumption is made that the absorptivity of an object is numerically equal to the emittance of the object at the same wavelengths. Therefore, the value of the emittance can be used to determine the portion of the energy received by the object which heats (or energy lost which cools) the object. Emittance is always less than 1.0.

Extraterrestrial solar radiation is that solar radiation received outside the Earth's atmosphere at one astronomical unit from the Sun. The term "solar spectral irradiance" is used when the extraterrestrial solar radiation is considered by wavelength intervals.

Fraunhofer lines are the dark absorption lines or bands in the solar spectrum caused by gases in the outer portion of the Sun and Earth's atmosphere. These lines may be of metals (sharp lines) or molecules (broad lines) in the gaseous state.

Horizontal solar radiation is the solar radiation measured on a horizontal surface. This is frequently referred to as "global radiation" or "total horizontal radiation" or "total hemispherical radiation" when solar and diffuse sky radiation are included.

Irradiation is the emitting of energy from an object. In this report the energy is black body radiation.

Normal incident (I_{DN}) solar radiation is the radiation received on a surface, normal to the direction of the Sun, direct from the Sun. A very small amount of diffuse sky radiation in a narrow band around the Sun is normally measured with normal incident measuring instruments.

Radiation temperature is the absolute temperature of a radiating blackbody determined by Wien's displacement law, expressed as

$$T_R = \frac{w}{\lambda \max} \tag{4.1}$$

where T_R is the absolute temperature of the radiating body (K), w is the Wien's displacement constant (0.2880 cm K), and λmax is the wavelength of the maximum radiation intensity for the blackbody.

Sky radiation temperature is the average radiation temperature of the sky when it is assumed to be a blackbody. Sky radiation is the radiation to and through the atmosphere from outer space. While this radiation is normally termed nocturnal radiation, it takes place under clear skies even during daylight hours, and is always much lower than the measured air temperature.

Solar constant is the intensity of solar radiation received outside the Earth's atmosphere on a surface normal to the incident radiation at the Earth's mean distance (1 au) from the Sun. The best value of the solar constant is 1,371±5 W m^{-2} at 1 au (ref. 4.2, with refs. 4.3, 4.4, and 4.5 providing prior background information).

Total solar radiation: When the word "Total" is used it means the wavelength band covering the entire solar spectrum from the extreme ultraviolet to the far infrared.

4.3 Spectral Distribution of Radiation

4.3.1 Introduction

All objects radiate energy in some portion of the electromagnetic spectrum. The amount and frequency of the radiation distribution is a function of temperature. The higher the temperature, the greater the amount of total energy emitted and the higher the frequency (shorter the wavelength) of the peak energy emission, according to Wien's displacement law,

$$\lambda_{max} = \frac{w}{T_R} \tag{4.1A}$$

Solar radiation and its transmittance characteristics through the atmosphere are presented in the following subsections.

4.3.2 Solar Radiation

The Sun emits energy in the electromagnetic spectrum from below 10^{-7} to greater than 10^{5} μm. This radiation ranges from cosmic rays through the very long wave radio waves. The total amount of radiation from the Sun is nearly constant in intensity with time.

Of the total electromagnetic spectrum of the Sun, only the radiant energy from that portion of the spectrum between 0.22 and 20.0 μm will be considered in this document since it contributes 99.8 percent of the total electromagnetic energy from the Sun. The spectral distribution of this region closely resembles the emission of a black body radiating at 5,762 K (T_{max}). This is the spectral region which causes nearly all of the heating of an object.

Solar radiation, observed at an altitude high enough that the Earth's atmosphere does not absorb the radiation, is distributed in a continuous spectrum with many narrow absorption bands caused by the

elements and molecules in the colder solar atmosphere. These absorption bands are the Fraunhofer lines, whose widths are usually very small ($<10^{-4}$ μm in most cases).

The Earth's atmosphere also absorbs a part of the solar radiation. The major portion of the solar radiation reaching the Earth's surface is between about 0.35 and 4.00 μm. The distribution of the solar energy outside the Earth's atmosphere* (extraterrestrial) is as follows:

Region (μm)	Distribution (%)	Solar Intensity* g-cal cm^{-2} (min^{-1})
Ultraviolet below 0.38	7.003	0.136
0.38 to 0.75	44.688	0.867
Infrared above 0.75	48.309	0.937

The first detailed information published for use by engineers on the distribution of solar radiation energy (solar irradiation) wavelengths was that by Parry Moon in 1940 (ref. 4.6). These data were generally based on theoretical curves but are still used as the basic solar radiation in design by many engineers.†

4.3.3 Solar Radiation Intensity Distribution

Table 4.1 presents data on the distribution with wavelength of solar radiation outside the Earth's atmosphere and at the Earth's surface after 1.0 atmosphere absorption on a very clear day. This "clear day" is based on a day where the value of the solar radiation at the surface equals the value of 1.64 g-cal cm^{-2} min^{-1}. It was determined by fitting a spectral curve to give the proper area under the curve from the data as shown in table 4.1.

In table 4.1, above a wavelength of 0.290 microns, the table is accurate to within ±30 percent. The smaller wavelength data are up to 5X low in some cases. For more precise data, reference 4.2 gives the recommended data for above the atmosphere, while data for below the atmosphere can be obtained by using LOWTRAN 7 model and computer code (ref. 4.7).

The solar radiation distribution outside the Earth's atmosphere (solar spectral irradiance) are defined for the average Sun-Earth distance of 1 au. This is based on data obtained from high flying aircraft, high altitude platforms, balloons, and the Mariner-Mars probe. Different types of instruments were used. The instruments were referred to three scales of radiometry, the absolute electrical units scale, the international pyrheliometric scale IPS 56, and the thermodynamic Kelvin temperature scale (ref. 4.4). The Earth is at 1 au on April 4 and October 5. At other times of the year the Earth is closer to, or farther away, from the Sun making the values increase or decrease by approximately 3.5 percent. Also, the cyclic variation in the solar energy output received from the Sun is about equal to the variation of the Earth's distance from the Sun. Therefore, any adjustment of the solar spectral irradiance would not be feasible.

The values of solar radiation given in table 4.1 for a one standard atmosphere absorption are representative of a very clear atmosphere which provides a minimum of atmospheric absorption. This gives a total solar radiation value (area under the spectral curve) equal to the highest values measured at the Earth's surface at sea level in mid-latitudes. These values are for use in solar radiation design when extreme solar radiation effects are desired at the Earth's surface. If data are required for less extreme

* At one astronomical unit (au) on a surface normal to the Sun.

†Additional information is provided by: Beckman, W.A., Klein, S.S., and Duffie, J.A.: "Solar Heating Design," John Wiley and Sons, New York, 1967; Daniels, G.E., Smith, O.E., and Greene, W.M.: "Application of Solar Radiation and Temperature in Design of Aerospace Vehicles," Internal Note IN-ES 42-76-1, NASA Marshall Space Flight Center, April 15, 1976.

Table 4.1 Solar spectral irradiance (outside atmosphere) and solar radiation after absorption by clear atmosphere

Wavelength (microns) λ	Solar Spectral Irradiance ($W\ cm^{-2}\ \mu^{-1}$)	Area Under Solar Spectral Irradiance Curve ($W\ cm^{-2}$)	Solar Radiation After One Atmosphere Absorption ($W\ cm^{-2}\ \mu^{-1}$)	Area Under One Atmosphere Solar Radiation Curve ($W\ cm^{-2}$)	Percentage of Solar Radiation After One Atmosphere Absorption for Wavelengths Shorter Than λ (%)
0.120	0.000010	0.00000060	0.000000	0.000000	0.00
0.140	0.000003	0.00000073	0.000000	0.000000	0.00
0.150	0.000007	0.00000078	0.000000	0.000000	0.00
0.160	0.000023	0.00000093	0.000000	0.000000	0.00
0.170	0.000063	0.00000136	0.000000	0.000000	0.00
0.180	0.000125	0.00000230	0.000000	0.000000	0.00
0.190	0.000271	0.00000428	0.000000	0.000000	0.00
0.200	0.00107	0.000010	0.000001	0.000000	0.00
0.210	0.00229	0.000027	0.000003	0.000000	0.00
0.220	0.00575	0.000067	0.000007	0.000000	0.00
0.225	0.00649	0.000098	0.000007	0.000000	0.00
0.230	0.00667	0.000131	0.000008	0.000000	0.00
0.235	0.00593	0.000162	0.000007	0.000000	0.00
0.240	0.00630	0.000193	0.000007	0.000000	0.00
0.245	0.00723	0.000227	0.000008	0.000000	0.00
0.250	0.00704	0.000263	0.000008	0.000000	0.00
0.255	0.0104	0.000306	0.000012	0.000000	0.00
0.260	0.0130	0.000365	0.000015	0.000000	0.00
0.265	0.0185	0.000443	0.000021	0.000000	0.00
0.270	0.0232	0.000548	0.000026	0.000000	0.00
0.275	0.0204	0.000657	0.000023	0.000000	0.00
0.280	0.0222	0.000763	0.000025	0.000000	0.00
0.285	0.0315	0.000897	0.000036	0.000001	0.00
0.290	0.0482	0.001097	0.000055	0.000001	0.00
0.295	0.0584	0.001363	0.000066	0.000001	0.00
0.300	0.0514	0.001638	0.006677	0.000035	0.03
0.305	0.0603	0.001917	0.019830	0.000134	0.12
0.310	0.0689	0.002240	0.029084	0.000279	0.25
0.315	0.0764	0.002603	0.038941	0.000474	0.42
0.320	0.0830	0.003002	0.047684	0.000712	0.64
0.325	0.0975	0.003453	0.062018	0.001022	0.92
0.330	0.1059	0.003961	0.073829	0.001392	1.25
0.335	0.1081	0.004496	0.080896	0.001796	1.61
0.340	0.1074	0.005035	0.084636	0.002219	1.99
0.345	0.1069	0.005571	0.087080	0.002655	2.39
0.350	0.1093	0.006111	0.091327	0.003111	2.80
0.355	0.1083	0.006655	0.092186	0.003572	3.40
0.360	0.1068	0.007193	0.092857	0.004036	3.63
0.365	0.1132	0.007743	0.099873	0.004536	4.08
0.370	0.1181	0.008321	0.105507	0.005063	4.55
0.375	0.1157	0.008906	0.104596	0.005586	5.03
0.380	0.1120	0.009475	0.102971	0.006101	5.49
0.385	0.1098	0.010030	0.102273	0.006613	5.95
0.390	0.1098	0.010579	0.103977	0.007132	6.42
0.395	0.1189	0.011150	0.114309	0.007704	6.93
0.400	0.1429	0.011805	0.137403	0.008391	7.55
0.405	0.1644	0.012573	0.158076	0.009181	8.26
0.410	0.1751	0.013422	0.168365	0.010023	9.02
0.415	0.1774	0.014303	0.170576	0.010876	9.79
0.420	0.1747	0.015183	0.167980	0.011716	10.54
0.425	0.1693	0.016043	0.162788	0.012530	11.28
0.430	0.1639	0.016876	0.157596	0.013318	11.99
0.435	0.1663	0.017702	0.159903	0.014117	12.71
0.440	0.1810	0.018570	0.174038	0.014988	13.40
0.445	0.1922	0.019503	0.184807	0.015912	14.30
0.450	0.2006	0.020485	0.192884	0.016876	15.19
0.455	0.2057	0.021501	0.195904	0.017656	16.07
0.460	0.2066	0.022532	0.196761	0.018839	16.96
0.465	0.2048	0.023560	0.196923	0.019824	17.84
0.470	0.2033	0.024580	0.195480	0.020801	18.72

Table 4.1 Solar spectral irradiance (outside atmosphere) and solar radiation after absorption by clear atmosphere (continued).

Wavelength (microns) λ	Solar Spectral Irradiance ($W\ cm^{-2}\ \mu^{-1}$)	Area Under Solar Spectral Irradiance Curve ($W\ cm^{-2}$)	Solar Radiation After One Atmosphere Absorption ($W\ cm^{-2}\ \mu^{-1}$)	Area Under One Atmosphere Solar Radiation Curve ($W\ cm^{-2}$)	Percentage of Solar Radiation After One Atmosphere Absorption for Wavelengths Shorter Than λ (%)
0.475	0.2044	0.025600	0.196538	0.021784	19.61
0.480	0.2074	0.026629	0.197523	0.022772	20.50
0.485	0.1976	0.027642	0.186415	0.023704	21.34
0.490	0.1950	0.028623	0.183962	0.024624	22.17
0.495	0.1960	0.029601	0.183177	0.025539	22.99
0.500	0.1942	0.030576	0.179814	0.026439	23.80
0.505	0.1920	0.031542	0.176146	0.027319	24.60
0.510	0.1882	0.032492	0.172660	0.028183	25.37
0.515	0.1833	0.033421	0.168165	0.029023	26.13
0.520	0.1833	0.034337	0.168165	0.029864	26.88
0.525	0.1852	0.035259	0.169908	0.030714	27.65
0.530	0.1842	0.036182	0.168990	0.031559	28.41
0.535	0.1818	0.037097	0.166788	0.032393	29.16
0.540	0.1783	0.037997	0.163977	0.033211	29.90
0.545	0.1754	0.038882	0.160917	0.034015	30.62
0.550	0.1725	0.039751	0.158256	0.034806	31.33
0.555	0.1720	0.040613	0.157798	0.035595	32.05
0.560	0.1695	0.041466	0.155504	0.036373	32.75
0.565	0.1705	0.042316	0.156422	0.037155	33.45
0.570	0.1712	0.043171	0.157064	0.037940	34.16
0.575	0.1719	0.044028	0.157726	0.038729	34.87
0.580	0.1715	0.044887	0.157339	0.039516	35.57
0.585	0.1712	0.045744	0.157064	0.040301	36.28
0.590	0.1700	0.046597	0.155963	0.041081	36.98
0.595	0.1682	0.047442	0.154311	0.041852	37.68
0.600	0.1666	0.048279	0.152844	0.042616	38.37
0.605	0.1647	0.049107	0.151100	0.043372	39.05
0.610	0.1635	0.049928	0.150000	0.044122	39.72
0.620	0.1602	0.051546	0.146972	0.045592	44.05
0.630	0.1570	0.053132	0.145370	0.047045	42.30
0.640	0.1544	0.054689	0.144299	0.048488	43.66
0.650	0.1511	0.056217	0.142547	0.049914	44.94
0.660	0.1486	0.057715	0.141523	0.051329	46.22
0.670	0.1456	0.059186	0.140000	0.052729	47.48
0.680	0.1427	0.060628	0.137211	0.054101	48.71
0.690	0.1402	0.062042	0.134807	0.055449	49.93
0.700	0.1369	0.063428	0.131634	0.056766	51.11
0.710	0.1344	0.064784	0.129230	0.058058	52.27
0.720	0.1314	0.066113	0.126346	0.059321	53.41
0.730	0.1290	0.067415	0.124038	0.060562	54.53
0.740	0.1260	0.068690	0.121153	0.061773	55.62
0.750	0.1235	0.069938	0.118750	0.062961	56.69
0.800	0.1107	0.075793	0.106442	0.068283	61.48
0.850	0.0988	0.081030	0.095000	0.073033	65.76
0.900	0.0889	0.085723	0.080090	0.077037	69.36
0.950	0.0835	0.090033	0.077314	0.080903	72.84
1.000	0.0746	0.093985	0.071730	0.084490	76.07
1.100	0.0592	0.100675	0.056923	0.090182	81.20
1.200	0.0484	0.106055	0.046538	0.094836	85.39
1.300	0.0396	0.110455	0.036000	0.098436	88.63
1.400	0.0336	0.114115	0.002240	0.098660	88.83
1.500	0.0287	0.117230	0.027333	0.101393	91.29
1.600	0.0244	0.119885	0.023461	0.103739	93.40
1.700	0.0202	0.122115	0.019423	0.105681	95.15
1.800	0.0159	0.123920	0.013826	0.107064	96.40
1.900	0.0126	0.125345	0.000126	0.107077	96.41
2.000	0.0103	0.126490	0.009809	0.108057	97.29
2.100	0.0090	0.127455	0.008653	0.108923	98.07
2.200	0.0079	0.128300	0.007596	0.109682	98.76
2.300	0.0068	0.129035	0.006538	0.110336	99.34

Table 4.1 Solar spectral irradiance (outside atmosphere) and solar radiation after absorption by clear atmosphere (continued).

Wavelength (microns) λ	Solar Spectral Irradiance ($W\ cm^{-2}\ \mu^{-1}$)	Area Under Solar Spectral Irradiance Curve ($W\ cm^{-2}$)	Solar Radiation After One Atmosphere Absorption ($W\ cm^{-2}\ \mu^{-1}$)	Area Under One Atmosphere Solar Radiation Curve ($W\ cm^{-2}$)	Percentage of Solar Radiation After One Atmosphere Absorption for Wavelengths Shorter Than λ (%)
2.4	0.0064	0.129695	0.006153	0.110951	99.90
2.5	0.0054	0.130285	0.001080	0.111059	100.00
2.6	0.0048	0.130795	0.000005	0.111060	100.00
2.7	0.0043	0.131250	0.000004	0.111060	100.00
2.8	0.00390	0.131660	0.000004	0.111061	100.00
2.9	0.00350	0.132030	0.000004	0.111061	100.00
3.0	0.00310	0.132360	0.000003	0.111061	100.00
3.1	0.00260	0.132645	0.000002	0.111062	100.00
3.2	0.00226	0.132888	0.000002	0.111062	100.00
3.3	0.00192	0.133097	0.000002	0.111062	100.00
3.4	0.00166	0.133276	0.000001	0.111062	100.00
3.5	0.00146	0.133432	0.000001	0.111062	100.00
3.6	0.00135	0.133573	0.000001	0.111062	100.00
3.7	0.00123	0.133702	0.000001	0.111062	100.00
3.8	0.00111	0.133819	0.000001	0.111063	100.00
3.9	0.00103	0.133926	0.000001	0.111063	100.00
4.0	0.00095	0.134025	0.000001	0.111063	100.00
4.1	0.00087	0.134116	0.000001	0.111063	100.00
4.2	0.00078	0.134198	0.000000	0.111063	100.00
4.3	0.00071	0.134273	0.000000	0.111063	100.00
4.4	0.00065	0.134341	0.000000	0.111063	100.00
4.5	0.00059	0.134403	0.000000	0.111063	100.00
4.6	0.00053	0.134459	0.000000	0.111063	100.00
4.7	0.00048	0.134509	0.000000	0.111063	100.00
4.8	0.00045	0.134556	0.000000	0.111063	100.00
4.9	0.00041	0.134599	0.000000	0.111063	100.00
5.0	0.0003830	0.13463906	0.000000	0.111063	100.00
6.0	0.0001750	0.13491806	0.000000	0.111063	100.00
7.0	0.0000990	0.13505506	0.000000	0.111063	100.00
8.0	0.0000600	0.13513456	0.000000	0.111063	100.00
9.0	0.0000380	0.13518356	0.000000	0.111063	100.00
10.0	0.0000250	0.13521506	0.000000	0.111063	100.00
11.0	0.0000170	0.13523606	0.000000	0.111063	100.00
12.0	0.0000120	0.13525056	0.000000	0.111063	100.00
13.0	0.0000087	0.13526091	0.000000	0.111063	100.00
14.0	0.0000055	0.13526801	0.000000	0.111063	100.00
15.0	0.0000049	0.13527321	0.000000	0.111063	100.00
16.0	0.0000038	0.13527756	0.000000	0.111063	100.00
17.0	0.0000031	0.13528101	0.000000	0.111063	100.00
18.0	0.0000024	0.13528376	0.000000	0.111063	100.00
19.0	0.0000020	0.13528596	0.000000	0.111063	100.00
20.0	0.0000016	0.13528776	0.000000	0.111063	100.00
25.0	0.000000610	0.13529328	0.000000	0.111063	100.00
30.0	0.000000300	0.13529556	0.000000	0.111063	100.00
35.0	0.000000160	0.13529671	0.000000	0.111063	100.00
40.0	0.000000094	0.13529734	0.000000	0.111063	100.00
50.0	0.000000038	0.13529800	0.000000	0.111063	100.00
60.0	0.000000019	0.13529829	0.000000	0.111063	100.00
80.0	0.000000007	0.13529855	0.000000	0.111063	100.00
100.0	0.000000003	0.13529865	0.000000	0.111063	100.00
1,000.0	0.000000000	0.13530000	0.000000	0.111063	100.00

or average values of solar radiation at the surface and for values for more than one standard atmosphere (air mass), values given in ref. 4.5, pages 36 through 39. Also ref. 4.8 or LOWTRAN 7 can be used.

Figure 4.1 shows in graphical form the solar spectral irradiance at 1 au, normal incident solar radiation at sea level on a clear day, and the blackbody spectral irradiance curve at T = 5,762 K.

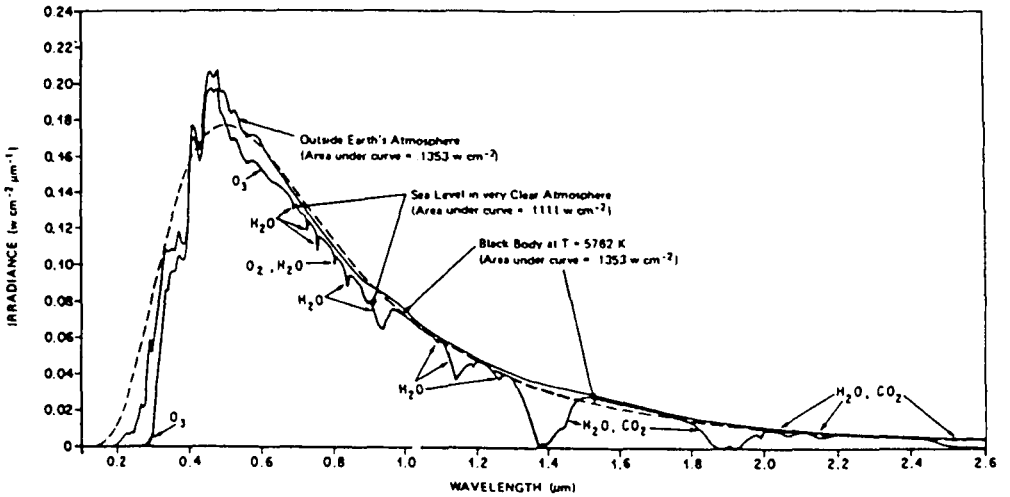

Figure 4-1. Normal incident solar radiation at sea level on very clear days, solar spectral irradiance outside the Earth's atmosphere at 1 au (ref. 4.4), and blackbody spectral irradiance curve at T = 5.762 K (normalized to 1 au).

4.3.4 Atmospheric Transmittance of Solar Radiation

The atmosphere of the Earth is composed of a mixture of gases, aerosols, and dust which absorb, scatter and emit radiation in different amounts at various wavelengths. If the ratio is taken of the solar spectral irradiance I_0 to that of the solar radiation after absorption through one air mass $I_{1.00}$ an atmospheric transmittance factor M can be found (equation (4.2)):

$$M = \frac{I_{1.00}}{I_0} \tag{4.2}$$

The atmospheric transmittance constant can be used in the following equation for computations of intensities for any other number of air masses:

$$I_N = I_0 \, (M^N) \tag{4.3}$$

where

I_N = intensity of solar radiation for N air mass thickness

N = number of air masses.

Equation (4.3) can also be used to obtain solar radiation intensities versus wavelengths for total normal incident solar radiation intensities (area under curve) by computing new values of atmospheric transmittance as follows:

$$M_N = M \frac{I_{TN}}{0.1111}, \tag{4.4}$$

where

I_{TN} = new value of total normal incident solar radiation intensity in W cm^{-2}

M = value for atmospheric transmittance given in table 4.1

M_N = new value of atmospheric transmittance.

Equations (4.3) and (4.4) are valid only for locations relatively near the Earth's surface (below 5 km altitude). For higher altitudes, corrections are needed for the change of the amount of ozone and water vapor in the atmosphere. Also, equation (4.4) should be used only for values of I_{TN} greater than 0.0767 W cm^{-2} (1.10 g-cal cm^{-2} min^{-1}). Values lower than this would indicate a considerably higher ratio of water vapor to ozone in the atmosphere and require that the curve be adjusted to give more absorption in the infrared water vapor bands at long wavelengths (infrared) and a small increase for the ozone at shorter wavelengths. Tables providing lower solar radiation values are given in refs. 4.5 and 4.8. Caution should be used in any analysis using lower values of solar radiation in areas where smoke (such as from forest fires), dust or sand from high winds, or other types of unusual particulate matter exist, since the shape of the curve with respect to wavelength will be entirely different than the normal curves. These particulate matters and aerosols will also give unusual diffuse radiation values.

4.3.5 Diffuse (Sky) Radiation

When solar radiation, which is a nearly parallel beam of light, enters the atmosphere of the Earth, molecules of air and aerosols such as dust particles and water vapor droplets diffuse and absorb a part of the radiation. The diffuse or scattered radiation then reaches the Earth as nonparallel light from all directions. This is described in the following subsection.

4.3.5.1 Scattered Radiation

Scattered radiation gives the sky its brightness and color. The color is a result of selective scattering at specific wavelengths as a function of the size and type of the molecules and particles. On a clear day, the amount of scattering is very low because there are fewer particles, water vapor, and water droplets present. The clear sky can be as little as 10^{-6} as bright as the surface of the Sun. This sky radiation will be referred to as "diffuse radiation." On a clear day, the total energy contribution from the diffuse radiation from the entire sky hemisphere to a horizontal surface is between 0.0007 and 0.014 W cm^{-2} (0.01 and 0.02 g-cal cm^{-2} min^{-1}). With clouds present, the amount of diffuse radiation can be much greater. The total sky hemisphere during an overcast day may contribute as much as 0.069 W cm^{-2} (1.0 g-cal cm^{-2} min^{-1}) of radiation to a horizontal surface.

Table 4.2 presents expected extremal surface temperatures and the sky radiation values for selected locations of interest to NASA. The surface temperatures are primarily the result of a balance between incoming and outgoing radiative energy along with convection effects. As a black-body radiator, the clear sky is considered equivalent to a cold surface. The radiation temperature of the clear sky is the same during the day as at night. It is the clear sky acting as a cold sink, without the incoming solar radiation heating of the surface, that causes air temperatures to be lower at night than during the day. At night, clouds act as a barrier to the outgoing radiation. Clouds absorb outgoing IR and emit radiation at lower temperature, making the effective atmospheric temperature warmer than the clear sky. Thus the air near the ground will not cool off to as low a temperature on a cloud covered night. Although not a significant factor, atmospheric dust, which is related to wind speed, and pollution aerosols behave in a similar fashion. Therefore, the greatest cooling of the Earth's surface occurs with calm winds (no mixing with warmer air) and clear skies.

Radiation interchange with the sky should be based on the design high and design low effective sky temperatures of 50 °F and –30 °F, respectively (ref. 4.9). These are representative of any global launch site or reentry region.

Table 4.2 Surface air and sky radiation temperature extremes.

Area		Surface Air Temperature Extremes[a]				Sky Radiation	
		Maximum		Minimum		Extreme Minimum Equivalent Temperature	Equivalent Radiation ($g\text{-}cal\ cm^{-2}\ min^{-1}$)
		Extreme	95%[b]	Extreme	95%[b]		
Huntsville, Alabama	°C	40.0	36.7	-23.9	-12.8	-30.0	0.28
	°F	104	98	-11	9	-22	
Kennedy Space Center, Florida[c]	°C	37.2	35.0	-7.2	0.6	-15.0	0.36
	°F	99	95	19	33	5	
Vandenberg AFB, California[c]	°C	37.8	29.4	-3.9	1.1	-15.0	0.36
	°F	100	85	25	34	5	
Edwards AFB, California	°C	45.0	41.7	-15.6	-7.8	-30.0	0.28
	°F	113	107	4	18	-22	
Honolulu, Oahu – Hickam Field	°C	33.9	32.8	11.1	15.6	-15.0	0.36
	°F	93	91	52	60	5	
Guam – Andersen AFB	°C	34.4	31.1	18.9	22.2	-15.0	0.36
	°F	94	88	66	72	5	
Santa Susana, California	°C	42.2	36.1	-2.2	1.7	-15.0	0.36
	°F	108	97	28	35	5	
Thiokol Wasatch Division, Utah[d]	°C	40.0	35.6	-29.4	-16.1	-30.0	0.28
	°F	104	96	-21	3	-22	
New Orleans, Lousiana[e]	°C	38.9	35.0	-10.0	-3.3	-17.8	0.35
	°F	102	95	14	26	0	
Stennis Space Center Mississippi[f]	°C	39.4	35.6	-14.4	-2.2	-17.8	0.35
	°F	103	96	6	28	0	
Continent Transportation (rail, truck, river barge)	°C	47.2	–	-34.4	–	-30.0	0.28
	°F	117	–	-30	–	-22	
Ship Transportation (West Coast, Panama Canal, Gulf of Mexico)	°C	37.8	–	-12.2	–	-15.0	0.36
	°F	100	–	10	–	5	
Johnson Space Center, Texas	°C	40.0	36.7	-9.4	-2.2	-17.8	0.35
	°F	104	98	15	28	0	
GSFC-Wallops Flight Facility, Virginia	°C	38.3	33.3	-20.0	-5.6	-17.8	0.35
	°F	101	92	-4	22	0	
White Sands Missile Range, New Mexico[g]	°C	44.4	38.9	-25.6	-10.0	-30.0	0.28
	°F	112	102	-14	14	-22	

a. The extreme maximum and minimum temperatures will be encountered during periods of wind speeds less than about 1 m/s.

b. Based on daily extreme (maximum or minimum) observations for worst month.

c. Sky temperature limits for shuttle launch at KSC and VAFB as given in NSTS 07700 Appendix 10.10 are 50 °F for a design high and -30 °F for a design low.

d. Includes extreme temperature observations at Bear River Refuge, UT.

e. Applies for the Michoud Assembly Facility (New Orleans, LA) and the Slidell Computer Complex (Slidell, LA).

f. Includes extreme temperature observations at Picayune, MS.

g. Also applies for Northrup Strip. Includes extreme temperature observations at Alamogordo and Holloman AFB, NM.

Maximum values of solar radiation for several locations, as a function of surface wind speed, are given in table 4.3. These decreased values are primarily the result of additional particulate matter in the atmosphere due to wind speed increases.

Table 4.3 Solar radiation maximum values associated with extreme wind values.

Maximum Solar Radiation (Normal Incident)						
Steady-State Ground Wind Speed at 18-m Height	Huntsville, New Orleans, Stennis, JSC, Gulf Transportation, Eastern Range, Western Range, West Coast Transportation and Wallops Flight Facility			White Sands Missile Range		
($m\ s^{-1}$)	($kJm^{-2}\ s^{-1}$)	($g\text{-}cal\ cm^{-2}\ min^{-1}$)	($Btu\ ft^{-2}\ h^{-1}$)	($kJm^{-2}\ s^{-1}$)	($g\text{-}cal\ cm^{-2}\ min^{-1}$)	($Btu\ ft^{-2}\ h^{-1}$)
10	0.84	1.20	265	1.05	1.50	322
15	0.56	0.80	177	0.70	1.00	221
≥20	0.35	0.50	111	0.56	0.80	177

4.3.5.2 Absorbed Radiation

The various gases in the atmosphere selectively absorb some of the incoming radiation. The absorbed energy warms the gas and is reradiated at different (typically longer) wavelengths. Absorption by gases is observed in the solar spectrum as bands of various widths. The major gases in the Earth's atmosphere, which show as absorption bands in the solar spectrum, are water vapor, carbon dioxide, ozone, and molecular oxygen.

4.4 Total Solar Radiation at the Earth's Surface

4.4.1 Introduction

This subsection presents a description of the total solar radiation, its definitions, and applications for use in design.

Standard solar radiation sensors measure the intensity of direct solar radiation from the Sun falling on a horizontal surface, plus the diffuse (sky) radiation from the total sky hemisphere at the Earth's surface where the instrument is located. This may not be at sea level. Diffuse radiation is lowest with dry, clean air; it increases with increasing water vapor, water droplets, or dust in the air. With extremely dense clouds or fog, the measured solar radiation will be nearly all diffuse radiation, with the total measured amount being much lower than the solar radiation on a clear day (see 4.3.5.1). The higher (≈95 percentile) values of measured horizontal solar radiation occur under very clear skies or under conditions of scattered fair weather cumulus clouds which reflect additional solar radiation onto the measuring sensor.

4.4.2 Use of Solar Radiation in Design

When radiation data are used in design studies, the direct solar radiation should be applied from one direction as parallel rays, and, at the same time, diffuse radiation must be applied as rays from all directions of a hemisphere (see fig. 4.2).

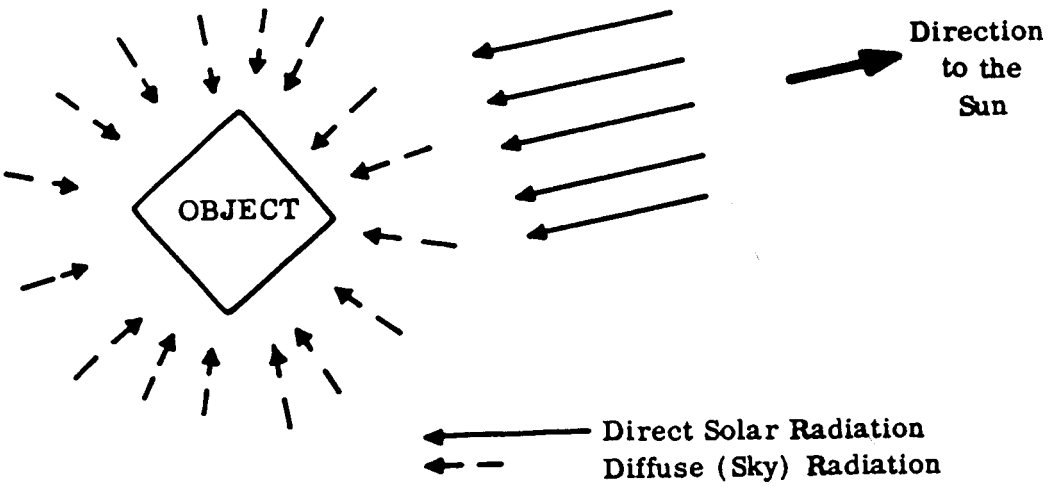

Figure 4.2 Method of applying radiation for design.

Because the Sun provides heat (from radiation) from a specific direction, differential heating of an object occurs; i.e., one part is heated more than another. This may result in stress and deformation. As an example, the side of the space shuttle vehicle facing the Sun is heated, while the sky cools the opposite side. This differential heating causes the vehicle to bend away from the Sun sufficiently, at the top, to be a required consideration in the design of platforms surrounding the vehicle. These platforms are used to ready the vehicle on the launch pad and must be designed so as to prevent damage to the vehicle skin from the platform, as the vehicle bends.

4.4.3 Total Solar Radiation Computations and Extreme Conditions

Ten years of total horizontal solar and diffuse (sky) radiation data were selected from measuring stations at two geographic locations for analysis to determine the frequency distribution of solar radiation for use in design. The data analysis was made by the National Oceanic and Atmospheric Administration (NOAA), National Climatic Data Center, under contract to NASA-Marshall Space Flight Center.

4.4.3.1 Computing Total Normal Incident Solar Radiation

The basic data used in computing the normal incident radiation (I_{TN}) were hourly totals of horizontal (direct) solar (I_{TH}) and diffuse (sky) radiation (I_{dH}) for each hour of the day for a 10-year period at each of two locations: Apalachicola, Florida (to represent Kennedy Space Center, Florida) and Santa Maria, California (to represent Vandenberg AFB, California). The hourly totals were divided by 60 to obtain the average solar radiation values per minute for each hour of the day. The units of this data are g-cal cm^{-2} min^{-1}. The average value per minute is numerically equal to intensity. These values were used in the computation of frequency distributions. The diffuse sky radiation intensities (I_{dH}) were empirically estimated for each value based on the amount of total horizontal (direct) solar radiation (I_{TH}) and diffuse (sky) radiation (I_{dH}) measured and the solar elevation angle, similar to the methods used in ref. 4.10. After the diffuse sky radiation (I_{dH}) is subtracted from the total horizontal solar and sky radiation, the resultant horizontal radiation (I) can be used to compute the direct normal incident radiation (I_{DN}) by using the following equation (refs. 4.11, 4.12, and 4.13).

$$I_{DN} = \frac{I}{\sin b} , \tag{4.5}$$

where

I_{DN} = direct normal incident solar radiation

I = horizontal solar radiation = $I_{TH} - I_{dH}$

b = solar elevation angle, in degrees (refs. 4.12 and 4.13).

Any of the solar radiation units, such as g-cal cm^{-2} min^{-1}, W cm^{-2}, W m^{-2}, Btu ft^{-2} h^{-1}, or other units may be used in any of the following equations depending on the source of the data (refs. 4.12 and 4.13).

The total normal solar radiation I_{TN} values were found by adding the direct normal incident solar radiation (I_{DN}) and the diffuse sky radiation (I_{dH}) as previously estimated from the contract with NOAA and presented in tables 4.4 and 4.5; i.e.,

$$I_{TN} = I_{DN} + I_{dH} \quad . \tag{4.6}$$

This method of finding the normal incident solar radiation may result in a slight overestimate of the value for low solar elevation because the sky hemisphere may be intercepted by the ground surface above the normal horizon. This error is insignificant, however, when extreme values are used and would be small for values equal to or greater than the mean plus one standard deviation.

To determine the amount of solar radiation on a south-facing surface, with the normal at some angle X to the horizon, the following equations may be used:

$$I_{D(X)} = I(\sin X \deg = \cot b \cos a \cos X \deg) \quad , \tag{4.7}$$

where

$I_{D(X)}$ =intensity of direct solar radiation on a south-facing surface, the normal being X degrees to the horizontal

I = horizontal solar radiation $I_{TH} - I_{dH}$

a = Sun's azimuth measured from the south direction, either east or west in degrees

b = Sun's elevation angle above the true horizon, in degrees

If we wish to include the diffuse radiation, we can use the following equation:

$$T_{TN} = I_{D(X)} + I_{dH} \quad . \tag{4.8}$$

4.4.3.2 Solar Radiation Extremals

To present the solar radiation data in a simplified form, the month of June was selected to represent the summer and the longest period of daylight, and December was selected for the winter and shortest period of daylight. The June Santa Maria, California, data for normal incident solar radiation (I_{DN}) were measured at the Earth's surface. These data were increased for the period from 1100 to 1900 hours to reflect the higher values which occur early in July (first week) during the afternoon. This was done because of the frequent fog which occurs in June and lasts most of the day.

Table 4.4 Extreme values of solar radiation for the Vandenberg AFB, West Coast Transportation, Santa Susana, White Sands Missile Range, Brigham City, and Edwards AFB.

Time of Day (Local Standard Time)	Total Horizontal Solar Radiation g-cal cm^{-2} min^{-1}		Diffuse Radiation* g-cal cm^{-2} min^{-1}		Total Normal Incident Solar Radiation g-cal cm^{-2} min^{-1}		Total 45° Surface Solar Radiation g-cal cm^{-2} min^{-1}	
	June							
	Extreme	95 Percentile	Extreme	95 Percentile	Extreme	95 Percentile	Extreme	95 Percentile
0500	0	0	0	0	0	0	0	0
0600	0.16	0.11	0.02	0.04	1.14	0.78	0.04	0
0700	0.46	0.40	0.05	0.08	1.34	1.08	0.19	0.16
0800	0.82	0.76	0.06	0.09	1.54	1.38	0.34	0.31
0900	1.16	1.11	0.04	0.08	1.74	1.62	0.84	0.77
1000	1.45	1.42	0	0.03	1.79	1.71	1.19	1.12
1100	1.64	1.56	0	0.10	1.79	1.69	1.39	1.31
1200	1.69	1.63	0	0.08	1.74	1.68	1.49	1.38
1300	1.69	1.64	0	0.07	1.74	1.68	1.49	1.40
1400	1.59	1.54	0.06	0.12	1.74	1.68	1.34	1.29
1500	1.45	1.39	0	0.06	1.79	1.70	1.14	1.09
1600	1.21	1.19	0	0.02	1.79	1.71	0.89	0.78
1700	0.87	0.83	0.03	0.05	1.69	1.60	0.34	0.18
1800	0.46	0.42	0.05	0.08	1.39	1.23	0.19	0.13
1900	0.14	0.12	0.02	0.04	1.19	0.93	0.04	0
2000	0	0	0	0	0	0	0	0
	December							
	Extreme	95 Percentile	Extreme	95 Percentile	Extreme	95 Percentile	Extreme	95 Percentile
0800	0	0	0	0	0	0	0	0
0900	0.35	0.32	0.04	0.05	1.59	1.39	0.99	0.85
1000	0.65	0.60	0.03	0.05	1.64	1.53	1.29	1.21
1100	0.86	0.80	0	0.04	1.84	1.64	1.64	1.49
1200	0.96	0.89	0.02	0.06	1.79	1.69	1.74	1.63
1300	0.99	0.89	0	0.06	1.84	1.70	1.79	1.64
1400	0.85	0.80	0.01	0.04	1.79	1.64	1.59	1.49
1500	0.66	0.60	0.02	0.05	1.69	1.54	1.34	1.21
1600	0.38	0.31	0.02	0.05	1.64	1.38	1.04	0.87
1700	0	0	0	0	0	0	0	0

*Diffuse radiation, associated with total horizontal solar radiation extremes.

Table 4.5 Extreme values of solar radiation for Eastern Range (KSC), Stennis Space Center, JSC, New Orleans, Gulf Transportation, and Huntsville.

Time of Day (Local Standard Time)	Total Horizontal Solar Radiation g-cal cm^{-2} min^{-1}		Diffuse Radiation* g-cal cm^{-2} min^{-1}		Total Normal Incident Solar Radiation g-cal cm^{-2} min^{-1}		Total 45° Surface Solar Radiation g-cal cm^{-2} min^{-1}	
	June							
	Extreme	95 Percentile	Extreme	95 Percentile	Extreme	95 Percentile	Extreme	95 Percentile
0500	0	0	0	0	0	0	0	0
0600	0.12	0.07	0	0	1.09	1.00	0	0
0700	0.42	0.36	0.05	0.07	1.29	1.04	0.19	0.16
0800	0.82	0.71	0.04	0.10	1.59	1.30	0.34	0.27
0900	1.23	1.02	0	0.10	1.59	1.48	0.49	0.41
1000	1.35	1.30	0.02	0.06	1.59	1.54	0.99	0.95
1100	1.52	1.45	0.03	0.09	1.59	1.54	1.19	1.14
1200	1.58	1.53	0.10	0.16	1.64	1.55	1.29	1.24
1300	1.58	1.50	0.10	0.20	1.64	1.53	1.29	1.24
1400	1.50	1.44	0.05	0.12	1.59	1.52	1.19	1.09
1500	1.35	1.30	0.02	0.06	1.59	1.52	1.04	0.95
1600	1.10	1.01	0.05	0.12	1.54	1.44	0.54	0.44
1700	0.77	0.72	0.05	0.09	1.49	1.33	0.34	0.30
1800	0.48	0.40	0.03	0.06	1.44	1.14	0.19	0.18
1900	0.11	0.08	0	0	1.14	1.00	0.14	0.03
2000	0	0	0	0	0	0	0	0
	December							
	Extreme	95 Percentile	Extreme	95 Percentile	Extreme	95 Percentile	Extreme	95 Percentile
0700	0	0	0	0	0	0	0	0
0800	0.16	0.10	0	0	1.34	1.12	0.64	0.50
0900	0.46	0.42	0.04	0.06	1.44	1.36	0.94	0.89
1000	0.79	0.71	0.01	0.07	1.69	1.60	1.39	1.29
1100	0.95	0.92	0.02	0.04	1.79	1.68	1.64	1.56
1200	1.09	1.02	0	0.03	1.79	1.70	1.74	1.66
1300	1.05	1.02	0	0.03	1.79	1.78	1.74	1.66
1400	0.94	0.89	0.02	0.05	1.74	1.67	1.59	1.63
1500	0.79	0.70	0	0.03	1.74	1.57	1.39	1.27
1600	0.46	0.41	0.04	0.06	1.54	1.40	0.99	0.91
1700	0.16	0.10	0	0	1.34	1.12	0.64	0.50
1800	0	0	0	0	0	0	0	0

*Diffuse radiation, associated with total horizontal solar radiation extremes.

Tables 4.4 and 4.5 give the frequency distributions for the extreme* values and the 95 percentile values for the different types of solar radiation as a function of hours of the day. The values given for diffuse radiation are the values which occurred in association with the extremes and the 95th percentiles of the other solar radiations given. Direct sunlight with surrounding cumulus clouds may give significantly higher values of radiation. Since the diffuse sky radiation decreases with increasing total horizontal solar radiation, the values given in tables 4.4 and 4.5 are lower than the highest values of diffuse radiation which occurred during the period of record. They should be used with the other extreme values. Tables 4.4 and 4.5 both present the total solar radiation intensities received on a south-facing surface, with the normal to the surface at 45° to the horizon, as dictated by equation (4.7). Solar radiation data recommended for use in design are given in table 4.6 and figure 4.3 versus time of day. The design high curve presents clear day direct incident solar radiation to a horizontal surface. The actual radiation absorbed by a surface would be a function of the surface optical properties and the surface geometry relative to the Sun vector. The design low curve presents cloudy day diffuse solar radiation which would apply to all surfaces. The actual radiation absorbed by these surfaces would also be a function of surface optical properties. These data should be used in conjunction with the sky temperature defined in section 4.3.5.1..

4.4.3.3 Variation With Altitude

Solar radiation intensity on a surface will increase with altitude above the Earth's surface, with clear skies, according to the following equation (the LOWTRAN 7 code can be used to calculate I_H):

$$I_H = I_{DN} + (1.94 - I_{DN}\left(1 - \frac{\rho_H}{\rho_S}\right), \tag{4.9}$$

where

I_H = intensity of solar radiation normal to surface at required height

I_{DN} = intensity of solar radiation normal to surface at the Earth's surface assuming clear skies ($I_{DN} = I_{TN} - I_{dH}$)

ρ_H = atmospheric density at required height (from U.S. Standard Atmospheres, U.S. Standard Supplemental Atmospheres, or this document) (kg m^{-3})

ρ_S = atmospheric density at sea level (from U.S. Standard Atmospheres, U.S. Standard Supplemental Atmospheres, or this document) (kg m^{-3})

S = solar constant (in g-cal cm^{-2}).

The diffuse radiation I_{dH} decreases with altitude above the Earth's surface, with clear skies. A good estimate of the value can be obtained from the following equation:†

$$I_{dH} = 0.7500 - 0.4076\ I_H\ , \tag{4.10}$$

where

I_{dH} = intensity of diffuse radiation

I_H = intensity of solar radiation normal to surface.

Equation (4.10) is valid for values of I_H from equation (4.9) up to 1.84 g-cal cm^{-2}. For values of I_H greater than 1.84 g-cal cm^{-2}, $I_{dH} = 0$.

* Extreme as used in this section is the highest measured value of record.

† Equation (4.10) is based on a cloudless and dust-free atmosphere.

4.4.3.4 Solar Radiation During Extreme Wind Conditions

When ground winds occur exceeding the 95, 99, or 99.9 percentile design winds given in section II of this document, the associated weather normally is such that clouds, rain, or dust is generally present; therefore, the intensity of the incoming solar radiation will be less than the maximum values given in tables 4.4 and 4.5. Maximum values of solar radiation intensity to use with corresponding wind speeds are given in table 4.3.

Table 4.6 Recommended design high and design low solar radiation (ref. 4.9).

Local Time of Day	Design High Solar Radiation		Local Time of Day	Design Low Solar Radiation	
Hour	Btu/ft^2/h	g-cal/cm^2/min	Hour	Btu/ft^2/h	g-cal/cm^2/min
0500	0	0.00	0655	0	0.00
1100	363	1.64	1100	70	0.32
1400	363	1.64	1300	80	0.36
2000	0	0.00	1710	0	0.00

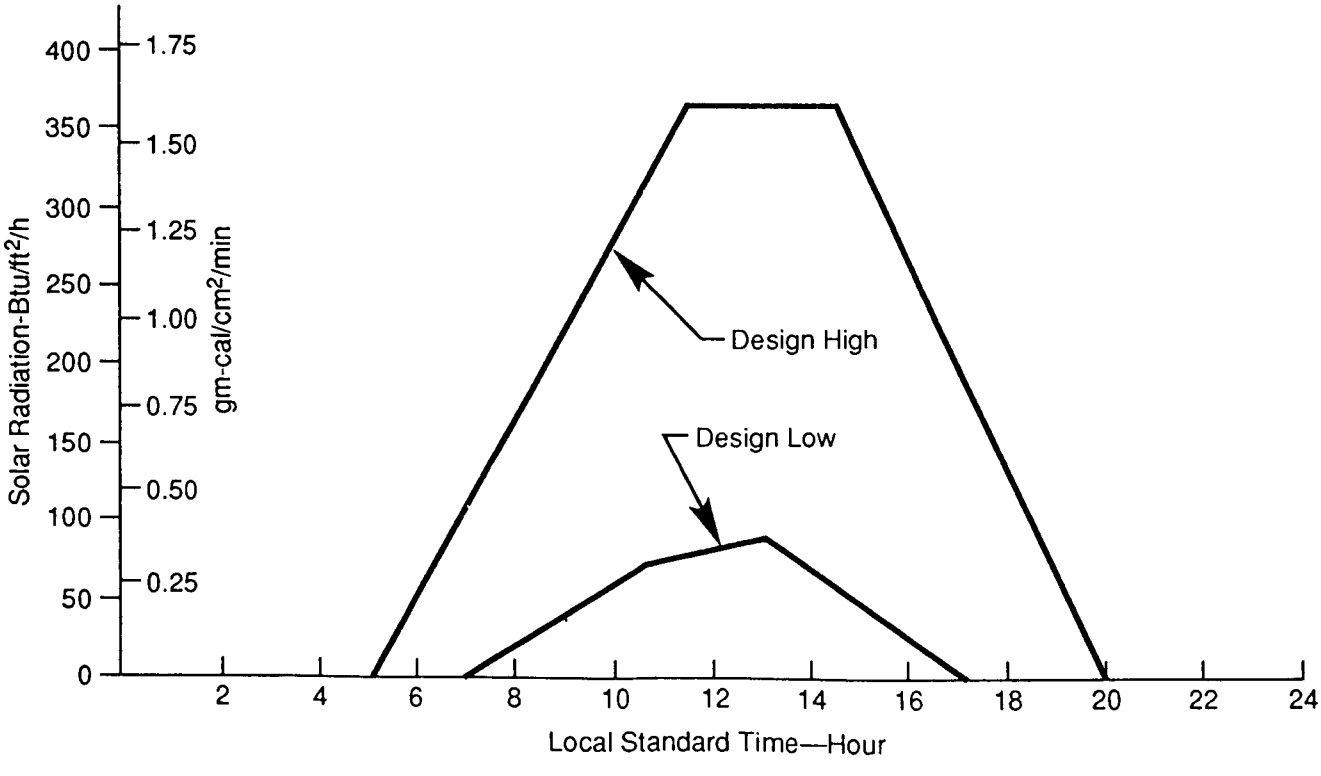

Figure 4.3 Recommended design solar radiation at ground level (ref. 4.9).

Note: Design high is direct incident solar radiation to a horizontal surface. Design low is diffuse incident radiation to any surface.

4.5 Reradiation and Temperature Effects

Objects receiving solar or other radiation absorb some of the energy and reradiate energy in the infrared band. The exchange of energy will heat or cool an object and may also affect surrounding objects.

4.5.1 Average Emittance of Objects

In thermal engineering studies, the color of a surface, especially when painted, is not important for low-temperature radiation (i.e., below about 0 °C for most painted surfaces). At such low temperatures, the absorptivity is about the same in the visible spectrum. The word "emittance" (or emissivity) is used to describe such data. Emittance is the ratio of the actual measured value to the emittance of a black body (considered "1.00") (ratio is always less than one). The emittance of some substances is essentially the same at all wavelengths. Such radiators are referred to as "gray" bodies. However, in most real substances the emittance varies as a function of wavelength and the temperature of the object. Colored surfaces may differ in absorptivity as was shown in tests with thermisters having different spectral responses when used on radiosondes at Marshall Space Flight Center (ref. 4.14) and also at Goddard Space Flight Center (ref. 4.15). A list of values of emissivity and absorptivity for various surfaces and different colors of paint exposed to solar radiation is presented in reference 4.11. Similar data are available in other publications. These give either a range of values for different wavelengths or mean values for each type of surface. Nearly all paints have very high emittances in the infrared region of the spectrum, yet most metals have lower emittance in the infrared. The change of temperature of an object (above or below the air temperature), which is the amount of heating or cooling, is proportional to the emittance or absorptivity. Therefore, the accuracy of determining the temperature of a surface exposed to radiation is related to the accuracy of the values of emittance and absorptivity available. Spectral distribution curves of emittance are available (or can be determined) for many surfaces. Knowing the emittance curve, the average emittance of any surface can be computed by the following method:

a. Divide the spectral emittance curve (i.e., that given in figure 4.4) into small intervals that have small or no change of emittance within the interval.

b. Using the same intervals from the spectral distribution of radiation (i.e., from table 4.1), multiply each value of emittance over the selected interval by the percentage of radient power over the interval.

c. Sum the resultant products to give the average emittance.

Table 4.7 and figure 4.4 give an example of such emittance computations for a white surface with data from figure 4.1 and table 4.1 being used. Similar computations can be accomplished for other sources of radiation such as the night sky or from cloudy skies.

4.5.2 Computation of Surface Temperature From One Radiation Source

Note: In the following computations, except in equation (4.13), degrees Kelvin must be used. In equation (4.13), any unit of temperature may be used. Units of solar radiation must be in the same unit system as the Stefan-Boltzmann constant.

The extreme value of temperature which a surface may reach when exposed to daytime (solar) or nighttime (night sky) radiation with no wind (calm), assuming it has no mass or heat transfer within the object, is

$$T_S = T_A + \mathrm{E}\,(\Delta T_{BS}) \ , \tag{4.11}$$

Table 4.7 Computation of emittance of white paint ($BaSO_4$ and MgO) exposed to direct solar radiation at the Earth's surface.

Wavelength (μ)	Emittance (Ratio)	Average Emittance (Ratio)	Solar Radiation, 1 Atmosphere (%)	Solar Radiation Over Interval (%)	Product of Average Emittance and Percent Solar Radiation Over Interval Divided by 100
0.300	0.73		0.03		
		0.590		1.22	0.0072
0.330	0.45		1.25		
		0.410		1.55	0.0063
0.350	0.37		2.80		
		0.365		21.00	0.0766
0.500	0.36		23.80		
		0.325		11.77	0.0382
0.580	0.29		35.57		
		0.260		15.54	0.0404
0.700	0.23		51.11		
		0.225		10.37	0.0233
0.800	0.22		61.48		
		0.260		7.88	0.0205
0.900	0.30		69.36		
		0.370		6.71	0.0248
1.000	0.44		76.07		
		0.520		9.32	0.0485
1.200	0.60		85.39		
		0.650		3.44	0.0224
1.400	0.70		88.83		
		0.745		4.57	0.0340
1.600	0.79		93.40		
		0.810		3.01	0.0244
1.900	0.83		96.41		
		0.830		3.59	0.0298
50.000	0.83		100.0		
Sum = average emittance = 0.396					

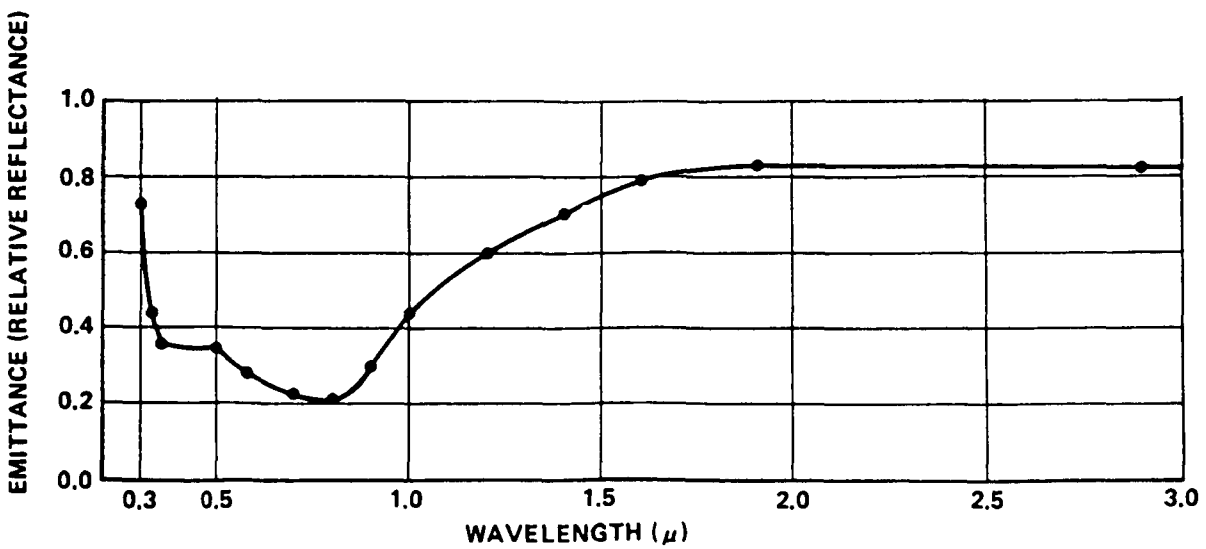

Figure 4.4 Plot of measured emittance of barium sulfate and magnesium oxide (white paint) versus wavelength when exposed to the solar spectrum.

where

T_S = surface temperature (K)

T_A = air temperature (K)

E = emittance of surface

ΔT_{BS} = Surface temperature differential resulting in an increase in blackbody temperature (K) from daytime solar radiation (plus); or a decrease in blackbody temperature (K) from day or nighttime sky radiation (minus), calculated from

$$\Delta T_{BS} = \left(\frac{I_{TS}}{\sigma}\right)^{1/4} - T_A \ . \tag{4.12}$$

Equation (4.12) gives the surface radiative balance, i.e., absorbed radiation = emitted radiation.

Extreme values of ΔT_{BS} can be obtained from figure 4.5A or table 4.8, where

I_{TS} = total radiation (solar by day) (sky for night) received at surface. These values can be extremes from tables 4.4, 4.5, or 4.2 from this report.

σ = Stefan-Boltzmann constant

$= 8.312 \times 10^{-11}$ g-cal cm^{-2} K^{-4}

$= 5.6697 \times 10^{-12}$ W cm^{-2} K^{-4}.

The term $(I_{TS}/\sigma)^{1/4}$ is equal to the extreme blackbody surface temperature.

If a correction for wind speed is desired, equation (4.11) can be used as follows:

$$T_S = T_A + E(\Delta T_{BS}) \frac{f_w}{100} \ , \tag{4.13}$$

where f_w is the correction for wind speed in percent from figure 4.5B. Equations (4.11), (4.12), and (4.13) are only for computing the effect of one source of radiation on a surface. When more than one radiation source is received by an object, then a more complex method must be used, as given in subsection 4.5.3. The value of f_w is for sea level (1.0 atmosphere pressure). For values at higher altitudes the value of

$$f_{w_{alt}} = f_w \ (\rho_{alt}/\rho_{sea\ level}) \ . \tag{4.13A}$$

4.5.3 Computation of Surface Temperature From Several Simultaneous Radiation Sources

If we have a blackbody with several radiation sources and no forced or natural convection (calm wind), then the total radiation balance (I) can be computed from the Stefan-Boltzmann law:

$$\sigma T^4 = \sum_i^n I_i \qquad i = 1, 2, 3, \ldots, n \ . \tag{4.14}$$

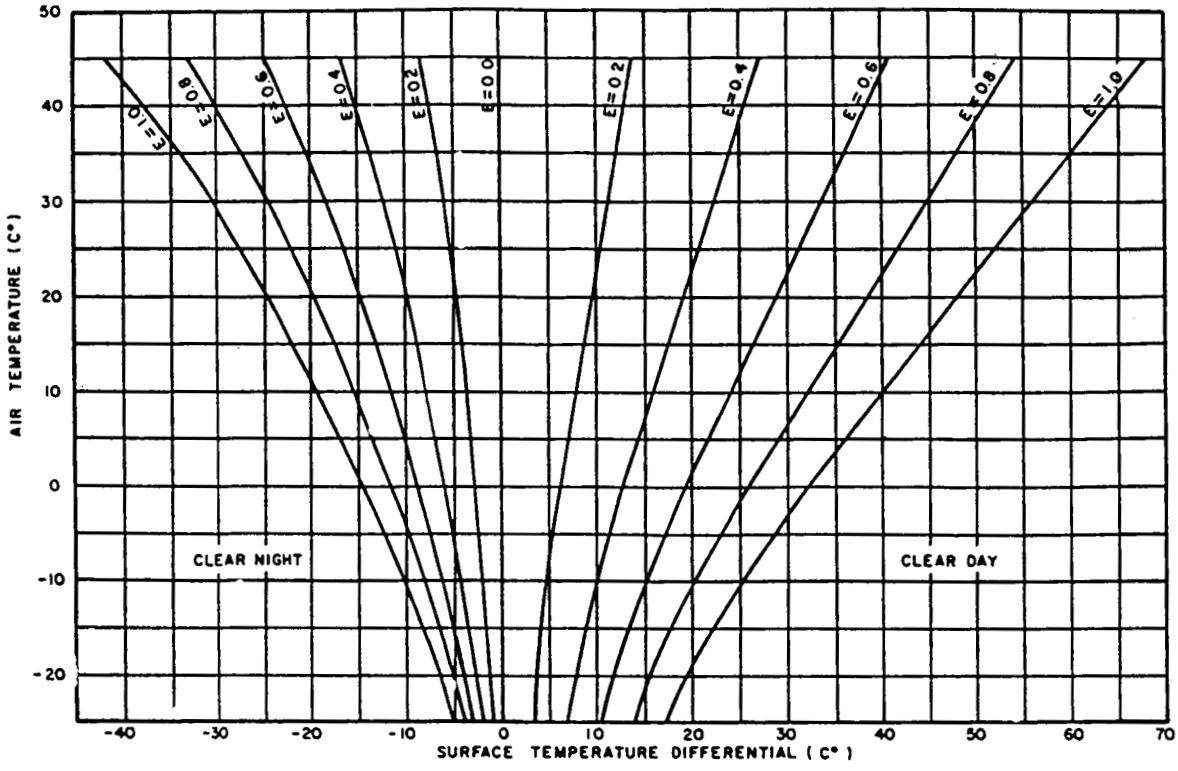

A. Surface temperature differential (ΔT_{BS}) with respect to air temperature for surface with emittance between 0.0 and 1.0 for a calm wind. The temperature difference, after correction for wind speed, is added or subtracted to the air temperature to give the surface (skin) temperature. Wind speed has a great effect, not because it changes the radiation part of the heat transfer, but because it makes the convective heat transfer very significant.

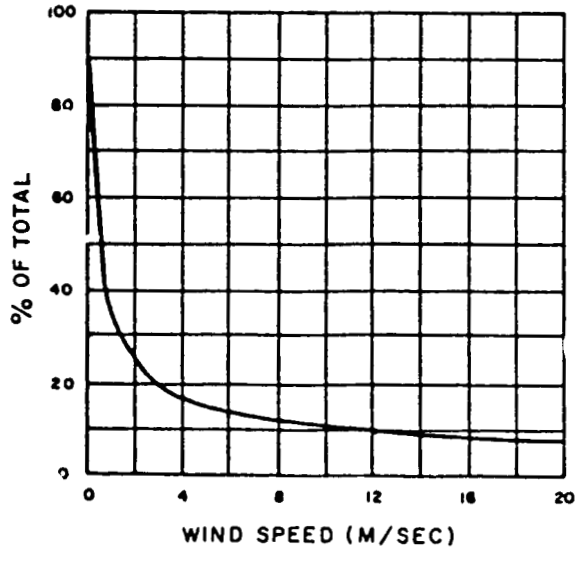

B. Correction (*fw*) for wind speed to the surface temperature difference (obtained from graph A). Valid only for a pressure of one atmosphere.

Figure 4.5 Extreme surface (skin) temperature of an object near the Earth's surface (0 to 300 m) for clear sky.

Table 4.8 Extreme surface (skin) temperature above or below air temperature of an object near the Earth's surface.

Air Temperature (°C)	Surface Temperature Differential (°C)									
	Clear Night					Clear Day				
	Wind Speed ($m\ s^{-1}$)					Wind Speed ($m\ s^{-1}$)				
	0	2	4	10	20	0	2	4	10	20
	Correction Factor					Correction Factor				
	1.00	0.25	0.17	0.11	0.08	1.00	0.25	0.17	0.11	0.08
-25	-5.0	-1.2	-0.8	-0.6	-0.4	16.9	4.2	2.9	1.9	1.4
-20	-6.5	-1.6	-1.1	-0.7	-0.5	19.2	4.8	3.3	2.1	1.5
-15	-8.2	-2.0	-1.4	-0.9	-0.6	22.0	5.5	3.7	2.4	1.8
-10	-10.2	-2.6	-1.7	-1.1	-0.8	25.1	6.3	4.3	2.8	2.0
-5	-12.2	-3.0	-2.1	-1.3	-1.0	28.5	7.1	4.8	3.1	2.3
0	-14.5	-3.6	-2.5	-1.6	-1.2	32.0	8.0	5.4	3.5	2.6
5	-16.9	-4.2	-2.9	-1.9	-1.4	36.0	9.0	6.1	4.0	2.9
10	-19.4	-4.8	-3.3	-2.1	-1.6	40.0	10.0	6.8	4.4	3.2
15	-21.9	-5.5	-3.7	-2.4	-1.8	44.0	11.0	7.5	4.8	3.5
20	-24.6	-6.2	-4.2	-2.7	-2.0	48.0	12.0	8.2	5.3	3.8
25	-27.4	-6.8	-4.6	-3.0	-2.2	52.0	13.0	8.8	5.7	4.2
30	-30.5	-7.6	-5.2	-3.4	-2.4	56.0	14.0	9.5	6.2	4.5
35	-34.0	-8.5	-5.8	-3.7	-2.7	60.0	15.0	10.2	6.6	4.8
40	-37.7	-9.4	-6.4	-4.1	-3.0	64.0	16.0	10.9	7.0	5.1
45	-41.7	-10.4	-7.1	-4.6	-3.3	68.0	17.0	11.6	7.5	5.4

NOTE: Values are given for solar absorbtivity and an emittance value of 1.0, i.e., black body. Temperature differences for other emittance can be determined by multiplying tabular value by the appropriate emittance.

Then

$$T - T_A = \Delta T_{BS} = \left(\frac{\sum_{1}^{n} I_i}{\sigma} \right) - T_A \ , \tag{4.15}$$

where T_A is the air temperature.

For any object exposed to any type of radiation in the Earth's atmosphere, the following function may be used.

$$\Delta T_{BS} = f_w \left(\frac{\sum_{1}^{n} E_i I_i}{\sigma} \right)^{1/4} - T_A \ , \tag{4.16}$$

where

E_i = emittance of object for corresponding radiation source I_i

$$\Delta T_{BS} = T - T_A \tag{4.17}$$

f_w = wind effect (convection)

$$f_w = \frac{0.325}{\sqrt{w}} \ , \tag{4.18}$$

w = wind speed (m/s).

4.6 Temperature

Several types of temperatures at the Earth's boundary layer must be considered in design. These are as follows:

a. Air temperatures at surface level (normally measured at a height of 1.22 m (4 ft) above a grass surface in special shelter) (see section 4.6.1). Temperatures at various altitudes above the surface are given in the Reference Atmosphere tables of section III.

b. Changes of air temperature with changes in solar radiation intensity (usually the rapid changes which occur in less than 24 hours) are given in section 4.6.2.

c. Measurement of surface or skin temperature of a surface exposed to radiation is presented in section 4.6.3.

d. Temperatures within a closed compartment. See section 4.6.4.

All of the above will be discussed in the following subsections.

4.6.1 Extreme Air Temperature Near the Surface

Surface air temperature extremes (maximum, minimum, and 95-percentile values) and the extreme minimum sky radiation (equal to the out-going radiation) are given in table 4.2 for various geographical areas. Maximum and minimum temperature values should be expected to last only a few hours during a daily period.* Generally, the maximum temperature is reached after 12 noon and before 5 p.m., while the minimum temperature is reached just before sunrise. Table 4.9 shows the maximum and minimum design air temperatures for each hour at Kennedy Space Center. These curves represent a cold and hot extreme day. The method of sampling the day (frequency of occurrence of observations) will result in the same extreme values if the same period of time for the data is used, but the 95-percentile values will be different for hourly, daily, and monthly data reference periods. Selection of the reference period depends on engineering application. Table 4.10 gives monthly mean temperatures, standard deviations, and 2.5 and 97.5 percentiles of temperature values for Kennedy Space Center, Florida, and Vandenberg AFB, California. United States and worldwide temperature extremes are given in section V.

4.6.2 Extreme Air Temperature Change Over Time

a. For all areas the design values of extreme air temperature changes (thermal shock) are:

(1) An increase of air temperature of 10 °C (18 °F) with a simultaneous increase of solar radiation (measured on a normal surface) from 0.50 g-cal cm^{-2} min^{-1} (110 Btu ft^{-2} h^{-1}) to 1.85 g-cal cm^{-2} min^{1} (410 Btu ft^{-2} h^{-1}) may occur in a 1-hour period. Likewise, the reverse change of the same magnitude may occur for decreasing air temperature and solar radiation.

(2) A 24-hour change may occur with an increase of 27.7 °C (50 °F) in air temperature in a 5-hour period, followed by 4 hours of constant air temperature, then a decrease of 27.7 °C (50 °F) in a 5-hour period, followed by 10 hours of constant air temperature.

---

* The equivalent radiation values given here were computed from the equivalent temperature minimum extremes by using the Stefan-Boltzmann law (σT^4).

Table 4.9 Maximum and minimum design surface air temperatures at each hour for the Kennedy Space Center.[a]

Time (LST)	Annual Maximum Temperature		Annual Minimum Temperature[b,c]	
Hours	°C	°F	°C	°F
1 a.m.	28.9	84	–3.3	26
2	28.9	84	–3.9	25
3	29.4	85	–4.4	24
4	28.3	83	–4.4	24
5	28.9	84	–5.0	23
6	29.4	85	–5.6	22
7	30.6	87	–6.1	21
8	31.1	88	–5.6	22
9	33.3	92	–3.9	25
10	34.4	94	–2.2	28
11	35.0	95	–1.7	29
12 noon	36.1	97	–0.6	31
1 p.m.	37.2	99	0.0	32
2	36.1	97	+2.8 (+3.3)	37 (38)
3	36.7	98	+2.8 (+3.9)	37 (39)
4	36.1	97	+2.2 (+4.4)	36 (40)
5	36.1	97	+1.1 (+4.4)	34 (40)
6	35.0	95	0.0 (+1.7)	32 (35)
7	33.3	92	–0.6	31
8	31.7	89	–1.1	30
9	31.1	88	–1.7 (–1.1)	29 (30)
10	30.0	86	–2.2 (–1.7)	28 (29)
11	30.0	86	–2.2	28
12 mid	30.0	86	–2.2	28

a. Data based on Patrick Air Force Base and Kennedy Space Center records.

b. Many KSC minimum temperatures are representative of the January 21–22, 1985, cold spell. This cold spell altered most minimum temperature values. These values given represent annual extreme conditions, but can also be used in a continuous 24-hour cycle of extreme KSC cold temperature conditions starting at 9 a.m. January 21 (25 °F) through 8 a.m. January 22 (22 °F). The minimum values given for 2, 3, 4, 5, 6, 9, and 10 p.m. are not representative of the January 1985 cold spell. Cold spell values for these hours in January 21, 1985, are presented in brackets to the right. Note that the maximum values cannot be used in a continuous time cycle.

c. Note that the minimum temperature of record for this location, as given in tables 3.4 and 4.2, is –7.2 °C (19 °F).

Table 4.10 Monthly mean, standard deviations (STD), and 2.5 and 97.5 percentile values of temperature for Kennedy Space Center, Florida and Vandenberg AFB, California.

	Kennedy Space Center				Vandenberg AFB			
			Percentiles				Percentiles	
Month	Monthly Mean or 50 Percentile (°F)	Standard Deviation 30-Day Average	30-Day 2.5%[a] (°F)	Average 97.5%[a] (°F)	Monthly Mean or 50 Percentile (°F)	Standard Deviation 30-Day Average	30-Day 2.5%[a] (°F)	Average 96.5%[a] (°F)
January	59.9	3.5	53.1	66.7	50.9	1.7	47.6	54.2
February	59.8	4.8	50.4	69.2	51.1	2.0	47.1	55.1
March	64.4	3.1	58.3	70.5	51.6	1.8	48.1	55.1
April	70.1	1.3	67.6	72.6	52.4	1.6	49.3	55.5
May	74.5	0.9	72.8	76.2	53.2	1.1	51.2	55.7
June	77.8	1.3	75.3	80.3	55.6	1.7	52.2	59.0
July	79.2	1.2	76.8	81.6	56.9	1.7	53.0	59.5
August	78.9	0.7	77.6	80.2	58.3	1.7	55.0	61.6
September	78.5	1.1	76.3	80.6	59.2	2.0	55.3	63.1
October	73.9	1.7	70.3	77.1	58.6	1.8	55.0	62.2
November	67.0	2.8	61.3	72.4	54.7	2.1	50.5	58.9
December	60.6	3.0	54.8	66.4	51.0	2.7	45.7	56.3

a. Recommended for use in solid rocket motor propellant bulk temperature predictions for design analyses. See (ref. 14.9) Natural Environment Design Requirements – Appendix 10.10 of NSTS 07700, Volume X.

b. For Eastern Range (Kennedy Space Center), the 99.9-percentile air temperature changes are as follows:

(1) An increase of air temperature of 5.6 °C (11 °F) with a simultaneous increase of solar radiation (measured on a normal surface) from 0.50 g-cal cm^{-2} min^{-1} (110 Btu ft^{-2} h^{-1}) to 1.60 g-cal cm^{-2} min^{-1} (354 Btu ft^{-2} hr^{-1}), or a decrease of air temperature of 9.4 °C (17 °F) with a simultaneous decrease of solar radiation from 1.60 g-cal cm^{-2} min^{-1} (354 Btu ft^{-2} h^{-1}) to 0.50 g-cal cm^{-2} min^{-1} (110 Btu ft^{-2} h^{-1}) may occur in a 1-hour period.

(2) A 24-hour temperature change may occur as follows: An increase of 16.1 °C (29 °F) in air temperature (wind speed under 5 m/s) in an 8-hour period, followed by 2 hours of constant air temperature (wind speed under 5 m/s), then a decrease of 21.7 °C (39 °F) in air temperature (wind speed between 7 and 10 m/s) in a 14-hour period.

4.6.3 Surface (Skin) Temperature

The temperature of the surface of an object exposed to radiation (solar, day sky, or night sky) is usually different from the air temperature (refs. 4.16 and 4.17). The amount of the extreme difference in temperature between a black body object and the surrounding air temperature is given in table 4.8 and figure 4.5A for exposure to a clear night (or day)* sky or to the Sun on a clear day with calm winds. A change in the flow of air across an object will change the balance between the heat transfer, resulting from radiation and convection-conduction. The difference in the temperature between air and the object will decrease with increasing wind speed (ref. 4.18). Part B of figure 4.5 provides information for making the correction for wind speed. These values are also given in table 4.8 for different wind speeds.

* Without the Sun's rays striking, the daytime sky is about as cold as the nighttime sky.

4.6.4 Compartment Temperatures

4.6.4.1 Introduction

A cover of material enclosing an air space will conduct heat to (or remove heat from) the inside air when the cover is heated by solar radiation (or cooled by the night sky). This results in the compartment air space being frequently considerably hotter or cooler than the surrounding air. The temperature reached in a compartment is dependent on the location of the air space with respect to the heated surface, the type, thickness, and optical properties of the surface material, the type of construction, and the insulating value of the material. Adding more layers of material with high insulating value on the inside surface of the compartment will greatly reduce the heating or cooling of the air in the compartment space (refs. 4.20 and 4.21).

4.6.4.2 Compartment High Temperature Extreme

A compartment probable extreme average high temperature of 87.8 °C (190 °F) for a period of 1 hour and an average high temperature of 65.6 °C (150 °F) for a period of 6 hours must be considered at all geographic locations while aircraft or other transportation equipment is stationary on the ground without air conditioning in the compartment. These extremes will be found at the top and center of the compartment (refs. 4.20 and 4.21).

4.7 Data on Air Temperature Distribution With Altitude

Data on air temperature distribution with altitude are given in section III.

REFERENCES

4.1 Middleton, W.E.K. and Spilhaus, A.F.: "Meteorological Instruments." University of Toronto Press, Third Edition, revised 1960.

4.2 SSP 30425, Revision A, "Space Station Program, Natural Environment Definition for Design," Rev. A, National Aeronautics and Space Administration, Reston, Virginia, June 1991.

4.3 "Solar Electromagnetic Radiation," NASA SP-8005, Rev. April 1971. National Aeronautics and Space Administration, Washington, DC.

4.4 Thekaekara, Matthew P. (Editor): "The Solar Constant and the Solar Spectrum Measured From a Research Aircraft." NASA TR R-351, National Aeronautics and Space Administration, Washington, DC, October 1970.

4.5 Thekaekara, Matthew P. (Editor): "The Energy Crisis and Energy From the Sun." Papers presented at the Symposium on Solar Energy Utilization and Panel Discussion on Solar Energy Programs and Progress, Shoreham American Hotel, Washington, DC, April 30, 1974. Supplement to the Proceedings of the 20th Annual Meeting of the Institute of Environmental Sciences.

4.6 Moon, Parry: "Proposed Standard Solar Radiation Curves for Engineering Use." Journal of the Franklin Institute, vol. 230, November 1940, pp. 583–617.

4.7 Kneizys, F.S., Shettle, E.P., Abreu, L.W., Chetwynd, J.H., Anderson, G.P., Gallery, W.O., Selby, J.E.A., and Clough, S.A.: "Users Guide to LOWTRAN 7." AFGL-TR-88-0177, Project 7670, August 1988, Air Force Geophysics Laboratory, Hanscom AFB, MA.

4.8 Thekaekara, M.P.: "Alternate Methods in Solarimetry: Remote Sensing and Computer Models." Solarimetry Workshop, February 24–28, 1975, Energy Task Group. Financiadora de Estudos e Projetos—FINEP, Rio de Janeiro, Brazil. Paper presented at the Brazilian National Academy of Sciences, February 24, 1975.

4.9 "Space Shuttle—Flight and Ground System Specification," Level II Program Definition and Requirements, NASA–JSC, NSTS 07700, Vol. X, Rev. J.; "Natural Environment Design Requirements," Appendix 10.10, June 14, 1990.

4.10 Parmalee, G.V.: "Irradiation of Vertical and Horizontal Surfaces by Diffuse Solar Radiation From Cloudless Skies." Heating, Piping, and Air Conditioning, vol. 26, August 1954, pp. 129–136.

4.11 ASHRAE Handbook of Fundamentals. American Society of Heating, Refrigerating, and Air Conditioning Engineers, New York, 1967.

4.12 Becker, C.F., and Boyd, J.S.: "Solar Radiation Availability on Surfaces in the United States as Affected by Season, Orientation, Latitude, Altitude, and Cloudiness." Journal of Solar Engineering, Science and Engineering, vol. 1, January 1957, pp. 13–21.

4.13 Ornstein, M.P.: ""Solar Radiation." Journal of Environmental Sciences, vol. 5, April 1962, pp. 24–27.

4.14 Daniels, Glenn E.: "Errors of Radiosonde and Rocketsonde Temperature Sensors." Bulletin American Meteorological Society, vol. 49, No. 1, January 1968, pp. 16–18.

4.15 Schmidlin, F.J., Luers, J.K., and Huffman, P.D.: "Preliminary Estimates of Rocketsonde Thermistor Errors." NASA TP-2637, National Aeronautics and Space Administration, Washington, DC, September 1986.

4.16 Fishenden, Margaret, and Saunders, Owen A.: "The Calculation of Heat Transmission." His Majesty's Stationary Office, London, 1932.

4.17 Daniels, Glenn E.: "Measurement of Gas Temperature and the Radiation Compensating Thermocouple." Journal of Applied Meteorology, vol. 7, 1968, pp. 1026–1035.

4.18 "Tables of Computed Altitude and Azimuth," Publication H.O. No. 214, United States Hydrographic Office, United States Government Printing Office, 1940.

4.19 Duffie, John A. and Beckman, William A.: "Solar Energy Thermal Processes." John Wiley & Sons, NY, 1974.

4.20 Porter, William L.: "Occurrence of High Temperatures in Standing Boxcars." Technical Report EP-27, Headquarters Quartermaster Research and Development Center, United States Army, Natick, Massachusetts, February 1956.

4.21 Cavell, W.W., and Box, R.H.: "Temperature Data on Standard and Experimental Cartridges in Pilot Ejection Devices in a B47E Aircraft Stationed at Yuma, Arizona." Memo Report No. M60-16-1, Frankford Arsenal, Pitman-Dunn Laboratories Group, Philadelphia, Pennsylvania, 1960.

SECTION V. U.S. AND WORLD SURFACE EXTREMES

5.1 United States Surface Extremes

Most NASA programs involving the launch and reentry of aerospace vehicles are conducted in the United States. This section provides the extremes of those atmospheric variables not included elsewhere in this document that are critical to such programs. Statistical data discussed in this section include air temperature, snowfall, hail, and atmospheric pressure. The second part of this section, World Surface Extremes, provides a more general discussion of atmospheric extremes on a global scale.

5.1.1 Environments Included

(a) Air temperature, extreme maximum and minimum;

(b) Snowfall: snow loads, 24-h maximum and storm maximum;

(c) Hail, maximum size;

(d) Atmospheric pressure, extreme maximum and minimum.

Information is available for other extreme atmospheric parameters relative to the principal locations covered by this document by consulting the appropriate section in this document.

5.1.2 Source of Data

The extremes presented have been prepared using data from National Weather Service stations and published articles, such as reference 5.1. These extremes represent the highest or lowest extreme value measured at each station. The length of record varies from station to station, but most values represent more than 15 years of record. Where unusual geographical features in a local area affect an extreme value (such as the minimum temperature on a high mountain peak), it will not, in general, be shown on the maps presented unless a National Weather Service station is located there.

The extremes noted reflect measurements during the available period of record for essentially all meteorological parameters. Because this period of record covers only a few decades for most locations, it is obvious that there is a finite risk that the extreme values presented will be exceeded in future years. However, the values shown are considered appropriate as criteria guidelines for use in critical engineering design studies relative to probable occurrence of atmospheric extremes during expected operational lifetime.

5.1.3 Extreme Design Environments

The values of extreme maxima and minima in this section are for design guidelines and may or may not exactly reflect extrapolation (theoretical or otherwise) of actual measured values over the available period of record.

5.1.3.1 Air Temperature

The distribution, by state and location, of extreme maximum air temperatures in the United States is shown in figure 5.1, while figure 5.2 shows the extreme minimum temperature distribution. Given in table 5.1 are the extreme U.S. temperatures (°F) together with their locations and dates of occurrence (ref. 5.2). To convert to °C, use the formula: °C = 5/9 (°F–32). The maps (figs. 5.3 and 5.4) from reference 5.3 show the mean temperature and standard deviations of the temperatures for January and July.

To estimate the temperature $\hat{T}$ that is less than or equal to a probability p (corresponding to the normal distribution), from figures 5.3 and 5.4, find from the appropriate figure, by interpolation as needed, the mean temperature $\bar{T}$ and the standard deviation S_T and substitute these in the equation

$$\hat{T}=\bar{T}+S_T y_s\,[°F]\,.$$

Values of y_s for various normal probability levels are shown below:

Cold Temperatures (fig. 5.3)		Hot Temperatures (fig. 5.4)	
p	y_s	p	y_s
0.20	0.84	0.80	+0.84
0.10	−1.28	0.90	+1.28
0.05	−1.65	0.95	+1.65*
0.025	−1.96	0.975	+1.96
0.01	−2.33	0.99	+2.33

*The 95th percentile value is recommended for hot-day design ambient temperatures over runways for landing-takeoff performance calculation using figure 5.4; the 5th percentile is recommended for cold-day design.

5.1.3.2 Snowfall—Snow Load

The maps in figures 5.5 and 5.6 show the maximum depth of snow and the corresponding snow loads for the contiguous United States. Figure 5.5 shows the maximum depth for a 24-h period; figure 5.6 shows the maximum depth and the corresponding snow loads for a snow period. The storm total map shows the same snow depth as in the 24-h map in the southern low elevation areas of the United States since snow storms seldom exceed 24 h in these areas. The greatest 24-h snowfall was 1,930 mm (76 in) at Silver Lake, Colorado, on April 14–15, 1921. One storm gave 4,800 mm (189 in) at Mt. Shasta Ski Bowl, California, from February 13 to 19, 1959 (ref. 5.4). The greatest snowfall in one calendar month is 9,906 mm (390 in) which occurred at Tamarack, California, during January of 1911.

The terrain combined with the general movement of weather patterns has a great effect on the amount of fall, accumulation, and melting of the snow. Also, the length of a single storm varies from various areas. In some areas in mountain regions, much greater amounts of snowfall have been recorded than shown on the maps. Also, the snow in these areas may remain for the entire winter. For example, in a small valley near Soda Springs, CA, a seasonal snow accumulation of 7.9 m (26 ft) with a density of about 0.35 g/cm^3 was recorded. This gives a snow load of 2,772 kg/m^2 (567.7 lb/ft^2). Such a snow pack at Soda Springs is the greatest on record in the United States and was nearly double the previous records in the same area. A study of the maximum snow loads in the Wasatch Mountains of Utah showed that for a 100-year return period at 2,740 m (9,000 ft) altitude, a snow load of 1,220 kg/m^2 (250 lb/ft^2) could be expected (ref. 5.5).

Snow characteristics and loading for particular sites are given in subsection 7.4.

5.1.3.3 Hail

The distribution of maximum-sized hailstones in the United States is shown in figure 5.7. The sizes are for single hailstones and not conglomerates of several hailstones frozen together. The largest officially recorded hailstone in the United States weighed 757 g (1.67 lb). It fell September 3, 1970, at Coffeyville, KS (ref. 5.4). Subsection 7.5 presents further information concerning hail characteristics and climatology.

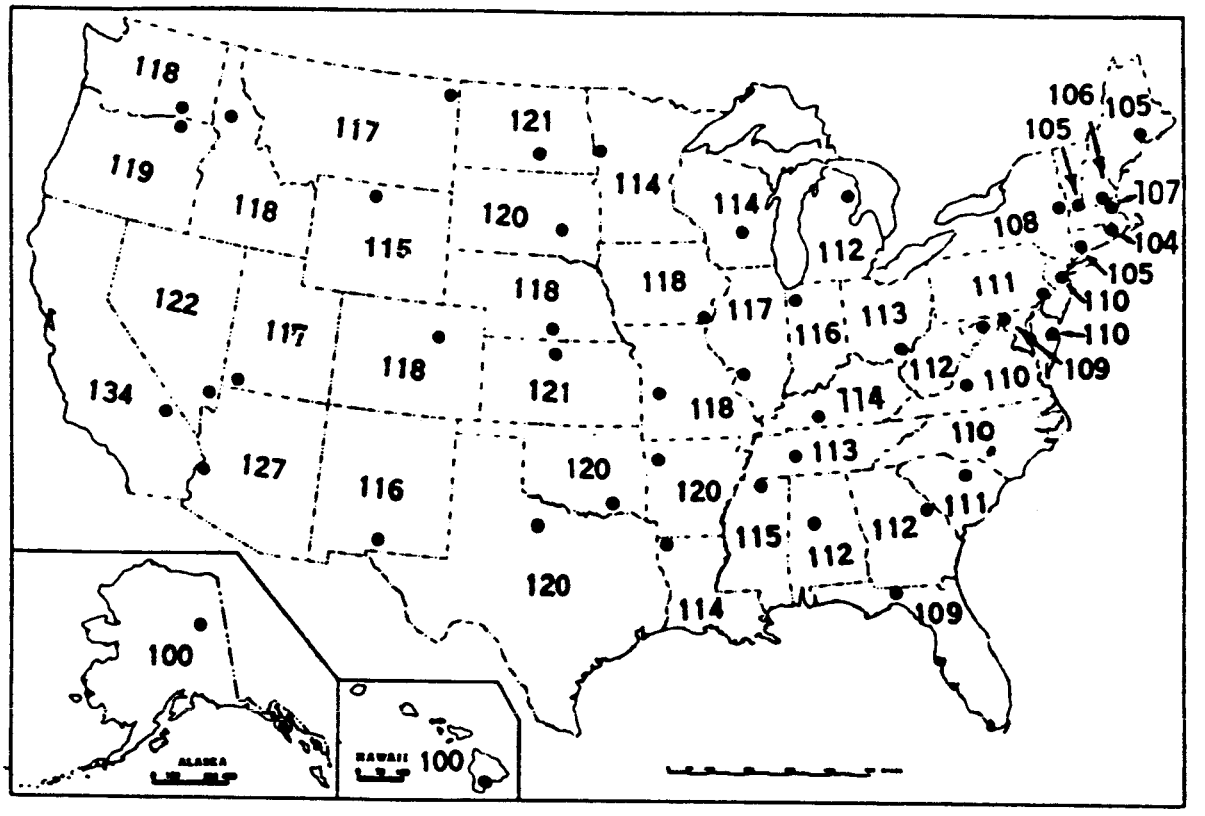

Figure 5.1 Highest temperatures (°F) of record and locations, by states.

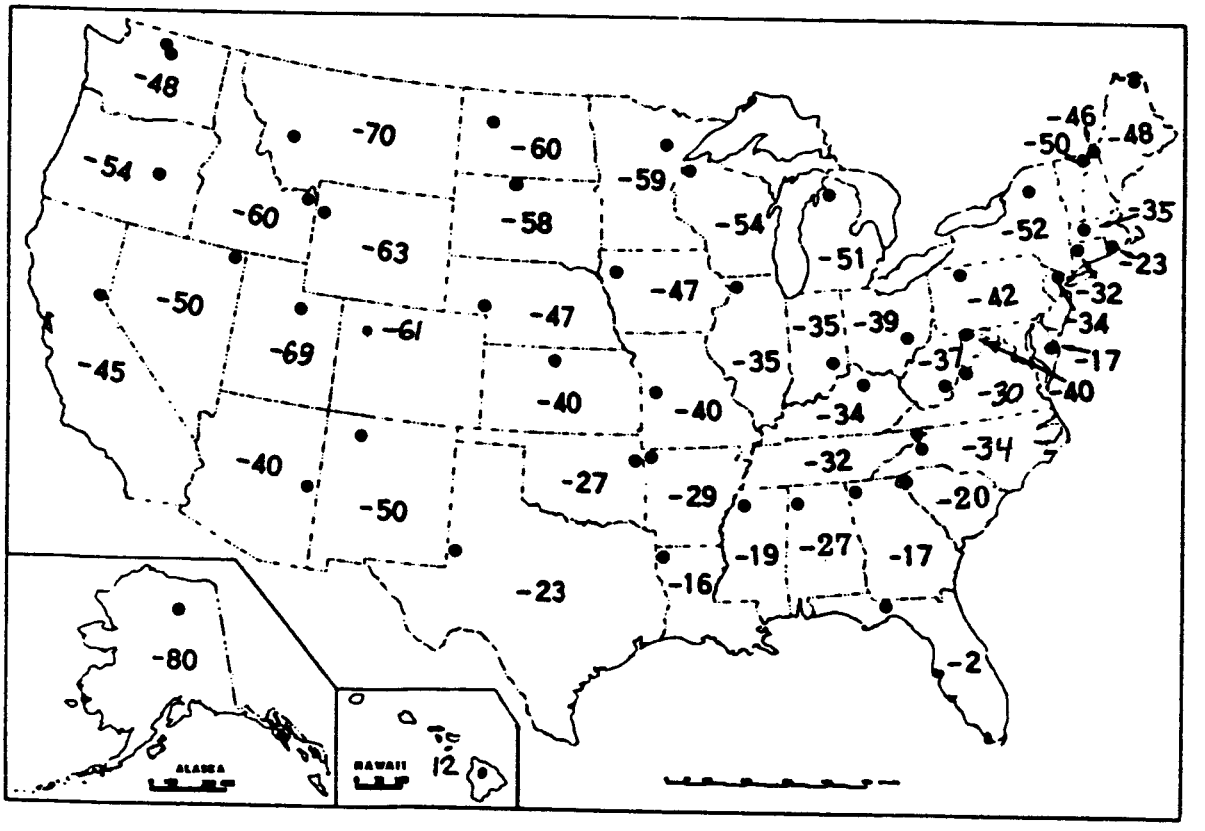

Figure 5.2 Lowest temperatures (°F) of record and locations, by states.

Table 5.1 Extremes of temperature and sea level pressure for the United States (ref. 5.1).

Temperature (°C (°F))		Location	Date	Sea-Level Pressure (N/m^2 (mb) (in))	Location	Date
High				High		
Contiguous United States	57 (134)	Greenland Ranch, CA	July 10, 1913	106,400 (1,064.0) (31.42)	Miles City, MT	Dec. 24, 1983
Hawaii	38 (100)	Pahala	April 27, 1931	102,670 (1,026.7) (30.32)	Honolulu	Feb. 10, 1919
Alaska	38 (100)	Fort Yukon	June 27, 1915	107,860 (1,078.6) (31.85)	Northway	Jan. 31, 1989
Low				Low		
Contiguous United States	–57 (–70)	Rogers Pass, MT	Jan. 20, 1954	95,490 (954.9) (28.20)	Canton, NY Block Island, RI	Jan. 3, 1913 Mar. 7, 1932
U.S. (Hurricane)	—	—	—	89,230 (892.3) (26.35)	Matecumbe Key, FL	Sept. 2, 1935
Hawaii	–11 (12)	Mauna Kea Observatory	May 17, 1979	97,200 (972.0) (28.70)	Barking Sands	Nov. 23, 1982
Alaska	–62 (–80)	Prospect Creek	Jan. 23, 1971	92,500 (925.0) (27.31)	Dutch Harbor	Oct. 25, 1977

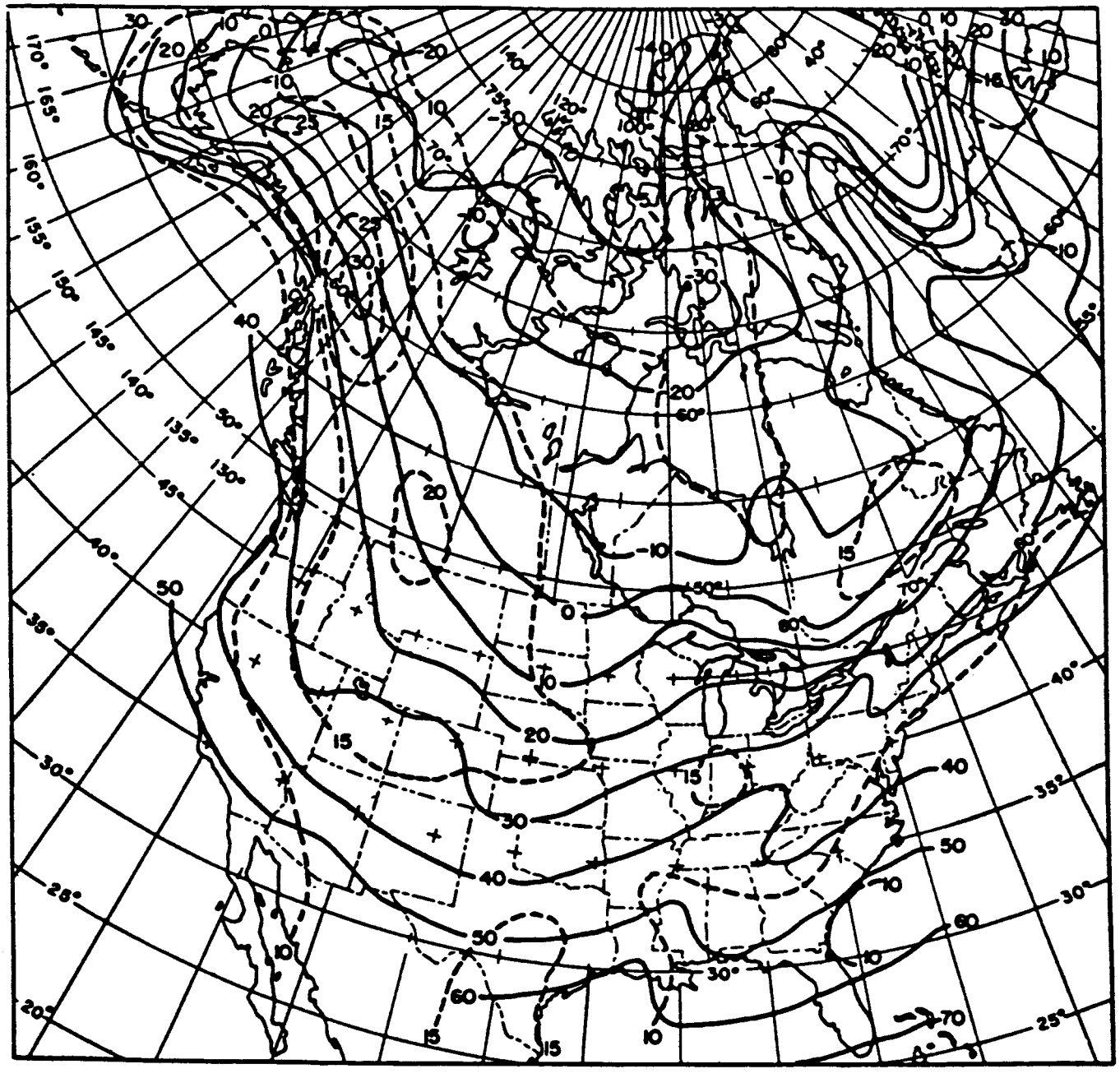

Figure 5.3 Isotherms of January hourly surface temperatures. (Approximate mean values (°F) are shown by solid lines, standard deviations (°F) by broken lines. The approximations were made to give best estimates of lower 1- to 20-percentile values of temperature by normal distribution (ref. 5.3).)

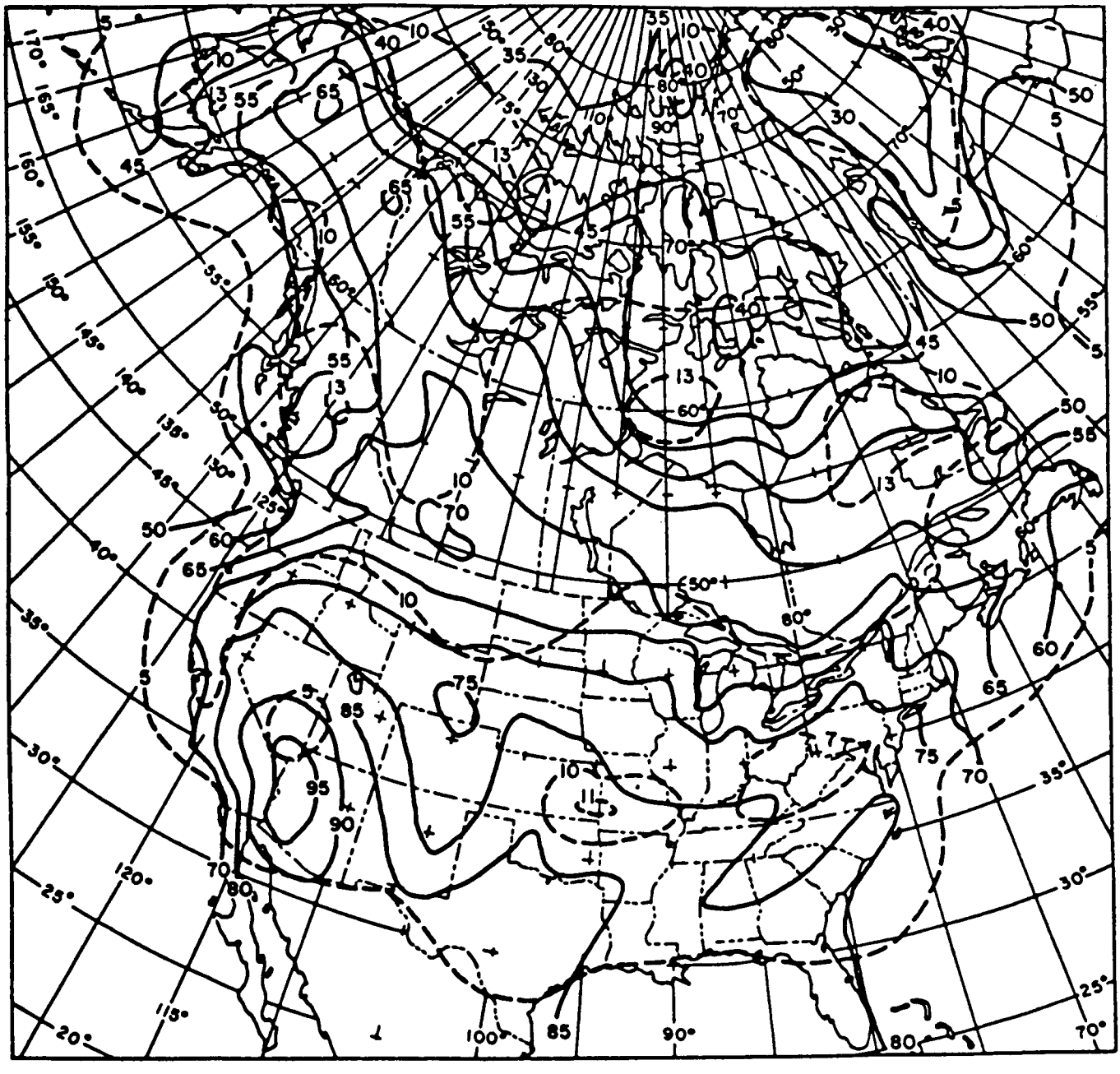

Figure 5.4 Isotherms of July hourly surface temperatures. (Approximate mean values (°F) are shown by solid lines, standard deviations (°F) by broken lines. The approximations were made to yield the best estimates of upper 80- to 99-percentile values by normal distribution (ref. 5.3).)

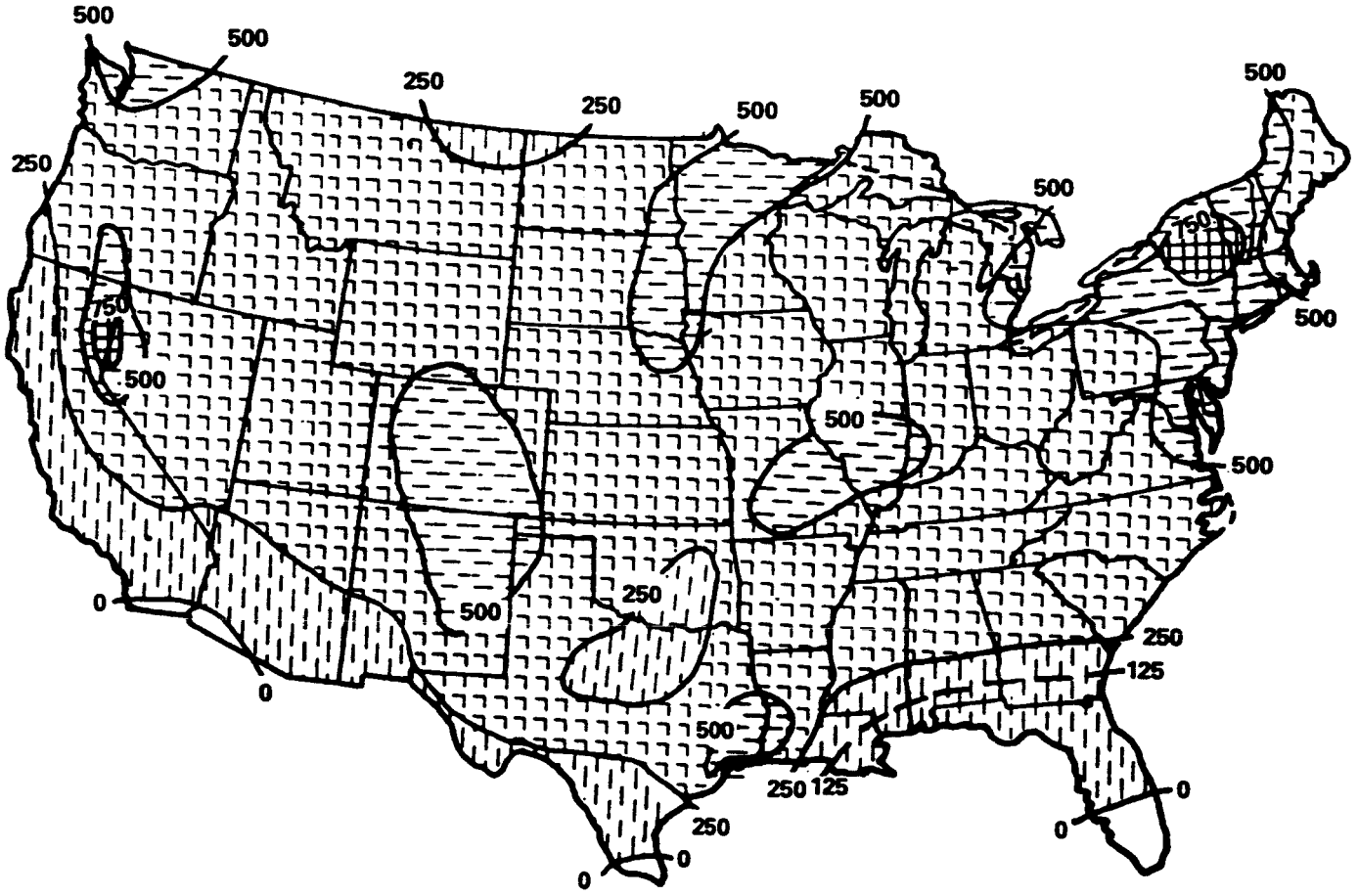

SNOW DEPTH (mm)	SNOW LOAD (kg/m^2)
0-250	25
250-500	50
500-750	75
over 750	100

Figure 5.5 Extreme 24-h maximum snowfall (mm) and maximum snow load.

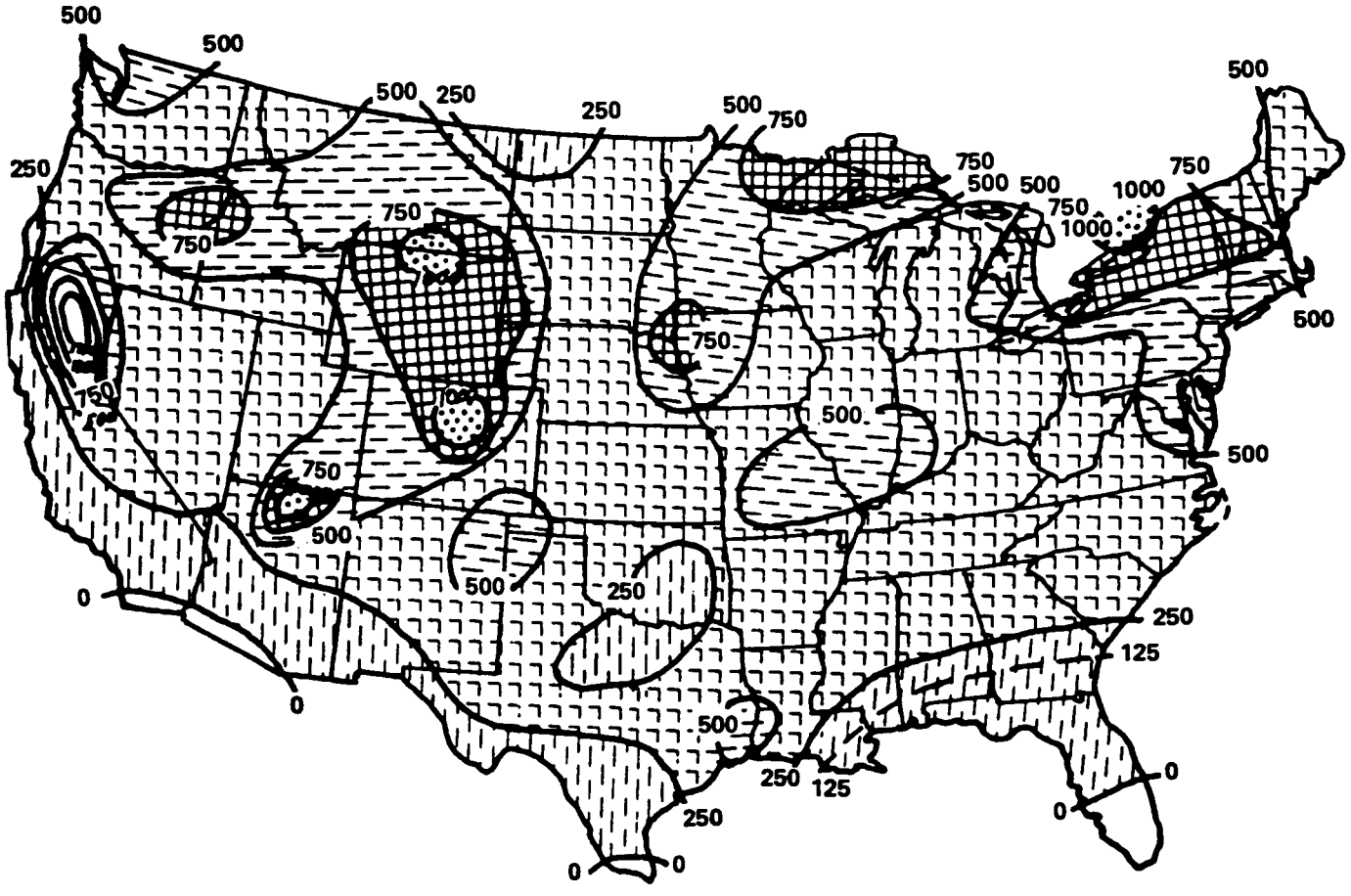

SNOW DEPTH (mm)	SNOW LOAD (kg/m^2)
0-250	25
250-500	50
500-750	75
750-1000	100
1000-1250	125

Figure 5.6 Extreme storm maximum snowfall (mm) and maximum snow load.

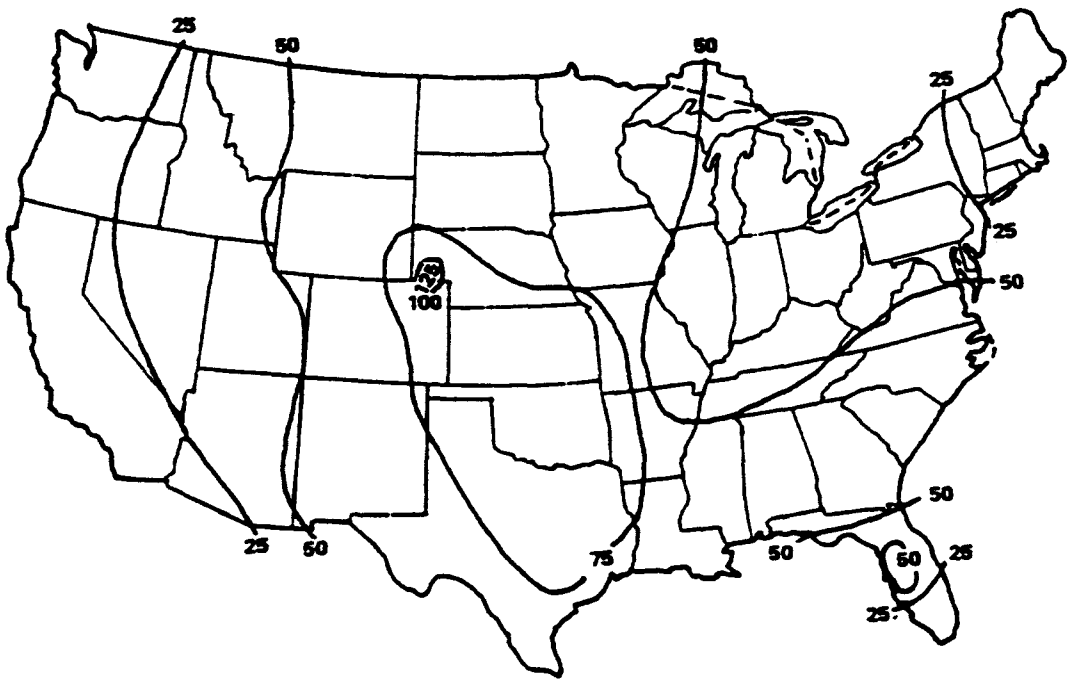

Figure 5.7 Extreme maximum hailstone diameters (mm).

5.1.3.4 Atmospheric Pressure

Atmospheric pressure extremes normally given in the literature are given as the pressure which would have occurred if the station were at sea level. The surface weather map published by the United States National Weather Service uses sea-level pressures for the pressure values to assist in map analysis and forecasting. These sea-level pressure values are obtained from the station pressures by use of the hydrostatic equation:

$$-dP = \rho g dZ \tag{5.1}$$

where

dP = pressure difference

ρ = density

g = gravity

dZ = altitude difference.

These sea level data are valid only for design purposes at locations with elevations near sea level. As an example, when the former highest officially reported sea level pressure observed in the United States of 106,330 N/m^2 (1,063.3 mb) occurred at Helena, MT (ref. 5.6), the actual station pressure was approximately 92,100 N/m^2 (921 mb) because the station is 1,187 m (3,893 ft) above mean sea level.

Figures 5.8 and 5.9 show the general distribution of extreme maximum and minimum station pressures in the United States. Because of the direct relationship between pressure and station elevation, figures 5.10 through 5.13 should be used with the station elevation to obtain the extreme maximum and minimum pressure values for any location in the United States. Similar maps and graphs in U.S. Customary Units are given in reference 5.7.

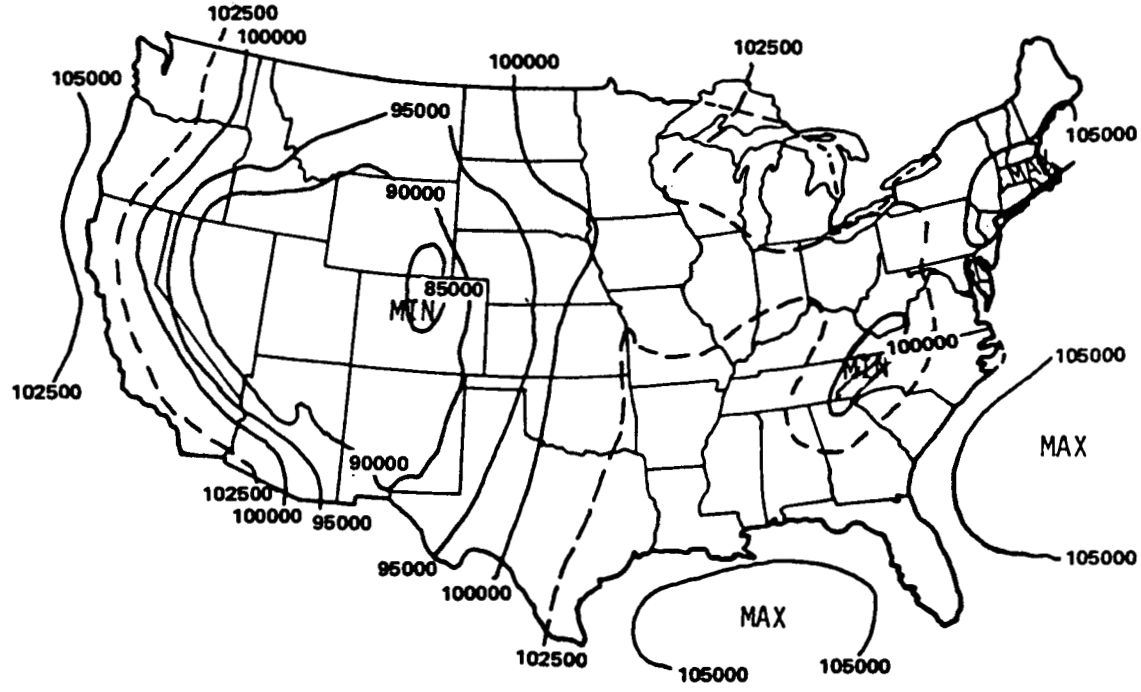

Figure 5.8 Maximum absolute station pressure (N/m^2).

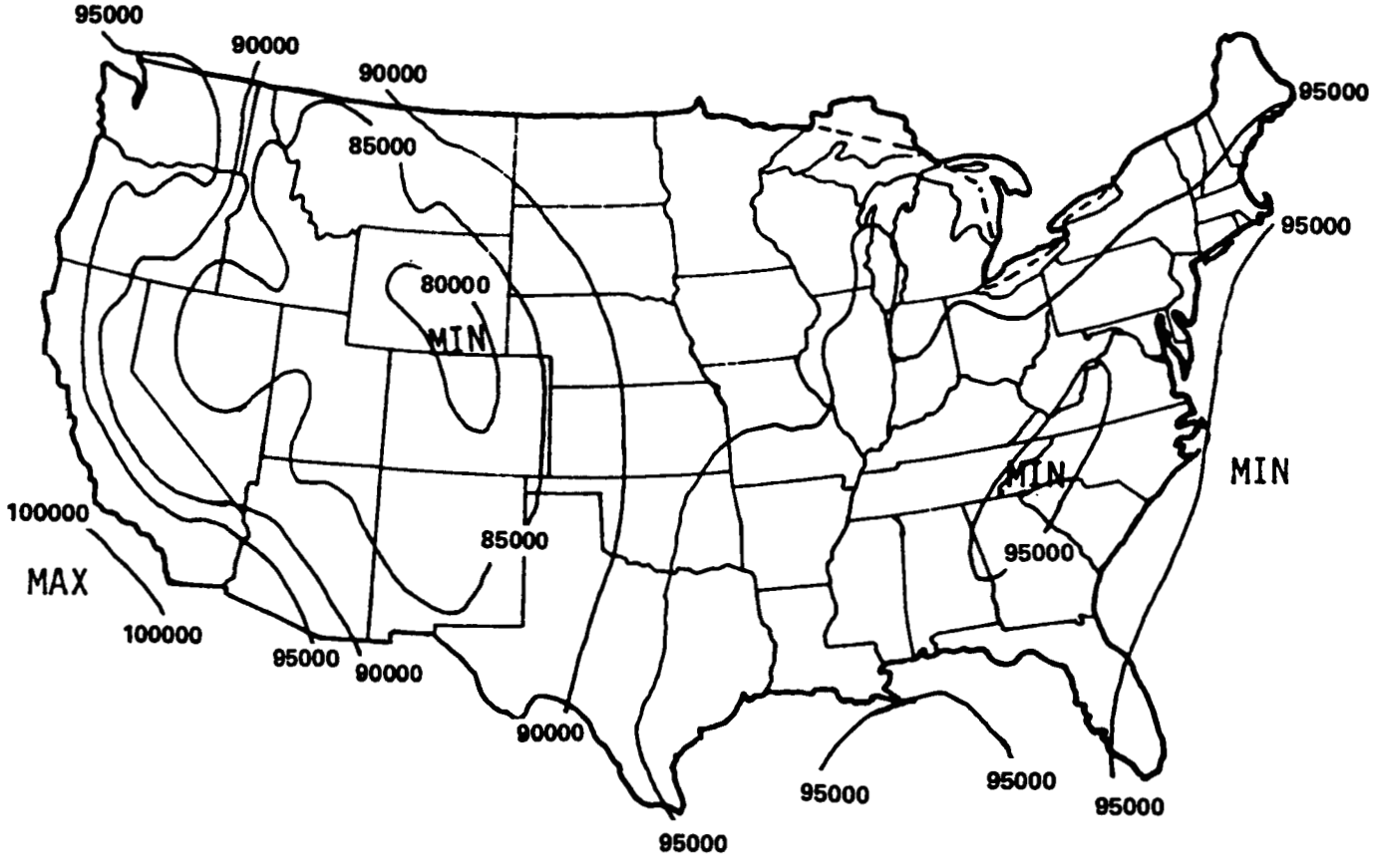

Figure 5.9 Maximum absolute station pressure (N/m^2).

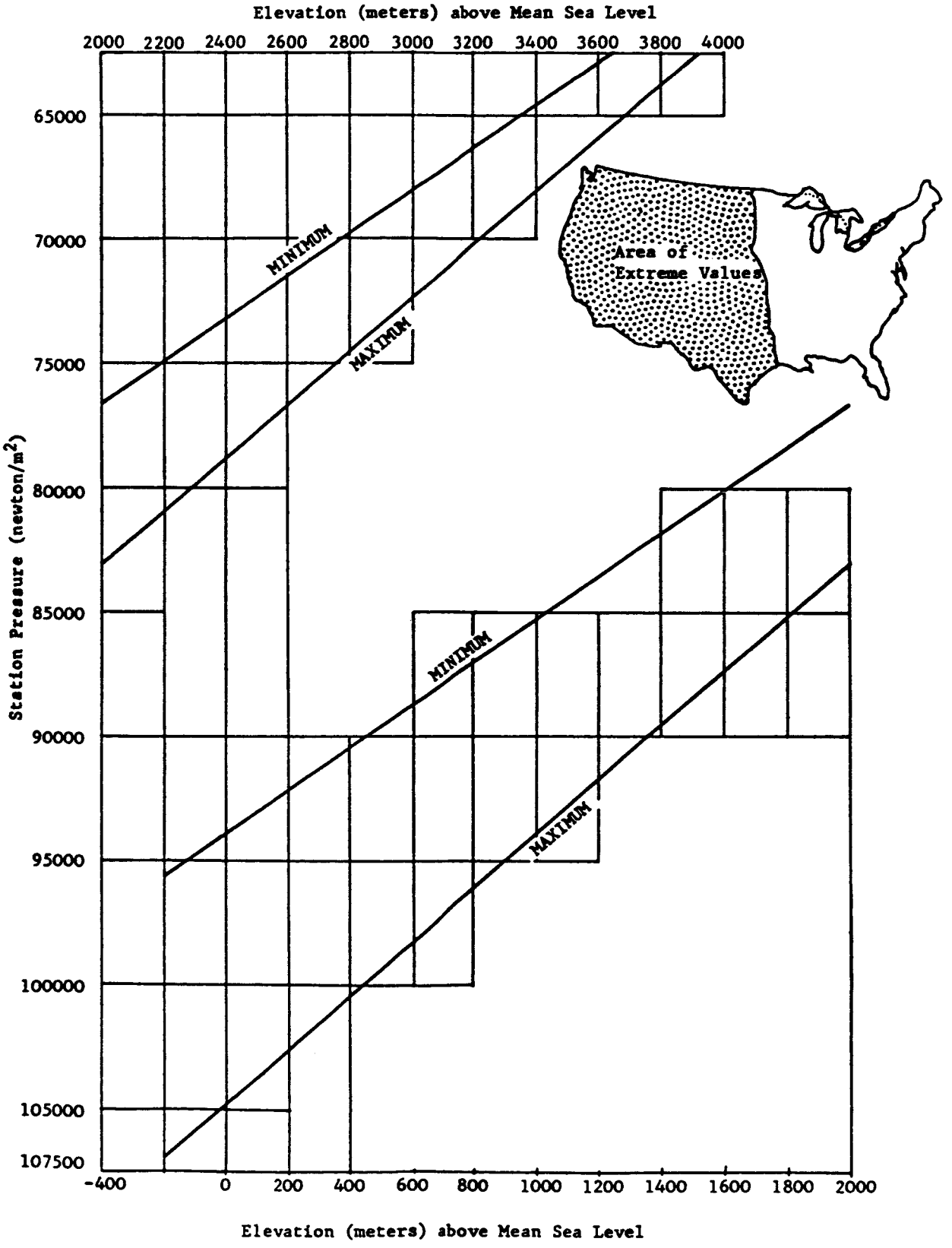

Figure 5.10 Extreme pressure values versus elevation for western United States.

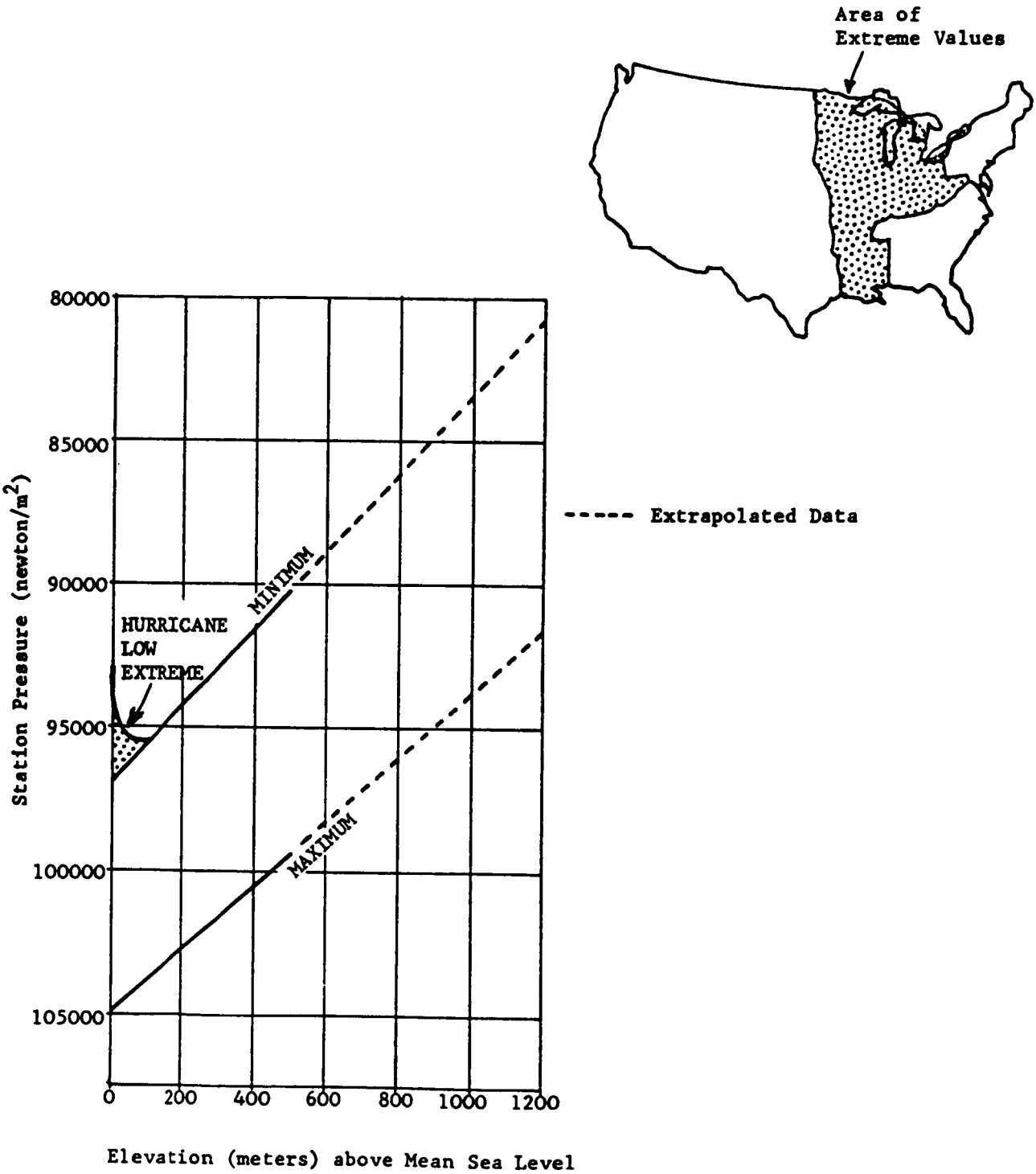

Figure 5-11 Extreme pressure values versus elevation for central United States.

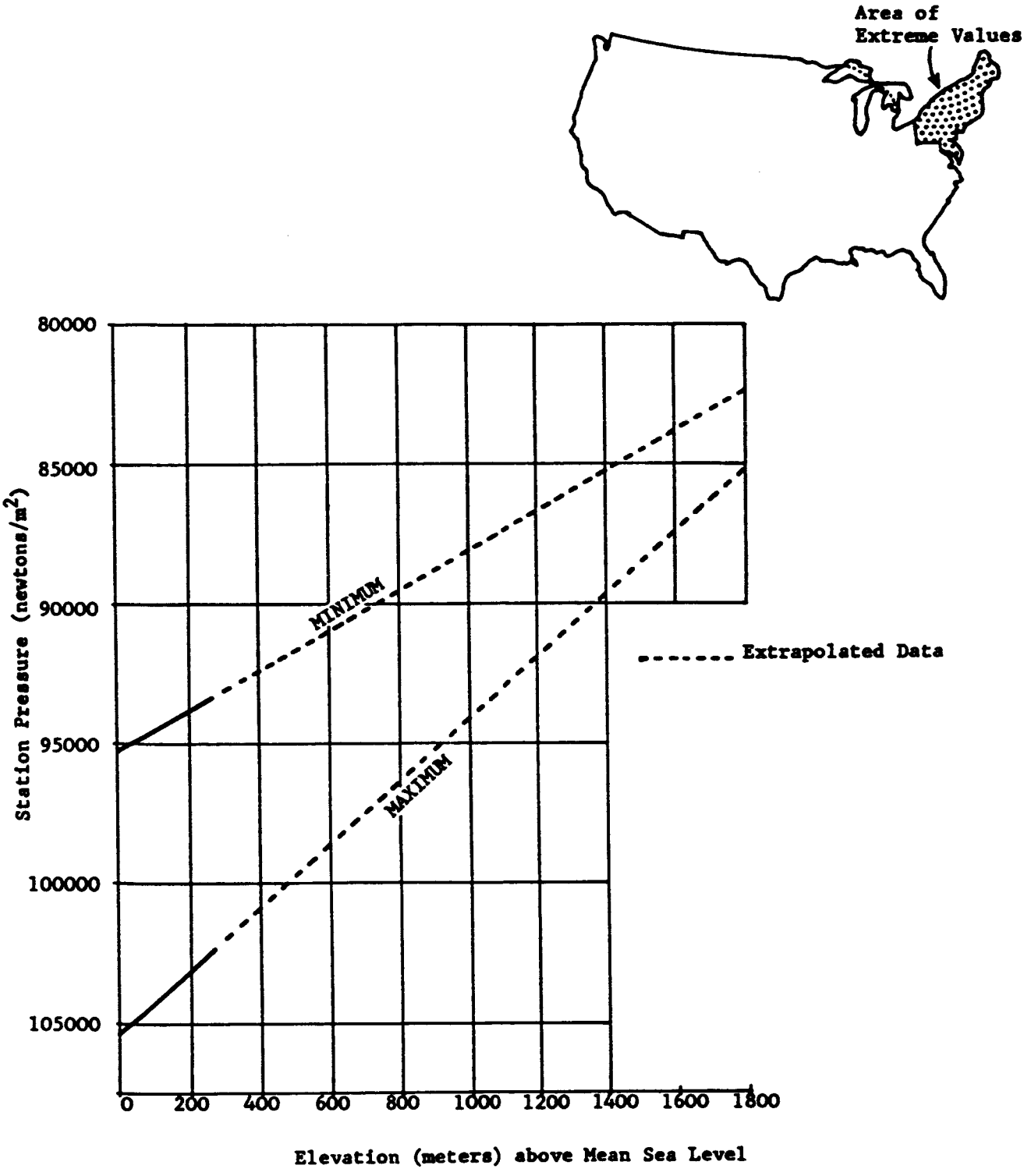

Figure 5.12 Extreme pressure values versus elevation for northeastern United States.

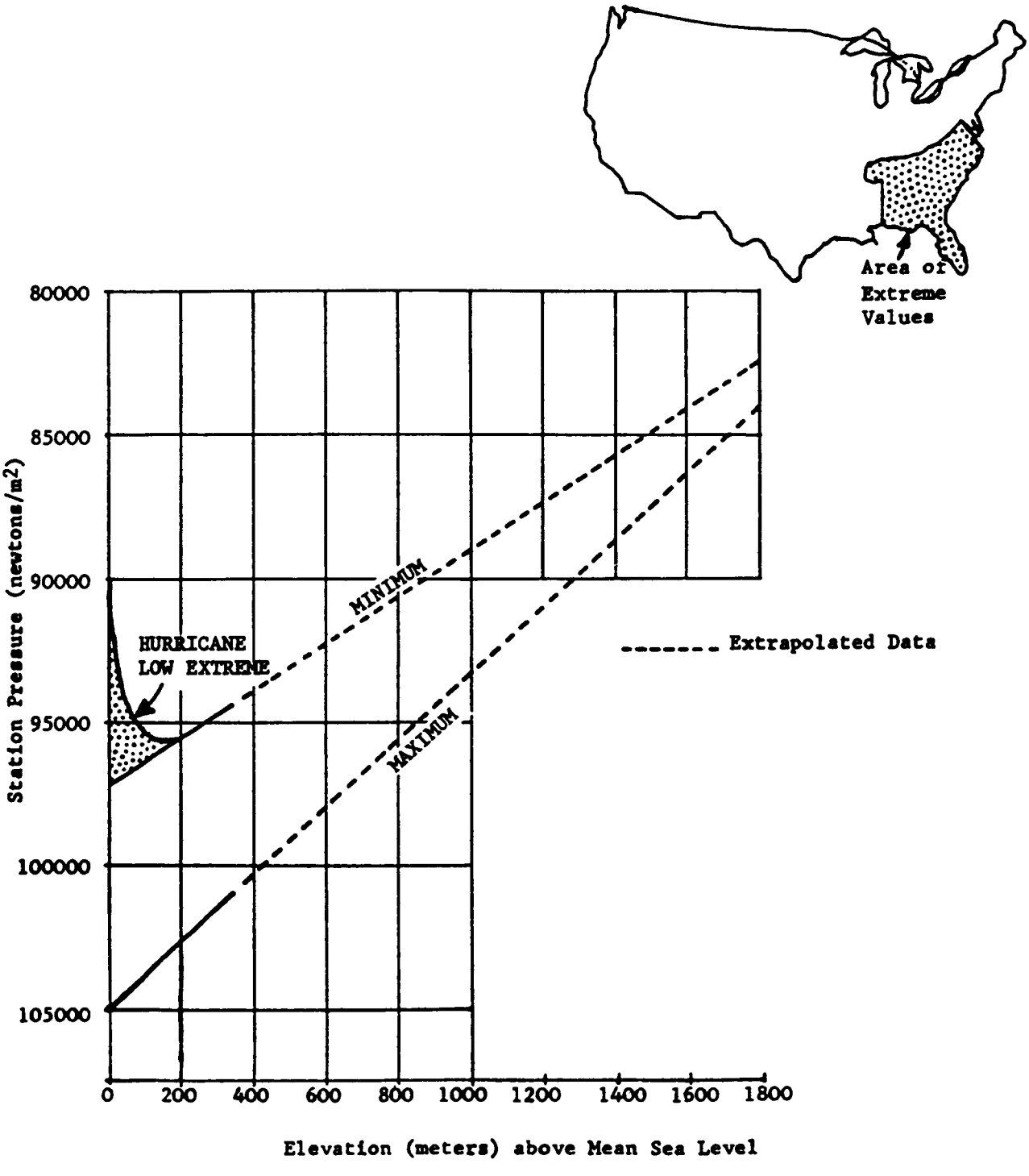

Figure 5.13 Extreme pressure values versus elevation for southeastern United States.

Extreme temperatures and sea-level pressures for the United States are given in table 5.1 (refs. 5.2, 5.6, 5.8, and 5.9). Reference 5.9 also contains surface atmosphere extreme criteria for vehicle launch and transportation areas.

5.2 World Surface Extremes

This section provides world extreme values for temperature, dew point, precipitation, pressure, wind speed, etc.

5.2.1 Sources of Data

A great amount of atmospheric data has been collected throughout the world. Various agencies have collected data in a form that may be used for statistical studies. "World Weather Records" (ref. 5.10), compiled by the National Oceanic and Atmospheric Administration, provides another summary of mean values of meteorological data. A publication entitled, "Weather Extremes" (ref. 5.1) is extremely valuable for its listing of extreme values of surface meteorological parameters.

The Earth Sciences Laboratory of the U.S. Army Topographic Laboratories at Fort Belvoir, VA, has collected worldwide data on meteorological extremes which are published in AR 70-38 (ref. 5.11). For AR 70-38, the Earth Sciences Laboratory prepared world maps that show worldwide absolute maximum and absolute minimum temperatures. These maps are reproduced in this section in figures 5.14 and 5.15.

5.2.2 World Extremes Over Continents

To present all the geographic extremes properly, many large maps similar to figures 5.14 and 5.15 would be required; therefore, only worldwide extremes of each parameter will be discussed, and available references on each parameter will be given. Individual geographic extremes will be mentioned when pertinent.

5.2.2.1 Temperature

Absolute maximum and absolute minimum world temperature extremes are shown in figures 5.14 and 5.15. Some geographical extreme air temperatures of record are given in table 5.2.

Temperatures of the ground are normally hotter than the air temperatures during the daytime. In Loango, Congo, Africa, temperatures of the ground as high as 82 °C (180 °F) have been measured. At Stuart, Australia, the sand has reached temperatures so hot that matches dropped into it burst into flame.

In the design of equipment for worldwide ground environment operations, MIL-STD-210C (ref. 5.12) now uses extreme temperature values of 58 °C (136 °F) for a hot temperature and –68 °C (–90 °F) for a cold temperature (excluding Antarctic extremes).

Long-term extremes of high temperature that would be expected to occur at least once during a 10 to 60 year period, in the hottest part of the world, are given in table 5.3 (ref. 5.12). These extreme temperature values were derived from a statistical analysis of 57 years of temperature data from Death Valley, CA, which is considered representative of conditions in the Sahara Desert. Such temperatures persist for 1 or 2 hours during the day.

Long-term extremes of low temperature that would be expected to occur at least once during a 10 to 60 year period, in the coldest area of the world, are presented in table 5.4 (ref. 5.12). These values were derived from a statistical analysis of 16 years of Ojmjakon, Russia, data. The extreme low temperatures will persist for longer periods since they occur during polar darkness. (Also see references 5.13 and 5.14 regarding probabilities of surface temperature extremes.)

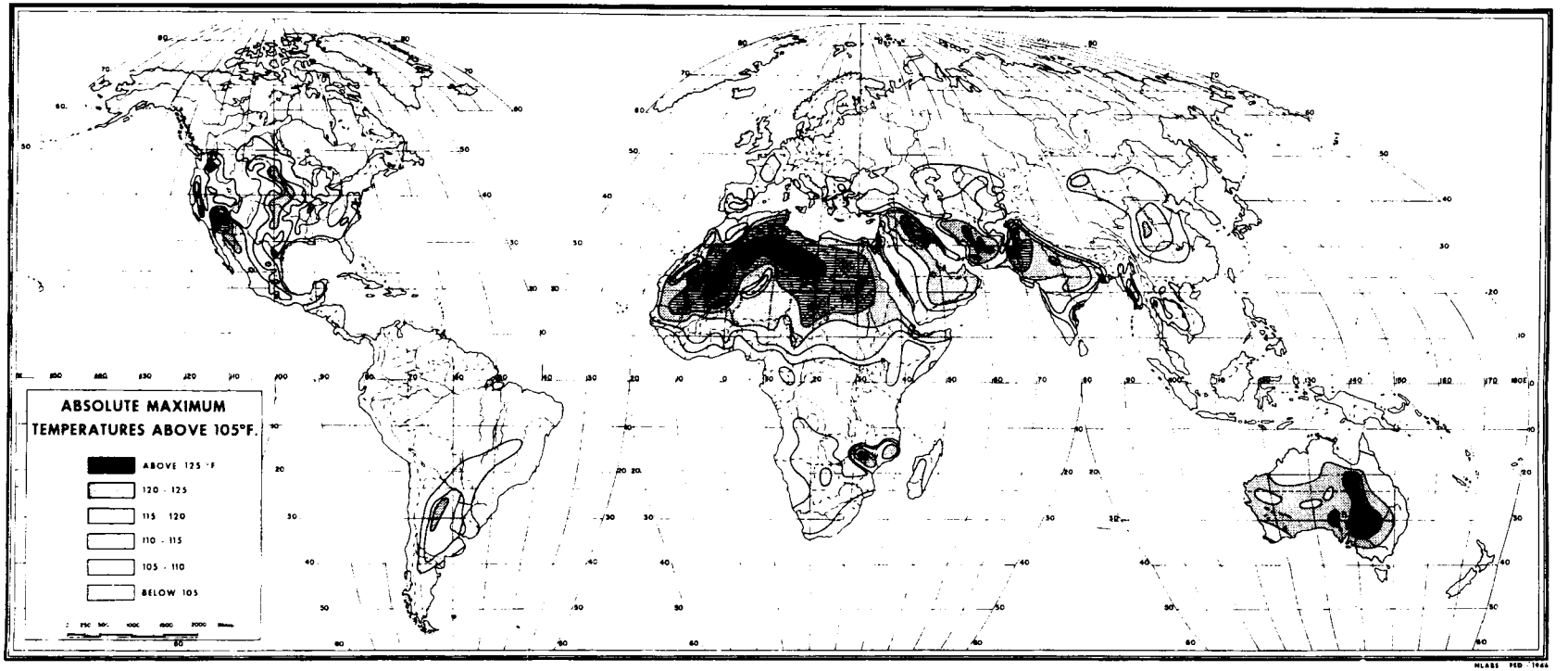

Figure 5.14 Worldwide geographic absolute maximum temperatures above 41 °C (105 °F) (ref. 5.11).

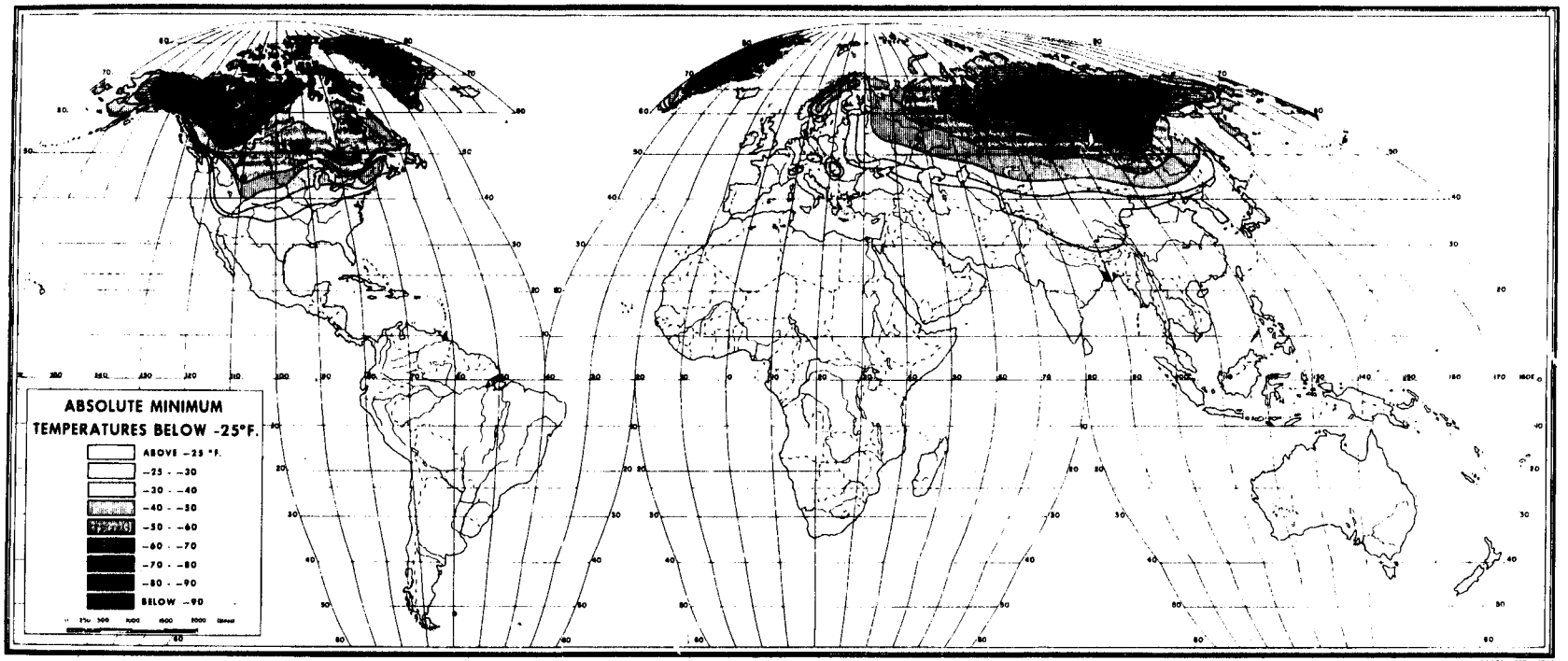

Figure 5.15 Worldwide geographic absolute minimum temperatures below –32 °C (–25 °F) (ref. 5.11).

Table 5.2 Extreme surface air temperatures of record.

Location	Air Temperature of Record (°C (°F))
Salah, Africa	48 (118), mean daily maximum for 45 days 53 (127), absolute maximum
El Azizia, Libya*	58 (136), absolute maximum
Tirat Tsvi, Israel	54 (129), absolute maximum
Death Valley, California*	57 (134), absolute maximum for U.S.
Cloncurry Queensland, Australia	53 (128), absolute maximum
Vostok, Antarctica	–89 (–129), absolute minimum
Ojmjakon, Siberia	–68 (–90), absolute minimum
Northice, Greenland	–66 (–87), absolute minimum
Prospect Creek Camp, Alaska	–62 (–80), absolute minimum
Rogers Pass, Montana	–57 (–70), absolute minimum for U.S.
Snag, Yukon Territory, Canada	–63 (–81), absolute minimum for North America

*The validity of these temperatures has been questioned; see reference 5.4.

Table 5.3 Extreme high surface temperatures[1] with relation to long-term exposure (ref. 5.12).

Temperatures (°C (°F))		
Exposure Period in Years		
10	30	60
53 (128)	54 (130)	55 (131)

[1] Based on Death Valley, CA, data.

Table 5.4 Extreme low surface temperatures[2] with relation to long-term exposure (ref. 5.12).

Temperatures (°C (°F))		
Exposure Period in Years		
10	30	60
–65 (–86)	–67 (–89)	–69 (–92)

[2] Based on Ojmjakon, Russia, data. Temperatures in Antactica were not considered in the study.

5.2.2.2 Dew Point

High dew points associated with high temperatures near large bodies of water can be detrimental to equipment and make living conditions very uncomfortable. Some examples of this atmospheric condition are:

a. The northern portion of the Arabian Sea in April and May, to 29 °C (85 °F) dew point.

b. The Red Sea in July, to 32 °C (89 °F) dew point.

c. The Caribbean Sea (includes the western end of Cuba and the Yucatan Peninsula, Mexico) in July, to 27 °C (81 °F) dew point.

d. The northern portion of the Gulf of California, to 30 °C (86 °F) dew point.

e. The Persian Gulf (Sharjah, Arabia) in July, to 34 °C (93 °F) dew point.

A discussion on atmospheric humidity is presented in section VI.

5.2.2.3 Precipitation

The worldwide distribution of precipitation is extremely variable; some areas do not receive rain for years, while others receive torrential rain many months of the year. Precipitation is also seasonal; for example, Cherrapunji, India, with its world record total of 2,647 cm (1,042 in) of precipitation in a year, has a mean monthly precipitation of less than 2.54 cm (1 in) in December and January. Arica, Chile, had no rain between October 1903 through December 1917. The longest dry period for a United States location was 767 days for Bagdad, CA (October 3, 1912, to November 8, 1914).

The heaviest precipitation for greater than 12 hours usually occurs in monsoon weather. High rates of rainfall for short periods (under 12 hours) usually occur during thunderstorms and over much smaller areas than the monsoon rain. Some world records for various periods of rainfall are given in table 5.5 (ref. 5.4).

For in-depth information on precipitation, see section VII.

Table 5.5 World rainfall records.

Station	Time Period	Amount (in) (cm)
Unionville, Maryland	1 min	1.23 (3.1)
Plum Point, Jamaica	15 min	8.0 (20)
Holt, Missouri	60 min	12.0 (31)
D'Hanis, Texas	3 h	20.0 (51)
Foc-Foc, LaReunion Island	12 h	45.0 (114)
Foc-Foc, LaReunion Island	1 day	72.0 (183)
Cherrapunji, India	30 days	366.14 (930)
Cherrapunji, India	1 year	1,041.73 (2,647)

Highest average annual precipitation:
World: 460 in (1,168 cm), Mt. Waialeale, Kauai, Hawaii
Contiguous U.S.: 144 in (366 cm), Wynoochee, Washington

Lowest average annual precipitation:
World: 0.03 in (0.08 cm), Arica, Chile
U.S.: 1.63 in (4.4 cm), Death Valley, California

5.2.2.4 Pressure

Surface atmospheric pressure extremes for use in design must be derived from the measured station pressures, not from the calculated sea level pressures that are usually published.

Station pressures have great variability between stations because of the difference in altitude of the stations. The lowest station pressures occur at the highest altitudes. The highest station pressures occur at either the lowest elevation stations (below sea level), or in the arctic regions in cold air masses at or near sea level.

Court (ref. 5.15) has published an interesting discussion on world pressure extremes. Some typical extreme high and low pressure values are given in table 5.6 (refs. 5.1 and 5.4).

Surface and aloft pressure values are given in subsections 3.3.2 and 3.4.2, respectively.

Table 5.6 Extreme pressure values for selected areas.

Station	Elevation Above Sea Level (m (ft))	Sea-Level Pressure (mb)	
		Lowest	Highest
Lahasa, Tibet	3,685 (12,090)	645*	652*
Sedom, Israel	–389 (–1,275)	—	1,081.8
Portland, Maine	19 (61)	—	1,056
Northway, Alaska	NA	—	1,078.6
Qutdligssat, Greenland	3 (10)	—	1,063.4
In the Typhoon Tip, 16°44' N., 137°46' E., October 12, 1979	0	870**	—
Agata, Siberia	261 (855)	—	1,083.8

*Monthly means.
**Lowest sea level pressure of record.

5.2.2.5 Ground Wind

World extreme surface winds have occurred in several types of meteorological conditions: tornadoes, hurricanes or typhoons, mistral winds, and Santa Ana winds. In design, each type of wind needs special consideration. For example, the probability of tornado winds is very low compared with the probability of mistral winds, which may persist for days. The world's highest recorded peak wind speed gust of 103 m/s (231 mph) occurred at Mt. Washington, New Hampshire, on April 12, 1934. The highest 5-min average wind speed of 84 m/s (188 mph) also occurred at Mt. Washington (ref. 5.1). Section II presents a complete discussion of winds.

5.2.2.5.1 Tornadoes and Whirlwinds

Tornadoes are rapidly revolving circulations (vortices) normally associated with a cold front squall line or with warm, humid, unsettled weather; they usually occur in conjunction with a severe thunderstorm. Although a tornado is extremely destructive, the average tornado path is only about 400 m (1/4 mi) wide and seldom more than 26 km (16 mi) long, but there have been a few instances in which tornadoes have caused heavy destruction along paths more than 1.6 km (1 mi) wide and 483 km (300 mi) long. The probability of any one point being in a tornado path is very small; therefore, design of structures to withstand tornadoes is usually not considered except for special situations. Velocities have been estimated to exceed 134 m/s (260 knots or 300 mi/h) in tornadoes. See section XII for further information regarding tornadoes.

A whirlwind is a small-scale, rotating column of air. The most extreme whirlwind is a tornado. Dust devils and waterspouts are the smaller and far less intense whirlwinds. The largest Florida Keys waterspouts can produce tangential wind speeds up to 90 m/s (200 mi/h); while large, mature dust devils have yielded wind velocities up to 40 m/s (90 mi/h).

5.2.2.5.2 Hurricanes (Typhoons)

Hurricanes (also called typhoons, willy-willies, tropical cyclones, and many other local names) are large storms of considerable intensity which originate in tropical regions between the equator and 25° latitude. Hurricanes are always accompanied by heavy rain. Since the hurricanes of the West Indies are as intense as others throughout the world, design winds based upon these hurricanes would be representative for any geographical area.

Section II gives hurricane design winds for the area of Kennedy Space Center, FL. Although the highest winds recorded in a hurricane in the area of KSC, FL, were lower than winds from thunderstorms in the same area, the probability still exists that much higher winds could result from hurricanes in the vicinity of KSC.

For extremes applicable to equipment, table 5.7 from a study of 19 years of wind data for Naha, Okinawa (in the Pacific typhoon belt) (ref. 5.12), is representative of all hurricane areas of the world. The maximum gust velocity observed in the United States is 89.4 m/s (174 knots or 200 mi/h), recorded during hurricane Camille. Elsewhere, typhoon winds have been recorded at speeds up to 100 m/s (195 knots or 224 mi/h) (ref. 5.4).

See section XII for further information regarding hurricanes.

5.2.2.5.3 Mistral Winds

The mistral wind is a strong polar current between a large anticyclone and a low pressure center. These winds frequently have a temperature below freezing. The mistral of the Gulf of Lions and the Rhone Valley, France, is the best known of these winds. Although winds of 37 m/s (83 mph) have been recorded in the area of Marseilles, France, much higher winds have occurred to the west of Marseilles in the more open terrain, where even railway trains have been blown over. Mistrals blow in the Rhone Valley for about 100 days a year.

5.2.2.5.4 Santa Ana Winds

In contrast to the mistrals, the Santa Ana winds, which occur in southern California west of the coast range of mountains, are hot and dry and have speed up to 21 m/s (41 knots). Similar winds, called Fohn winds, occur in the Swiss Alps and in the Andes, but, because of the local topography, they have lower speeds. The destructiveness of these winds is not from their speeds, but from their high temperatures and dryness, which can do considerable damage to blooming trees, crops, exposed equipment and instruments that may be sensitive to prolonged heat and dryness.

Table 5.7 Extreme winds in hurricane (typhoon) areas with relation to risk and desired lifetime (3.1 m reference height).

Extreme Wind Speeds ($m\ s^{-1}$)*†				
Planned Lifetime (years)				
Risk (%)	2	5	10	25
10	*69 †61	79 72	86 80	97 91

*Based on 2-s gusts (annual extreme)
†Based on 1-min steady wind associated with the 2-s gust

REFERENCES

5.1 Schmidli, R.J.: "Weather Extremes," NOAA Technical Memorandum NWS WR-28, revised October 1991.

5.2 "Temperature Extremes in the United States." Environmental Information Summaries, C-5, NOAA Environmental Data Service, Asheville, NC, December 1987.

5.3 Valley, S.L.: "Handbook of Geophysics and Space Environments." McGraw-Hill Book Company, Inc., New York, 1965.

5.4 Riordan, P., and Bourget, P.G.: "World Weather Extremes." Report ETL-0416, U.S. Army Engineer Topographic Laboratories, Ft. Belvoir, VA, December 1985.

5.5 Brown, M.J., and Williams, P., Jr.: "Maximum Snow Loads Along the Western Slopes of the Wasatch Mountains of Utah." Journal of Applied Meteorology, vol. 15, No. 3, 1962, pp. 123–126.

5.6 Ludlum, D.M.: "Extremes of Atmospheric Pressure in the United States." Weatherwise, vol. 15, No. 3, 1962, pp. 106–115.

5.7 Daniels, G.E.: "Values of Extreme Surface Pressure for Design Criteria." 1965 Proceedings, Institute of Environmental Sciences, Mt. Prospect, IL, pp. 283–288.

5.8 Ludlum, D.M.: "Extremes of Atmospheric Pressure." Weatherwise, vol. 24, No. 3, 1971, pp. 130–131.

5.9 Surface Atmospheric Extremes (Launch and Transportation Areas) NASA Space Vehicle Design Criteria (Environment), NASA SP-8084, May 1972.

5.10 "World Weather Records," U.S. Department of Commerce, Weather Bureau, Superintendent of Documents, U.S. Government Printing Office, Washington, DC, 1968.

5.11 "Research, Development, Test, and Employment of Material for Extreme Climate Conditions," AR-70-38, July 1, 1969.

5.12 Military Standard 210C: "Climatic Information to Determine Design and Test Requirements for Military Standards and Equipment," Department of Defense, MIL-STD-210C, January 9, 1987.

5.13 Tattleman, P., and Kantor, A.J.: "Atlas of Probabilities of Surface Temperature Extremes: Part I—Northern Hemisphere," AFGL-TR-76-0084, 1976.

5.14 Tattleman, P., and Kantor, A.J.: "Atlas of Probabilities of Surface Temperature Extremes: Part II—Southern Hemisphere," AFGL-TR-77-0001, December 27, 1976.

5.15 Court, A.: "Improbable Pressure Extreme: 1,070 mb," Bulletin of the American Meteorological Society, vol. 50, No. 4, April 1969, pp. 248–250.

SECTION VI. HUMIDITY

6.1 Introduction

The water vapor or moisture content of the atmosphere plays a significant role in the fabrication, test, operations, and flight of aerospace vehicles because it can cause both physical and chemical deterioration of materials as well as affect vehicle functions. Some effects atmospheric moisture may have on aerospace vehicles are:

1. Minute particulates can be corrosive when they settle from the air. The rate of corrosion increases with humidity.

2. Humidity can affect the performance of electronic equipment, i.e., changes the dielectic constants of capacitors, decreases the breakdown voltage between potentials, and causes deterioration of electronic components through metallic corrosion or electrode chemical reactions.

3. Organic growth, bacteria, and fungi thrive in warm, moist air, consequently degrading performance of aerospace systems and sensors.

4. The low temperature of the cryogenic fuels cools the moist air, often resulting in condensation and icing or frost which can be detrimental to vehicle operation.

This section will define some terminology associated with water vapor and discuss some of the effects of the vapor. Various tests are required to measure the effects of water vapor as early as possible in a program development cycle. Most of these tests are outlined in references 6.1 and 6.2; however, some test criteria for specific sites are described herein.

6.2 Definitions (ref. 6.3)

Absolute Humidity: In a system of moist air, the ratio of the mass of water vapor present to the volume occupied by the mixture; that is, the density of the water vapor component.

Condensation: The physical process by which a vapor becomes a liquid or solid; the opposite of evaporation.

Critical Point: The thermodynamic state in which the liquid and gas phases of a substance coexist in equilibrium at the highest possible temperature. (At higher temperatures the liquid phase will not exist.)

Dew-Point Temperature: The temperature to which a given parcel of air must be cooled at constant pressure and constant water-vapor content in order for saturation to occur.

Dry-Bulb Temperature; The temperature of the air. The temperature registered by the dry-bulb thermometer of a psychrometer (sometimes referred to as ambient temperature).

Evaporation: The phase transition in which the liquid or solid is transformed into the gaseous state; the opposite of condensation. In meteorology, evaporation is usually restricted to a liquid becoming a gas, while sublimation refers to phase changes between solids and gases.

Frost Point: The highest temperature at which sublimation directly from water vapor to ice crystals occurs. It is analogous to the dew point at 0 °C, but below 0 °C, the frost point becomes greater than the dew point since the saturation vapor pressure over ice is less than the saturated vapor pressure over water.

Humidity: A general measure of the water vapor content in air. (See absolute humidity, relative humidity, specific humidity, mixing ratio, and dew point.)

Hydrology: The branch of physical geography which deals with the waters of the Earth exclusive of the oceans. The moisture (vapor, liquid, and solid) in the atmosphere is one phase of the "hydrologic cycle."

Hygrometer: An instrument which measures the water vapor content of the atmosphere.

Hygrometery: The study which deals with the measurements of the humidity and other gases of the atmosphere.

Latent Heat of Condensation: The heat released per unit mass as water vapor condenses to form water droplets or ice crystals.

Latent Heat of Vaporization: The heat absorbed per unit mass as water or ice is vaporized into the gaseous state. The inverse of the latent heat of condensation can be estimated within 0.8 percent for temperature T within the range of meteorological interest by the equation:

$$L_v = (2{,}500 - 2.274T\ ^\circ C)\ J/g \quad \text{(ref. 6.4)} \tag{6.1}$$

More precise values are available from a table in reference 6.5.

Mixing Ratio: In a system of moist air, the dimensionless ratio of the mass of water vapor to the mass of dry air.

Moisture: A term usually referring to the water vapor content of the atmosphere, or to the total water substance (gaseous, liquid, and solid) present in a given volume of air.

Moisture Inversion: An increase with altitude of the moisture content of the air; specificially, the layer through which this increase occurs, or the altitude at which the increase begins.

Relative Humidity: The dimensionless ratio of the actual water vapor pressure of the air to the saturation vapor pressure. Relative humidity above 100 percent occurs (particularly with respect to ice) which gives rise to dew and frost. This may be relevant to surfaces which are locally colder (by radiation or otherwise).

Saturation: The condition in which the partial pressure of any fluid constituent is equal to its maximum possible partial pressure under the existing environmental conditions, such that any increase in the amount of that constituent without a change in the surrounding conditions will create a thermodynamically unstable environment where, if a nucleation site exists, condensation will occur.

Specific Humidity: In a system of moist air, the dimensionless ratio of the mass of water vapor to the total mass of the system.

Sublimation: The transition of a substance from the solid phase directly to the vapor phase, or vice versa, without passing through an intermediate liquid phase.

Supersaturation: The condition existing in a given portion of the atmosphere (or other space) when the relative humidity is greater than 100 percent; that is, when it contains more water vapor than is needed to produce saturation with respect to a plane surface of pure water or pure ice.

Vapor: A substance existing in a gaseous state at a temperature lower than that of its critical point. It is formed by evaporation or sublimation and can become liquefied with compression.

Vapor Concentration: (previously called absolute humidity (ref. 6.6)). The ratio of the mass of water vapor present to the volume occupied by the mixture, i.e., the density of the water content. This is usually expressed in grams of water vapor per cubic meter of air.

Vapor Pressure: The pressure exerted by the molecules of a given vapor. For a pure, confined vapor, vapor pressure is the pressure on the walls of its containing vessel; and for a vapor mixed with other vapors or gases, it is that vapor's contribution to the total pressure (i.e., its partial pressure).

Wet-Bulb Temperature: The temperature read from the wet-bulb thermometer. More formally: "The temperature an air parcel would have if cooled adiabatically to saturation at constant pressure by evaporation of water into it, all latent heat being supplied by the parcel." The thermometer reading can be used on a psychrometry chart to determine the corresponding value of relative humidity.

6.3 Vapor Concentration

6.3.1 Background Information

A significant amount of moisture exists in the atmosphere, the majority of which comes from the Earth's surface. The equatorial region of the Earth is the main source from which moisture is supplied to the atmosphere. Broad-scale evaporation takes place in this area due to the vast oceanic area and moist land regions in addition to the warm climatic conditions.

Since the molecular weight of water vapor is less than the molecular weight of dry air, moist air is less dense than dry (drier) air. This contributes to the lower atmospheric pressure which is common to warm, moist air masses. To a great extent, the dynamic variations of global circulation are due to the pressure difference between moist (warm) and dry (cold) air.

The various measures of water vapor are related, as shown by table 6.1 (ref. 6.7) as well as the following approximated equations:

1. Vapor pressure in terms of frost point

$$\log_{10} e = -2{,}485.0/T_F + 3.5665 \log_{10} T_F - 0.0032098 T_F + 2.0702 \tag{6.2}$$

2. Vapor pressure in terms of dew point

$$\log_{10} e = -2{,}949.1/T_D - 5.028 \log_{10} T_D + 23.832 \tag{6.3}$$

3. Absolute humidity (g/m^3) (vapor concentration) in terms of vapor pressure and air temperature

$$\rho_v = 216.68\ e/T \tag{6.4}$$

4. Mixing ratio (g/kg) in terms of vapor pressure and atmospheric pressure

$$r = 621.97\ e/(p-e)\ , \tag{6.5}$$

where

e = vapor pressure (mb)

T = air temperature (K)

T_D = dew point temperature (K)

T_F = frost point temperature (K)

p = atmospheric pressure (mb)

ρ_v = absolute humidity (g/m^3)

r = mixing ratio (g/kg).

6.3.2 Testing

Testing is a necessary precaution in order to minimize failure due to atmospheric moisture. The effects of moisture are measured by humidity cycling, a procedure in which test items are placed in a closed chamber where temperature and relative humidity are closely regulated to simulate environmental conditions (ref. 6.2). Chamber test procedures and criteria for various systems and their associated electrical-mechanical components are usually identified in the various system requirements documents. This document recommends criteria based on actual environmental records, including extreme values, in component testing to promote realism about the actual environment.

NASA's External Tank Verification Plan (ref. 6.8) lists the following general statements under Test Controls and Test Methods: (1) the item is sealed or potted and subjected to a seal test, (2) the item is located in a controlled-humidity or air-conditioned environment during operation and is protected from humidity when nonoperating, (3) the item is subjected to propellant compatibility testing which is considered to be a more severe environment, and (4) the item is fabricated from materials which preclude corrosion by humidity. This requires additional and different quality control standards than those discussed previously.

The space shuttle program, shuttle master verification plan document, states that the humidity and other environmental parameter tests will use the procedures outlined in "Military Standard 810" (ref. 6.2 is the latest version, i.e., MIL-STD 810D).

A temperature of 71 °C (160 °F) and 95-percent relative humidity represent a dew-point temperature of 69 °C (156 °F), which is much higher than any natural extreme in the world. Dew points above 32 °C (90 °F) are extremely unlikely in nature (ref. 6.9), since the dew-point temperature is limited by the source of the water vapor, i.e., the surface temperature of the water body from which the water evaporates (ref. 6.10). The following paragraphs contain site-specific humidity criteria to be used in aerospace vehicle testing.

6.3.2.1 High Vapor Concentration at Surface

a. Huntsville, New Orleans, and Kennedy Space Center:

(1) An extreme humidity cycle of 24 hours with a wind of less than 5 m/s (9.7 knots): Three hours of 37.2 °C (99 °F) air temperature at 50-percent relative humidity and a vapor concentration of 22.2 g/m^3 (9.7 gr/ft^3), 6 hours of decreasing air temperature to 24.4 °C (76 °F) with relative humidity increasing to 100 percent (saturation), 8 hours of decreasing air temperature to 21.1 °C (70 °F) with a release of 3.8 grams of water as liquid per cubic meter of air (1.7 grains of water per cubic foot of air) with relative humidity remaining at 100 percent, * and 7 hours of increasing air temperature to 37.2 °C (99 °F) and a decrease to 50-percent relative humidity (fig 6.1).

*The release of water as a liquid on the test object may be delayed for several hours after the start of this part of the test because of thermal lag in a large test object. If the lag is too large, the test should be extended in time for each cycle to allow condensation.

Table 6-1. The correspondence between the several measures of water vapor content (ref. 6.7).

Dew Point (K)	Frost Point (K)	Vapor Pressure (mb)	Absolute† Humidity (g/m^3)	Mixing Ratio (g/kg)								
				1,000 mb	850 mb	700 mb	500 mb	400 mb	100 mb	50 mb	10 mb	1 mb
313		7.378+1	5.119+1	4.980+1	5.941+1	7.361+1	1.080+2	1.411+2	*	*	*	*
308		5.624+1	3.963+1	3.725+1	4.427+1	5.456+1	7.910+1	1.020+2	8.008+2	*	*	*
303		4.243+1	3.038+1	2.769+1	3.282+1	4.029+1	5.786+1	7.399+1	4.590+2	*	*	*
298		3.167+1	2.305+1	2.044+1	2.417+1	2.959+1	4.219+1	5.363+1	2.886+2	*	*	*
293		2.337+1	1.730+1	1.495+1	1.766+1	2.156+1	3.059+1	3.870+1	1.899+2	5.462+2	*	*
288		1.704+1	1.283+1	1.083+1	1.278+1	1.557+1	2.201+1	2.775+1	1.279+2	3.217+2	*	*
283		1.227+1	9.399	7.762	9.146	1.113+1	1.569+1	1.973+1	8.707+1	2.024+2	*	*
278		8.719	6.797	5.495	6.471	7.870	1.107+1	1.389+1	5.946+1	1.314+2	*	*
273	273.0	6.108	4.847	3.839	4.519	5.492	7.710	9.664	4.049+1	8.659+1	9.764+2	*
268	268.6	4.215	3.407	2.644	3.112	3.780	5.300	6.637	2.739+1	5.728+1	4.533+2	*
263	264.1	2.863	2.358	1.794	2.110	2.562	3.590	4.492	1.834+1	3.779+1	2.495+2	*
258	259.6	1.912	1.605	1.197	1.408	1.709	2.393	2.993	1.213+1	2.474+1	1.470+2	*
253	255.1	1.254	1.074	7.847–1	9.227–1	1.120	1.568	1.960	7.903	1.601+1	8.919+1	*
248	250.5	8.070–1	7.047–1	5.048–1	5.936–1	7.204–1	1.008	1.260	5.603	1.021+1	5.461+1	*
243	245.8	5.088–1	4.534–1	3.182–1	3.742–1	4.540–1	6.352–1	7.938–1	3.183	6.397	3.335+1	6.443+2
238	241.2	3.139–1	2.856–1	1.963–1	2.308–1	2.801–1	3.918–1	4.896–1	1.960	3.931	2.016+1	2.846+2
233	236.5	1.891–1	1.757–1	1.183–1	1.390–1	1.687–1	2.360–1	2.948–1	1.179	2.362	1.199+1	1.450+2
273.0	273	6.107	4.847	3.839	4.518	5.492	7.709	9.668	4.048+1	8.658+1	9.759+2	*
267.3	268	4.015	3.246	2.518	2.963	3.599	5.047	6.322	2.604+1	5.433+1	4.722+2	*
261.8	263	2.597	2.139	1.627	1.913	2.324	3.255	4.075	1.660+1	3.409+1	2.182+2	*
256.2	258	1.652	1.387	1.034	1.216	1.476	2.067	2.592	1.045+1	2.126+1	1.231+2	*
250.8	253	1.032	8.835–1	6.456–1	7.592–1	9.214–1	1.289	1.613	6.490	1.311+1	7.158+1	*
245.3	248	6.323–1	5.521–1	3.955–1	4.650–1	5.643–1	7.895–1	9.872–1	3.961	7.969	4.199+1	*
239.9	243	3.798–1	3.385–1	2.375–1	2.792–1	3.388–1	4.740–1	5.926–1	2.373	4.763	2.456+1	3.809+2
234.6	238	2.233–1	2.032–1	1.396–1	1.642–1	1.993–1	2.787–1	3.483–1	1.393	2.791	1.420+1	1.788+2
229.3	233	1.283–1	1.192–1	8.026–2	9.434–2	1.144–1	1.600–1	2.001–1	7.996–1	1.601	8.084	9.154+1
224.1	228	7.198–2	6.836–2	4.503–2	5.293–2	6.422–2	8.981–2	1.122–1	4.483–1	8.970–1	4.510	4.824+1
	223	3.935–2	3.821–2	2.463–2	2.895–2	3.512–2	4.910–2	6.135–2	2.450–1	4.901–1	2.457	2.548+1
	218	2.092–2	2.078–2	1.309–2	1.539–2	1.867–2	2.611–2	3.261–2	1.302–1	2.604–1	1.304	1.329+1
	213	1.080–2	1.098–2	6.761–3	7.947–3	9.640–3	1.347–2	1.684–2	6.723–2	1.344–1	6.725–1	6.791
	208	5.006–3	5.627–3	3.386–3	3.979–3	4.826–3	6.749–3	8.427–3	3.365–2	6.728–2	3.362–1	3.381
	203	2.615–3	2.784–3	1.639–3	1.926–3	2.336–3	3.265–3	4.076–3	1.628–2	3.254–2	1.627–1	1.631
	198	1.220–3	1.334–3	7.646–4	8.986–4	1.090–3	1.524–3	1.902–3	7.593–3	1.518–2	7.590–2	7.597–1
	193	5.472–4	6.138–4	3.423–4	4.023–4	4.882–4	6.828–4	8.530–4	3.406–3	6.810–3	3.404–2	3.405–1
	188	2.353–4	2.710–4	1.472–4	1.730–4	2.099–4	2.936–4	3.668–4	1.465–3	2.928–3	1.464–2	1.464–1
	183	9.672–5	1.144–4	6.051–5	7.111–5	8.629–5	1.207–4	1.508–4	6.020–4	1.204–3	6.016–3	6.016–2

† At saturation only.
* Atmospheric saturation is not possible at this ambient temperature and pressure

(2) An extreme relative humidity between 75 and 100 percent and air temperature between 22.8 °C (73 °F) and 27.8 °C (82 °F), which would result in corrosion and bacterial and fungal growths, can be expected for a period of 15 days. A humidity of 100 percent occurs one-fourth of the time at the lower temperature in cycles not exceeding 24 hours. Any loss of water vapor from the air by condensation is replaced from outside sources to maintain at least 75-percent relative humidity at the higher temperature.

b. The Vandenberg AFB:

(1) An extreme humidity cycle of 24 hours with a wind of less than 5 m/s (9.7 knots): Three hours of 23.9 °C (75 °F) air temperature at 75-percent relative humidity and a vapor concentration of 16.2 g/m^3 (7.1 gr/ft^3), 6 hours of decreasing air temperature to 18.9 °C (66 °F) with relative humidity increasing to 100 percent, 8 hours of decreasing air temperature to 12.8 °C (55 °F) with a release of 5.0 grams of water as liquid per cubic meter of air (2.2 grains of water per cubic foot of air) with relative humidity remaining at 100 percent, and 7 hours of increasing air temperature to 23.9 °C (75 °F) and a decrease to 75-percent relative humidity (fig. 6.2).

(2) Bacterial and fungal growth should present no problem because of the lower temperatures in this area. For corrosion, an extreme relative humidity of between 75 and 100 percent and air temperature between 18.3 °C (65 °F) and 23.3 °C (74 °F) can be expected for a period of 15 days. The humidity should be 100 percent during one-fourth of the time at the lower temperature in cycles not exceeding 24 hours. Any loss of water vapor from the air condensation is replaced from outside sources to maintain at least 75-percent relative humidity at the higher temperature.

c. White Sands Missile Range:

This area is located at 1,216 m (4,000 ft) above sea level and is on the eastern side of higher mountains. The mean annual rainfall of 250 cm (10 in) is rapidly absorbed in the sandy soil. Fog rarely occurs; therefore, at this location, a high vapor concentration over periods longer than a few hours need not be considered.

6.3.2.2 Low Vapor Concentration at Surface

6.3.2.2.1 Introduction

Low water-vapor concentration can occur at very low or at high temperatures when the air is very dry. In both cases, the dew points are very low. However, in the case of low dew points and high temperatures, the relative humidity is low. When any storage area or compartment of a vehicle is heated to temperatures well above the ambient air temperature (such as the high temperatures of the storage area in an aircraft standing on the ground in the Sun), the relative humidity will be even lower than the relative humidity of the ambient air. These two types of low water-vapor concentrations have entirely different environmental effects. In the case of low air temperatures, ice or condensation may form on equipment, while in the high-temperature, low-humidity condition, organic materials may dry and split or otherwise deteriorate. When a storage area (or aircraft) is considerably warmer than the ambient air (even when the air is cold), the drying increases even more. Low relative humidities may also result in another problem—that of static electricity. Static electrical charges on equipment may ignite fuel, result in shocks to personnel when discharged, or interfere with performance of the microelectronic components of the system. Because of these dangers, the two types of low water-vapor concentrations (dry extreme) are given for testing criteria in the following paragraph.

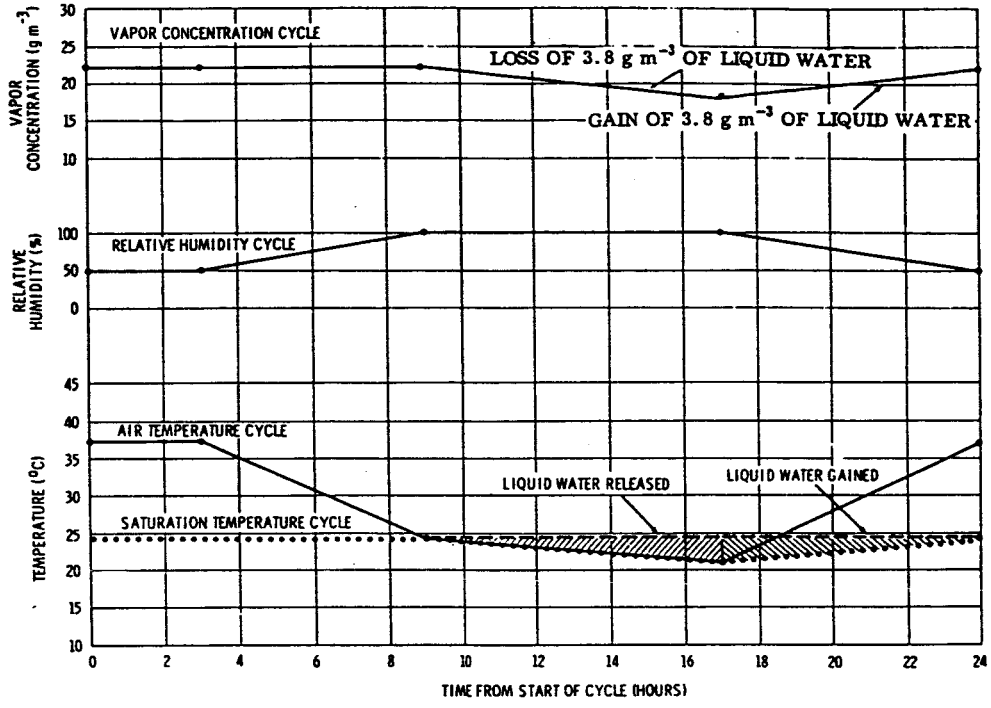

Figure 6.1 Extreme high vapor concentration cycle for Huntsville, New Orleans, and Kennedy Space Center.

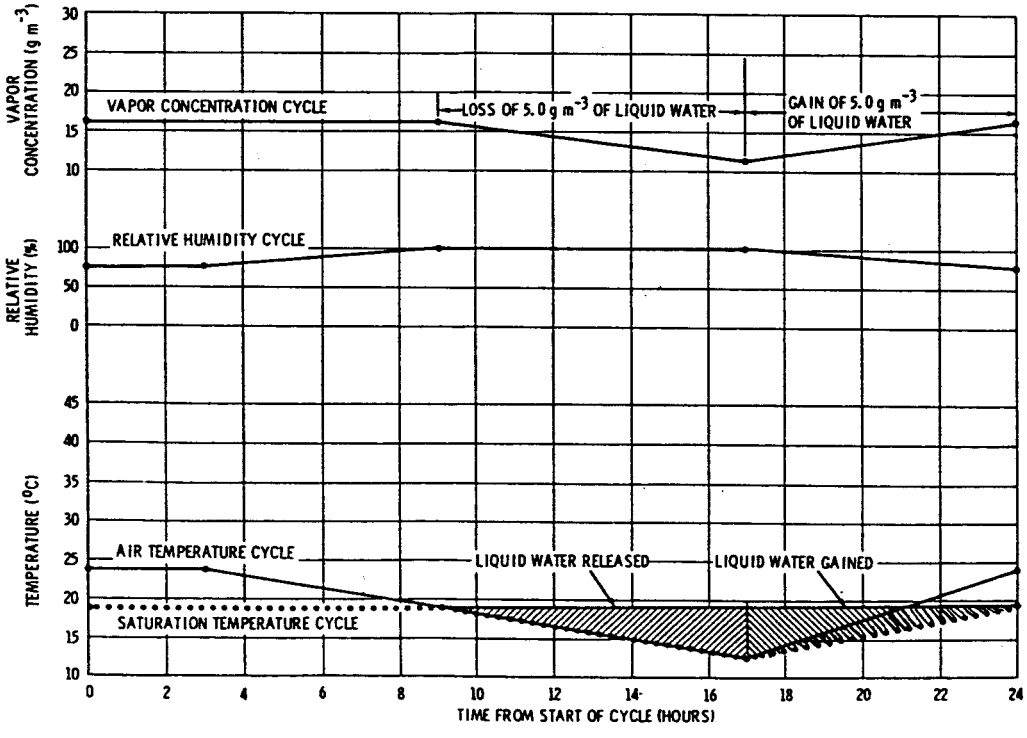

Figure 6.2 Extreme high vapor concentration for the Vandenberg AFB.

6.3.2.2.2 Surface Extremes of Low Vapor Concentration

a. Huntsville and White Sands Missile Range:

(1) An air temperature of –11.7 °C (+11 °F) and a vapor concentration of 2.1 g/m^3 (0.9 gr/ft^3), with a relative humidity between 98 and 100 percent for a duration of 24 hours.

(2) An air temperature of 28.9 °C (84 °F), a vapor concentration of 4.5 g/m^3 (2.0 gr/ft^3) (corresponding to a dew point of 1.1 °C (30 °F)), and a relative humidity of 15 percent occurring for 6 hours; a maximum relative humidity of 34 percent at an air temperature of 15.6 °C (60 °F) for the remaining 18 hours of the day for a 10-day period.

b. New Orleans and Kennedy Space Center:

(1) An air temperature of –2.2 °C (28 °F) and a vapor concentration of 4.2 g/m^3 (1.8 gr/ft^3), with a relative humidity between 98 and 100 percent for a duration of 24 hours.

(2) An air temperature of 22.2 °C (72 °F), a vapor concentration of 5.6 g/m^3 (2.4 gr/ft^3) (corresponding to a dew point of 2.2 °C (36 °F)), and a relative humidity of 29 percent occurring for 8 hours; a maximum relative humidity of 42 percent at an air temperature of 15.6 °C (60 °F) for the remaining 16 hours of the day for a 10-day period.

c. Vandenberg Air Force Base:

(1) An air temperature of –2.2 °C (28 °F) and a vapor concentration of 4.2 g/m^3 (1.8 gr/ft^3), with a relative humidity between 98 and 100 percent for a duration of 24 hours.

(2) An air temperature of 37.8 °C (100 °F), a vapor concentration of 4.8 g/m^3 (2.1 gr/ft^3) (corresponding to a dew point of 0.0 °C (32 °F)), and a relative humidity of 11 percent occurring for 4 hours; a maximum relative humidity of 26 percent at an air temperature of 21.1 °C (70 °F) for the remaining 20 hours of the day for a 10-day period.

6.3.3 Compartment Vapor Concentration at Surface

For testing to simulate conditions in the interior of an aircraft or space vehicle compartment, the following criteria should be used for all locations: a low water vapor concentration extreme of 10.1 g/m^3 (4.4 gr/ft^3), corresponding to a dew point of 11.1 °C (52 °F) at a temperature of 87.8 °C (190 °F) and a relative humidity of 2 percent occurring for 1 hour, a linear change over a 4-hour period to an air temperature of 37.8 °C (100 °F) and a relative humidity of 22 percent occurring for 15 hours, then a linear change over a 4-hour period to the initial conditions.

6.4 Vapor Concentration at Altitude

In general, the vapor concentration decreases with altitude in the troposphere, because of the decrease of temperature with altitude. Stratospheric and mesospheric levels of atmospheric moisture are small. Figure 6.3 presents an interim reference model for the mean and variability of middle atmospheric water vapor (ref. 6.11). It represents mean, Northern Hemisphere, mid-latitude, springtime, mixing ratios (ppmv) along with its variability (bars) and accuracies (brackets). The data presented in the following paragraphs are appropriate for design purposes.

6.4.1 High Vapor Concentration at Altitude

The following tables present the relationship between maximum vapor concentration and the associated temperature normally expected as a function of altitude.

a. Maximum Vapor Concentrations for Kennedy Space Center, table 6.2.

b. Maximum Vapor Concentrations for White Sands Missile Range, table 6.3.

c. Maximum Vapor Concentrations for Vandenberg AFB, table 6.4.

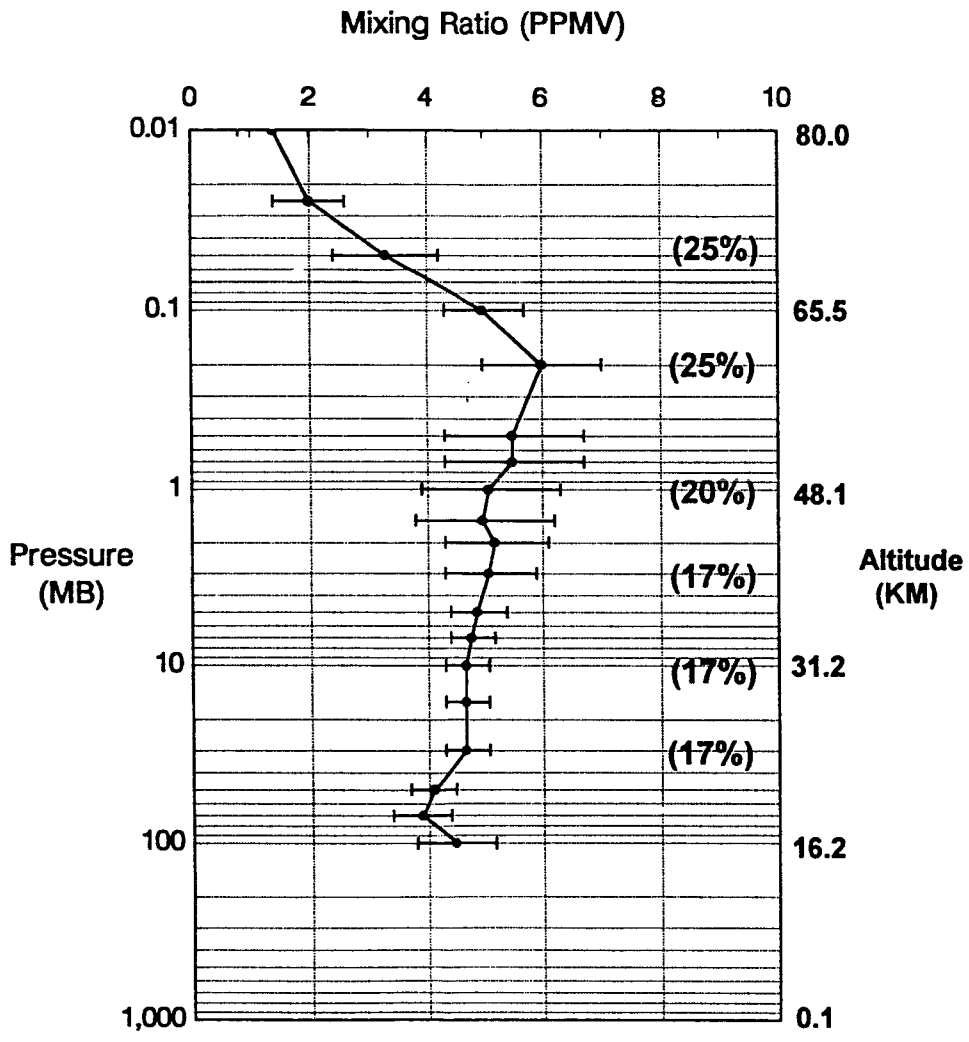

Figure 6.3. Reference profile of middle atmosphere mixing ratio mean, variability, and accuracy; representative of Northern Hemisphere, mid-latitude, springtime conditions (ref. 6.11).

6.4.2 Low Vapor Concentration at Altitude

The values presented as low extreme vapor concentrations in the following tables are based on data measured by standard radiosonde equipment.

a. Minimum Vapor Concentrations for Kennedy Space Center, table 6.5.

b. Minimum Vapor Concentrations for White Sands Missile Range, table 6.6.

c. Minimum Vapor Concentrations for Vandenberg AFB, table 6.7.

Table 6.2 Maximum vapor concentration for Kennedy Space Center.

Geometric Altitude		Maximum Vapor Concentration		Temperature Associated With Maximum Vapor Concentration	
(km)	(ft)	(g m^{-3})	(gr ft^{-3})	(°C)	(°F)
SFC (0.005 m.s.l.)	(16)	27.0	11.8	30.5	87
1	3,300	19.0	8.8	24.5	76
2	6,600	13.3	5.8	18.0	64
3	9,800	9.3	4.1	12.0	54
4	13,100	6.3	2.8	5.5	42
5	16,400	4.5	2.0	–0.5	31
6	19,700	2.9	1.3	–6.8	20
7	23,000	2.0	0.9	–13.0	9
8	26,200	1.2	0.5	–20.0	–4
9	29,500	0.6	0.3	–27.0	–17
10	32,800	0.3	0.1	–34.5	–30
16.2	53,100	0.025	0.01	–57.8	–72
20	65,600	0.08	0.03	–47.8	–54

Table 6.3 Maximum vapor concentration for White Sands Missile Range.

Geometric Altitude		Maximum Vapor Concentration		Temperature Associated With Maximum Vapor Concentration	
(km)	(ft)	(g m^{-3})	(gr ft^{-3})	(°C)	(°F)
SFC (1.2 m.s.l.)	(3,989)	16.0	7.0	21.5	71
2	6,600	13.2	5.8	18.9	66
3	9,800	9.0	3.9	12.8	55
4	13,100	6.8	3.0	7.8	46
5	16,400	4.9	2.1	2.2	36
6	19,700	3.4	1.5	–2.2	28
7	23,000	2.2	1.0	–10.0	14
8	26,200	1.3	0.6	–16.1	3
9	29,500	0.6	0.3	–22.8	–9
10	32,800	0.2	0.1	–30.0	–22
16.5	54,100	0.08	0.03	–47.8	–54
20	65,600	0.05	0.02	–52.2	–62

Table 6.4 Maximum vapor concentration for Vandenberg AFB.

Geometric Altitude		Maximum Vapor Concentration		Temperature Associated With Maximum Vapor Concentration	
(km)	(ft)	(g m^{-3})	(gr ft^{-3})	(°C)	(°F)
SFC (0.113 m.s.l.)	371	17.5	7.6	30.5	87
1	3,300	14.8	6.5	24.2	76
2	6,600	10.0	4.4	20.6	69
3	9,800	7.5	3.3	11.0	52
4	13,100	5.0	2.2	4.7	41
5	16,400	3.7	1.6	−1.4	30
6	19,700	2.3	1.0	−8.1	17
7	23,000	1.6	0.7	−12.5	10
8	26,200	0.8	0.3	−20.2	−4
9	29,500	0.4	0.2	−28.2	−19
10	32,800	0.2	0.1	−34.3	−30

Table 6.5 Minimum vapor concentration for Kennedy Space Center.

Geometric Altitude		Minimum Vapor Concentration		Temperature Associated With Minimum Vapor Concentration	
(km)	(ft)	(g m^{-3})	(gr ft^{-3})	(°C)	(°F)
SFC (0.005 m.s.l.)	(16)	1.5	0.7	7.0	45
1	3,300	0.5	0.2	6.0	42.8
2	6,600	0.2	0.1	0.0	32.0
3	9,800	0.1	0.04	−11.0	12.2
4	13,100	0.1	0.04	−14.0	6.8

Table 6.6 Minimum vapor concentration for White Sands Missile Range.

Geometric Altitude		Minimum Vapor Concentration		Temperature Associated With Minimum Vapor Concentration	
(km)	(ft)	(g m^{-3})	(gr ft^{-3})	(°C)	(°F)
SFC (1.2 m.s.l.)	(3,989)	1.2	0.5	–1.0	30
2	6,600	0.9	0.4	–5.0	23
3	9,800	0.6	0.3	–12.0	10
4	13,100	0.4	0.2	–20.0	–4
5	16,400	0.2	0.1	–26.0	–15
6	19,700	0.1	0.04	–36.0	–33
7	23,000	0.09	0.03	–42.0	–44
8	26,200	0.07	0.03	–49.0	–56
9	29,500	0.03	0.01	–55.0	–67
10	32,800	0.02	0.01	–60.0	–76

Table 6.7 Minimum vapor concentration for Vandenberg AFB.

Geometric Altitude		Minimum Vapor Concentration		Temperature Associated With Minimum Vapor Concentration	
(km)	(ft)	(g m^{-3})	(gr ft^{-3})	(°C)	(°F)
SFC (0.113 m.s.l.)	371	1.6	0.7	4.5	40
1	3,300	0.7	0.3	–1.4	30
2	6,600	0.4	0.2	–7.5	19
3	9,800	0.3	0.1	–12.6	9
4	13,100	0.1	0.04	–19.4	–3
5	16,400	0.07	0.03	–27.3	–17
6	19,700	0.03	0.01	–35.1	–31
7	23,000	0.02	0.009	–39.5	–39

REFERENCES

6.1 "Military Standard, Climatic Information to Determine Design and Test Requirements for Military Systems and Equipment." MIL-STD-210C, January 9, 1987.

6.2 "Military Standard, Environmental Test Methods." MIL-STD-810D, July 31, 1986.

6.3 "Glossary of Meteorology." American Meteorological Society, Boston, MA, 1959.

6.4 Fleagle, R.G. and Businger, J.A.: "An Introduction to Atmospheric Physics." Academic Press, New York, NY, 1965, p. 96.

6.5 "Smithsonian Meteorological Tables, Sixth Edition." Prepared by Robert List. Smithsonian Institution Press, Washington, DC, 1984.

6.6 Sheppard, P.A.: "The Physical Properties of Air With Reference to Meteorological Practice and the Air-Conditioning Engineer." ASME, vol. 71, 1949, pp. 915–919.

6.7 "Handbook of Geophysics and Space Environment." Air Force Geophysics Laboratory, Air Force Systems Command, United States Air Force, 1985.

6.8 "External Tank Verification Plan." MMC-ET-TM01-B, Contract No. NAS8-30300, WBS No. 1.6.6.2., DR. NO. TM01, Martin Marietta, Michoud Assembly Facility, New Orleans, LA, September 9, 1974.

6.9 Sissenwine, N. and Court, A.: "Climate Extremes for Military Equipment," Report No. 146, Environmental Protection Branch, Research and Development Division, Office of the Quartermaster General, Washington, DC, 1951.

6.10 Sverdrup, H.V.: "Oceanography for Meteorologists." Prentice-Hall, Inc., New York, NY, 1942.

6.11 Remsberg, E.E., Russell, J.M. III, and Wu, C.-Y.: "An Interim Reference Model for the Variability of the Middle Atmosphere Water Vapor Distribution." Adv. Space Res., vol. 10, No.6, 1990, pp. (6)51–(6)64.

SECTION VII. PRECIPITATION, FOG, AND ICING

7.1 Introduction

Precipitation, fog, and icing are atmospheric phenomena of interest to the design, fabrication, and flight of aerospace vehicles. In some arid areas of the world, however, precipitation does not occur for several years. Likewise, in areas of moderate to heavy rainfall, there are periods of time without rain. Because precipitation does occur in discrete events, statistical representation may be misleading; therefore, caution must be taken to ensure that data relative to the desired location are used. Definitions used in this section are given in the following paragraphs. For definition of size ranges see reference 7.21.

7.2 Definitions

Precipitation: Precipitation is usually defined as all forms of hydrometeors, liquid or solid, which are free in the atmosphere and reach the ground. In this report, the definition is extended to those hydrometeors which do not reach the ground but impinge on a flying surface, such as space vehicles. Accumulation is reported in depth over a horizontal surface, i.e., millimeters or inches for liquid phase, and in depth or depth-of-water equivalent for the frozen phase.

Icing: In general, any deposit or coating of ice on an object, caused by the impingement and freezing of liquid hydrometers. Aircraft "icing" forms by the freezing of supercooled cloud drops and is always determined by aerodynamical considerations.

Mist: Mist is composed of a suspension of very small (from submicrometer to ~20 μm in diameter) water droplets in the air. Mist reduces the horizontal visibility at the Earth's surface, as does fog, rain, snow, and other hydrospheric and lithospheric substances.

Drizzle: Drizzle consists of droplets which are so small that they make no precipitable impact on surfaces. If individual droplets make a distinct splash on striking the ground or a water surface, they should be recorded as rain (ref. 7.1).

Glaze: A coating of ice, generally clear and smooth but usually containing some air pockets, formed on exposed objects by the freezing of a film of supercooled water deposited by rain, drizzle, fog, or possibly condensed from supercooled water vapor.

Rain: There is no universal agreement on the precise dividing line between drizzle and rain. However, many texts suggest diameters near 0.5 mm or larger. Regardless, most observers can easily determine when moisture begins to fall as visibly separate drops, which then becomes the practical differentiation between the two terms.

Freezing Rain: Rain that falls in liquid form but freezes upon impact to form a coating of glaze upon the ground or exposed objects.

Fog: A visible mist.

Hail: Precipitation in the form of balls or irregular lumps of ice and is always produced by convective clouds. Through established convention, to be classified as hail the diameter of the ice must be 5 mm or more and the specific gravity must be between 0.60 and 0.92.

Rime: A white or milky and opaque granular deposit of ice formed by the rapid freezing of supercooled water drops as they impinge upon an exposed object.

Sleet: A mixture of rain and snow, or partially melted snow.

Small Hail: Precipitation in the form of semitransparent round or conical grains of frozen water under 5 mm in diameter. Each grain consists of a nucleus of soft hail (ball of snow) surrounded by a very thin ice layer. The grains are not crisp and do not usually rebound when striking a hard surface.

Snow: All forms of frozen precipitation except large hail. It encompasses snow pellets, snow grains, ice crystals, ice pellets, and small hail.

The previously described precipitation forms are sufficiently different that each must be considered separately in design problems.

7.3 Rainfall

There are four major rainfall-producing atmospheric conditions: (1) the monsoon, which produces the heaviest precipitation over long periods (most world records of rainfall rates for periods greater than 12 hours are a result of monsoons); (2) thunderstorms, which generate high rates of precipitation for short periods; (3) cold and warm frontal systems, frequently accompanied by bands of steady light rain. Frontal-produced rain can persist for several days depending upon the movement of synoptic scale weather systems (thunderstorms may occur with frontal systems to give heavier rain), and (4) hurricanes, which produce heavy rain associated with winds. These four rainfall types are defined in the following paragraphs.

Monsoon: The monsoon is a seasonal wind which blows for long periods of time, usually several months from one direction. When these winds blow from the water to land with increasing elevation from the water, the orographic lifting of the moisture-laden air releases precipitation in heavy amounts. In Cherrapunji, India, 9,144 mm (360 in) of rain has fallen in a 1-month period from monsoon rains. The amount of rain from monsoons at low elevations is considerably less than at higher elevations.

Thunderstorm: In general, the thunderstorm (local storm) is produced either by lifting of unstable moist air, heating of the land mass, lifting by frontal systems, or a combination of these conditions. Cumulonimbus clouds, which are produced by these storms, are always accompanied by lightning and thunder. The thunderstorm is a consequence of atmospheric instability and is defined loosely as an overturning of air layers in order to achieve a stable condition. Strong wind gusts, heavy rain, severe electrical discharges, and sometimes hail occur with the thunderstorm, with the most frequent and severe occurrences in the late afternoons and evenings.

Rain shower: Precipitation from a convective cloud. Showers are characterized by the suddenness with which they start and stop, by the rapid changes of intensity, and usually by rapid changes in the appearance of the sky.

Cold and warm front precipitation: When two masses of air meet—one more dense than the other —the lighter air mass (warm) will slide up over the more dense air mass (cold). If sufficient moisture is in the air mass being lifted, then the moisture will be condensed out and fall as precipitation, either rain or snow, depending on the temperature of air masses.

Hurricanes: A hurricane is a severe "tropical storm" which forms over the various oceans and seas, nearly always in tropical latitudes. At maturity the tropical cyclone (storm) is one of the most intense and feared storms in the world: Winds exceeding 90 m/s (175 kn) have been measured, and rainfall can be torrential. The wind speed must exceed 33 m/s (64 kn) for the storm to be classified as a hurricane.

Orographic effects should not be overlooked in a discussion of rainfall. Islands located in persistent moist air flow receive extreme rainfall as a result of the moist air being lifted to the condensation level (frequently over 2,000 to 5,000 ft altitude), with resulting persistent rain. This phenomenon accounts for wide variations in precipitation amounts between locations in close proximity in mountainous areas.

7.3.1 Record Rainfall

In design analysis, the maximum amounts of rainfall for various periods need to be considered. These extreme values vary considerably in different areas of the world, but in areas of similar climatic conditions the extreme values are similar.

7.3.1.1 World Record Rainfall

To best study the maximum amounts of rainfall that have occurred worldwide for different periods, log-log graph paper is used. Figure 7.1 shows these worldwide values and the envelope of these values as a straight line with the equation

$$R = 363.0\sqrt{D_h}\ \text{(mm)} \qquad \text{or} \qquad R = 14.3\sqrt{D_h}\ \text{(in)} \tag{7.1}$$

where R is the depth or rainfall in millimeters for period D, and D_h is the duration of rainfall in hours. Due to the lack of sufficient objective data at less than about 20 min duration, much greater scatter in individual measurements is observed, which reduced the reliability of the straight line graph in this region.

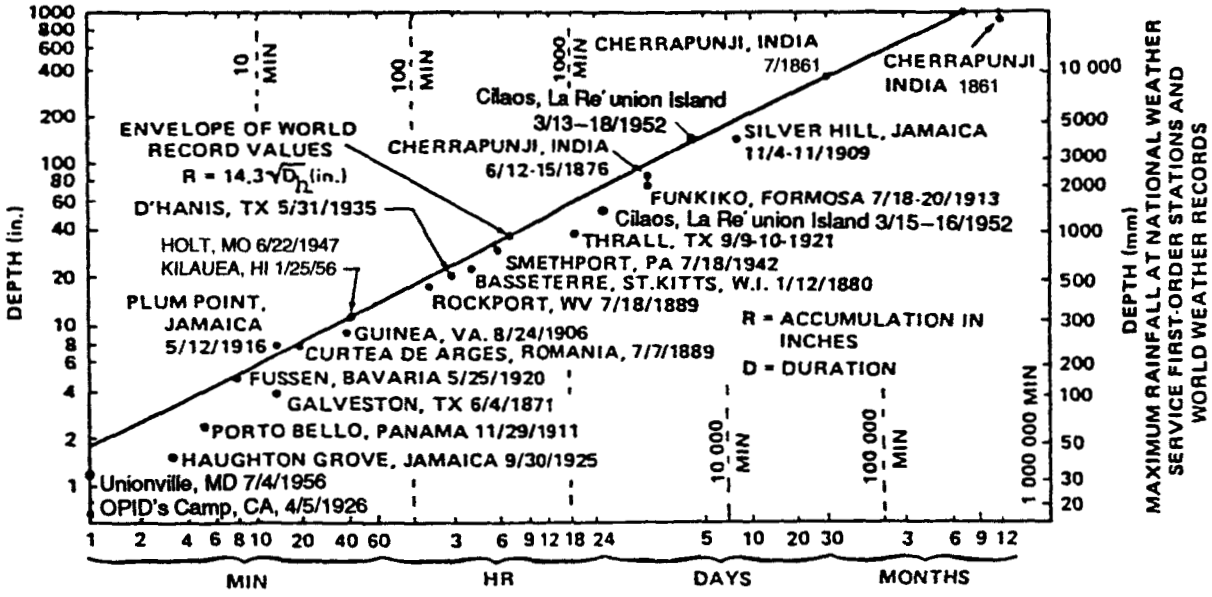

Figure 7.1 World record rainfalls and an envelope of world record values (after R.D. Fletcher and S. Sartos, Air Weather Service Tech. Report No. 105-81, 1951 and ref. 7.2).

7.3.1.2 Design Rainfall Rates

For design and testing, the rate of rainfall per unit time is more useful than the total depth of rainfall. The normal rates used are shown in millimeters per hour or inches per hour. Figure 7.2 shows the envelope of world record values plotted as the rate per hour (inches and millimeters) versus duration.

The Kennedy Space Center and Vandenberg AFB design rainfall rate curves are also shown in figure 7.2 with the 5-year and 100-year return periods for a few select stations. The 5-year and 100-year return period data were taken from rainfall intensity-duration-frequency curves published by the U.S. Department of Commerce, Weather Bureau (ref. 7.3). These data were analyzed by the extreme value method of Gumble (ref. 7.4).

The term "return period" is a measure of the average time interval between occurrences of a specific event. For example, the 99th percentile rainfall rate for Tampa, Florida, is approximately 10 in/hr for a duration of 6 min (from fig. 7.2 and table 7.1). On the average this rainfall rate can be expected to return in 100 years at Tampa. Return periods can be expressed as probabilities, as shown in table 7.1.

Values of design rainfall for various locations and worldwide extremes of rainfall are given in tables 7.2, 7.3, 7.4, and 7.5 with values of the corresponding drop size. The worldwide extremes would not normally be used for design of space vehicles but may be needed for facility design, tracking stations, etc. The values of rainfall rates are represented with the following equation:
7-4

$$r=\frac{C\sqrt{D_m}}{D_m}=\frac{C}{\sqrt{D_m}}, \tag{7.2}$$

where

r = rate in inches per hour or mm per hour

D_m = time in minutes

C = constants for locations are given in table 7.6.

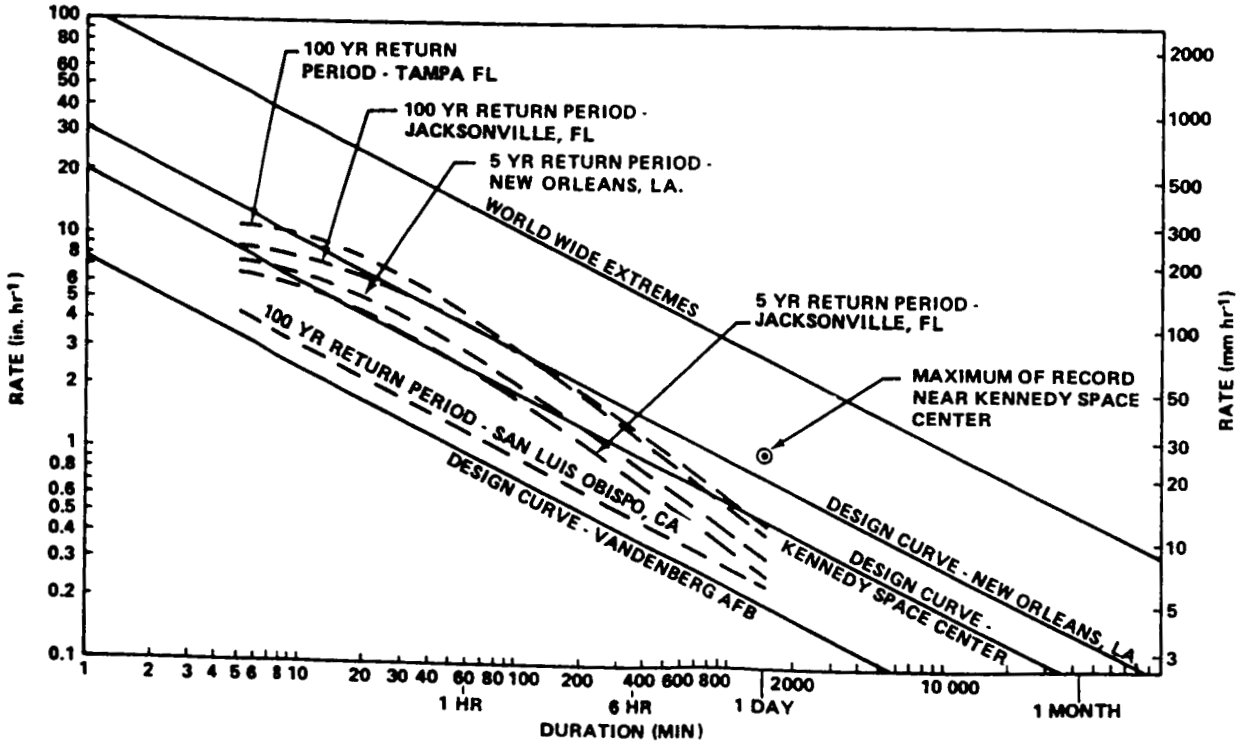

Figure 7.2 Design rainfall rates.

Table 7.1 Relationship of return periods to probabilities.

Return Period	Percentile	Return Period	Percentile
(year)	(%)	(year)	(%)
2	50	50	98
5	80	100	99
10	90	1,000	99.9

Table 7.2 Design rainfall, Kennedy Space Center, FL, and Huntsville, AL, based on yearly largest rate for stated time periods.*

Time Period	Rainfall Rate (r)		Rainfall Total Accumulation		Raindrop Size	
					Average	Largest
	mm h^{-1}	in h^{-1}	mm	in	mm	mm
1 min	492	19.4	8	0.3	2.0	6.0
5 min	220	8.7	18	0.7	2.0	5.8
15 min	127	5.0	32	1.25	2.0	5.7
1 h	64	2.5	64	2.5	2.0	5.0
6 h	26	1.0	156	6.1	1.8	5.0
12 h	18	0.7	220	8.7	1.6	4.5
24 h	13	0.5	311	12.2	1.5	4.5

*Use average rate of fall for raindrops of 6.5 m/s for all time periods.

Table 7.3 Design rainfall, New Orleans, LA, based on yearly largest rate for stated time periods.*

Time Period	Rainfall Rate (r)		Rainfall Total Accumulation		Raindrop Size	
					Average	Largest
	mm h^{-1}	in h^{-1}	mm	in	mm	mm
1 min	787	31.0	13	0.5	2.1	6.0
5 min	352	13.9	29	1.2	2.0	6.0
15 min	203	8.0	51	2.0	2.0	5.7
1 h	102	4.0	102	4.0	2.0	5.5
6 h	41	1.6	249	9.8	1.9	5.0
12 h	29	1.2	352	13.9	1.8	5.0
24 h	21	0.8	498	19.6	1.6	5.0

*Use average rate of fall for raindrops of 6.5 m/s for all time periods.

Table 7.4 Design rainfall, Vandenberg AFB, CA, Edwards AFB, CA, and White Sands Missile Range, NM, based on yearly largest rate for stated time periods*.

Time Period	Rainfall Rate (r)		Rainfall Total Accumulation		Raindrop Size	
					Average	Largest
	mm h^{-1}	in h^{-1}	mm	in	mm	mm
1 min	197	7.7	3	0.1	2.0	5.6
5 min	88	3.5	7	0.3	2.0	5.3
15 min	51	2.0	13	0.5	2.0	5.0
1 h	25	1.0	25	1.0	1.8	5.0
6 h	10	0.4	62	2.4	1.5	4.6
12 h	7	0.3	88	3.5	1.3	4.3
24 h	5	0.2	124	4.9	1.3	4.0

*Use average rate of fall for raindrops of 6.5 m/s for all time periods; except use 6.0, 5.8, and 5.5 m/s for 6, 12, and 24 h, respectively.

Table 7.5 Design rainfall, worldwide extremes, based on yearly largest rate for stated time periods.*

Time Period	Rainfall Rate (r)		Rainfall Total Accumulation		Raindrop Size	
					Average	Largest
	mm h^{-1}	in h^{-1}	mm	in	mm	mm
1 min	2,813	110.8	47	1.8	2.5	8.0
5 min	1,258	49.5	105	4.1	2.2	8.0
15 min	726	28.6	182	7.1	2.1	8.0
1 h	363	14.3	363	14.3	2.0	8.0
6 h	148	5.8	890	35.3	2.0	5.8
12 h	105	4.1	1,258	49.5	2.0	5.5
24 h	74	2.9	1,779	70.1	2.0	5.2

*Use average rate of fall for raindrops of 6.5 m/s for all time periods.

Table 7.6 Constants to use with equation (7.2) for rainfall rates.

	Kennedy Space Center, Huntsville	New Orleans	Vandenberg AFB, Edwards AFB, White Sands Missile Range	World Extremes
in h^{-1} mm h^{-1}	19.365 491.87	30.984 786.99	7.746 196.75	110.767 2,813.48
Values of r given in Table No.	7.2	7.3	7.4	7.5

7.3.2 Raindrop Size

A knowledge of raindrop sizes is required to (1) simulate rainfall tests in the laboratory, (2) know the rate of fall of the raindrops and impact energy, and (3) use in erosion tests of materials.

At the surface, the size of the raindrops varies with the rate of rainfall per unit time; the heavier the rainfall, the larger the drops. Any one rainstorm will contain a variety of sizes of raindrops ranging from less than 0.5 mm (the lower limit of size measurement) to greater than 4.0 mm. The more intense the storm (the higher the rate of rainfall), the larger some of the drops will be. Reference 7.5 shows data on probability of occurrence of various raindrop sizes with relation to types of rain-producing storms: (1) thunderstorms, (2) rain showers, and (3) continuous rain. Thunderstorms have the greatest occurrence of the larger drops (over 2 mm). Rain showers have the next greatest occurrence, while the continuous rain produces the lowest occurrence of the larger drops. Rain drop sizes below 2 mm in diameter occur with near equal probability from all types of storms. In comparing drop sizes with various rainfall rates, the larger drops occurred with the highest probability from the highest rainfall rates. Raindrops over 8 mm in diameter are not expected to occur frequently because the rate of fall breaks these large drops into smaller ones (ref. 7.6).

The raindrop size distribution depends critically on the origin of the rain. In particular, very large drops can exist when they are stabilized by a little unmelted ice as from a thunderstorm soft hail shower.

7.3.3 Statistics of Rainfall Occurrences

One set of statistical data on precipitation will not be satisfactory for all needs in design; therefore, several sets of statistical data are presented in this section as follows.

7.3.3.1 Design Rainfall Rates

The design rainfall rates in figure 7.2 and tables 7.2, 7.3, 7.4, and 7.5 are based on precipitation occurrences; i.e., if precipitation is occurring, what is the probability of exceeding a given rate? These data are based on occurrences over a year and would be used in design of items continuously exposed, such as launch facilities.

7.3.3.2 Probability That Precipitation Will Not Exceed a Specific Amount in Any One Day

Values for each month with the probability that precipitation will not exceed a specified amount in any one day are given for several selected sites of aerospace vehicle design interest—Kennedy Space Center, FL; Edwards AFB, and Vandenberg AFB, CA, and New Orleans, LA—in tables 7.7 through 7.10, respectively. The values in the tables should not be interpreted to mean that the amount of precipitation

occurs uniformly over the 24-h period, since it is more likely that most or all of the amounts occurred in a short period of the day.

7.3.3.3 Rainfall Rates Versus Duration for 50th, 95th, and 99th Percentile, Given a Day With Rain for the Highest Rain Month, KSC, FL

Rainfall rates for various durations for the 50th, 95th, and 99th percentile, given a day with rain in the highest rain month, are given in table 7.11 for the Kennedy Space Center, FL. The precipitation amounts should not be interpreted to mean that the rain fell uniformly for a brief period for the referenced time periods with no rain the remainder of the time period. As an example, the 99th percentile total of 49 mm (1.93 in) (i.e., left column, 99th percentile, 1-h duration as shown on table 7.11) could have occurred as follows: 25 mm (0.98 in) could have fallen during a 5-min period within a particular hour, with an additional 24 mm (0.95 in) of rainfall for another 5-min period, making a total of 49 mm (1.93 in) for a total of about 10 min. Subsequently, no rain would have fallen for 50 min of the hypothetical 1-h period. The 99th percentile rainfall data are referenced in that such extremes are important to consider in vehicle and facility design studies. Table 7.2 has rainfall rates listed as well as total accumulation, raindrop size, etc., for various periods for Kennedy Space Center and Huntsville, which are also valuable data to use as vehicle criteria.

7.3.4 Distribution of Rainfall Rates With Altitude

Rainfall rates normally decrease with altitude when rain is striking the ground. The rainfall rates at various altitudes in percent of the surface rates are given in table 7.12 for all areas (ref. 7.7). Table 7.12 values are representative of summer rain rates (from 2.8 through 10.3 mm/h) in temperate latitudes for updrafts from 0.1 to 0.4 m/s.

Tattelman (ref. 7.5) models the mil-standard, world-wide, extreme rainfall rates with height based on estimates of surface rates occurring 0.5, 0.1, and 0.01 percent of the time for the worst month in the severest rain areas of the world, also for the 42- and 1-min world record rainfalls. These five extreme cases are representative of surface rainfall rates of 36 to 1,872 mm/h.

Precipitation above the ground is generally colder than at the ground and frequently occurs as supercooled drops which may cause icing on objects moving through the drops. Such icing can be expected to occur when the air temperature is about -2.2 °C (28 °F). The major factors that influence the rate of ice formation are (1) the amount of liquid water, (2) the droplet size, (3) air speed, and (4) the size and shape of the airfoil (ref. 7.8). Terminal fall velocities for various raindrops with diameters from 0.05 to 0.70 cm are given in table 7.18.

7.3.5 Types of Ice Formation

The type of ice which will form on the outside exposed surfaces of cryogenic tanks is related to the temperature of the tank surface, the precipitation rate, drop size, and wind velocity (or tank velocity). In general, the larger the drop size and the higher the temperature, precipitation rate, and wind speed, the denser the ice will form until a condition is reached where surface temperatures are too high for ice formation. If the precipitation is at too high a temperature at relatively high precipitation rates and wind speed, it may warm the tank sufficiently to melt ice which formed previously.

Table 7.13 summarizes ice types for various tank wall temperatures with moderate precipitation (over 10 mm h^{-1}).

Table 7.7 Probability that precipitation will not exceed a specific amount in any one day, Kennedy Space Center, FL.

Amount		Jan.	Feb.	March	Apr.	May	June
(in)	(mm)	%	%	%	%	%	%
0.00	0.00	68.1	60.8	62.2	70.6	64.2	54.7
Trace	Trace	77.1	71.4	71.3	80.0	76.2	65.7
0.01	0.25	79.0	74.3	72.5	82.7	79.4	68.4
0.05	1.27	84.8	79.4	77.5	86.6	84.7	74.1
0.10	2.54	87.1	82.3	81.6	89.3	89.4	75.8
0.25	6.35	90.0	85.8	87.8	93.5	92.9	82.8
0.50	12.70	93.9	91.6	91.6	95.9	96.4	90.8
1.00	25.40	97.1	96.1	96.3	98.0	99.3	97.1
2.50	63.50	99.4	100.0	99.5	99.5	100.0	99.8
5.00	127.00	100.0	100.0	99.8	99.8	100.0	100.0
Amount		July	Aug.	Sept.	Oct.	Nov.	Dec.
(in)	(mm)	%	%	%	%	%	%
0.00	0.00	56.8	52.6	40.0	47.4	62.1	64.2
Trace	Trace	65.8	63.9	53.9	61.6	74.2	78.1
0.01	0.25	68.4	66.2	57.5	63.9	77.2	81.0
0.05	1.27	73.2	69.4	62.7	72.0	83.9	86.8
0.10	2.54	75.8	74.9	67.9	76.8	86.9	89.4
0.25	6.35	83.5	80.7	75.8	85.5	90.8	93.3
0.50	12.70	88.3	88.4	83.7	91.3	92.6	96.5
1.00	25.40	93.8	93.6	92.2	95.5	96.2	99.1
2.50	63.50	99.6	99.7	97.4	99.4	99.2	100.0
5.00	127.00	99.6	100.0	99.8	99.7	99.5	100.0

The 100 percent values in the table indicate no chance of exceeding certain amounts of precipitation during most of the months, however, it should be realized that the length of available data records is not long and that there is always a chance of any meteorological extreme of record being exceeded.

Table 7.8 Probability that precipitation will not exceed a specified amount in any one day, Edwards AFB, CA.

Amount		Jan.	Feb.	March	Apr.	May	June
(in)	(mm)	%	%	%	%	%	%
0.00	0.00	81.7	81.8	82.6	86.7	95.1	98.8
Trace	Trace	88.0	88.9	89.6	93.8	98.6	99.5
0.01	0.25	88.9	89.5	91.3	94.8	99.0	99.5
0.05	1.27	91.7	92.1	93.8	96.4	99.1	99.5
0.10	2.54	93.5	93.5	95.5	97.6	99.4	99.5
0.25	6.35	96.9	95.6	98.0	99.0	100.0	99.9
0.50	12.70	98.8	98.3	99.1	99.6	100.0	100.0
1.00	25.40	99.8	99.6	99.8	100.0	100.0	100.0
2.50	63.50	100.0	100.0	99.9	100.0	100.0	100.0
5.00	127.00	100.0	100.0	100.0	100.0	100.0	100.0
Amount		July	Aug.	Sept.	Oct.	Nov.	Dec.
(in)	(mm)	%	%	%	%	%	%
0.00	0.00	94.7	95.2	94.6	93.0	89.8	85.2
Trace	Trace	99.0	98.1	97.8	95.8	94.2	90.8
0.01	0.25	99.3	98.1	98.2	96.1	94.4	91.4
0.05	1.27	99.7	98.9	98.9	97.2	96.4	93.7
0.10	2.54	99.7	99.3	98.9	98.2	97.0	94.9
0.25	6.35	100.0	99.6	99.2	99.2	98.4	96.7
0.50	12.70	100.0	99.9	99.8	99.6	99.3	99.0
1.00	25.40	100.0	100.0	99.9	99.7	100.0	99.9
2.50	63.50	100.0	100.0	100.0	100.0	100.0	100.0
5.00	127.00	100.0	100.0	100.0	100.0	100.0	100.0

The 100 percent values in the table indicate no chance of exceeding certain amounts of precipitation during most of the months, however, it should be realized that the length of available data records is not long and that there is always a chance of any meteorological extreme of record being exceeded.

Table 7.9 Probability that precipitation will not exceed a specific amount in any one day, Vandenberg AFB, CA.

Amount		Jan.	Feb.	March	Apr.	May	June
(in)	(mm)	%	%	%	%	%	%
0.00	0.00	69.4	70.4	61.7	70.4	71.8	70.0
Trace	Trace	79.1	75.9	72.2	80.4	94.0	94.8
0.01	0.25	81.1	76.9	74.6	82.5	96.8	97.7
0.05	1.27	83.5	81.4	83.9	87.9	98.0	100.0
0.10	2.54	88.3	84.4	85.9	90.8	98.8	100.0
0.25	6.35	91.5	90.4	91.5	95.4	99.6	100.0
0.50	12.70	95.1	94.4	96.3	97.5	100.0	100.0
1.00	25.40	98.3	96.9	98.7	99.2	100.0	100.0
2.50	63.50	99.9	99.9	99.5	100.0	100.0	100.0
5.00	127.00	100.0	100.0	99.9	100.0	100.0	100.0
Amount		July	Aug.	Sept.	Oct.	Nov.	Dec.
(in)	(mm)	%	%	%	%	%	%
0.00	0.00	62.4	63.4	77.9	79.4	73.3	73.8
Trace	Trace	98.2	94.9	95.4	95.1	82.6	80.6
0.01	0.25	98.9	98.1	95.8	95.5	83.3	83.1
0.05	1.27	100.0	98.8	97.5	95.9	85.9	87.4
0.10	2.54	100.0	99.5	97.9	96.7	87.4	89.2
0.25	6.35	100.0	99.9	98.7	97.5	90.0	93.5
0.50	12.70	100.0	100.0	99.9	98.7	94.4	97.1
1.00	25.40	100.0	100.0	100.0	99.5	98.8	99.6
2.50	63.50	100.0	100.0	100.0	99.9	99.9	100.0
5.00	127.00	100.0	100.0	100.0	100.0	100.0	100.0

The 100 percent values in the table indicate no chance of exceeding certain amounts of precipitation during most of the months, however, it should be realized that the length of available data records is not long and that there is always a chance of any meteorological extreme of record being exceeded.

Table 7.10 Probability that precipitation will not exceed a specific amount in any one day, New Orleans, LA.

Amount		Jan.	Feb.	March	Apr.	May	June
(in)	(mm)	%	%	%	%	%	%
0.00	0.00	77.1	70.2	73.6	79.7	75.9	72.2
0.01	0.25	77.7	71.1	74.1	79.9	76.4	72.6
0.05	1.27	80.9	74.5	78.1	81.9	78.0	77.7
0.10	2.54	85.7	76.4	81.0	83.6	82.9	82.3
0.20	5.08	89.1	80.4	82.8	87.0	86.5	85.3
0.50	12.70	94.0	88.8	88.6	91.2	92.2	90.3
1.00	25.40	97.4	93.8	92.9	95.3	95.6	93.8
2.00	50.80	98.9	97.8	97.9	97.8	99.0	98.8
5.00	127.00	99.7	99.7	99.7	100.0	100.0	100.0
10.00	254.00	100.0	100.0	100.0	100.0	100.0	100.0
Amount		July	Aug.	Sept.	Oct.	Nov.	Dec.
(in)	(mm)	%	%	%	%	%	%
0.00	0.00	54.5	70.1	69.2	84.4	83.4	77.6
0.01	0.25	55.8	71.3	71.1	85.6	84.7	78.2
0.05	1.27	61.4	74.4	76.3	88.2	85.7	80.7
0.10	2.54	67.4	79.3	79.2	90.5	87.4	83.2
0.20	5.08	73.3	83.5	84.4	93.4	89.4	85.2
0.50	12.70	81.5	92.4	90.3	96.0	94.0	91.9
1.00	25.40	91.5	95.7	94.5	98.0	97.3	95.2
2.00	50.80	96.7	98.2	98.0	99.7	98.3	99.4
5.00	127.00	100.0	100.0	99.0	100.0	99.7	99.7
10.00	254.00	100.0	100.0	100.0	100.0	100.0	100.0

The 100 percent values in the table indicate no chance of exceeding certain amounts of precipitation during most of the months, however, it should be realized that the length of available data records is not long and that there is always a chance of any meteorological extreme of record being exceeded.

Table 7.11 Highest rainfall rate versus duration for various probabilities, given a day with rain for the highest rain month, Kennedy Space Center, FL.

Duration	Percentile											
	50				95				99			
	(in)	(mm)	in h^{-1}	mm h^{-1}	(in)	(mm)	in h^{-1}	mm h^{-1}	(in)	(mm)	in h^{-1}	mm h^{-1}
5 min	0.22	5.6	2.6	66.0	0.72	18.0	8.7	221.0	1.00	25.0	12.0	305.0
15 min	0.23	5.8	0.93	24.0	0.88	22.0	3.5	89.0	1.30	33.0	5.2	132.0
1 h	0.25	6.4	0.25	6.4	1.17	30.0	1.17	30.0	1.93	49.0	1.93	49.0
6 h	0.28	7.1	0.05	1.3	1.55	39.0	0.26	6.6	3.18	81.0	0.53	13.0
24 h	0.43	10.9	0.02	0.5	2.62	67.0	0.11	2.8	5.00	127.0	0.21	5.3

Table 7.12 Distribution of rainfall rates with height.

For All Four Locations*		For World Extremes†	
Height (Geometric) Above Surface (km)	Percent Surface Rate	Height Above Surface (km)	Percent Surface Rate
SFC	100	SFC	100
1	90	2	100
2	75	4	100
3	57	6	100
4	34	8	74
5	15	10	51
6	7	12	35
7	2	14	22
8	1	16	11
9	0.1	18	8
10 and over	<0.1	20	0

*Summer type rainfall in temperate latitudes representing 2.8 through 10.3 mm/h rain rates (ref. 7.7).

†Mil-Std: For worst month, in severest rain area, representing 36 through 1,872 mm/h rain rates (ref. 7.5).

Table 7.13 Ice types as a function of tank wall temperatures.

Temperature of Tank Wall		Type of Ice	Density Range		Remarks
°F	°C		lb ft^{-3}	g cm^{-3}	
23 to 32	–5 to 0	clear ice	60	0.69	hard dense ice
15 to 23	–9 to –5	milky ice or clear ice with air bubbles	43 to 53	0.69 to 0.85	
below 15	below –9	rime ice	18 to 25	0.29 to 0.40	crumbly

Table 7.14 Summary of hydrometeor characteristics (ref. 7.9).

Type of Hydrometeor	Altitude (km)	Drop Diameter (μm)		Concentration per Unit Volume (cm^3)		Liquid Water Content Per Unit Volume ($g\ m^{-3}$)		Ambient Temperature (°C)
	Range	Range	Rep.[1]	Range	Rep.	Range	Rep.	Range≈
Layer Clouds	sfc–1.5	<1–40	11	<10–10,000	500	<0.1–1	0.2	+30 to –15
Layer Clouds	2.5–7.5	<1–50	12	<20–1,000	100	<0.1–1	0.2	+20 to –25
Layer Clouds (ice crystals)	7.5–15.0	<10–10,000	100	<0.1–10	0.2	<0.01–0.1	0.02	–10 to –55
Convective Clouds								
Fair Weather Cumulus	0.5–8.0	<1–75	12	<10–10,000	300	<0.1–1	0.5	+20 to –30
Cumulus Congestus	0.5–13.0	<1–200	25	<10–10,000	150	<1–10	4.0	+20 to –55
Continuous Type Rain	sfc–6.0	<500–3,000	1,000	<50–3,000*	500*	<0.05–0.7	0.1	+30 to –15
Shower Type Rain	sfc–13.0	<500–7,000	2,000	<10–3,000*	500*	<0.1–30	1.0	+30 to –55
Coalescence (Warm) Rain	sfc–5.0	<100–1,000	500	<500–50,000*	3,000*	<0.05–0.1	0.1	+30 to 0
Hail	sfc–13.0	<0.01–13 cm	0.8 cm	<0.5–1,000*	50*	<0.1–0.9**	0.8**	+30 to –55
Ice and Snow Crystals	sfc–13.0	<100–20,000	5,000	<1–1,000*	100*	<0.001–0.7***	0.07***	+5 to –55

1. Rep.: Representative value or value most frequently encountered.
* Per m^3
** Density of particles ($g\ cm^{-3}$)
*** Mass of crystals (mg)

7.3.6 Hydrometeor Characteristics With Altitude

Raindrops falling on the surface may originate at a higher altitude as some other form of hydrometeor, such as ice or snow. The liquid water content of these hydrometeors per unit volume would have a distribution similar to that given in table 7.14 for rainfall. A summary of the hydrometeor characteristics from reference 7.9 is given in table 7.14.

7.4 Snow

The accumulation of snow on a surface produces stress. For a flat horizontal surface, the stress is proportional to the weight of the snow directly above the surface. For long narrow objects, such as pipes or wires lying horizontally above a flat surface (which can accumulate the snow), the stress can be figured as approximately equal to the weight of the wedge of snow with the sharp edge along the object and extending above the object in both directions at approximately 45° to the vertical. (In such cases, the snow load would be computed for the weight of the snow wedge above the object and not the total snow depth on the ground). The weight of new-fallen snow on a surface varies between 0.5 kg m^{-2} per cm of depth (0.25 lb ft^{-2} in^{-1}) and 2.0 kg m^{-2} per cm of depth (1.04 lb ft^{-2} in^{-1}), depending on the atmospheric conditions at the time of the snowfall. Snow near 0 °C (wet snow) can build up on power lines to >10 times line diameter and lead to failure. Wind can cause galloping (wind induced oscillations) which enhance failure.

7.4.1 Snow Loads at Surface

Maximum snow loads of the following areas are:

a. Huntsville and Edwards AFB. For horizontal surfaces a snow load of 25 kg m^{-2} (5.1 lb ft^{-2}) per 24-h period (equivalent to a 10-in snowfall) to a maximum of 50 kg m^{-2} (10.2 lb ft^{-2}) in a 72-h period, provided none of the snow is removed from the surface during that time, should be considered for design purposes.

b. Vandenberg AFB and White Sands Missile Range. For horizontal surfaces, a maximum snow load of 10 kg m^{-2} (2.0 lb ft^{-2}) per one 24-h period (equivalent to a 4-in snowfall) should be considered for design purposes.

c. Kennedy Space Center and New Orleans area snow loads need not be considered.

7.4.2 Snow Particle Size

Snow particles may penetrate openings (often openings of minute size) in equipment and cause a malfunction of mechanical or electrical components, either before or after melting. Particle size, associated wind speed, and air temperature to be considered are as follows:

a. Huntsville and Edwards AFB. Snow particles 0.1-mm (0.0039-in) to 5-mm (0.20-in) diameter; wind speed 10 m s^{-1} (19 kn); air temperature -17.8 °C (0 °F).

b. Vandenberg AFB and White Sands Missile Range. Snow particles 0.5-mm (0.020-in) to 5-mm (0.20-in) diameter; wind speed 10 m s^{-1} (19 knots); air temperature -5.0 °C (24 °F).

7.5 Hail*

Hail is precipitation in the form of balls or irregular lumps of ice and is always produced by convective clouds. By definition, hail has a diameter of 5 mm (0.2 in) or more. Hailfalls are small-scale areal phenomena, with a relatively infrequent occurrence rate at any given geographical point. The resulting time and space variability of hail is its prime characteristic.

There are two areas of confusion regarding hail: (1) definition and (2) assessment of damage due to hail. First is the question of whether snow or ice pellets (often called "small hail") are hailstones. Sleet has also been confused with small hail, but convective cloud origin and size of stone are two factors which separate hail from any other form of frozen hydrometeors. The second area of confusion associated with hail concerns delineating crop loss due to hail. This type of loss often includes damage by wind, either that with the hail or that before or after the hail. The wind-induced damage can easily be mistaken as damage due to hail.

While North American hail data and information are generally sparse, there is much more information available than for any other location. In North America, very extensive hail data information are available for Alberta, Canada, and Illinois and Colorado in the United States. Hail phenomena studies have generally centered on hailstones, point hailfalls, hailstreaks, hailstorms, hailswaths, and hail days over areas of various sizes.

The principal hail area on the North American continent is located on the lee side of the Rocky Mountains where frequent and intense hail causes great damage over the Great Plains region. Another high-frequency hail area, related to spring storms, extends from Michigan to Texas. However, less crop damage is observed here because hail activity largely precedes the crop season.

The worldwide hail occurrence pattern is characterized by a greater hail frequency in continental interiors of mid-latitudes, with decreasing frequencies seaward, poleward, and equatorward. Most all hail is either orographically or frontally induced, although the Great Lakes affect the frequency close to that region. There are very few local-type hailstorms away from the mountains. The United States hail-days pattern is shown in figure 7.3.

Four key hail characteristics (average frequency, primary cause of hail, peak hail season, and hail intensity) were analyzed in order to delineate hail regions within the United States. Figure 7.4 indicates that 14 hail regions exist across the United States, with a marine-effect influence on the West Coast and in the lee of the Great Lakes.

Although most hail is produced by thunderstorms, the special climatologies of these two phenomena differ in some respects. The main difference is that thunderstorms generally exhibit a latitudinal distribution across North America, whereas hail has an inner-continental maxima wih frequency decreasing outward in all directions, as mentioned previously.

The "intensity" of hail produces the damage. Intensity is a direct function of the number of stones, their size, and the wind. A hail intensity pattern has been developed specifically for potential property loss. The development of this pattern incorporated insurance data, stone size data, and extreme wind frequency data. The hail intensity pattern is shown in figure 7.5, which indicates a north-south oriented maximum located in the Great Plains region. This is the region of the continental United States in which large hailstones (the major factor in property loss) are most frequent and high winds occur most often.

An important difference between soft hail and hailstones (in the conventional sense) is the density—hailstones are close to ice (0.92 g cm^{-3}). The damage can be computed from the stone's kinetic energy (KE) = $^1/_2\, mV^2$.

$$\left.\begin{array}{c} m \propto r^3 \\ V_{\text{terminal}} \propto \sqrt{r} \end{array}\right] KE \propto r^{\frac{7}{2}}$$

This needs to be integrated over a size distribution to assess the overall effect. Also a specific critical size may exist for damage to specific surfaces.

*Subsection 7.5 contains figures and information from reference 7.10.

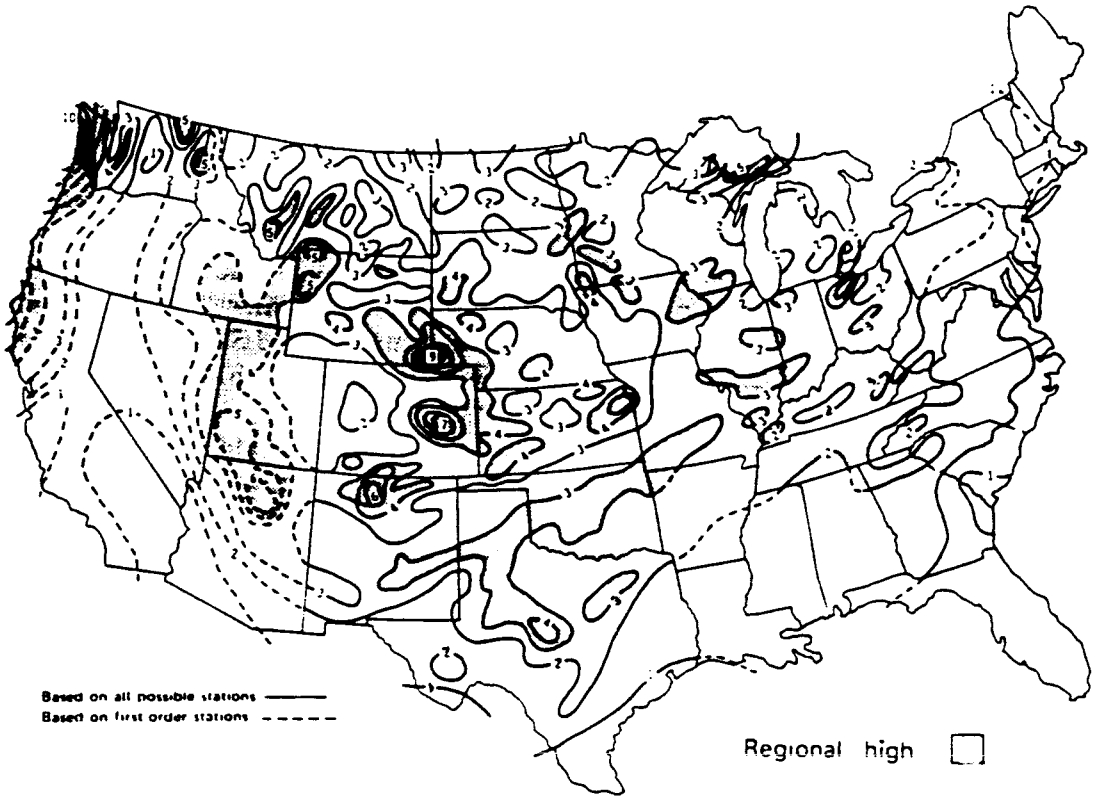

Figure 7.3 Average number of hail days based on point frequencies.

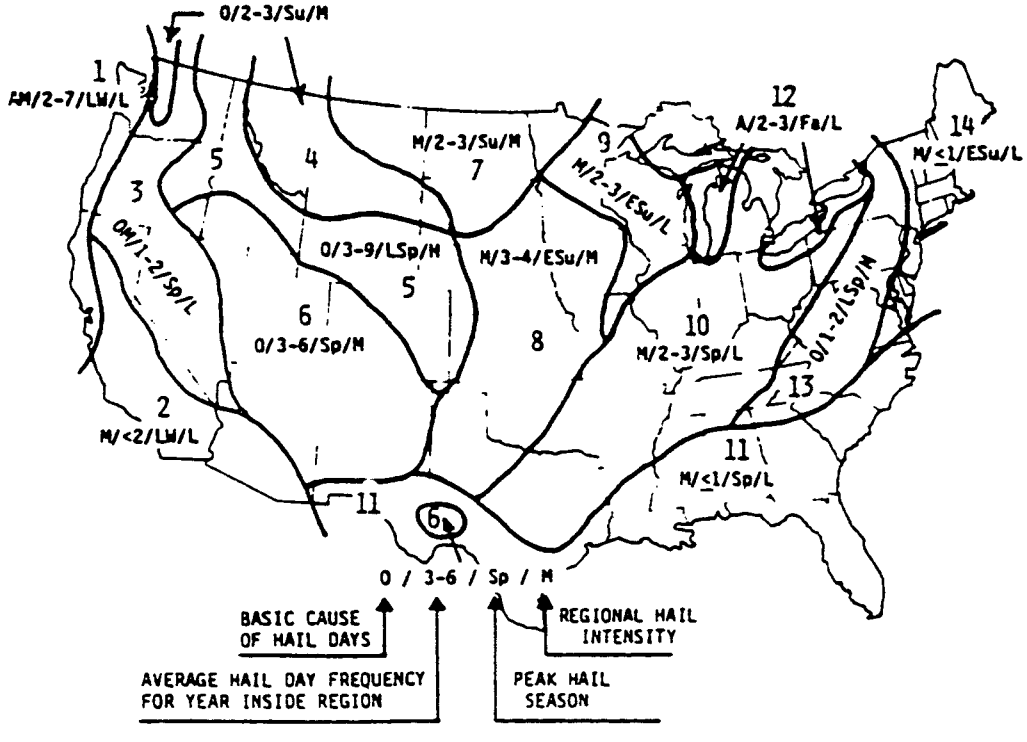

Figure 7.4 Hail regions of the United States.

Since hailstone sizes as well as the number of stones are important to intensity, size distributions help account for regional differences. Hailstone sizes have not been systematically measured throughout the United States, but small-area studies have provided some information. Figure 7.6 indicates that the greatest frequency of large stones is found in the lee of mountain localities like Colorado. Small hailstones dominate in Illinois, New England, and mountain-top areas of Arizona. An Illinois hailfall averages 24 stones per hailpad (1 ft^2 or 930 cm^2), and only approximately 2 percent of these are more than 1.3 cm in diameter. In northeast Colorado, a hailfall averages 202 stones/ft^2, and more than half (51 percent) of these are larger than 1.3 cm.

The season of high hail activity varies across the country. East of the Great Plains, maximum hail activity occurs in the spring months, starting in March in the far south and in May in the northern states. In the lee-of-the-mountain states, maximum hail activity occurs in the summer months. The Great Lakes area is the only place in North America where maximum hail occurs in fall months. Along the West Coast certain areas have maximum hail in late winter or spring.

The duration of hailstorms is also variable. The average duration of hail near the mountains is 10 to 15 min, while in the Midwest it is 3 to 6 min. Hailstreaks, which have a median size of 20.7 km^2 (8 square miles), last an average of 10 min. A hailstreak is an area hit by a single volume of hail produced in a storm. A single storm may produce one or many hailstreaks.

In large areas, such as Iowa, Illinois, or Colorado, hail occurs on approximately 70 percent of all days with thunderstorms. In the Midwest, 50 percent of all thunderstorms connected with warm fronts and low pressure centers produce hail, but 75 percent of the thunderstorm days associated with cold fronts or stationary fronts are hail days.

Hail may also be accompanied by moderate to heavy rainfall, tornadoes, or wind. Crop-damaging hailstorms in Nebraska, Colorado, and Kansas are generally associated with moderate rains of 0.2 to 1.0 in, and 25 percent of the rain through the entire crop season falls with damaging hail. Hail days in Illinois typically have rainfall so heavy it averages nearly half (48 percent) of the monthly average. There have been cases where hailstones, falling at the same time or immediately before heavy rains, have blocked drains and downspouts, preventing much of the rain runoff from flat roofs and thereby causing roof collapse from the weight of the rainfall (ref. 7.11).

A study of tornadoes in Illinois shows that major large tornadoes—those having tracks longer than 40 km (>25 mi)—always have hailfalls somewhere near their track. During 1951 to 1960, nearly 96 percent of the 103 tornado days in Illinois were also hail days, and 12 percent of all hail days in Illinois were tornado days as well.

Wind with hail is another critical factor in crop loss, and the Illinois studies show that windblown hailstones occurred in 60 percent of all hailfalls. Whenever this happens, an average of 66 percent of the hailstones at any one point are windblown.

7.5.1 Hail at Surface

An estimate has been made of hail characteristics at selected space vehicle development and test locations. Figures 7.7, 7.8, 7.9, and table 7.15 give estimated hail characteristics for Kennedy Space Center, Vandenberg AFB, Edwards AFB, White Sands Missile Range, Northrup Strip, Marshall Space Flight Center, and Stennis Space Center. Since no direct measurements, except for the number of hail days, exist for these locations, all other items were estimated from Illinois hailpad measurements reported by Changnon (7.8). Hail characteristics estimated for use in evaluating hail protection needs and requirements are:

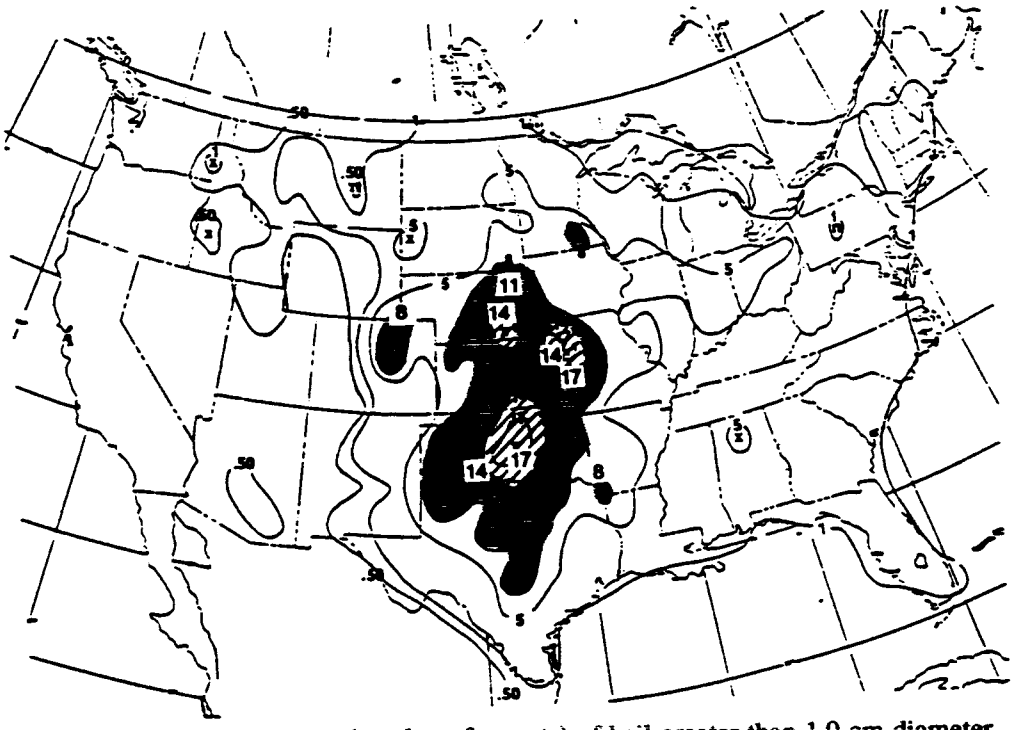

Figure 7.5 Frequency (number of reports) of hail greater than 1.9 cm diameter per 26,000 km^2 per year. (Ref. 7.11)

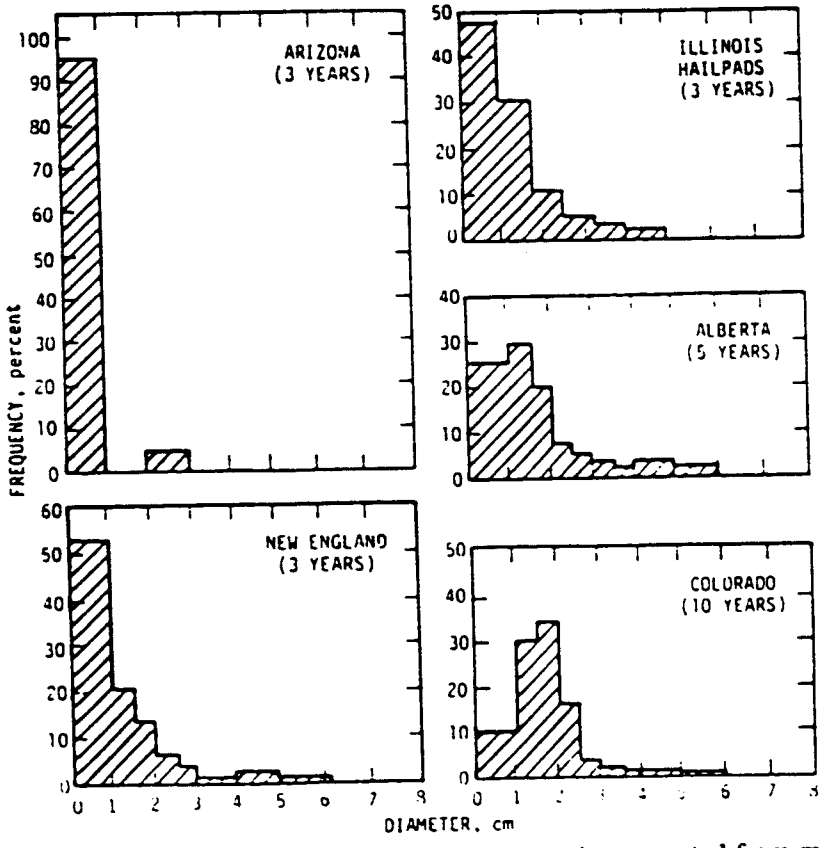

Figure 7.6 Frequency distributions of maximum hailstone sizes reported from many hailfalls at different locales.

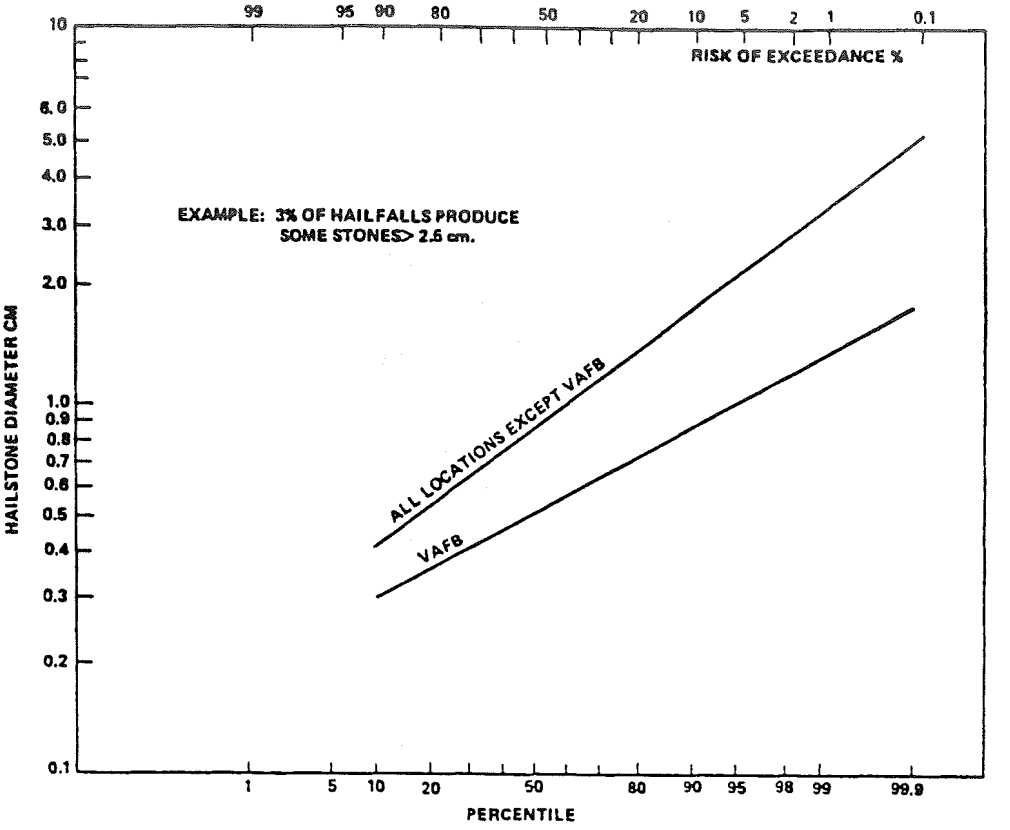

Figure 7.7 Maximum hailstone size per point hailfall.

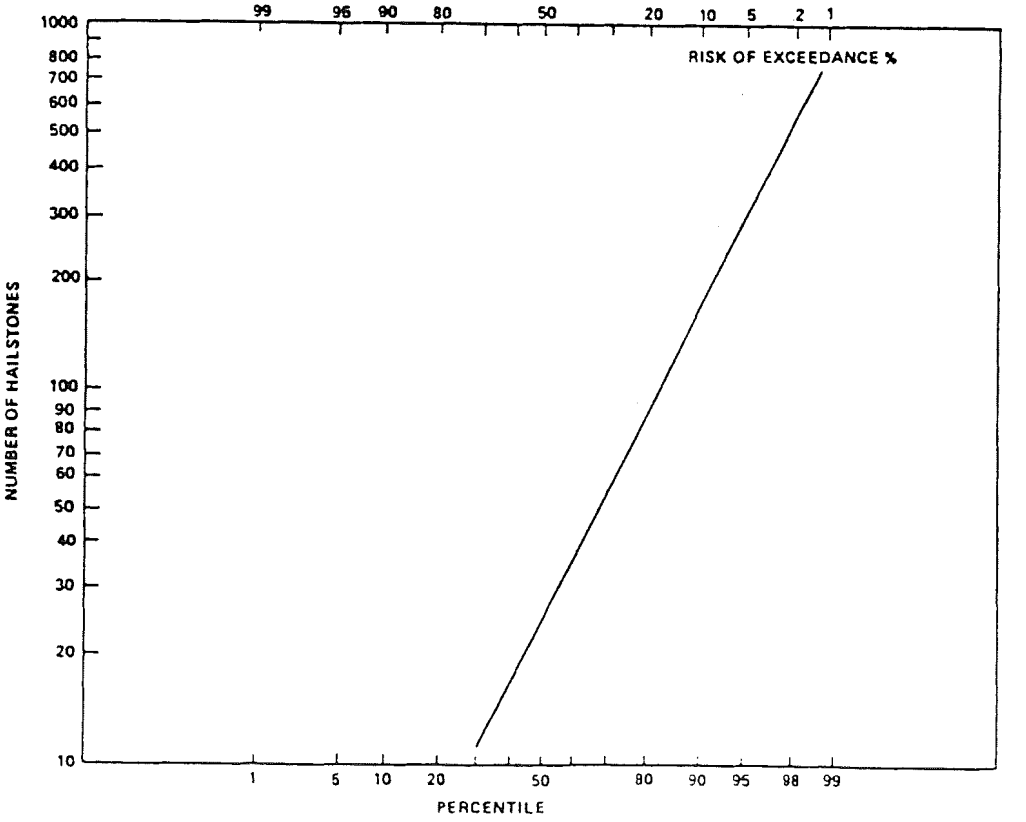

Figure 7.8 Probability (percent) of number of stones per hailfall on hailpad of 930 cm^2 (1 ft^2).

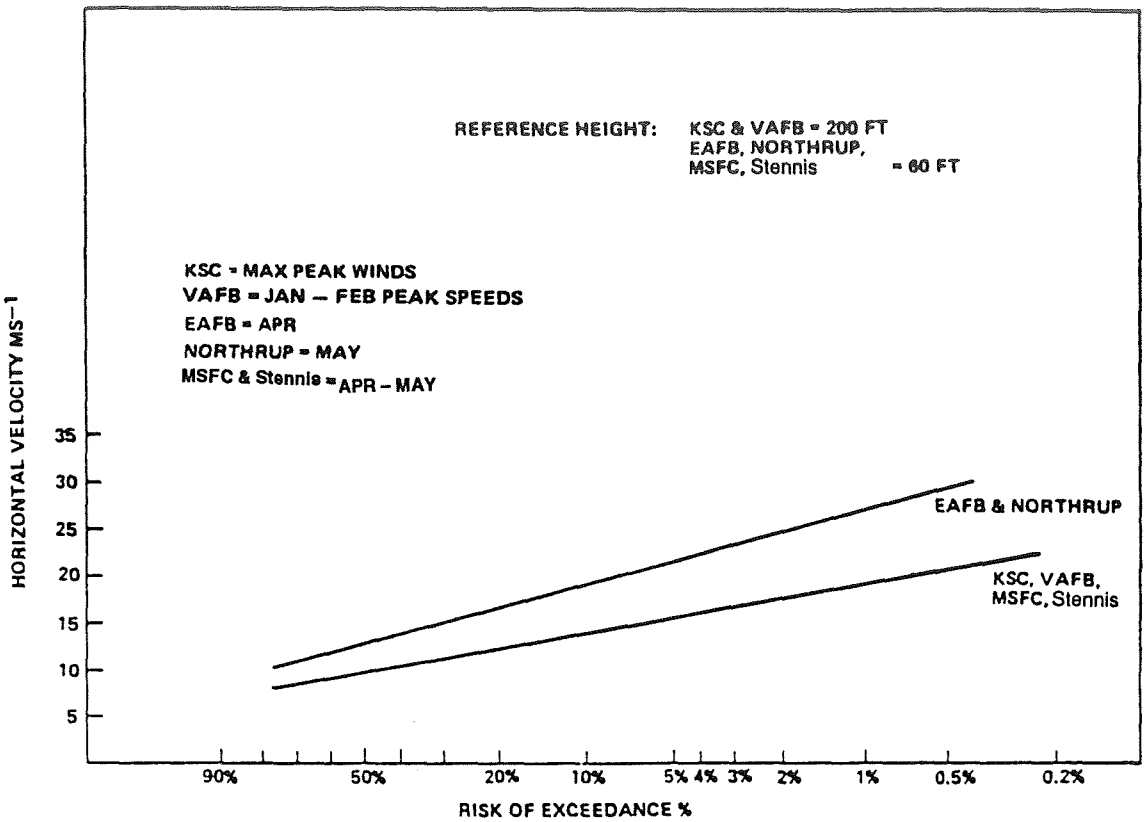

Figure 7.9 Horizontal hailstone velocity.

Table 7.15 Estimated hail characteristics at selected space vehicle locations.

Estimated Hail Characteristics	KSC	VAFB	EAFB	Northrup	MSFC	Stennis
Exposure Time Risk (%)						
Worst Month Reference Period	1	8	5	12	17	3
Worst 6 Months Reference Period	7	41	25	53	67	18
Mean Number of Hailstorm Days Per Year	0.1	1.1	0.6	1.5	2.2	0.4
Average Point of Duration of Hailfall (min)	5	5	5	5	5	5
Average Number of Hailstones Per 930 cm^2 (1 ft^2)	24	24	24	24	24	24
Density of Hailstones (g/cm^3)	0.9	0.9	0.9	0.9	0.9	0.9
Size-diameter (cm) and Terminal Velocity (m/s)						
Representative Size (50-percent Risk)	0.9	0.5	0.9	0.9	0.9	0.9
Terminal Velocity	11	8	11	11	11	11
Large Size (5-percent Risk)	2.2	1.0	2.2	2.2	2.2	2.2
Terminal Velocity	17	11.5	17	17	17	17
Horizontal Velocity (m/s)—All Directions*						
Mean Speed	9	9	13	13	9	9
5-percent Risk Speed	15	15	22	22	15	15
Months of Max Frequency	May	Jan–Feb	Feb–Apr	May–July	April	Apr–May
Period of Record—Years	22	20	28	30	9	28

*KSC and VAFB reference height = 61 m (200 ft). All others = 18 m (60 ft).

a. Hailstone Size. Figure 7.7 gives the risk in percent of a point hailfall producing stones larger than indicated sizes. For example, only 3 percent of the hailfalls at Kennedy Space Center will produce stones larger than 2.5 cm, while 50 percent will produce some stones larger than 0.9 cm.

b. Terminal Velocity. The general expression for the terminal velocity of a sphere is given in ref. 7.2. However, for quick calculations, the best estimate of hailstone terminal velocity, as reported by several investigators, is given by the expression:

$$W = K\sqrt{D}\ , \tag{7.1}$$

where

W = terminal velocity in m s^{-1}

D = hailstone diameter in cm

$K = 11.5$.

c. Number of Hailstones Per Hailfall. Values used for space vehicle locations were taken from Illinois measurements which showed that point hailfalls average 24 stones and that only 5 percent of the storms produced more than 300 stones per hailpad of 930 cm^2 (1 ft^2). These numbers were used to prepare figure 7.8.

d. Horizontal Velocity of Hailstones. These values (fig. 7.9) were derived from peak wind speed distributions for each space vehicle location. These wind speeds may be different from other shuttle design values because only hail season winds were used rather than the windiest period concept.

The reference height at Kennedy Space Center and Vandenberg AFB is 61 m (200 ft). At all other locations it is 18.3 m (60 ft).

e. Density of Hailstones. A generally accepted value for the density of hail at all locations is 0.89 g cm^{-3} (56 lb ft^{-3}).

f. Recommended Procedures for Evaluating Protection Requirements.

(1) Use 50 percent values for stone size and number of stones.

(2) Use 5 percent risk horizontal wind speeds.

(3) Calculate risk of experiencing a hailfall during a specified continuous exposure period from:

$$\text{Risk} = 1 - e^{-\lambda t} \tag{7.2}$$

where

λ = mean number of independent hailstorm days per year

t = exposure time in years

7.5.2 Distribution of Hail With Altitude

Although it is not the current practice to design space vehicles for flight in thunderstorms, data on distribution with altitude are presented as an item of importance. In general, the probability of hail increases with altitude from the surface to about 5 km and then decreases rapidly with increasing height. Above about 9 km, infrequent hail encounters have occurred, but cannot be completely discounted. Data on hailstone size versus altitude, with a 0.1-percent encounter probability while enroute aloft for 200 miles (322 km), in the worst month, worst area, are given in table 7.16. When including thunderstorm data from several areas, investigators have estimated probabilities of encountering hail versus altitude, as presented in table 7.17 (ref. 7.14). This supports the general shape of the vertical distribution. Further, it appears expedient to assume that any level between 3 and 6 km can become one of maximum hail concentration at any one time.

Table 7.16 Estimate of hailstone size equaled or exceeded, with a 0.1-percent probability of encounter while enroute aloft for 200 miles (322 km), in most severe month and area (ref. 7.13).

Altitude (km)	Estimate of Hailstone Size (inch)	(cm)
1.5	1.2	3.1
3.0	2.4	6.1
6.1	2.4	6.1
7.6	1.9	4.8
9.1	1.7	4.3
10.7	1.5	3.8
12.1	1.1	2.8
13.7	0	0

Table 7.17 Estimates of the probability of encountering hail of any size at a single-point location by altitude (ref. 7.14).

Altitude (km)	Probability
Ground Level	0.000448
1.5	0.000448
3.0	0.00314
4.6	0.00314
6.1	0.00314
7.6	0.00134
9.1	0.00100
10.7	0.00067
12.2	0.00034
13.7	0.000

7.6 Laboratory Test Simulation

In the laboratory, simulated rain droplets are usually produced by use of a single orifice, mounted above the equipment being tested. Such a test will not necessarily duplicate the natural occurrence of precipitation and may or may not reflect the true effect of natural precipitation on the equipment since a single orifice produces drops all nearly the same size.

Each test should be evaluated to determine if the following factors which occur in natural precipitation are important in the test.

7.6.1 Rate of Fall of Rain Droplets

Natural rain droplets will have usually fallen a sufficient distance to reach their terminal velocity (maximum rates of fall). Simulation of such rates of fall in the laboratory requires the droplets to fall a suitable distance. Large droplets (4-mm diameter and greater) will require approximately 12 m (39 ft) to reach terminal velocity.

Values of terminal velocities of water droplets were measured by Gunn and Kinzer (ref. 7.15). Their results gave the values in table 7.18. Reference 7.15 should be consulted for more detailed information. Gunn and Kinzer found that water droplets greater than 5.8 mm would usually break up before the terminal velocity was reached.

Table 7.18 Values of terminal velocities of raindrops (ref. 7.15).

Drop Diameter (mm)	Terminal Velocity ($m\ s^{-1}$)
1	4.0
2	6.5
3	8.1
4	8.8
5	9.1
6	9.1
7	9.1

7.6.2 Raindrop Size and Distribution

Normal rainfall has a variety of drop sizes with a distribution as shown in figure 7.10 (ref. 7.15), which illustrates the wider distribution of droplet sizes in the heavier rain which has the larger droplets. The maximum drop diameter distribution could be adequately simulated by a number of orifices, all at the same water pressure, to produce droplets of approximately 1-, 2-, 3-, and 4- and 5-mm diameter. For the median drop diameter, the use of a single orifice to produce 1-mm droplets would be suitable.

7.6.3 Wind Speed

In most cases of natural rain there will be wind blowing near horizontal. This wind will modify the droplet paths from a vertical path to a path at some angle to the vertical, thus causing the rain droplets to strike at an angle. In addition, unless the equipment is streamlined in the direction of the wind, small vortices may develop at the surface of the equipment. These vortices may cause a considerable amount of the precipitation to flow in a variety of directions, including upward against the bottom of the equipment.

Studies of thunderstorms with rainfall rates from 12.7 to 76.2 mm h^{-1} (0.5 to 3.0 in h^{-1}) with relationship to wind speeds occurring at the same time have shown an average mean wind speed of 5 m s^{-1} for all storms combined. Peak winds were as high as 16 m s^{-1}. All storms, except one with rates exceeding 25 mm h^{-1}, had peak winds at least 5 m s^{-1} greater than the mean wind for the same storm.

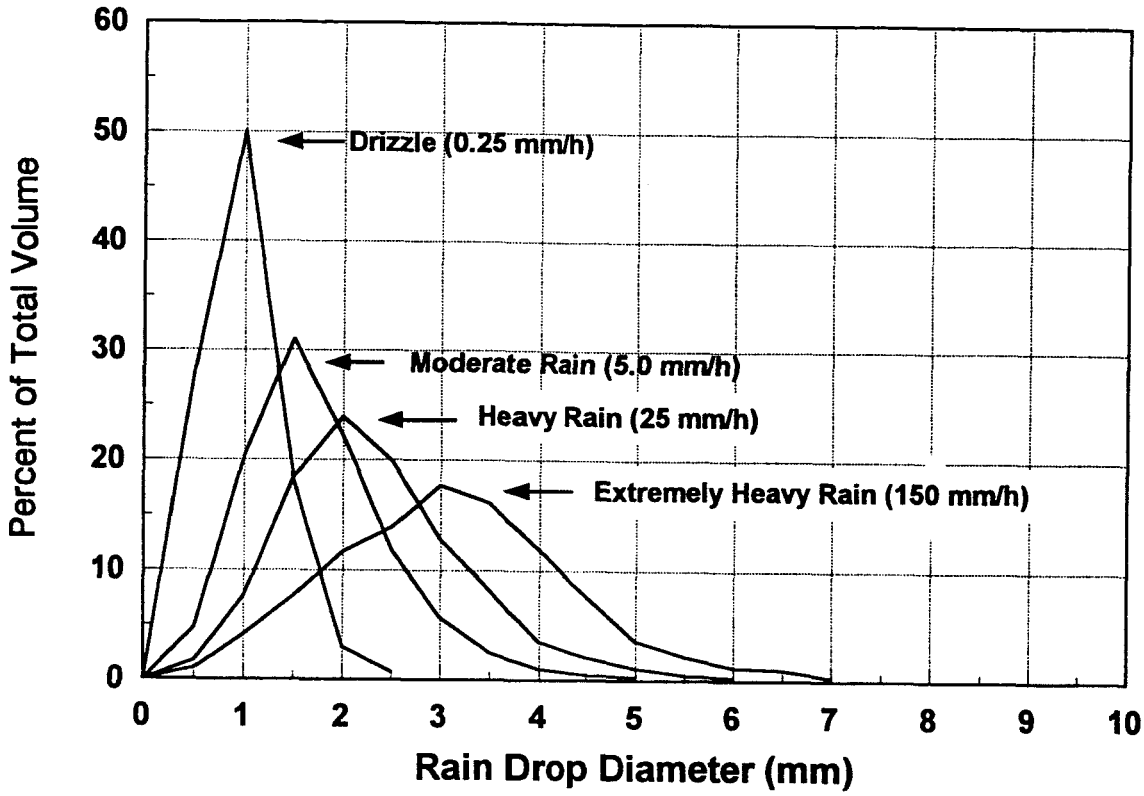

Figure 7.10 Distribution of drop sizes of rain (ref. 7.15).

7.6.4 Temperatures

The air temperature at the ground usually decreases several degrees at the start of rainfall. The amount of the temperature decrease is greatest in the summer, about 8 °C (14 °F), when the temperature is high (greater than 32 °C (90 °F), with the final temperature approximately 24 °C (75 °F). In the winter the temperature decrease is usually about 2.8 °C (5 °F). At the end of the rainfall the summer temperature will increase again to nearly the same values as before the storm, but in the winter there is no general pattern of warming. This decrease in temperature is caused by the water droplets being colder than the surface air temperature.

7.6.5 Recommended Items to Include in Laboratory Rainfall Tests

The following items need to be considered in rainfall tests in the laboratory:

a. Raindrop size distribution.

Rates less than 25 mm h^{-1}, drop size of 1 mm.

Rates greater than 25 mm h^{-1}, drop size from 1 to 5 mm.

b. Rate of fall of drops. Drops should fall at least 12 m to obtain terminal velocity.

c. Wind Speed. A mean wind of 5 m s^{-1} with gusts of 15 m s^{-1} of 30-s duration at least once in each 15-min period.

d. Temperature. The temperature in the chamber should decrease from 32 °C (90 °F) to 24 °C (75 °F) at the start of rainfall for representative summer tests and should be maintained at 10 °C (50 °F) for winter tests. The decrease in air temperature may be obtained by using water at, or slightly below 24 °C for the summer tests.

7.6.5.1 Idealized Rain Cycle, KSC, FL

For some studies and laboratory tests, it may be desirable to use an extreme rain cycle with associated drop sizes, wind speeds, and temperatures. The values from table 7.11 can be used in any combination of rainfall rate and duration such that the total accumulation does not exceed the table 7.11 value for the selected time period and percentile level. The percentile level should be compatible with the risk the operator is willing to accept. The 95 percentile values have a 5 percent risk of being exceeded—the 99 percentile values only a 1-percent risk.

If wind speed, temperature, and raindrop size are to be included in the test, the following values may be used with both 95- and 99-percentile rain rates:

Wind speed: 5.1 m s^{-1}, gusts to 15.4 m s^{-1}
10 knots, gusts to 30 knots
guat lasting 2 min applied every 15 min.

	Summer		Winter	
	Before	During	Before	During
Temperature:	32 °C (90 °F)	24 °C (75 °F)	13 °C (55 °F)	10 °C (50 °F)

Drop size: Average = 2 mm
Largest 1% = 5.9 mm

The following are some rain cycle examples using 95-percentile values from table 7.11:

Period of Rainfall		Rate (in/h)	Total Accumulation (in)
1 hr		1.17	1.17
3 hr		0.47	1.41
(1 h)	10 min	0.5	1.17
	3 min	8.7	
	5 min	3.5	
	42 min	0.51	
(3 h)	15 min	0.2	1.41
	30 min	0.5	
	5 min	3.5	
	25 min	0.5	
	105 min	0.35	

7.7 Rain Erosion

7.7.1 Introduction

Rain erosion is caused by the stress resulting from liquid droplets impinging a solid surface. This stress may dent or crack the surface or result in a mass loss (ref. 7.15). Multiple impacts can cause three times the damage of a single impact (ref. 7.16). With the advent of high-speed aircraft, careful consideration must be given in selecting materials to prevent erosion of paint coatings, structural plastics, and metallic parts.

7.7.2 Rain Erosion Criteria

The magnitude of rain erosion may be influenced by many parameters, such as impact velocity, drop size, density, viscosity, and surface tension. Different techniques have been applied to determine the effects of impact velocities on erosion. Tables listing erosion rates for various materials at specific velocities are found in references 7.17 and 7.18.

Tests by A. A. Fyall at the Royal Aircraft Establishment (ref. 7.19) on single rain droplets have shown that the rain erosion rate may increase considerably with lower air pressure (higher altitude) because of the lower cushioning effect of the air on the droplets at impact.

7.8 Fogs

Fogs are classified as either warm or supercooled fog, depending upon whether the ambient temperature is above or below 0 °C. In either case, fog consists of a considerable number of minute water drops suspended in the atmosphere near the Earth's surface and which reduce visibility to less than 1 km (American Meteorological Society's Glossary of Meteorology—Definitions).

The conditions most favorable for the formation of fog are high relative humidity, light surface winds, no overcast so that radiative cooling is most effective, and an abundance of condensation nuclei. Fog occurs more frequently in coastal areas than in inland areas since there is an abundance of water vapor.

Fogs are formed either by cooling the air until the water vapor condenses or by the evaporation of additional water vapor into the air. Common types are (1) radiation fogs, (2) advection fogs, (3) up-slope fogs, (4) frontal fogs, and (5) steam fogs. A brief description of each fog type follows.

Radiation fog forms on clear nights when the Earth loses heat very rapidly to the atmosphere. When humidity is high and cooling takes place rapidly, condensation occurs. If there are no winds, the fog will be very shallow or will be reduced to a dew or frost deposit. If winds are present (about 5 kn), then the fog will thicken and deepen. These fogs do not occur at sea since the sea surface does not cool as the land does.

Advection fog forms as warm, moist air moves over a colder surface. These fogs occur in coastal areas because the moist air moves inland by breezes over the colder land in the winter. In summer the warm, moist air is carried out to sea, where it forms a fog over the cool water and then the sea breezes advect the fog inland. These fogs are common along the coast of California in the summer.

Up-slope fog forms when stable, moist air moves up sloping terrain and is cooled by expansion. This cooling produces condensation, and fog forms. An up-slope wind is necessary for the formation and maintenance of this type of fog. Usually these fogs produce low stratus-type clouds.

Frontal fog forms in the cold air mass of the frontal system. The precipitation from the warm air mass, overrunning the cold air mass, evaporates as it falls through and saturates the cold air, thus producing the frontal-type fog. These fogs form rapidly, cover large areas, occur frequently in winter, and are associated with slow-moving or stationary fronts.

Steam fog forms by the movement of cold air over a warmer water surface. Steam fog rises from the surface of lakes, rivers, and oceans.

Although not classified as a common-type fog, there is a fog type called the ice (crystal) fog which is of interest. This fog occurs when the air temperature is approximately -34 °C, and as water vapor from the exhaust of aircraft engines, automobiles, etc., is produced, the vapor changes directly to ice crystals instead of condensing directly to liquid drops. The suspension of the ice crystals in the atmosphere produces the ice fog. These fogs can persist from a few minutes to several days and are quite a problem in arctic or polar regions. Salt fog, which develops along a coastal area, is presented in subsection 10.3.2.1.

Some typical microphysical characteristics of both radiation and advection types of fogs are as follows:

a. Radiation Fog (Inland)

   (1) Diameter of drops (av)—10 μm

   (2) Typical drop size—5 to 35 μm

   (3) Liquid water content—110 mg/m^3

   (4) Droplet concentration—200 cm^{-3}

   (5) Vertical depth

      (a) Typical—100 m

      (b) Severe—300 m

   (6) Horizontal visibility—100 m

b. Advection Fog (Coastal)

   (1) Diameter of drops (av)—20 μm

   (2) Typical drop size—7 to 65 μm

   (3) Liquid water content—170 mg/m^3

   (4) Droplet concentration—40 cm^{-3}

   (5) Vertical depth

      (a) Typical—200 m

      (b) Severe—600 m

   (6) Horizontal visibility—300 m.

7.9 Precipitation or Fog (VAFB and KSC)

Figures 7.11 and 7.12, showing the percentage frequency of precipitation or fog with visibility ≤0.8 km (0.5 mi) at Vandenberg AFB and Kennedy Space Center, were developed from historical records of hourly observations. Certain Vandenberg and Kennedy Space Center climatic characteristics that may be of significance to aerospace mission planning and operations are immediately apparent. That is, potentially unfavorable climatic conditions occur mainly during summer night and early morning hours at Vandenberg AFB but during summer afternoons at Kennedy Space Center. This, of course, is due to the high frequency of fog at Vandenberg AFB and summer afternoon showers in central Florida.

For climatological studies useful in operational design data for spacecraft and aircraft operations, the Department of Transportation-Federal Aviation Administration has produced a tabulation of ceilings, visibilities, wind, and weather data by various periods of the day and by various temperature and wind categories for 41 airports (ref. 7.20).

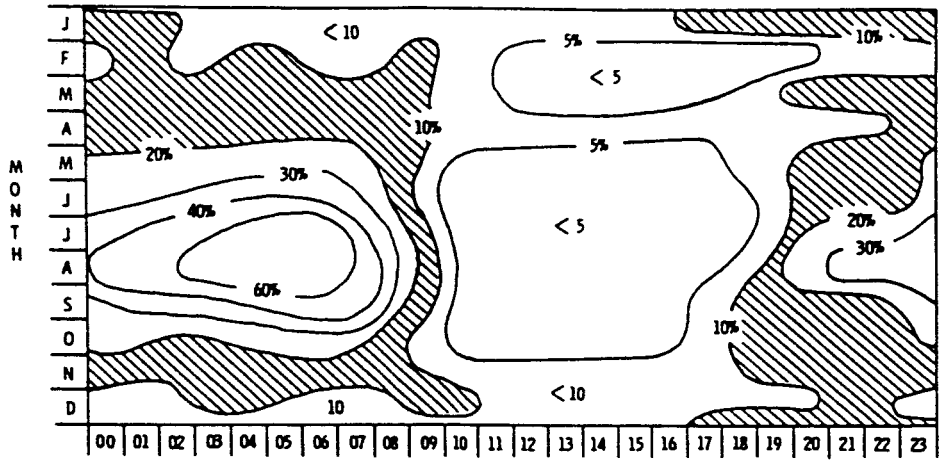

VANDENBERG AFB

Figure 7.11 Probability of precipitation or fog with visibility ≤0.8 km (0.5 mi).

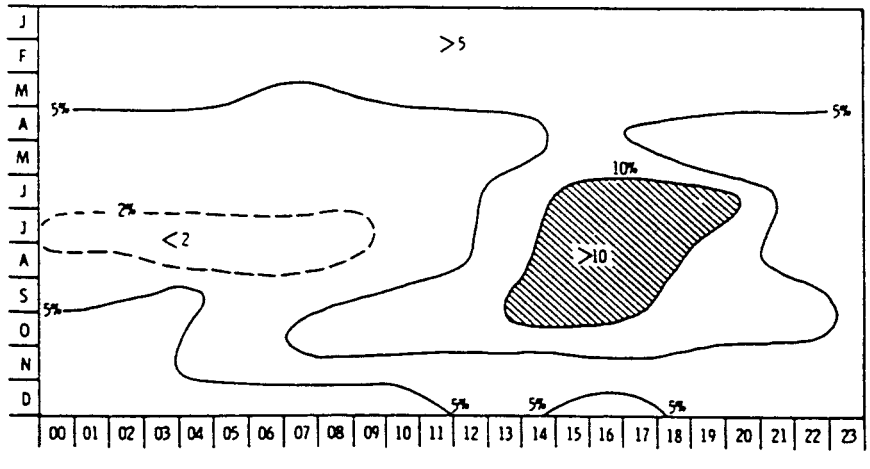

KENNEDY SPACE CENTER (KSC)

Figure 7.12 Probability of precipitation or fog with visibility ≤0.8 km (0.5 mi).

REFERENCES

7.1 "Handbook of Meteorology, Second Edition." Her Majesty's Stationary Office, London, 1971.

7.2 Riordan, P. and Bourget, P.G.: "Worldwide Weather Extremes." ETL-0416, Engineer Topographic Laboratories, U.S. Corps of Engineers, Fort Belvoir, VA, December 1985.

7.3 "Rainfall Intensity-Duration-Frequency Curves for Selected Stations in the United States, Alaska, Hawaiian Islands, and Puerto Rico." Technical Paper No. 25, U.S. Department of Commerce, Washington, DC, December 1955.

7.4 Gumble, E.J.: "Statistics of Extremes." Columbia University Press, 1958.

7.5 Tattleman, P., and Willis, P.T.: "Model Vertical Profiles of Extreme Rainfall Rate, Liquid Water Content, and Drop-Size Distribution." AFGL-TR-85-0200, ERP No. 928, September 6, 1985.

7.6 Beard, K.V., Johnson, D.B., and Baumgardner, D: "Aircraft Observations of Large Raindrops in Warm, Shallow, Convective Clouds." Geophysical Research Letters, vol. 13, October 1986, pp. 991–994.

7.7 Valley, S.L.: "Handbook of Geophysics and Space Environments." McGraw-Hill Book Company, Inc., New York, April 1965.

7.8 "Aviation Weather for Pilots and Flight Operations Personnel." Federal Aviation Agency, Department of Commerce, Weather Bureau, Washington, DC, 1975.

7.9 Vaughan, W.W.: "Distribution of Hydrometeors With Altitude for Missile Design and Performance Studies." ABMA DA-TM-138-59, U.S. Army Ballistic Missile Agency, Huntsville, AL, 1959.

7.10 Changnon, S.A., Jr.: "The Scale of Hail." Journal of Applied Meteorology, vol. 16, No. 6, July 1977, pp. 626–648.

7.11 Kelly, D.L., Schaefer, J.T., and Doswell, C.A.: "Climatology of Non-Tornadic Severe Thunderstorm Events in the United States." Monthly Weather Review, vol. 113, No. 11, November 1985.

7.12 Changnon, S.A., Jr.: "Heavy Falls of Hail and Rain Leading to Roof Collapse." Journal of the Structural Design, ASCE, vol. 104, No. ST1, Technical Note, January 1978, pp. 198–200.

7.13 Kissel, G.J.: "Rain and Hail Extremes at Altitude." AIAA paper No. 79-0539, AIAA 15th Annual Meeting, Washington, DC, February 6–8, 1979.

7.14 "Handbook of Geophysics and the Space Environment." Air Force Geophysics Laboratory, Air Force Systems Command, U.S. Air Force, 1986.

7.15 Houghton, D.D.: "Handbook of Applied Meteorology." John Wiley and Sons, Inc., 1985.

7.16 Springer, G.S.: "Erosion by Liquid Impact." Scripta Publishing Company, 1976.

7.17 Reinecke, W.G.: "High Speed Erosion in Rain and Ice." Erosion by Liquid and Solid Impact; Proceedings Held at Newnham College, Cambridge, U.K., vol. 5, section 8, September 1979.

7.18 Heymann, F.J.: "Conclusions from the ASTM Interlaboratory Test Program with Liquid Impact Erosion Facilities," Erosion by Liquid and Solid Impact; Proceedings Held at Newnham College, Cambridge, U.K., vol. 5, section 20, September 1979.

7.19 Moteff, J.: "Pneumatic Erosion Effects on Microstructure of Metals and Alloys." TLSP: Progress Report for January to April 1982.

7.20 "Climatological Summaries—Visibilities Below 1/2 Mile and Ceilings Below 200 Feet." FAA-RD-69-22, FA-67-WAI-12, National Weather Record Center, Asheville, NC, June 1969.

7.21 Hinds, W.C.: "Aerosol Technology: Properties, Behavior, and Measurement of Airborne Particles." John Wiley and Sons, Inc., 1982.

SECTION VIII. CLOUD PHENOMENA AND CLOUD COVER MODELS

8.1 Introduction

This section presents cloud cover and atmospheric moisture models that can be applied in various NASA mission planning and attenuation studies. There is also a discussion and criteria regarding the high altitude/high latitudinal cloud phenomena existing at stratospheric and mesospheric levels.

A most useful tool in planning experiments and applying space technology to Earth observation is a model of atmospheric parameters. For example, cloud cover data might be used to predict mission feasibility or the probability of observing a given target area in a given number of satellite passes.

To meet the need for atmospheric models, NASA-MSFC sponsored the development of the four-dimensional atmospheric models (subsection 8.4) and the worldwide cloud model (subsection 8.3). The goal of this work was to produce atmospheric attenuation models to predict degradation effects for all classes of sensors for application to Earth-sensing experiments from spaceborne platforms. To ensure maximum utility and application of these products, NASA-MSFC also sponsored the development of an "Interaction Model of Microwave Energy and Atmospheric Variables," a complete description of the effects of atmospheric moisture upon microwaves (ref. 8.1).

Cloud related phenomena are presented in other sections of this report such as: precipitation/icing hail/fog in section VII, humidity in section VI, and atmospheric electricity in section IX.

8.2 Interaction Model of Microwave Energy and Atmospheric Variables

While the visible and infrared wavelengths find clouds opaque, the microwave part of the electromagnetic spectrum is unique in that cloud and rain particles vary from very weak absorbers and scatterers to very significant contributors to the electromagnetic environment. This is illustrated in figures 8.1, 8.2, and 8.3, which are extracted from the final report on the interaction model (ref. 8.1).

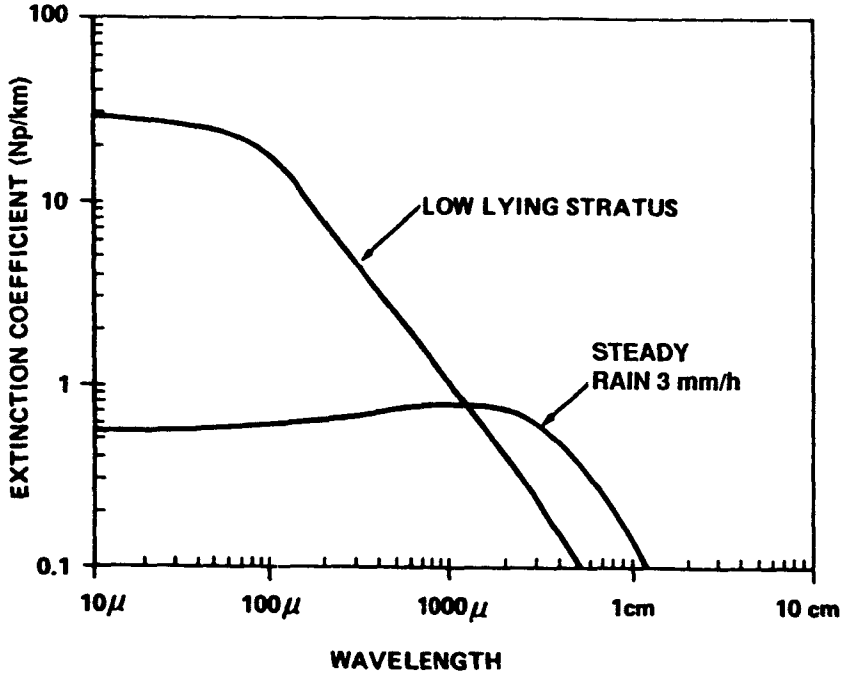

Figure 8.1 Extinction coefficient as a function of wavelength.

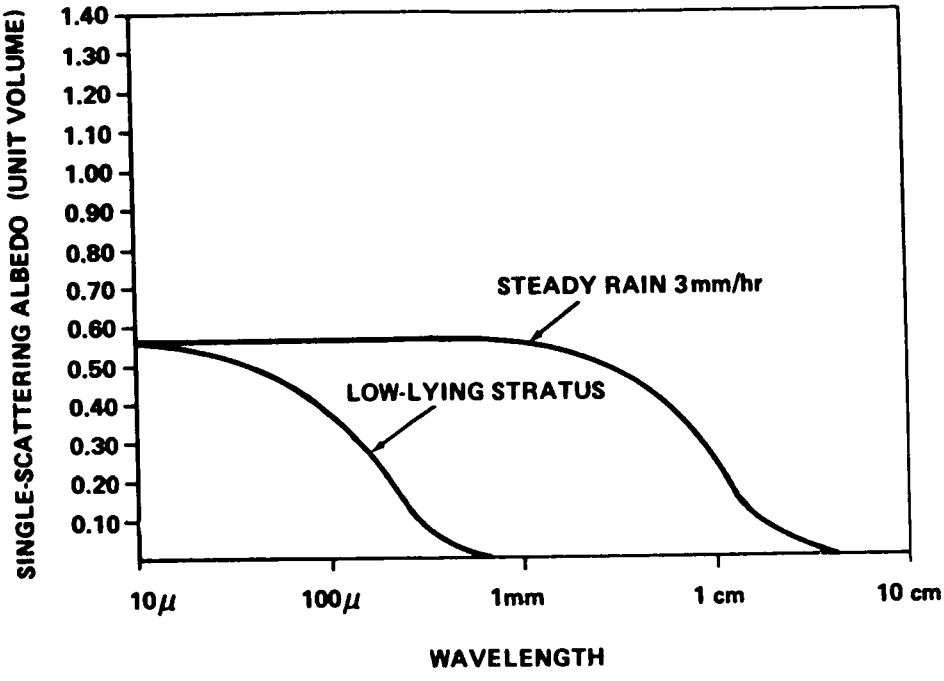

Figure 8.2 Single scattering albedo for two cloud models.

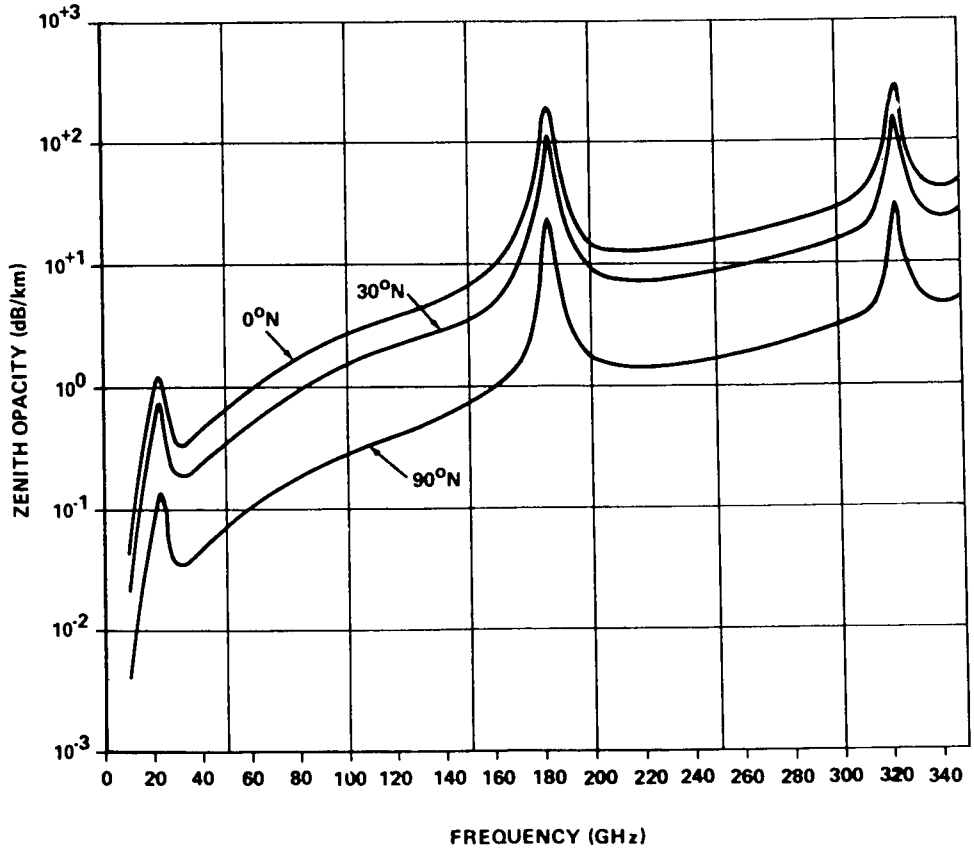

Figure 8.3 Zenith opacity.

8.2.1 Scattering and Extinction Properties of Water Clouds Over the Range 10 cm to 10 μm

Figures 8.1 and 8.2 show the unit-volume scattering and extinction properties of two modeled cloud drop distributions computed using the Mie theory. Figure 8.1 gives the extinction coefficient, in units of Neper (Np), as a function of wavelength. Figure 8.2 presents the single scattering albedo for two cloud models representing low stratus clouds and rainy conditions. The curves show the wavelength regimes appropriate to the two cloud types in which scattering effects are relatively unimportant, and in which the extinction coefficient follows the simple Rayleigh ($1/\lambda^2$) dependence.

8.2.2 Zenith Opacity Due to Atmospheric Water Vapor as a Function of Latitude

In the preparation of figure 8.3, 5 years of climatological data from the MIT Planetary Circulations Project were used to obtain mean water vapor distributions applicable to the latitudes 0° N., 30° N., and 90° N., corresponding to tropical, midlatitude, and arctic conditions. The total water vapor content for the three cases is 4.5, 2.5, and 0.5 g/cm^3, respectively. The curves demonstrate the effect of climatological extremes in simulating and predicting the influence of atmospheric water vapor upon surface observations from a space observer, over the range from 10 to 350 gigahertz. A detailed report on the interaction model (ref. 8.1) is available upon request to the Earth Science and Applications Division, Space Scienee Laboratory, NASA/Marshall Space Flight Center.

8.3 Global Cloud Cover Models and Data Bases

8.3.1 Introduction

When an aircraft or spacecraft is above the tropospheric cloud altitudes, the NASA-MSFC Global Cloud Data Base Model (ref. 8.6) can be used for Earth observation applications, mission feasibility/ planning purposes, or for climate studies. Calculating the probability of viewing a given land target area below, for any given month and time, is possible using this data base. Cloud cover is a key element in the research strategy of the U.S. Climate Program. Cloud information is needed to develop an understanding of the role played by clouds in the radiation balance and to aid in the parameterization of clouds in climate models.

Clouds are also a key factor to be considered in the planning of remote sensing missions of the Earth's surface. Depending upon the extent and thickness of a cloud and upon the wavelengths used by the spaceborne sensor, a cloud has effects on the measured radiation ranging from slight attenuation to total absorption. The complexity of modern sensing systems, with wavelengths in the visible, infrared, and microwave, necessitates detailed information on expected cloud cover to permit intelligent planning and studies. In an earlier recognition of the need for a global cloud data set, the Earth Science and Applications Division at the Marshall Space Flight Center (MSFC) sponsored the development of a global data bank of cloud statistics (ref. 8.2) and computer techniques to utilize the statistics in various simulation studies (ref. 8.3). This effort employed only standard ground-based cloud observations.

Concurrent with these studies, MSFC also sponsored the development of another data bank (refs. 8.4, 8.5). This data bank, known as the four-dimensional (4-D) atmospheric model, contains means and variances of atmospheric pressure, temperature, water vapor, and density from the surface to 25 km above the Earth. Related computer programs were also written to permit the use of this data bank in specifying atmospheric profiles for any latitude, longitude, and month of the year. This 4-D model evolved into the Global Reference Atmosphere Model, 1990 (GRAM-90), as published in reference 8.16.

By using the global cloud cover statistics and the simulation procedure, it was possible to provide an evaluation of the consequence of cloud cover on Earth-viewing space missions or receipt of solar radiation for individual target areas of swaths over small areas.

Although this earlier data set has received extensive use, it has some major limitations. The number of cloud climatic regions was limited by data volume handling capability and by the amount of suitable data available. The entire United States, for example, is effectively covered in only four or five regions. Also, each region is assumed to be completely homogeneous. That is, the base station cloud distribution applies everywhere within that region. The cloud climatologies for nine of the Southern Hemisphere (SH) regions were taken as being seasonal reversals of similar Northern Hemisphere (NH) regions. For some oceanic regions, where representative data could not be obtained, statistics were modified from those of other regions based upon climatological considerations. The satellite-derived data base for the conditional statistics is generally weak. It was necessary to compute conditional probabilities on a seasonal basis to produce an adequate sample size for statistical manipulations. The inconsistency between ground-observed basic or unconditional statistics and satellite-observed conditional distributions has introduced uncertainties in the combined utilization of the two data bases.

The techniques for changing the cloud distributions to make them applicable to larger area sizes, temporal separations other than 24 h, and spatial distances other than 200 nmi, are all theoretical and have not been adequately verified. Finally, the original model is more than 15 years old, and much better data have since been acquired. Consequently, in mid-1981, in an effort to overcome some of these limitations, MSFC sponsored the development of a global cloud cover data base (ref. 8.6) comprised of one parameter, observed total sky cover, and which became initially available in late 1981.

8.3.2 Background

An extensive investigation revealed no suitable summarized or statistical cloud distributions and only one source of cloud observations that provides global coverage and diurnal variation in a manageable volume. This is the three-dimensional (3-D) NEPH automated cloud analysis prepared by the Air Force Global Weather Center (refs. 8.7, 8.8). Archived SMS/GOES VISSR data do not provide global coverage and contain eight observations daily from both positions (east and west) only since September 1978 (ref. 8.9). The polar orbiter satellite data provide global coverage, but only daily hemispheric polar stereographic mosaics are archived (ref. 8.10). The 3-D NEPH analysis, on the other hand, though possessing some limitations in cloud typing (ref. 8.11) which are minimized by using total measurements and other known shortcomings (ref. 8.12) provides the only global coverage of cloud cover amounts at frequent time intervals. These data are directly applicable to mission simulations and for other endeavors.

The 3-D NEPH analysis, a global cloud analysis, is prepared eight times (00Z, 03Z, 06Z, ...) daily by the Air Force Global Weather Central (GWC), Offutt Air Force Base, Nebraska. In the past, it was prepared only four times daily for the SH. The analysis, made from all available cloud data, includes satellite, aircraft, and ground/ship observations. These observations are fitted into a coherent global cloud structure through a scheme that has been fully described by Coburn and by Fye, which largely eliminates the risk of incorporating erroneous data or interpreting snow or sand as clouds. The analysis encompasses 15 altitude layers and includes 22 parameters on a fine mesh grid (approximately 25 nmi spacing at 45° latitude).

The 3-D NEPH analysis has all the attributes required for adequate mission simulations except that it is too voluminous to handle. Fortunately, the data processing at the archiving location reduces the volume to a manageable amount. To further reduce the volume of data, only one parameter—total cloud cover—was selected for the new NASA cloud cover data base, which is described in detail in reference 8.6.

8.3.3 Discussion of Validation

To ensure that the cloud cover amounts in the new NASA cloud cover data base are representative of the real world, several comparisons with ground observed sky cover were made. Figure 8.4 shows a comparison of single year-month statistics for a few U.S. locations where surface reports were available. The NASA cloud data are from the gridpoint nearest the ground location. U.S. locations were chosen for this comparison since satellite values tend to dominate U.S. portions of the data base.

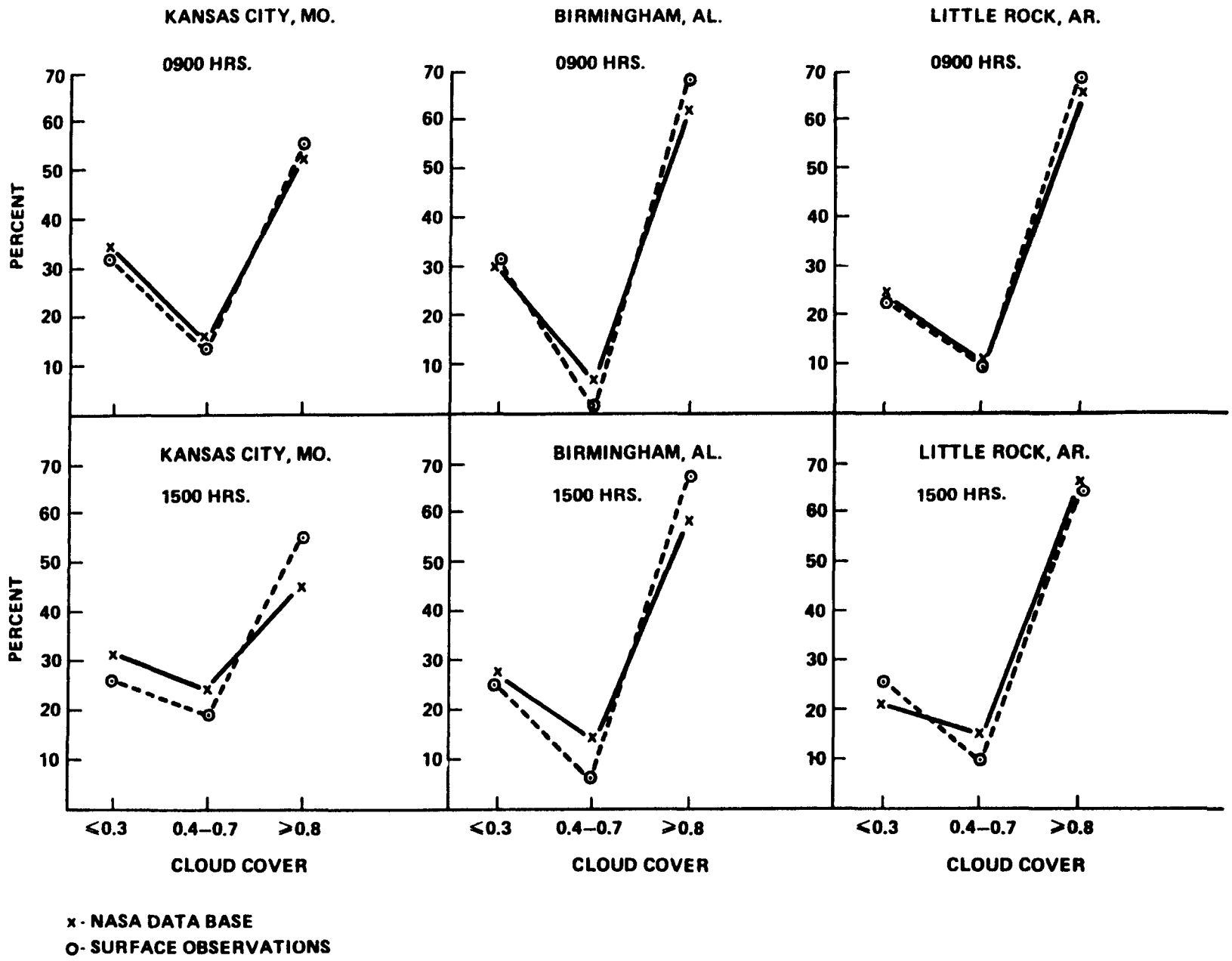

Figure 8.4 Cloud cover comparison—surface observations and NASA data base, January 1973.

Table 8.1 shows cloud cover statistics calculated from the 5 years of this new data base compared with long term ground observed statistics extracted from the previous data base (ref. 8.9).

As in the figure 8.4 case, the new statistics apply to the grid point closest to the ground station—in some cases they may be as much as 25 nmi apart. This geographic separation, especially in coastal or mountainous areas, might produce different cloud regimes at the two locations. Cloud amount differences can also be expected between the ground climatology versus satellite (NASA) observations and the different period of record of the two samples. Still, there is good agreement between the two data bases. For example, the percent frequency of ≥0.8 cloud cover at 1,500-h local time for the ground stations averaged 5-percent higher in winter and 10-percent higher in summer as seen in table 8.1. Still other investigators have used different validation procedures to verify the basic 3D NEPH data (refs. 8.11, 8.13, 8.14).

Figures 8.5 and 8.6 illustrate some hemispheric cloud cover values developed from this new data base. Both figures show a rather dramatic increase in NH cloudiness in 1977. For that year, the mean NH cloud cover was 57 percent. January showed the minimum coverage (49 percent) and July the maximum (62 percent). All available months except mid-1975 were consistently much less for 1972 through 1975 in the NH, yielding a 5-year mean of 46 percent. Mean 1977 coverage for the SH was also 57 percent with the minimum in September (54 percent) and the maximum in February (63 percent). Except for the first two-thirds of 1976, all available months for 1976 through 1980 consistently varied within ±7 percent of this mean value in the SH, yielding a 5-year mean of 56 percent. In general, the data depict scattered conditions in the NH for the first half of the decade of the 70's with a possible trend toward broken conditions during the latter half. However, broken conditions prevail in the SH over the entire last half of the decade.

Large variations were observed in the 1975–76 data, attributable in part to modifications in the automated analysis program. However, such variations scarcely negate the usefulness of this new data base for certain purposes since earlier NH data exhibit strong internal consistency, as does later SH data.

Furthermore, it should be remarked that the 3-D NEPH data were derived from a program which had one major objective; i.e., producing operationally significant, Earth-orbital viewing data in a quasi-real-time mode. The program's continual thrust was toward greater and greater clarity of such satellite-derived data. Minimal consideration was necessarily given to possible variations between past, current, and future data except as they impacted client missions. In short, as those who have ever been involved in such efforts are fully aware, "yesterday" is passe, "today" is paramount, and "tomorrow" is problematical though being planned. Archival of data was essentially undertaken in acknowledgment of the waste of data destruction and because such action was only minimally more troublesome or costly than any destruction.

This effort was only one of several which were undertaken in an attempt to revitalize the usefulness of these archived data. Naturally, because of its nature, discrepancies in the 3-D NEPH archive are to be expected. Future investigations of these variations are planned; but, as others have suggested, the 3-D NEPH data is probably the best of its kind currently available (refs. 8.14, 8.15).

8.3.4 The Earth-Viewing Simulation Procedure

The great attribute of this data base in Earth viewing applications is the direct use of observed cloud cover instead of a Monte Carlo selected cloud amount. This is especially advantageous when the Earth target area is larger than the area viewed by the sensing instrument. For example, suppose the desired target area is 1,000 × 100 nmi and a camera acquires a series of pictures 100 × 100 nmi which are pieced together to cover the desired area. To simulate this situation using a statistical cloud cover data base requires a Monte Carlo draw of cloud cover encountered in the initial 100 × 100 nmi picture. This first part is a reasonable approach which should give good results for the first picture. For the remainder of the 1,000 nmi swath, however, the Monte Carlo procedure becomes more complicated and less likely to produce reasonable results—due to the spatial (and sometimes temporal) continuity of clouds. To avoid unreasonable cloud patterns such as alternating clear and overcast in the remaining nine 100 × 100 nmi squares, the statistical data base must have additional time and space conditional probability distributions—which induces a further departure from reality.

Table 8.1 Comparison of climatology with NASA data base.

Probability of ≤0.3 and ≥0.8 cloud cover at 0900 and 1500 hours in December and July.

Station	December								July							
	≤0.3				≥0.8				≤0.3				≥0.8			
	0900		1500		0900		1500		0900		1500		0900		1500	
	C	N	C	N	C	N	C	N	C	N	C	N	C	N	C	N
Dhahran, Saudia Arabia	0.49	0.37	0.53	0.36	0.22	0.32	0.25	0.28	0.81	0.83	0.84	0.85	0.09	0.01	0.07	0.00
Tripoli, Libya	0.38	0.28	0.33	0.29	0.35	0.35	0.35	0.36	0.89	0.74	0.91	0.83	0.02	0.03	0.03	0.00
Angeles, Luzon, P.I.	0.16	0.13	0.10	0.02	0.58	0.55	0.60	0.59	0.01	0.01	0.01	0.00	0.76	0.74	0.80	0.80
Tampa, Florida	0.39	0.34	0.37	0.30	0.37	0.39	0.36	0.36	0.20	0.20	0.07	0.10	0.38	0.38	0.55	0.40
Mountain Home, Idaho	0.22	0.14	0.22	0.15	0.62	0.62	0.60	0.59	0.74	0.66	0.65	0.59	0.11	0.10	0.14	0.15
Fort Yukon, Alaska	0.31	0.48	0.34	0.41	0.55	0.29	0.54	0.39	0.28	0.27	0.21	0.38	0.48	0.37	0.43	0.28
Belleville, Illinois	0.29	0.21	0.28	0.23	0.57	0.65	0.58	0.60	0.31	0.46	0.25	0.31	0.41	0.32	0.36	0.25
Ban Me Thuot, Vietnam	0.07	0.30	0.14	0.26	0.40	0.44	0.36	0.44	0.03	0.26	0.00	0.28	0.51	0.47	0.51	0.38
Ship D (Atlantic)	0.13	0.06	0.04	0.04	0.60	0.67	0.68	0.73	0.15	0.32	0.15	0.35	0.61	0.35	0.55	0.32
Adak, Alaska	0.04	0.02	0.03	0.03	0.71	0.69	0.71	0.73	0.02	0.01	0.03	0.02	0.84	0.87	0.80	0.83
Resolute, NWT, Canada	0.64	0.65	0.50	0.61	0.31	0.08	0.37	0.15	0.20	0.12	0.17	0.13	0.64	0.38	0.66	0.45
Fort Kobbe, Canal Zone	0.26	0.28	0.16	0.10	0.37	0.27	0.48	0.30	0.03	0.00	0.00	0.01	0.80	0.67	0.82	0.70
Bangalore, India	0.30	0.47	0.26	0.45	0.31	0.18	0.34	0.17	0.00	0.01	0.00	0.06	0.80	0.79	0.77	0.67
San Francisco, California	0.32	0.24	0.39	0.26	0.55	0.41	0.46	0.41	0.72	0.35	0.84	0.50	0.16	0.23	0.08	0.18
Shreveport, Louisiana	0.33	0.32	0.36	0.38	0.53	0.51	0.48	0.46	0.34	0.30	0.27	0.27	0.33	0.34	0.34	0.26
Ship V (Pacific)	0.17	0.35	0.18	0.32	0.54	0.32	0.53	0.34	0.16	0.39	0.25	0.48	0.56	0.30	0.52	0.25

C = Climatology N = NASA

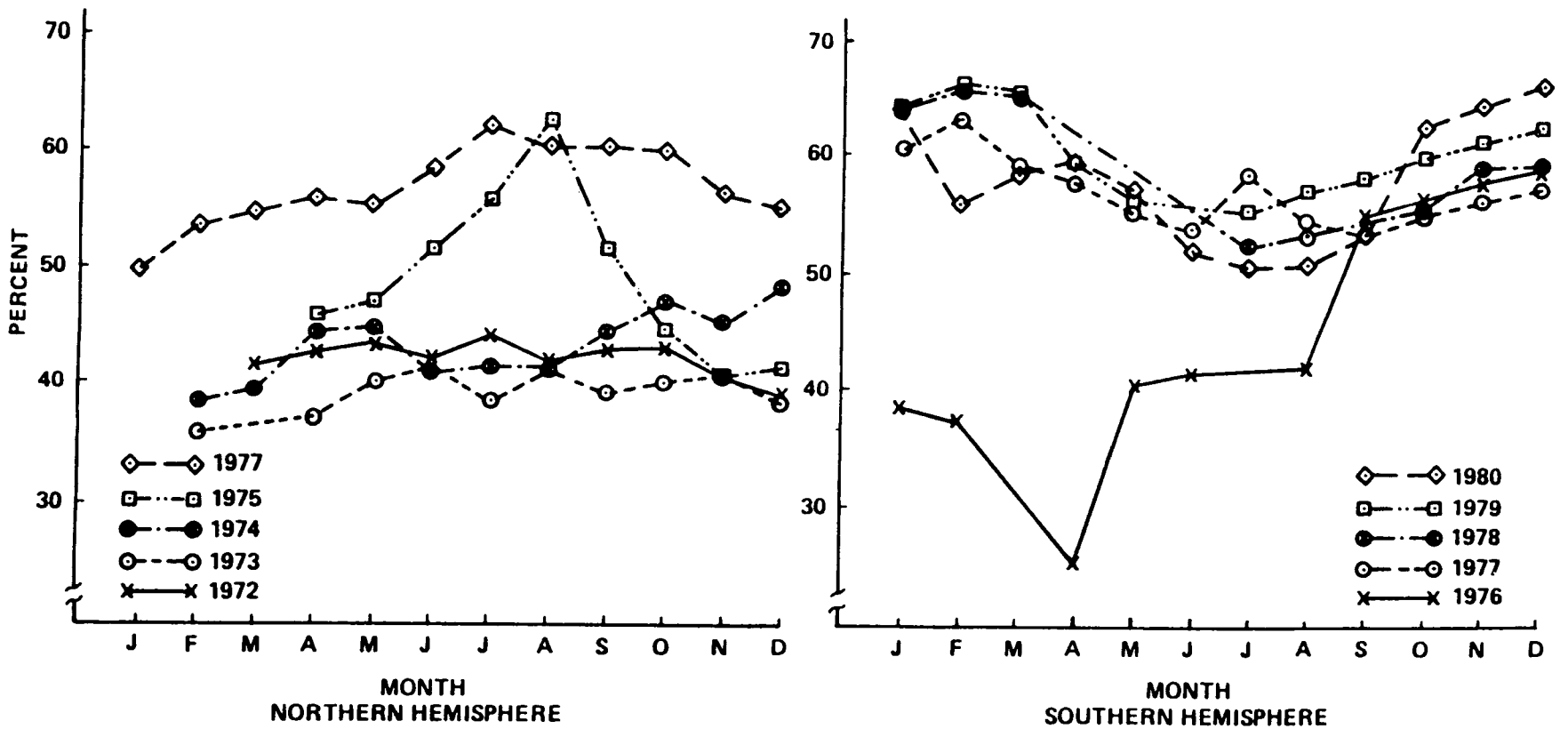

Figure 8.5 Mean hemispheric cloud cover.

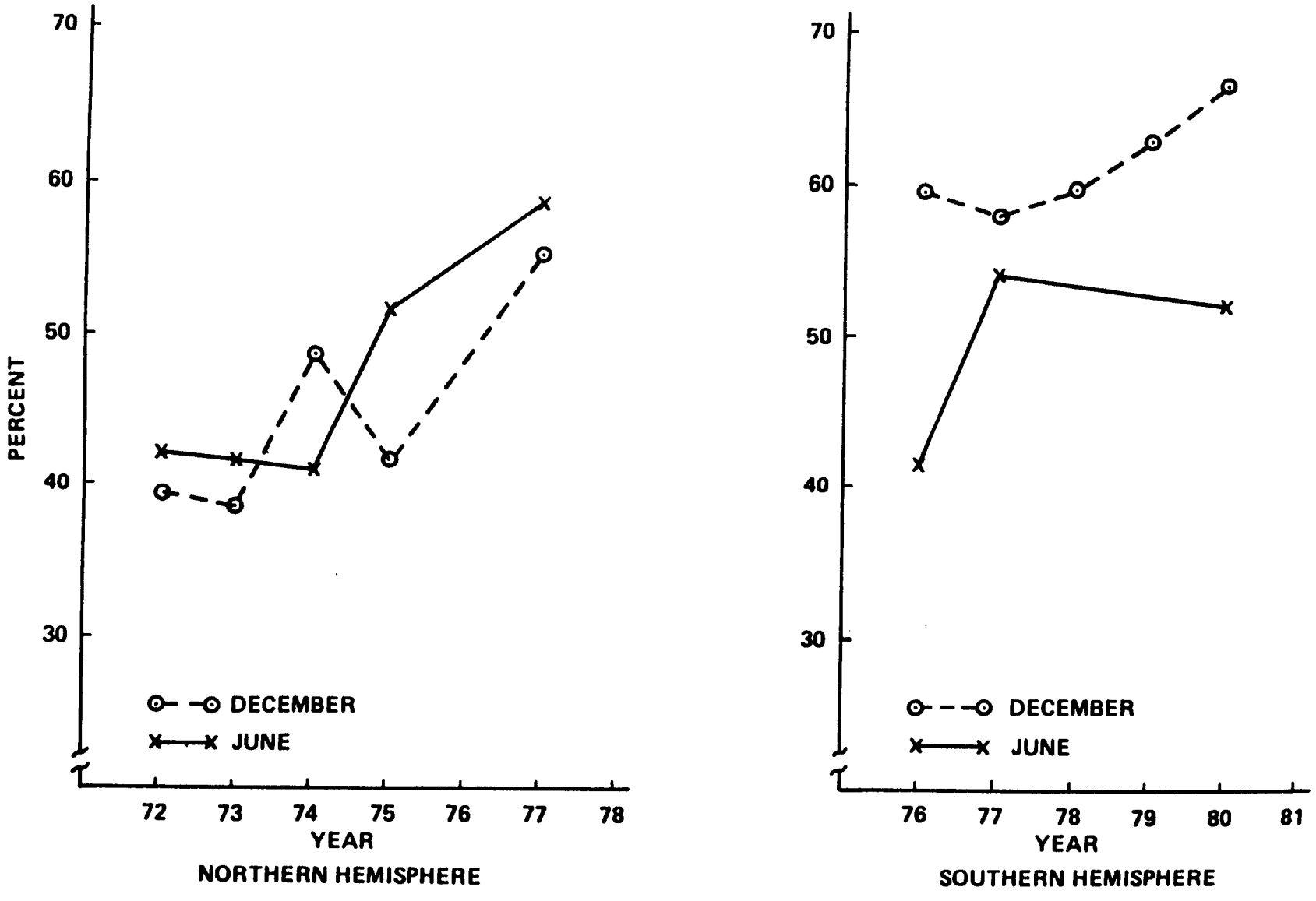

Figure 8.6 Mean monthly cloud cover.

Earth viewing simulations, using the new data base, bypass the time and space conditional probability problem by always using observed cloud cover. Although no missions have yet been analyzed with this NASA data base, the mechanics of the simulation procedure have been developed along with an ephemeris program and a program to locate gridpoints from latitude/longitude coordinates.

To illustrate the simulation procedure, consider, for example, the case described above where it is required to photograph a swath 1,000 nmi long and 100 nmi wide.

(1) Step 1—Locate the gridpoint closest to the center of the first 100 × 100 nmi square and the four surrounding gridpoints; i.e., I+1, I-1, J+1, J-1.

(2) Step 2—Calculate the mean cloud cover of those five points for the appropriate date/time and assign that value to the first square.

(3) Step 3—Move 100 nmi along the ground track and repeat step 1 and step 2. Repeat until all ten 100 nmi squares have an assigned cloud cover.

(4) Step 4—Average the ten values from above to obtain a single cloud cover for the entire swath. One minus the cloud cover is the fraction of Earth viewed on the first pass or revolution over the target area. Store this value.

(5) Step 5—Repeat the entire process the number of times in the month or season the actual mission will be flown.

(6) Step 6—Summarize the results to show: (a) The probability of success (where success is defined as photographing some specified percent of the swath) versus number of satellite passes over the target (fig. 8.7). (b) Probability versus area photographed for a specified number of satellite passes over the target (fig. 8.8).

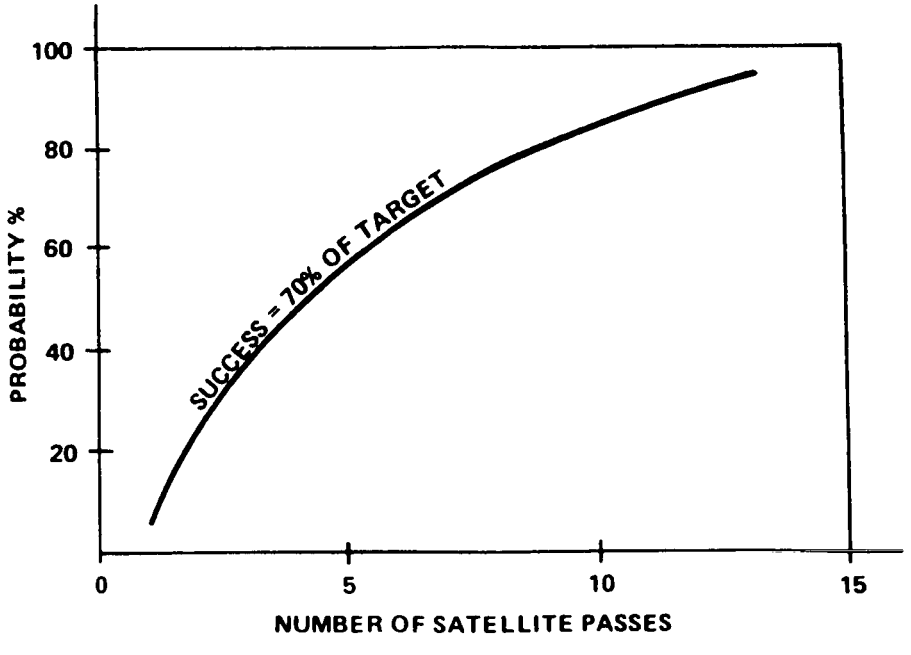

Figure 8.7 Probability of success.

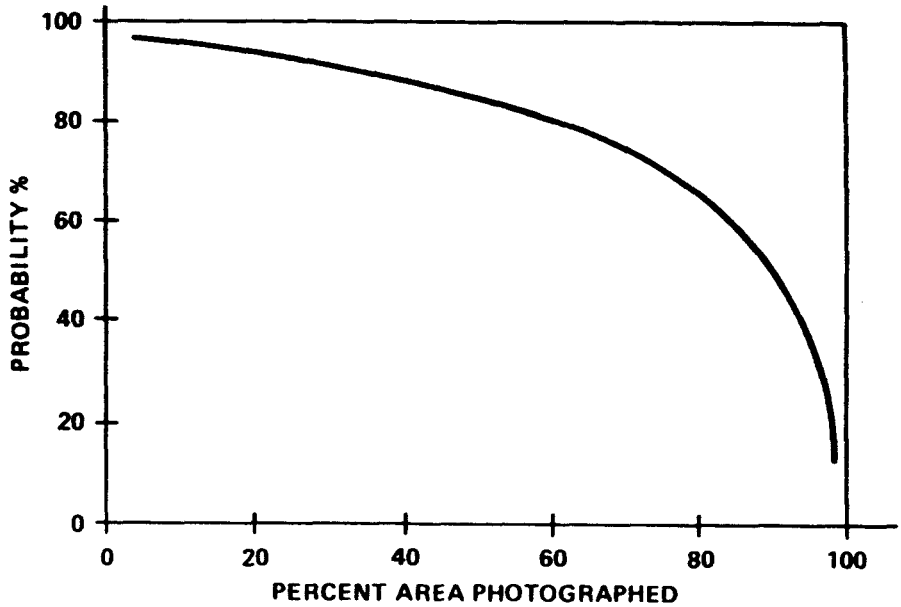

Figure 8.8 Photographic coverage of target area after 10 satellite passes.

While the example specified a 1,000 × 100 nmi swath, the simulation procedure can be applied to any size area from a single grid point to a continent. Also, details as fine as single grid points within larger areas can be analyzed. For example, perhaps the mission requirements can be satisfied by incremental photographic coverage, i.e., forming a montage from parts of the area acquired on separate satellite revolutions, rather than acquiring the necessary amount on a single try. In this case, single grid points within the area can be cleared on successive passes to contribute to the area coverage. There is enough built-in flexibility to accommodate a wide variety of mission requirements.

8.4 Four-Dimensional Atmospheric Models

In this part of the attenuation model project, the emphasis is placed on water vapor rather than clouds. Also, since attenuation calculations are usually made from reference atmosphere inputs, the other atmospheric parameters found in reference atmospheres were included in the MSFC 4-D model. The basic data comprise monthly statistics (mean and standard deviations) of pressure, temperature, density, and moisture content from 0- to 25-km altitude on a global grid network. These data provide information on latitudinal, longitudinal, altitudinal, and temporal variations of the parameters; hence the name "four-dimensional atmospheric models." Of course, a profile of temperature, pressure, density, and moisture content for any global location may be retrieved from these data. Still, to reduce the data to a more manageable amount it was decided to outline homogeneous moisture content regions for which a single set of profile statistics would apply. This procedure would permit the use of one set of profiles for all locations within a homogeneous region. For each region, analytical functions have been fitted to the statistical data. For moisture, exponential functions were most appropriate, while for temperature, a series expansion technique was used. Fitting analytic functions to the statistical climatological profile data produces a library of coefficients for the temperature and moisture profiles. These coefficients are then used to develop computer subroutines to regenerate the model profiles of temperature and moisture which are a function of the homogeneous region and month of the year.

In the compilation of the global statistics, pressure and density were determined from the hypsometric equation and the equation of state, rather than linear or logarithmic interpolation. The purpose of this was to insure hydrostatic consistency; thus, the pressure and density profiles can be generated from the temperature profile and the hydrostatic assumption.

The final result of this 4-D model analysis is a computer program that provides mean and variance profiles of moisture, temperature, pressure, and density from the surface to 25-km altitude for any location on the globe and month of the year. The computer program contains the equations, data, and library of coefficients necessary to produce the desired results. The thermodynamic parameters from this model were subsequently used to produce the lower segment (0- to 25-km altitude) for the Global Reference Atmosphere Model, 1990 (GRAM-90) (Ref. 8.16). However the GRAM-90 does not output any moisture parameters. The MSFC 4-D atmospheric model is described in references 8.4 and 8.5.

8.5 Stratospheric and Mesospheric Clouds

Four types of high-altitude clouds are presented in this subsection to alert designers and planners to the fact that there exists cloud systems/particles above the troposphere which need to be considered when observations or vehicle reentry, launch or horizontal flight above 12-km altitude is desired. Two related types of stratospheric cloud phenomena are presented here which occur at stratospheric altitudes (15 to 30 km) and are called polar stratospheric clouds (PSC), and nacreous clouds (NAC). Two similar types of upper mesospheric clouds (80- to 85-km altitude) called polar mesospheric clouds (PMC) and noctilucent clouds (NLC) will also be discussed briefly. The polar stratospheric clouds can be frozen aerosol particles, whereas the mesospheric clouds consist mainly of water ice. A global tropospheric cloud cover model is described in paragraph 8.3. See section X for more information on atmospheric constituents, aerosols, and chemistry.

8.5.1 Stratospheric Clouds

8.5.1.1 Polar Stratospheric Clouds

Polar stratospheric clouds were discovered in the late 1970's when they were observed as extinction amounts in the SAM II and LIMS satellite data (ref. 8.17). They are probably not the visually observed nacreous clouds, but nacreous is a special subset of PSC's (ref. 8.18). They appear not to be related to orographic features and appear larger and more persistent than nacreous clouds, PSC's may not even be visible to the ground observer. Therefore these high extinction stratospheric layers (aerosol related) were named polar stratospheric clouds (ref. 8.17 and 8.19).

Polar stratospheric clouds are frozen aerosol particles observed in local winter over both polar regions whenever the ambient temperature falls below about 195 K. On one occasion they were observed extending continuously from 80° N. to the pole. The clouds are layered with the maximum amount near 20 km, close to the region of minimum stratospheric temperature. The layers are thin; <1 to 2 or more km thick (thicker in the Antarctic) in the altitude range from 10 to 30 km. Multiple layers of PSC's can exist. PSC's descend in altitude during the course of the winter until they reach an altitude of about 15 kms at the end of the winter. Antarctic PSC's generally occur at lower altitudes (<17 km) than Arctic PSC's (17 to 25 km). PSC's are also linked to the ozone depletion/hole over the poles (ref. 8.25). This is in agreement with the predicted mean flow in the polar vortex. This results in a strong gradient across the polar night jet stream which lasts until the springtime breakup. This feature is in good agreement with the observed aerosol properties. The cloud characteristics change rapidly, most probably due to fluctuations in local temperature, water vapor, or wind shear. The clouds are apparently formed from frozen nuclei consisting primarily of either a nitric acid mixture (type I), or water ice particles (type II). Small admixtures of other compounds such as sulfuric and hydrochloric acid in solid solution also can exist with these two mixtures in the formations of PSC's (ref. 8.20). The clouds are much more prevalent in the Antarctic with their colder (by 3.5 K) stratospheric temperatures than they are in the Arctic. If they were illuminated, these polar stratospheric clouds would have the appearance of a thin cirrus or cirrostratus veil. The clouds are not formed at the level of maximum aerosol concentration but near the level of minimum temperature. References 8.17 through 8.24 describe polar stratospheric clouds and their characteristics. Although different kinds of polar stratospheric clouds exist which may have different compositions, they exist as highly supercooled/supersaturated liquid drops.

8.5.1.2 Polar Stratospheric Clouds (PSC) Design Criteria[1]

	PSC Type I		PSC Type II
Composition/phase	HNO_3[2]/Ice		H_2O/Ice
Concentration	2 cm^{-3}		0.03 cm^{-3}
General Range	1 to 10 cm^{-3} (at 20 km)		0.005 to 0.1 cm^{-3} (at 15 km)
Mass Density	20 ppbm*		400 ppbm
Radius	0.5 μm		≥6 μm
Range		0.1 to 10 μm	
Temperature	<195 K		<195 K
	Antarctic		Arctic
Altitude	15 km		20 km
Range	11 to 22 km		17 to 25 km
Time of Occurrence	June to October		December to March
Associated Stratospheric Water Vapor Content: Avg		7 ppmv*	
Upper Limit	15.5 ppmv		21.5 ppmv
Horizontal Extent		10 to 10^3 km	
Geographic Extent		from 70° to Pole	
Duration		Hours to Months	

(1.) Much is based on ref. 8.24.
(2.) Nitric acid mixture, >40-percent concentration
*ppbm = parts per billion mass and ppmv = parts per million volume.

8.5.1.3. Nacreous Clouds

Nacreous clouds, also called "mother-of-pearl clouds" (MPC), luminous clouds, or stratospheric veil clouds are infrequently observed, thin stratospheric clouds appearing brilliantly colored and stationary (lenticular) in wintertime over high latitudes in both hemispheres, i.e., Scandinavia, Alaska and Antarctica, when the Sun is below the horizon. Over 155 dates in which northern hemispheric sightings (for undisturbed stratosphere only, no aircraft contrails included), of NAC's have been observed over 100 years during winter (December to February). Somewhat more frequent are NAC's over the Antarctic winter (June to September) where over 140 sightings in 100 years have occurred in these sparse reporting areas (ref. 8.26). NAC's have been sighted between 17- to 31-km altitude (average 23 km), and set-up preferentially downwind of mountain ranges. This indicates orographic origin with lee waves producing up to 40-km

wavelengths present in the NAC bands. NAC's are a special subset of polar stratospheric clouds, but it is not yet clear that the two-cloud phenomena are the same (ref. 8.18). NAC's are composed of micrometer-sized water ice particles (crystals) with sizes of the order of 1 to 2 μm in radius, and life times are >10 min at 20 km, 1 ppm of water is equivalent to 5 particles cm^{-3} of size 1.5 μm. An approximate maximum radius of about 4 μm at 20 km altitude may be determined, assuming 3 ppm of water condensing to form 1 particle cm^{-3}. It is generally believed that NAC's form by deposition of H_2O on pre-existing stratospheric aerosol particles (sulfate), when stratospheric temperatures are typically at or below –85 °C. Therefore, the number concentration of NAC particles should be equal to that of the stratospheric aerosols (~5 to 20 cm^{-3} at 20 km).

8.5.2 Mesospheric Clouds

Mesospheric clouds fall into two separate, but similar, cloud (water ice) phenomena that occur at cold, summertime, high latitude mesopause altitudes. Such phenomena are known as noctilucent clouds in their twilight manifestation between 50° and 65° latitude, via ground based observations; and as polar mesospheric clouds in their extension into the entire polar/daytime regions (65° to 85° latitude, with some occurrences as low as 55° latitude). PMC's are believed to be the brighter extension of NLC's into the northern and southern polar cap region. Both phenomena are similar and keyed to the summer solstice when temperatures fall below 140 K at mesopause heights. This suggests that variations of temperature and/or the accompanying upward advective water vapor flux are responsible for the seasonal variations of PMC and NLC (ref. 8.27).

8.5.2.1 Polar Mesospheric Clouds

PMC's are scattering layers observed by satellite that occur at high latitude, summertime, mesopause regions over extensive areas of both poles. PMC's develop at the coldest point over the planet as small ice particles grow by sublimation on available nuclei. Nucleation upon meteoric dust (or condensed vapor) and/or hydrated ions has been investigated and both routes are plausible (ref. 8.28).

8.5.2.2 PMC Seasonal Climatology

Comparison of PMC seasonal properties for 1981–1985 with NLC (1885–1972). Times are given in days after summer solstice (ref. 8.27).

	South PMC	North PMC	North NLC
Beginning date[1]	–32	–23	–38
Ending date	61	64	50
Time of maximum	7–16	16–22	16–20
Duration of season	93	87	88
Lower latitude boundary	65° (PM)[2]	60° (PM)[3]	45° N./50° S.
Months observed		June–August	
Interannual variability	±15 percent	±15 percent	
Altitude, km	83.2±1.5	85.0±1.5	

1. Begins at high latitude 10 to 20 days before lower latitude observation. South Pole season begins earlier and lasts longer than North Pole season.

2. 55° (AM)
3. 60° (AM)

8.5.2.3 PMC Properties

Ice particle size: 35- to 70-nm range

Ice particle concentration: 190 cm^{-3} (5- to 500-cm^{-3} range)

Ice particle column number: 10^6- to 10^8-cm^{-2} range

Water mixing ration (w): 1 to 4 ppmv

Temperature: <140 K

Cloud thickness: 2 to 3 km

Cloud extent: 100 × 100 km.

8.5.2.4 Noctilucent Clouds

8.5.2.4.1 Background

Noctilucent clouds were once thought to be very rare, especially in the Southern Hemisphere; however, observations from space have shown that they occur almost continuously during some periods of time. In both hemispheres their coverage can be quite extensive. Noctilucent clouds are composed of submicro- sized water ice particles growing in supersaturated air and occurring in a few-kilometer thick layer, only during summer over higher latitudes (poleward of 45° N. and 50° S.) at cold (<140 K) mesopause altitudes (85 km). These clouds have been observed only from the ground over the past 100 years, at twilight (morning or evening) when the Sun is between 6° and 16° below the horizon, so that the 80- to 85-km level is still in sunlight. Whether NLC and PMC both represent the same phenomenon currently remains an open question. The exact relationship between NLC and PMC is not yet known (ref. 8.28). The NLC season begins and ends much earlier than PMC, and occurs at significantly lower latitudes than do PMC. Jensen and Thomas have stated that they feel PMC and NLC could actually be the same phenomenon with their cloud property differences noted, being due to their variation with local time, since the two phenomena are observed at different diurnal times. The following was extracted from references 8.27, 8.29, 8.30, and 8.31.

8.5.2.4.2 Types

Fogle and Haurwitz (ref. 8.31) have classified noctilucent clouds as follows:

TYPE I. VEILS—These are the simplest. They are very tenuous with no well-defined structure, and are often present as a background for other categories or forms. They are somewhat like cirrus clouds of uncertain shape; however, occasionally they exhibit a faintly visible fibrous structure. They often flicker.

TYPE II. BANDS—These are long streaks with diffuse edges (type IIa) or sharply defined edges (type IIb). They are sometimes hundreds of kilometers long and often occur in groups arranged roughly parallel to each other or interwoven at small angles (perhaps visible evidence of the gravity waves propagating through the region). Occasionally an isolated band is observed. Bands change very little with time and blurred bands with little movement are often the predominant structure in the noctilucent cloud field. When they do move, it is often in a direction and with a speed that is different than that of the display as a whole. Very closely spaced thin streaks, called serrations, are occasionally seen in the veil background. They look like a continuous cloud mass since the serrations are separated by only a few kilometers.

TYPE III. BILLOWS—These are groups of closely spaced short bands which sometime consist of straight and narrow, sharply outlined parallel short bands (type IIIa). Sometimes they exhibit a wave-like

structure (type IIIb). The distance separating pairs of billows is about 10 km. Billows sometimes lie across the direction of the long bands and their alignment usually differs noticeably in close portions of the sky. Unlike the long bands billows may change their form and arrangement or even appear and disappear within a few minutes.

TYPE IV. WHIRLS—Whirls of varying degrees of curvature are also observed in veils, bands, and billows; infrequently, complete rings with dark centers are formed. Whirls of small curvature (less than 1.0°) are classified as type IVa while whirls having a single simple band or several bands with a radius of 3° to 5° are classified as type IVb. Larger scale whirls are classified as type IVc.

TYPE V. AMORPHOUS—These are similar to veils in that they have no well-defined structure but they are brighter and more readily visible than the veil type NLC.

8.5.2.4.3 Characteristics

Typical characteristics of NLC based on ground-based observations in the Northern Hemisphere are given in the following from Fogle and Haurwitz (ref. 8.31) and references 8.27, 8.29, and 8.30:

Color	Bluish-white
Height (average)	82.7 km, maximum 95, minimum 73
Latitude of observations	45 to 80°; best about 60°
Season of observation	Northern Hemisphere: March through October, best June through August Southern Hemisphere: December through January
Time	While the solar depression angle varies from 6° to 16°
Spatial extent	10^4 to more than 4×10^7 km^2; can cover considerable parts of latitudinal belts north of 45°
Duration	Several minutes to more than 5 hours
Average velocity	40 m s^{-1} towards the southwest. Individual bands often move in different directions and at speeds differing from the NLC display as a whole.
Thickness in the vertical	0.5 to 2.0 km
Vertical wave amplitude	1.5 to 3.0 km
Average particle diameter	3×10^{-5} cm
Particle number density	10^{-2} to 1/cm^3
Ambient temperature when NLC present	135 K
Brightness	<0.4 candles/cm^3
Albedo	2.3×10^{-5} to 4.7×10^{-5}
Polarization	Strongly polarized in same sense as but less sharply than twilight sky.

8.5.2.4.4 Particle Size and Number Density

It is generally agreed that noctilucent clouds consist of ice particles; however, there is disagreement as to whether or not they are aligned or randomly oriented. There is general agreement that they consist principally of particles of a radius of 0.1 to 0.2 μm; however, there is evidence to indicate that some particles may be larger than 1 μm in radius. Number densities range from 10^{-2} to 1 cm^{-3}. The particle size distribution is given by the Junge law (ref. 8.29):

$$dn(r) = c \times r^{-\nu}\, d(\ln r) \tag{8.1}$$

where r is the radius, c is a measure of the turbidity depending upon the density per cubic centimeter, and $2<\nu<3$.

8.5.2.4.5 Composition

There is disagreement as to what the growth mechanism is, condensation or coagulation; however, there is agreement that supersaturated conditions can be expected to occur at the mesopause in the summer hemisphere. The question still remains as to whether or not there is enough moisture to generate the amount of clouds observed. Figure 8.9 shows the water vapor content of the atmosphere to an altitude of 100 km. Observations show that nickel, iron, carbon, copper, etc. are present in the nuclei. These are possibly of extraterrestrial origin. There is further evidence to support the concept that the nuclei could be ion clusters.

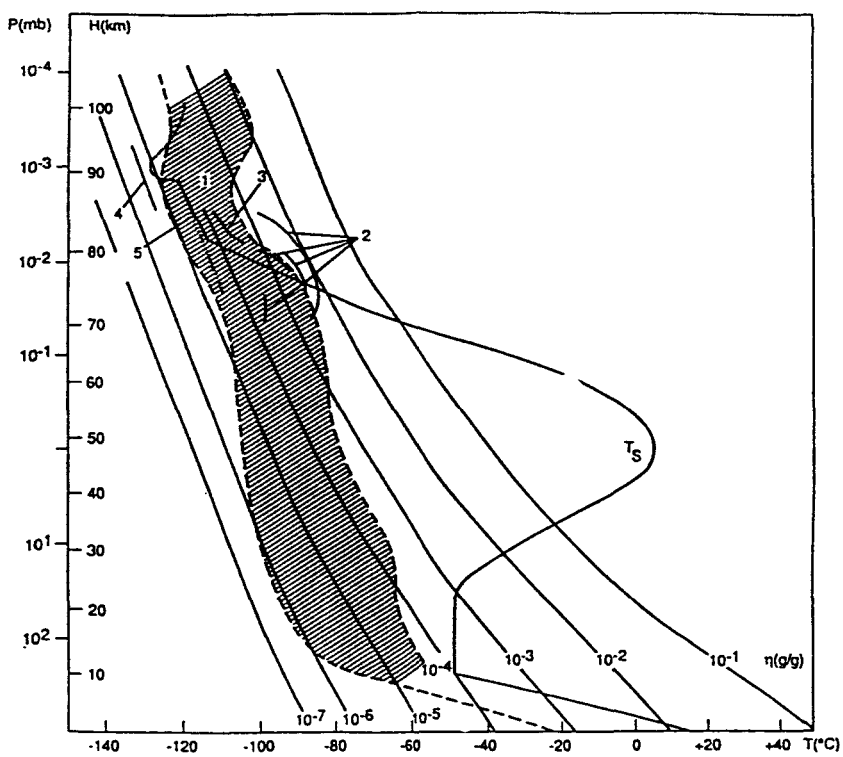

Figure 8.9 Water vapor mixing ratio versus altitude: data generalized by (1) Sonntag, 1974, (2) measurements by Perov and Fedynsky, 1968; (3) by Chyzhov and Kim, 1970; (4) by Arnold and Krankovsky, 1977; and (5) by Quessette, 1968. Curve T_S gives the mean temperature at 60° N. in July by Cole and Kantor, 1978. Also ascending smooth mixing curves from 10^{-1} through 10^{-7} are plotted.

8.5.2.4.6 Optical Properties

Results of analyses to date indicate that the optical thickness in the 0.2 to 0.4 μm wavelength interval can be approximated by:

$$\tau\lambda = \tau\lambda_0 \times 5.5\ \lambda^{0.6} \exp(-2\ \lambda^{0.65}) \tag{8.2}$$

where $\lambda_0 = 0.55$ μm.

REFERENCES

8.1 Gaut, N.E., and Reifenstein, E.C., III: "Interaction Model of Microwave Energy and Atmospheric Variables." Environmental Research and Technology, Inc., final report of contract NAS8-26275, February 1971.

8.2 Sherr, P.E., et al.: "World Wide Cloud Cover Distribution for Use in Computer Simulations." Allied Research Associates, NASA CR-61226, June 14, 1968.

8.3 Greaves, J.R., et al.: "Development of a Global Cloud Model for Simulating Earth-Viewing Space Missions." Allied Research Associates, final report of contract NAS8-25812, January 1971.

8.4 Spiegler, D.B., and Greaves, J.R.: "Development of Four-Dimensional Atmospheric Models (Worldwide)." Allied Research Associates, Inc., NASA CR-61362, August 1971.

8.5 Spiegler, D.B., and Fowler, M.G.: "Four-Dimensional Worldwide Atmospheric Models (Surface to 25-km Altitudes)." Allied Research Associates, Inc., NASA CR-2082, July 1972.

8.6 Brown, S.C., and Jeffries, W.R., III: "A New NASA/MSFC Mission Analysis Global Cloud Cover Data Base." NASA TR-2448, March 1985.

8.7 Coburn, A.R.: "Improved Three-Dimensional Nephanalysis." U.S. Air Force Global Weather Center, AFGWC Technical Memorandum 71-2, 1971.

8.8 Fye, F.K.: "The AFGWC Automated Cloud Analysis Model." U.S. Air Force Global Weather Center, AFGWC Technical Memorandum 78-002, 1978.

8.9 Anonymous: "VISSR Digital Archive User's Guide." National Climatic Center, Satellite Data Services Division, Applications Branch, 1978.

8.10 Kidwell, K.B.: "NOAA Polar Orbiter Data (TIROS-N) User's Guide (Preliminary Version)." National Climatic Center, Satellite Data Services Division, 1979.

8.11 d'Entremont, R.P., Hawkins, R.S., and Bunting, J.T.: "Evaluation of Automated Imagery Analysis Algorithms for Use in the Three-Dimensional Nephanalysis Model at AFGWC." AFGL Technical Report 82-0397, 1982.

8.12 Davis, P.A., and Wolf, D.E.: "Specifications of Cloud Cover Using Multispectral Satellite Radiometry Data." U.S. Dept. of Commerce Final Report PB-281160, 1978.

8.13 Henderson-Sellers, A., Hughes, N.A., and Wilson, M.: "Cloud Cover Archiving on a Global Scale: A Discussion of Principles." Bull. Am. Meteorol. Soc., vol. 62, 1981, pp. 1300–1307.

8.14 Hughes, N.A., and Henderson-Sellers, A.: "A Preliminary Global Oceanic Cloud Climatology From Satellite Albedo Observations." Jour. of Geophys. Res., vol. 88, C2, 1983, pp. 1475–1483.

8.15 Gordon, A., and Hovanec, R.: "The Sensitivity of Model-Derived Radiation Fluxes to the Monthly Mean Specification of Cloudiness." Clouds in Climate, Goddard Institute for Space Studies, NASA, 1981.

8.16 Justus, C.G., Alyea, F.N., Cunnold, D.M., Jeffries, W.R., III, and Johnson, D.L.: "The NASA/MSFC Global Reference Atmospheric Model—1990 Version (GRAM-90), Part 1: Technical/Users Manual." NASA TM-4268, April 1991.

8.17 Farrukh, U.O.: "Polar Stratospheric Cloud Sightings by SAM II: 1978–1982." NASA CR-177995, March 1986.

8.18 McCormick, M.P., and Hamill, P.: "Characteristics of Polar Stratospheric Clouds as Observed by SAM II, SAGE, and Lidar." Jour. Meteor. Soc. of Japan, vol. 63, No. 2, April 1985, pp. 267–276.

8.19 Hamill, P., and McMaster, L.R.: "Polar Stratospheric Clouds—Their Role in Atmospheric Processes." NASA CP-2318, 1984.

8.20 Hamill, P., Turco, R.P., and Toon, O.B.: "On the Growth of Nitric and Sulfuric Acid Aerosol Particles Under Stratospheric Conditions." JAC, vol. 7, 1988, pp. 287–315.

8.21 McCormick, M.P., and Trepte, C.R.: "Polar Stratospheric Optical Depth Observed Between 1978 and 1985." JGR, vol. 92, No. D4, April 20, 1987, pp. 4297–4306.

8.22 Kent, G.S., Poole, L.R., and McCormick, M.P.: "Characteristics of Arctic Polar Stratospheric Clouds as Measured by Airborne Lidar." JAS, vol. 43, No. 20, October 15, 1986, pp. 2149–2161.

8.23 Steele, H.M., Hamill, P., McCormick, M.P., and Swissler, T.J.: "The Formation of Polar Stratospheric Clouds." JAS, vol. 40, August 1983, pp. 2055–2067.

8.24 Kinne S., et al.: "Measurements of Size and Composition of Particles in Polar Stratospheric Clouds From Infrared Solar Absorption Spectra." JGR, vol. 94, No. D14, November 30, 1989, pp. 16481–16491.

8.25 Hofmann, D.J., et al.: "Stratospheric Clouds and Ozone Depletion in the Arctic During January 1989." Nature, vol. 340, July 13, 1989, pp. 117–121.

8.26 Stanford, J.L., and Davis, J.S.: "A Century of Stratospheric Clouds Reports: 1870–1972." Bull. AMS, vol. 55, No. 3, March 1974.

8.27 Thomas, G.E., and Olivero, J.J.: "Climatology of Polar Mesospheric Clouds 2, Further Analysis of Solar Mesosphere Explorer Data." JGR, vol. 94, No. D12, October 20, 1989, pp. 14673–14681.

8.28 Jensen, E., and Thomas, G.E.: "On the Diurnal Variation of Noctilucent Clouds." JGR, vol. 94, No. D12, October 20, 1989, pp. 14693–14702.

8.29 Kaufman, J.W.: "Noctilucent Clouds." NASA-MSFC/ES42 preliminary report, January 1989.

8.30 Toon, O.B., and Farlow, N.H.: "Particles Above the Tropopause." Ann. Rev. Earth Planet Sci., vol. 9, 1981, pp. 19–58.

8.31 Fogle, B., and Haurwitz, B.: "Noctilucent Clouds." Space Science Reviews, vol. 6, No. 3, 1966, pp. 279–340.

SECTION IX. ATMOSPHERIC ELECTRICITY

9.1 Introduction

Atmospheric electricity must be considered in the design, transportation, and operation of aerospace vehicles. Aerospace vehicles that are not adequately protected can be upset, damaged, or destroyed by a direct lightning stroke to the vehicle or the launch support equipment while on the ground or after launch (e.g., refs. 9.1, 9.2, and 9.3). Damage can also result from the current induced in the vehicle from changing electric fields produced by a nearby lightning stroke. The effect of the atmosphere as an insulator and conductor of high-voltage electricity at various atmospheric pressures must also be considered. High voltage systems aboard the vehicle which are not properly designed can arc or breakdown at low atmospheric pressure.

This section provides an introductory description of the electrification of thunderclouds and thundercloud electrical structure (section 9.2) and gives the reader a basic understanding of the frequency of occurrence of thunderstorms across the United States (section 9.3). The characteristics of cloud-to-ground lightning discharges are then discussed in detail in section 9.4 with emphasis on lightning damage and protection. In section 9.4, four lightning current damage parameters that are important in determining protective measures against lightning are described, and estimates of these parameters from tower strike measurements, rocket triggered lightning experiments, and field inferred methods are given.

Finally, section 9.5 is devoted to lightning current test standards that have recently been adopted for improving the protection of aerospace vehicles (refs. 9.4 and 9.5). Severe lightning strike current test waveforms are provided that are more realistic than the test waveforms provided in the prior revision of this document (NASA TM 82473). In this section, five current test waveforms are given which can be used in the design, development, and test of aerospace vehicles. These test waveforms represent components of a severe lightning strike event.

9.2 Cloud Electrification

Under the proper meteorological conditions, a moist region of the atmosphere may be lifted by a variety of external forcings (e.g., surface heating, terrain effects, fronts, etc.). In very unstable atmospheres, this lifting may result in the development of a cumulonimbus cloud (or thundercloud) whose cloud top extends to altitudes where the ambient air temperature is well below freezing. The electrified nature of a thundercloud is fundamentally related to processes occurring at both the microphysical and cloud-size scales.

9.2.1 Charge Separation Mechanisms

There have been important recent developments in understanding the processes responsible for the electrification of thunderstorms due to increasingly realistic laboratory simulations, and cooperative experiments combining simultaneous observations of electrical and microphysical parameters and the use of sophisticated methods of following air motions.

Table 9.1 summarizes a variety of charge separation processes that occur at the microphysical and cloud-size scales (ref. 9.6). These processes vary in importance depending on the developmental stage of convective clouds. However, it has been suggested that both induction and interface charging are the primary electrification mechanisms in convective clouds (ref. 9.7). Inductive charging involves bouncing collisions between particles in the external field. The amount of charge transferred between the polarized drops at the moment of collision depends on the time of contact, the contact angle (no charge transferred at grazing collisions), the charge relaxation time, and the net charge on the particles. Interface charging involves the transfer of charge due to contact or freezing potentials during the collisions between riming precipitation particles and ice crystals. The sign and magnitude of the charge transfer depended on the temperature, liquid water content, and the ice crystal size and impact velocity.

Table 9.1 Charging mechanisms in clouds and thunderstorms (ref. 9.8).

Mechanism	Microscale	Cloud Scale	Major Roles
1. Diffusion charging	Ion capture by diffusion		Removes ions within cloud
2. Drift charging	Ion capture in drift currents	Drift currents Convection (Sedimentation)	Charges particles Enhances field
3. Selective ion charging	Ion capture by polarized drops	Sedimentation (Convection)	Charges particles Enhances fields
4. Breakup charging	Collisional breakup of polarized drops	Sedimentation (Convection)	Charges drops
5. Induction charging	Charge transfer between polarized particles	Sedimentation (Convection)	Charges particles Enhances field
6. Convection charging	Space-charge production Ion capture in drift currents	Convection	Enhances field (Charges particles)
7. Thermoelectric charging	Charge transfer between particles of differing temperatures	Sedimentation (Convection)	(Charges particles)
8. Interface charging	Charge transfer between particles involving contact potentials (freezing potentials)	Sedimentation (Convection)	Charges particles Enhances field

9.2.2 Thundercloud Electrical Structure

Figure 9.1 illustrates the vertical charge structure of a thundercloud for different geographical locations. A tripolar charge structure is often evident, with a spatially extended region of positive charge at high altitudes, a narrow band of negative charge at lower altitudes, and a small pocket of positive charge near cloud base (ref. 9.8). The thundercloud charge distribution has been inferred using a variety of in situ (e.g., balloon, aircraft) and remote measurements. For instance, ground-based measurements of lightning field changes obtained from a field mill network at the Kennedy Space Center (KSC) have been analyzed to determine the charges deposited by lightning in Florida thunderstorms (ref. 9.9). Figure 9.2 summarizes some of these results. The circles represent negative charge centers associated with cloud-to-ground lightning, while the vectors indicate moment charges due to cloud discharges. These results are consistent with the charge distribution given in figure 9.1.

9.3 Frequency of Occurrence of Thunderstorms

An important phenomenological parameter that aids in the design of lightning protection systems is the average lightning flash density, i.e., the number of lightning ground strikes per square kilometer per year. This parameter is critical in almost all lightning protection designs (such as the lightning overvoltage protection of a utility power line), since the number of power outages or related failures are directly proportional to the number of cloud-to-ground discharges per unit area per year (ref. 9.10). Various ways of obtaining flash densities are given below along with some results.

9.3.1 Flash Counters

Most available data on lightning flash densities have been derived from flash counters. Reference 9.11 has summarized much of the published and unpublished data on average flash density that have been obtained using flash counts, visual observations, and electric field change meters. The mean annual flash density for the United States is given in figure 9.3.

9.3.2 Lightning Location Systems

The development of techniques during the last decade for the automatic detection and location of cloud-to-ground lightning strike points represents an important recent advance in lightning and thunderstorm observations. Systems based on magnetic direction finding (ref. 9.12) and on time-of-arrival techniques have been developed and deployed in networks that cover large regions worldwide, including the continental United States and Alaska. With these systems, thunderstorms can conveniently be monitored and tracked from the cloud-to-ground lightning that they produce. Climatic statistics on ground strike flash densities derived from these lightning location systems are now becoming available.

9.3.3 Satellite Observations

Satellites represent ideal platforms for observing lightning over large regions of the Earth. Already, instruments carried on satellites in low-Earth orbit have provided additional data on the geographical and seasonal distribution of thunderstorms and lightning. New information has been gathered, in particular, for regions over the oceans which could not be monitored using flash counters or lightning location systems. These measurements have suffered from low detection efficiency, poor spatial resolution, and the inability to continuously monitor specific storms or storm systems.

Using results of recent thunderstorm investigations that include observations with high altitude NASA U-2 aircraft, space sensors capable of mapping both intracloud and cloud-to-ground lightning discharges during the day and night with a spatial resolution of 10 km (i.e., storm scale resolution) and high detection efficiency (i.e., 90 percent) are planned for the late 1990's. One such instrument, the lightning mapper sensor (LMS), is planned for placement in geostationary Earth orbit on a geostationary operational

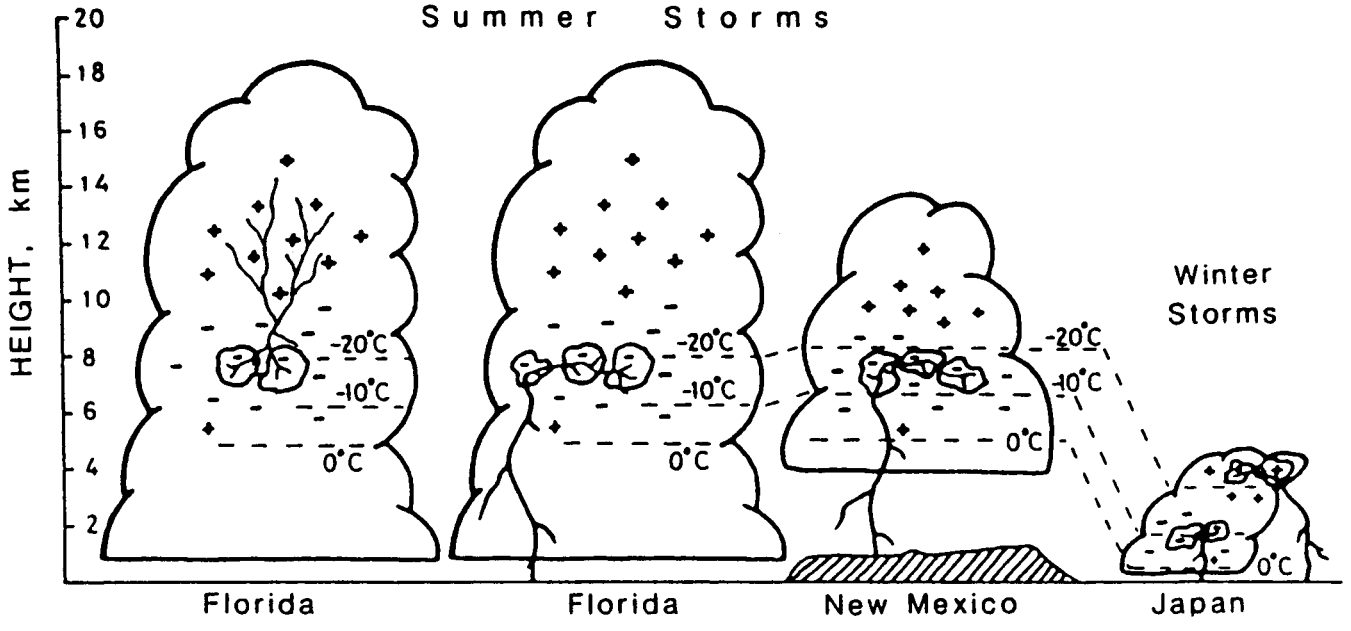

Figure 9.1 Negative charge centers at similar temperature levels for storms in different locations (ref. 9.8).

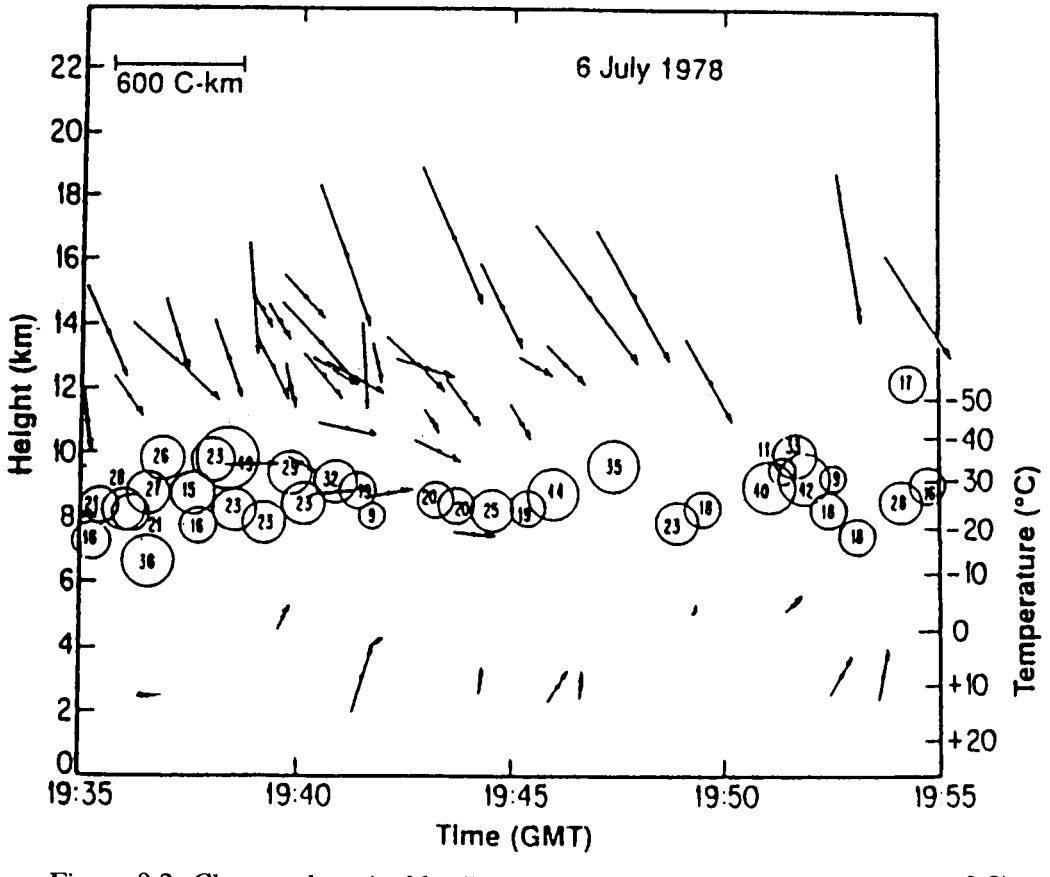

Figure 9.2 Charges deposited by lightning in a Florida thunderstorm (ref. 9.9).

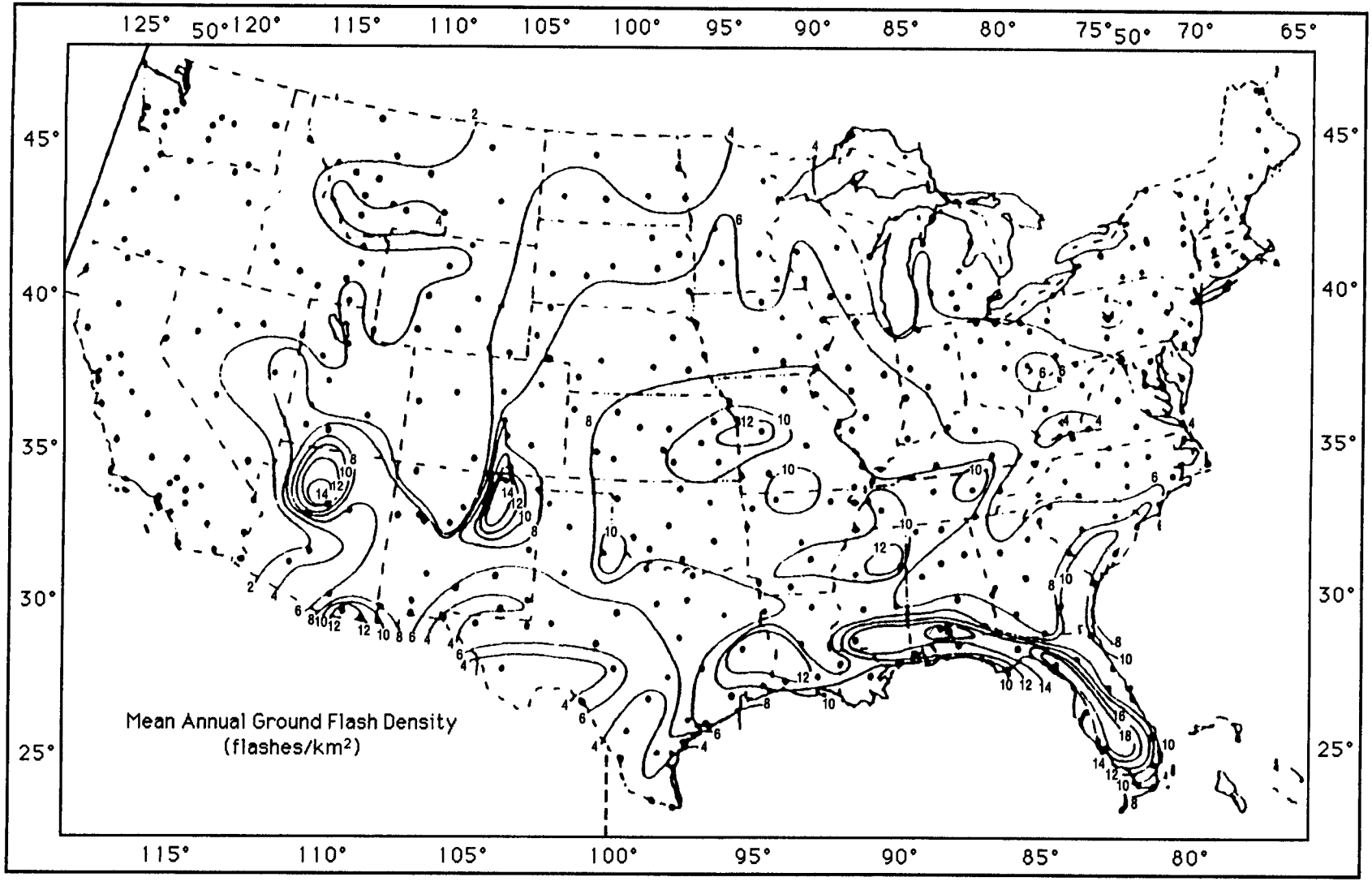

Figure 9.3 Mean annual U.S. ground strike density (ref. 9.14).

environmental satellite (GOES) (ref. 9.13). Another instrument called the lightning imaging sensor (LIS) has been selected for the Tropical Rainfall Measuring Mission (TRMM) and a lightning detector system with significantly improved capabilities can be expected for the geostationary platform. The LMS, LIS, and other satellite-based lightning detection systems will support Earth system science studies in the next decade and beyond.

9.3.4 Thunder Day and Thunder Hour Statistics

Audible thunder is an indication of nearby thunderstorm activity, and its occurrence is recorded routinely at meteorological stations around the world. If thunder is heard one or more times in a day, that day is counted as one "thunder day." These data provide the most readily available and longest-term measurement of world-wide thunderstorm occurrence. A compilation of world-wide thunder day data has been given by the World Meteorological Organization (ref. 9.14) and the isoceraunic level, or number of thunder days per year, is plotted in reference 9.15. Thunder day data from 227 global stations have recently been examined for secular variations during the period 1901 to 1980 (ref. 9.16).

Thunder day statistics for the 33-year period from 1957 to 1989 at KSC are given in tables 9.2 and 9.3 as a function of year, month, and time of day. Figure 9.4 presents the incidence of thunderstorm days (days thunderstorms observed) annually for the United States (ref. 9.17a). Monthly U.S. thunderstorm frequencies can be obtained from reference 9.17b.

For many applications, however, thunder day statistics are inadequate because (1) the duration of lightning activity is unknown, (2) the data do not provide a measure of lightning flashing rates, (3) there is no distinction made between intracloud and cloud-to-ground discharges, and (4) the range of audibility of thunder may be quite variable and depends on station location and atmospheric conditions.

A somewhat more precise measurement of thunderstorm activity is by thunderstorm duration (measured in thunder hours). It is defined as the difference between the time thunder was first heard and a time 15 minutes after the last occurrence of thunder. Since it is the ground flash density (N_g) that is important in lightning protection design, empirical relations have been found to relate thunder days (T_D) and thunder hours (T_H) to N_g. These relations are of the form:

$$N_g = a(T_D)^b$$
$$N_g = c(T_H)^d \ , \qquad (9.1)$$

where the values of the constants a, b, c, and d vary from study to study as indicated in reference 9.10.

9.3.5 Thunderstorm Characteristics

The frequency of thunderstorm durations across the U.S. can be obtained from ref. 9.18, whereas the diurnal variation of U.S. thunderstorms is available from ref. 9.19. A specific climatological study of Florida summer thunderstorms is documented in ref. 9.20. A severe thunderstorm climatology presenting extreme hail-fall and the associated strong winds is given in ref. 9.21. The extreme hail characteristics given in ref. 9.21 are also presented in section 7.5 of this document.

9.4 Cloud-to-Ground Lightning Damage and Protection

Damaging effects due to lightning include human injury or death, forest fires, communication and power system failures, and hazards to civil, commercial, and military aircraft and aerospace vehicles. In order to determine valid protection standards, it is necessary to investigate the basic characteristics of a lightning discharge. Knowledge of lightning currents and radiation fields is fundamental in this understanding, and recent data on these quantities are discussed below. This section will concentrate primarily on ground discharges.

Table 9.2 Number of thunderstorm days at KSC by month, for each year.

	MONTHS												
YEAR	1	2	3	4	5	6	7	8	9	10	11	12	YRSUM
1957	0	0	3	1	12	9	16	15	10	2	1	2	71
1958	1	2	4	3	5	10	8	14	9	2	1	0	59
1959	1	1	2	5	9	11	10	10	11	5	0	0	65
1960	0	2	4	3	6	17	21	11	9	4	0	0	77
1961	0	0	4	3	6	13	8	14	7	2	0	1	58
1962	0	3	3	3	4	17	19	22	10	3	1	0	85
1963	1	1	2	2	8	11	13	14	3	3	1	0	59
1964	0	0	1	4	2	7	9	17	6	0	3	2	51
1965	1	1	5	2	3	13	21	11	2	2	1	0	62
1966	0	1	1	1	14	9	10	11	17	1	0	0	65
1967	0	1	1	0	2	21	23	9	7	1	0	2	67
1968	1	1	2	3	7	12	10	11	6	11	0	0	64
1969	0	1	3	5	8	10	19	18	9	3	1	1	78
1970	0	2	4	1	1	9	15	11	9	2	0	1	55
1971	0	4	4	1	5	20	19	11	6	13	3	1	87
1972	4	3	5	3	10	8	11	17	1	5	3	1	71
1973	1	0	4	4	7	9	13	11	10	1	1	1	62
1974	0	0	3	3	10	16	21	15	12	3	1	1	85
1975	0	0	2	2	10	21	15	18	15	5	0	0	88
1976	0	0	4	0	17	10	19	10	14	1	0	2	77
1977	2	1	1	1	10	13	17	15	12	3	2	3	80
1978	2	0	1	2	8	12	24	6	8	3	1	1	68
1979	1	2	2	1	11	13	16	15	10	2	1	0	74
1980	2	1	0	4	8	13	13	7	9	4	1	0	62
1981	0	2	1	1	5	7	14	14	8	2	0	3	57
1982	1	2	3	6	7	14	17	16	8	1	3	3	81
1983	2	4	4	3	4	13	13	17	8	7	1	6	82
1984	2	3	1	4	6	9	11	10	5	0	3	1	55
1985	0	0	1	4	9	14	13	19	11	10	1	1	83
1986	2	2	4	0	5	16	15	16	7	4	2	1	74
1987	1	3	7	2	5	10	15	10	13	0	5	0	71
1988	1	0	2	2	5	6	13	15	5	2	1	1	53
1989	1	2	3	6	7	17	15	11	9	5	1	0	77
NOBS	1,013	924	1,009	990	1,023	990	1,023	1,023	990	1,023	990	1,023	12,021
N TSTRMS	27	45	91	85	236	410	496	441	286	112	39	35	2,303
PERCENT	2.7	4.9	9.0	8.6	23.1	41.4	48.5	43.1	28.9	10.9	3.9	3.4	19.2

Table 9.3 Percentage frequency of thunderstorms at KSC, during the day, for each month.

HOUR (EST)	1	2	3	4	5	6	7	8	9	10	11	12
0	0.0	0.1	0.5	0.6	0.7	0.9	1.2	2.2	2.6	0.8	0.2	0.1
1	0.1	0.2	0.6	0.4	0.7	0.6	1.1	1.3	2.4	1.4	0.1	0.0
2	0.4	0.0	0.8	0.3	0.7	0.9	0.7	0.7	1.6	1.1	0.3	0.0
3	0.1	0.2	1.0	0.1	0.4	0.9	0.2	0.9	1.3	0.9	0.4	0.1
4	0.3	0.3	0.8	0.2	0.7	1.0	0.6	0.9	1.6	1.1	0.3	0.3
5	0.3	0.3	1.2	0.2	0.4	0.5	0.9	0.5	1.0	0.8	0.2	0.1
6	0.0	0.3	0.7	0.1	0.3	0.8	0.4	1.2	1.3	0.5	0.2	0.1
7	0.0	0.1	0.8	0.3	0.3	0.5	1.4	1.0	1.2	0.5	0.3	0.0
8	0.1	0.1	0.6	0.4	0.3	0.5	1.3	0.8	0.8	0.7	0.2	0.0
9	0.3	0.2	0.6	0.2	0.5	0.5	0.9	1.3	1.2	0.4	0.3	0.2
10	0.2	0.3	0.8	0.5	1.0	1.0	1.0	1.2	2.4	0.3	0.3	0.3
11	0.2	0.5	0.8	0.8	1.8	2.9	2.5	4.1	2.4	0.4	0.2	0.0
12	0.2	0.4	1.2	1.2	3.2	5.0	6.6	5.8	2.2	1.2	0.4	0.5
13	0.1	0.8	1.1	1.7	3.7	9.1	11.7	8.5	4.9	1.1	0.6	0.6
14	0.1	0.3	1.2	1.9	5.3	12.8	17.0	14.0	7.0	1.2	0.5	0.3
15	0.2	0.8	0.8	1.9	5.8	14.0	19.1	16.8	7.6	1.9	0.6	0.7
16	0.3	0.5	1.0	1.8	6.3	14.9	19.5	16.2	6.9	2.2	0.6	0.5
17	0.1	0.6	0.8	1.8	7.4	13.6	18.8	14.0	7.4	1.8	0.6	0.9
18	0.2	0.2	1.3	1.2	7.1	11.4	15.5	12.0	6.4	2.3	0.8	0.5
19	0.4	0.4	1.6	1.4	5.3	8.6	10.7	6.3	6.1	2.5	0.3	0.2
20	0.4	0.6	1.2	1.0	4.6	6.4	6.5	5.6	4.8	1.9	0.5	0.1
21	0.0	0.6	1.1	0.8	3.3	4.3	4.9	3.6	3.8	1.1	0.6	0.1
22	0.1	0.4	0.9	0.9	1.6	2.6	2.6	2.2	3.0	0.9	0.4	0.2
23	0.2	0.4	0.7	0.6	1.4	1.6	2.2	1.9	1.9	0.8	0.3	0.0
NOBS	24,265	22,175	24,190	23,756	24,548	23,758	24,550	24,548	23,758	24,550	23,756	24,539
NTSTRMS	43	84	221	203	640	1,144	1,504	1,255	812	281	92	58
PCT	0.2	0.4	0.9	0.9	2.6	4.8	6.1	5.1	3.4	1.1	0.4	0.2

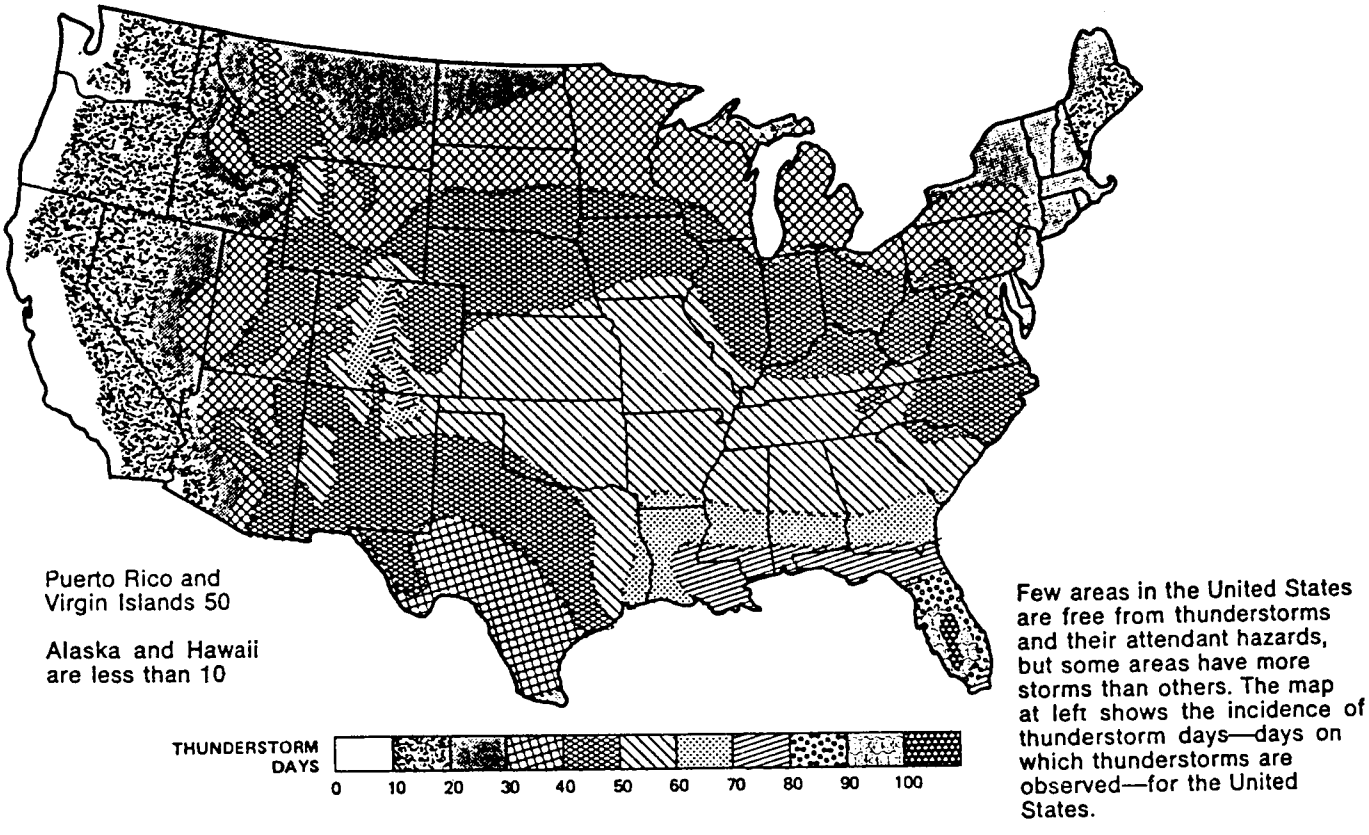

Figure 9.4 Incidence of thunderstorm days, per year (ref. 9.17).

9.4.1 Characteristics of Cloud-to-Ground Discharges

As shown in figure 9.5, a cloud-to-ground lightning begins in the cloud with a preliminary breakdown process that is not well understood. There seems to be fairly good agreement, however, that this process takes place at roughly the 0 °C to –20 °C level in the cloud, in the region from which negative charge is eventually lowered to ground. This initial breakdown is followed by the stepped leader process that lowers negative charge to ground in a series of steps that typically last 1 μs and are each about 50 m in length. As the stepped leader approaches the Earth, the fields near exposed objects on the ground may become large enough that one or more upward discharges are initiated. This begins the attachment process. One or more of the upward connecting discharges will move up to intersect the stepped leader channel, usually a few tens of meters above the ground. The distance between the tip of the stepped leader and the object about to be struck, at the time when the connecting discharge is initiated is referred to as the striking distance and is an important parameter in lightning protection design.

When contact between the stepped leader and the connecting discharge occurs, the first return stroke is initiated; this high-current breakdown wave effectively carries ground potential upward at roughly 1/3 the speed of light. If additional charge is made available in the cloud by J and K processes, a dart leader may propagate down the residual first return stroke channel. Once electrical connection is made between the dart leader and the ground, a second return stroke is possible (second, third, etc., return strokes are collectively referred to as subsequent strokes). Currents that follow return strokes and that persist for up to several hundreds of milliseconds are sometimes observed and are called continuing currents. Table 9.4 summarizes the important physical characteristics of (negative) cloud-to-ground discharges, i.e., those that bring negative charge to Earth as described above.

9.4.2 Lightning Current Damage Parameters

There are several lightning current parameters that are important in assessing the potential for lightning damage: the peak current, i; the peak current derivative, di/dt; the charge transfer (the integral of current over time), Q; and the action integral (the integral of the square of the current over time), $\int i^2 dt$.

For objects that have primarily a resistive impedance, the peak voltage that develops across the object will depend on the peak current. A large voltage that develops at one end or across an object may lead to discharges through the air and around the object (creating a short circuit) or from the object to ground.

For objects and systems that consist primarily of an inductive impedance, such as cabling in electronics systems or electrical connections on printed circuit cards, the peak voltage will be proportional to the time derivative of the current. For example, if a current with a peak di/dt of 1 kA/μs (one hundredth of a typical lightning peak di/dt value) is injected into a straight length of wire with an inductance of 1 μH/m, a voltage of 1,000 V will develop across 1 m of the wire. It is easy to imagine the damage this could produce in solid-state electronic systems that are sensitive to transient voltages in the tens-of-volts range.

The heating or burn-through of metal sheets such as airplane wings or metal roofs is, to a crude approximation, proportional to the charge transferred during a lightning strike. Generally, large charge transfers occur during the long-duration, low-current amplitude portions of lightning discharges such as the continuing current phase, rather than during the short-duration, high-current amplitude return stroke processes.

The heating of electrically conducting materials and the explosion of nonconducting objects is, to a first approximation, determined by the value of the action integral since the quantity $\int i^2 R dt$ is the Joule heating (R is the resistive impedance). Generally, electrical heating vaporizes internal material, and the resulting increase in pressure causes a fracture or explosion to occur.

9.4.3 Tower Measurements of Current

Table 9.5 summarizes typical lightning current parameter values obtained from tower measurements performed atop Mt. San Salvatore in Switzerland (ref. 9.22). The data in parentheses are from tower measurements conducted in Italy (ref. 9.23).

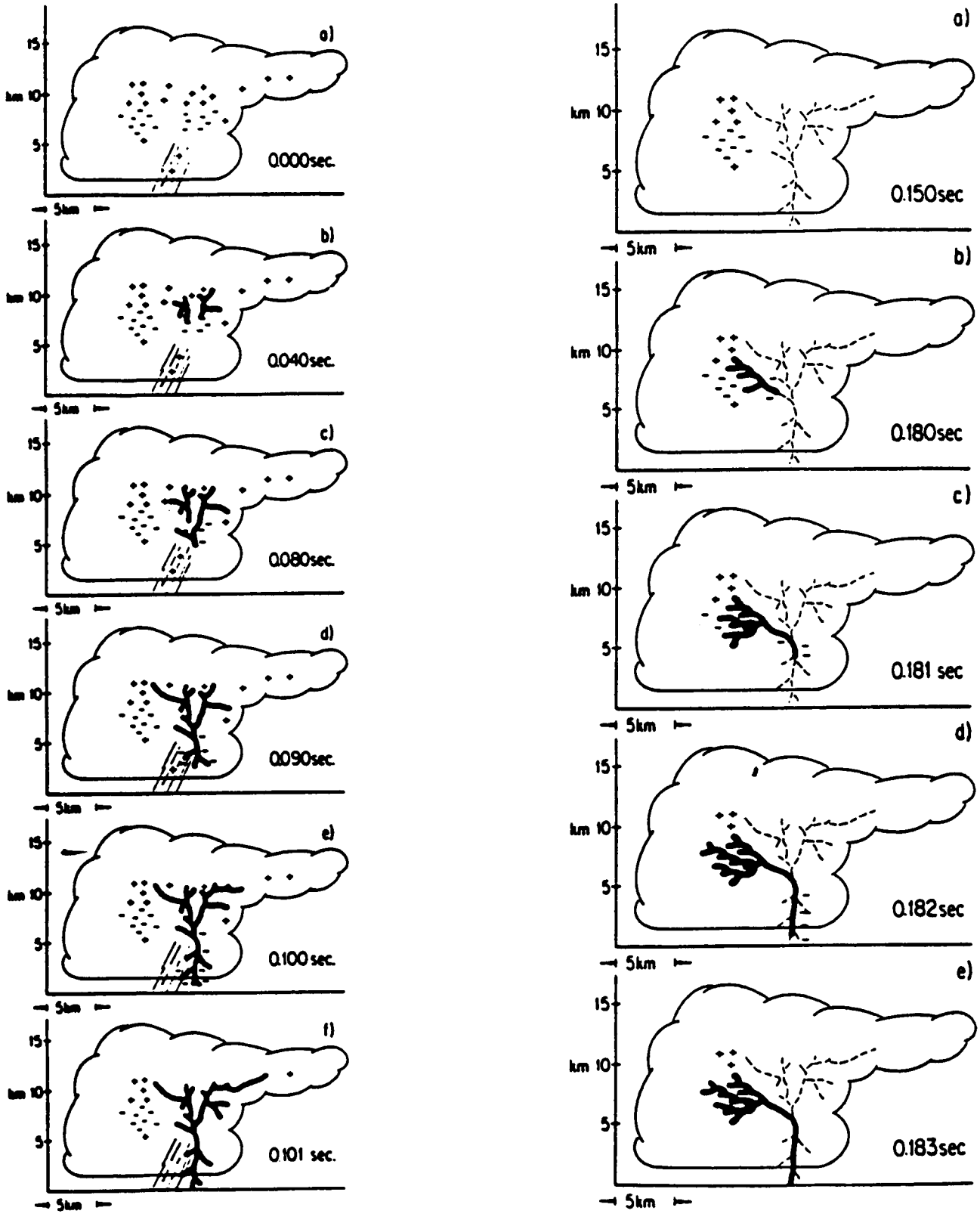

Figure 9.5 First column is a sketch of the luminous processes that form the stepped leader and the first return stroke in a cloud-to-ground lightning flash. Second column shows the development of a lightning dart-leader and a return stroke subsequent to the first in a cloud-to-ground lightning (ref. 9.22).

Table 9.4 Typical negative cloud-to-ground lightning characteristics (adapted from ref. 9.10).

Cloud-to-Ground Flash	
Number of return strokes	3 to 4
Time between return strokes	50 ms
Duration of flash	0.5 s
Charge transferred	25 C
Stepped Leader	
Duration	10 to 30 ms
Step length	50 m
Step interval time	50 μs
Average velocity	1 to 2×10^5 m/s
Step velocity	$>5\times10^7$ m/s
Charge lowered	10 C
Average current	100 to 1,000 A
Peak step current	≥1 kA
Upward Discharge	
Length	10 to 20 m (above flat terrain) 20 to 100 m (above tall structures)
First Return Stroke	
Peak current	10 to 30 kA
Peak current rate of rise	100 kA/μs
Velocity	1×10^8 m/s
Dart Leader	
Duration	2 ms
Average velocity	0.5 to 1×10^7 m/s
Charge lowered	1 C
Average current	1 kA
Dart-Stepped Leader	
Step length	10 m
Step interval time	10 μs
Average velocity	1×10^6 m/s
Subsequent Return Strokes	
Peak current	10 kA
Current rate of rise	100 kA/μs
Velocity	1×10^8 m/s
Continuing Current	
Duration	0.1 s
Current	100 to 300 A
Charge transfer	10 C

Table 9.5 Negative cloud-to-ground lightning current parameters measured in strikes to instrumented towers (refs. 9.22 and 9.23).

Parameter (Units)	Number Events	Percentage of Cases Exceeding Tabulated Value 95%	50%	5%
Peak Current (kA)				
First strokes	101	14	30	80
	(42)		(33)	
Subsequent strokes	135	4.6	12	30
	(33)		(18)	
Peak dI/dt (kA/μs)				
First strokes	92	5.5	12	32
	(42)		(14)	
Subsequent strokes	122	12	40	120
	(33)		(33)	
Charge (C)				
First strokes	93	1.1	5.2	24
Subsequent strokes	122	0.2	1.4	11
Flash (all strokes)	94	1.3	7.5	40
Action Integral (A^2 s)				
First strokes	91	6.0×10^3	5.5×10^4	5.5×10^5
Subsequent strokes	88	5.5×10^2	6.0×10^3	5.2×10^4
Front Duration (μs)*				
First strokes	89	1.8	5.5	18
	(42)		(9)	
Subsequent strokes	118	0.22	1.1	4.5
	(33)		(1.1)	
Stroke Duration (μs)**				
First strokes	90	30	75	200
	(42)		(56)	
Subsequent strokes	115	6.5	32	140
	(33)		(28)	
Time Between Strokes (ms)	133	7	33	150
Flash Duration (ms)				
(including single stroke flashes)	94	0.15	13	1,100
(excluding single stroke flashes)	39	31	180	900

Notes:
*2 kA to peak
**2 kA to half-peak amplitude value

9.4.4 Triggered Lightning Current Measurements

It is often argued that triggered lightning realistically simulates natural lightning and may be used in studies of lightning physics and lightning protection technology. The first successful attempts to trigger lightning over land were performed at the St. Privat d'Allier station in south-central France. In this and similar experiments that followed, a small antihail rocket, approximately 85-cm tall and weighing 2.7 kg, was fired upward into a thundercloud and carried a wire that unspooled from the ground. The rocket developed a maximum speed of about 200 m/s and could reach an altitude of about 700 m in 5 s. Cotton-covered steel wire (0.18-mm diameter) was used. An upward leader was initiated from the top of the rocket when the rocket had reached an altitude of typically 200 to 300 m. A triggering attempt was generally successful if the static field at the ground was equal to or greater than 10 kV/m, though success also depended on the storm and on the amount of natural lightning activity. Rocket heights at the time of initiation were between 50 and 530 m with a mean of 210 m. Fields at the time of successful launches ranged from –6 to –17 kV/m with a mean of 10 kV/m.

Since the initial experiments at St. Privat d'Allier in France, additional experiments have been performed in Japan, New Mexico, and Florida. The results of these experiments are summarized in table 9.6. Note that the four basic lightning current "damage parameters" discussed above are included in the table. These data represent the best estimates of natural lightning peak *di/dt* amplitudes available at the present time.

9.4.5 Inferring Damage Parameters From Lightning Fields

Aside from measuring lightning current parameters directly from tower strikes as sited above, one can infer values of the current and current derivative from measurements of the radiated fields. The variety of discharge processes which occur during a lightning flash generate electromagnetic radiation over a very broad range of frequencies ranging from near dc to microwave band. A variety of lightning processes including leaders, certain intracloud discharges, and return strokes all produce large-amplitude radiation field changes in a fraction of a microsecond. Abruptly changing fields have important implications in the design of lightning protection equipment and are also of interest because they imply large and rapid current variations.

It is only in about the last 10 years that accurate measurements of the fastest lightning field variations have been made. This is due partly to the increased availability of suitable recording equipment. It is due also to the realization that, since high frequency content of lightning fields is degraded by propagation over land, fast-field changes can be adequately observed only if the propagation path from the lightning to the recording station is entirely over salt water.

Figure 9.6 is a schematic representation of simultaneous photographic and electric field measurements for a multiple-stroke, cloud-to-ground lightning flash. This will serve to illustrate typical lightning field variations in different frequency intervals and on different time scales.

Electric field variations below a few tens of megahertz are commonly measured using broadband antenna systems. The sensing element is often a flat conductor which is placed horizontally on the Earth's surface (e.g., ref. 9.24). A current flows to and from the antenna in response to a changing external electric field. The antenna current is then integrated to give an output voltage proportional to E. In "slow antenna" systems, an amplifier decay time constant of several seconds is used. This is several times longer than the duration of the flash, and an accurate record of the entire field change is obtained. "Fast antenna" systems have a shorter decay time constant, typically hundreds of microseconds, so that the amplifier output voltage will recover to near zero between separate events. In this way, the structure of each impulsive component within a discharge can be studied with the full dynamic range of the amplifier.

Note that the schematic slow E-field record is dominated by large transitions produced by the separate return strokes. More slowly varying fields, representing charge transport occurring during leader processes and continuing currents are also detected with slow antenna systems.

Table 9.6 Mean lightning current parameters for rocket-triggered lightning events.*

Parameter (units)	Number of Events	Percentage of Cases Exceeding Tabulated Value 90%	50%	10%	Maximum Value
Peak Current (kA)					
France (a)	94	2	12	29	42
New Mexico (a)	35	4	18	30	40
Florida (1985–1988)	231	5.5	12	26	60
France (1986)	9		13		48
Peak dI/dt (kA/μs)					
Florida (1985)	31	61	102	171	250
Florida (1987, 1988)	74	42	125	215	411
France (1986)	9		78		139
Charge (C) Per Stroke					
New Mexico	35		0.35 (b) 0.95 (c)		
Charge (C) Per Flash					
France	94	4	50	100	140
New Mexico	35	6	35	175	
Action Integral (A^2 s)					
France	94	3×10^2	6×10^3	5×10^4	3×10^5
Flash Duration (ms)					
France	94	70	350	850	1,300
New Mexico	35	250	470	940	
Percentage of Flashes With Only a Continuous Current Phase	France New Mexico	40% 20%			
Number of Pulses Per Flash					
France (b)	94	4	11	15	53
New Mexico (b)	35		10(b) 2(c)		

Notes:
(a) Distribution of only the largest peak current in each flash.
(b) Only pulses with peak currents ≥3 kA were included.
(c) Only pulses with peak currents ≥10 kA were included.

*This table is from data found in refs. 9.40 through 9.46.

The fine structure of large amplitude fast E-field impulses is shown on expanded time scales below the fast E-field record in figure 9.6. These highly time-resolved E-field signatures are complicated by a variety of discharge processes. At the bottom of figure 9.6 is a schematic depiction of VHF lightning radiation such as would be detected using a tuned, narrowband receiver. Radiation at these frequencies is currently being used in time-of-arrival and interferometric systems to locate and follow lightning channel growth and propagation in thunderstorm clouds.

To infer lightning current and current derivative from the radiated fields, one begins by considering the fields emitted by a straight, vertical current element of length H above a perfectly conducting ground (ref. 9.25). The geometry for this calculation is given in figure 9.7. At the ground, at a distance D from the ground-strike point, the field in MKS units is given by:

$$\vec{E}_{\text{total}} = \frac{1}{2\pi\varepsilon_0}\int_0^H (E_R + E_I + E_S)\, dz'\hat{z}\,, \tag{9.2}$$

where

$$E_R = -\frac{\sin^2\alpha}{c^2 R}\frac{\partial i}{\partial t}(z', t-R/c) = \text{radiation term}$$

$$E_I = \frac{(2-3\sin^2\alpha)}{cR^2}\, i(z', t-R/c) = \text{induction term}$$

$$E_S = \frac{(2-3\sin^2\alpha)}{R^3}\int_0^t i(z', \tau-R/c)\, d\tau = \text{electrostatic term}\,.$$

where ε_0 is the permitivity of free space.

The radiation or "far-field" component decays more slowly with distance than the other components and thus becomes dominant at large distances.

It is not possible to solve equation (9.2) for the current in terms of measured electric fields. Rather, it is necessary to assume a functional form for the channel current (a function of time and channel height). If it is possible to adjust current model parameters until good agreement with measured fields and the observed wave front speed is obtained, then the model current is assumed to be a realistic approximation to the true current. A realistic current model would be of practical importance because (1) return stroke currents and statistical distributions of current parameters could be determined from remote measurements of lightning fields, and (2) realistic fields could be calculated for use in "coupling" calculations, such as might be used to determine voltages induced on power lines from a nearby lightning strike.

The model most widely used to derive lightning currents from measured fields is the transmission-line (TL) model (ref. 9.26). The TL model assumes that the current which is measured at the ground propagates up the channel at a constant velocity, without distortion, much as it would along a lossless transmission line. The TL model current has the following functional dependence:

$$\begin{aligned} i(z',t) &= i(0, t-z'/v) \quad z' \le L(t) \\ i(z',t) &= 0 \qquad\qquad z' > L(t) \end{aligned} \tag{9.3}$$

Here, $L(t)$ is the height of the return stroke wavefront at time t. A particularly simple relationship between the currents and the radiation belts, at a distance r, is obtained for the TL model current:

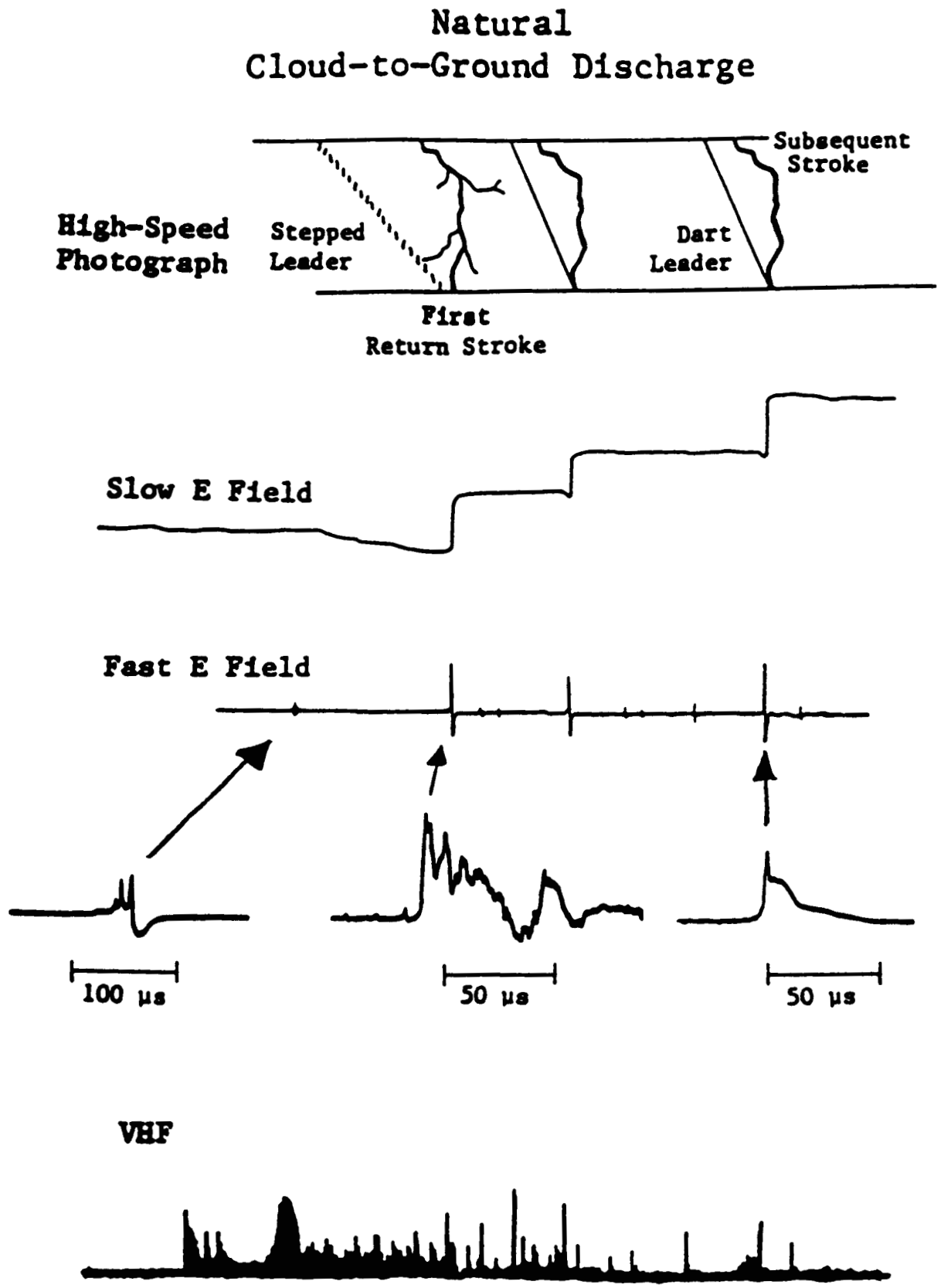

Figure 9.6 Simultaneous photographic and electric field measurements for a multiple stroke, cloud-to-ground lightning flash. The schematic at the bottom is an example of a VHF lightning radiation signature (adapted from ref. 9.10).

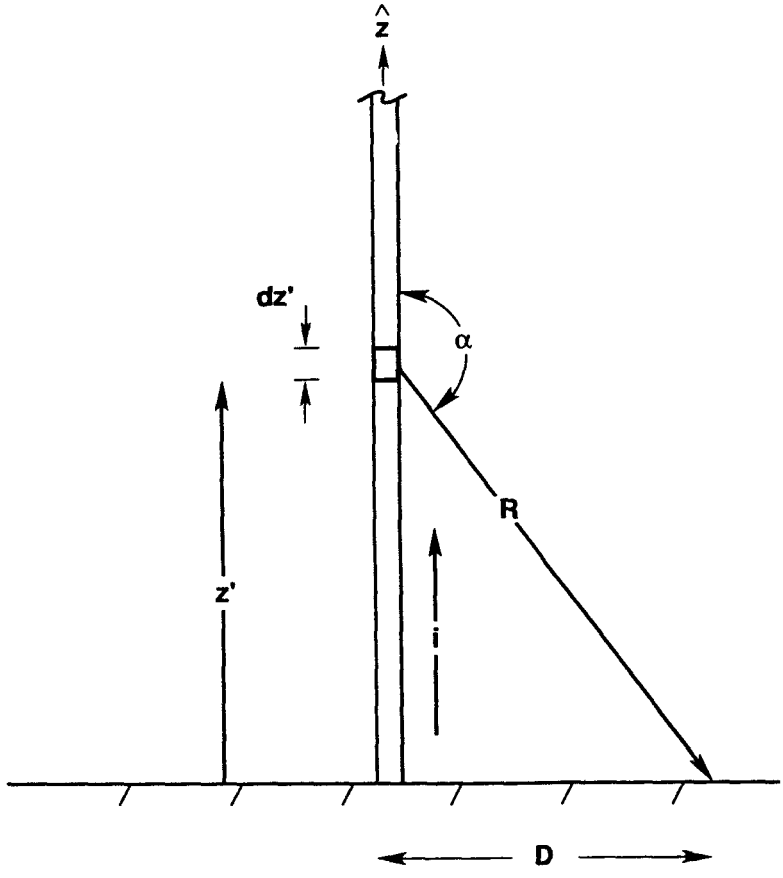

Figure 9.7 Geometry used to infer lightning current characteristics from the radiated field (ref. 9.25).

$$i(t) = \frac{2\pi\varepsilon_0 c^2 r}{v} E_R(r, t+r/c)$$

$$\frac{di}{dt}(t) = \frac{2\pi\varepsilon_0 c^2 r}{v} \frac{dE_R}{dt}(r, t+r/c) \; . \tag{9.4}$$

These equations are the basis for field-inferred current parameters. In the TL model, since the same current wave shape passes all points on the channel, charge is only transferred from the bottom of the channel to the top, and the leader channel is not discharged. There is poor agreement, therefore, between model and measured fields at longer times. In practice, these relations are applied at or before the time of peak return stroke current. Typical value of peak field derivative for cloud-to-ground return strokes is about 40 V/m/μs.

9.5 Lightning Test Standards

In this section we will review lightning current standards that have recently been adopted for the design and verification of lightning protection for aerospace vehicles. The aerospace industry has generally kept better pace with advancements in our understanding of lightning processes and changes in vehicle design

than has been the case for most ground-based systems. Reviews of lightning test standards used in the aerospace industry have been given by reference 9.27. A discussion of lightning protection techniques is beyond the scope of this report. A comprehensive treatment of lightning protection of aircraft may be found in reference 9.28.

9.5.1 Historical Perspective

The first airplane lightning protection test standards were published in the mid-1950's by the Federal Aviation Administration (FAA) (ref. 9.29) and the U.S. Department of Defense (DOD) (ref. 9.30). MIL-B-5087 dealt exclusively with the electrical bonding of aircraft components. Bonding refers to a low-resistance electrical connection between components that is sufficient to withstand lightning currents. At the time, it was generally believed that the damaging effects of lightning were limited to the exterior of the aircraft or structures directly exposed to a lightning strike (see ref. 9.31 for a review of the direct effects of lightning). It was felt that sufficient protection would be provided if these components were adequately bonded to the main air frame. The FAA circular dealt exclusively with the protection of aircraft fuel systems.

Two spectacular incidents in the 1960's indicated clearly that other lightning related effects could lead to catastrophic accidents. On December 8, 1963, a lightning strike ignited fuel in the reserve tank of a Boeing 707 commercial airliner. The left wing of the aircraft was destroyed and 81 people on board were killed. In 1969, Apollo 12 was launched into clouds that had not been producing lightning. The Saturn V rocket artificially triggered two discharges. The lightning strikes produced major system upsets, but only minor permanent damage and the vehicle and crew survived and were able to complete their mission (ref. 9.1). These and accidents motivated the FAA and the DOD to request that the Society of Automotive Engineers (SAE) committee on electromagnetic compatability (SAE-AE4) formulate improved lightning protection design and test standards. The report issued by that group (ref. 9.32) quickly became the standard for the U.S. civil aviation industry. A revision of that report followed in 1978 (ref. 9.33). The 1978 report, given a blue cover, became known as the "blue book" and was adopted for both civil and military aircraft and by foreign certification agencies. The SAE defined lightning environment was formally incorporated into military protection specifications in MIL-STD-1757 (ref. 9.34), and a revision MIL-STD-1757A (ref. 9.35), and by the FAA in advisory circular 20-53A (ref. 9.36).

A panel was also convened in the early 1970's to formulate lightning protection standards for the NASA space shuttle program. The result of that activity was the publication of the "Shuttle Lightning Protection Criteria Document," NSTS-07636 (ref. 9.37). The lightning environment defined in that document predated and differed somewhat from that in the SAE 1978 report, but the key aspects of the current test waveforms were nearly the same.

Several more recent trends in the design of aerospace vehicles have resulted in an increased vulnerability to the indirect effects of lightning. These developments include the use of nonmetallic, lightweight, composite materials in the skin and structure of the vehicle which do not shield the interior of the aircraft as efficiently as a metal body, and an increased reliance on digital flight control electronics as opposed to analog and mechanical systems. In these cases, the lightning damage occurs not as a direct result of the lightning currents, but from spurious signals that are induced or coupled into the interior of the vehicle where they may damage or upset electronic processing equipment (ref. 9.38). A recent example of the hazards associated with indirect lightning effects is provided by the Atlas/Centaur accident which occurred in March 1987 (ref. 9.3). Investigation of that incident determined that the vehicle was struck by a triggered cloud-to-ground flash. The lightning current caused a transient signal to be coupled into the Centaur digital computer unit where data in a single memory location was changed. The computer subsequently issued an erroneous yaw command which resulted in large dynamic stresses being placed on the vehicle and caused the vehicle to breakup.

Indirect lightning hazards have required additional changes in protection design philosophy. Also, in an effort to better evaluate the lightning hazards, new research programs were undertaken in the 1980's by NASA, the U.S. Air Force, the FAA, and the French Government. Experimental results from these studies have been incorporated into the most recent aerospace vehicle lightning standards (refs. 9.4, 9.5, 9.39).

9.5.2 Severe Direct Lightning Strike Current Test Waveforms

Five current component waveforms which would represent a severe lightning strike event are specified in the SAE 1987 report (ref. 9.5) which is the industry standard for transport aircraft. The SAE 1987 test specifications have also been incorporated into a recent revision of the "Shuttle Lightning Protection Criteria Document" (ref. 9.4). The SAE 1987 current waveforms are illustrated in figure 9.8 and consist of:

Component A

This waveform represents a first return stroke with a peak current of 200 kA, and is defined mathematically by:

$$I(t) = I_o(e^{-at} - e^{-bt}) \ , \tag{9.5}$$

where I_o is 218,810 A, a = 11,354 s^{-1}, b = 647,265 s^{-1}, and t is time in seconds. This waveform component has a very large peak current, peak current derivative, and action integral.

Component B

This component represents an intermediate current following the first return stroke. Component B has an average amplitude of 2 kA and transfers 10 C of charge. This component is described by a double exponential of the form shown in equation (9.5) with I_o = 11,300 A, a = 700 s^{-1}, and b = 2,000 s^{-1}.

Component C

This waveform represents a continuing current. Component C is a square waveform with a current amplitude between 200 and 800 A and a duration of 1 to 0.25 s chosen to give a total charge transfer of 200 C. The primary purpose of this waveform is charge transfer.

Component D

Component D represents a subsequent stroke with a peak current of 100 kA. This component is described by a double exponential of the form shown in equation (9.5) with I_o = 109,405 A, a = 22,708 s^{-1}, and b = 1,294,530 s^{-1}.

Component H

Component H is a short duration, high rate of rise current pulse with a peak current amplitude of 10 kA. This test waveform incorporates important characteristics of lightning discharges recorded during triggered strikes to instrumented aircraft in flight. This waveform is also defined by a double exponential with I_o = 10,572 A, a = 187,191 s^{-1}, and b = 19,105 s^{-1}. Component H has a peak current derivative of 2×10^{11} A/s.

Figure 9.9 depicts and lists the key aspects of a current waveform consisting of the sum of components A, B, C, and D. The test values, a peak current of 200 kA, a charge transfer of 200 C, and an action integral of 2×10^{6} A^2 s, occur at the 1-percent level or less in negative ground discharges. Approximately 10 percent of positive ground discharges, however, while generally more infrequent, would be expected to exceed these test values. The peak current derivative test value, 1.4×10^{11} A/s, probably does not represent a severe level test. Referring back to table 9.6, we note that 10 percent of the return strokes triggered in Florida during 1987 and 1988 had current derivatives which exceeded 215 kA/μs. A maximum

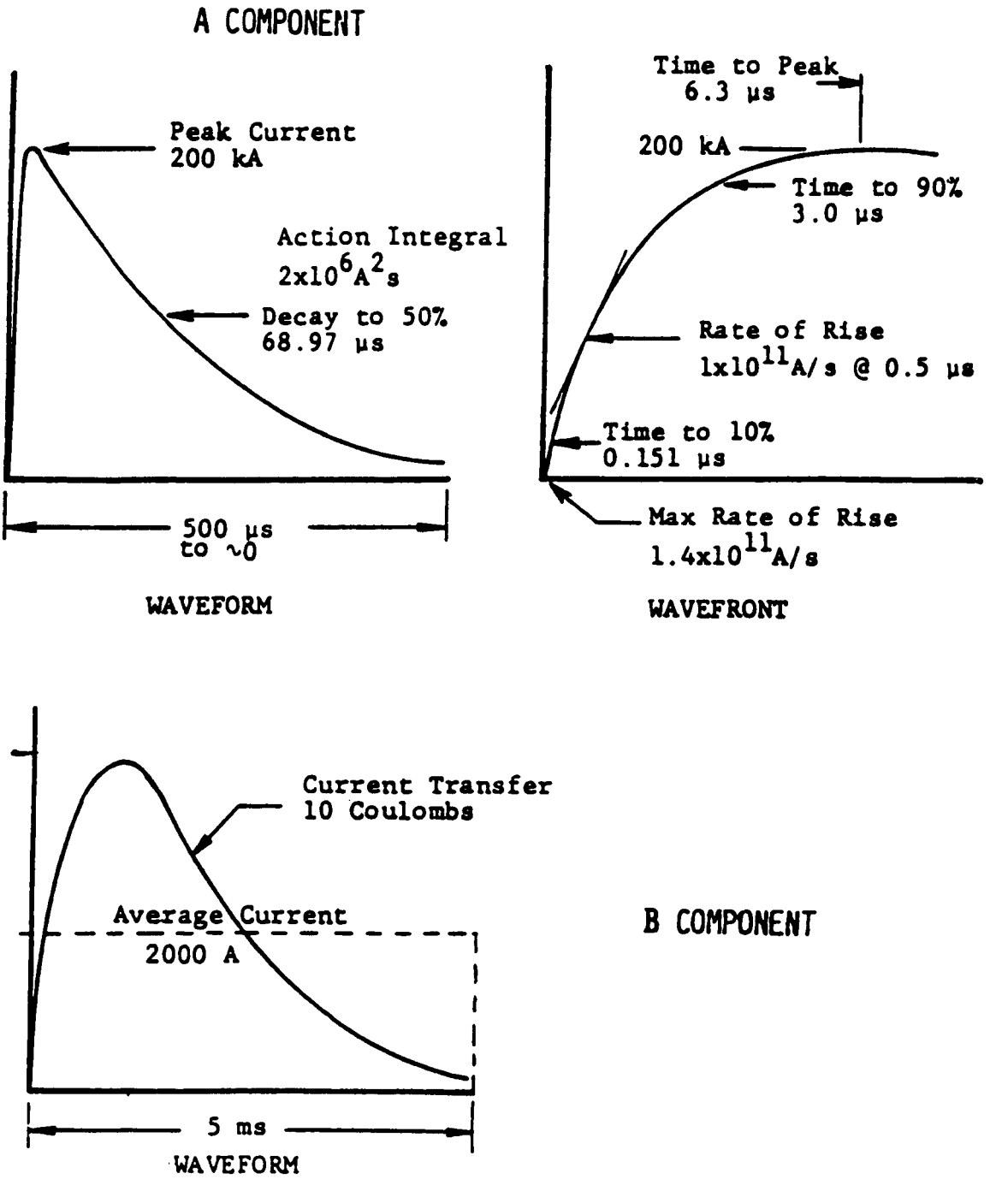

Figure 9.8 The SAE 1987 current test waveforms for severe direct lightning strikes to aircraft (ref. 9.5).

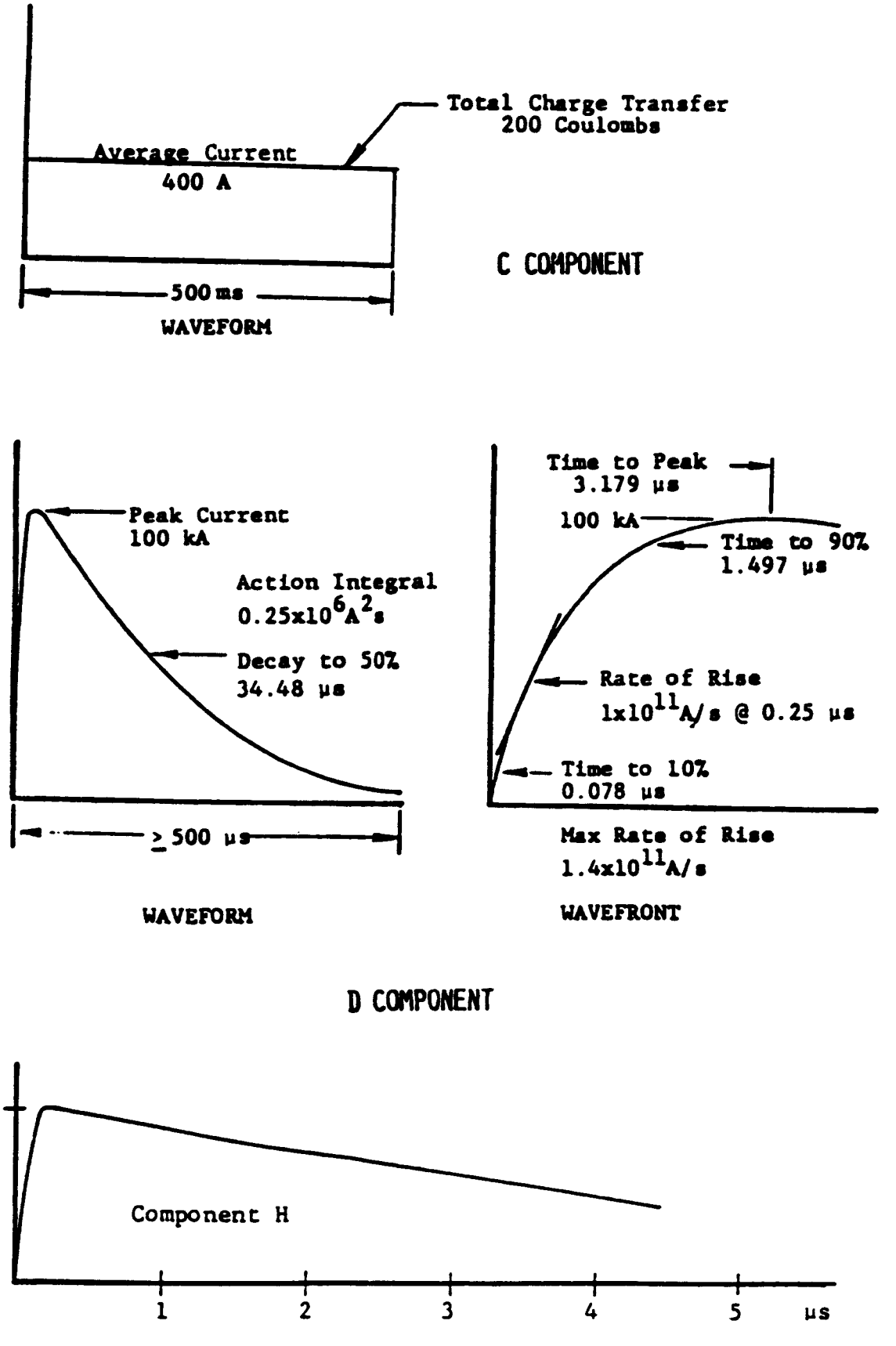

Figure 9.8 The SAE 1987 current test waveforms for severe direct lightning strikes to aircraft (ref. 9.5) (continued).

peak *dI/dt* value of 411 kA/μs has been measured in Florida, for a stroke with a peak current of about 60 kA, and a *dI/dt* value of 380 kA/μs was recorded during measurements conducted with the NASA F-106 aircraft.

A typical ground flash consists of a first return stroke followed by several subsequent strokes. For protection against direct effects, it is adequate to consider only one return stroke (component A or D). For a proper evaluation of indirect effects, such as coupling into the interior of aerospace vehicles, it is necessary to consider the multiple stroke nature of an actual flash. For this purpose, a multiple stroke consisting of a component A current pulse followed by 23 randomly spaced subsequent strokes of 50 kA peak amplitude (component D divided by 2), all occurring within 2 s, has been defined. The multistroke test waveform is illustrated in figure 9.10.

Rapid sequences of pulses with low-peak current amplitude, but large current derivative values, were observed during the lightning strike measurements made with instrumented aircraft. While a single current pulse, like component H, is not likely to cause physical damage, a burst of randomly distributed pulses may cause interference or upset in some systems. A test standard consisting of component H current pulses occurring repetitively, in a 2 s period, in 24 randomly spaced groups of 20 pulses each, has been defined. This multiple burst waveform is illustrated in figure 9.11.

The idealized waveforms described above are appropriate for design analyses. The cost of constructing a simulator capable of delivering these test waveforms to actual vehicles may be prohibitive. In that case, actual testing may involve the use of different waveforms. It must be possible, however, to extrapolate or scale the test results made with the alternate waveforms to the severe hazard level described above.

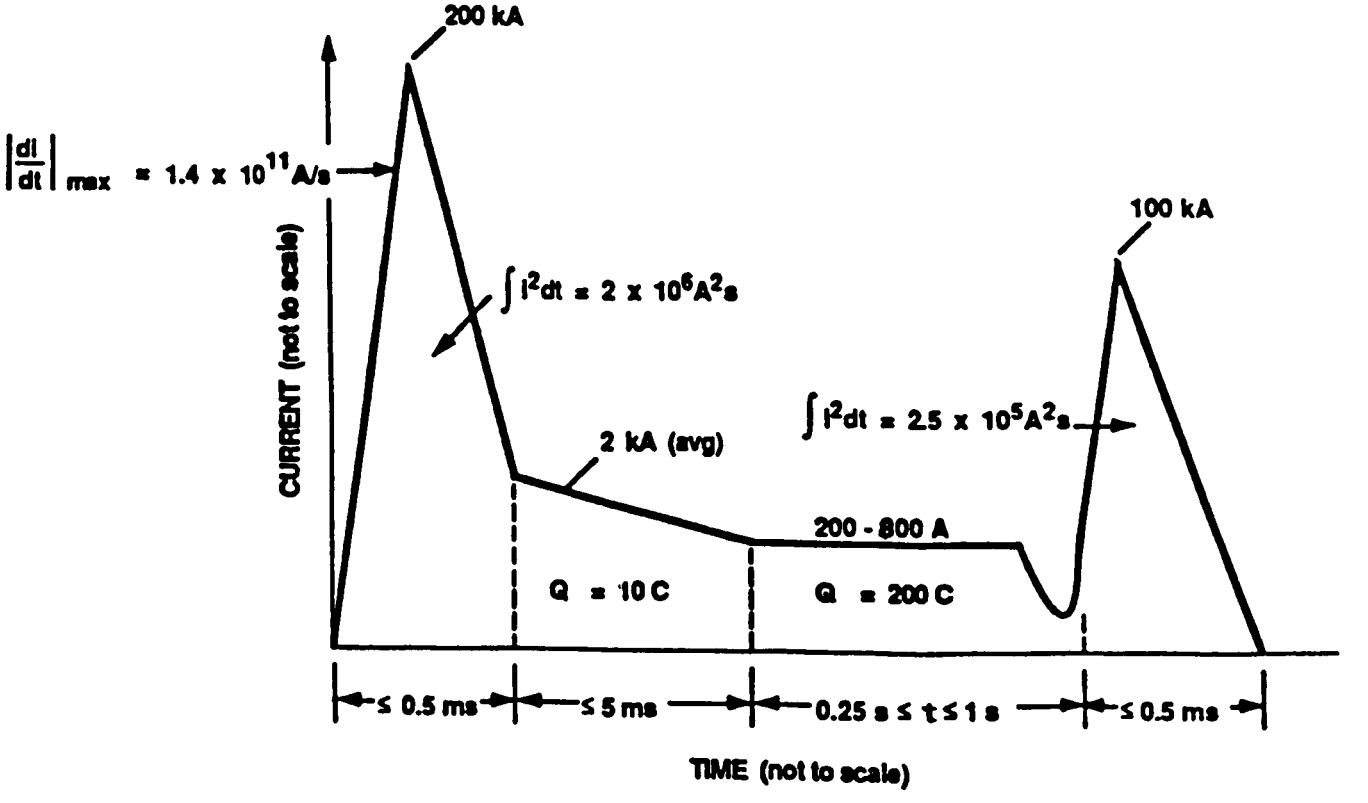

Figure 9.9 Current waveform composed of the four components A, B, C, and D shown in figure 9.8 (ref. 9.5).

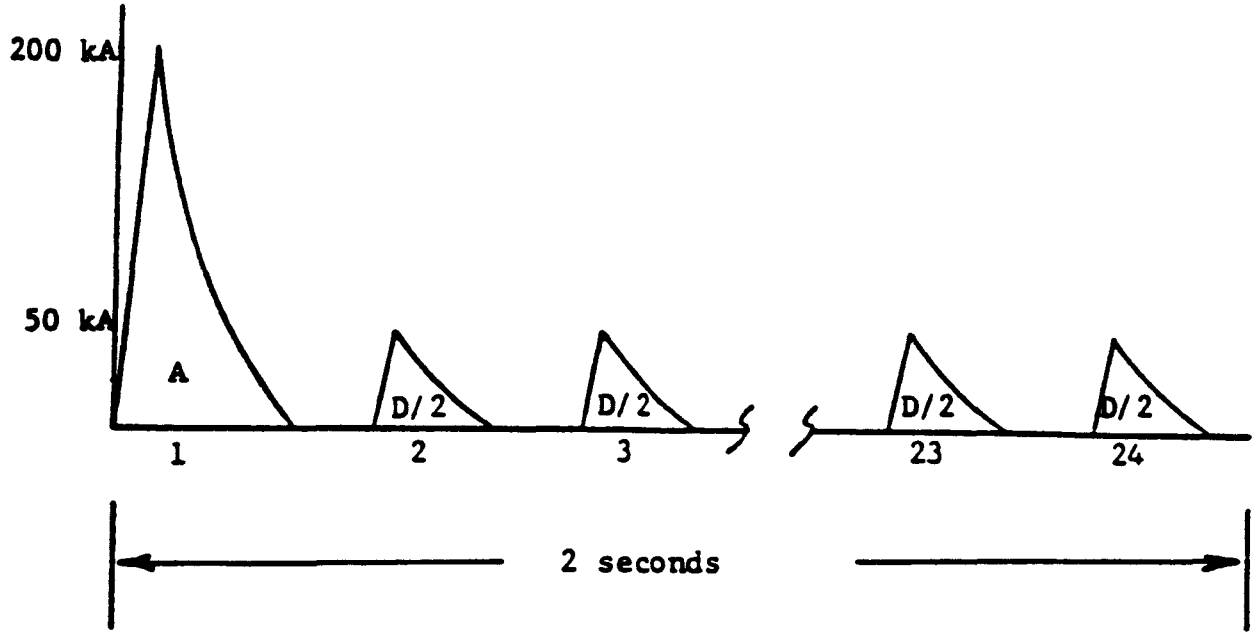

Figure 9.10 Multiple stroke lightning current test waveform consisting of a first stroke (component A) and followed by 23 subsequent strokes (attenuated D components) (ref. 9.5).

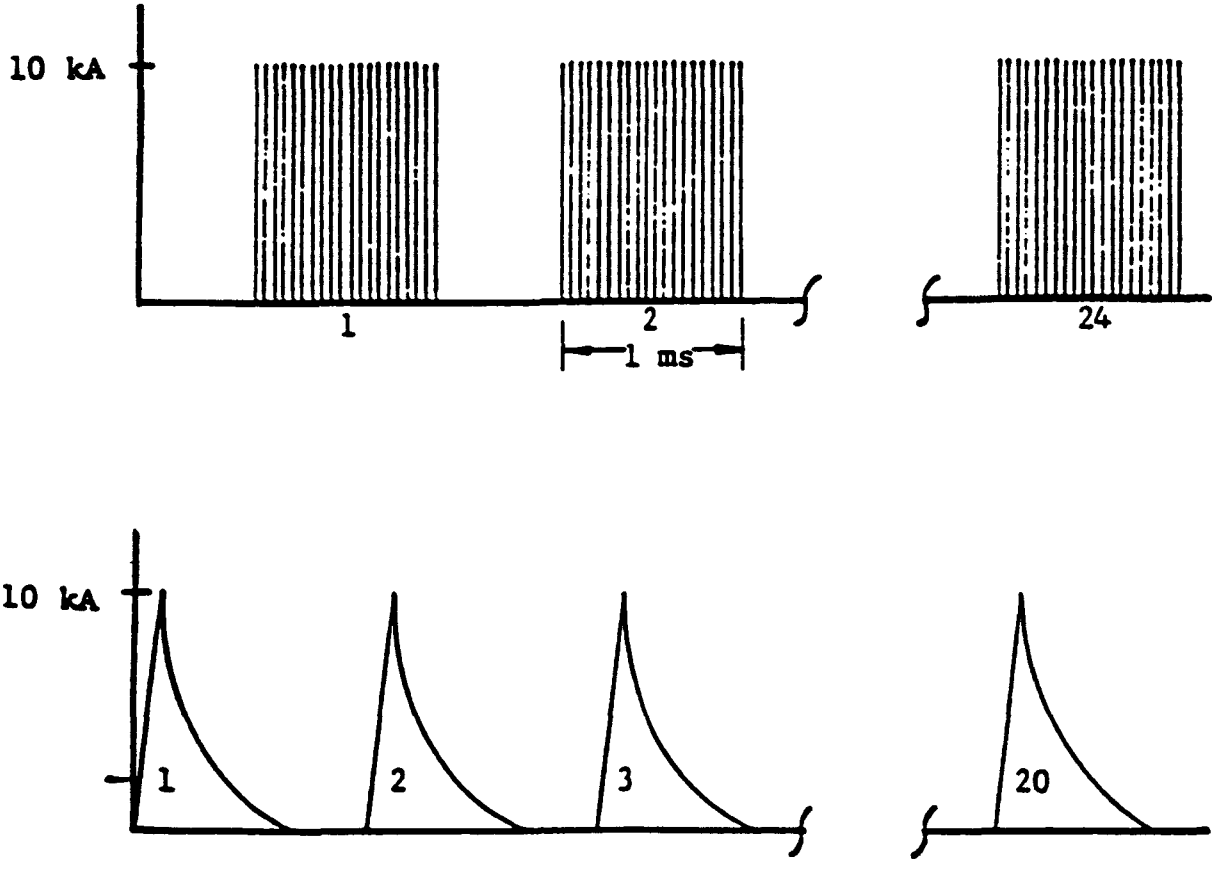

Figure 9.11 A current test waveform composed of 24 bursts (top figure) that are randomly spaced within a 2-s period. Each burst (bottom figure) consists of 20 pulses randomly spaced within a 1-ms period (ref. 9.5).

REFERENCES

9.1 "Analysis of Apollo 12 Lightning Incident," Document No. MSC-01540, prepared jointly by Marshall Space Flight Center, Kennedy Space Center, and Manned Spacecraft Center, National Aeronautics and Space Administration, February 1970.

9.2 Brook, M., Holmes, C.R., and Moore, C.B.: "Lightning and Rockets—Some Implications of the Apollo 12 Lightning Event." Naval Research Reviews, vol. 23, No. 4, April 1970, pp. 1–17.

9.3 Christian, H.J., Mazur, V., Fisher, B.D., Ruhnke, L.H., Crouch, K., and Perula, R.P.: "The Atlas/Centaur Lightning Strike Incident." J. Geophys Res., vol. 94, 1989, pp. 13169–13177.

9.4 National Aeronautics and Space Administration, "Lightning Protection Criteria Document," NSTS-07636, Revision E., Lyndon B. Johnson Space Center, March 18, 1988.

9.5 Society of Automotive Engineers, Recommended Draft Advisory Circular: "Protection of Aircraft Electrical/Electronic Systems Against the Indirect Effects of Lightning," Report of SAE Committee AE-4L, February 4, 1987.

9.6 Beard, K.V.K., and Ochs, H.T.: "Charging Mechanisms in Clouds and Thunderstorms," in The Earth's Electrical Environment, E.P. Krider and R.G. Roble (eds.), National Academy Press, Washington, DC, 1986, pp. 114–130.

9.7 Lhermitte, R., and Williams, E.: "Cloud Electrification." Rev. Geophys. Space Phys., vol. 21, 1983, pp. 984–992.

9.8 Krehbiel, P.R.: "The Electrical Structure in Thunderstorms," in The Earth's Electrical Environment, E.P. Krider and R.G. Roble (eds.), National Academy Press, Washington, DC, 1986, pp. 90–113.

9.9 Koshak, W.J., and Krider, E.P.: "Analysis of Lightning Field Changes During Active Florida Thunderstorms." J. Geophys. Res., vol. 94, 1989, pp. 1165–1186.

9.10 Uman, M..A.: "The Lightning Discharge." Academic Press, Orlando, Florida, 1987.

9.11 Prentice, S.A.: "The Frequency of Lightning Discharges in Lightning," vol. 1, R.H. Golde (ed.), Academic Press, New York, New York, 1977, pp. 465–495.

9.12 Krider, E.P., Noggle, R.C., and Uman, M.A.: "A Gated Wideband Magnetic Direction Finder for Lightning Return Strokes." J. Appl. Meteorol., vol. 15, 1976, pp. 301–306.

9.13 Christian, H.J., Blakeslee, R.J., and Goodman, S.J.: "The Detection of Lightning From Geostationary Orbit," J. Geophy. Res., vol. 94, 1989, pp. 13329–13337.

9.14 WMO, World Distribution of Thunderstorm Days, Part I: Tables, WMO/OMM—No. 21, TP. 6, World Meteorological Organization, Geneva, 1953. (WMO Publications Center, P.O. Box 433, New York, New York 10016.)

9.15 WMO, World Distribution of Thunderstorm Days, Part II: Tables of Marine Data and World Maps, WMO/OMM—No. 21, TP. 21, World Meteorological Organization, Geneva, 1956.

9.16 Changnon, S.A., Jr.: "Secular Variations in Thunder-Day Frequencies in the Twentieth Century." J. Geophys. Res., vol. 90, 1985, pp. 6181–6194.

9.17a "Thunderstorms and Lightning," NOAA/PA 83001 pamphlet, GPO, 1984.

9.17b Changery, M.J.: "National Thunderstorm Frequencies for the Contiguous United States." NUREG/CR-2252, U.S. Nuclear Regulatory Commission, Washington, DC, November 1981.

9.18 Robinson, P.J., and Easterling, D.R.: "The Frequency Distribution of Thunderstorm Durations." Journal of Applied Meteorology, vol. 27, January 1988.

9.19 Easterling, D.R., and Robinson, P.J.: "The Diurnal Variation of Thunderstorm Activity in the United States." Journal of Climate and Applied Meteorology, vol. 24, October 1985.

9.20 Michaels, P.J., et al.: "Composite Climatology of Florida Summer Thunderstorms." Monthly Weather Review, vol. 115, November 1987.

9.21 Kelly, D.L., and Schaefer, J.T.: "Climatology of Nontornadic Severe Thunderstorm Events in the United States." Monthly Weather Review, vol. 113, No. 11, November 1985.

9.22 Berger, K., Anderson, R.B., and Kroninger, H.: "Parameters of Lightning Flashes." Electra, No. 41, 1975, pp. 23–37.

9.23 Garbagnati, E., and Lo Pipero, G.B.: "Parameter von Blitzstromen." Elektrotech. Z., ETA-A, vol. 103, 1982, pp. 61–65.

9.24 Krider, E.P., Weidman, C.D., and Noggle, R.C.: "The Electric Fields Produced by Lightning Stepped Leaders." J. Geophys. Res., vol. 82, 1977, pp. 951–960.

9.25 Uman, M.A., Brantley, R.D., Tiller, J.A., Lin, Y.T., Krider, E.P., and McLain, D.K.: "Correlated Electric and Magnetic Fields From Lightning Return Strokes." J. Geophys. Res., vol. 80, 1975, pp. 373–376.

9.26 Uman, M.A., and McLain, D.K.: "Lightning Return-Stroke Current From Magnetic and Radiation Field Measurements." J. Geophys. Res., vol. 75, 1970, pp. 5143–5147.

9.27 Clifford, D.W., Crouch, K.W., and Schulte, E.H.: "Lightning Simulation and Testing." IEEE Trans. Electromag. Comp., EMC-24, 1982, pp. 209–224.

9.28 Fisher, F.A., Plumer, J.A., and Perala, R.A.: "Lightning Protection of Aircraft." Lightning Technologies Inc., Pittsfield, Massachusetts, 1990.

9.29 Federal Aviation Administration: "Protection of Aircraft Fuels Systems Against Lightning," U.S. FAA Advisory Circular 25-3, Washington, DC, November 10, 1965.

9.30 U.S. Department of Defense: "Bonding, Electrical, and Lightning Protection for Aerospace Systems." U.S. Military Specification MIL-B-5087B, October 15, 1964.

9.31 Plumer, J.A., and Robb, J.D.: "The Direct Effects of Lightning on Aircraft." IEEE Trans. on Electromag. Comp., EMC-24, 1982, pp. 158–172.

9.32 Society of Automotive Engineers: "Lightning Test Waveforms and Techniques for Aerospace Vehicles and Hardware." Report of SAE Committee AE-4, Special Task F, May 5, 1976.

9.33 Society of Automotive Engineers: "Lightning Test Waveforms and Techniques for Aerospace Vehicles and Hardware." Report of SAE Committee AE-4L, June 20, 1978.

9.34 U.S. Department of Defense: "Lightning Qualification Test Techniques for Aerospace Vehicles and Hardware." U.S. Military Standard MIL-STD-1757, June 17, 1980.

9.35 U.S. Department of Defense: "Lightning Qualification Test Techniques for Aerospace Vehicles and Hardware." U.S. Military Standard MIL-STD-1757A, 20 June 1983.

9.36 Federal Aviation Administration: "Protection of Airplane Fuel Systems Against Fuel Vapor Ignition Due to Lightning." U.S. FAA Advisory Circular 20-53A, Washington, DC, April 12, 1985.

9.37 National Aeronautics and Space Administration: "Lightning Protection Criteria Document," NSTS-07636, Lyndon B. Johnson Space Center, 1973.

9.38 Perala, R.A., Rudolph, T., and Eriksen, F.: "Electromagnetic Interaction of Lightning With Aircraft." IEEE Trans. on Electromag. Comp., EMC-24, 1982, pp. 173–203.

9.39 U.S. Department of Defense: "Lightning Protection of Aerospace Vehicles and Hardware," DOD Standard DOD-STD-1795, May 30, 1986.

9.40 Saint Privat d'Allier Research Group: "Eight Years of Lightning Experiments at Saint Privat d'Allier." Revue Generale de l'Electricite, No. 9, 1982, pp. 561–582.

9.41 Hubert, P., Laroche, P., Eybert-Berard, A., and Barret, L.: "Triggered Lightning in New Mexico." Journal of Geo. Research, vol. 89, 1984, pp. 2511–2521.

9.42 Leteinturier, C., Weidman, C., and Hamelin, J.: "Current and Electric Field Derivatives in Triggered Lightning Return Strokes." Journal of Geo. Research, vol. 95, 1990, pp. 811–828.

9.43 Eybert-Berard, L., Barret, L., and Berlandis, J.P.: "Campagne Foudre aux Etats Unis, Kennedy Space Center (Florida), Programme RTLP 85." Report SST/ASP 86-01. Centre d'Etudes Nucleaires de Grenoble, Box 85 X, 38041 Grenoble Cedex, France, 1986 (in French).

9.44 Barret, L., Boulay, G., and Eybert-Berard, A.: "Campagne Foudre RTLP 86, Kennedy Space Center (Florida) USA, Recueil des Resultats Bruts au 01.12.86." Report STT/ASP 86-12/LB-mA. Centre d'Etudes Nucleaires de Grenoble, Box 85 X, 38041 Grenoble Cedex, France, 1986 (in French).

9.45 Eybert-Berard, A., Barret, L., and Berlandis, J.P.: "Campagne d'Experimentations Foudre RTLP 1987 (NASA Kennedy Space Center, Florida, USA)." Report STT/Lasp 88-21-AEB/LB/JPB-pD. Centre d'Etudes Nucleaires de Grenoble, Box 85 X, 38041 Grenoble Cedex, France, 1988 (in French).

9.46 Eybert-Berard , A., Barret, L., Berlandis, J.P., and Terrier, G.: "Characterisations des Decharges Electomagnetiques Provoquees, Campagne RTLP 1988, NASA Kennedy Space Center, Florida (USA)." Report STT/LASP 89-21/AEB/LB/JPB/GT-pD. Centre d'Etudes Nucleaires de Grenoble, Box 85 X, 38041 Grenoble Cedex, France, 1989 (in French).

SECTION X. ATMOSPHERIC CONSTITUENTS

10.1 Introduction

Gases and particles in the atmosphere must be considered during aerospace vehicle development in order to avoid detrimental effects to the vehicle on the ground or in flight. Some of these effects include corrosion, abrasion, and optical hinderances. These effects are explained later in this section. The intensity of damage depends on the source (type), location, and concentration of the particles. The particles together with the air that suspends them are termed aerosols.

10.1.1 Sources of Particles

Airborne particles develop from both primary (direct) and secondary (indirect) sources (ref 10.1).

10.1.1.1 Primary Sources

a. Meteorites—extraterrestrial or interplanetary dust

b. World Oceans—sea-salt particles

c. Arid and Semiarid Regions—soil dust, road dust, etc.

d. Terrestrial Materials—volcanic debris

e. Terrestrial Biota—biological material

f. Combustion—carbonaceous materials, ash.

10.1.1.2 Secondary Source

The secondary source of atmospheric particles is gas to particle conversions (GPC) where chemical reactions convert natural and man-made atmospheric trace gases into liquid and solid particles.

10.1.2 Distribution of Particles

The distribution of aerosols is regionally dependent. Particles may have a "local" distribution as well as a "regional" distribution. The "local" aerosol takes place in the area surrounding factories, volcanoes, and other direct sources of aerosol. Since this aerosol can greatly affect an aerospace facility, the site should be surveyed for possible problems. Factors such as wind speed, distance from source, altitude, and particle size play an important part in determining the makeup and concentration of a "local" aerosol. These same factors also affect "regional" aerosol. On a regional scale, number concentrations of particles in the atmosphere increase rapidly with decreasing particle size, to sizes smaller than 0.1 μm radius. Work cited in references 10.2 and 10.3 shows that the concentrations and size distributions are highly variable with altitude. Some examples of these variations are given in subsection 10.3.

Natural aerosol size distribution is trimodal and dependent on number, surface, and volume. Aerosol particles ranging from 0.1 to 1.0 μm are in the "accumulation mode" because they tend to grow from smaller particles by coagulation or condensation. The "transient mode" consists of particles around 0.01 μm, usually resulting from combustion or anthropogenic nuclei sources. Dust, fly-ash, sea spray, and other particles that are larger than 1 μm make up the "coarse particle mode." This mode is usually derived from mechanical processes (ref. 10.4).

10.1.3 Upper Atmospheric Aerosols

Atmospheric aerosols can exist at stratospheric levels (15- to 30-km altitude) as well as in the troposphere. The stratospheric aerosols, consisting mainly of liquid sulfuric acid droplets, are divided into three catogories: (1) background aerosols, (2) volcanic aerosols, and (3) polar stratospheric cloud particles (PSC's) (ref. 10.5). Section 8.5.1.1 gives more information regarding PSC's. Table 10.1 presents the basic characteristics of stratospheric aerosols.

Table 10.1 Characteristics of stratospheric aerosols (ref. 10.6).

Particle Type	Sulfate Aerosol	Type-I PSC	Type-II PSC	Meteoric Dust	Rocket Exhaust
Physical state	Liquid or slurry with crystals	Solid nitric acid trihydrate, solid solutions	Solid crystal, hexagonal or cubic basis	Solid granular irregular or spherical	Solid spheres or irregular surface ablated debris
Particle radius (μm, 10^{-6} m)	0.01 – 0.5, Amb. 0.01 – 10, Volc.	0.3 – 3	1 – 100	1 – 100, Micro-meteorites 0.01 – 0.1, smoke	0.1 – 10
Number (# cm^{-3})	~1 – 10	~0.1 – 10	<<1	10^{-6}, 100 μm 10^{-3}, 1 μm	10^{-4}, 10 μm 10^{-2}, 1 μm
Principal composition	H_2SO_4/H_2O ~70%/30%	HNO_3/H_2O ~50%/50%	H_2O	SiO_2, Fe, Ni, Mg; C	Al_2O_3
Trace composition	NH_4^+, NO_3	HCl SO_4^{2-}	HNO_3, HCl	SO_4^{2-} (surface)	Cl^-, SO_4^{2-} (surface)
Physical characteristics	Dust inclusions, in solution	Equidimensional crystalline or droplets	Elongated crystals with polycrystalline structure	Irregular mineral grains, grain defects	Homogeneous composition; smooth spheres
Distribution	Global, Amb. Region, Volc, 12–35 km alt.	Polar winter 14–24 km alt.	Polar winter 14–24 km alt.	~Global >12 km alt.	Global >12 km alt.
Residence Time	~1–2 yr. Amb. ~1–3 yr. Volc.	~1 day to weeks	~ hours	<1 mo. (micro-meteorites) 1–10 yr. (meteoritic smoke)	<1 yr.

Background aerosols are those aerosols observed under normal stratospheric temperatures higher than 195 K (not volcanic) and are primarly supercooled H_2SO_4 (75 percent by weight) in H_2O solution. They are formed by heterogeneous nucleation on preexisting particles. Small amounts of ammonium ions or meteoritic material may also be present.

Large volcanic eruptions can inject both sulfurous gases and ash (radii <3 μm) into the stratosphere. These gases are responsible for the rapid generation (within a few weeks or months) of sulfuric acid aerosols which remain at stratospheric levels for several months or even years. The exponential 1/e decay time for the integrated aerosol backscattering was found to range between 12 and 18 months. Low levels of other species

such as chlorine and NO_x can also be observed. Abundant halide particles (radii of 2 to 3 μm), probably derived from the chlorine-rich alkali magma, are also present (ref. 10.5).

The size distributions of volcanic aerosols (shown in figure 10.1 for an El Chichon simulation) exhibit a tri-modal structure that evolves with time. The principal size modes are: (1) a nucleation mode, which is most prominent at early times and at sizes near 0.01 μm; (2) a sulfate accumulation mode, which evolves initially from the nucleation mode (by coagulation and condensation) and increases in size to about 0.3 μm after 1 year; and (3) a large-particle "ash" mode (of solid mineral and salt particles) that settles out of the layer in 1 or 2 months. A primary feature of the volcanic aerosol size distribution after several months is a greatly enhanced sulfate accumulation mode. The increased aerosol size is caused by accelerated growth in the presence of enhanced sulfuric acid vapor concentrations that are maintained by continuing SO_2 chemical conversion (ref. 10.6).

PSC's form when aerosol particles encounter cold temperatures (<195 K) in wintertime polar regions and are formed by excess condensation of water vapor on background stratospheric sulfate particles. Nitric and hydrochloric acids may also be impinging onto the PSC particles. Section VIII provides a more in-depth study of PSC's.

Aerosol particles with a radius greater than 0.1 μm typically obey a size distribution of the form (ref. 10.4);

$$n(r) = dN/d(\log r), \tag{10.1}$$

where

r = radius of particle

dN = number of particles in the radius interval $d(\log r)$.

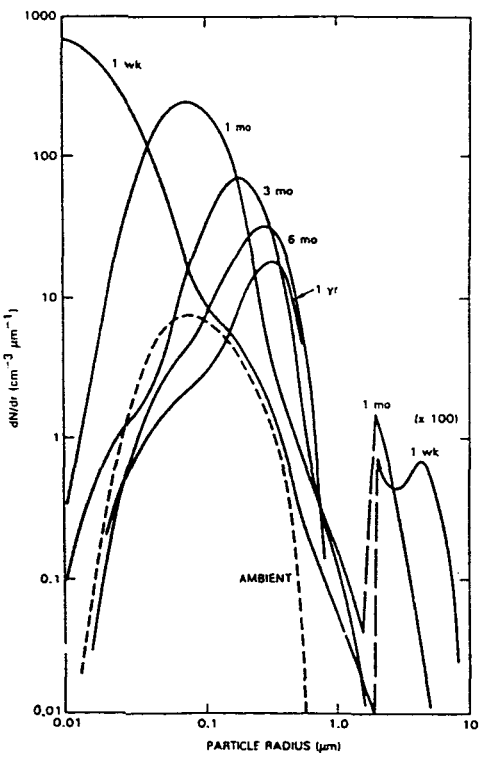

Figure 10-1. Evolution of the volcanic aerosol size distribution at 20 km in the simulated El Chichon eruption cloud. Size distributions are shown at various times, and are compared to the ambient size distribution (ref. 10.6).

10.2 Threats Caused by Atmospheric Particles

Abrasion, optical hindrances, and corrosion are the main problems caused by gases and airborne particles that must be considered during aerospace vehicle development. For an example of specific launch related threats, refer to subsection 10.3.5.

10.2.1 Abrasion

When an aerosol exists around an object, the particles usually follow the airflow around the object. However, if the momentum of the particles is sufficiently great, they will deviate from the flow path to impact the surface. Whether or not impaction occurs depends on the particle size, shape, and density and on air density; the relative speed of the aerosol and object; and the size and shape of the object. Impaction theory is reviewed in reference 10.7. The greater the size and density of the particles and the greater the relative aerosol velocity, the greater is the likelihood of impact.

The effect of the impact depends on the physical characteristics of the particle, and the impact surface, the velocity of the particle, and the angle of impact. Direct impact of dry particles on a surface may cause abrasion, and, when voids are filled with dry particles, they may interfere with or cause wear on moving parts. Particles may also clog various mechanisms or produce electrical shorts.

The degree of hardness, i.e. the resistance offered by a mineral to abrasion or scratching, is often compared using the Mohs' scale of hardness. This scale of mineral hardness was devised in 1822 by a German mineralogist, Fredrich Mohs, and has been used since because of its simplicity and usefulness. This scale is made up of a number of minerals of increasing hardness, as given in table 10.2 with a comparison of other materials given in table 10.3 (ref. 10.8). A complete listing as well as mineral breaking or cleaving shapes can be found in reference 10.9.

The Mohs' scale of hardness is used as a guide to determine which materials will abrade or scratch other materials. A material can be scratched by another material of the same hardness or a higher hardness number.

Two minerals included in table 10.3 are halite (NaCl) and kaolinite ($H_4Al_2Si_2O_9$). Halite, a naturally occurring salt, indicates the general hardness of sea-salt particles. Although NaCl is usually cube-shaped, it may be an irregular shape if broken. Kaolinite, an aluminum silicate, is a common clay mineral (usually a crystal plate) which makes up many of the fine particles in the air from sandy soils.

Table 10.2. Mohs' scale-of-hardness for minerals.

Moh's Relative Hardness	Mineral
1	Talc
2	Gypsum
3	Calcite
4	Fluorite
5	Apatite
6	Orthoclase
7	Quartz
8	Topaz
9	Carborundum
10	Diamond

Table 10.3. Mohs' hardness values for some other materials.

Material	Hardness
Lead	1.5
Aluminum	2–2.5
Halite (sea-salt)	2–2.5
Kaolinite	2–2.5
Zinc	2.5
Copper	2.5–3
Gold	2.5–3
Brass	3–4
Iron	4–5
Platinum	4.3
Glass	4.5–6.5
Steel	5–8.5
Volcanic Ash	6–7

The larger and harder sand particles, primarily quartz (SiO_2), are usually rounded but may be jagged. Volcanic ash particles, consisting of SiO_2, orthoclase ($KAlSi_3O_8$) and various other minerals, are usually jagged. Gypsum particles, ($CaSO_4$, $2H_2$), are at times raised by winds over arid areas, especially in the White Sands, New Mexico area which is almost entirely gypsum. Most smog particles are droplets of soft organic particles or salts, although some harder particles such as fly ash from power plants may be present.

A discussion of rain erosion is covered in section VII.

10.2.2 Optical Hindrances

Atmospheric aerosols affect optical properties in a variety of ways. The optical effects of an aerosol depend on the sizes, optical constants, and shapes of the aerosol (ref. 10.10). One of the most evident manifestations of air pollution is the production of haze which causes a reduction in visibility or visual range. Other particles may coat optical and transparent surfaces to affect visibility. The effect of aerosols on optical and infrared transmission can be assessed using the LOWTRAN 7 computer code.

10.2.3 Corrosion

Certain atmospheric gases may cause engineering metals to react chemically and cause atmospheric corrosion. Atmospheric corrosion is the degradation of a material exposed to the air and its pollutants and is the cause of more failures in terms of cost and tonnage than any other single environment. The basic types of atmospheric corrosion are often classified and defined as follows (ref. 10.11):

a. Dry corrosion—Corrosion which occurs in the absence of moisture. Usually, this corrosion occurs very slowly unless elevated temperatures exist.

b. Damp corrosion—Corrosion occurring when there is some moisture in the air. When the relative humidity reaches a specific critical value, around 70 percent, a thin layer of moisture on the metal surface provides an electrolyte for current transfer, and consequently increases the rate of corrosion.

c. Wet corrosion—Visible water layers caused by sea spray, dew, or rain cause wet corrosion. Wet corrosion usually occurs most rapidly due to the high conductivity.

10.2.3.1 Rate of Atmospheric Corrosion

The rate of atmospheric corrosion depends on many different atmospheric variables. Some of these variables are temperature, humidity, and other climatic conditions, as well as surface shape and properties. Table 10.4 provides average corrosion rates over 10- and 20-year intervals for certain surface metals (ref. 10.11).

Table 10.4 Average atmospheric-corrosion rates of various metals for 10- and 20-year exposure times (ref. 10.11).

Corrosion rates are given in mils/yr (1 mil/yr = 0.025 mm/yr). Values cited are one-half reduction of specimen thickness.

Metal	Atmosphere					
	New York, NY (Urban-Industrial)		La Jolla, CA (Marine)		State College, PA (Rural)	
	10	20	10	20	10	20
Aluminum	0.032	0.029	0.028	0.025	0.001	0.003
Copper	0.047	0.054	0.052	0.050	0.023	0.017
Lead	0.017	0.015	0.016	0.021	0.019	0.013
Tin	0.047	0.052	0.091	0.112	0.018	...
Nickel	0.128	0.144	0.004	0.006	0.006	0.009
65% Ni, 32% Cu, 2% Fe, 1% Mn (Monel)	0.053	0.062	0.007	0.006	0.005	0.007
Zinc (99.9%)	0.202	0.226	0.063	0.069	0.034	0.044
Zinc (99.0%)	0.193	0.218	0.069	0.068	0.042	0.043
0.2% C Steel(a) (0.02% P, 0.05% S, 0.05% Cu, 0.02% Ni, 0.02% Cr)	0.48	...	...	...	...	...
Low-Alloy Steel(a) (0.1% C, 0.2% P, 0.04% S, 0.03% Ni, 1.1% Cr, 0.4% Cu)	0.09	...	...	...	...	...

10.2.3.2 Protection From Atmospheric Corrosion

Prevention from atmospheric corrosion can be temporary or permanent. During transport or storage, lowering the atmospheric humidity by artificial methods may temporarily prevent corrosion. Changing the surface material or applying a coating can provide a longer term solution. In determining the materials, the type of environment must be considered. Table 10.5 and table 10.6 list the corrosivities for iron, steel, and zinc for various environments (ref 10.12).

10.3 Characteristics of Specific Particles

Included in this section are characteristics of some particles that should be considered in aerospace vehicle design. Table 10.7 gives estimates of the sizes of various particles (refs. 10.1 and 10.13), but the actual sizes may vary greatly depending on the specific atmospheric conditions. Typical sizes for suspended water droplets (fog) can be found in section VII.

Table 10.5 Relative corrosivity of atmospheres at different locations (ref. 10.12).

Location	Type of Atmosphere	Average Weight Loss of Iron Specimens in 1 Year mg/cm^2	Relative Corrosivity
Khartoum, Sudan	Dry island (arid)	0.08	1
Singapore	Tropical/marine	0.69	9
State College, PA	Rural	1.90	25
Panama Canal Zone	Tropical/marine	2.28	31
Kure Beach, NC (250-m, or 800-ft, lot)	Marine	2.93	38
Kearny, NJ	Industrial	3.92	52
Pittsburgh, PA	Industrial	4.88	65
Frodingham, UK	Industrial	7.50	100
Daytona Beach, FL	Marine	10.34	138
Kure Beach, NC (25-m, or 80-ft, lot)	Marine	35.68	475

Table 10.6 Measured atmospheric-corrosion rates for steel and zinc (ref. 10.12).

Site	Location	Type of Atmosphere	Relative Corrosivity	
			Steel	Zinc
1	Normal Wells, Northwest Territory	Rural	0.02	0.2
2	Saskatoon, Saskatchewan	Rural	0.2	0.2
9	State College, PA(a)	Rural	1.0	1.0
17	Pittsburgh, PA (roof)	Industrial	1.8	1.5
18	London (Battersea), UK	Industrial	2.0	1.2
27	Bayonne, NJ	Industrial	3.4	3.1
28	Kure Beach, NC (250-m, or 800-ft, site)	Marine	3.6	1.9
31	London (Stratford), UK	Industrial	6.5	4.8
33	Point Reyes, CA	Marine	9.5	2.0
37	Kure Beach, NC (25-m, or 80-ft, site)	Marine	33.0	6.4

(a) The average weight losses on two 100- by 150-mm (4- by 6-in) specimens after 1 year of exposure at the indicated site were used to calculate the relative corrosivity of the site. The losses in the rural atmosphere at State College, PA, were taken as unity and the relative corrosiveness at each of the other sites is given in this table as a fraction or a multiple of unity.

Table 10.7 Estimated size ranges of natural occurring atmospheric particles.

Particle Type	Radii Size (μm)
Extraterrestrial	0.1–1,000
Sea-Salt	0.02–60
Crustal Aerosol	0.02–100
Volcanic Ash[1]	0.1–10
Combustion and Secondary Particles (average)	<1.0
Indirect Sources	under 0.1

[1]Directly after the eruption particles as large as 5 mm can be found (ref. 10.13).

10.3.1 Extraterrestrial Dust

Extraterrestrial dust is usually formed by the breakup of meteoroids and orbital debris. It reaches the troposphere through processes such as gradual sedimentation, stratospheric subsidence, followed by a rapid pursing from the stratosphere into the troposphere in the "stratospheric folds." Within the troposphere, the extraterrestrial dust is concentrated around the polar regions. The larger dust particles are "fluffy and compacted aggregates" while the smaller particles (submicrometer) are more dense (ref. 10.1). The residence time for these particles in the stratosphere and troposphere ranges from months to years.

10.3.2 Sea-Salt Particles

Sea-salt particles are the most common aerosol component (ref. 10.1). Most airborne sea-salt droplets are formed by the breaking of myriads of air bubbles at the surface of the sea. The bubbles are produced by the breaking of small waves or the larger surf, and, to a lesser extent, by rain or snow falling on the water. The droplets, thus formed, evaporate when the humidity falls below 75 percent. If humidities above 75 percent are encountered, the sea-salt particles become droplets again (ref. 10.14).

Atmospheric temperature inversions over the oceans, such as the tropical inversion, tend to keep sea-salt particles below a few kilometers in altitude. Above such inversions the particles are largely of continental origin, except near clouds or near the residues from dissipated clouds. Table 10.8 lists a few average concentrations of sea-salt with respect to altitude (ref. 10.14).

Table 10.8 Mean sea-salt particle concentrations in maritime air masses and corresponding altitudes.

Altitude (m)	Concentration (cm^{-3})
Sea level	200–300
600–800	10–20
1,200	2–4

Sea-salt particle concentrations also depend on the wind speed. In figure 10.2, the concentrations at two altitudes are shown as a function of wind speed (ref. 10.13).

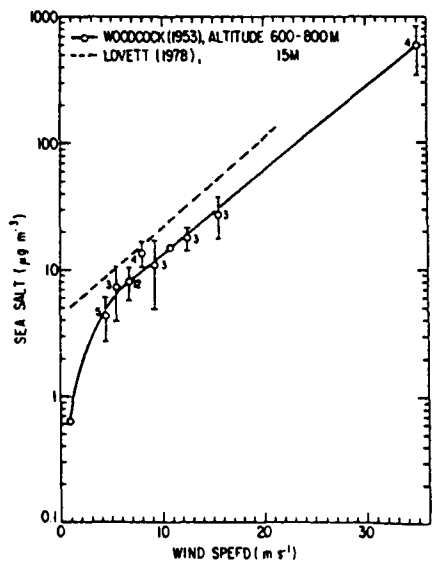

Figure 10.2. Sea-salt concentration at two altitudes as a function of wind speed near the surface of the sea. The number of observations averaged for each data point is given, as well as standard deviation (ref. 10.13).

Salt (sodium chloride (NaCl)) particles, whether from the ocean or areas where salt occurs in nature on the continents, may be detrimental to space vehicles and associated systems because of their corrosive actions and their ability to coat transparent areas until they become opaque. Salt attacks many metals, and the corrosion is especially rapid at high humidities and high temperatures. Salt solutions also provide a conductive path that can alter or short electrical circuits.

10.3.2.1 Salt Fog

Fog developing over a coastal area can be influenced by the marine environment and can contain sea salt (NaCl) which can degredate equipment and materials. The salt fog test (method 509.3) as outlined in MIL-STD-810E (ref. 10.15) should be followed to determine the resistance of equipment to the effects of an aqueous salt atmosphere. This type of atmosphere could impose three degradation effects on materials and equipment, i.e., corrosion, electrical, and physical effects.

The characteristics of marine fog droplets and salt nuclei are presented in references 10.16 and 10.17. Subsections 7.8 and 7.9 present a general and a location-specific discussion of fog.

10.3.3 Crustal Derived Aerosols

Dust and sand are transported through the air by wind blowing across a disturbed soil area. Strong winds are required to uplift the submicron sand and dust particles, because strong adhesive forces exist between the particles and the ground (ref. 10.18). Dense vegetation and ground cover also provide considerable protection from strong winds (ref. 10.19). The concentration of these particles is highly dependent on wind speed (the higher the speed, the greater the volume of sand and dust), the nature of the soil, and the amount of moisture in the soil and in the air (refs. 10.20 and 10.21). Threshold air velocities for the input of soil particles into the air increase with different types of soil surfaces in the following order: disturbed soils (except disturbed heavy clay soils), sand dunes, alluvial and aeolian sand deposits, disturbed playa (dry lake) soils, skirts of playa centers, and desert pavements (alluvial deposits) (ref. 10.22).

The larger, more abrasive particles in dust and sand storms are mostly in the lower 2 km of the atmosphere, although fine dust can reach great heights and travel great distances, e.g., approximately 10 million tons of red dust from northwest Africa was deposited on England in 1903. California experiences dust in two general regions. One region extends into southwestern Arizona and covers all the southeastern California with a maxima north of the Salton Sea and the western Mojave Desert. The second region is situated in central California. Figures 10.3 through 10.7 give maps on the characteristics of dust storms in the Southwest United States. In urban areas, the resuspension of dust by traffic or other methods must also be considered (ref. 10.10).

10.3.4 Volcanic Ash

Volcanic eruptions are normally followed by an emission of dust or ash and release of significant quantities of reactive gases. The emission rate, occurrence, and size distribution of the ash cannot be predicted by common meteorological methods because of the unpredictable timing and the different levels of intensity of volcanoes.

During the few days following an eruption, the distribution of the ash and gases is concentrated around the volcanic site, but over the following few months, a 2- to 4-km layer is formed above the troposphere over much of the world (ref. 10.14). Although most volcanic aerosol is found in the stratosphere, some of the aerosol is transported to high tropospheric layers and polar regions (ref. 10.1).

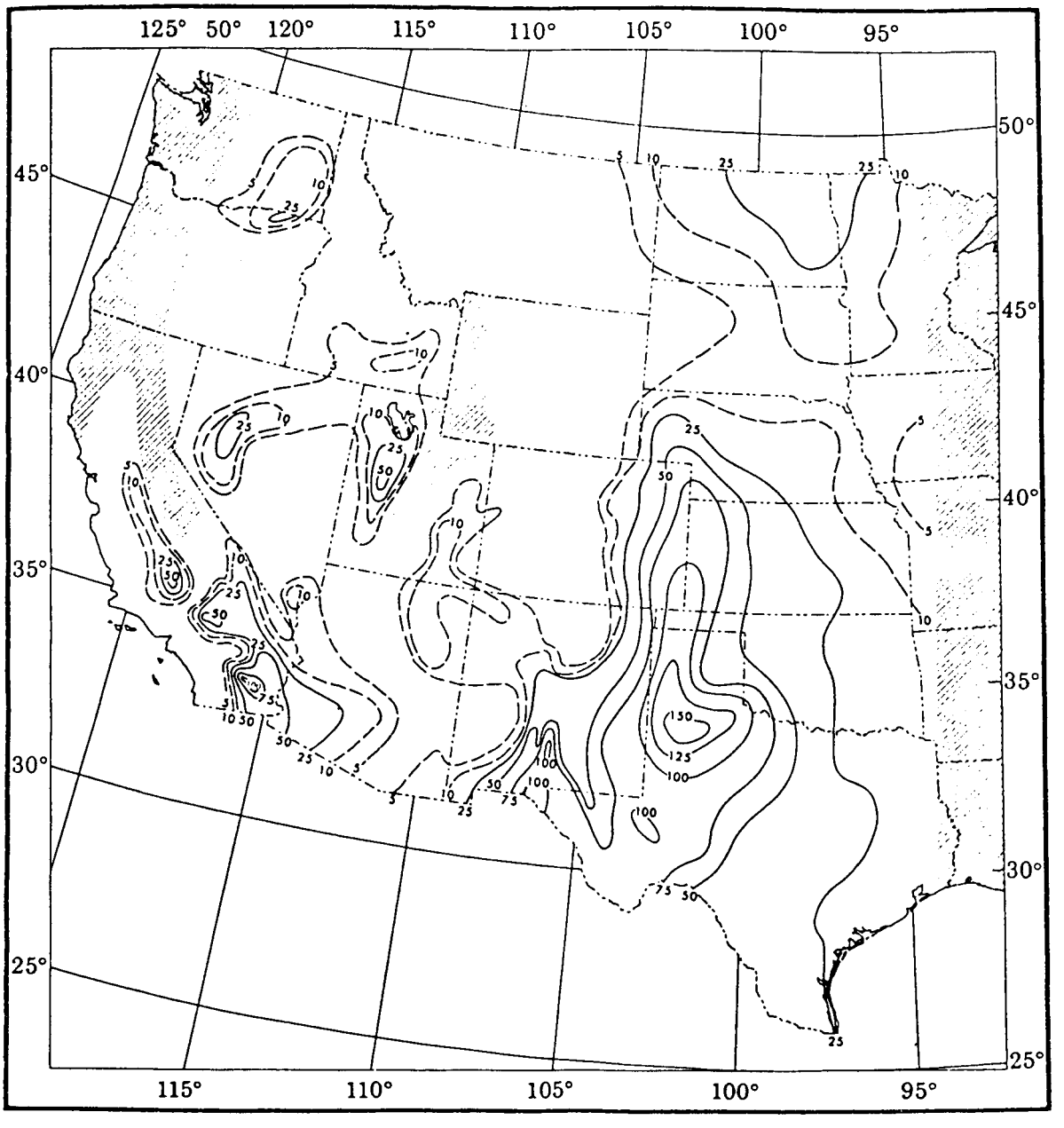

Figure 10.3. Annual average number of hours of dust episode visibility less than 7 miles (ref. 10.19).

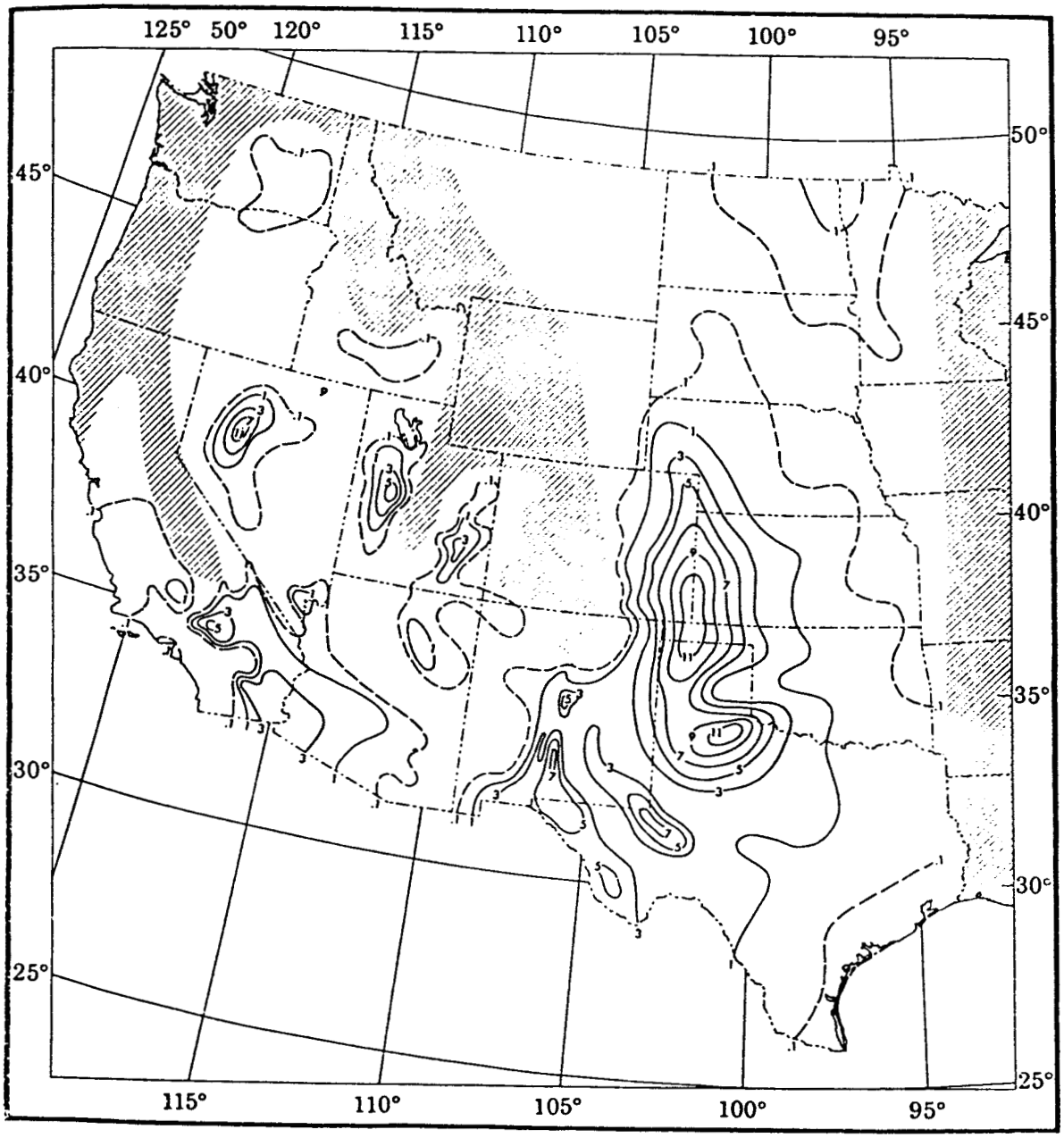

Figure 10.4. Annual average number of hours of dust episode visibility less than 5/8 mile (ref. 10.19).

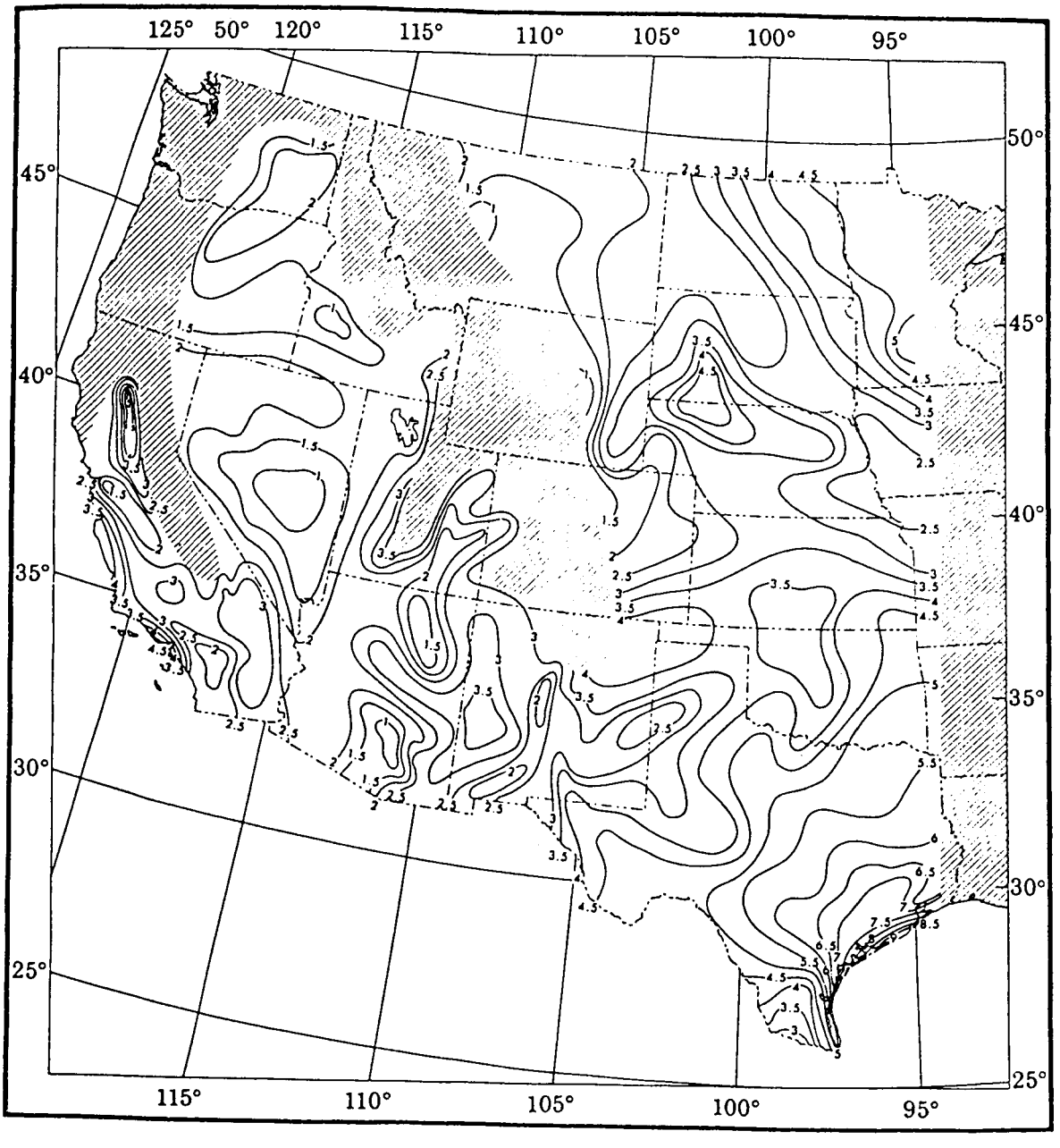

Figure 10.5. Average duration (hours) of dust episodes with visibility less than 7 miles (ref. 10.19).

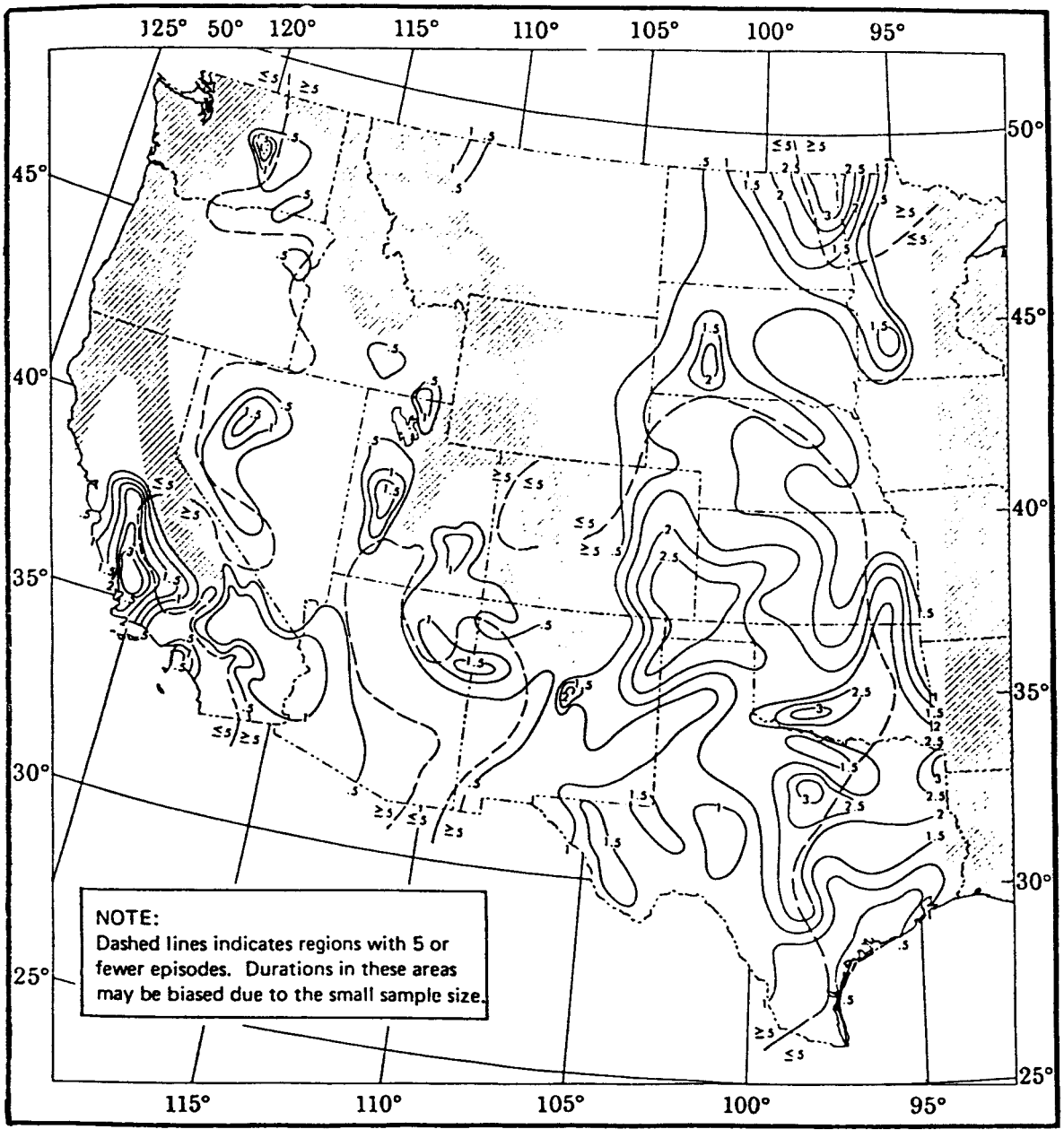

Figure 10-6. Average duration (hours) of dust episodes with visibility less than 5/8 mile (ref. 10.19).

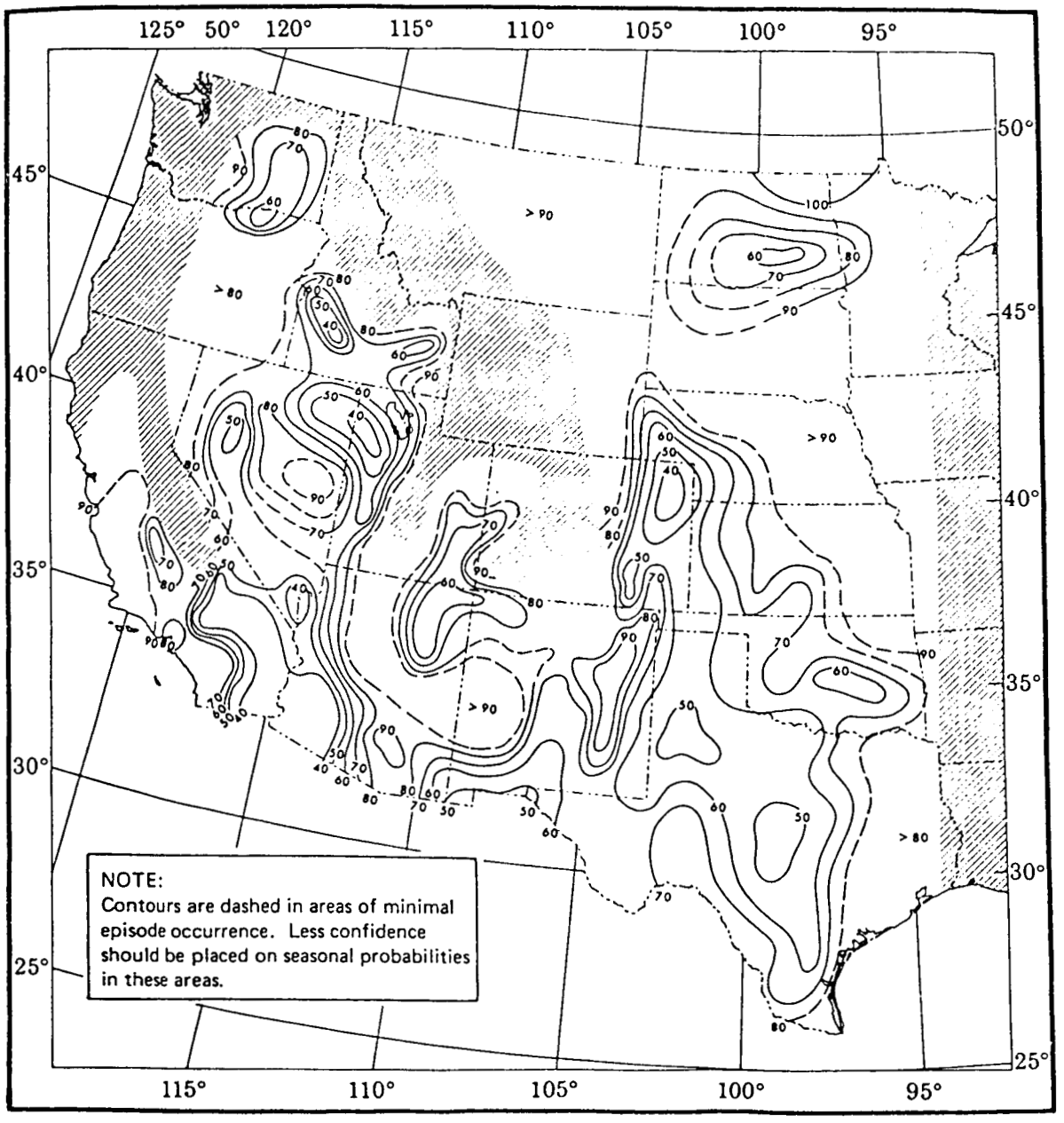

Figure 10-7. Probability (percent) of dust episodes with visibility less than 5/8 mile occurring during primary season (ref. 10.19).

10.3.5 Combustion and Other Man-Induced Aerosol

Secondary and combustion aerosols are formed by three major processes: gas-to-particle conversion resulting from physical or chemical changes; condensation of a supersaturated gas; and direct emissions of solids or liquids from the combustion sources (ref. 10.10). The particles resulting from primary combustion are carbonaceous (soots) or noncarbonaceous (fly-ash). The inorganic ionic aerosols, which include sulfate and nitrate aerosol particles are produced by secondary processes through condensation. These aerosols are usually submicron size unless further aggregation of the particles occurs. The number and mass concentrations are highly dependent on location and time (ref. 10.23).

The industrial and anthropogenic activities in eastern North America provide a major source of secondary and combustion aerosol. Atmospheric pollutants tend to be trapped beneath atmospheric temperature inversions. Incidents of severe smog usually are associated with such inversions. In the Los Angeles Basin, the pollutants are frequently trapped and cannot disperse because the basin is surrounded on the north, east, and south by mountain ranges higher than the inversions, with frequent prevailing easterly winds.

The firing of solid rocket motors (SRM's) during a rocket launch or static test is an example of an emission source which is of particular importance for aerospace activities. The byproducts of the SRM's include a significant amount of gaseous hydrogen chloride (HCl) and particulate aluminum oxide (Al_2O_3). The mass fractions of HCl and Al_2O_3 in SRM exhaust are 0.21 and 0.30, respectively. In test and launch configurations which utilize substantial amounts of cooling or sound suppression water, or when rain, fog, or other natural sources of water are present, the HCl gas and Al_2O_3 particulates will combine with the water yielding an acidic deposition which will be dispersed by the exhaust plume over the facility and may be carried downwind as well. The amounts and location of deposition are strongly influenced by the configuration of the water spray, as well as by wind and other meteorological factors. Concentrations of a few deposition spots per square centimeter are typical within a few kilometers of a shuttle launch. In one extremely windy case (STS-2), trace amounts of deposition were found up to 22 km downwind from the launch site. (See section XI for additional discussion.)

For the aerospace design engineer, the most serious issue is usually the heavy deposition which occurs (for systems like shuttle which use large quantities of sound suppression water) within 1 km of the firing location. For the shuttle, the initial deposition is usually about one-third Al_2O_3 solids by volume in a moderately acidic (~2N) solution. Once dispersed over the facility the solution generally evaporates quite rapidly. However, the water vaporizes more rapidly than the acid, resulting in a highly concentrated acidic solution for a short time—typically a few minutes on an open surface. The rate of evaporation depends on wind speed, ambient humidity, air temperature, and surface temperature. For the shuttle launch system, there are sufficient quantities of deposition to impact both vegetation and animal life within 1 km of the launch facility, as well as to be corrosive to manmade structures. When the evaporation potential of the HCl is high (warm temperatures, low humidity, and moderate to high wind speeds), the immediate corrosion damage is typically not evident except on the most sensitive surfaces. However, even in this situation the acid greatly increases the bonding between the aluminum oxide particulates and the exposed surface. The surface may be coated with particulates which will not come off without direct scrubbing. This material is hygroscopic and will enhance corrosion over long periods of time. The addition of chemical additives to the water source is an option for reducing the bonding potential.

Gaseous HCl, which is either released during a firing or is the result of evaporation of this deposition, can also be a corrosion hazard at or near the facility, especially for sensitive electronic systems. Concentrations in the 5 to 10 ppm range have been measured at the shuttle launch site in the hours following a launch. As one would expect, the most severe cases tend to correlate with times when the ground was wet from rain prior to the launch. Special precautions should be taken whenever extensive electronic equipment is to be located close to the launch pad or test site. Computer or other electronic equipment is usually very sensitive to HCl gas; an 8- to 10-h exposure may render a system inoperable. Electronics are often sensitive to gas concentrations of 10 to 100 ppb, and concentrations above this level may be encountered intermittently for at least 2 days following a SRM firing. The threshold limit value for HCl exposure for workers is 5 ppm, and the exposure limit for the public is 1 ppm (ref. 10.24). (See section XI for a discussion of far field effects.)

10.3.5.1 Acid Rain

Acid rain is rain with a pH in the range of 4 to 5 and is common in the northeastern United States, southeastern Canada, and in Europe. This rain is a result of the HNO_3 vapor, H_2SO_4 vapor, and HCl vapor being dissolved in rain drops. A pH of 5.6 has been selected to be the neutral point below which precipitation is said to be acidified (ref. 10.26). Acid rain can occur anywhere in the United States. The maximum

concentrations occur in the northeastern United States over the Ohio River Valley, southern Ontario, Canada, and western New York State. The lowest (highest acidity) observed values of annual pH are between 4.0 and 4.2 and are centered in this area. Table 10.9 gives mean annual values of ion concentrations, deposition, and pH for this area in 1982 (ref. 10.26).

Acidic deposition can also occur in dry (in gaseous or particulate form) as well as in the wet form with precipitation. Acid rain measurements are generally expressed in terms of constituent concentration (mg/l) and deposition (g/m^2) of sulfate (SO_4^{2-}), or nitrate (NO_3^-), and hydrogen ions (H^+) in precipitation or in terms of pH.

The availability of the hydrogen ion allows acid rain to react with materials (including minerals and plants) that it contacts. The other sulfate, nitrate, chloride, ammonium, and calcium ions are also more abundant in acid rain and contribute to its detrimental effects (ref. 10.26).

Increases in the acidity of precipitation are caused by the many industrial, energy producing, and transportation-related activities which release acidic wastes into the atmosphere. At the present time, between 75 and 100 million metric tons of anthropogenic, or man-made, sulfur emissions are released into the atmosphere yearly (ref. 10.27).

At the Eastern Range, annual average pH values of 4.58 are observed (ref. 10.25).

Table 10.9 Mean, annual concentration, and deposition in 1982 of hydrogen, sulfate, and nitrate ion in wet deposition for sites in the precipitation chemistry data base, when pH < 4.2 (ref. 10.26).

	Concentration (mg/L)	Deposition (g/m^2)
H^+	0.073	0.065
SO_4^{2-}	3.497	3.079
NO_3^-	2.240	1.984

10.4 Gaseous Constituents

Gaseous as well as particulate matter can cause detrimental effects on aerospace vehicles and ground equipment due to various chemical reactions/processes. Nitrogen (N_2) and oxygen (O_2) make up approximately 99.0 percent by volume (98.6 percent by weight) of the lower atmosphere. These two atmospheric constituents along with carbon dioxide, water vapor, and ozone are the gases of primary concern. Water vapor (H_2O) is discussed in section VI of this document. Stratospheric ozone depletion is discussed in section 8.5.1.1.

10.4.1 Average Atmospheric Constituents

The variability (range) of many atmospheric trace gases is quite large. However, given in table 10.10 are the average or typical gas concentration values expected at both ground level and with altitude. Seasonal, diurnal, locational, and other changes can all add to the variability of various atmospheric constituents. The mean values presented in table 10.10 are based on model information taken from references 10.27 and 10.28.

Table 10.10 Average concentrations (standard atmosphere values) of various gaseous constituents from the Earth's surface up to 900-km altitude.[a] (Refs. 10.27, 10.28)

Constituent	Typical Concentration (ppbv*)	
	Altitude (km)	ppbv
N_2	0 and above	7.81×10^8
O_2	0 and above	2.09×10^8
Rare Gases	0	very small
O_3	0	27
	7	50
	22	3,650
	40	7,300
	75	250
	90	700
N_2O	0	320
	9	320
	32	117
	49	5
	90	0.5
NO [b]	0	0.3
	12	0.3
	18	0.2
	40	11
	70	11
	90	213
NO_2 [b]	0	0.02
	10	0.02
	18	0.8
	35	7.3
	50	0.4
	90	0.2
H_2S [b]	0	0.1
	2	0.03
	10	0.01
	26 and above	10^{-15}
CS_2 [b]	0	0.07
	14	0.03
	32 and above	10^{-15}
COS	0	<0.05
NH_3 [b]	0	0.5
	12 and above	<0.01
H_2	0 to 90	560
CH_4	0	1,700
	10	1,700
	40	564
	50	210
	90	140
SO_2 [b]	0	0.3
	30	0.01
	70	0.04
	90	0.002
CO	0	150
	10	100
	21	12
	50	46
	90	5,840
CO_2	0	330,000
	75	330,000
	90	310,000
HNO_3 (vapor) [b]	0	0.05
	15	0.45
	22	5.5
	50	0.06
	90	0.03
H_2SO_4 (vapor)	0 to 90	small except in localized areas

a. This table gives average values such that a constituent value at altitude can be obtained by linear interpolation between the listed altitude/concentration values. See references 10.27 and 10.28 for more exact curves.
b. These gases have a very large latitudinal and longitudinal gradient, due to short lifetimes, causing a large range of local concentrations with altitude to exist.
* ppbv = parts per billion volume.

REFERENCES

10.1 d'Almeida, G.A., Koepke, P., and Shettle, E.P.: "Atmospheric Aerosols Global Climatology and Radiative Characteristics." 1991, pp. 11–24.

10.2 "U.S. Standard Atmosphere." United States Government Printing Office No. 003-017-00323-0, Washington, DC, October 1976.

10.3 Blifford, I.H. and Ringer, L.D.: "The Size and Number Distribution of Aerosols in the Continental Atmosphere." Journal of Atmospheric Sciences, vol. 26. 1969, pp. 716–726.

10.4 Jennings, S.G.: "Physical Characteristics of the Natural Atmospheric Aerosol." TSLP: Final Technical Report, March 1975–September 1976, p. 2.

10.5 Kent, G.S., and Yue, G.K.: "The Modeling of CO_2 Lidar Backscatter From Stratospheric Aerosols." Journal of Geophy. Res., vol. 96, No. D3, March 20, 1991, pp. 5279–5292.

10.6 Turco, R.: "Upper-Atmosphere Aerosols: Properties and Natural Cycles." Chapter 3B of "The Atmospheric Effects of Stratospheric Aircraft: A First Program Report," NASA RP-1272, January 1992, pp. 63–91.

10.7 Cadle, R.D.: "The Measurement of Airborne Particles." Wiley-Interscience, New York, 1975, p. 342.

10.8 "CRC Handbook of Chemistry and Physics." 73rd Edition, CRC Press, Inc., Boca Raton, Florida, 1992.

10.9 Ford, W.E.: "Dana's Manual of Meteorology." John Wiley & Sons, Inc., New York and Chapman & Hall, London, 13th Edition, 1912.

10.10 Patterson, E.M.: "Size Distributions, Concentrations, and Composition of Continental and Marine Aerosols." Atmospheric Aerosols: Their Formation, Optical Properties, and Effects. Spectrum Press, Hampton, Virginia, 1982.

10.11 Pohlman, S.L.: "General Corrosion." Metals Handbook, Ninth Edition, Volume 13–Corrosion. ASM International, United States, 1987, pp. 80–83.

10.12 Money, K.L.: "Corrosion Testing in the Atmosphere." Metals Handbook, Ninth Edition, Volume 13–Corrosion. ASM International, United States, 1987, pp. 204–206.

10.13 Prata, A.J.: "Observations of Volcanic Ash Clouds in the 10–12 μm Window Using AVHRR/2 Data." International Journal of Remote Sensing, vol. 10, Nos. 4 and 5, 1989, pp. 751–761.

10.14 Blanchard, Duncan C.: "The Production, Distribution, and Bacterial Enrichment of Sea-Salt Aerosol." Air-Sea Exchange of Gases and Particles, D. Reidel Publishing Company, 1983, pp. 407–454.

10.15 Military Standard: Environmental Test Methods and Engineering Guidelines, MIL-STD-810E, AMSC F4766, 14 July 1989.

10.16 Woodcock, A.H.: "Marine Fog Droplets and Salt Nuclei—Part I." J. of the Atmos. Sci., vol. 35, April 1978, pp. 657–664.

10.17 Woodcock, A.H.: "Marine Fog Droplets and Salt Nuclei—Part II." J. of the Atmos.. Sci., vol. 38, January 1981, pp. 129–140.

10.18 Twomey, S.: "Atmospheric Aerosols." Elsevier Scientific Publishing Company, New York, 1977, p. 27.

10.19 Changery, M.J.: "A Dust Climatology of the Western United States." NUREG/CR-3211. National Oceanic and Atmospheric Administration, prepared for U.S. Nuclear Regulatory Commission. National Climatic Data Center, Asheville, NC 28801-2696, April 1983.

10.20 Gillette, D.A., Clayton, R.N., Mayeda, T.K., Jackson, M.L., and Sridhag, K.: "Tropospheric Aerosols From Some Major Dust Storms of the Southwestern United States." Journal of Applied Meteorology, vol. 17, 1978, pp. 832–845.

10.21 Gillette, D.A.: "Fine Particulate Emissions Due to Wind Erosion." Transactions of American Society of Agricultural Engineers, vol. 20, 1977, pp. 890–897.

10.22 Gillette, D.A., Adams, J., Endo, A., and Smith, D.: "Threshold Velocities for Input of Soil Particles Into the Air of Desert Soils." Journal of Geophysical Research, vol. 85, 1980, pp. 5621–5630.

10.23 Cadle, R.D., Kiang, C.S., and Louis, J.F.: "The Global Scale Dispersion of the Eruption Clouds From Major Volcanic Eruptions." Journal of Geophysical Research, vol. 81, 1976, pp. 3125–3132.

10.24 Anderson, B.J. and Keller, V.W.: "A Field Study of Solid Rocket Exhaust Impacts on Near-Field Environment." NASA TM 4172, MSFC, Alabama, January 1990.

10.25 Madsen, B.C., et al.: "Characterization and Evaluation of Acid Rain in Central Florida From 1978 to 1987—Ten Year Summary Report." NASA TM-102149, January 1989.

10.26 Barchet, W.R.: "Acid Rain: A Primer on What, Where, and How Much." Pacific Northwest Laboratory Report PNL-SA-13199, April 1985.

10.27 Anderson, G.P., et al.: "AFGL Atmospheric Constituent Profiles (0–120 km)." AFGL-TR-86-0110, Environmental Research Papers, No. 954, Air Force Geophysics Laboratory, Hanscom AFB, MA 01731, May 15, 1986.

10.28 Smith, M.A.H.: "Compilation of Atmospheric Gas Concentration Profiles From 0 to 50 km." NASA TM-83289, March 1982.

SECTION XI. AEROSPACE VEHICLE EXHAUST AND TOXIC CHEMICAL RELEASE

11.1 Introduction

This section of the guidelines is intended to provide aerospace engineers and scientists with background information in the areas of tropospheric air quality and environmental assessment to assist them in the planning, design, testing, and operation of space vehicle systems. It deals primarily with the release of hazardous materials from the launch of space vehicle systems, spills of toxic fuels, and potential accidents.

Including the introduction, this section is organized into eight major subsections. The contents of the remaining subsections are summarized as follows:

11.2 TERMS—Definition of terms used in this section.

11.3 ENVIRONMENTAL THREATS—Overview of the atmospheric environmental threats that may be caused by the handling, testing, and launch of space vehicle systems.

11.4 METEOROLOGICAL EFFECTS—Overview of the concepts of atmospheric transport and diffusion.

11.5 SPECIFIC SOURCES—Description of the specific sources of air pollutants such as rocket exhaust products, fuel spills, fires, and accidents.

11.6 TOXICITY CRITERIA—Toxicity criteria for materials that have the potential of being released into the atmosphere during the handling, testing, and launch of space vehicle systems.

11.7 HAZARD ASSESSMENT AND MITIGATION—Discussion of procedures for identifying and dealing with potential atmospheric environmental threats.

11.8 COMPUTER MODELS—Discussion of computerized models that can be employed to evaluate different atmospheric hazards. Model applicability, data requirements, necessary hardware, and output are discussed.

11.2 Definition of Terms

ACGIH—American Council of Government and Industrial Hygienists.

AFTOX—U.S. Air Force toxic chemical dispersion model.

Al_2O_3—Aluminum oxide.

Ambient—Encompassing or surrounding.

Atmospheric Diffusion—The spreading of gaseous and/or particulate matter by turbulent motions in the atmosphere (often used interchangeably with dispersion).

Atmospheric Stability—A measure of the thermal stability or instability of the atmosphere, especially its lowest layers.

BLAST—Acoustics effects model.

BOOM—Acoustics effects model.

Ceiling—(1) Maximum short-term average concentration above which exposure should never occur. (2) Lowest height above ground level at which the clouds at and below that level obscure more than five-tenths of the total sky.

Cloud Stabilization—The point at which a cloud with initial vertical momentum and/or buoyancy ceases to rise because it has reached approximate equilibrium with ambient conditions.

Concentration—The amount (mass) of a substance in a given volume of air (as in milligrams per cubic meters) or the relative amount of a substance given as a ratio (as in parts per million).

Confidence Level—The probability that a specified concentration or dosage will not be exceeded.

Conflagration—A raging fire that results when solid fuels or propellants are ignited.

Continuous Release—A release of air pollutants over an extended period of time, as in the case of evaporation from a liquid spill or stack emissions.

CO—Carbon monoxide.

CO_2—Carbon dioxide.

Deflagration—An explosion and raging fire that occur when hypergolic liquid propellants are mixed together.

Deposition—Material deposited on the ground surface in mass per unit area (see gravitational deposition and washout).

Dispersion—The spreading of gaseous and/or particulate matter by turbulent motions in the atmosphere (often used interchangeably with diffusion).

Doppler Acoustic Sounder—A remote sensing device that uses the doppler shift of acoustic waves to measure vertical wind profiles up to a maximum of 600 to 1,000 meters above the surface.

Dosage—Time-integrated concentration (typical units are milligram minutes per cubic meter).

D2—U.S. Army chemical hazard prediction model.

D2PC—Updated version of the D2 model that is designed specifically for personal computers.

Emission Rate—Mass or quantity of an air pollutant released to the atmosphere per unit time (typical units are grams per second).

Entrain—To draw or pull into.

EPA—Environmental Protection Agency.

Evaporation Rate—Amount of vapor released to the atmosphere per unit time from the surface of a liquid (typical units are milligrams per minute).

FDH—Formaldehyde dimethylhydrazone.

Gravitational Deposition—Surface deposition (fallout) due to gravitational settling of particles or drops.

HARM—Hypergolic Accidental Release Model.

Hazard Distance—The maximum distance to a concentration, dosage, or deposition greater than or equal to a specified critical value.

HCl—Hydrogen chloride.

Hypergolic Reaction—An explosive chemical reaction that takes place when hypergolic propellants (liquid fuel and oxidizer) are mixed together.

Instantaneous Release—A short-term release of air pollutants by an explosion, flash fire, etc.

Inversion—A thermally stable atmospheric layer within which the temperature increases with increasing height.

Isopleth—A constant value line or contour level.

Lapse Rate—The rate of atmospheric temperature decrease with height.

mg/m^3—Milligrams per cubic meter.

Mixing Layer—Atmospheric layer above the surface within which vertical turbulent mixing takes place (also referred to as the mixed layer or surface mixing layer).

Mixing Layer Height—Height (depth) of surface mixing layer.

MSHA—Mine Safety and Health Administration.

NDMA—Nitrosodimethylamine.

NIOSH—National Institute of Occupational Safety and Health.

N_2H_4—Hydrazine.

NO_2—Nitrogen dioxide.

N_2O_4—Nitrogen tetroxide.

OBDG—Ocean Breeze/Dry Gulch model.

p/m or ppm—Parts per million.

Pasquill Stability Category—A letter indicator for the following six atmospheric stability categories: very unstable (A), unstable (B), slightly unstable (C), neutral (D), stable (E), and very stable (F). An extremely stable (G) category is sometimes used.

Permissable Exposure Limit (PEL)—An allowable average concentration of a pollutant, usually for an 8-hour work day.

Precipitation Scavenging—See washout.

Rawinsonde—A balloon-borne meteorological instrument package used to obtain upper-air measurements of winds, barometric pressure, temperature, and humidity.

REEDM—Rocket Exhaust Effluent Diffusion Model.

Spill Rate—Amount (mass or volume) of a chemical that escapes or spills from a casing or container per unit time.

SPILLS—A dispersion model developed by Shell Oil Company for evaporative spills.

SRB—Solid rocket booster.

SRM—Solid rocket motor.

Surface Roughness Length—A micrometeorological measure of how rough the surrounding terrain is, depending on obstacles to wind flow such as buildings, hills, trees, and vegetation.

Time-Mean Concentration—The mean concentration over a specified averaging time.

Time-Weighted Average (TWA)—See permissible exposure limit.

Troposphere—The first 10 to 17 kilometers of the atmosphere within which, on average, temperature decreases with height.

UDMH—Unsymmetrical dimethylhydrazine.

Upper-air Sounding—Vertical profiles of temperature, relative humidity, winds, and pressure versus altitude, usually obtained from rawinsonde measurements.

UTM—Universal Transverse Mercator (planetary grid system).

Vapor Pressure—The pressure of vapor in equilibrium with a liquid at a given temperature.

Washout—Surface deposition of a substance removed from the atmosphere by precipitation.

11.3 Potential Environmental Threats

11.3.1 Overview

The handling, test firing, and launching of aerospace vehicle systems involve hazardous materials that present many potential environmental threats. Personnel, flora, fauna, equipment, and facilities are all threatened to some degree, depending on their sensitivity and the hazardous materials involved. Contact with a hazardous material may be direct (at the source) or indirect (arising from the atmospheric transport and diffusion (dispersion) of the material). In addition to hazardous materials, the launch and reentry of aerospace vehicles produce sonic booms that occasionally have adverse impacts.

The primary atmospheric environmental hazards associated with the handling, test firing, and launch of aerospace vehicle systems are produced by the fuels and propellants used by these systems. Modern space vehicle systems use both liquid and solid propellants. Although storage and handling normally do not present hazards for solid rocket motors, they do for liquid fuels. Liquid hydrogen and liquid oxygen are highly explosive, but are not otherwise a threat to the environment. Hypergolic liquid fuels, on the other hand, are extremely hazardous if released to the atmosphere by a leak or spill. The pollutants of concern in the exhaust from a liquid fueled rocket consist of both combustion products and unburned fuel

and oxidizer. The unused hypergolic fuel and oxidizer in a space vehicle that returns to Earth present a hazard that should not be overlooked.

The pollutants of principal concern in current rocket exhaust clouds are aluminum oxide (Al_2O_3), hydrogen chloride (HCl), carbon monoxide (CO), hydrazine (N_2H_4), unsymmetrical dimethylhydrazine (UDMH), formaldehyde dimethylhydrazone (FDH), nitrogen tetroxide (N_2O_4), and hydrazine hydrochloride. The toxic effects of aluminum oxide are those of a nuisance dust such as irritation to the eyes and mucous membranes of the respiratory tract. Hydrogen chloride is highly corrosive to human tissue, and its inhalation can damage the teeth and irritate or damage the mucous membranes of the upper respiratory tract, depending on the concentration. Carbon monoxide has an affinity for hemoglobin 210 times that of oxygen and, by combining with hemoglobin, renders blood incapable of carrying oxygen to the tissues. Thus, carbon monoxide can cause hypoxia (oxygen deficiency), followed by unconsciousness or death at higher concentrations. Exposure to hydrazine can cause irritation of the nose and throat, followed by itching, burning, and swelling of the eyes (temporary blindness may occur) and damage the kidney, liver, and blood systems. Hydrazine also possesses carcinogenic properties. When heated, hydrazine hydrochloride decomposes into hydrazine and hydrogen chloride and may therefore have the toxic potential of both chemicals. UDMH exposure at high concentrations can lead to tremors and then seizures, and it has both mutagenic and carcinogenic properties. Because FDH breaks down into reaction products similar to those of UDMH, it is assumed to have similar toxicological properties. Nitrogen tetroxide decomposes into various nitrogen oxides of which nitrogen dioxide (NO_2) is of greatest concern. Toxic effects produced by nitrogen dioxide range from irritation of the eyes and nose to lung damage to death, depending on the exposure time and concentration.

11.3.2 Static Firings and Launches

The potential environmental threat presented by normal firings of liquid-fueled engines is small because the major pollutants in the exhaust are carbon dioxide and small amounts of nitrogen oxides and carbon monoxide. The pollutants of primary concern in the exhaust from a solid-fueled rocket motor are aluminum oxide and hydrogen chloride. Aluminum oxide, an abrasive used in many types of sanding and grinding materials, can damage optical and precision equipment. As a dust, it is subject to EPA and state ambient air quality standards for particulates with aerodynamic equivalent diameters less than 10 micrometers. However, because these standards are for long-term exposures (the standards are 24-hour average and annual geometric mean concentrations of 150 and 50 micrograms per cubic meter, respectively), the short-term impacts caused by rocket launches and test firings generally do not threaten them. Hydrogen chloride, which can exist as a vapor or in water as an acid, is both corrosive and toxic. There is some evidence that hydrogen chloride in low concentrations can adversely affect electronic equipment (ref. 11.1). In systems where deluge and/or sound suppression water is directed into the exhaust of SRM's, airborne droplets containing hydrogen chloride and other exhaust products are likely.

The degree of damage to flora by contact with a hazardous material depends on the species, the hazardous material, the magnitude of the exposure, and the ambient humidity. The presence of water on a leaf generally enhances damage. Potential threats range from partial but recoverable foliage damage to total destruction. The Air Pollution Control Association publication "Recognition of Air Pollution Injury to Vegetation: A Pictorial Atlas" (ref. 11.2), illustrates and discusses the effect on flora of many air pollutants. Experience at Kennedy Space Center (ref. 11.3) reveals that a single launch of the space shuttle can cause severe plant damage within 1 km of the launch facility, and minor loss of photosynthetic tissue due to deposition of water droplets containing aluminum oxide and hydrogen chloride has been observed more than 10 km from the launch pad. The degree of damage is spotty and varies widely with distance and from launch to launch. Over a 30-month period covering the first nine space shuttle launches, the number of plant species in the vicinity of launch complex 39A declined from an average of 7.8 per study area to 5.1. Heartier plant species have taken over the areas where other species were destroyed.

11.3.3 Accidental Releases

Many hazardous materials must be stored near rocket test or launch facilities because they are used as fuels, oxidizers, solvents, and cleaners. As indicated by the toxicity tables in section 11.6, the accidental release of any of these materials poses a serious threat to the environment. Indeed, accidental releases of hazardous materials are a far greater threat to personnel safety, flora, and fauna than are normal rocket firings. Section 11.5 provides additional information about accidental releases.

11.3.4 Acoustic Threats

The atmosphere acts as a lens that can refract acoustic (sound) waves upward or downward, depending on the vertical profile of the speed of sound. At any height in the atmosphere, the speed of sound is equal to the sum of the temperature-dependent acoustic wave propagation speed and the wind-speed component in the direction of propagation. If the speed of sound decreases with height, the acoustic wave will be refracted upward. Conversely, if the speed of sound increases with height, the acoustic wave will be refracted downward. Because the acoustic wave propagation speed increases with height in a temperature inversion (an atmospheric layer within which temperature increases with height), an inversion layer above an acoustic source (explosion, rocket firing, etc.) will cause a portion of the wave front to be refracted back to the surface with a resulting sound enhancement, especially downwind of the source. The noise produced by the firing of a space vehicle system generally does not present an environmental threat other than startling animals or triggering the fall of loose plaster on buildings in the vicinity. The launch and reentry of space vehicles usually produce sonic booms. Depending on the meteorological conditions, these booms may be focused to yield large overpressures capable of causing damage such as broken windows. The magnitude of a sonic boom, which depends on the flying vehicle's speed and size, is measured in decibels, pascals, kilograms per square meter (kg/m^2), or pounds per square foot (lb/ft^2) of overpressure. The sonic booms from conventional aircraft typically cause overpressures of 2.44 to 9.76 kg/m^2 (0.5 to 2.0 lb/ft^2), while those from the space shuttle have been as high as 29.3 kg/m^2 (6.0 lb/ft^2).

11.4 Atmospheric Effects on Transport and Diffusion

Some of the most serious environmental threats associated with the handling, test firing, and launching of space vehicle systems occur when hazardous materials are transported by the atmosphere to long downwind distances. Atmospheric conditions govern the speed and direction of downwind travel of the airborne material, the rate of dilution, and the rate of evaporation. A brief discussion of the phenomena that control atmospheric transport and diffusion processes is given below. A more detailed discussion can be found in references such as the "Handbook of Applied Meteorology" (ref. 11.4) and "Atmospheric Science and Power Production" (ref. 11.5).

Wind direction determines the direction of travel for material released into the atmosphere, and wind speed determines the time required for material to travel from the point of release to a downwind point of concern, which is often called a receptor. Wind directions are reported as directions from which the wind is blowing. For example, a north wind will transport material to the south. Calm or light and variable winds present very difficult cases because the travel path of released material is unpredictable. Consequently, precautions must be taken in all directions.

The atmospheric diffusion of a cloud or plume of gases or aerosols (small drops or particles) released near the surface is determined by atmospheric turbulence (wind fluctuations caused by atmospheric eddies) and the depth of the surface mixing layer. Wind fluctuations caused by eddies smaller than the cloud or plume mix it with ambient air, while larger wind fluctuations move the cloud or plume in its entirety. Turbulence consists of mechanical and convective components. The mechanical component is produced by forced airflow over surface roughness elements, which include vegetation, terrain, and manmade structures. Mechanical turbulence increases as the wind speed or roughness of the surface

increases. Convective turbulence is caused by the eddies that occur as a result of thermal instability. The atmosphere is thermally unstable if the adiabatic (no exchange of heat with the surroundings) cooling of a small "parcel" of air displaced upward results in a parcel that is warmer (less dense) than the surrounding air. Because the parcel will then continue to rise, thermal instability acts to increase vertical motions. On the other hand, if the atmospheric temperature decreases with height less rapidly than the adiabatic rate, an air parcel adiabatically displaced upward will be colder (denser) than the surrounding air. In this case of thermal stability, buoyancy forces will act to suppress the vertical motion and return the parcel to its original level. The neutral case occurs when the atmospheric temperature decreases with height at the adiabatic rate of 0.01 °C per meter. In general, the convective component is the dominant component of atmospheric turbulence on days when winds are light and solar heating of the surface results in thermal instability, while the mechanical component is dominant at night or whenever there is an adiabatic thermal stratification. Because lower atmospheric turbulence is produced by surface effects (flow over surface roughness and surface heating), atmospheric turbulence extends through only a finite depth of the lower atmosphere. This layer in which turbulent mixing occurs is called the surface mixing layer.

Diffusion models use turbulence (wind fluctuation) measurements or stability parameters to characterize diffusion rates. The standard deviations of the wind direction and elevation angles are the most common turbulence measurements. Some stability parameters vary continuously and others divide diffusion rates into discrete categories. One of the simplest and most widely used stability classification techniques is a modified version of the scheme proposed by Pasquill (ref. 11.6). The six or seven Pasquill stability categories range from A for very unstable conditions to F or G for very or extremely stable conditions. The popularity of the Pasquill stability categories is in part explained by the fact that they can be determined from standard airport surface weather observations of wind speed, cloud cover, and ceiling height. Wind speed is used as an indicator of the mechanical component of atmospheric turbulence, while the cloud cover and ceiling height are used to modify the solar radiation incident at the top of the atmosphere. This modified solar radiation is used as an indicator of the convective component of turbulence.

Precipitation falling through an atmosphere containing a hazardous gas or aerosol tends to scavenge it and deposit it at the surface. The amount of material scavenged depends on the type and rate of precipitation and the material being scavenged. Some pollutants such as hydrogen chloride are readily absorbed by water, while others such as particulate matter depend on impaction as the removal process. Small particles may also act as nuclei for the formation of clouds and precipitation. Although precipitation scavenging can significantly reduce atmospheric concentrations of the scavenged material, the amount of material deposited at the surface can also be dramatic because material is removed from the entire vertical column through which the precipitation is falling.

Evaporative spills of hazardous liquids used as rocket propellants or for other purposes, such as cleaning solvents, are among the most serious potential environmental threats. The evaporation rate is controlled by the liquid's physical characteristics such as molecular weight and vapor pressure and meteorological factors such as the temperature and wind speed. In general, evaporation increases as the wind speed and/or temperature increase. Also, evaporative losses to the atmosphere increase as the evaporating surface area increases.

11.5 Specific Sources of Air Pollutants

11.5.1 Storage

The major threat to the environment from a stored toxic liquid such as a hypergolic fuel or oxidizer is that a leak, spill, or handling accident may release the material into the atmosphere. In addition to the obvious threat presented by the storage of toxic fuels and oxidizers, the toxicity of other chemicals such as cleaning solvents and payload materials must be considered. Hypergolic materials (nitrogen tetroxide in particular) evaporate at ambient temperatures, producing vapors that are transported downwind and

dispersed by normal atmospheric processes. Not only are hypergolic materials toxic to most life, they are highly flammable and some are corrosive. The probability of an accidental release of toxic materials from a storage facility is highest when material transfers take place. Potential release scenarios include broken transfer lines, connection failures, accidents by vehicles transporting hazardous materials, and damage to the storage facility resulting from a vehicle accident.

11.5.2 Static Firings and Launches

The exhaust products of rocket motor firings may contain hazardous materials, depending upon the chemical mix of the fuel. In general, the exhaust from rocket engines that exclusively burn liquid oxygen and liquid hydrogen or RP-1 contain water and carbon dioxide, which are not considered hazardous. All other fuels produce materials that have effects on the environment ranging from a nuisance to an extreme hazard. The current SRM's produce exhaust clouds containing aluminum oxide, hydrogen chloride, carbon dioxide, water, nitrogen, and various other trace materials after the rapid chemical reactions have been completed. Of these materials, hydrogen chloride and aluminum oxide are hazardous. Some SRM's contain other metals such as beryllium, which is very toxic and requires special precautions if released into the atmosphere.

Water is often injected into the exhaust of SRM's to protect the launch pad or test facility or to suppress sound. Much of this water is atomized by the mechanical shears and turbulence generated by the exhaust flows. If large quantities are used, water may be expelled onto the area near the launch pad or mixed with the exhaust gas. Droplets carried aloft with the exhaust plume may rain out of the exhaust cloud as it travels downwind, as is the case of the space shuttle (ref. 11.7). Significant quantities of hydrogen chloride and aluminum oxide can be scavenged from the exhaust cloud by this process. Water droplets which come in contact with the exhaust gases, whether from rain or dewfall prior to the launch or from the launch pad ground system, mix with the exhaust gases and leave small pools and drops of dilute hydrochloric acid on the ground in the vicinity of the launch pad. This acid is initially 2 normal, but as the water evaporates it increases to approximately 11 normal where it remains until the drop is completely evaporated. At this point, the hydrogen chloride evaporates along with the water. As the deposited acid solution evaporates, the ambient concentration of gaseous hydrogen chloride rises to a peak and then decreases as the drops are depleted, and only the acid in the surface soil and the more slowly evaporating pools are available to fuel the ambient concentration. The peak ambient hydrogen chloride concentrations measured at Kennedy Space Center after the launches of space shuttle missions 41D and 51A were 3 and 9 ppm, respectively. These peak concentrations occurred 1.5 to 2 hours after the launches. Although the ambient hydrogen chloride concentration after both missions gradually decreased to about 1 ppm within several more hours, small rises in ambient concentration were reported after sunrise for 2 days after mission 51A.

In addition to a normal firing, exhaust products can be released into the atmosphere by the accidental breakup of a SRM and the subsequent burning of its pieces on the ground, which is called a conflagration. Although the exhaust products are nearly identical to those of a normal firing, changes in the heat produced and the time elapsed while burning can cause both the magnitude of the hazard and the downwind hazard distance to be greatly increased.

As noted above, liquid-fueled rocket engines other than those fueled with liquid oxygen and hydrogen or RP-1 produce exhaust clouds that contain hazardous materials. The current hypergolic-fueled rocket engines primarily burn hydrazine-based fuels with nitrogen tetroxide as the oxidizer. The exhaust products from a normal firing of these engines include nitrogen oxides that can be toxic. A greater threat than a conflagration for these vehicles is a deflagration in which the fuel and oxidizer come in contact with each other, resulting in a hypergolic explosion. The hypergolic explosion is a fairly common event that usually takes place when a space vehicle is aborted in flight. However, there also have been cases that occurred on or near the Earth's surface. For example, a Titan II missile was involved in a hypergolic explosion near Demascus, Arkansas in 1980. More recently, a Titan 34D mission was aborted shortly after launch from Vandenberg Air Force Base, California. Hypergolic explosions produce clouds that

contain nitrogen tetroxide, hydrazine, and other hazardous products. In the case of the Titan 34D event, fragments of burning solid propellant fell to the ground and produced ground fires with toxic plumes, and the hypergolic fuels of the upper stages combined to produce a toxic cloud in the lower atmosphere. Long downwind hazard distances can result from deflagrations of hypergolic-fueled space vehicle systems because of the quantities and toxicities of the materials that are released.

11.5.3 Fires

Fires that involve toxic propellants or other hazardous materials are another potential threat to the environment. In general, air pollutants released by these fires include both uncombusted toxic materials and toxic products of combustion. Because the heat generated by a fire usually is small compared to that produced by a rocket launch, the buoyant rise of the plume from a fire is generally less than that of an exhaust cloud. Consequently, fires can produce toxic clouds relatively close to the Earth's surface, resulting in little chance for dispersion to take place before the toxic clouds mix to the surface. The hazards produced by fires are very difficult to evaluate because it is difficult to quantify the amount of material involved, the efficiency of combustion, the chemical reactions that take place, and the effects of fire fighting on the combustion chemistry. Most of what is known about these fires comes from test burns of toxic materials under controlled conditions.

11.5.4 Transportation

The transportation of toxic materials presents threats to the environment resulting from numerous scenarios that are beyond the scope of the current discussion. These scenarios range from small leaks to the rupture of rail cars containing toxic materials. The U.S. Department of Transportation and most State and local governments have established rules, guidelines, and procedures for the transportation of toxic materials. These rules and procedures are established by material classification and, in some cases, by individual materials.

11.5.5 Payloads

The upper stages and the payloads of some space vehicle systems contain hazardous materials. The contents of these stages must therefore be investigated as part of the hazards analysis for the system. In addition to fuels and oxidizers, electrical and other power sources may contain hazardous materials. Also, nuclear power sources are common for some types of payloads. Although the threat of radioactive hazards goes beyond the scope of this document, it is mentioned here for completeness.

11.6 Toxicity Criteria

The chemical formulas, molecular weights, and chemical abstract service (CAS) numbers for air pollutants that are contained in rocket exhaust clouds or that may be released by spills of liquid rocket fuels are listed in tables 11-1 and 11-2, respectively. Table 11-2 also includes other hazardous liquids such as cleaning solvents that are commonly found at test and launch facilities. The exposure criteria that have been established for the toxic pollutants in tables 11-1 and 11-2 by the Occupational Safety and Health Administration (OSHA), the Mine Safety and Health Administration (MSHA), the National Institute of Occupational Safety and Health (NIOSH), and the American Council of Government and Industrial Hygienists (ACGIH) are summarized in tables 11-3 and 11-4. The exposure criteria used by the U.S. Air Force and implemented in its AFTOX dispersion model for fuel spills (ref. 11.8) are listed in table 11-5. There are two types of exposure criteria. The first, a permissible exposure limit (PEL) or time-weighted average (TWA), usually represents an allowable average concentration for an 11-hour work day. The second is a ceiling or maximum short-term average concentration above which exposure should never occur. In 1989, OSHA promulgated PEL's and ceilings and proposed new values to take effect in 1992 (Ref. 11.9). Both sets of exposure criteria are listed in tables 11-3 and 11-4. In addition to

Table 11-1. Chemical formulas, molecular weights, and chemical abstract service numbers for rocket exhaust products.

Chemical	Chemical Formula	Molecular Weight	CAS No.
Aluminum Oxide	Al_2O_3	101.96	1344-28-1
Hydrogen Chloride	HCl	36.46	7647-01-0
Carbon Monoxide	CO	28.01	630-08-0
Hydrazine	N_2H_4	32.06	302-01-2
Unsymmetrical (1,1-) Dimethylhydrazine (UDMH)	$(CH_3)_2N_2H_2$	60.12	57-14-7
Formaldehyde Dimethylhydrazone (FDH)	$(CH_3)_2N-N=CH_2$	72.11	2035-89-4
Nitrogen Tetrozide	N_2O_4	92.02	10544-72-6
Hydrazine Hydrochloride	$N_2H_4 \cdot HCl$	68.52	2644-70-4

Table 11-2. Chemical formulas, molecular weights, and CAS numbers for liquid rocket fuels, solvents, and cleaners.

Chemical	Chemical Formula	Molecular Weight	CAS No.
Aerozine-50	$(CH_3)_2N_2H_2 \cdot N_2H_4$	41.81	8065-75-6
Hydrazine	N_2H_4	32.06	302-01-2
Hydrazine (54%)	$N_2H_4 \cdot H_2O$	50.07	7803-57-8
Unsymmetrical (1,1-) Dimethylhydrazine (UDMH)	$(CH_3)_2N_2H_2$	60.12	57-14-7
Monomethylhydrazine (MMH)	$CH_3N_2H_3$	46.09	60-34-4
Fuming Nitric Acid (IRFNA)	HNO_3	57.20	7697-37-2
Nitrogen Tetroxide	N_2O_4	92.02	10544-72-6
n-Butyl Alchohol	$CH_3(CH_2)_3OH$	74.12	71-36-3
t-Butyl Alchohol	$(CH_3)_3COH$	74.12	75-65-0
Benzene	C_6H_6	78.12	71-43-2
Freon 12	Cl_2CF_2	120.91	75-71-8
Isopropyl Ether	$(CH_3)_2CHOCH(CH_3)_2$	102.18	108-20-3
Acetone	CH_3COCH_3	58.08	67-64-1
Xylene	C_8H_{10}	106.17	1330-20-7

Table 11-3. Exposure criteria for rocket exhaust products.

Chemical	OSHA[a]			MSHA[b]		NIOSH[b]		ACGIH[b]	
		PEL	Ceiling	TWA	Ceiling	TWA	Ceiling	TWA	Ceiling
Aluminum Oxide	1989: 1992:	15(10)mg/m^3[c] 10(5)mg/m^3[c]	— —	—	—	—	—	—	—
Hydrochloric Acid	1989: 1992:	— —	5.0 p/m* 5.0 p/m	—	5.0 p/m	—	—	—	—
Carbon Monoxide	1989: 1992:	50 p/m 35 p/m	— 200 p/m	50 p/m	—	35 p/m (10-h)	200 p/m	50 p/m	400 p/m (15-min)
Hydrazine	1989: 1992:	1.0 p/m 0.1 p/m	— —	1.0 p/m	—	—	0.04 mg/m^3 (2-h)	0.1 p/m	—
Unsymmetrical (1,1-) Dimethylhydrazine (UDMH)	1989: 1992:	0.5 p/m 0.5 p/m	— —	0.5 p/m	—	—	0.15 mg/m^3 (2-h)	0.5 p/m	—
Formaldehyde Dimethylhydrazone (FDH)	1989: 1992:	0.5 p/m 0.5 p/m	— —	0.5 p/m	—	—	0.15 mg/m^3 (2-h)	0.5 p.m	—
Nirogen Tetroxide	1989: 1992:	— —	5.0 p/m[d] 1.0 p/m[d] (15-min)	—	5.0 p/m[d]	—	1.0 p/m[d] (15-min)	3.0 p/m[d]	—
Hydrazine Hydrochloride	1989: 1992:	— —	— —	—	—	—	0.04 mg/m^3 (2-h)	—	—

a. PEL is 8-h average and ceiling is maximum instantaneous concentration unless otherwise specified.
b. TWA is 8-h average and ceiling is maximum instantaneous concentration unless otherwise specified.
c. Total dust (respirable dust).
d. Exposure criteria are for NO_2; molecular weight for NO_2 of 46.01 should be used to convert hydrazine concentrations to p/m for comparison with exposure criteria.
* p/m = parts per million.

Table 11-4. Exposure criteria for liquid rocket fuels.

Chemical	OSHA[a]		MSHA[b]		NIOSH[b]		ACGIH[b]	
	PEL	Ceiling	TWA	Ceiling	TWA	Ceiling	TWA	Ceiling
Aerozine–50	—	—	—	—	—	—	—	—
Hydrazine	1989: 1.0 p/m* 1992: 0.1 p/m	— —	1.0 p/m		—	0.04 mg/m^3 (2-h)	0.1 p/m	—
Hyrazine (54%)	1989: 1.0 p/m 1992: 0.1 p/m	— —	1.0 p/m	—	—	0.04 mg/m^3 (2-h)	0.1 p/m	—
Unsymmetrical (1,1-) Dimethylhydrazine (UDMH)	1989: 0.5 p/m 1992: 0.5 p/m	— —	0.5 p/m	—	—	0.15 mg/m^3 (2-h)	0.5 p/m	—
Monomethylhydrazine (MMH)	1989: — 1992: —	0.2 p/m 0.2 p/m	—	0.2 p.m	—	0.08 mg/m^3 (2-h)	—	0.2 p/m
Fuming Nitric Acid (IRFNA)	1989: 2.0 p/m 1992: 2.0 p/m	— —	2.0 p/m	—	2.0 p/m (10-h)	—	—	—
Nitrogen Tetroxide	1989: — 1992: —	5.0 p/m[c] 1.0 p/m[c] (15-min)	—	5.0 p/m[c]	—	1.0 p/m[c] (15-min)	3.0 p/m[c]	—
n-Butyl Alcohol	1989: 100 p/m 1992: —	— 50 p/m	100 p/m	—	—	—	—	50 p/m
t-Butyl Alcohol	1989: 100 p/m 1992: 100 p/m	— —	100 p/m	—	—	—	100 p/m	
Benzene	1989: — 1992: —	— —	—	25 p/m	0.1 p/m (10-h)	1.0 p/m (15-min)	10 p/m	—
Freon 12	1989: 1,000 p/m 1992: 1,000 p/m	— —	1,000 p/m	—	—	—	—	—

Table 11-4. Exposure criteria for liquid rocket fuels (continued).

Chemical	OSHA[a]		MSHA[b]		NIOSH[b]		ACGIH[b]	
	PEL	Ceiling	TWA	Ceiling	TWA	Ceiling	TWA	Ceiling
Isopropyl Ether	1989: 500 p/m 1992: 500 p/m	— —	250 p/m	—	—	—	250 p/m	—
Acetone	1989: 1,000 p/m 1992: 750 p/m	— —	1,000 p/m	—	590 mg/m^3 (10-h)	—	750 p/m	—
Xylene	1989: 100 p/m 1992: 100 p/m	—	—	—	100 p/m (10-h)	200 p/m (10-min)	—	—

a. PEL is 8-h average and ceiling is maximum instantaneous concentration unless otherwise specified.
b. TWA is 8-h average and ceiling is maximum instantaneous concentration unless otherwise specified.
c. Exposure criteria are for NO_2; molecular weight for NO_2 should be used to convert hydrazine concentrations to p/m for comparison with exposure criteria.
* p/m = parts per million.

Table 11-5. U.S. Air Force exposure criteria for rocket exhaust products and liquid rocket fuels.

Chemical	TWA[a]
Hydrogen Chloride	3.0 p/m
Carbon Monoxide	100 p/m
Nitrogen Tetroxide	2.0 p/m
Aerozine-50	0.03 p/m
Hydrazine (54%)	0.02 p/m
Fuming Nitric Acid (IRFNA)	2.0 p/m
n-Butyl Alcohol	50 p/m
t-Butyl Alcohol	100 p/m
Benzene	10 p/m
Freon-12	100 p/m
Isopropyl Ether	250 p/m
Acetone	1,000 p/m
Xylene	100 p/m

a. TWA is 8-h average.
p/m = parts per million

the toxicity criteria in tables 11-3 and 11-4, there may also be state, local, or other criteria applicable to a specific facility. For space shuttle firings, the Committee on Toxicology (ref. 11.10) recommends 1-hour and 24-hour short-term public exposure emergency guidance levels of 1 ppm of HCl.

11.7 Standard Hazard Assessment and Mitigation Procedures

11.7.1 General

Standard assessment and mitigation procedures for the potential atmospheric hazards associated with the handling, test firing, and launching of space vehicle systems typically consist of identification and quantification of the threats, preparation of operations and contingency plans, training, and implementation. At most installations, a team under the direction of the safety office or similar organization is in place to perform these tasks. Each activity or process that could release a hazardous material to the atmosphere should be identified in advance (see section 11.3 for a discussion of the most common threats and section 11.5 for additional details). Mathematical simulation models such as those described in section 11.8 can then be used to quantify the magnitude of each potential hazard. Based on the results of this quantitative hazard assessment, operations and contingency plans should be developed to minimize each potential hazard. For example, transfer operations for toxic liquids can be restricted to periods when meteorological conditions are such that an accidental release would be unlikely to produce hazardous concentrations in downwind areas where access cannot be restricted. Operations and contingency plans with clearly defined responsibilities must be developed, and employees must be trained in their required actions under both routine and emergency conditions. All employees should know and be trained to perform their responsibilities in the event of a planned or accidental release long before the release occurs. It is highly desirable to test operations and contingency plans in simulated routine and emergency scenarios to refine and improve these plans as well as to train employees.

Preplanning for possible events that may threaten the environment is a management responsibility, but management must be provided with sufficient information to make informed decisions when developing routine operational procedures, contingency plans, and emergency response procedures such as evacuation and decontamination procedures. The availability of the necessary resources under adverse conditions must be addressed as part of the planning process. For example, if computer facilities are required, arrangements must be made for backups in the event of a power failure. Similarly, provision must be made for communications in the event of a power outage that would render most telecommunication systems unusable. Also, if predictive models are used in hazard assessment during routine or emergency operations, the data required to execute these models must be routinely acquired and available for use.

11.7.2 Storage

A procedure should be established to maintain a current inventory of all materials located at each installation where space vehicle activities take place. This inventory should include the materials, amounts, locations, possible hazards, toxicity levels, and any special emergency procedures to be followed. Liquid hydrogen, liquid oxygen, and hypergolic materials require special storage facilities. Housekeeping and inspection programs must be ongoing because neglect and corrosion are likely causes of leaking containers. Evaporative losses to the atmosphere increase as the evaporating surface area increases. Consequently, containment is generally required to retain any spilled material within a specific area and prevent the development of a large evaporating surface. Many storage facilities include a means of covering the containment area to prevent evaporation into the atmosphere. The possibility of vandalism must be considered at every storage site. Preventive measures such as security, restricted access, and shielding may be required. Proper controls and accurate inventories must be maintained for all hazardous materials. Employees at storage sites must be trained in all aspects of hazardous material storage and handling. Plans for a material transfer and the necessary precautions must be completed well in advance of the actual transfer. All potential release scenarios should be considered, and responses to these scenarios such as decontamination and/or cleanup should be part of employee training. Employees must be kept in a ready state and must be thoroughly familiar with their responsibilities in order to prevent breakdowns and confusion in the event of an accident.

11.7.3 Static Firings and Launches

The static firing of a rocket engine or motor or the launch of an aerospace vehicle system produces a large, thermally buoyant cloud of exhaust products that usually includes toxic materials. This cloud grows rapidly through the entrainment of ambient air and rises until it reaches approximate equilibrium with the surrounding atmosphere. Because this exhaust cloud cannot be prevented, a static firing or launch must be planned and conducted so as to minimize its downwind impact. This mitigation is typically accomplished by restricting static firings and launches to periods when atmospheric conditions are not conducive to pollutant concentration, dosage, or deposition values that may have an unacceptable impact in uncontrolled areas. Atmospheric transport and diffusion (dispersion) models normally are used to define the atmospheric constraints on a static firing or launch and may be used in near real time to assist in operational go/no-go decisions. In addition to considering normal firings and launches, model calculations should be performed for all credible accident scenarios (i.e., conflagrations and deflagrations). Sound propagation models can be used in a similar manner to minimize adverse noise impacts.

11.7.4 Mathematical Modeling

Mathematical models such as those described below in section 11.8 often play a key role in hazard assessment and mitigation procedures. If so, procedures for the routine execution of the selected models must be established and followed. Also, the individuals responsible for performing the model calculations must have a working knowledge of the concepts upon which they are based as well as be entirely familiar with their operational details. If a model is only executed on occasion or the person performing the model calculations is not qualified, erroneous predictions, breakdowns, and confusion can

be expected, especially under the pressure of an emergency. As indicated above, all required model inputs must be readily available on a timely basis.

It is important that the output of mathematical models used for hazard assessment meet the requirements of the end user, typically the safety office, program manager, or other decision makers. Thus, several different output formats such as overlays and tabular listings may be required. Because the units of the model output should be clearly understood by the end user, provisions should always be made for conversion between metric and English units.

As an example of a typical procedure for using a hazard assessment model, assume that a dispersion model is routinely used at the launch complex for a hypergolic-fueled space vehicle. The meteorological parameters required as input to the model are routinely measured and also forecasted. At the start of each day, the planned operations are reviewed and the model is executed for all possible release scenarios for the toxic propellants under existing or forecast meteorological conditions. The model's predictions are then presented in an appropriate format to the safety office or other users, and the predictions are also filed for future reference. The model predictions are updated as required throughout the day's operations to reflect changes in meteorological or other conditions. In the event that a release to the atmosphere occurs, a post-event analysis is performed to determine the model's performance through a comparison of model predictions with all available measurements.

11.7.5 Briefings

The manner in which a mathematical model's predictions are presented to management and others is as important as the accuracy of the predictions themselves. During the planning stages, management and other users should be provided with a detailed explanation of the selected models, and they should participate in the development of formats for briefing materials that best meet their needs. If a selected model is designed to be safe-sided (i.e., biased toward overestimation of potential hazards), as is the case with most hazard assessment models, decision makers should be made aware of this fact. The information presented to decision makers should avoid superfluous details in order to avoid confusion. Graphical presentations, such as the depiction of the predicted hazard area on an installation map, can be a very effective means of providing readily understandable results. However, too much graphical detail (for example, concentration isopleths well below the hazard criterion that cover large areas) can be misleading and should be avoided. In general, a briefing should not go beyond describing the magnitude and area of the potential hazard in the user's terms. If there is no predicted hazard, a simple statement to that effect is usually all that is needed.

11.7.6 Public Awareness

Contingency plans for planned or accidental releases of toxic materials to the atmosphere must recognize the possibility that these materials could be transported to uncontrolled areas in hazardous concentrations. The elected and appointed public officials responsible for these uncontrolled areas should be briefed on the potential hazards and the actions that have and will be taken to prevent or minimize adverse impacts. Written agreements between the test or launch facility and external agencies such as fire and police departments should be negotiated to define areas of responsibility and actions to be taken in the event of a planned or accidental release. To the extent possible, external agencies should be encouraged to participate in the routine training exercises in order to test the contingency plans. If it is anticipated that planned test or launch activities will require temporary restricted access to or evacuation of some normally uncontrolled areas, the general public as well as their officials should be made aware of these requirements and the reasons why they are necessary. Press releases to the local news media and public meetings are some techniques used to inform the public of plans to protect their safety.

11.8 Computer Models

11.8.1 Background

Table 11-6 summarizes the computerized models most frequently used in quantitative hazard assessments for rocket motor or engine test firings, space vehicle launches, and related activities that could release hazardous materials to the atmosphere. The computer resources required by these models are summarized in table 11-7. With the exception of the BLAST and BOOM sound propagation models, all of the models in table 11-6 are atmospheric transport and diffusion (dispersion) models. (In addition to the dispersion models in table 11-6, a products of combustion atmospheric dispersion (PCAD) model is currently being privately developed.) Although all of the dispersion models in table 11-6 except the empirical OB/DG model are based on widely used Gaussian diffusion model concepts, there are significant differences in model complexity and the applications for which they are designed. An overview of each model is given below with greatest emphasis placed on the rocket exhaust effluent diffusion model (REEDM) because it is the only model applicable to static firings, normal launches, conflagrations, and deflagrations. REEDM was originally developed under the sponsorship of the NASA George C. Marshall Space Flight Center (MSFC), Space Science Laboratory (ref. 11.11) to provide near real-time predictions of rocket exhaust concentrations in support of space shuttle missions. The NASA/MSFC multilayer diffusion model (ref. 11.12) was used to test and develop the procedures and algorithms used within REEDM (refs. 11.13–11.15) before the model was used to support the first launches of the space shuttle from Kennedy Space Center. REEDM has been and is undergoing continuous improvement under the sponsorship of the U.S. Air Force and NASA for use at Kennedy Space Center and Vandenberg Air Force Base. Requests for information pertaining to this diffusion model technology should be directed to the Environmental Analysis Branch, Earth Sciences and Application Division Space Science Laboratory at NASA Marshall Space Flight Center.

11.8.2 REEDM Version 7

The REEDM version 7 computer program (ref. 11.16) is used to assess the air quality impacts of the exhaust products produced by large rocket motors or the burning of rocket fuels. The model is designed to calculate peak and time-mean concentration, dosage, and surface deposition (resulting from both gravitational settling and precipitation scavenging) of exhaust cloud constituents downwind of normal launches, launch failures, and static firings. There are several modes which this model can be used: normal launch mode in which everything operates normally, conflagration mode where an on pad explosion ruptures the SRB's casings, and finally the deflagration mode which simulates a catastrophic fireball caused by a hypergolic liquid reaction.

REEDM also incorporates three modes of operation: operational, research, and diagnostic. The operational mode is designed for launch-support operations and automatically calculates many necessary program input variables. The research mode permits the user to examine and change program parameters (e.g., fuel loads, diffusion parameters, etc.). In the diagnostic mode, a very detailed output of the model calculations may be obtained.

The main input requirements of the REEDM program are meteorological data in the form of rawinsonde measurements and rocket vehicle parameters. Rawinsonde profiles of wind speed and direction, temperature and dew point, barometric pressure, relative humidity, and air density are required up to approximately 3,000 m (10,000 ft). Meteorological tower and doppler acoustic sounder measurements of wind direction and elevation angle standard deviations may optionally be used to specify atmospheric turbulence. Other meteorological parameters required by the model include the cloud cover, cloud ceiling height, and mixing depth. Rocket vehicle parameters (source inputs) required by REEDM depend on the vehicle and launch scenario. Default rocket vehicle parameters are provided in a data base file for the space shuttle, Titan II, Titan 34D, Titan IV, Delta 2914, Delta 3914, and Minuteman II. In general, the required vehicle parameters for SRB's are the solid fuel load, the solid fuel burn rate, the heat released per unit mass of the solid fuel, and the pollutant (hydrogen chloride, aluminum oxide, etc.) emissions per unit

Table 11-6. Summary of computer models available for hazard assessment.

Model	Type	Applicability	Meteorological Inputs	Source Inputs	Output
REEDM	Gaussian diffusion model coupled to a wind field model.	Static firings, normal launches, conflagrations, and deflagrations.	Rawinsonde profiles, cloud cover, ceiling height, and mixing depth. If available, tower or Doppler acoustic sounder wind direction and elevation angle measurements may be used as turbulence inputs.	Fuel load, fuel burn rate, fuel heat content, and pollutant emissions per unit weight of fuel burned. Coefficients of vehicle time-height curve also required for normal launches and deflagarations.	Peak concentration and dosage; time-mean concentration; cloud arrival and departure times; gravitational deposition and precipitation washout (maximum deposition or minimum pH). Plume rise, cloud position, and turbulence parameters may also be output. Graphics output is available.
HARM	Gaussian diffusion model.	Hypergolic expolsions above ground or in silos.	Rawinsonde profiles, cloud cover, ceiling height, and mixing depth.	Accident type and quantities of fuel and oxidizer released.	Peak concentration and dosage; time-mean concentration; cloud arrival and departure times; and precipitation washout. Graphics output is available.

Table 11-6. Summary of computer models available for hazard assessment (continued).

Model	Type	Applicability	Meteorological Inputs	Source Inputs	Output
AFTOX	Gaussian diffusion model.	Instantaneous and continuous liquid and gas releases. Includes buoyant rise for stack plumes and evaporation for spills.	Surface roughness length, cloud cover, ceiling height, wind speed and direction, air temperature, and mixing depth. Standard deviation of wind direction is optional turbulence input.	Type of release and quantity, molecular weight, and vapor pressure of chemical released. Contains data base of properties for 76 chemicals. Additional inputs required for stack releases.	Concentration at user-specified times. Graphics output is available, including 90 percent confidence limits on hazard distances.
D2PC	Gaussian diffusion model.	Instantaneous, quasi-continuous and continuous liquid and gas releases. Includes evaporation for spills. Designed primarily for application to chemical warfare agents.	Cloud cover, ceiling height, wind speed and direction, air temperature, barometric pressure, and mixing depth. Pasquill stability category can be entered to replace category determined from cloud cover/ceiling height and wind speed.	Essentially the same as AFTOX.	Peak concentration and dosage. Hazard distances to 1-percent lethality, no deaths, and no effects for chemical munitions.
OB/DG	Empirical diffusion model equation.	Continuous release at the surface (usually an evaporative spill).	Wind direction, wind direction standard deviation, and temperature difference between 56 and 6 ft.	Evaporation rate.	Downwind distance to specified concentration. Some versions predict 95-percent confidence limit on hazard distance.

Table 11-6. Summary of computer models available for hazard assessment (continued).

Model	Type	Applicability	Meteorological Inputs	Source Inputs	Output
BLAST	Acoustic.	Sonic boom propagation.	Rawinsonde profiles.	Vehicle flight profile.	Focus overpressures. Some versions estimate window damage.
BOOM	Acoustic.	Maximum overpressure for a surface noise source.	Rawinsonde profiles.	TNT equivalent of noise source.	Instantaneous overpressure.

Table 11-7. Summary of computer resources required by hazard assessment models.

Model	Computer Language	Specific Computers	Program Size	Comments
REEDM	FORTRAN 77	Mainframe IBM compatible PC-AT	Source code: 1.3 Mbytes Executable code: 1.33 Mbytes	Program can be segmented to reduce memory requirements.
HARM	FORTRAN 77	Mainframe	750,000 bytes	
AFTOX	BASIC	IBM compatible PC Zenith-100 Zenith-248		Two versions, one for Zenith-100 and one for Zenith-248.
D2PC	FORTRAN 77	Mainframe or PC	<200,000 bytes	
OB/DG	Many different versions exist	Scientific calculator		Many computerized versions exist for different applications.
BLAST	FORTRAN 77	Mainframe		
BOOM	BASIC	Microcomputer Radio Shack TRS-80 PC-2		

mass of the solid fuel. Similarly, the required vehicle parameters for hypergolic rocket engines are the total liquid fuel and oxidizer loads, the fuel and oxidizer flow rates, and the time after SRB ignition of the ignition of the liquid engine. Rocket vehicle parameters required for both solid motors and liquid hypergolic engines include the coefficients a, b, and c of the equation

$$t = ah^b + c \ , \tag{11.1}$$

where t is time and h is vehicle height above ground level. Finally, the REEDM program has an option to use a mesoscale wind field model to account for the effects of complex terrain on the low-level circulation (fig. 11-1). The use of this feature required terrain elevations for a grid system surrounding the launch site.

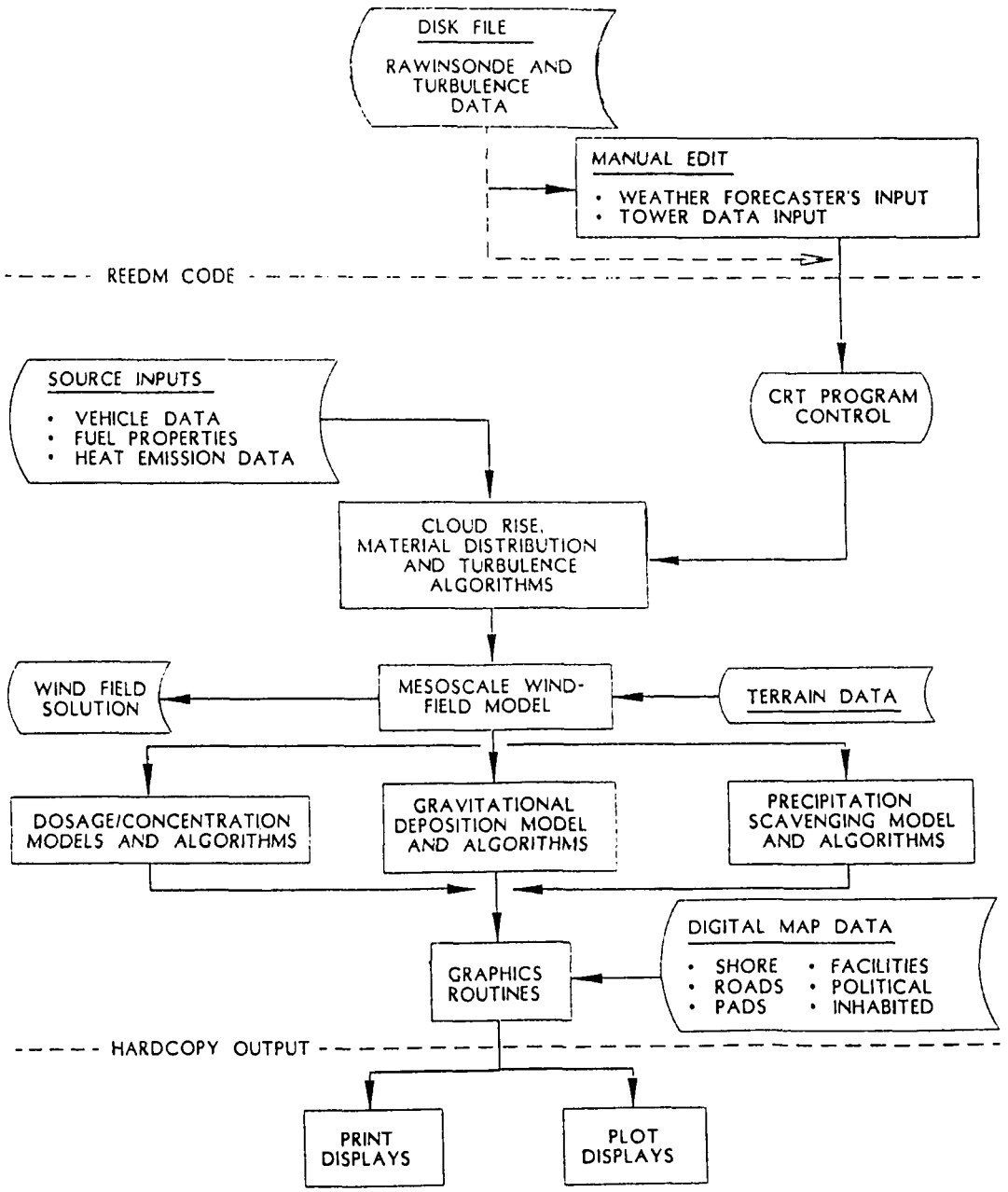

Figure 11-1. Schematic diagram illustrating the major components of the REEDM computer program.

The REEDM program output options include tables of peak concentrations, total dosages, cloud arrival and departure times, and time-mean concentrations at user-specified downwind distances; tables of maximum ground-level deposition at user-specified downwind distances; and tables of precipitation deposition expressed as either maximum deposition or minimum surface water pH at user-specified downwind distances. The program produces a summary or very detailed print output, depending on the mode of operation. The more detailed print output includes intermediate calculations such as plume rise, cloud position, and turbulence parameters. Graphics output options consist of plots of vertical profiles of the meteorological data; plots of centerline peak or time-average concentration, dosage, or deposition versus downwind distance; and isopleth (contour) plots of peak or time-mean concentration, dosage, and deposition. Examples of REEDM plots of centerline peak concentration and peak concentration isopleths are shown in figures 11-2 and 11-3, respectively.

The REEDM version 7 computer program is written in FORTRAN 77 and is designed for use on CDC CYBER 700, UNIVAC 1100, HP9000/800, and VAX 780 or 8000 series computers. The source program is 1.3 megabytes in length and the executable program requires approximately 1.33 megabytes of memory. The graphics output requires either a Calcomp 36-in drum plotter or a Tektronix 41xx terminal. An IBM PC-AT compatible adaptation of the REEDM version 7 code has recently been completed.

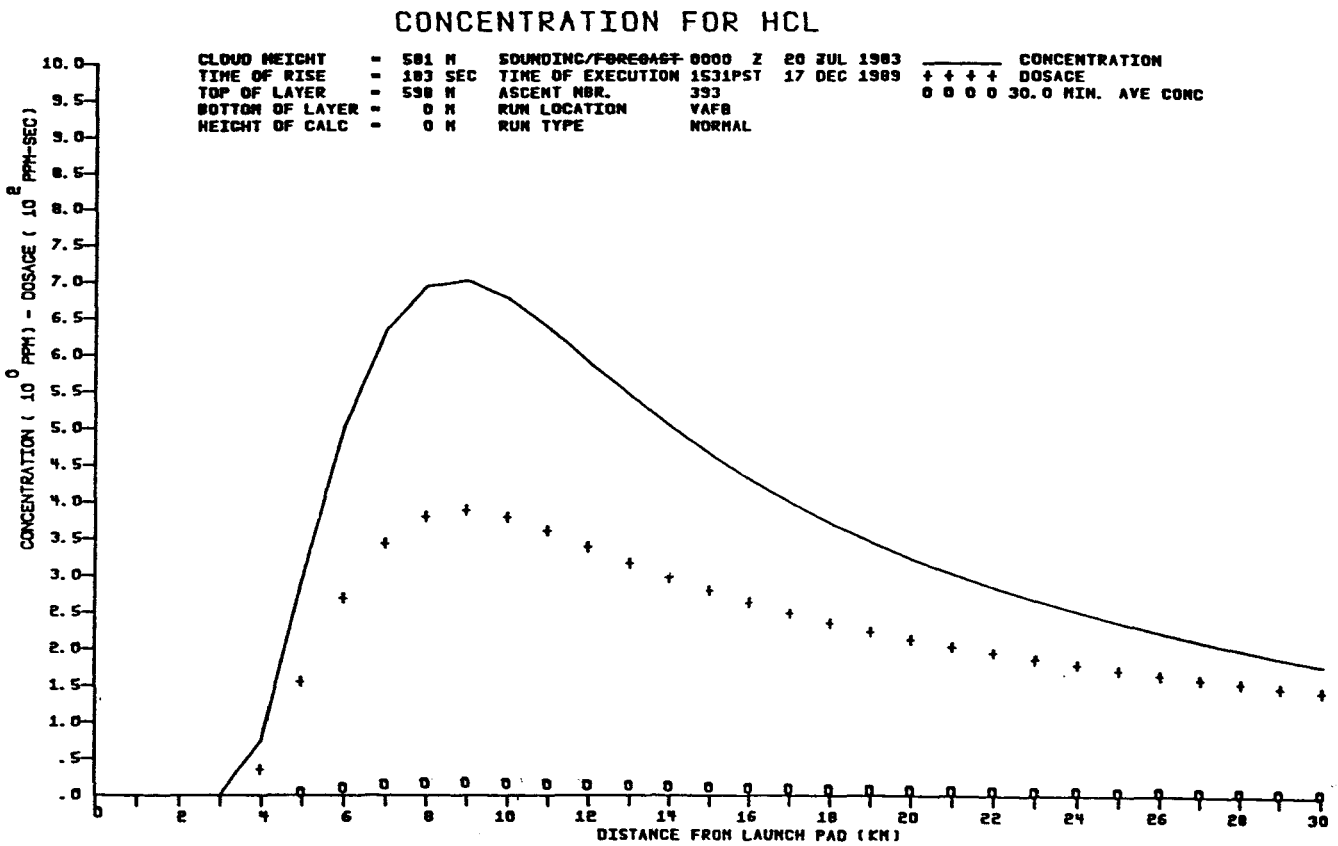

Figure 11-2. Example REEDM plot of centerline peak HCl concentration versus downwind distance for a space shuttle launch.

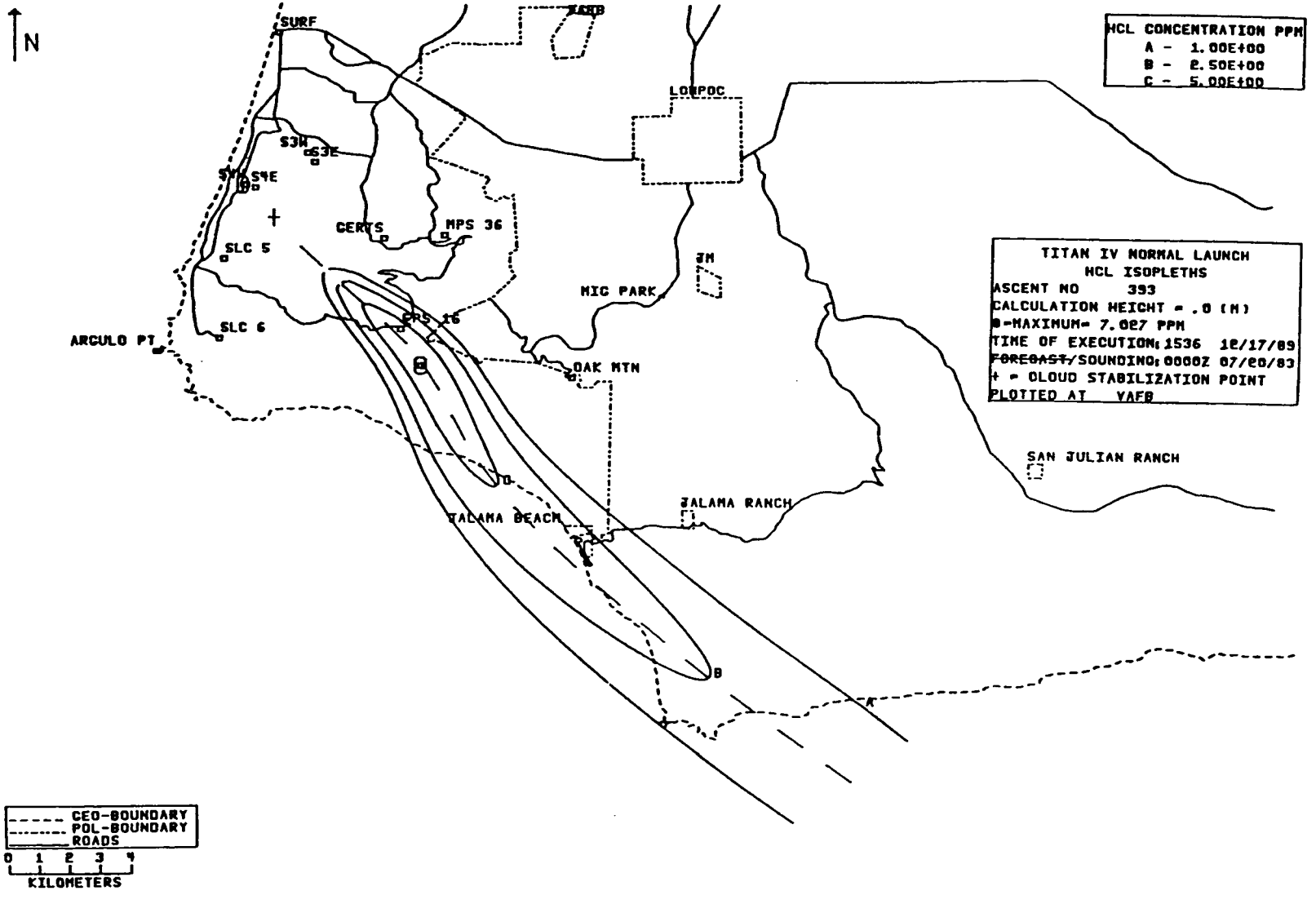

Figure 11-3. Example REEDM plot of peak HCl concentration in parts per million for a space shuttle launch.

11.8.3 HARM

The hypergolic accidental release model (HARM) (ref. 11.17) combines source characterization algorithms for hypergolic reactions (refs. 11.18 and 11.19) with the REEDM cloud rise and dispersion algorithms to predict the transport and dispersion of toxic clouds produced by hypergolic reactions. The four hypergolic accident scenarios that can be considered by the model are: (1) above ground, (2) in-silo with the silo door closed, (3) in-silo with the silo door open, and (4) ejected second stage detonation resulting from an in-silo explosion. The HARM computer program calculates peak concentration, dosage, time-mean concentration, and deposition due to precipitation scavenging (washout) at points downwind from the accident site. If the precipitation scavenging option is selected, the user may direct the program to predict either the maximum possible washout for the user-specified rainfall rate or the washout expected for the user-specified rainfall rate and precipitation start and end times.

The HARM computer program has operational, research, and production run modes. The operational mode, which is designed for real-time use during emergencies or accidents, automatically selects many of the required input parameters. The research mode allows the user greater freedom in specifying inputs and provides more detailed output, while the production mode is used to process multiple cases, usually in a batch environment.

The HARM program's meteorological inputs consist of rawinsonde profiles, the depth of the surface mixing layer, and the base and top of an elevated layer within which concentration or dosage predictions are desired. Other inputs include the cloud cover and ceiling height, the accident type, and the quantities of fuel and oxidizer released.

The HARM program's printed output consists of tables listing the upper-air sounding; stabilized cloud parameters; peak concentration, time-mean concentration, and dosage values along with range, bearing, and cloud arrival and departure times; and precipitation washout along with range and bearing. Graphics output options consist of: (1) vertical profiles of meteorological parameters plus the cloud shape at stabilization; (2) profiles of centerline concentration, dosage, and time-mean concentration or washout versus downwind distance for user-specified toxic chemicals; and (3) isopleths of concentration, dosage, and time-mean concentration or washout. The isopleths can be plotted on a standard map of the area.

The HARM computer code is written in FORTRAN 77 and requires no special computer facilities. Hardcopy printing and plotting facilities are helpful, but not required. Approximately 750,000 bytes of memory are used by the HARM code.

11.8.4 AFTOX

The U.S. Air Force toxic chemical dispersion model (ref. 11.20) is an interactive computer program designed to predict toxic chemical concentrations and dosages downwind of an accidental release. The program can also predict the dispersion of a buoyant stack plume. AFTOX is based on SPILLS, a model developed by the Shell Oil Company (ref. 11.21).

The AFTOX model requires chemical, source, and meteorological inputs. The AFTOX program contains a data file of the properties of 76 toxic chemicals. If the chemical to be modeled is not in this file, the model will request the chemical's molecular weight and vapor pressure. The molecular weight is used to convert concentrations to units of parts per million, while the vapor pressure is used in the evaporation calculations. If the molecular weight is not known, concentrations must be output in units of milligrams per cubic meter. If the vapor pressure is not known, AFTOX makes the worst-case assumption that the evaporation rate equals the spill rate. The program allows the user to update or modify its chemical data file. The AFTOX model's source inputs consist of the type of release (continuous or instantaneous, liquid and/or gas) and parameters that are dependent on the type of release. For a stack, these inputs include the emission rate, volumetric flow rate, and exit temperature. For a chemical spill, these inputs include the spill rate, total time of release, height of release, area of spill, and pool temperature. The AFTOX model's

meteorological inputs consist of the air temperature, wind speed and direction, standard deviation of wind direction (optional), sky cover and cloud category (low, middle, or high), ground condition, and mixing layer height.

Three output options are available with the AFTOX program: (1) a plot of concentration isopleths for up to three user-specified contour values, (2) the concentration at a user-specified location and time, and (3) the maximum concentration at a user-specified height and time after the spill. If the plot option is selected, the isopleth plot includes a hazard sector that represents the area expected to contain the minimum contour value approximately 90 percent of the time. This feature accounts for the fact that the concentration predicted by a diffusion model at a given downwind distance is the mean value that would be expected at that distance if the same release were made a number of times under similar meteorological conditions. Thus, hazard distances longer than indicated by the concentration isopleth can be expected about 50 percent of the time. All AFTOX output is directed to the user's terminal.

There are two versions of AFTOX, both written in the BASIC language. Version 1 was designed specifically for use on the Zenith-100 microcomputer and version 2 was designed for the Zenith-248 microcomputer. Both versions are IBM compatible, with version 2 having an enhanced color graphics capability. Hardcopy graphics and text output can be sent to a printer if available. Execution times for AFTOX can become large for cases with long downwind hazard distances. These times can be reduced by approximately a factor of 10 if a BASIC compiler is used to produce a directly executable binary copy of AFTOX.

11.8.5 D2PC

The U.S. Army chemical hazard prediction model D2PC (ref. 11.22) calculates peak concentrations and dosages and downwind hazard distances for continuous, instantaneous, or variable releases of toxic chemicals. The D2PC program is a revised version of the D2 program (Ref. 11.23) that includes a more user-friendly input environment and a vapor depletion option that considers losses by deposition/ground absorption and/or atmospheric chemical reactions. The D2PC program is primarily designed to provide the U.S. Army's chemical weapons storage facilities with a tool to estimate downwind hazard distances for accidental releases of chemical agents. Although the release scenarios built into D2PC are for chemical weapons, the program can estimate downwind concentrations and dosages for releases of most toxic materials by entering user-defined input parameters.

The D2PC program contains a rather broad data base that includes: (1) the location, average pressure, and seasonal average mixing layer heights of 11 U.S. Army chemical storage sites; (2) source parameters for 10 different chemical munitions; and (3) the physical constants, such as molecular weight, for 17 different toxic chemicals (including UDMH and hydrazine). If the accident/incident site, type of munition, or toxic chemical of interest is not in the D2PC data base, the user must provide the required information. Additional input parameters include the amount of chemical released, the type of release (explosion, evaporation, flash fire, etc.), the surface type and puddle dimensions for a spill, and the meteorological conditions (atmospheric stability, wind speed, ambient air temperature, barometric pressure, and mixing height). The user can select a Pasquill stability category or have the program estimate the stability category from the wind speed, cloud cover and height, date and time, and location. If the model is used in a wooded area, stability is not required because the dispersion rate is assumed to be a function only of the wind speed outside the woods.

The D2PC program provides print output only, and the user determines how descriptive this output will be. The output consists of a listing of the input parameters and the results of the concentration or dosage calculations. The default output, which is specifically designed for application to chemical agents, provides the approximate downwind hazard distances for 1-percent lethality, no deaths, and no effects. The user can also choose to have downwind distances calculated for specified dosage or concentration values.

The D2PC program is written in FORTRAN 77 for use on IBM-compatible personal computers. A hardcopy output device is useful but not necessary. The program requires less than 200,000 bytes of memory to execute. The program has also been run on mainframe computer systems. Because D2PC is written in FORTRAN 77, it is an alternative to the BASIC-coded AFTOX spill model.

11.8.6 Ocean Breeze/Dry Gulch (OB/DG)

The Ocean Breeze and Dry Gulch (OB/DG) diffusion model (ref. 11.24) is an empirical equation that predicts centerline concentration as a function of downwind distance for a ground-level release. The OB/DG equation was developed by the U.S. Air Force to consider the downwind hazards of accidental spills of propellants from the Titan II missile at Cape Canaveral, Florida and Vandenberg Air Force Base, California. The model is based on three field experiments conducted by the Air Force Cambridge Research Laboratories. The first, Project Prairie Grass (refs. 11.25–11.27), was conducted near O'Neill, Nebraska. The other two diffusion experiments took place at Cape Canaveral and Vandenberg Air Force Base and were named Ocean Breeze (ref. 11.28) and Dry Gulch (ref. 11.29), respectively. The composite data set from the Prairie Grass, Ocean Breeze, and Dry Gulch experiments was divided into two, with the first half of the data used to derive the OB/DG model equation and the second half used to test it. The regression fit to the first half of the data yielded

$$Cp/Q = (0.00211)\, X^{-1.96}\, \sigma_\theta^{-0.506}\, (\Delta T + 10)^{4.33}\,, \tag{11.2}$$

where

Cp = peak (centerline) concentration (g/m^3) at downwind distance X(m)

Q = release rate (g/s)

σ_θ = standard deviation of wind direction (degree)

ΔT= temperature difference (°F) between 56 and 6 ft.

Wind speed was initially considered in deriving the OB/DG equation, but was deleted because it did not significantly improve prediction accuracy. Because of the difficulty in obtaining σ_θ from the traces produced by the analog recorders in use at Titan II sites at that time, a second regression equation was derived in which ΔT is the only meteorological predictor.

The second half of the composite data set from the Prairie Grass, Ocean Breeze, and Dry Gulch experiments was used to evaluate the OB/DG equation and determine confidence limits. The peak concentrations predicted by the equation agreed to within a factor of 2 of the observed concentrations for 72 percent of the cases and to within a factor of 4 for 97 percent of the cases. After solving the OB/DG equation for the downwind distance to a hazard concentration, the Air Force normally multiplies this distance by 1.63 to obtain a 95-percent confidence that concentrations above the hazard level will not occur at longer downwind distances.

The OB/DG model is limited by its empirical basis. For example, it generally predicts shorter hazard distances than other diffusion models at night with stable meteorological conditions because it is principally based on day-time trials. Also, it is not applicable to instantaneous releases or to large buoyant clouds or plumes. Because the OB/DG model considers peak concentrations only, it cannot provide information on ground-level concentration patterns.

The advantage of the OB/DG model is that it requires minimal meteorological inputs and computer resources. Consequently, it has served for decades as a simple way of estimating hazard distances downwind of spills of toxic propellants. Over the years, the OB/DG equation has been implemented in

forms ranging from nomograms to computer programs. Many variations and modifications such as changes in units of input parameters have been made for specific applications. If an existing OB/DG computer program is used, the exact model formulation should therefore be determined.

11.8.7 BLAST

The BLAST model is designed to predict the propagation of sonic booms. Based on the original work by Plotkin (ref. 11.30), BLAST was developed for use by the U.S. Air Force at the Eastern and Western Test Ranges. The model uses rawinsonde profiles of pressure, temperature, and winds as meteorological inputs and the flight profile as source inputs. Some versions of BLAST go beyond the prediction of sonic boom focus overpressures and combine population densities with predicted overpressures to estimate window damage. Worst-case analyses can be performed by allowing BLAST to modify the rawinsonde profiles in order to maximize the overpressures predicted at the surface. The interpretation of the BLAST computer program's output is rather difficult and requires experience.

11.8.8 BOOM

The blast operational overpressure model (BOOM) (ref. 11.31) was developed by the U.S. Air Force to predict the far-field acoustic overpressures produced by explosions at the surface. Rather than use computer intensive ray tracing techniques, BOOM uses a simple, semi-empirical equation to predict the instantaneous overpressure. This equation is based on the maximum value of $\Delta v/\Delta z$, where Δv is the difference in sound between the surface and height Δz above the surface. The BOOM computer program determines the vertical profile of the speed of sound from rawinsonde profiles of pressure, temperature, and winds. The model's empirical coefficients are based on data from two sets of surface detonations. Although BOOM is specifically designed for application to explosions at the surface, it can be applied to any surface sound source that can be defined in terms of the TNT equivalent explosive weight. The BOOM computer code is written in BASIC and is specifically designed for use on a Radio Shack TRS-80 PC-2 portable microcomputer.

An elaborate, site-specific, sound propagation model (ref. 11.32) called "Noise Assessment and Prediction System" (NAPS), is now in place at Aberdeen Proving Ground, MD. However, it is currently being made transportable for use at other ranges. It is an automated program/system which includes ray-tracing and sound-level contouring, etc.

REFERENCES

11.1 Anderson, J., and Keller, V.W.: "A Field Study of Solid Rocket Exhaust Impact on the Near-Field Environment." NASA Technical Memorandum, October 1989.

11.2 Jacobson, J.S., and Hill, A.C.: "Recognition of Air Pollution Injury to Vegetation—A Pictorial Atlas." Air Pollution Control Association, Pittsburgh, PA, 1970.

11.3 Schmalzer, P.A., Hinkle, C.R., and Breininger, D.: "Effects of Space Shuttle Launches STS-1 Through STS-9 on Terrestrial Vegetation of the John F. Kennedy Space Center." NASA Technical Memorandum 83103, September 1985.

11.4 Houghton, D.D. (ed.): "Handbook of Applied Meteorology." John Wiley & Sons, New York, 1985.

11.5 Randerson, D. (ed.): "Atmospheric Science and Power Production." DOE/TIC-27601 (NTIS Accession No. DE84005177), Technical Information Center, U.S. Department of Energy, 1984.

11.6 Pasquill, F.: "The Estimation of the Dispersion of Windborne Material." Meteorology Magazine, vol. 90, 1961, pp. 33–49.

11.7 Anderson, B.J., and Keller, V.W.: "Acidic Deposition Production Mechanism—Space Shuttle Environmental Effects—The First Five Flights," 1983, pp. 155–156.

11.8 Kunkel, B.A.: "AFTOX Computer Program Software, Version 2—CH.DAT Chemical Data File." Air Force Geophysics Laboratory, Hanscom Air Force Base, MA, 1986.

11.9 Registry of Toxic Effects of Chemical Substances. Department of Health and Human Services, Washington, DC, January to September 1989.

11.10 Emergency and Continuous Exposure Guidance Levels for Selected Airborne Contaminants, Volume 7, Ammonia, Hydrogen Chloride, Lithium Bromide, and Toluene, Board on Environmental Studies and Toxicology, Commission on Life Sciences, National Research Council, National Academy Press, Washington, DC, 1987.

11.11 Bjorklund, J.R., et al.: "User's Manual for the REEDM (Rocket Exhaust Effluent Diffusion Model) Computer Program." NASA Contractor Report 3646, December 1982.

11.12 Bjorklund, J.R., and Dumbauld, R.K.: "User's Instructions for the NASA/MSFC Cloud-Rise Preprocessor Program—Version 6, and the NASA/MSFC Multilayer Diffusion Program—Version 6." NASA Contractor Report 2945, January 1971.

11.13 Stevens, J.B., Susko, M., Kaufman, J.W., and Hill, C.K.: "An Analytical Analysis of the Dispersion Predictions for Effluent From Saturn V and Scout-Algol III Rocket Exhausts." George C. Marshall Space Flight Center, NASA Technical Memorandum X-2935, October 1973.

11.14 Kaufman, J.W., Susko, M., and Hill, C.K.: "Prediction of Engine Exhaust Concentrations Downwind from the Delta-Thor Telsat-A Launch of November 9, 1972." George C. Marshall Space Flight Center, NASA Technical Memorandum X-2939, November 1973.

11.15 Susko, M., Hill, C.K., and Kaufman, J.W.: "Downwind Hazard Calculations for Space Shuttle Launches at Kennedy Space Center and Vandenberg Air Force Base." George C. Marshall Space Flight Center, NASA Technical Memorandum X-3162, December 1974.

11.16 Bjorklund, J.R.: "User's Manual for the REEDM Version 7 (Rocket Exhaust Effluent Diffusion Model) Computer Program, Volume I." H.E. Cramer Co., Inc., Salt Lake City, UT, 1989.

11.17 Bjorklund, J.R., et al.: "User`s Manual for the Hypergolic Accidental Release Model (HARM) Computer Program." H.E. Cramer Co., Inc., Salt Lake City, UT, 1984.

11.18 Prince, S.: "Atmospheric Dispersion of Hypergolic Liquid Rocket Fuels—Phase I: Source Characterization." Martin Marietta Aerospace Division, Denver, CO, 1982.

11.19 Prince, S.: "Atmospheric Dispersion of Hypergolic Liquid Rocket Fuels—Phase II: Atmospheric Dispersion Modeling." Martin Marietta Aerospace Division, Denver, CO, 1983.

11.20 Kunkel, B.A.: "User`s Guide for the Air Force Toxic Chemical Dispersion Model (AFTOX)." Report No. AFGL-TR-811-0009, ERP No. 992, Air Force Geophysics Laboratory, Hanscom Air Force Base, MA, 1981.

11.21 Fleischer, M.T.: "SPILLS—An Evaporation/Air Dispersion Model for Chemical Spills on Land." Shell Development Company, NTIS Accession No. PB 83109470, 1980.

11.22 Whitacre, C.G., Grimes, J.H., Myirski, M.M., and Sloop, D.W.: "Personal Computer Program for Chemical Hazard Prediction (D2PC)." CRDEC-TR-87021, Aberdeen Proving Ground, MD, 1987.

11.23 Whitacre, C., and Myirski, M.: "Computer Program for Chemical Hazard Prediction (D2)." ARCSL- TR-82014, Chemical Systems Laboratory, DRDAR-CLO-R, Aberdeen Proving Ground, MD, 1982.

11.24 Kunkel, B.A.: "An Evaluation of the Ocean Breeze/Dry Gulch Dispersion Model (OB/DG)." AFGL-TR-84-0313 ERP. No. 900, Air Force Geophysics Laboratory, Hanscom Air Force Base, MA, 1984.

11.25 Barad, M.L. (ed.): "Project Prairie Grass, A Field Program in Diffusion, Volume I." AFCRC-TR-511-235(I), AD-152573, 1951.

11.26 Barad, M.L. (ed): "Project Prairie Grass, A Field Program in Diffusion, Volume II." AFCRC-TR-511-235(II), AD-152573, 1951.

11.27 Haugen, D.A. (ed.): "Project Prairie Grass, A Field Program in Diffusion, Volume III. AFCRC-TR-511-235(III), AD-217076, 1959.

11.28 Haugen, D.A., and Fuguay, J.J. (eds.): "The Ocean Breeze and Dry Gulch Diffusion Programs, Volume 1." AFCRL-63-791(I), AD-428436, 1963.

11.29 Haugen, D.A., and Taylor, J.H. (eds.): "The Ocean Breeze and Dry Gulch Diffusion Programs, Volume 2. " (AFCRL-63-791(II), AD-427687, 1963.

11.30 Plotkin, J.K., and Cantrill, J.M.: "Prediction of Sonic Boom at a Focus. Wyle Laboratories," WR75-7, October 1975.

11.31 Douglas, D.A.: "Blast Operational Overpressure Model (BOOM): An Ambient Prediction Method." AFWL-TR-85-150, Air Force Weapons Laboratory, Kirtland Air Force Base, NM, 1987.

11.32 Olsen, R.O., and Noble, J.M.: "A Noise Assessment and Prediction System." NASA-LaRC Fourth International Symposium on Long-Range Sound Propagation, December 1990, pp. 231–244.

SECTION XII OCCURRENCES OF TORNADOES AND HURRICANES

12.1 Introduction

Severe weather may adversely affect the design, transportation, test, and operation of aerospace vehicles. This section contains a discussion of such atmospheric phenomena. (The reader is referred to section IX for a discussion of lightning and thunderstorm activity and to section V for information regarding severe worldwide weather conditions, including tornado, waterspout, dust devil, and hurricane extreme winds. Hail criteria is presented in section VII.)

12.2 Tornadoes

A tornado is a violently rotating column of air in contact with the ground which can be seen when it contains either surface dust and debris or condensation. Water spouts are tornadoes occurring on a water surface, and a funnel cloud occurs when the air column does not reach the ground. Although tornadoes are regarded as the most destructive wind force, most tornadoes (62 percent) are weak tornadoes. Weak tornadoes have wind speeds close to or below 100 miles per hour (mi/h), while strong tornado speeds may be in excess of 200 mi/h (ref. 12.1). Due to differential pressures created by tornadoes, buildings have been known to literally explode. Tornadoes are sometimes observed in association with hurricanes in Florida and along the coastal states. A subsection is presented here on this topic. Fortunately, the aerial extent of tornadoes is small compared with hurricanes. Tornado paths are predominately from the southwest direction (59 percent), with 72 percent of all F5 scale tornadoes being from the southwest (ref. 12.2). Figure 12.1 is a United States contour map showing the average annual tornado incidence per 10,000 mi^2 between 1953 and 1980. On this map, the months of peak tornado activity and average number of annual occurrences are given for each state (ref. 12.1). The three main centers of highest tornado incidence occur around Florida, Oklahoma, and Indiana.

The Fujita tornado intensity scale (F-scale) was introduced by Fujita (ref. 12.2) in 1971. Table 12.1 describes some characteristics of this six-point scale. The five most deadly (loss of life) individual tornadoes that have occurred over a 40-year time span in the U.S. since 1950 are shown in table 12.2 (ref. 12.3). Note that the associated F-scale is given, whereby indicating that loss of life is indeed more frequent in violent tornadic storms. The most individual tornadoes to occur on a single tornado day (i.e., tornado outbreak) is 144 on April 3, 1974, with path lengths totaling 2,452 miles (ref. 12.2). Tornado length, width, and area characteristics are presented in table 12.3 (ref. 12.4) for various states of interest to NASA. Fujita calculated what the maximum tornadic windspeeds would be with a 10^{-7} or 1/10,000,000 per year probability of occurrence. These windspeed categories are presented in fig. 12.2 for the continental United States. The highest windspeed of 308 mi/h with a 10^{-7} per year probability was found to be located in both central Oklahoma and northern Alabama. Windspeeds of 320 mi/h appear to be a reasonable maximum speed for tornadoes east of 105° longitude (eastern and central U.S.); while 180 mi/h maximum is reasonable west of 105° longitude (ref. 12.4).

Based on Thom's analysis of the number of tornado occurrences (ref. 12.5), table 12.4 has been prepared giving tornado statistics for stations of interest. The statistics included in table 12.4 are based upon an area (A_2) of a 1° square of latitude and longitude on the Earth's surface. The period of record is 1954 to 1983 (ref. 12.3). The probability of one or more tornadoes in N years in an area (A_1) is given by[1]

$$P(A_1;N) = 1-\exp[(-\bar{x}*A_1*N)/A_2] \ , \tag{12.1}$$

where $\bar{x}$ is the mean number of tornadoes per year in a 1° square. The area size for A_1 was chosen as 7.3 km^2 (2.8 mi^2) because Thom (ref. 12.5) reports that 7.2572 km^2 (2.8209 mi^2) is the average ground area covered

[1] Credit is due Dr. J. Goldman, International Center for the Solution of Environmental Problems, Houston, Texas, for this form of the probability expression.

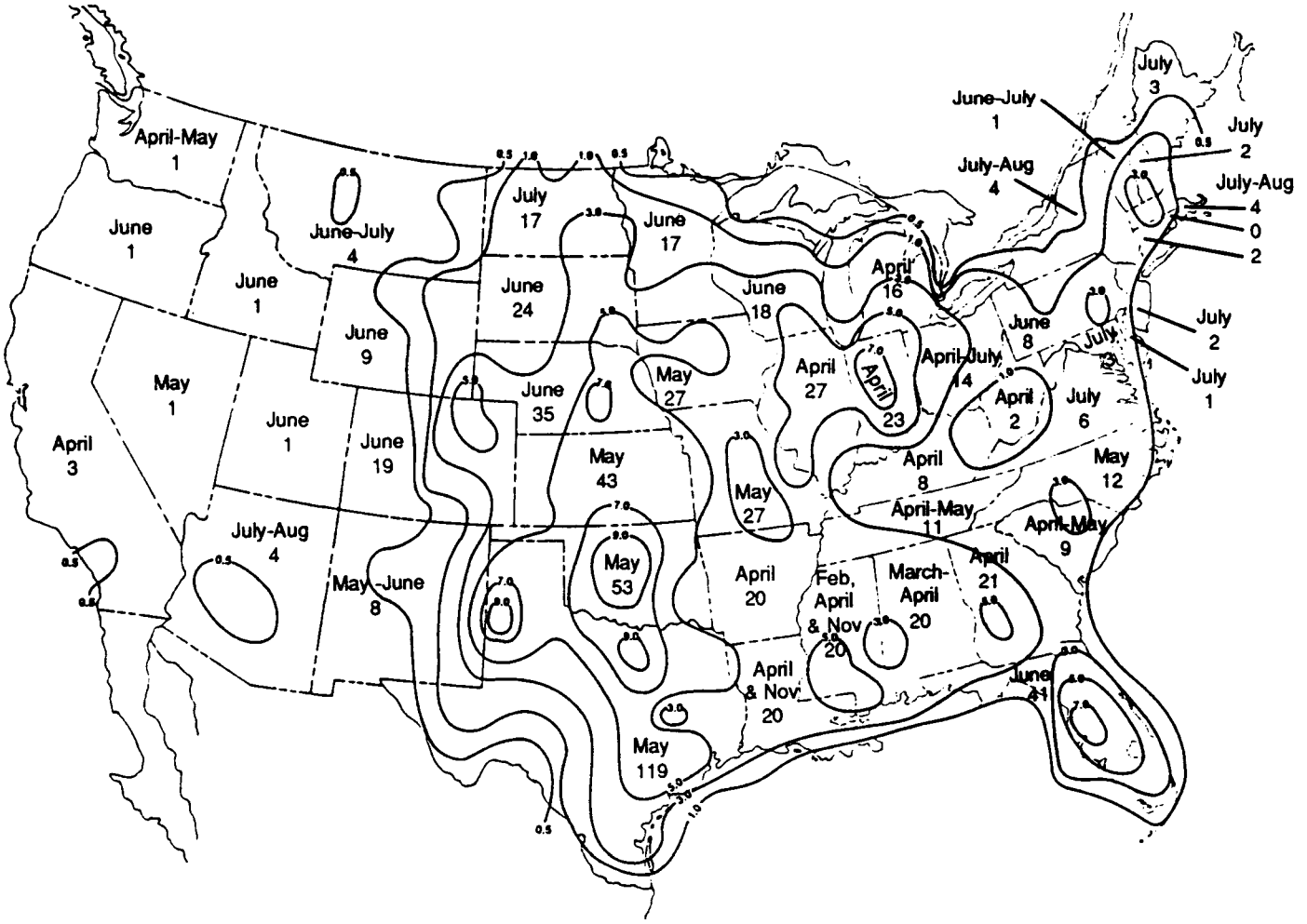

[1]Month of peak tornado activity given on each state.

[2]Lower figure is average, annual tornadoes for each state.

Figure 12.1 Contours of average annual tornado incidence per 10,000 square miles, 1953–1980[1,2] (ref. 12.1).

Table 12.1 F-scale tornado intensities and corresponding windspeed ranges and characteristics (ref. 12.2)

Tornado Intensity	F-Scale	Sustained Damage	Windspeed (mi/h)	F-Scale Percent Occurrence	Mean Path Length (mi)	Path Length Percent Occurrence
Weak	0	Light	40–72	25.5	1.2	7.3
	1	Moderate	73–112	37.3	2.6	22.9
Strong	2	Considerable	113–157	25.6	5.4	32.5
	3	Severe	158–206	9.3	10.0	21.8
Violent	4	Devastating	207–260	2.0	27.2	13.2
	5	Incredible	>261*	0.3	35.5	2.4

*Up to ~318 mph.

Table 12.2 Five deadliest individual tornadoes 1950–1989 (ref. 12.3).

Date	Place	Deaths	F-Scale
1. June 8, 1953	Flint, MI	116	F5
2. May 11, 1953	Waco, TX	114	F5
3. June 9, 1953	Worcester, MA	90	F4
4. May 25, 1955	Udall, KS	80	F5
5. February 21, 1971	Pugh City, MS	58	F4

Table 12.3 Tornado event characteristics, 1954–1983 (ref. 12.4).

State	No. of Events	Tornado Length (mi)			Tornado Width (mi)			Tornado Area (mi^2)		
		Average	F0 95%	F4 95%*	Average	F0 95%	F4 95%	Average	F0 95%	F4 95%
Alabama	685	7.25	42.7	53.5	0.099	0.327	0.677	1.048	8.02	19.1
California	111	1.87	7.55	—	0.059	0.223	—	0.239	0.645	—
Florida	1,328	2.67	8.70	—	0.028	0.074	—	0.137	0.368	—
Louisiana	703	4.56	20.2	36.6	0.055	0.161	1.43	0.379	1.76	17.0
Mississippi	744	8.72	47.8	58.2	0.106	0.341	0.616	1.093	7.39	11.2
New Mexico	250	3.54	15.5	—	0.100	0.483	—	0.291	3.19	—
Texas	4,008	3.42	13.9	44.5	0.063	0.184	1.23	0.453	1.43	26.2
Utah	36	0.89	3.53	—	0.049	0.328	—	0.069	0.629	—
Eastern U.S. Longitude <105°	21,583	4.44	18.5	113.0	0.068	0.224	0.968	0.512	2.08	39.5
Western U.S. Longitude >105°	779	2.29	8.03	—	0.049	0.163	—	0.137	0.514	—

*Assume log-normality distribution.

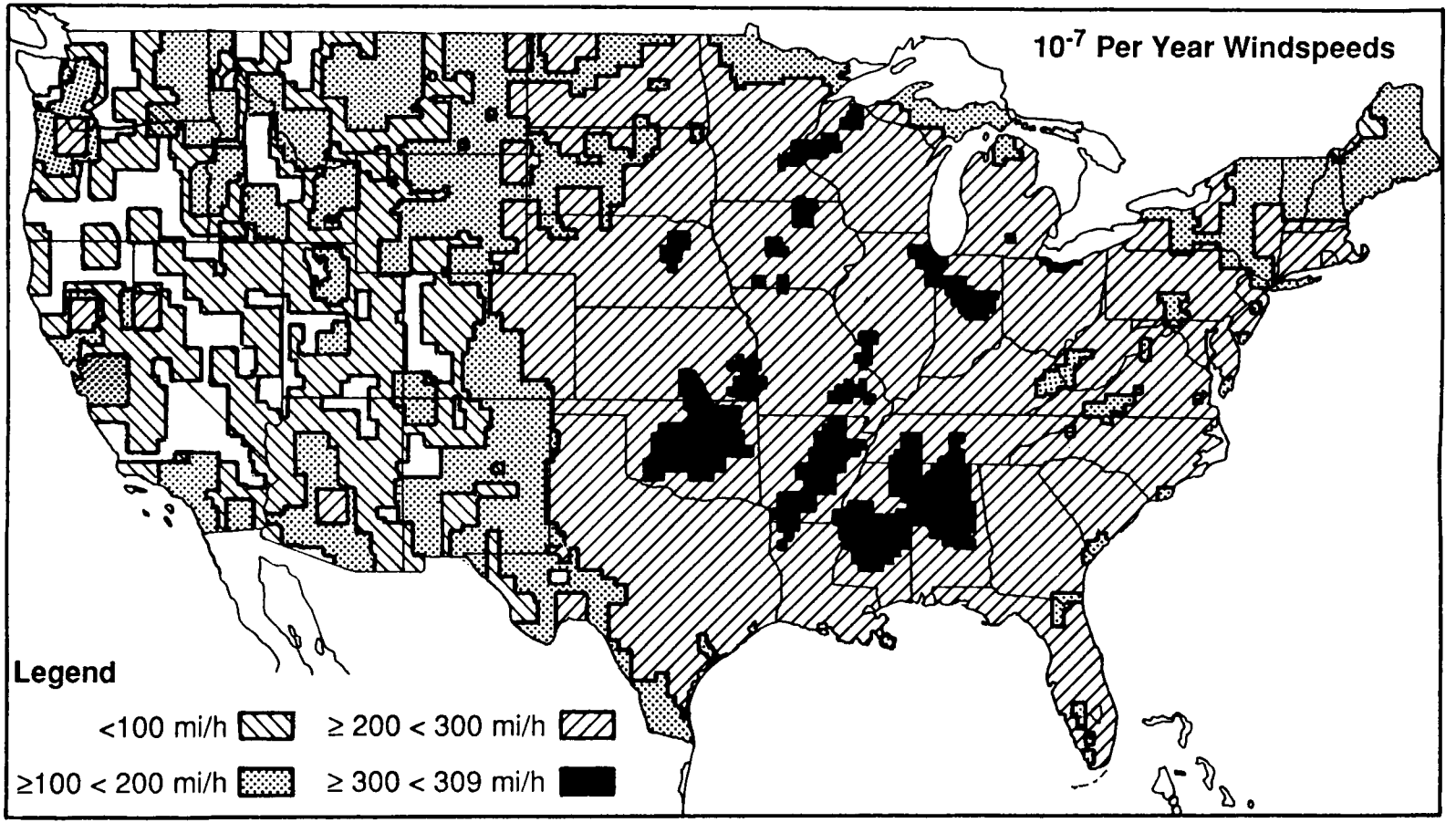

Figure 12.2 Distribution of the maximum windspeeds of tornadoes expected to occur with a 10^{-7} or 1/10,000,000 per year probability which is required for protecting nuclear power plants in the United States (ref. 12.2).

Table 12.4 Tornado statistics for stations specified, 1954–1983.

Station	Number of Tornadoes in 1° Square	Mean ($\bar{x}$) Number of Tornadoes Per Year in 1° Square	Area (A_2) of 1° Square km² (mi²)	Mean (P) Probability of a Tornado Striking a Point in Any Year in 1° Square	Mean (R) Recurrence Internal (yr) for a Tornado Striking a Point in a 1° Square
Huntsville	95	3.17	10,179 (3,930)	0.002275	440
Kennedy Space Center	59	1.97	10,839 (4,185)	0.001328	753
Vandenberg AFB	2	0.07	10,179 (3,930)	0.000050	19,902
Edwards AFB	11	0.37	10,179 (3,930)	0.000266	3,759
New Orleans	75	2.50	10,645 (4,110)	0.001716	583
NSTL, Bay St. Louis	72	2.40	10,645 (4,110)	0.001647	607
Houston	187	6.23	10,736 (4,145)	0.004240	236
White Sands	7	0.23	10,412 (4,020)	0.000161	6,211

$P = 2.8209\,\bar{x}/A_2$, $R = 1/P$

Table 12.5 Probability of one or more tornadoes in a 7.3-km² area and a 2.59-km² area in 1, 10, and 100 years.

Station	Mean ($\bar{x}$) Number of Tornadoes Per Year in 1° Square	$P(A_1;N)$ for A_1 = 7.3 km² (2.8 mi²)			$P(A_1;N)$ for A_1 = 2.59 km² (1.00 mi²)		
		N=1 Year	N=10 Years	N=100 Years	N=1 Year	N=10 Years	N=100 Years
Huntsville	3.17	0.002256	0.022585	0.202164	0.000807	0.008066	0.077494
Kennedy Space Center	1.97	0.001317	0.013180	0.131804	0.000471	0.004707	0.045982
Vandenberg AFB	0.07	0.000050	0.000499	0.004975	0.000018	0.000178	0.001780
Edwards AFB	0.35	0.000249	0.002494	0.024936	0.000089	0.000891	0.008866
New Orleans	2.50	0.001702	0.016887	0.170316	0.000608	0.006083	0.059014
NSTL, Bay St. Louis	2.40	0.001634	0.016217	0.150837	0.000584	0.005839	0.056722
Houston	6.23	0.004199	0.041211	0.343508	0.001503	0.015030	0.139552
White Sands	0.23	0.000160	0.001601	0.015892	0.000057	0.000572	0.005705

$P(A_1;N) = 1 - e^{-\bar{x}(A_1/A_2)N}$

by tornadoes in Iowa, and the vital industrial complexes for most locations are of this general size. Thus defining A_1 as 7.3 km^2 (2.8 mi^2) and 2.59 km^2 (1.0 mi^2) and evaluating equation 12.1 for the values of $\bar{x}$ and A_2 for the stations given in table 12.4 yields the data in table 12.5. Table 12.5 gives the probability of one of more tornadoes in 7.3 km^2 and 2.59 km^2 areas in one year, 10 years, and 100 years for the indicated eight locations. It is noted that for $A_1 << A_2$ and N < 100, equation (12.1) can be approximated by

$$P(A_1;N) = (\bar{x} * A_1 * N)/A_2 \ . \qquad (12.2)$$

An interpretation of the statistics in table 12.5 is given using Kennedy Space Center (KSC) as an example. There is a 13.2 percent chance that at least one tornado will "hit" within a 7.3 km^2 (2.8 mi^2) area at KSC in 100 years. For a 2.59 km^2 (1 mi^2) area at KSC, the chance of at least one tornado hit in 100 years is 4.6 percent. If several structures within a 7.3 km^2 area at KSC are vital to a space mission and these structures are not designed to withstand the wind and internal pressure forces of a tornado, then there is a 13.2 percent chance that one or more of these vital structures will be damaged or destroyed by a tornado in 100 years. If the desired lifetime of these structures (or 7.3 km^2 industrial complex) is 100 years and the risk of destruction by tornadoes is accepted in the design, then the design risk or calculated risk of failure of at least one structure due to tornado occurrences is 13.2 percent. This example serves to point out that the probability of occurrence of an event which is rare in 1 year becomes rather large when taken over many years, and that estimates for the desired lifetime versus design risk for structures discussed in subsection 2.2.10 of section II should be made with prudence.

12.3 Tornadoes Generated From Hurricanes

From a study by R. Gentry (ref. 12.6), which used a 22-year data base, it was determined that in nearly all full-intensity hurricanes, whose centers cross the U.S. coastline (south of Long Island, NY, and east of Brownsville, TX), have tornadoes associated with them. Also approximately 60 percent of tropical storms crossing into land develop tornadoes.

Most tornadoes (~20 percent) form near the hurricane core, or form within 100 km (~80 percent) of the hurricane center and frequently northeast and east of the center (between 20° and 120° azimuth) where the tipping and convergence terms of the vorticity equation are the largest. That is where the lower atmospheric layers are slowed by ground friction, but the upper (850-mb level) winds are still moving at high hurricane speeds, thus creating strong vertical shears in the horizontal wind component. Satellite-observed cloud-top temperatures were also very low in these tornadoes, or the tornado formed in areas of existing strong temperature gradients. Generally the air that goes into and forms a tornado does not travel far from the ocean before genesis. In most cases, the tornadoes formed closer to the water (coastline) than to the hurricane center (with the center being farther inland). Finally, as a hurricane moves farther inland and loses its tropical characteristics, some tornadoes do form, but these do not have the genesis characteristics of the classical hurricane-spawned tornado. Hurricane-generated tornadoes can occur at any local time, but 50 percent were found to occur between 1200 and 1800 l.s.t. Figure 12.3 presents the locations of all hurricane-associated tornadoes, occurring between 1972 and 1980 (ref. 12.6), as a function of distance from the coastline. The hurricane David ground track is plotted in figure 12.3, as a reference for the David tornado occurrences.

12.4 Hurricanes and Tropical Storms

The occurrence of hurricanes at KSC and other locations for the Eastern range is of concern to the space program because of high winds and because the range support for space operations is closed during passage or near approach of a hurricane. This discussion will be restricted to the frequency of tropical storms, hurricanes, and tropical cyclones (tropical storms combined with hurricanes) for annual reference periods and certain monthly groupings, as a function of radial distances from KSC as well as some information about tropical storms in the Gulf Coast area.

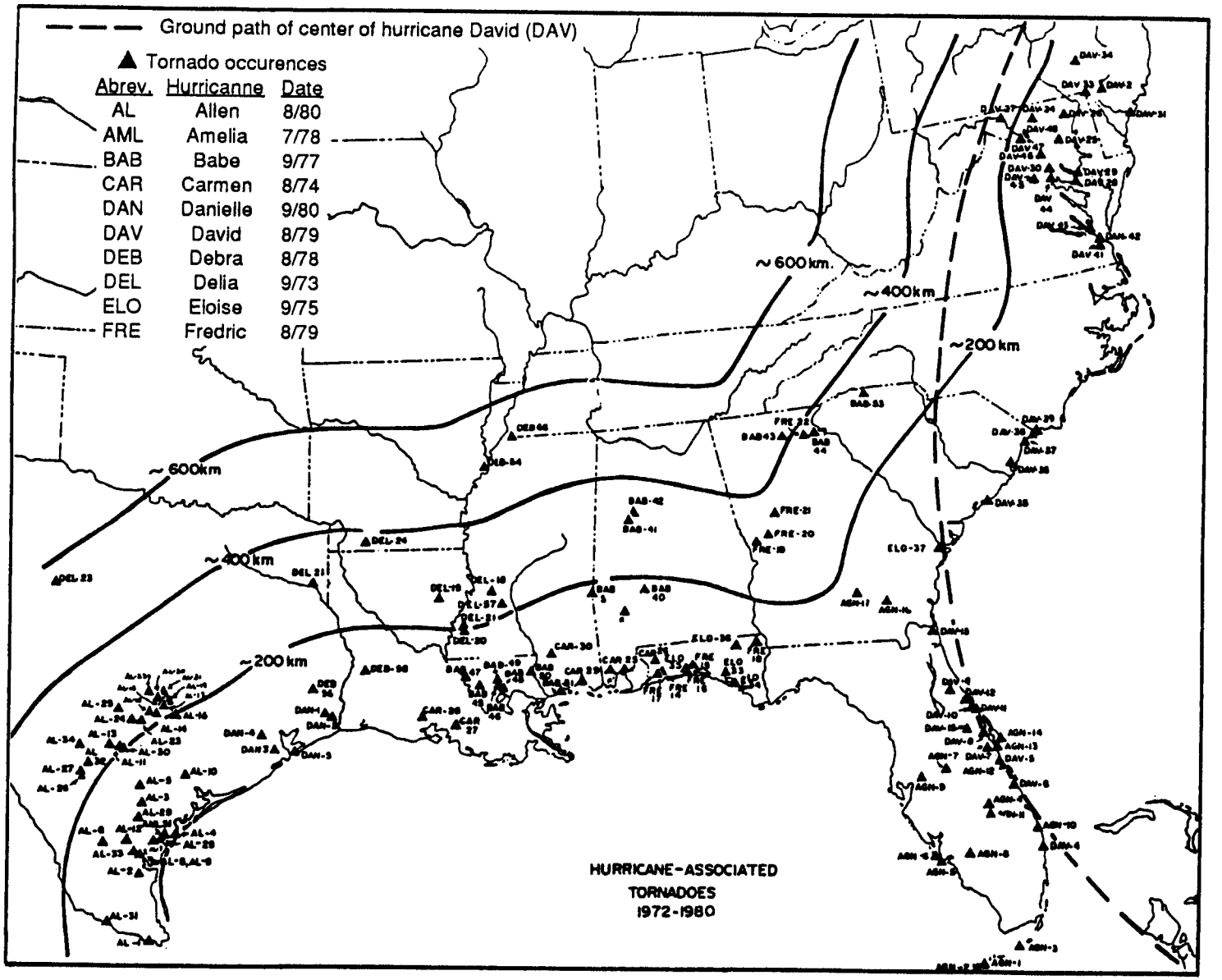

Figure 12.3 Location of tornadoes associated with hurricanes for the period 1972–80 with indications of the distance from the coast (ref. 12.4).

Table 12.6 Saffir/Simpson scale of hurricane intensity (ref. 12.7).

Storm Category	Storm Surge (feet)	Mean Wind Speed (knots)
1. Weak	4–5	64–82
2. Moderate	6–8	83–95
3. Strong	9–12	96–112
4. Very Strong	13–18	113–135
5. Devastating	18–?	136–?

By definition, a hurricane is a storm of tropical origin with maximum sustained (1-min mean) surface winds greater than or equal to 34 m/s (65 knots). A tropical storm is a cyclone whose origin is in the tropics with sustained winds equal to or less than 33 m/s (64 knots) but greater than or equal to 18 m/s (35 knots).

There is an established hurricane intensity scale which categorizes a hurricane's mean windspeed (and surge) versus its severity. It is called the Saffir/Simpson scale of hurricane intensity (ref. 12.7) and is presented in table 12.6. There is no upper limit for windspeed in hurricanes, but speeds exceeding 90 m/s (175 knots) have been measured. In the United States, maximum hurricane windspeeds of 89.4 m/s (173.9 knots) have been recorded at Matecubme Key, FL, in 1935 and during Hurricane Camille on the Louisiana/Mississippi coast in 1969 (ref. 12.8). Tornadoes have also been observed in association with hurricanes as previously mentioned in subsection 12.3.

Tables 12.7 and 12.8 give a general indication of the frequency of tropical storms and hurricanes by months within 161- and 644-km (100- and 400-nmi) radii of KSC. From table 12.7, it is noted that hurricanes within these radii of KSC have been observed as early as May and as late as November, with highest frequency during August and September. In the 102-year period (1886–1987), there were 34 hurricanes that came within a 161-km (100-nmi) radius of KSC during this period. Although a hurricane path may come within a radius of 161 km (100 nmi), the windspeeds observed at KSC are not always greater than 33 m/s (64 knots). The highest recorded KSC hurricane-associated wind gust speed was 45.5 m/s (88.4 knots) measured atop (96 m) the launch complex 34 service structure during hurricane Dora on September 9, 1964. A simultaneous measurement of 42.4 m/s (82.3 knots) from the 21-m level, blockhouse location, was also recorded (ref. 12.9). Hurricanes at distances greater than 161 km (100 nmi) from KSC can possibly produce hurricane force winds at KSC.

Severe thunderstorms, and hurricanes downgraded to tropical storms, have also produced strong peak winds in the KSC area; i.e., peak speeds of 38.8 m/s at 150 m and 34.2 m/s at 18 m were recorded from downgraded Hurricane Abby in June 1968. Nonhurricane-associated winds at KSC have reached 26.2 m/s at 18 m and 32.6 m/s at 150-m levels (ref. 12.9). In general, hurricanes approaching KSC from the east (from the sea) will produce higher winds than those approaching KSC after crossing the peninsula of Florida (from the land). Hurricane David, September 1979, was the first hurricane to strike the Cape Canaveral area directly since 1926. The eastern edge of the eye passed within an estimated 1.5 mi of the space shuttle runway. Hurricane David's peak speed of 34.5 m/s (measured at 10.4 m) exceeded the design launch peak wind speed profile of the space shuttle natural environment requirements for a 5-percent risk of exceeding a 10-m level peak windspeed of 15.8 m/s (30.8 knots) for the windiest 1-h exposure period (ref. 12.10).

Table 12.7 Number of hurricanes in a 102-yr period (1886–1987) within a 161- and 644-km radius of KSC.

Number of Hurricanes Within		
Month	161-km (100-nmi) Radius	644-km (400-nmi) Radius
January	0	0
February	0	0
March	0	0
April	0	0
May	1	2
June	1	11
July	3	15
August	13	51
September	8	51
October	7	41
November	1	8
December	0	0
Total	34	179

Table 12.8 Number of tropical storms in a 117-yr period (1871–1987) within a 161-644-km radius of KSC

Number of Tropical Storms Within		
Month	161-km (100-nmi) Radius	644-km (400-nmi) Radius
January	0	0
February	1	1
March	0	0
April	0	0
May	2	4
June	7	31
July	6	29
August	23	69
September	24	112
October	33	103
November	1	17
December	1	1
Total	98	367

12.4.1 Distribution of Hurricane and Tropical Storm Frequencies

Knowing the mean number of tropical storms or hurricanes (events) per year that come within a given radius of KSC, without knowing other information, is of little use. Assuming the distribution of the number of tropical storms or hurricanes is a Poisson-type distribution, the mean number of events per year (or any reference period) can be used to completely define the Poisson distribution function as demonstrated below.

From figure 12.4 the probability of no event, $P(E_o,r)$ where r = radius, for the following can be read: (1) tropical storms and hurricanes for annual reference periods; (2) tropical storms and hurricanes for July-August-September; and (3) tropical storms and hurricanes for July-August-September-October, versus radius, in kilometers, from KSC. To obtain the probability for one or more events, $P(E_1,r)$ from figure 12.4 the reader is required to subtract the $P(E_o,r)$, read from the abscissa, from unity; that is $[1-P(E_0,r)] = P(E_1,r)$. For example, the probability that no hurricane path (eye) will come within 556 km (300 nmi) of KSC in a year is 0.33 [$P(E_o,r=300) = 0.33$], and the probabilty that there will be one or more hurricanes within 556 km (300 nmi) of KSC in a year is 0.67 (1–0.33 = 0.67).

Figure 12.5 shows the average number of tropical cyclones entering on land in the Gulf Coast/Atlantic Coast areas per 100 years and per 10 nmi of coast in the time period from 1871 to 1984 (ref. 12.11).

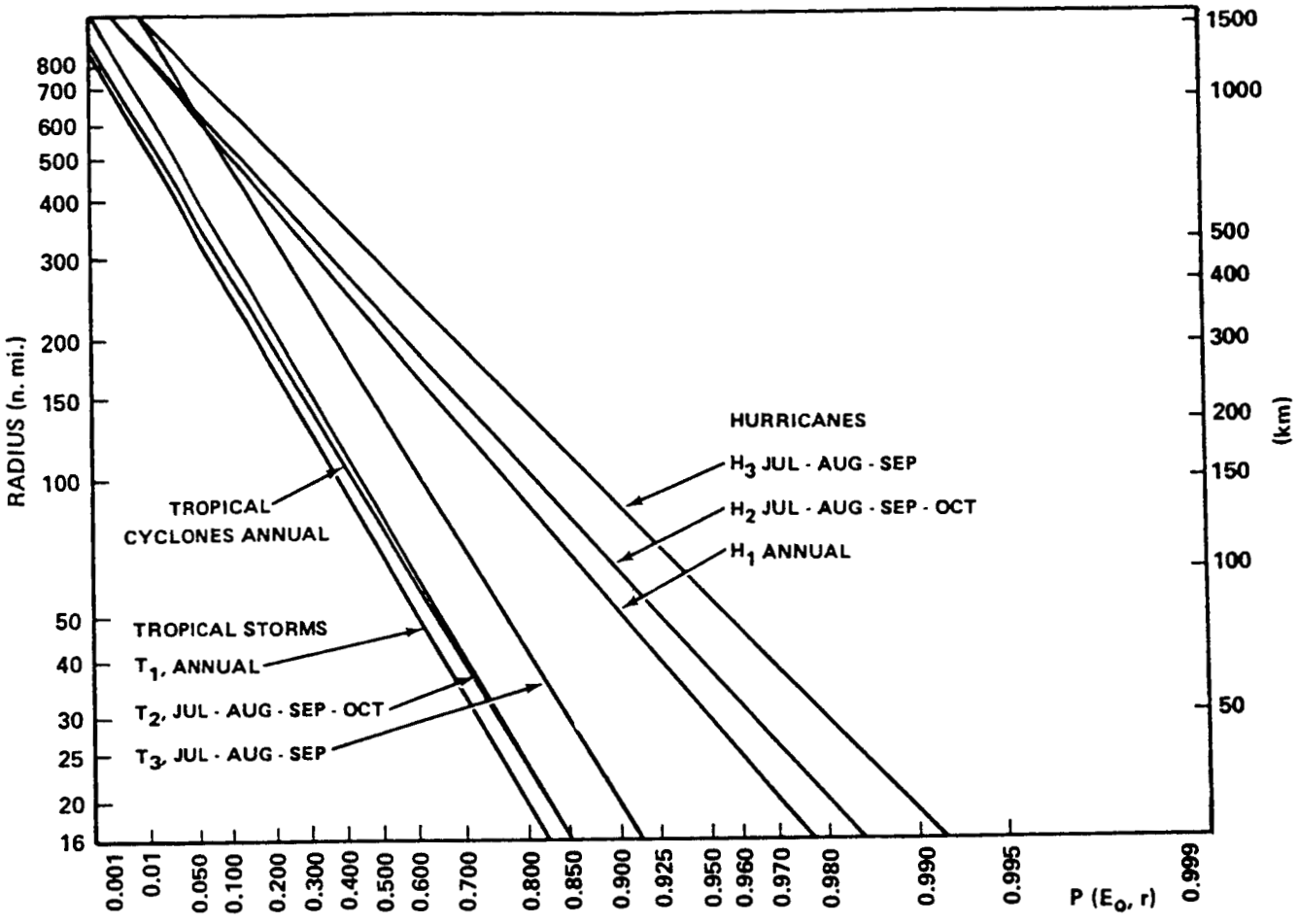

Figure 12.4 Probability of no tropical storms or hurricanes for various reference periods versus various radii from KSC.

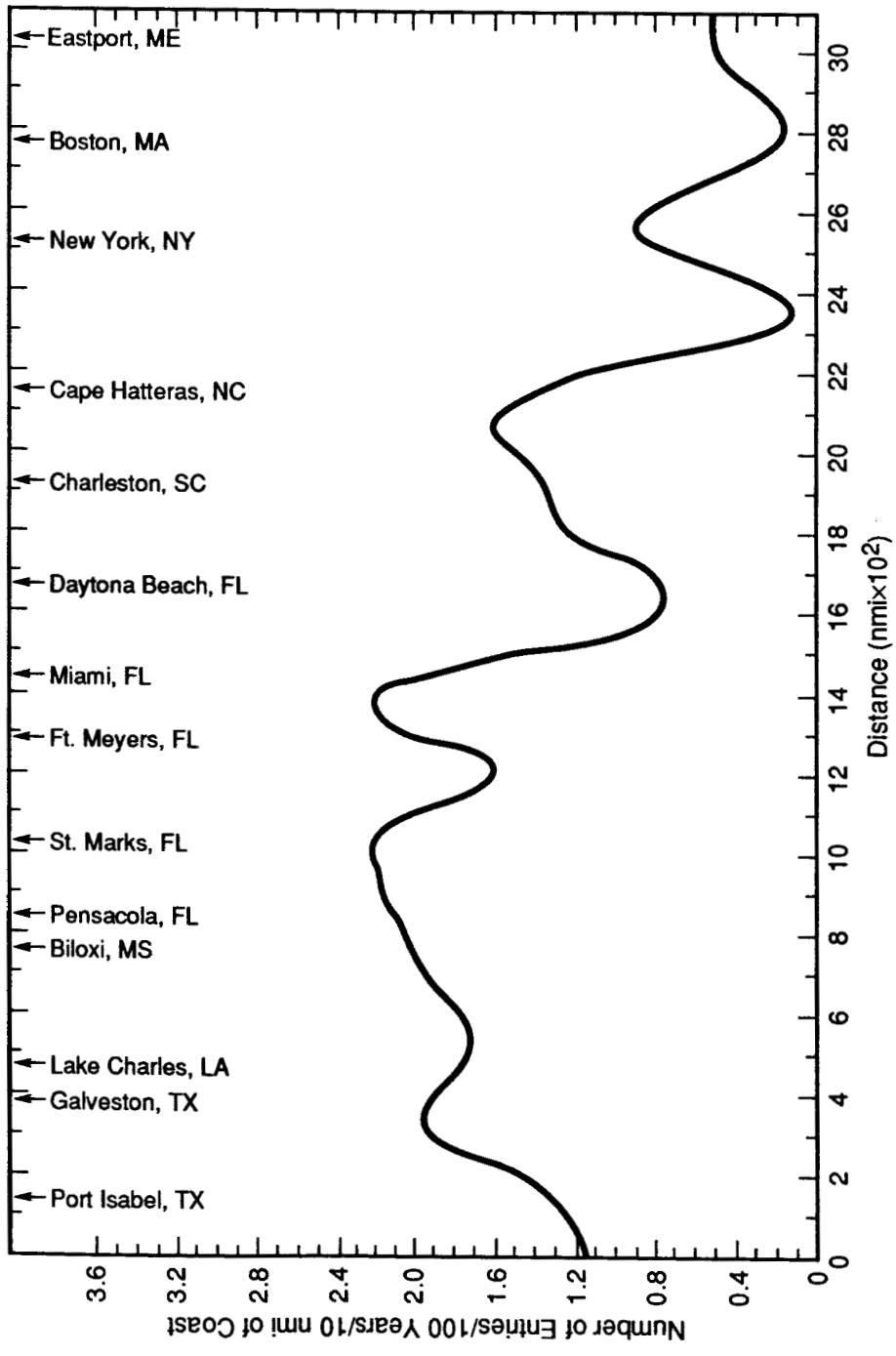

Figure 12.5 Smoothed frequency of landfalling tropical storms and hurricanes (1871–1984) by 50-nmi segments of a smoothed coastline for the Gulf and Atlantic coasts of the United States (ref. 12.9).

REFERENCES

12.1 "Tornado Safety—Surviving Nature's Most Violent Storms (With Tornado Statistics for 1953–1980)." U.S. Department of Commerce, NOAA, National Weather Service pamphlet NOAA/PA 82001 (January 1982), reprinted 1989.

12.2 Fujita, T.T.: "U.S. Tornadoes, Part One, 70-Year Statistics." The University of Chicago, SMRP-RP #218, 1987.

12.3 Grazulis, T.P.: "Significant Tornadoes, 1880–1989; Vol. II–A, Chronology of Events." Environmental Films, St. Johnsburg, VT, November 1990.

12.4 Ramsdell, J.V., and Andrews, G.L.: "Tornado Climatology of the Contiguous United States." NUREG/CR-4461, Battelle-Pacific Northwest Laboratory, May 1986.

12.5 Thom, H.C.S.: "Tornado Probabilities." Monthly Weather Review, vol. 91, No. 10–12, October–December 1963, pp. 730–736.

12.6 Gentry, R.C.: "Genesis of Tornadoes Associated With Hurricanes." Monthly Weather Review, vol. 111, September 1983, pp. 1793–1805.

12.7 NOAA: "Storm Data With Annual Summaries." Department of Commerce/NOAA/NCDC publication, vol. 30, No. 12, December 1988.

12.8 Riordan, P., and Bourget, P.G.: "World Weather Extremes." Report ETL-0416, U.S. Army Corps of Engineers, Engineer Topographic Laboratories, Fort Belvoir, VA, December 1985.

12.9 Alexander, M.B.: "An Analysis of Maximum Horizontal Wind Speeds Recorded Since 1961 at Kennedy Space Center, Florida." NASA TM-78177, Marshall Space Flight Center, Alabama, May 1978.

12.10 Alexander, M.B.: "Hurricane David Wind Velocities." NASA MSFC ES82 Memorandum for Record, September 20, 1979.

12.11 Ho, Su, Hanevich, Smith, and Richards: "Hurricane Climatology for the Atlantic and Gulf Coasts of the United States." NOAA-TR-NWS-38, National Weather Service, Silver Springs, MD, April 1987.

SECTION XIII. GEOLOGIC HAZARDS

13.1 Introduction

The American Geological Institute (AGI) Glossary of Geology defines a geologic hazard as "a naturally occurring or man-made geologic condition or phenomenon that presents a risk or is a potential danger to life and property." In this chapter these hazards are discussed as they pertain to Vandenberg and Edwards Air Force Bases, California; and Cape Canaveral, Florida. A section on seismic environment, prepared for space shuttle ground support equipment (GSE) design, has also been included.

13.2 Specific Hazards

Geologic hazards include: earthquakes, tsunamis and seiches, slope processes, floods, volcanic activity, expanding ground, and ground subsidence.

13.2.1 Earthquakes

Earthquakes are due to sudden releases of tectonic stresses which result in relative movement of rocks on opposite sides of a fault plane, as well as shaking of ground in areas near (and sometimes far from) the actual fault movement. Ground movement and shaking can trigger numerous other disasters, including landslides; liquefaction and sliding of unconsolidated sediments; destruction of buildings, dams, and roads; fires; tsunamis; seiches; changes in ground water level; and uplift of subsidence. They can also bring about far-reaching atmospheric pressure changes and sound waves and oscillations of the ionosphere (ref. 13.1).

Relative movement of different sections (plates) of the Earth's crust causes stresses to build up near the boundaries between them. Movement along faults, releasing seismic waves, takes place when the effective stresses exceed either the strength of the solid rock or the frictional resistance between rocks on either side of a pre-existing break or fault. Since pre-existing fault surfaces usually have lower strength than the surrounding rock, movement takes place along them.

Many microearthquakes take place along active faults, such as in parts of the San Andreas. But a greater number do not correspond to any known surface fault. Many of the earthquakes that are not associated with surface faults occur under folds—geologic structures formed when layered sediments are buckled upward in a broad arch called an anticline. The presence of an anticline reflects crustal compression as two moving tectonic plates collide, in the same way a carpet wrinkles when pushed across the floor. An unanswered question is whether these active folds conceal large faults, which could provide the sites for large shocks (ref. 13.2).

Earthquakes have proven to be one of the most disastrous and insurmountable of geologic hazards. Buildings constructed to withstand them have crumbled under their forces (ref. 13.1). Prediction of earthquake likelihood, intensity, and timing for a given location has not yet proved reliable (see subsection 13.2.1.1). Experience has shown that, to date, the best protection against earthquakes is identification of high-risk areas and avoidance of construction in them.

Definition of high-risk areas, a complicated process, includes mapping faults, dating movement on them to determine whether they are or might still be active, calculating theoretical maximum possible earthquake intensity for active faults, and predicting effects of possible earthquakes on sediments and rocks in the area. This information is then used to judge the safety of the area for construction.

Presented in figure 13.1 is a depiction of damaging earthquake potential occurring in the contiguous United States, based on where damaging earthquakes have occurred in the past. Five categories of damaging quakes are presented here, ranging from most damaging, indicated by the zone 4 to no major quakes, indicated by zone 0 (ref. 13.3a). The earthquakes that occurred in the Mississippi Valley (New Madrid) in late 1811 and early 1812 rank as the largest known shocks, with the largest potential damage and felt areas known, since the settlement of America began. An estimated area of 600,000 km^2 had potential damage of modified Mercalli intensity (MMI) equal to level VII or greater. The 1964 Alaska earthquake yielded a similar damage area of about 210,000 to 250,000 km^2, while the 1906 San Francisco earthquake had an area with MMI ≥ VII of about 30,000 km^2.

The Mississippi Valley map as presented in figure 13.2 (ref. 13.3b) presents hypothetical maximum intensities (modified Mercalli intensity scale of 1931) that would result from a magnitude M_S = 8.6, maximum intensity $I_o = XI$, earthquake anywhere along the New Madrid seismic zone. Magnitude 8.6 was chosen because that is the estimated magnitude of the December 16, 1811, New Madrid earthquake. This composite intensity map shows a more widespread distribution of effects than would result from a single earthquake of magnitude 8.6 because the distributions of effects were plotted for magnitude 8.6 earthquakes that could occur anywhere from the northern to the southern end of the seismic zone, and the maximum of the resulting intensities was chosen for each point on the map. This composite intensity map is believed to represent the upper level of shaking likely to occur within this area regardless of the location of the epicenter within the seismic zone.

13.2.1.1 California Earthquakes

Since subsections 13.3 and 13.4 present and discuss earthquake and seismic activity potential related to the Edwards and Vandenberg Air Force Bases (AFB), California sites, it was felt appropriate that a brief general discussion on California earthquakes and predictions be given here.

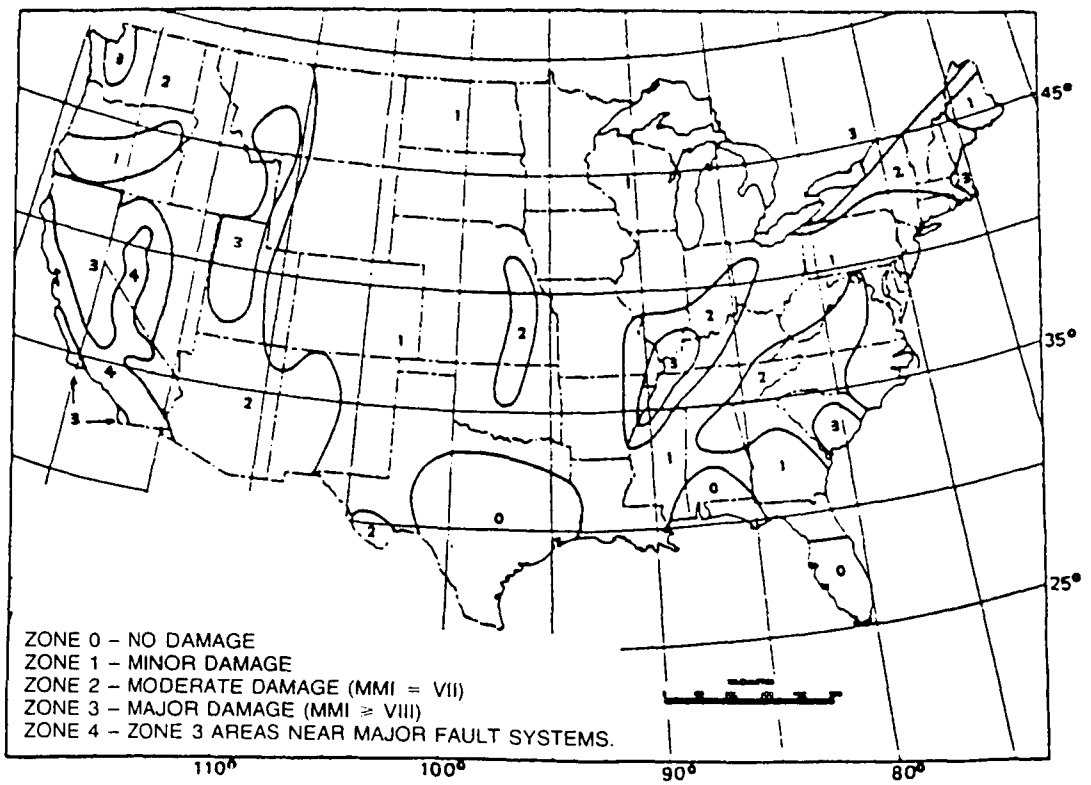

Figure 13.1 Seismic risk map of the contiguous United States: Uniform Building Code, 1979 (ref. 13.3a).

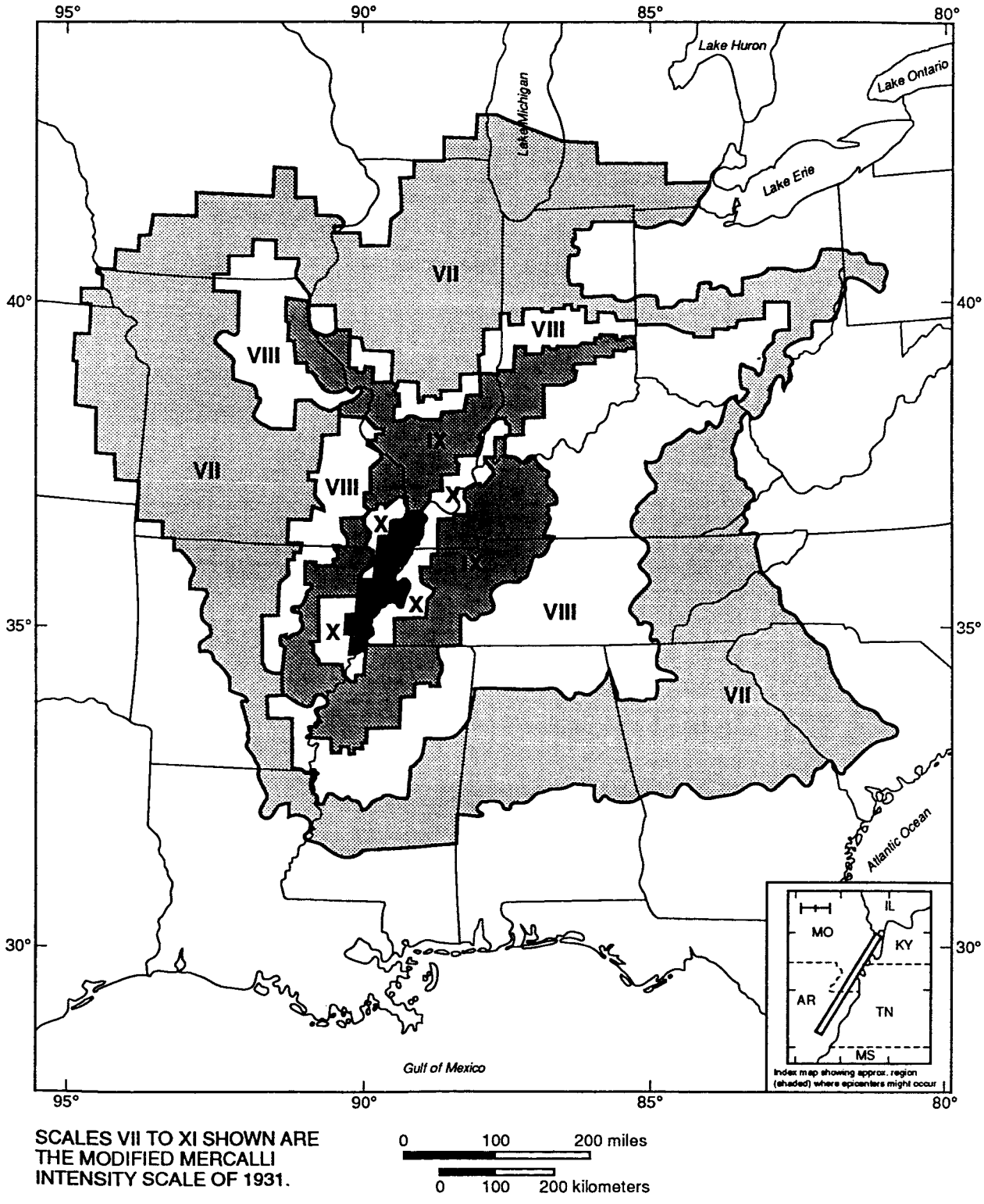

Figure 13.2 Estimated maximum regional seismic intensities associated with great earthquakes that could occur along the New Madrid seismic zone (ref. 13.3b).

Between 1912 and 1984 there have been 38 recorded southern California earthquakes with magnitudes of 6.0 or greater (ref. 13.4). Cousineau selectively lists 46 active and potentially active southern California faults which all have a maximum credible earthquake magnitude potential of 6.25 and higher. The San Andreas fault poses the greatest hazard to a NASA site from the standpoint of accelerations or shaking intensity. Detailed geologic studies indicate that this fault is likely to generate the largest earthquake of any fault in southern California and such an event is imminent (ref. 13.4).

Cousineau presents the work of Krinitizsky and Chang (ref. 13.5), in figure 13.3a, in which western U.S. earthquakes have been analyzed relating intensity to epicentral distance over a range of earthquake magnitudes. Also presented in figure 13.3b is the relationship between fault length (length of surface rupture) and earthquake magnitude, based on the work of Bonilla (ref. 13.6) and then Greensfelder (ref. 13.7).

Preliminary ground motion statistics, i.e., horizontal accelerations and velocities in rock, caused by earthquakes for the contiguous United States are mapped and presented in reference 13.8 for exposure times of 10, 50, and 250 years at the 90-percent probability level.* The velocity and acceleration map for an exposure time period of 50 years at the 90-percent probability level is presented in figures 13.4 and 13.5, respectively. As more data becomes available, these statistical maps will be updated. The ground motion maps can be used mainly in building code applications, design of structures, and in land use planning. The associated velocity and acceleration attenuation curves versus distance for areas east and west of the Rocky Mountains are presented in figures 13.6 and 13.7, respectively (ref. 13.8).

Finally, the USGS Working Group on California Earthquake Probabilities (ref. 13.9) has recently published their first conditional probabilities (fig. 13.8) for the occurrence of major earthquakes along the San Andreas fault between 1988 and 2018, with a 0.9 probability that the Parkfield, California, area will experience a significant earthquake before 1993. Since this publication, the San Francisco and Santa Cruz areas (Loma Prieta) experienced a magnitude 7.1 earthquake on October 17, 1989 (ref. 13.10). The USGF Working Group had assigned a 0.20 to 0.30 probability for major earthquake occurrence in the San Francisco area. An event of magnitude 7.5 or larger on the San Andreas fault is more likely in southern California than in the northern part of the State. Such an event in the south could occur on the Carrizon, Mojave, San Bernardino Mountains, or Coachella Valley segments. The combined probability of an earthquake rupturing at least one of these segments in the next 30 years is 60 percent.

Fault rupture poses a threat to structures that cross active faults. History of actual fault breaks at the ground surface in southern California shows only 11 such breaks. In general, the locations of the surface breaks themselves are largely unpredictable except for those along the largest faults. In summary, there are considerably more active and potentially active faults than historic fault ruptures. The latter occurrence is rare but merits consideration, particularly if serious consequences of the break are possible (ref. 13.4).

13.2.2 Tsunamis and Seiches

Tsunamis are seismic sea waves. They can be generated by submarine earthquakes that suddenly elevate or lower portions of the sea floor, by submarine landslides, or by submarine volcanic eruptions. Tsunamis travel on the order of 500 km per hour and can cross an ocean in less than 1 day. Their wavelengths are long—100 to 200 km. Their amplitudes in deep water are low, less than 1 m, but as they approach a shoreline, their large volume of water piles up into sizable "tidal waves." Configuration of the shoreline and tidal and wind conditions can help to form waves over 10-m high. In 1948, the U.S. Coast and Geodetic Survey established a seismic sea wave warning system for the Pacific Ocean, so the arrival of tsunamis from distant sources can now be anticipated by a few hours.

*These map analyses of 1982 have been updated with velocity and acceleration plots being reissued in 1984 (ref. 13.8b).

A seiche is a long surface wavelength occurring in an enclosed body of water. Its period can vary from a few minutes to several hours and is very dependent on the dimensions of the basin, pond, lake, or enclosed bay. Commonly, seiches are low in amplitude and are not noticeable. When a large-scale disturbance takes place, however, larger amplitude waves result and can continue to be reflected back and forth across the body of water for hours or days. Large seiches can be caused when tsunamis arrive in bays, or when earthquakes and large slope movements initiate them in an enclosed body of water. Seiches can also cause the piling up of water at one end of a lake or bay, given the proper steady wind conditions acting on a large fetch area. Near enclosed bodies of water investigation of possible damaging seiche activity should be considered as a part of earthquake and slope movement studies.

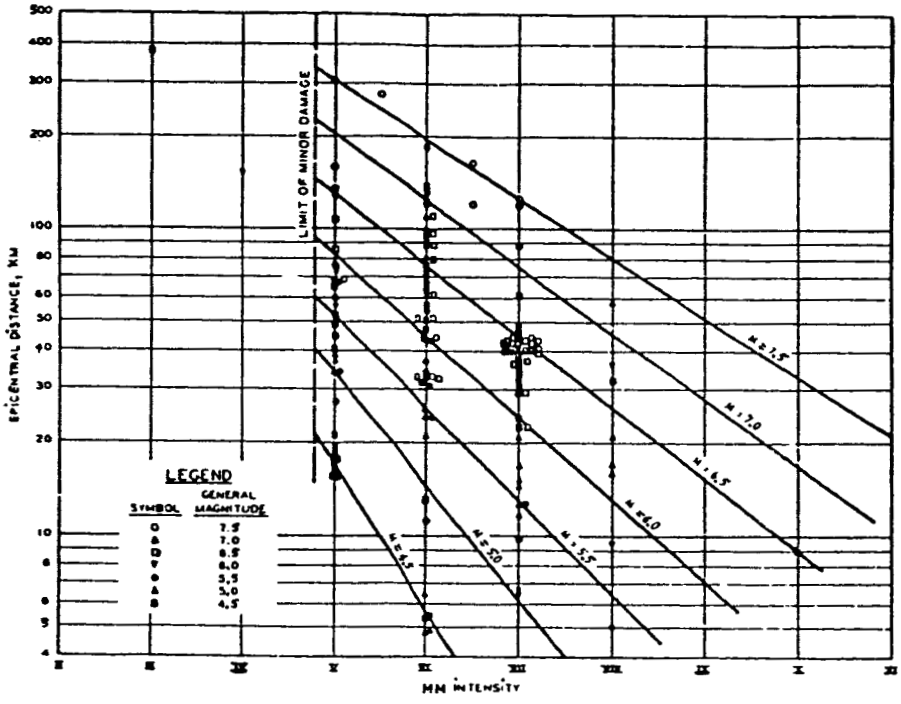

Figure 13.3a Intensity versus magnitude and epicentral distance (ref. 13.4).

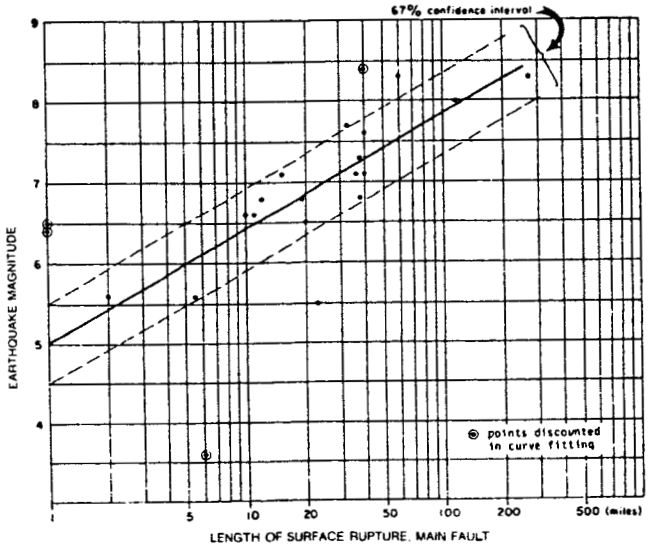

Figure 13.3b Earthquake magnitude versus fault rupture length (taken from Greensfelder, CDMG MS 23, 1974 (ref. 13.4)).

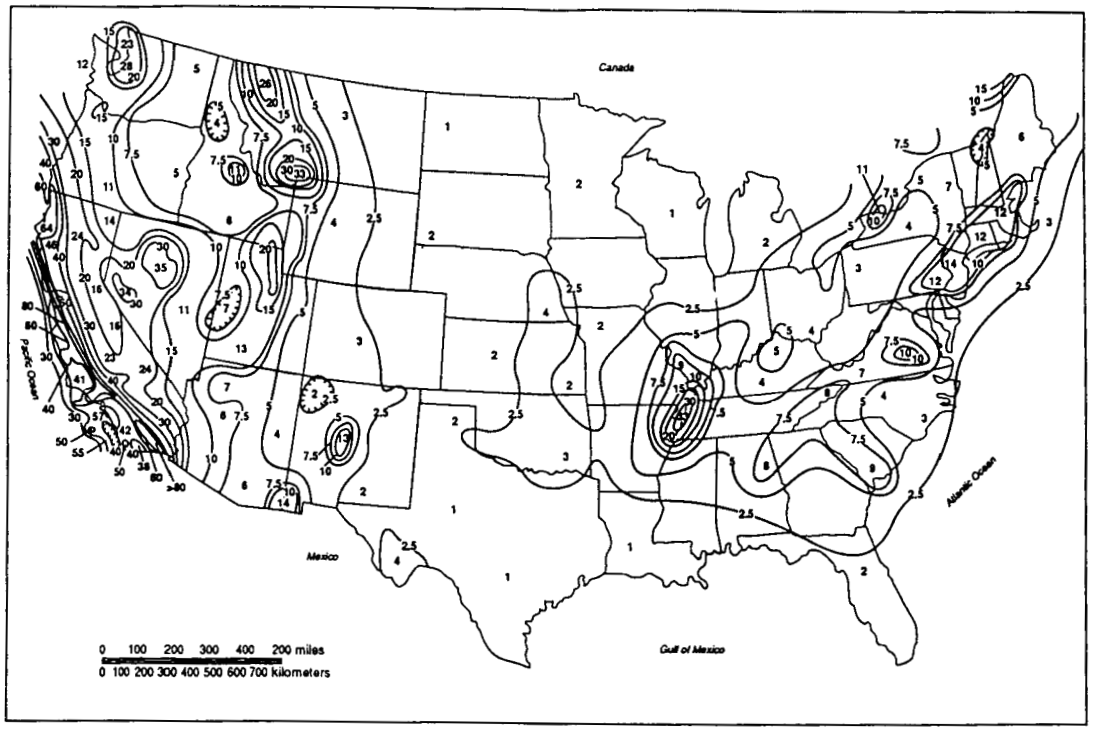

Figure 13.4 Preliminary map of horizontal velocity (expressed in cm/s) in rock with 90-percent probability of not being exceeded in 50 years (ref. 13.8b).

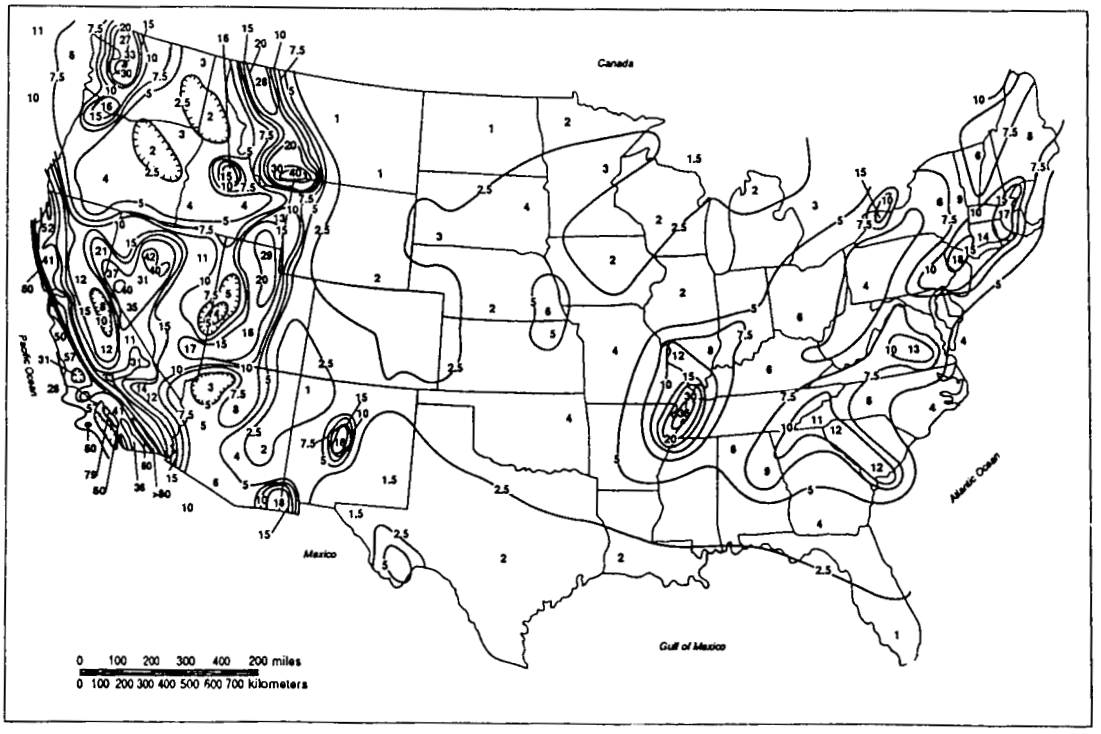

Figure 13.5 Preliminary map of horizontal acceleration (expressed as percent of gravity) in rock with 90-percent probability of not being exceeded in 50 years (ref. 13.8b).

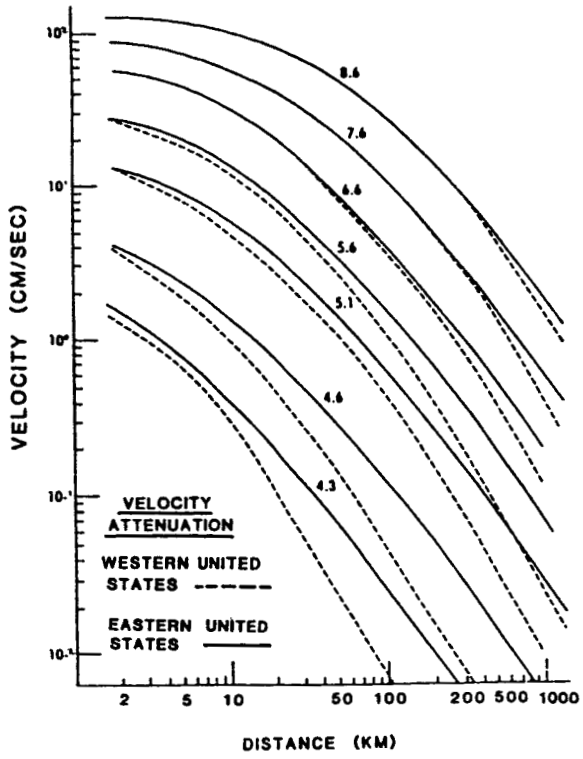

The solid lines are curves used for the eastern region. The dashed lines together with solid lines (in some instances) at close distances are the attenuation curves used for the western region.

Figure 13.6 Velocity attenuation curves (ref. 13.8a).

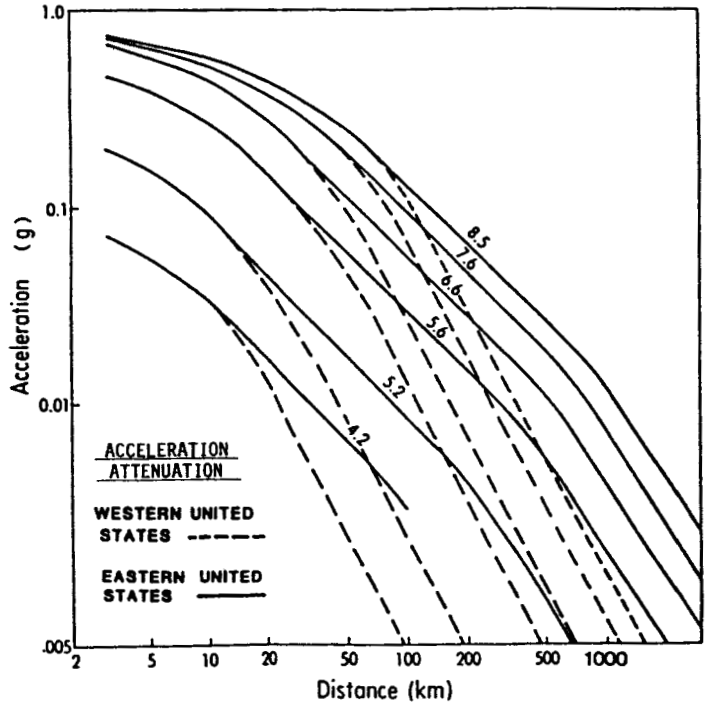

The solid lines are curves used for the eastern region (see text for definition). The dashed lines together with solid lines at close distances are the attenuation curves used for the western region and are taken from Schnabel and Seed (1973).

Figure 13.7 Acceleration attenuation curves (ref. 13.8a).

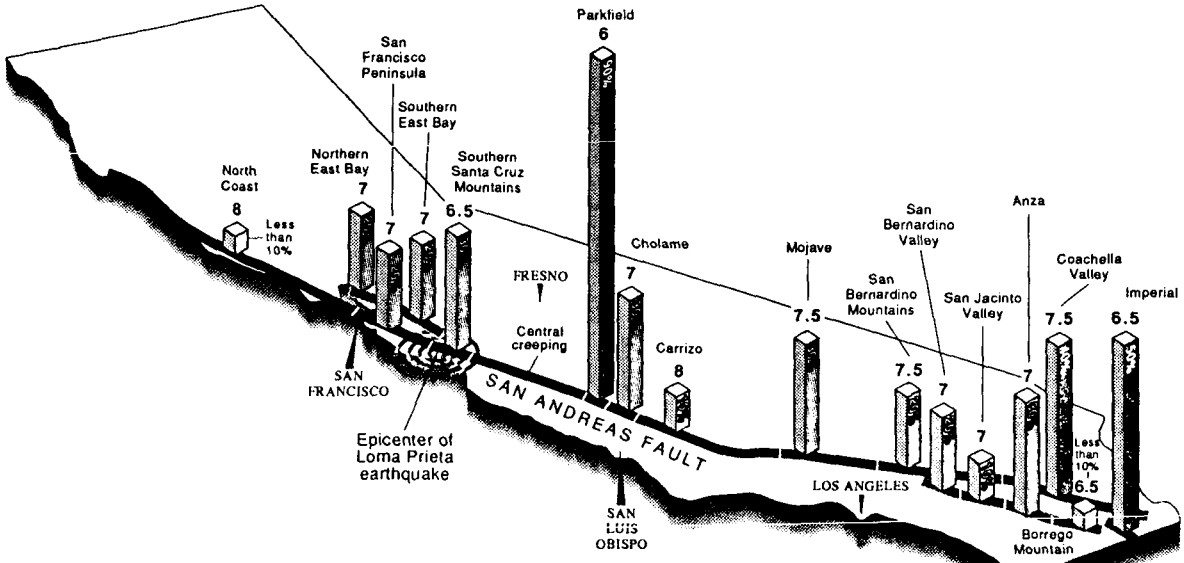

The expected magnitude for an earthquake on each segment is shown at the top of each box. The height of each box is proportional to the probability of the expected earthquake for that segment.

Figure 13.8 Conditional probability of the occurrence of major earthquakes along the four major California faults in the 30-year interval from 1988–2018 (refs. 13.9, 13.10).

13.2.3 Slope Processes

Slope processes refer to all types of movement of loose or solid materials (soil and rock) on slopes. These processes range from imperceptible slow creep to land slide, rock-falls, and mud-flows which can travel more than 100 m per second. Mass movements are often seasonal or periodic, but they may be catastrophic or spasmodic. The nature of slope instabilities and resultant downslope transferences depend upon:

(1) Type and structure of materials, including composition, size of their particles, degree of consolidation, and structural discontinuities (cleavages, bedding, contacts, fractures, etc.).

(2) Geomorphic setting, including climate, vegetation, shape and degree of slope, and slope orientation.

(3) Triggering mechanisms, external factors which upset the delicate balance which maintains slope stability. These mechanisms include natural and man-caused activities such as earthquakes, explosions, addition of excessive fluids (especially water), and alteration of hillslope configuration (undercutting, etc.).

Tables 13.1a and 13.1b describe various types of mass movements, and figure 13.9 depicts several forms of this class of hazards (ref. 13.11).

Although some problem areas can be detected by examination of aerial photos, infrared photography, and topographic maps, potential-use areas should be examined on-site by competent engineering geologists and/or geotechnical engineers.

Historically, several methods of prevention and control of slope processes have been used with varying degrees of success. They are:

1. Avoidance of problem areas;

2. Water control (drains, surface water diversions);

Table 13.1a Slope processes.

Movement		Composition of Mass and Process			Favoring Conditions
Kind	Rate	Material dry or with minor ice or water	Material and water	Material and ice	
Creep	Very slow	Soil creep	Rock creep Talus creep	Solifluction	Unconsolidated sediment or structurally modified rock. Bedded or alternate resistant and weak beds. Rock broken by fractures, joints, etc. Slight to steep slopes. High daily and annual temperature ranges; high frequency of freeze and thaw; alternate abundant rainfall and dry periods. Balance of vegetation to inhibit runoff but not to anchor movable mass.
Flowage	Slow to rapid		Earth flow Mudflow Debris avalanche	Debris avalanche	Unconsolidated materials, weathering products; poorly consolidated rock. Alternate permeable and impermeable layers; fine-textured sediment on bedrock. Beds dipping from slight to steeper angles; beds fractured to induce water in cracks. Scarps and steep slopes well gullied. Alpine, humid temperature, semiarid climate. Absence of good vegetative cover such as forest.
Sliding	Slow to very rapid	Slump Debris slide Debris fall	Rockslide Rockfall		Inherently weak, poorly cemented rocks; unconsolidated sediments. One or more massive beds overlying weak beds; presence of one or more permeable beds; alternate competent and incompetent layers. Steep or moderate dips of rock structures; badly fractured rock; internal deforming stress unrelieved; undrained lenses of porous material. Scarps or steep slopes. Lack of retaining vegetation.
Subsidence	Slow to very rapid		Subsidence		Soluble rocks; fluent clays or quicksand; unconsolidated sediments or poorly lithified rocks; materials rich in organic matter, water, or oil. Permeable unconsolidated beds over fluent layers. Rocks crushed, fractured, faulted, jointed inducing good water circulation. Level or gently sloping surface.

Compiled and modified from Sharpe (13.12), by permission.

Table 13.1b Factors causing slope processes.

Wedging and prying: by plant roots; swaying of trees and bushes in wind; expansion of freezing water and hydrostatic pressure of water in joints and cracks; diurnal, annual, irregular expansion due to heating; expansion due to wetting; animal activity. Filling and closing of cracks and voids caused by: burrowing of animals; decay of plant roots and other organic matter; gullying or undercutting by streams; removal of soluble rocks and minerals; erosion of fine particles by sheet wash and rills; downslope mass movement; shrinkage due to drying or cooling. Increase in load: addition of material upslope; rainfall, snow, or ice; traffic of vehicles or animals; tectonic, meteorologic, or animal disturbance.
Reduction in internal friction due to excessive amounts of water in mass. May start as slide; causes similar to landslides.
Removal of support: oversteepening of natural or artificial slopes by erosion; outflow, compaction, softening, burning out, solution, chemical alteration of subadjacent layer; disappearance of buttress against slope such as ice front. Overloading: by other mass-movement processes; by rain, snow, ice, and saturation, overburden in excavation. Reduction if internal friction and cohesion: by surface and ground water, oil seeps, chemical alteration by weathering. Wedging and prying: as in creep. Earth movement: produced by earthquakes; storms, traffic of vehicles and animals; drilling, blasting, gunfire, Earth strains due to temperature and atmospheric pressure and tidal pull.
Removal of support of adjacent layers: by solution or chemical alteration; by outflow of fluent material; by natural or artificial excavation; by compaction caused by natural or artificial overloading, by reduction of internal friction, by desiccation. Earth movement: by warping; by natural or artificially induced vibrations. Overloading: natural or artificial.

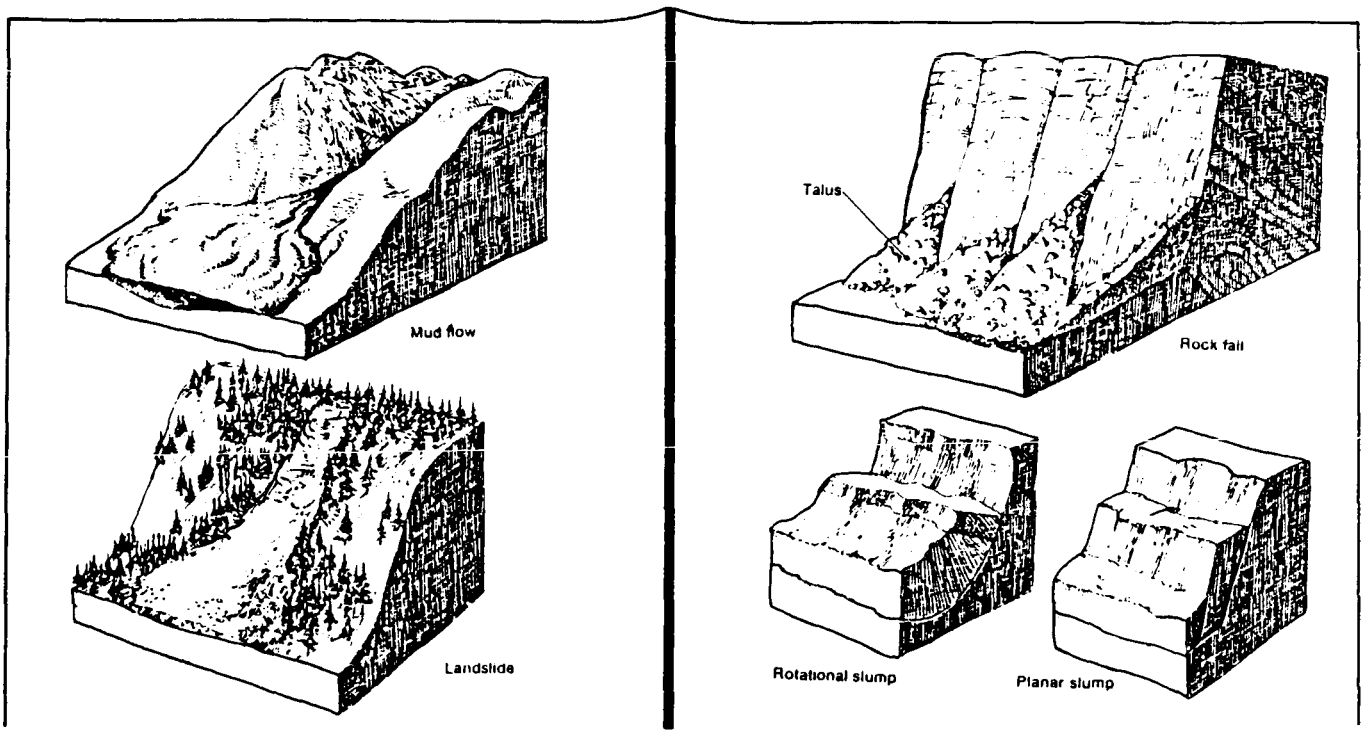

Figure 13.9 Illustrations of slope processes.

3. Excavations (slope reduction, unloading, terracing, total removal of slides);

4. Restraining structures (walls, piles, bolts, grout, nets); and

5. Planting, effective only in controlling shallow, small-scale slope processes.

13.2.4 Floods

Floods are defined as "any relatively high streamflow which overtops the natural or artificial banks in any reach of the stream." As a result, water and its sediment load are spread over the adjoining ground. Floods are natural, recurring events which become a problem only when they compete with man for the floodplain or flood channel. Rare catastrophic floods, in which water flows above and beyond the floodplains, may have disastrous consequences. Historically, catastrophic floods have resulted in loss of life and enormous property destruction. Initially, the greater than normal volumes of water, moving at abnormal velocities, are able to erode very quickly, picking up large volumes of sediment and debris. As water and its debris load continue downstream, large amounts of material (including man-made objects) are picked up or covered.

Floods normally occur as a result of cloudbursts, extended rain, and/or rapid snowmelt accompanied by rapid runoff. Natural dams such as those caused by landslide (as well as man-made dams) result in flooding of land upstream. Disastrous floods may also occur as a result of sudden release of large amounts of water by dam failures.

Several approaches have been used to avoid the damaging effects of floods. All these approaches make use of flood predictability from stream flow records and historical flooding recurrences. Flood hazard maps are compiled as various areas and assigned risk factors. The type of approach used to reduce flood damage will depend upon the calculated or assumed risk:

1. Avoidance of high-risk areas for construction activities.

2. Detention or delay of runoff in smaller tributaries at higher reaches of the watershed.

3. Modification of the lower reaches of rivers, where floodplain inundation is expected, by channels and levees.

13.2.5 Volcanic Hazards

Volcanic hazards fall into two categories: hazards near the volcanic activity and hazards distant from it (refs. 13.13 and 13.14).

13.2.5.1 Hazards Near Volcanic Activity

Within a few tens of miles of a volcanic center, hazards include: lava flows, nuées ardentes (hot ash flows) and poisonous gases, ash falls and bombs, earthquakes, debris, and mud flows.

1. Some lava flows are much more dangerous to man than others. Lava flows vary a great deal in viscosity, depending on their chemistry and temperature. They can be up to 10-m thick, travelling a meter per hour, or they can form a sheet as thin as 1 m which travels up to 50 km per hour. The latter have been the most hazardous to man in the past. A trained geologist can predict, to some extent, the type of flow most likely to occur in a given volcanic area. If fast fluid flows are likely, guiding levees can be built to shunt them away from populous or otherwise valuable areas.

2. Nuées ardentes are heavier than air, gas-borne flows of incandescent volcanic ash released during explosive volcanic eruptions. Temperatures in the flows reach 800 °C, and the gases that carry them may be poisonous. These flows, though gas-borne, are extremely dense. Their physical force is great enough to snap large trees and crumble strong buildings. It was a nuée ardent from Mt. Pelée that devastated St. Pierre, Martinique, in 1902, completely destroying the town and killing an estimated 40,000 people. Hot, dense, poisonous gases can also be emitted without ash.

3. Ashfalls in the immediate vicinity of a volcano can be up to a few tens of meters deep and very hot. Near the eruption center they may contain sizable volcanic bombs of solid or solidifying rock, as well as pebble-sized fragments of pumice. They may give off gases for some time.

4. Earthquakes (see section 13.2.1) usually accompany volcanic activity and often trigger debris flows and mud flows.

5. Debris and mud flows form from the unconsolidated material that makes up the flanks of active stratovolcanoes. The material becomes unstable because of doming of the volcano, rapid melting of snow by hot ash or lava, and/or percolation of hot volcanic gases through snow masses. Volcanic mud and debris flows have been known to travel 80 km at speeds of several tens of km per hour. Some flows from major volcanoes contain on the order of 2 to 4 cubic kilometers of material. Dams in the paths of mud flow may break and contribute to the volume of flows that overtop them. In some places where mudslide hazard has been recognized, dams have been built and reservoirs kept empty to absorb them. In addition to downstream damage, volcano-caused landslides can cause instability at their point of origin: When a large volume of material is removed suddenly from the flank or summit of an active volcano, pressure is released and an eruption may be triggered (as in the May 18, 1980, eruption of Mt. St. Helens).

13.2.5.2 Hazards Distant from Volcanic Activity

Far from volcanic centers, volcanic ash and tsunamis can still be serious hazards.

1. An ashfall's total volume depends on the size of the eruption that brought it about. Its distribution depends on the elevation reached by the volcanic cloud and on wind conditions at the time of the eruption. A sizable ashfall can damage areas several hundred kilometers from the eruption site. Ash is detrimental to human health and damaging to mechanical equipment. It reduces visibility if there is wind or traffic, and must be removed from buildings and pavement. Fine ash, if it reaches the stratosphere, may remain there for months or years, affecting climate by reducing insolation. See section X concerning aerosols in the atmosphere.

2. Tsunamis (see section 13.2.2) may be caused by submarine volcanic explosions and debris slides, which can travel thousands of kilometers from the volcanism that caused them. They endanger life and all coastal construction within 40 m of sea level.

When considering volcanic hazards, it is important to realize that in any area volcanism is sporadic. A volcanic area which has been inactive throughout historic times may reawaken to violent activity in a few days or weeks, or it may remain inactive for centuries into the future. Earthquakes, almost always felt or recorded several days or weeks before activity commences, serve as a warning of impending danger. Once volcanism commences, danger is greatest within a few tens of kilometers of the eruption. The effects of volcanism can easily be catastrophic, especially since volcanoes are virtually uncontrollable by man. Important constructions should not be located in the immediate vicinity of active or dormant volcanoes, or in areas likely to be affected by distant volcanism.

13.2.6 Expanding Ground

Expanding ground is caused by freezing and/or expansive soil or anhydrous expansion (without freezing) of moisture in the ground or by rock components that expand when wet. Expansive soils are found throughout the U.S. The soil can increase its volume as high as 1,000 percent if it is allowed to. The actual expansion depends upon the amount of water available and the overburden on the soil. The process of the expansion is generally slow. The heaving force can cause serious damages to foundations and structures.

When water freezes, its volume increases by approximately 9 percent. When water in fine-grained, unconsolidated material freezes, additional water from the atmosphere and from unfrozen ground below slowly adds to the already frozen mass. Eventually, lenses of ice build up, lifting the soil above them. In areas where winters are cold and moist, or where day-night temperatures differ markedly, freezing and thawing may cause marked dislocation of surface and near-surface materials. Some clays contain minerals that increase in volume upon wetting and decrease in volume upon drying. The most common of these minerals are anhydrite and of the montomorillonite clay group. Problems with expansive clays and the rocks and soil in which they occur are most frequently encountered in arid or semiarid areas with strong seasonal changes in soil moisture.

Expansive clays are particularly associated with volcanically derived materials. Shales containing clays of the montomorillonite group (including bentonite derived from volcanic ash) commonly swell 25 to 50 percent in volume (ref. 13.15). Such swelling results from chemical attraction of water molecules and their subsequent incorporation between submicroscopic, platelike clay molecules. As more water becomes available, it infiltrates between the clay plates and, with freezing, pushes them farther apart. Similarly, hydration of the mineral anhydrite induces a chemical change, causing 40-percent expansion and altering the anhydrite to the mineral gypsum.

These large increases in volume upon freezing or hydration, and associated decreases in volume with thawing or drying, can be very destructive. Volume increases of only 3 percent are considered to be potentially damaging and to require specially designed foundations. James and Holtz (ref. 13.16) report that shrinking and swelling damage to foundations, roads, and pipelines in the United States amounts to more than twice the dollar value of damage incurred by floods, hurricanes, tornadoes, and earthquakes combined.

On-site inspection by a competent soil engineer or engineering geologist may pinpoint potential clay-expansion problems. Engineering soil tests are required to evaluate the extent and severity of the problem in construction sites.

Installation of well-designed drainage systems using chemical treatment, or complete removal of expansive materials, may lessen the potential damage from expansive ground.

13.2.7 Ground Subsidence

Ground subsidence is characterized by downward movement of surface material, caused by natural phenomena such as removal of underground fluid, consolidation, burning of coal seams, or dissolution of underground materials. It may also be caused by man's removal or compaction of Earth materials.

Ground subsidence is ordinarily a relatively slow process; it has been known to continue for many decades. Usually the result is broad warping and flexing, with some cracking and offset at the ground surface. If the process causing subsidence persists, the surface may suddenly collapse. Foundation failures, ruptures of pipe and utility lines, dam collapses, salt water invasion, and disruption of roads and canals have all been directly attributable to ground subsidence.

Potential causes for ground subsidence include:

1. Removal of solids: Removal of the solid subsurface support base involves mining, natural or human solution of carbonate and other easily soluble minerals (including salt and sulfur), and underground burning of organic beds. Cavern collapse is the most catastrophic result. Alternatives to avoiding such areas for heavy loads include subsurface backfilling, cement-grouting, and installation of underground support pillars.

2. Withdrawal of fluids: Subsidence due to withdrawal of fluids (including gas, oil, and water) is the most common type of man-caused regional ground subsidence. As fluids are removed, and fluid pressure within the aquifer or reservoir rock is reduced, the aquifer skeleton must bear an increased grain-to-grain load. In permeable media, the increase in effective stress and subsequent compaction is immediate. Increasing percentages of clays in the aquifer cause the adjustment to take place more slowly. In extreme cases, subsidence of more than 7 m over a 60-year period has been directly attributed to withdrawal of water and/or petroleum. Injection of fluids back into the aquifer might arrest the subsidence.

3. Oxidation of organic beds: Oxidation of organic beds, such as layers of peat, and resultant breakdown of support structures have been known to follow drainage of peat bogs. Raising the water table can inhibit this oxidation.

4. Application of surface loads: Compaction due to surface loading alone commonly results in only minor ground subsidence. However, application of surface loads may trigger more severe subsidence when added to already weakened substratum conditions.

5. Hydrocompaction: Wetting of some clays in moisture-deficient, low-density soils may lead to weakening of clay bonds which support soil voids, and ultimately to collapse of internal soil structure and compaction. Hydrocompaction commonly occurs in wind-deposited silts and fine-grained colluvial soils

which have a high clay content. Some areas near the south and west borders of the San Joaquin Valley dropped 1.5 to 5 m in the early 20th century after application of water. Drainage installations and replacement of the offending clay-bearing materials are modifications used to circumvent potential hydrocompaction problems.

6. Tectonic movements: These movements include earthquakes and man-caused explosions which directly cause reordering and subsidence, and which commonly cause additional ground subsidence in already unstable areas. Some materials such as quick clays and quicksands lose all their cohesive strength and acquire the properties of a liquid upon being violently disturbed. Such materials can flow and envelope buildings constructed on them.

7. Liquefaction: When loose saturated soils are subjected to cyclic or impact loads, they tend to compact, thereby developing excess pore water pressures which may in turn result in complete loss of interparticle friction in the soil mass. Such a state is called liquefaction. A liquefied soil behaves like a fluid and cannot carry any shear loads. As a result, buildings can sink into a liquefied ground mass, earth slopes cannot be sustained, dams and bridges may collapse, or large landslides may occur. Liquefaction is a common phenomenon during earthquakes and it can also be triggered by strong explosions, pile driving, wave action, etc.

Ground subsidence is commonly caused by a combination of factors. Geologic conditions which are favorable for its occurrence include the presence of mines, soluble or flammable materials, oil, water or gas, windblown soils, fluent clays or quicksand, faults or fractured rocks, and good water circulation. It is imperative to recognize these potential problems *before* construction commences and to take corrective measures where they are called for.

13.2.8 Other Hazards

Geologic hazards such as avalanches and other snow and ice processes do not influence the three areas concerned and are not discussed here.

13.2.9 Conclusions

A word should be added to the preceding description of geologic hazards. Many of those described occur suddenly, while others take place over a long period of time. Almost all of these "hazardous" events are normal geologic processes and should be expected to occur from time to time. We have learned to predict and control some of these processes, but for others the best we can do is study the likelihood of their occurrence in different areas and avoid building where danger is great.

13.3 Geology and Geologic Hazards at Edwards Air Force Base, California

13.3.1 Geology

Edwards Air Force Base is covered by rock materials of three distinct age groups (ref. 13.17). The oldest rocks are pre-Tertiary (pre-65 million years ago) granite instrusive and metamorphic units (Ig on fig. 13.10). These rocks are similar in age and composition to the Sierra Nevada Batholith. They form most of the ridges and hills within the air base boundaries.

Minor amounts of Tertiary age rocks (3 to 65 million years old) are exposed at Edwards Air Force Base (Tvi on fig. 13.10). Most of these are dikes and sills of fine-grained rock. A few volcanic flows and pyroclastics, with interbedded sediments, crop out along the eastern boundary of the base. Some bentonite layers occur within the sedimentary units. Although the dikes and sills form stable slopes, some of the slopes covered by the pyroclastic and sedimentary interbeds are unstable.

Most of the terrain within the boundaries of Edwards Air Force Base is covered with thick units of Quaternary and Recent (3 million years old) unconsolidated and weakly consolidated materials which include alluvial sand and gravel (Qa on fig. 13.10), beach dunes and bars (also Qa), playa clays (Qc), windblown sands (Qcs), and older, partly consolidated gravels (Qf). These deposits generally occupy areas of low relief.

Alluvial sand and gravel, deposited by action of flowing water, form channel and fan deposits. Wave-deposited bars and wind-deposited dunes occur along the northern "shore" of Rogers Lake. Minor clay balls occur in the wave-deposited bars. Windblown sand forms small dunes elsewhere within the base, and also covers parts of the desert floor with a thick veneer of sand.

The playa clays are mudflat facies of the alluvium. They are hard when dry but become soft and sticky when wet. Studies by Droste (ref. 13.18) found that playa clays from Rogers Lake consist of 40 to 50 percent montmorillonite and 40 to 50 percent illite. Clays from Rosamond Lake consist of 20 to 30 percent montmorillonite, 50 percent illite, and 20 to 30 percent chlorite. Although in the desert climate thorough wetting of the playas is rare, these high-montmorillonite clays are subject to severe swelling and shrinking, which should be considered when planning construction activities near the dry lake beds.

Several high-angle, northwest-trending faults have been mapped in the southern and eastern parts of the air base. They have small displacements and seem to edge granitic domal features. The faults are at present inactive.

13.3.2 Geologic Hazards

The following subsections describe the general locations of potential geologic hazards which exist at Edwards Air Force Base (fig. 13.11). On-site investigations and engineering properties tests are recommended on a location-by-location basis before initiation of any construction activities.

13.3.2.1 Earthquakes

There were no recorded earthquakes with epicenter magnitude of 4 or greater at Edwards Air Force Base or within 25 miles of it between 1910 and the present (refs. 13.19, 13.20). The base is located on a relatively stable wedge between the San Andreas and Garlock faults, both of which are less than 40 miles from the base. The proximity of these major active faults indicates regional tectonic instability. However, the known faults mapped in the eastern and southern parts of the base seem to be inactive, and earthquake hazards are judged to be negligible.

The likelihood of surface fault rupture at the Edwards Air Force Base NASA Dryden site is considered to be very remote. However, it cannot be dismissed completely because it is not presently known if any buried faults underlie the site which may belong to the group of Mojave block faults. Another risk, albeit a low one, is the possibility of sympathetic movement, including fault rupture extending to the ground surface, of these possible underlying faults in response to large motions from a great earthquake on the San Andreas fault (ref. 13.4).

Recommendations for Edwards Air Force Base Seismic Design Criteria

It is recommended that facilities that are to be constructed on Edwards Air Force Base be evaluated for their resistance to the two following earthquakes (ref. 13.4).

1. A magnitude 8.5 event on the nearest approach of the San Andreas Fault, ~29 miles, would impose an acceleration of 0.40 g on the site with a bracketed duration of 40 s. It is suggested that a scaled trace of the N21E component of the Taft accelerogram of the 1952 Kern County earthquake is an adequate model.

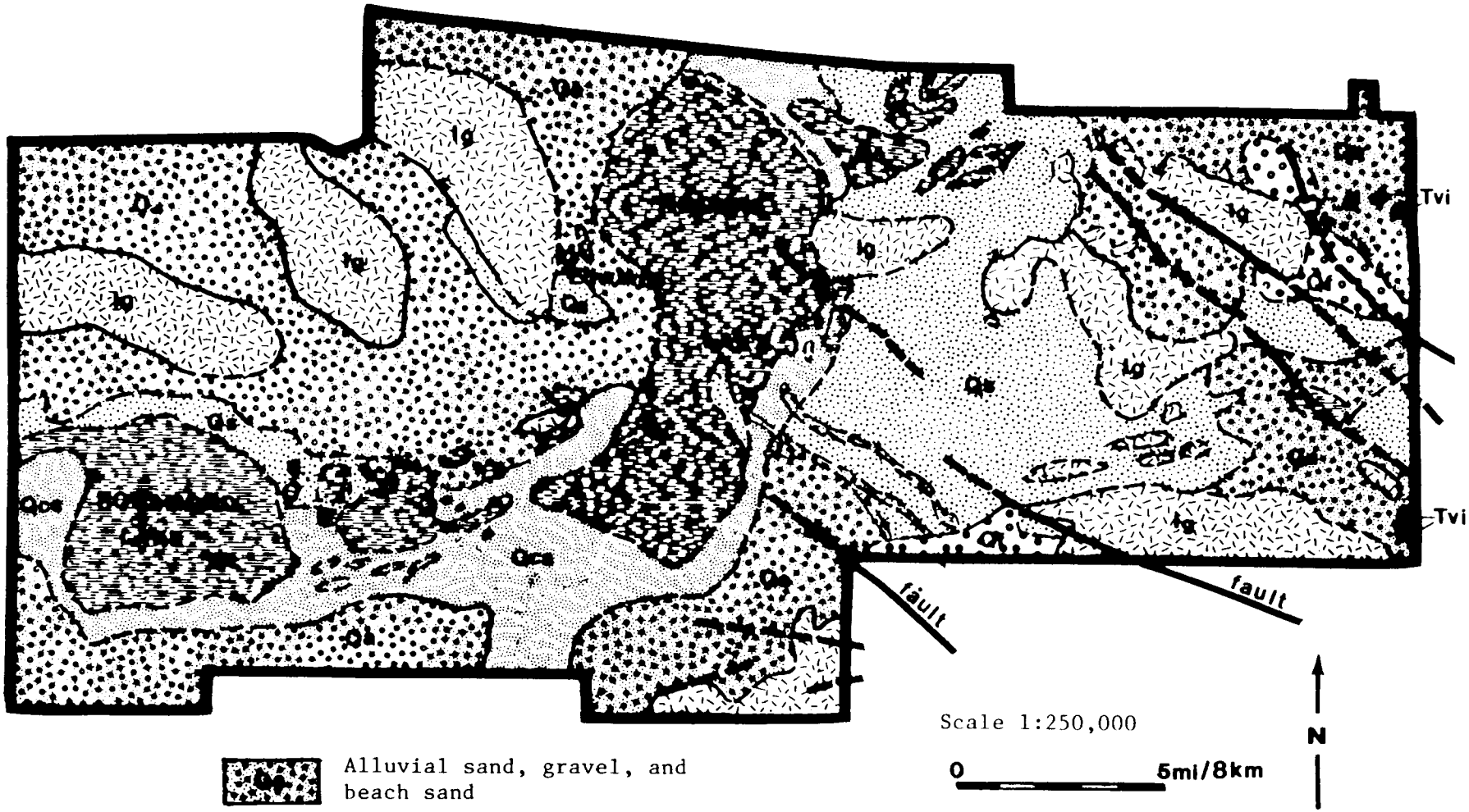

(Boundaries dashed where inferred or shifting)

Figure 13.10 Geology of Edwards AFB, California (after Dibblee, ref. 13.17).

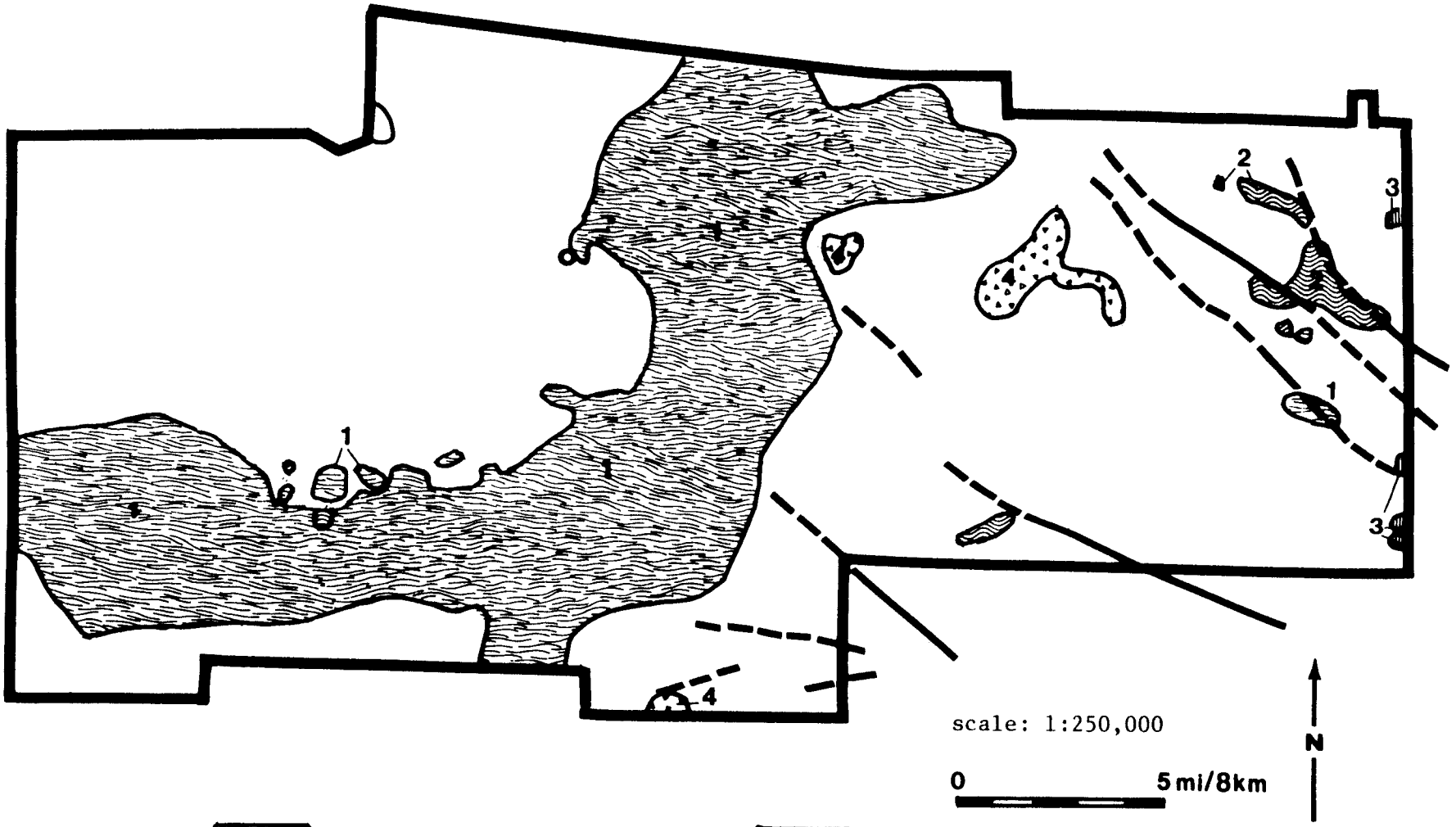

Figure 13.11 Geological hazards of Edwards AFB, California.

2. A near-field magnitude 4.5 event from a Mojave block fault would impose an acceleration of 0.20 g at the site with a short bracketed duration of 6 s. It is suggested that the unscaled trace of the Lake Hughes No. 4 S69E component from the San Fernando Valley earthquake of 1971 be used as an appropriate model.

13.3.2.2 Slope Processes

All of the air base lies within an area designated as 1 by Radbruch and Crowther (ref. 13.21). This designation identifies areas in California which have the lowest number and volume of landslides per given area. Hilly parts within a unit 1 area may experience landslides, but because of the overall low-to-moderate relief, few problems from slope processes are expected. Some hazards may exist on steep gravel-covered slopes. The fanglomerate units that form steep slopes in the Kramer Hills, near Jackrabbit Hill, and elsewhere on the base should be considered susceptible to mass movement. Slopes covered by Tertiary pyroclastics and interbedded sedimentary layers along the eastern boundary are potentially hazardous. Rockfall problems may exist at the bases of granite cliffs.

13.3.2.3 Flooding

Except for very local flash flooding, no flood hazards are likely. Flash flooding may turn playas into shallow temporary lakes.

13.3.2.4 Expanding Ground

Careful examination of the engineering properties of the playa clays should precede construction activities. The high montmorillonite content of these clays leads to swelling and shrinking when they are alternately wet and dry. Similar caution should be exercised when dealing with the Tertiary pyroclastics and their sedimentary interbeds.

13.3.2.5 Subsidence

Localized subsidence may occur near old mine diggings. There is also the possibility of hydro-compaction in playa clays.

13.3.2.6 Conclusions

Edwards Air Force Base, though mostly underlain by granite, is 65 percent covered by Pleistocene and recent unconsolidated sand, clay, and gravel. Despite proximity of major active faults, seismic risk is low. Slopes are generally less than 10 percent, so geologic hazards resulting from slope processes are localized and probably restricted to steep slopes consisting of weakly consolidated fanglomerate.

Approximately 30 percent of the air base is covered by unconsolidated clay-rich material. The clays include a high proportion of montmorillonite and are susceptible to expansion and shrinking. However, low precipitation of the Mojave Desert region greatly reduces the potential for such problems.

In summary, Edwards Air Force Base is located in a geologically low-risk area.

13.4 Geology and Geologic Hazards of Vandenberg Air Force Base, California

13.4.1 Introduction

Land use planning for Vandenberg Air Force Base should take into account possible danger from earthquakes, seismic waves, slope instability, floods, and burning ground. Volcanism, expanding clays and rocks, and subsidence are not expected to interfere with activities on the base.

13.4.2 Geology

Figure 13.12 is a geologic map of the Vandenberg Air Force Base area. The oldest rocks on the base, found in its northwest end, are Franciscan mafic and ultramafic igneous rocks and the sedimentary Knoxville Formation of Jurassic age. The remaining rocks, which cover the greater part of the base, are much younger, ranging in age from Oligocene to Recent. Oligocene poorly consolidated nonmarine sediments crop out near the older rocks. Miocene diatomaceous earth underlies the rest of the base and is overlain extensively by younger sediments. At most of its outcroppings, the diatomaceous earth is soft, lightweight, and porous, but resistant to weathering. It contains abundant water-soluble salts, which form an efflorescence on outcrops. This rock is a source and a reservoir for gas, oil, and tar, which have been removed in oilfields north and east of the base. Pliocene to Recent sediments are generally unconsolidated, fine-to-coarse sand and conglomerate. These sediments form terraces, fill valley bottoms, and are piled into extensive sand dunes near the coast. Sediments of Pliocene age contain hydrocarbons of Miocene derivation. Pliocene and older rocks have been extensively folded and locally faulted, probably as they were compressed during western drift of the continent (ref. 13.22).

13.4.3 Geologic Hazards

The following subsections describe general locations of potential geologic hazards which exist at Vandenberg Air Force Base (fig. 13.13). On-site investigations and engineering properties tests are recommended on a location-by-location basis before initiation of any construction activities.

13.4.3.1 Earthquakes

Although no recent fault scarps are known on Vandenberg Air Force Base, earthquakes pose an everpresent threat to it. The base is in one of the most earthquake-prone parts of the country. Between 1910 and 1971, five earthquakes with magnitude between 4.0 and 4.9 had foci within 3 miles of the base (ref. 13.23). See figure 13.14 for a depiction of earthquake epicenters around VAFB. Ground shaking has been felt on the base during many other earthquakes. Although usually of short duration, such shaking can trigger building collapse, water waves and flooding, slope movements and/or release of flammable gases. Earthquakes are a definite hazard at Vandenberg Air Force Base.

Vandenberg AFB, California (VAFB) is situated in one of the more seismically active regions of the United States and is characterized by a number of fault systems capable of generating major earthquakes. The air base is located between two physiographic regions. The Transverse Ranges Province at the south and the Coastal Ranges in the north.

Battis (ref. 13.24) presents a statistical and a nonstatistical approach in predicting maximum credible earthquakes and associated ground motion attenuation for VAFB. Battes' statistical hazard analysis, based on the historic earthquake (epicenter data) catalogue for a regional seismic risk study, gave 11 significant source regions identified within a 500-km radius of VAFB. Estimates of the maximum magnitude earthquake (M_L) possible from each source region gave results ranging from an M_L maximum of 6.1 (from the Coastal Ranges) to an 8.25 (from the Nevada Fault Zone). Maximum ground motion attenuation (acceleration, velocity, and displacement) levels were calculated at the Point Arguello site (SLC6) and are shown in figure 13.15.

Battis also presented a nonstatistical approach in predicting maximum magnitude earthquakes and ground motion. The majority of the faults within 50 km (and faults with quaternary displacements within 100 km) of Point Arguello gave maximum credible earthquakes between 6.75 (Santa Rosa Island fault) and 8.5 M_L (San Andreas Fault Zone). See Table 13.2 which presents these maximum credible earthquake potentials using Battis' calculation of maximum displacements at the Point Arguello site (at the 90 percent confidence level). The Hosgri and San Andreas Fault Zones produce the maximum credible ground motions possible for Point Arguello.

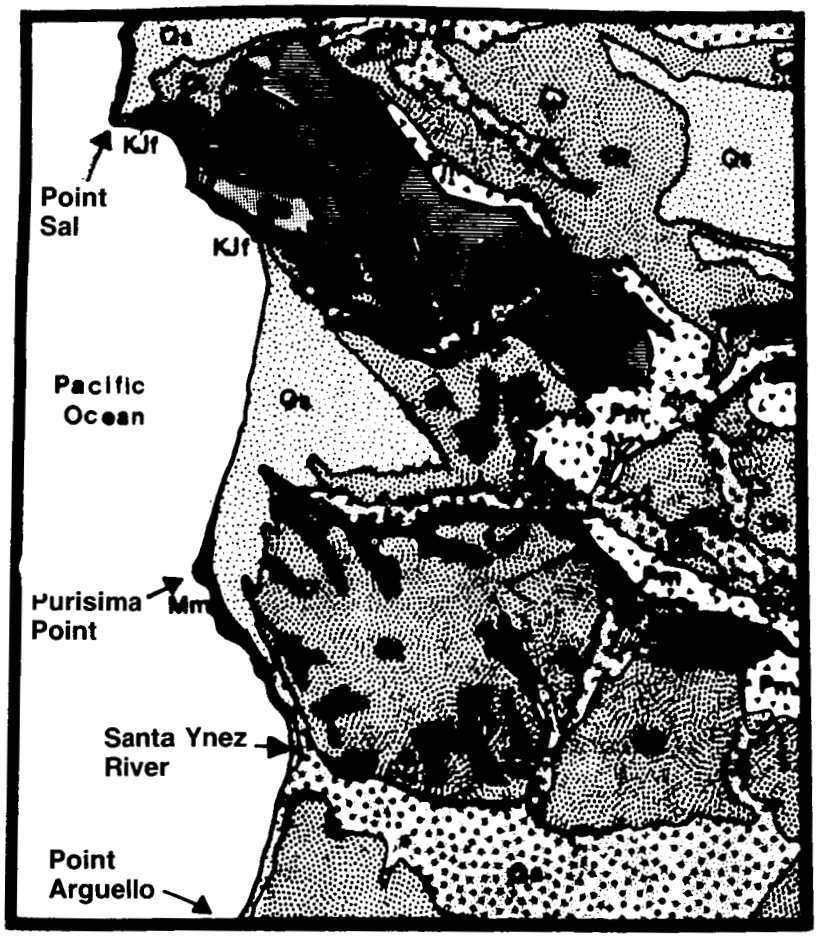

Figure 13.12 Geology of the Vandenberg AFB area (after Jennings, ref. 13.22).

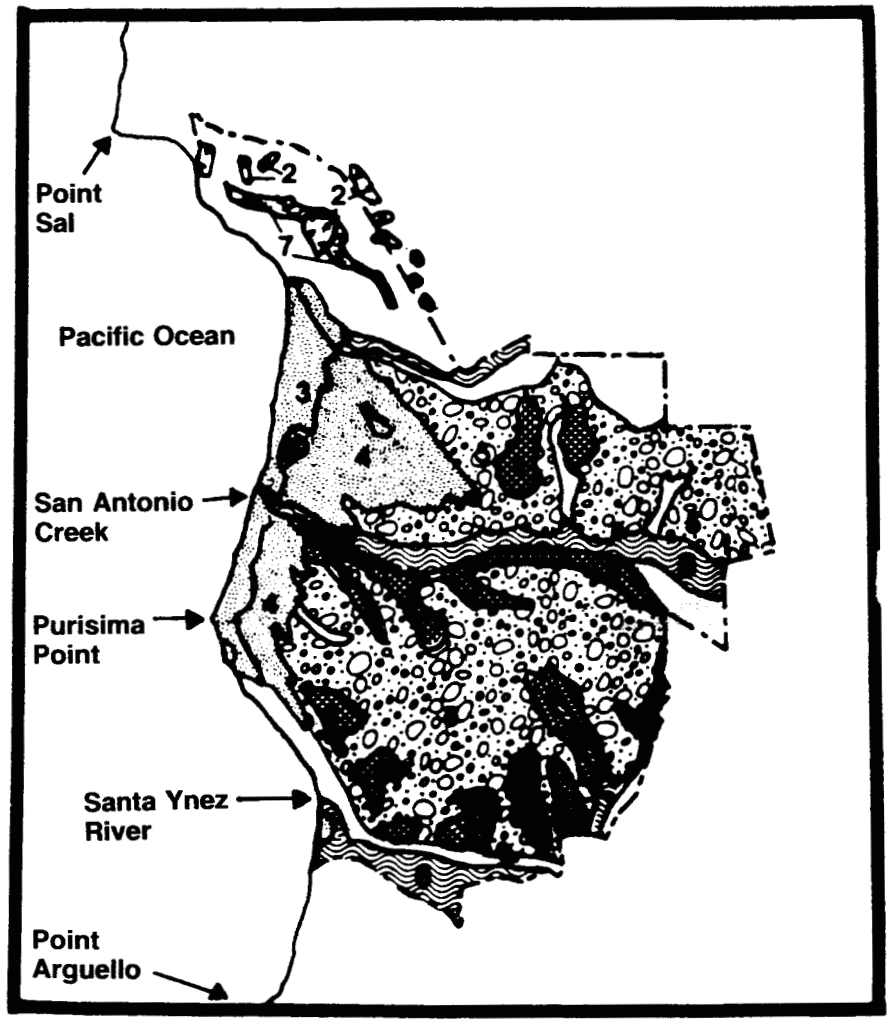

1 Gullying and resultant slope instability.

2 Recent landslides.

3 Active dunes.

4 Inactive dunes (anchored by vegetation).

Hazardous during Earthquakes

Unconsolidated terrace deposits.

Area of possible flash flooding. These areas, along with coastal areas, are also endangered by tsunamis or seiching.

Gypsiferous, clayey rock.

0 5mi/8km

scale: 1:250,000

Figure 13.13 Geologic hazards of Vandenberg AFB, California.

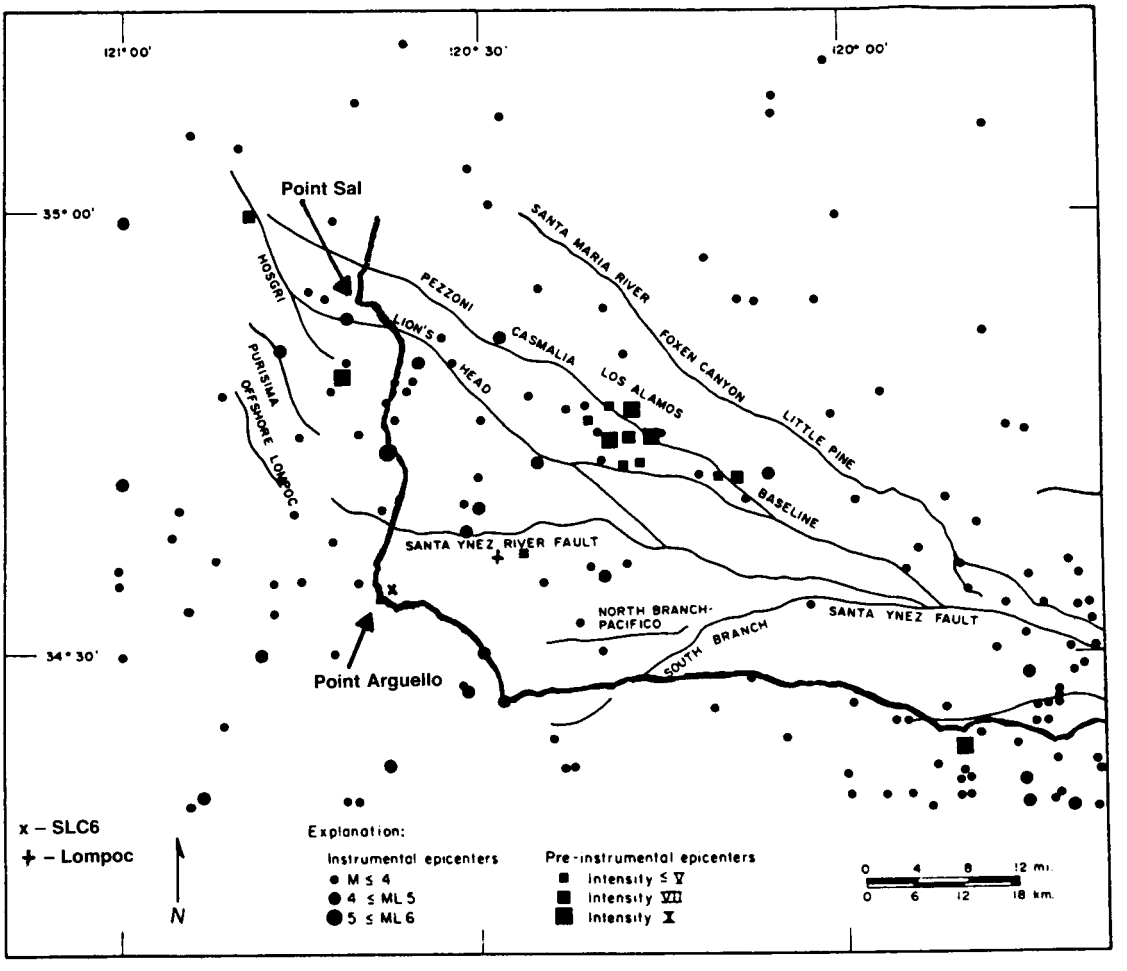

Figure 13.14 VAFB area and western Santa Barbara County, California, earthquake epicenters (ref. 13.24).

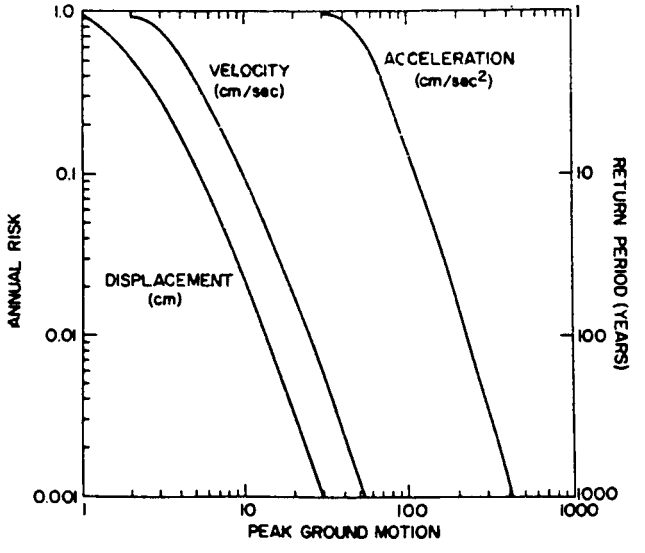

Figure 13.15 Annual seismic risk curves for peak ground motions at VAFB (SLC6), given at the 90-percent confidence level. Based on reference 13.24 statistical method.

Table 13.2 Major faults near VAFB and associated maximum credible earthquakes and ground motions (90-percent confidence level) at Point Arguello site.[1]

Fault	Maximum Credible Earthquake (M_L)	Maximum Credible Ground Motions at Point Arguello[2,3]		
		Acceleration (cm/s^2)	Velocity (cm/s)	Displacement (cm)
San Andreas Fault Zone	8.5	387.2	91.4	64.6
Hosgri Fault Zone	7.5	678.6	110.8	54.3
Big Pine Fault	7.5			
Santa Ynez Fault	7.5			
Rinconada Fault	7.5			
Nacimiento Fault Zone	7.0			
Santa Cruz Island Fault	6.75			
Santa Rosa Island Fault	6.75			

1. Based on reference 13.24 nonstatistical method.
2. Point Arguello and Point Sal are at the extremes of maximum credible ground motion for this area. Therefore, at the Point Sal site the maximum acceleration, velocity, and displacement values of 1,288.8 cm/s^2, 200.2 cm/s, and 83.8 cm, respectively, are possible.
3. Other fault ground motion statistics were not available from ref. 13.24.

However it is felt that the majority of faults very near VAFB have maximum credible earthquake potentials of between 6 and 6.5 M_L. In actuality, from 1932 to 1975 there have been 135 earthquakes with magnitudes between 2.5 to 4.9 M_L within 50 km of Point Arguello. The largest recent event to effect the VAFB region was the 1927 Lompoc earthquake with a reported magnitude of 7.3 M_L (Modified Mercalli Intensity IX), with its epicenter appearing to lie on an off-shore fault west of Point Arguello (ref. 13.24). Figure 13.14 presents a plot of these earthquake epicenters that have occurred in western Santa Barbara County, California. Battis' work indicates that VAFB should experience a Modified Mercalli Intensity of V somewhat less than once a year, which agrees with historical data.

13.4.3.2 Tsunamis and Seiches

Seismic water waves (tsunamis) must be considered as a threat all along the shore of the Pacific Ocean. Land within 12 m of sea level is in the tsunami danger zone. (Actually, few documented tsunamis have reached that height.) Fresh-water dams should be examined to determine their strength should seiching take place. Areas on the base which could be affected by tsunamis or by seiching are given in figure 13.13.

13.4.3.3 Slope Processes

The potential for slow or fast slope changes exists in several parts of Vandenberg Air Force Base. These areas are described later and are illustrated on figure 13.13.

a. Gullying is cutting away diatomaceous earth around the edges of Burton Mesa and San Antonio Terrace. This slow, almost continuous process has formed very steep slopes which would be unstable in a strong earthquake.

b. Several large landslides have occurred in the Casmalia Hills, in or near the north end of the base. Surface material there is obviously unstable and should be examined carefully on site before any construction.

c. Roughly one quarter of Vandenberg Air Force Base is covered by recent sand dunes. Though much of the dune area is anchored by vegetation, including windbreaks at the landward edge of the dunefield, sand blasting should be expected on San Antonio Terrace and Burton Mesa during times of high winds (see section II on Winds).

d. Although their surfaces are flat and nearly level, San Antonio Terrace and Burton Mesa are likely to be strongly affected by earthquake-induced surface movements because of the thick layer of unconsolidated sand and gravel terrace deposits which cover them. Shaking is highly amplified by thick, loose material, and buildings or other constructions on such material are at risk, especially if they are several stories high.

13.4.3.4 Floods

Three flood plain systems exist on the base. From north to south they are Shuman Canyon, San Antonio Valley, and Santa Ynez Valley. All three should be considered possible sites for flash flooding, especially since, during times when their rivers are dry, dune and bar sand partially block their outlets to the ocean. In addition, small dams in the Santa Ynez drainage basin could break and cause flooding during an earthquake.

13.4.3.5 Volcanic Hazards

No volcanic hazards are expected to affect this area, although tsunamis caused by distant volcanism are an always-present danger (see subsection 13.4.3.2).

13.4.3.6 Expanding Clays and Rocks

Expanding clays and rocks are not a major hazard on most of the base. Several hundred feet of gypsiferous, clayey, alkaline shale are present in the Casmalia Hills and should be avoided when locating construction sites.

13.4.3.7 Subsidence

Burning of hydrocarbon-rich layers of diatomaceous earth is well documented in historic time in the Casmalia Hills area. Burnt ground has been encountered to depths as great as 300 m in nearby oil wells (ref. 13.25). Red, hard, vesicular, scoriaceous rock ("clinker") results from this burning. However, no change in the volume of the burnt rock has been documented. Burning itself poses a threat, as it is next to impossible to stop once it has been started (by lightning or man).

13.4.4 Conclusions

Numerous potential geologic hazards exist within Vandenberg Air Force Base. Earthquakes occur from time to time, and could set off other dangerous events. Tsunamis caused by remote earthquakes or volcanism could affect the area of the base within 12 m of sea level. Seiching may pose a danger to small dams on the base. Widespread slope and surface instability is likely in the event of a strong earthquake. Blowing sand at times reduces the usefulness of some areas. Flash floods are possible in the valleys during rainy seasons. In some areas, hydrocarbon-soaked rocks have been known to catch fire. Use of different areas of the air base should take these hazards into account. True, the surface of the base is stable until rare hazard-causing events occur. But if they do, extensive destruction is possible.

13.5 Geology and Geologic Hazards at Cape Canaveral and KSC, FL

13.5.1 Introduction and Geology

Cape Canaveral, on the eastern coast of the Florida peninsula, covers an expanse of barrier bars, swamps, and lagoons between the Atlantic Ocean and the mainland. The entire Kennedy Space Center lies within 8 m of sea level. Surficial deposits on the center are roughly 30 m of Miocene to Recent shelly sand and clay and medium to fine-grained sand and silt (ref. 13.26) (fig. 13.16). These sediments overlie Eocene limestone and dolomite.

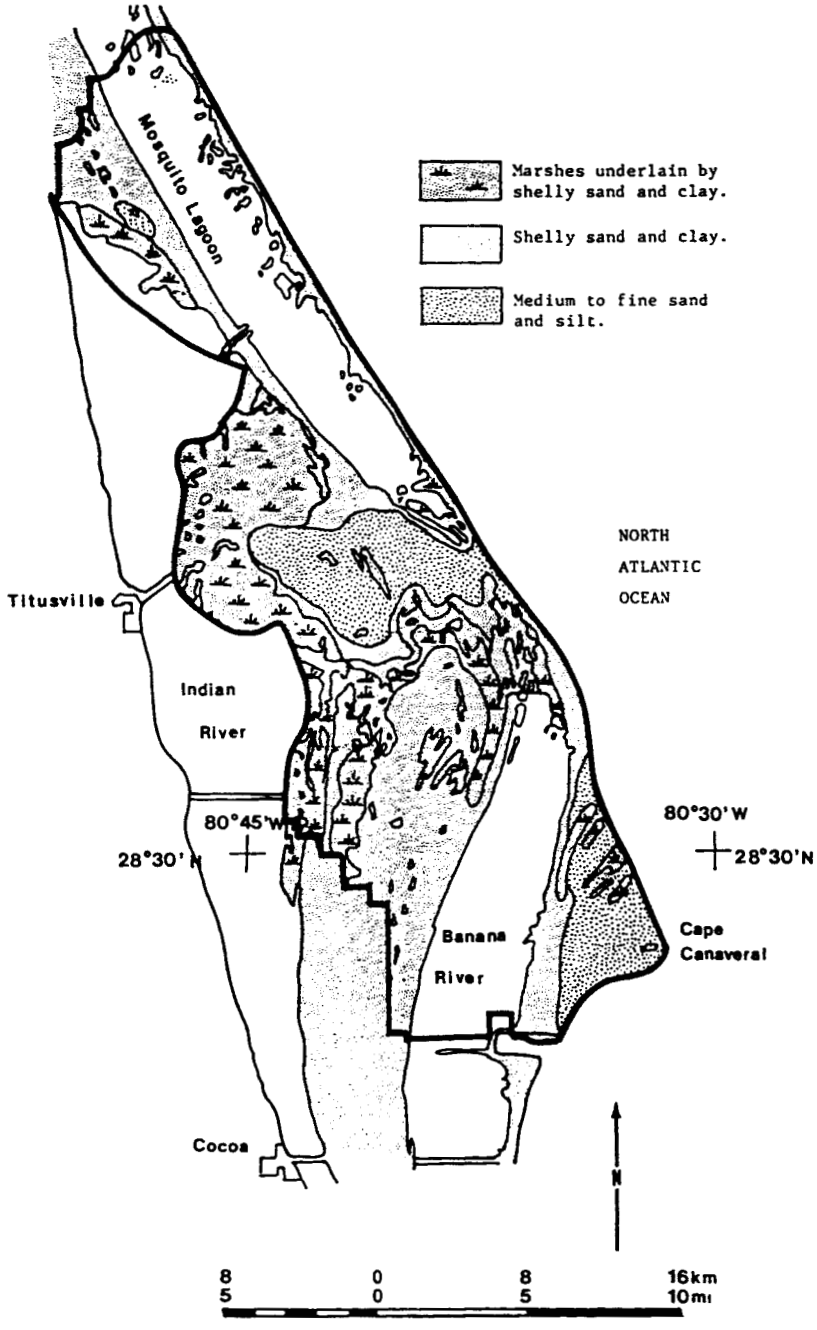

Figure 13.16 Geology of Cape Canaveral, Florida.

13.5.2 Geologic Hazards at Cape Canaveral and KSC

13.5.2.1 Earthquakes

Earthquakes are extremely unlikely in this corner of the United States and should not be considered a hazard.

13.5.2.2 Tsunamis and Seiches

Sea waves (tsunamis) induced by earthquakes and/or volcanism elsewhere could be a hazard to the entire space center because of its low elevation. However, tsunamis are not common in the Atlantic Ocean and, although not impossible, are considered unlikely. Nor are the lagoons and rivers likely to develop seiches.

13.5.2.3 Slope Stability

The lack of topographic relief on Cape Canaveral and Kennedy Space Center means slope stability is not a problem there.

13.5.2.4 Floods

Flooding could be a hazard to the space center if high water is brought about by hurricane winds (see sections II and XII on wind and severe weather).

13.5.2.5 Volcanic Hazards

Volcanism near Cape Canaveral is unknown in recent time. The only volcanic hazards to the Cape are tsunamis caused by distant volcanism.

13.5.2.6 Expanding Soils and Rocks

Expanding soils and rocks are not a hazard to the Kennedy Space Center because of the high sand content of sediments and the consistently high humidity.

13.5.2.7 Subsidence and Uplift

Drilling results indicate the presence of caverns in the limestone and dolomite units which underlie the space center (ref. 13.26); therefore, there is potential for eventual caving. There is no apparent evidence of karst topography in the space center area, nor is collapse expected in the foreseeable future. However, test drilling should always precede building location and construction.

13.5.2.8 Conclusions

Cape Canaveral/Kennedy Space Center is a low risk area for geologic hazards. Only flooding, due to hurricanes or seismically induced waves, is considered to be of possible importance. Crucial structures which would not survive high water should be protected by dikes.

13.6 Seismic Environment

Government support equipment (GSE), which may be subjected to a high risk potential, seismic environment, should be designed considering the geologic hazards defined in this section. The following are recommendations to consider during the design process.

13.6.1 GSE Categories and Recommendations

For seismic purposes, two categories of GSE have been established:

I. Equipment that can inflict structural damage on the space shuttle vehicle (SSV) elements during and after a seismic event by its operation or by its failure to operate.

II. Equipment located in close proximity to the SSV elements that can cause major structural damage due to support failure or physical contact with the integrated SSV or SSV elements.

All GSE elements should remain integrally constrained in their packages. The equipment should not be allowed to separate from the unit and become missiles. This recommendation does not include equipment which is already separated from SSV elements by strong physical barriers, such as walls or enclosures sufficient to prevent equipment contact with SSV elements.

13.6.2 Types of Design Analyses

Recommendations for typical dynamic or static analyses follow.

13.6.2.1 Dynamic Analysis

A rigorous dynamic analysis should be made to demonstrate that the equipment and its supporting mechanism/structure will withstand, without collapse or excessive deflection, the design loads induced in the system by a major seismic event. The effect of such an event on the system can be determined using the GSE design response spectra for major seismic events at Vandenberg Air Force Base shown in figure 13.17. The design loads should equal the root-sum-square (RSS) of the modal responses, where natural frequencies are determined by modal analysis and whose damping values are estimated by damping analysis, or by similarity to structures whose damping has been measured under actual or simulated earthquake motion.

13.6.2.2 Static Analysis

The following criteria are recommendations for designing GSE for seismic resistance:

1. GSE weighing less than 100 lb should have restraints to resist a horizontal force of $\times 1.5$ equipment weight from any direction applied to its center of gravity.

2. For GSE weighing between 100 and 1,000 lb, the following equation can be used to determine the recommended restraints:

$$F = ZKCW, \tag{13.1}$$

where

F = equivalent static lateral force in pounds applied at the center of gravity

Z = seismic probability coefficient (no units), where $Z = 1.5$ for high-loss potential equipment (damages SSV element), $Z = 1.0$ for low-loss potential equipment (damages GSE only)

C = seismic force coefficient (no units)

K = coefficient based on building type (no units)

W = weight in pounds of item under consideration.

C may be calculated using the following equation:

$$C = (C_s)\ (A_h)\ (MF)\ , \tag{13.2}$$

where

C_s = soil constant (no units) = 2.25–0.125 $f_b \geq 1$

f_b = allowable soil bearing value in kips per square foot (see Geophysical Investigation Supplement for VAFB Station Set V23 (VCR-77-067 of 20 January 1977) (1 kip = 1,000 lb))

A_h = design acceleration = 0.10+0.15 (h/h_t)

h = height of equipment in building above building base

h_t = height of building.

Now, MF = magnification factor (no units)

$$= \frac{1}{\sqrt{[1-(T_a/T)^2]^2 + [0.04\ T_a/T]^2}}\ , \tag{13.3}$$

where

T_a = period of item under consideration in seconds

T = period of building in seconds

(for graphical solution to equation see figures 13.18 and 13.19).

The building characteristic constants for the mobile service tower (MST), the payload changeout room (PCR), and the access tower (AT) are shown in table 13.3. For equipment in contact with the soil, buried in the soil, or supported by footings, pedestals, or slaps supported by soil, use the following coefficients: $K = 1.00$ and $C = 0.15$.

3. Also recomended is that items weighing more than 1,000 lb be subjected to dynamic analysis. Items weighing more than 1,000 lb and having a ratio of 4 to 1 or greater between structural strength of tie down and limit load, as defined in paragraph 2, are exempt from dynamic analysis.

Equipment that is to be in use for not longer than 8 hours in close proximity to, or supporting SSV elements, are exempt from these requirements.

Equipment that is mounted on casters or wheels should have lockable casters/wheels and be rigidly tied to primary or substantial secondary structure.

Table 13.3 Building characteristic constants.

	K	h (ft)	T (s)
MST	0.8	275	1.23
PCR	0.8	160	0.93
AT	0.8	192	0.61

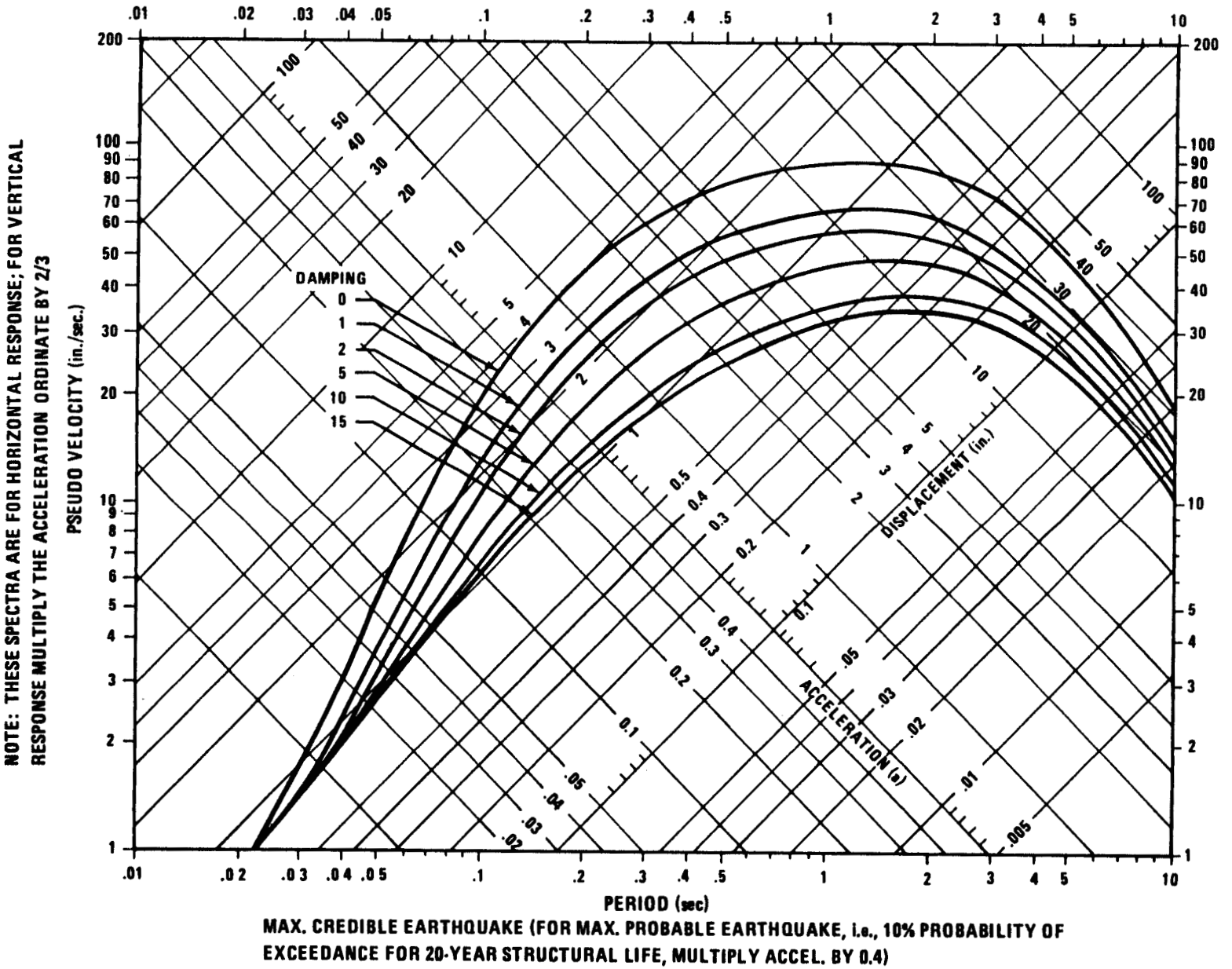

Figure 13.17 0.70E elastic design spectra for strongest potential vibratory ground motion.

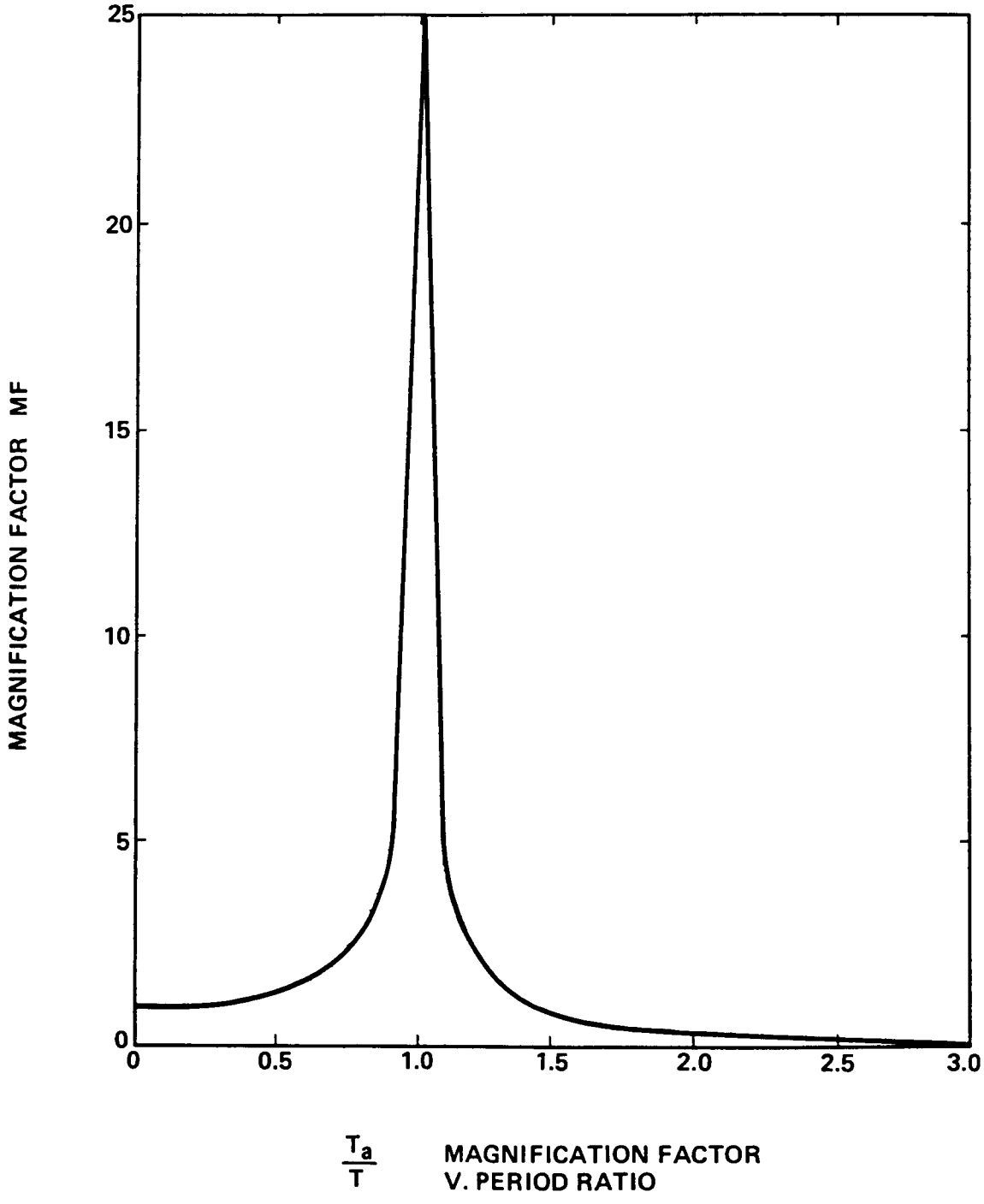

Figure 13.18 Magnification factor versus period ratio.

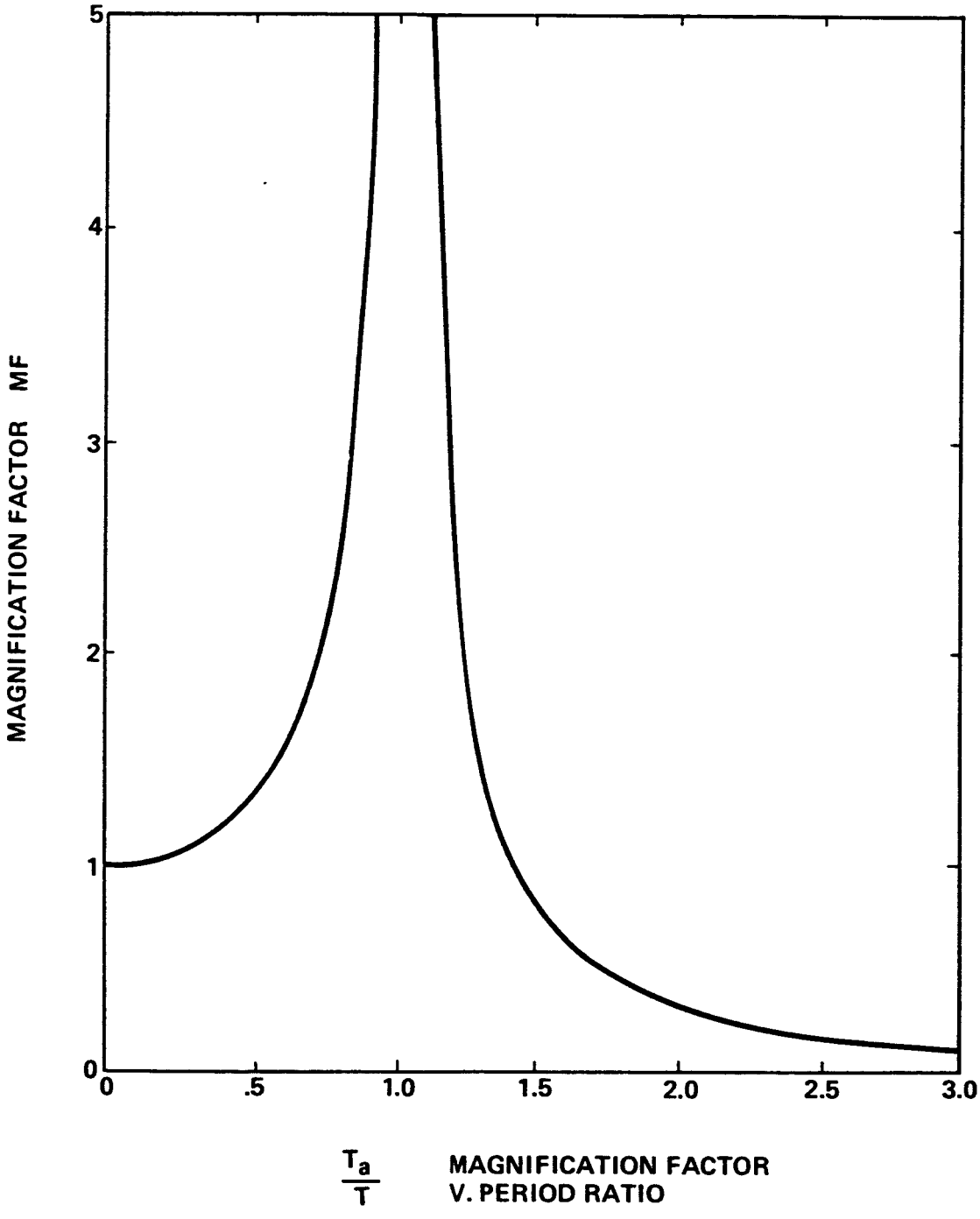

Figure 13.19 Magnification factor versus period ratio.

REFERENCES

13.1 Van Dorn, W.G.: "Source Mechanism of the Tsunami of March 27, 1964." Alaska: Coastal Eng. Conf., 9th, Lisbon, 1964 Proc., pp. 166–190, 1964.

13.2 Stein, R.S. and Yeats, R.S.: "Hidden Earthquakes." Scientific American, pp. 48–57, June 1989.

13.3a Algermissen, S.T.: "An Introduction to the Seismicity of the United States." Earthquake Engineering Research Institute Monograph, 1983.

13.3b Algermissen, S.T., and Hopper, M.G.: "Estimated Maximum Regional Seismic Intensities Associated With an Ensemble of Great Earthquakes That Might Occur Along the New Madrid Seismic Zone, East Central United States." Misc. Field Studies Map MF-1712, U.S. Geological Survey, 1984 (reprinted 1990).

13.4 Cousineau, R.D., et al.: "Investigation of Seismicity and Related Effects at NASA Ames-Dryden Flight Research Facility, Computer Center, Edwards, California." NASA CR-170415, November 1985.

13.5 Krinitizsky, E.L., and Chang, F.K.: "Earthquake Intensity and the Section of Ground Motions for Seismic Design." Corps of Engineers Waterways Experiment Station, Misc. Paper S-73-1.

13.6 Bonilla, M.: "Surface Faulting and Related Effects." In Earthquake Engineering, Prentice-Hall, 1970.

13.7 Greensfelder, R.W.: "Map of Maximum Bedrock Acceleration From Earthquakes in California." California Division of Mines and Geology, Map Sheet 23, 1974.

13.8a Algermissen, S.T., et al.: "Probabilistic Estimates of Maximum Acceleration and Velocity in Rock in the Contiguous United States." U.S. Geological Survey, Open File Report 82-1033, 1982.

13.8b Algermissen, S.T., et al.: "Probabilistic Earthquake Acceleration and Velocity Maps for the United States and Puerto Rico." Misc. Field Studies Map MF-2120, U.S. Geological Survey, 1990.

13.9 Working Group on California Earthquake Probabilities, U.S. Geological Survey Open File Report No. 88-398, 1988.

13.10 The Loma Prieta Earthquake of October 17, 1989, U.S. Geological Survey pamphlet, 1989.

13.11 Ruhe, R.V.: Geomorphology. Houghton Mifflin Co., Boston, Mass., pp. 99–123, 1975.

13.12 Sharpe, C.F.S.: "Landsides and Related Phenomena." New York, Columbia University Press, 1938.

13.13 Mullineaux, D.R.: "Preliminary Map of Volcanic Hazards in the Conterminous United States." U.S. Geological Survey, Misc. Field Inv. MF-786, scale 1:7,500,000, 1976.

13.14 Bolt, B.A., et al.: "Geologic Hazards: New York." Springer-Verlag, 328 pp. (Chapter on evaluation of volcanic hazards), 1975.

13.15 Rogers, W.P., et al.: "Guidelines and Criteria for Identification and Land Use Controls of Geologic Hazard and Mineral Resource Areas." Colo. Geol. Survey Special Pub. No. 6, pp. 68–76, 1974.

13.16 James, D.E., Jr. and Holtz, W.G.: "Expansive Soils—The Hidden Disaster." Civil Eng., 43, No. 8, 1973.

13.17 Dibblee, T.W., Jr.: "Geology of the Rogers Lake and Kramer Quadrangle." U.S. Geol. Survey Bull. 1089-B, pp. 73–139, 1960.

13.18 Droste, J.B.: "Clay Minerals in the Playa Sediments of the Mojave Desert, California." California Div. Mines and Geol. Special Report 69, 1961.

13.19 Mortan, D.M.: "Geologic Hazards in Southwestern San Bernardino County, California." California Div. Mines and Geol. Special Report 113, 1976.

13.20 Real, C.R., et al.: "Earthquake Epicenter Map of California, 1900–1974." California Div. Mines and Geol. MS 39, 1978.

13.21 Radbruch, D.H. and Crowther, K.C.: Maps showing areas of estimated relative amounts of landslides in California. U.S. Geol. Survey Misc. Geol. Inv. Map 747, 1973.

13.22 Jennings, C.W.: Santa Maria Sheet, Geologic Map of California. California Div. of Mines, 1:125,000, 1959.

13.23 Fife, D.L., et al.: "Geologic Hazards in Southwestern San Bernardino County, CA." California Division of Mines and Geology Special Report 113, plate 7, Earthquake Epicenters in Southern California, 1910–1917, 1976.

13.24 Battis, J.C.: Seismic Hazards Estimation Study for Vandenberg AFB. AFGL-TR-79-0277, AFSIG No. 418, November 14, 1979.

13.25 Arnold, R. and Anderson, R.: "Geology and Oil Resources of the Santa Maria Oil District, Santa Barbara County, California." U.S. Geol. Survey Bull. 322, map (1:125,000), 1907.

13.26 Scott, T.M.: Orlando Sheet, Environmental Geology Series. Florida Geol. Survey MS 85, 1978.

SECTION XIV. SEA STATE

14.1 Introduction

Natural environment design specifications for all applicable space shuttle activities are given in the appropriate level II (ref. 14.1) or level III (ref. 14.2) program requirement documents. Since those documents are controlled by the program or project manager, it is not appropriate to repeat the design values here. Instead, this section contains the empirical distributions of several natural environment parameters that may be useful in operational analyses, design tradeoff studies or to develop specific design specifications. The National Launch System (NLS) potential recovery areas sea state statistics are also described in this section.

In deep water, sea state is determined by the mean wind speed, the fetch (the distance over which it blows), and the duration of the wind over the open water. A sea state is generally described by significant wave height, which is the average height of the one-third highest waves. Higher waves exist in any given sea state. For example, from the relationship between wind speed and wave height for a fully arisen sea, as shown in figure 14.1, it can be seen that in a code 3 sea state with significant wave heights about 1.4 m, 10 percent of the waves will average about 1.7 m. In other words, a wind speed of 8.2 m s^{-1} (fetch and duration unlimited) will produce a sea with the highest one-third waves averaging about 1.4 m and the highest one-tenth waves about 1.7 m.

Figure 14.1 shows the distribution of wave heights versus wind speed at any given instant. This information is applicable to vehicle water entry. For all other operations (afloat, secure, towback recovery) where some considerable time interval is involved, the exposure period concept must be considered; that is, the longer the exposure period, the greater the probability of encountering a larger wave. Wave heights at the 5-percent risk level for exposure periods from 1 to 100 hours in sea-state codes 3, 4, and 5 are shown in figure 14.2. From 14.2, for example, it can be seen that exposure for 1 hour in sea-state code 4 entails a 5-percent risk of encountering at least one wave greater than 5.3 m. If the exposure time is increased to 48 hours in the same sea-state code 4 condition, the wave height at the 5 percent risk level becomes 6.3 m.

14.2 Sea States

The foregoing paragraphs dealt with general sea-state relationships valid in any deep-water area. This part will present statistical values applicable to aerospace vehicle ocean recovery areas off Kennedy Space Center (KSC) and Vandenberg Air Force Base (VAFB). The wind and wave duration statistics were taken from the "U.S. Navy Hindcast Spectral Ocean Wave Model Climatic Atlas" (ref. 14.3 and 14.4). While these publications contain comprehensive wind and wave descriptions, comparisons with other sources indicate that the Spectral Ocean Wave Model underestimates wind speed and wave height near U.S. east coast areas. For this reason the wind speeds and wave heights (except durations and intervals) from conventional sources (ship observations) are considered more appropriate for planning ocean operations in the Atlantic Ocean areas under discussion. The Spectral Ocean Wave Model is the only known source for duration/interval statistics.

Additional climatic and sea state statistics for these two areas can be found in references 14.5 and 14.6.

The following tables were generated from observations of significant waves ($H_{1/3}$ equals the average height of the one-third highest waves) without regard to fetch or duration (ref. 14.7). In any given sea state there will always be waves higher than the significant heights. Also, exposure time increases the chances of higher waves occurring.

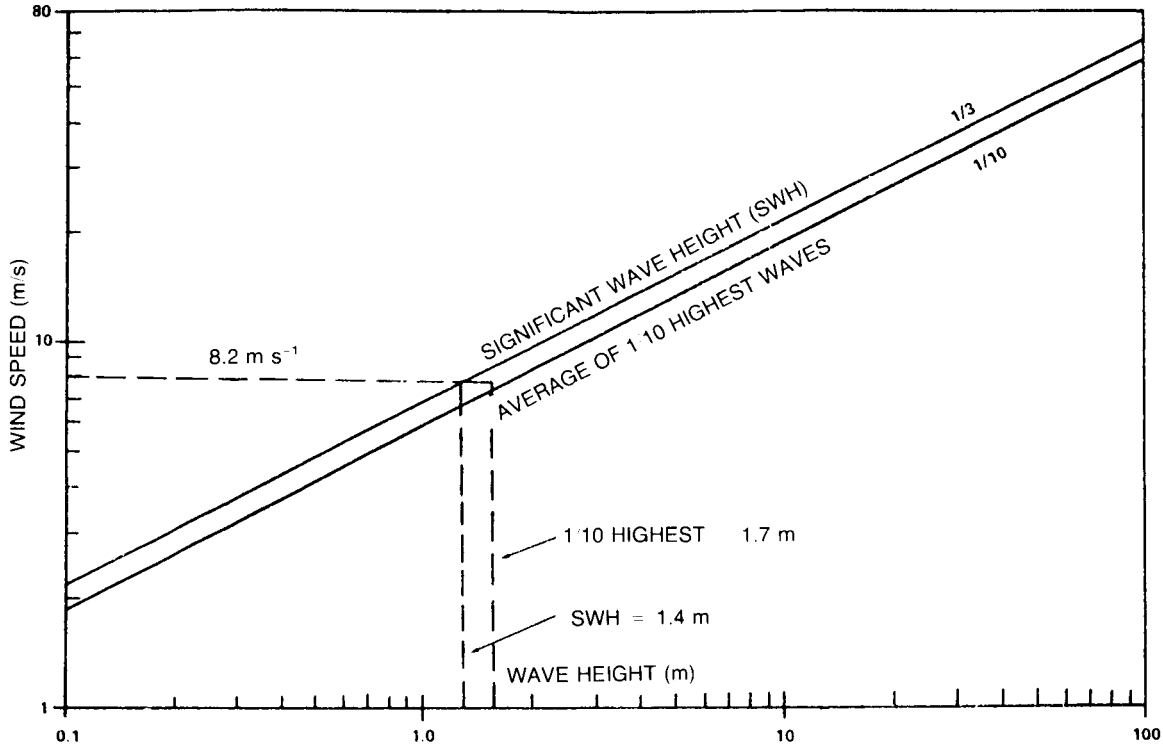

Figure 14.1. Relationship between wave height and wind speed in a fully arisen sea.

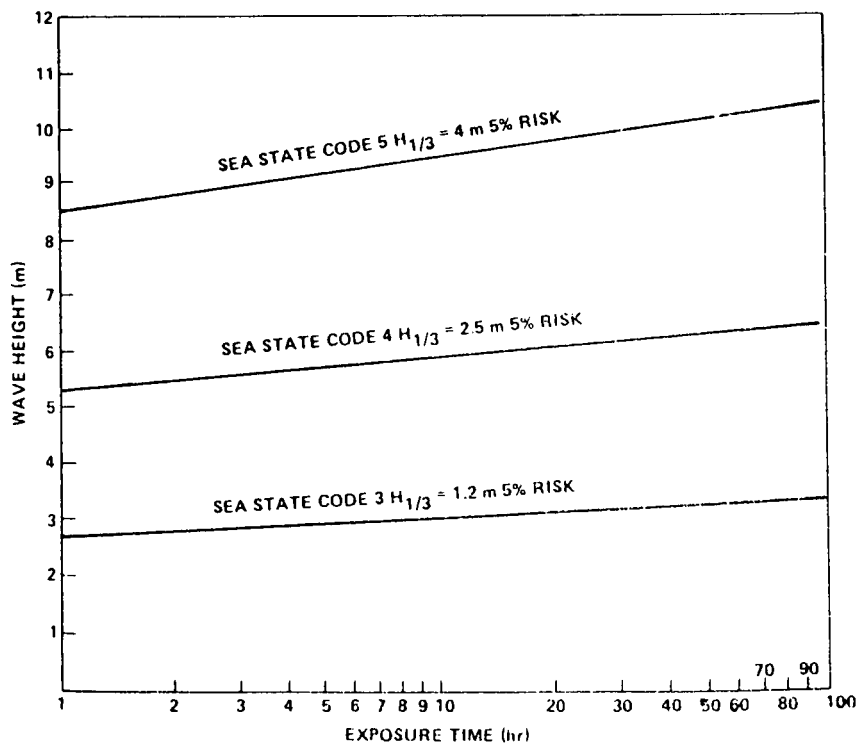

Figure 14.2. Five-percent risk wave height versus exposure time (assuming sea-state category remains unchanged for duration of exposure period).

From Table 14.1, there is a 3-percent risk of exceeding sea-state code 5 and a 68-percent risk of exceeding sea-state code 3 in February. Also, in February there is a 95-percent chance that the significant wave height will be ≤3.7 m and, conversely, a 5-percent chance that it will exceed 3.7 m. On an annual basis, the 95th percentile wave height is 2.9 m in the KSC recovery area versus 2.8 m in the VAFB recovery area (table 14.2). While the annual $H_{1/3}$ values are very similar, some monthly distributions show considerable differences. In general, the KSC area shows a somewhat greater seasonal variation and, consequently, a more severe environment.

Table 14.3 presents the international meteorological codes for the state of the sea (ref. 14.8).

Table 14.1. KSC recovery area sea states.
(24° to 32° N. latitude; 72° to 80° W. longitude)

Significant Wave Heights, Avg. of 1/3 Highest		Sea State Codes	Percent Probability of Exceeding Indicated Heights												
m	ft		J	F	M	A	M	J	J	A	S	O	N	D	Avg.
0.6	2	2	86	90	84	87	68	70	68	58	82	82	84	84	80
1.2	4	3	60	66	54	50	27	35	30	22	55	58	56	56	50
2.4	8	4	14	20	10	8	5	6	3	2	15	12	13	10	9
4.0	13	5	2	3	1	0.5	0.8	0.8	0.2	0.2	2	1.8	1.2	0.8	1
6.1	20	6	0.2	0.3	0.2	<0.1	0.2	0.2	<0.1	<0.1	0.2	0.3	<0.1	<0.1	0.1
			Significant Wave Height (m)												
Percentiles			J	F	M	A	M	J	J	A	S	O	N	D	Avg.
50th			1.4	1.6	1.4	1.2	0.8	0.9	0.8	0.7	1.3	1.4	1.4	1.4	1.2
95th			3.3	3.7	2.8	2.7	2.4	2.6	2.2	2.1	3.3	3.2	3.0	2.8	2.9

Table 14.2. VAFB recovery area sea states.
(25° to 34° N. latitude; 119° to 124° W. longitude)

Significant Wave Heights, Avg. of 1/3 Highest		Sea State Codes	Percent Probability of Exceeding Indicated Heights												
m	ft		J	F	M	A	M	J	J	A	S	O	N	D	Avg.
0.6	2	2	74	67	76	78	82	82	81	83	77	58	69	74	76
1.2	4	3	42	38	45	49	50	51	47	45	44	37	34	49	44
2.4	8	4	9	9	10	11	10	9	5	6	6	5	4	13	8
4.0	13	5	1.4	1	1.8	1.8	1.2	0.4	0.2	0.1	0.4	0.4	0.5	3	1
6.1	20	6	<0.1	<0.1	<0.1	<0.1	<0.1	<0.1	<0.1	<0.1	<0.1	<0.1	<0.1	<0.5	<0.1
			Significant Wave Height (m)												
Percentiles			J	F	M	A	M	J	J	A	S	O	N	D	Avg.
50th			1.0	0.9	1.1	1.2	1.2	1.2	1.1	1.1	1.1	0.7	0.9	1.2	1.1
95th			2.9	3.2	3.2	3.0	3.2	2.8	2.4	2.5	2.6	2.4	2.4	3.5	2.8

Table 14.3. International meteorological codes, code 3700, state of sea.

Code Figure	Descriptive Terms	$H_{1/3}$ of Waves	
		m	ft
0	Calm (Glassy)	0	0
1	Calm (Rippled)	0–0.1	0–0.33
2	Smooth (Wavelets)	0.1–0.5	0.33–1.6
3	Slight	0.5–1.25	1.6–4.1
4	Moderate	1.25–2.5	4.1–8.2
5	Rough	2.5–4	8.2–13.1
6	Very Rough	4–6	13.1–19.7
7	High	6–9	19.7–29.5
8	Very High	9–14	29.5–45.9
9	Phenomenal	Over 14	Over 45.9

Note: Exact bounding height is assigned to lower code; e.g., a height of 4 m is coded 5.

14.3 Surface Currents

a. KSC Solid Rocket Booster (SRB) Recovery Area. The dominant current, which is south to north, in the KSC SRB recovery area is the Gulf Stream. Although the mean speed and position of the maximum current shows little change from season to season, daily synoptic changes may be rapid and intense (ref. 14.9).

The following means and standard deviations may be applied to all seasons (fig. 14.3):

Area	Mean	Standard Deviation
B	0.4 m s^{-1} (0.8 knots)	0.7 m s^{-1} (1.27 knots)
A	1.3 m s^{-1} (2.5 knots)	0.6 m s^{-1} (1.25 knots)

b. VAFB SRB Recovery Area. While the predominant direction is north to south in all seasons, the currents are generally weak in the VAFB SRB recovery area—less than 1 knot.

The following mean and standard deviation may be used for the entire recovery area for all seasons:

Mean	Standard Deviation
0.3 m s^{-1} (0.54 knots)	0.3 m s^{-1} (0.56 knots)

14.4 Wave Slope

The wave slopes shown in tables 14.4A and 14.4B for Kennedy Space Center and Vandenberg AFB were calculated along the wind direction after assuming a Gaussian distribution in a fully aroused sea. The entire distribution of significant wave heights was used for the calculations.

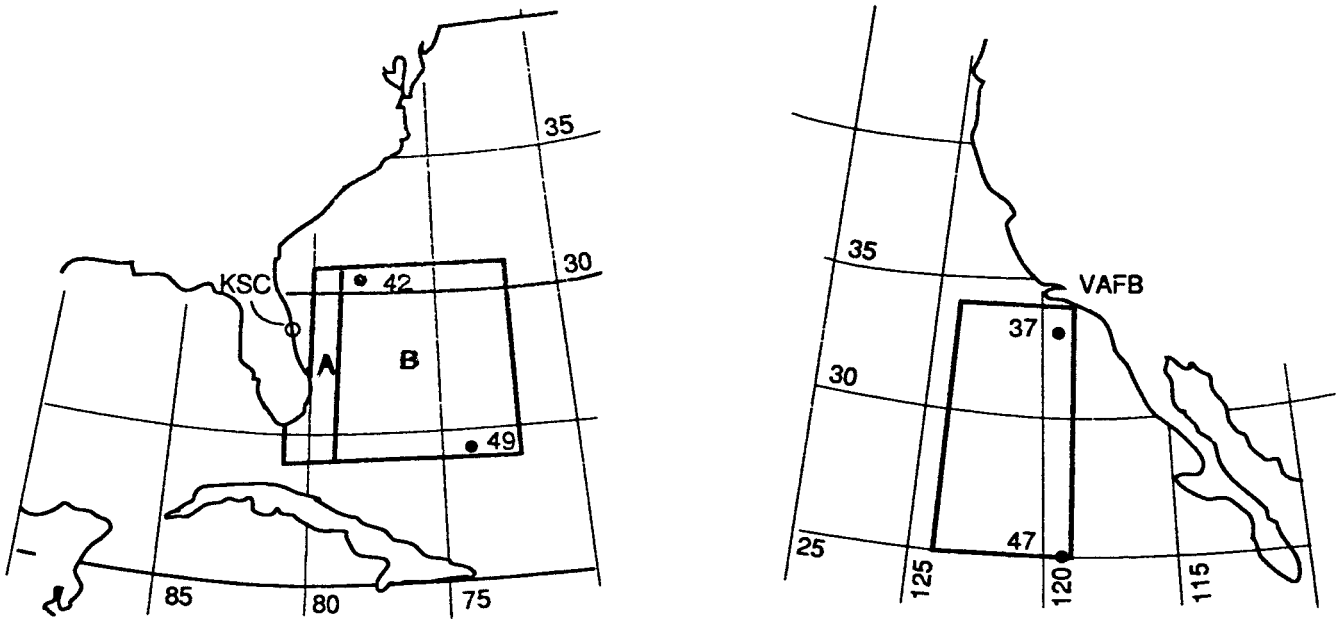

Figure 14.3. KSC and VAFB booster recovery areas. Includes special Gulf Stream current areas (A) and wind speed duration grid points.

Table 14.4A. KSC recovery area wave slopes (calculated from significant wave heights).

Risk of Exceeding	J	F	M	A	M	J	J	A	S	O	N	D	Avg.
5%	11°	12°	11°	10°	10°	10°	10°	9°	11°	11°	11°	11°	10°

Table 14.4B. VAFB recovery area wave slopes (calculated from significant wave heights).

Risk of Exceeding	J	F	M	A	M	J	J	A	S	O	N	D	Avg.
5%	10°	10°	10°	10°	11°	11°	10°	10°	10°	10°	10°	11°	10°

14.5 Ocean Temperatures

Maximum, mean, and minimum water temperatures for 3-month periods from the surface to depths of 50 m for KSC and VAFB booster recovery areas are given in tables 14.5 and 14.6 (ref. 14.10).

14.6 Atmospheric Conditions

Climatological information applicable to KSC and VAFB booster recovery and retrieval areas is given in tables 14.7 and 14.8 (refs. 14.7 and 14.11). These values, developed from observations made at 00, 06, 12, and 18 Z time by ships passing through the area, show the percent frequency of the indicated atmospheric condition. For example, off KSC in January the sky cover was 0, 1/8, or 2/8 (≤2/8) on 20.3 percent of the observations. The sky was completely covered (8/8) on 20.8 percent of the observations.

14.7 Wind Speed and Wave Height Durations and Intervals

The following duration and interval tables, taken from the "U.S. Navy Hindcast Spectral Ocean Wave Model Climatic Atlases" (refs. 14.3 and 14.4), are given for two Atlantic Ocean grid points (Nos. 42 and 49) near Cape Canaveral, FL and two Pacific Ocean grid points (Nos. 37 and 47) near Vandenberg AFB, CA (fig. 14.3). Even though the statistics are given at grid points they are representative of surrounding areas. Also, interpolation may be used for areas between grid points. The Atlantic Ocean data base of 20 years was considered large enough to produce reliable monthly statistics. The Pacific Ocean data base of 12.5 years, however, was not large enough for monthly summaries. The statistics were prepared for seasons as follows:

Winter = January, February March
Spring = April, May, June
Summer = July, August, September
Fall = October, November, December

Atlantic Ocean duration and interval tables were published for only 6 months—January, February, April, July, August, October—and a summary table which includes all the hindcasts. These months were chosen to show detail in winter (January and February) and summer (July and August), with only one month for each transition season (April and October). Episodes of durations (continuous hours or days) of events and episodes of intervals (continuous hours or days) between events were tallied for various thresholds. These tables give an indication of how long an episode is likely to last once it has begun. For convenience, the time an episode persisted above a given threshold is arbitrarily referred to as a "duration" of the event. The times in between episodes have been termed "intervals."

14.7.1 Legends For Duration and Interval Tables

Table 14.9 gives the legends for duration and interval tables (tables 14.10 through 14.25).

14.7.2 Applications of Durations and Interval Tables

When answering questions using the duration and interval tables, it is important to distinguish between questions that require the use of the number of episodes and those that require the number of hindcasts. Answers for questions regarding the percentage of time at or above, or below, certain thresholds require the use of the number of hindcasts. On the other hand, questions concerned with the percentage of episodes at or above, or below, certain thresholds demand the use of episode frequencies, where a 1-day episode and a 60-day episode will each count as one episode.

Table 14.5 Ocean tempeatures (°C) in the KSC booster recovery areas.

Months	January to March			April to June			July to September			October to December		
Depth (m)	Max.	Mean	Min.	Max.	Mean	Min.	Max.	Mean	Min.	Max.	Mean	Min.
0	26	23	16	29	26	21	31	29	27	29	26	19
10	26	23	16	29	26	20	30	29	26	29	26	19
20	26	23	17	29	26	19	30	28	23	29	26	20
30	26	23	16	28	26	17	29	28	21	29	26	21
50	26	23	17	28	25	17	29	27	19	28	26	22

Table 14.6 Ocean temperatures (°C) in the VAFB booster recovery areas.

Months	January to March			April to June			July to September			October to December		
Depth (m)	Max.	Mean	Min.	Max.	Mean	Min.	Max.	Mean	Min.	Max.	Mean	Min.
0	17	14	12	19	14	11	21	17	13	20	17	13
10	17	14	11	18	14	11	21	17	11	20	17	13
20	17	14	11	17	14	11	20	16	10	20	16	12
30	17	14	11	17	14	10	20	16	10	20	16	11
50	17	14	10	17	13	9	19	14	9	20	14	10

Table 14.7. KSC booster recovery area atmospheric conditions.

Percent Frequency of Occurrence									
	Visibility		Total Precip.	Sky Cover			Wind Speed (knots)		
Month	≤2	≥10	(in)	0-2/8	8/8	Mean*	≤10	≥17	Mean†
J	1.3	89.4	4.0	20.3	20.8	0.62	29.0	35.8	15.2
F	1.9	88.4	4.5	21.3	22.1	0.62	29.9	39.2	15.9
M	0.5	88.6	2.6	26.5	19.2	0.58	30.0	37.9	15.2
A	1.0	89.6	1.3	36.2	9.6	0.47	34.4	30.6	14.0
M	0.9	88.7	2.2	37.5	12.7	0.47	48.2	18.6	11.9
J	2.4	86.2	4.5	24.2	17.2	0.57	49.7	17.8	11.9
J	1.3	92.0	3.8	30.8	12.4	0.52	50.6	14.6	11.5
A	1.1	90.0	4.5	22.5	11.8	0.55	57.6	13.4	11.2
S	2.2	87.3	4.9	25.4	16.2	0.56	50.6	19.1	12.0
O	0.6	90.6	2.3	28.5	13.7	0.53	36.5	28.7	13.6
N	1.1	92.7	3.4	28.7	11.6	0.53	33.8	33.2	14.7
D	0.9	92.7	2.1	29.0	14.3	0.56	41.3	28.6	14.7

Table 14.8. VAFB booster recovery area atmospheric conditions.

Percent Frequency of Occurrence									
	Visibility		Total Precip.	Sky Cover			Wind Speed (knots)		
Month	≤2	≥10	(in)	0-2/8	8/8	Mean*	≤10	≥17	Mean†
J	2.3	76.9	5.1	30.5	25.2	0.59	41.2	27.5	13.1
F	4.6	76.3	4.9	27.8	29.3	0.60	38.6	32.5	13.8
M	0.8	81.0	3.2	30.4	23.9	0.58	35.1	40.4	14.8
A	1.6	75.2	3.0	25.0	30.3	0.63	29.1	43.6	15.7
M	0.3	84.1	2.1	24.0	31.8	0.65	26.5	43.5	15.8
J	1.1	71.5	2.7	21.7	49.2	0.71	28.1	42.4	15.5
J	1.2	74.1	2.3	16.5	60.4	0.79	34.7	34.8	14.0
A	0.8	72.8	1.4	16.1	58.6	0.79	32.9	33.5	13.9
S	0.5	77.0	1.9	26.4	39.4	0.66	35.4	33.3	13.7
O	1.0	79.1	1.3	33.9	33.1	0.58	40.7	30.8	13.4
N	1.9	77.5	3.8	32.9	26.0	0.56	44.2	26.2	12.7
D	1.2	83.3	3.2	32.8	20.5	0.55	46.5	28.2	12.7

*Mean sky cover is expressed in one-hundredths of the sky being covered.
†Mean wind speed values are expressed in knots, not in percent.

The following four examples are provided to illustrate applications of the duration and interval tables.

Question 1: Of all the events with wind speeds (Ws) ≥ 22 knots at grid point 42 in January (table 14.10), what percentage had durations of longer than 1 day?

Answer: Consult table 14.10. The number of events (or episodes) of Ws ≥ 22 k (from TE column) is 72. The number of events of wind speeds ≥22 knots lasting more than 1 day is $2+1+2+1+1=7$. The percentage of events of wind speed ≥22 knots lasting more than 1 days is then $7+72\times100=9.7$ percent.

Question 2: What percentage of the time during January at Atlantic grid point No. 42 can waves greater than or equal to 9 ft be expected to persist longer than 24 hours?

Answer: This problem involves computations using hindcasts from the monthly duration table (table 14.14) rather than episodes from the duration table since we are answering a question regarding the percentage of time. The solution can be found by computing the joint percentage as follows: percent of waves ≥9 ft times percent of ≥9-ft waves that persist longer than 24 hours. Note that the percent of ≥9-ft waves that lasted <24 hours plus the percent of ≥9-ft waves that lasted ≥24 hours is 100 percent so we can compute whichever is easier and subtract from 100 percent if necessary. Percentages are used because of the difference between T and T^* caused by missing data.

Step 1, Compute the percent of ≥9-ft waves that lasted >24 hours. In this example it will be easier to find the percent for ≤24 hours then subtract from 100 percent to obtain the percent we require. This requires the calculation of the total number of hindcasts meeting this criterion.

This procedure is as follows:

Duration	Hindcasts Per Event		Frequency (From Table)		Hindcasts ≥9 ft Lasting ≤24 hours
6 hours	1	×	8	=	8
12 hours	2	×	10	=	20
18 hours	3	×	5	=	15
24 hours	4	×	3	=	12
			TOTAL:		55

Thus, the percent of ≥9-ft waves that lasted ≤24 hours is (55+146)×100 = 37.7 percent. The percent of ≥9-ft waves lasting >24 hours is 100 percent – 37.7 percent = 62.3 percent.

Step 2. The percent of waves ≥9 ft is (T^*/TH)×100 or (146÷2.439)×100 = 6 percent.

Step 3. The answer is 62.3 percent ×6 percent = 3.7 percent.

Question 3: Suppose a certain operation to be conducted in February near grid point No. 42 requires that the significant wave height must remain less than 9 ft for at least 24 hours. What is the climatological probability that the operation can be conducted successfully?

Answer: This problem involves the use of the wave height interval tables, since we want intervals between wave height ≥9 ft. The number of intervals between events of waves ≥9 ft is 74 (from

the TI column of the interval table (table 14.16)). The number of intervals between events (episodes) of wave height ≥9 ft lasting 24 hours or less is 5 + 6 + 1 + 1 = 13. The percentage of intervals between waves ≥9 ft lasting 24 hours or less is thus (13÷74) ×100 = 17.6 percent. In other words, 17.6 percent of all the episodes with waves <9 ft persisted 24 hours or less, and the percentage of <9-ft wave episodes lasting longer than 24 hours is 100 percent –17.6 percent = 82.4 percent. Thus, the climatological probability that the operation can successfully be conducted is 82.4 percent.

Question 4: What percentage of the time can significant wave heights less than 9 ft be expected to persist longer than 2 days in February at Atlantic grid point No. 42?

Answer: This problem requires the use of hindcast frequencies from the interval table (table 14.16) for February. We proceed following the steps outlined in Question 2.

Step 1. Compute the percent of <9-ft waves that lasted >2 days. This requires estimation of the total number of hindcasts meeting this criterion. Estimation is necessary because beyond 1 day, the 0.25 day resolution of the hindcasts is lost in the summary process, so we must approximate the average number of hindcasts per interval. Since the 1 to 2 day interval includes episodes consisting of 1.25, 1.5, 1.75, and 2 days (that is 5, 6, 7, and 8 hindcasts), the average hindcasts per interval is 6.5. In this example it will be easier and more accurate to find the percent for ≤2 days then subtract from 100 to obtain the percent we require. The procedure is as follows:

Interval	Hindcasts Per Interval		Frequency (From Table)		Hindcasts ≥9 ft Lasting ≤2 Days
0.25 day	1	×	5	=	5
0.50 day	2	×	6	=	12
0.75 day	3	×	1	=	3
1 day	4	×	1	=	4
1–2 days	6.5	×	5	=	32.5
			TOTAL:		56.5

Thus, the percent of <9-ft waves that lasted <2 days is (56.5÷2,565) ×100 = 2.2 percent. The percent of <9-ft waves that lasted >2 days is 100 percent –2.2 percent = 97.8 percent.

Step 2. The percent of waves <9 ft is (T^*/TH) ×100 or (2,618÷2,862) ×100 = 91.5 percent.

Step 3. The answer is 97.8 percent ×91.5 percent = 89.5 percent.

Table 14.9. Legends for duration and interval tables.

WIND SPEED DURATIONS – MONTHLY SEASONAL

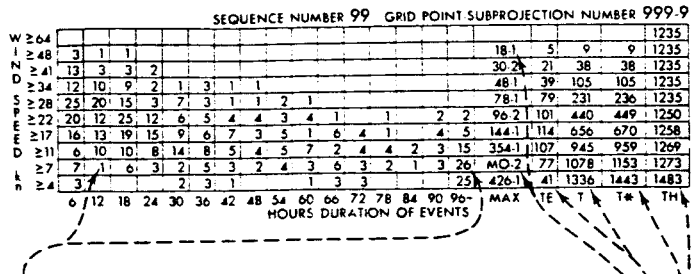

1 Event with wind speeds ≥7 kn. persisted 12 hours; 26 events persisted ≥96 hours.

The longest event with wind speeds ≥7 kn. persisted for 1 month or more and it occurred 2 times.
The longest event with wind speeds ≥48 kn. persisted 18 hours and it occurred 1 time.

41 Events had wind speeds ≥4 kn. which comprised a total of 1,336 hindcasts.

1,483 Hindcasts were examined, and 1,443 had wind speeds ≥4 kn.

Durations for a particular month extend from the time the event begins (or the first of the month if already in progress), and terminate when the event ends. Events become undefined if missing data is encountered. Durations lasting a month or more are categorized together. Durations may persist into the next month(s).

WIND SPEED INTERVALS – MONTHLY/SEASONAL

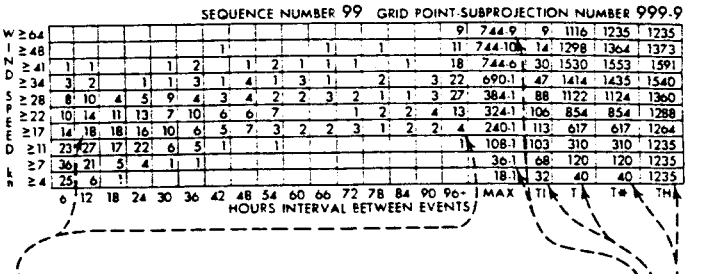

There were 18 12-hour intervals between events of wind speeds ≥17 kn.; 4 intervals persisted 96 hours or more.

The longest interval between events of wind speeds ≥7 kn. was 36 hours and it occurred 1 time.
The longest interval between events of wind speeds ≥64 kn. was 1 month or more and it occurred 9 times.

There were 32 intervals between events of wind speeds ≥4 kn. which comprised a total of 40 hindcasts.

1,235 Hindcasts were examined, and 40 had wind speeds <4 kn.

Intervals for a particular month extend from the time the event ends (or the first of the month if the event is not in progress), and terminate when the event begins. Intervals become undefined if missing data is encountered. Intervals lasting a month or more are categorized together. Intervals may persist into the next month(s).

WAVE HEIGHT DURATIONS – MONTHLY/SEASONAL

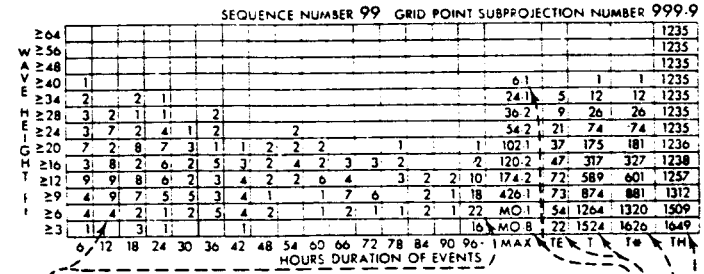

4 Events with wave heights ≥6 ft. (1.8m) persisted 12 hours; 22 events persisted ≥96 hours.

The longest event with wave heights ≥3 ft. (0.9m) persisted 1 month or more and it occurred 8 times.
The longest event with wave heights ≥40 ft. (12.2m) persisted for 6 hours and it occurred 1 time.

22 Events had wave heights ≥3 ft. (0.9m) which comprised a total of 1,524 hindcasts.

1,649 Hindcasts were examined, and 1,626 had wave heights ≥3 ft. (0.9m).

Durations for a particular month extend from the time the event begins (or the first of the month if already in progress), and terminate when the event ends. Events become undefined if missing data is encountered. Durations lasting a month or more are categorized together. Durations may persist into the next month(s).

WAVE HEIGHT INTERVALS – MONTHLY/SEASONAL

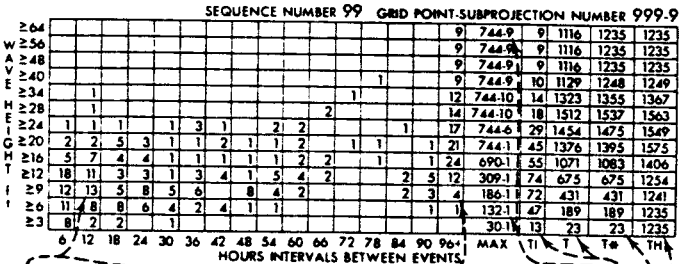

There were 13 12-hour intervals between events of wave heights ≥9 ft. (2.7m); 4 intervals persisted 96 hours or more.

The longest interval between events of wave heights ≥6 ft. (1.8m) was 132 hours and it occurred 1 time.
The longest interval between events of wave heights ≥64 ft. (19.5m) was 1 month or more and it occurred 9 times.

There were 13 intervals between events of wave heights ≥3 ft. (0.9m) which comprised a total of 23 hindcasts.

1,235 Hindcasts were examined, and 23 had wave heights <3 ft. (0.9m).

Intervals for a particular month extend from the time the event ends (or the first of the month if the event is not in progress), and terminate when the event begins. Intervals become undefined if missing data is encountered. Intervals lasting a month or more are categorized together Intervals may persist into the next month(s).

ABBREVIATIONS

MAX: Maximum duration or interval, followed by the number of occurrences.
TE or TI: Total number of events or intervals.
T: Total number of hindcasts included in TE or TI.
T*: Total number of hindcasts that met the stated criteria.
TH: Total number of hindcasts examined.

MO: Month
SEA: Season

Table 14.10 Wind speed durations, Atlantic grid point 42, location 30.4 N. latitude, 77.9 W. longitude.

January

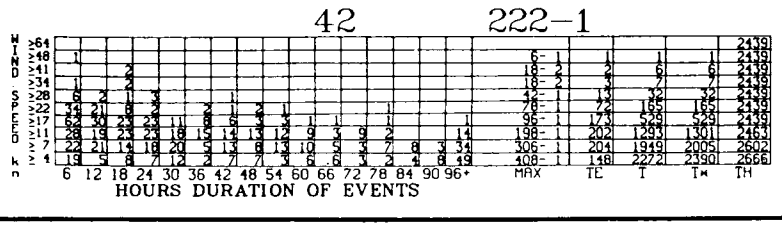

February

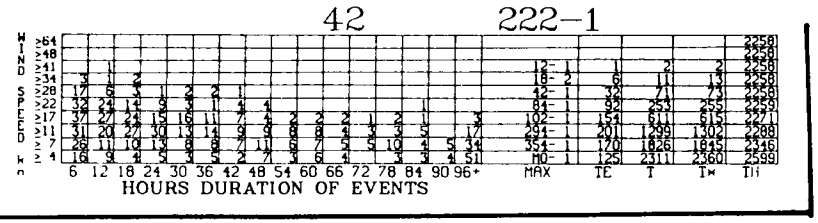

April

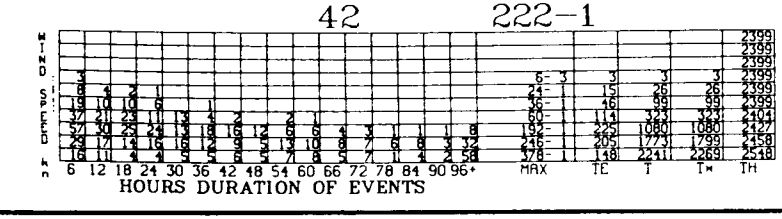

July

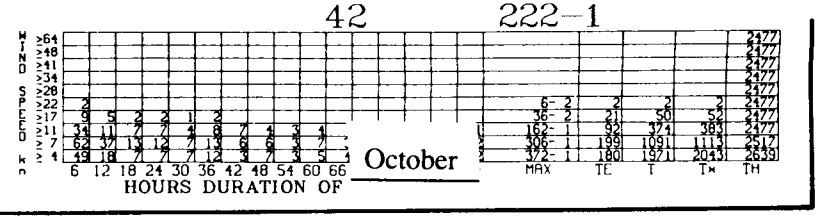

August

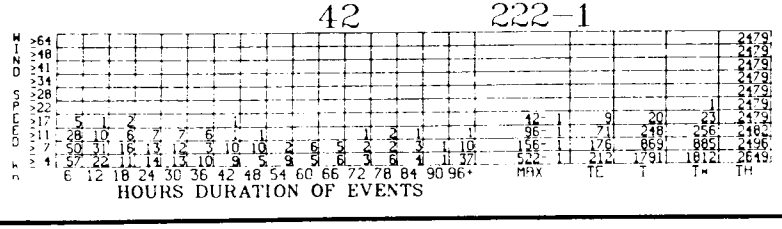

October

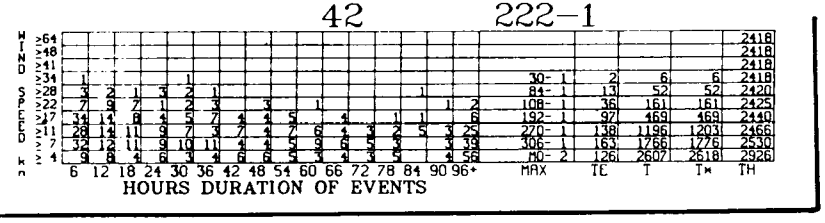

Table 14.11 Wind speed durations, Atlantic grid point 49, location 24.2 N. latitude, 72.9 W. longitude.

January

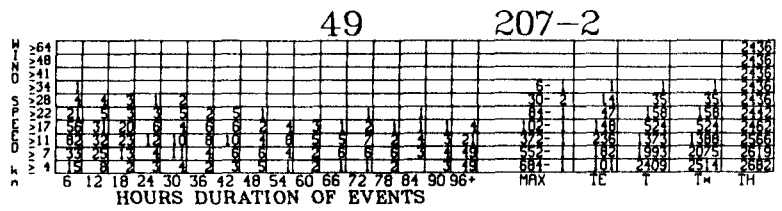

February

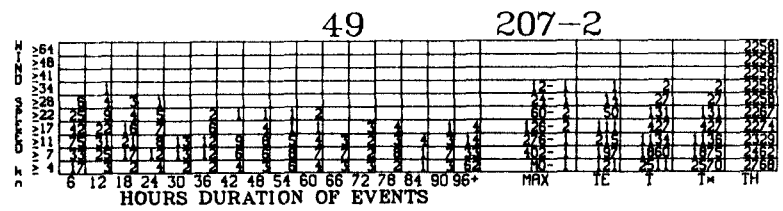

April

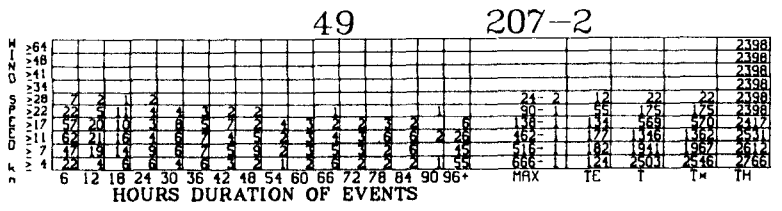

July

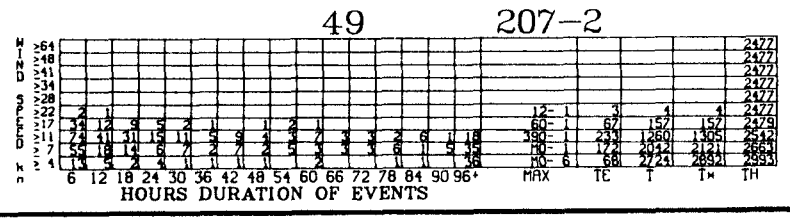

August

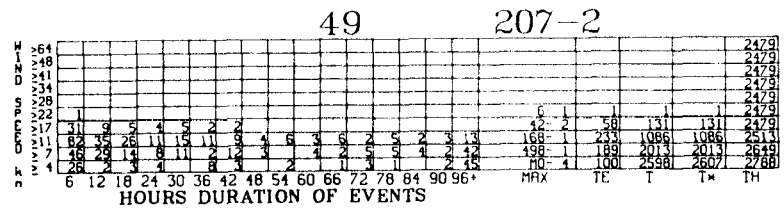

October

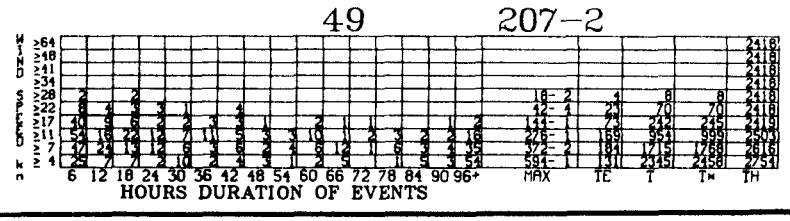

Table 14.12 Wind speed intervals, Atlantic grid point 42, location 30.4 N. latitude, 77.9 W. longitude.

January

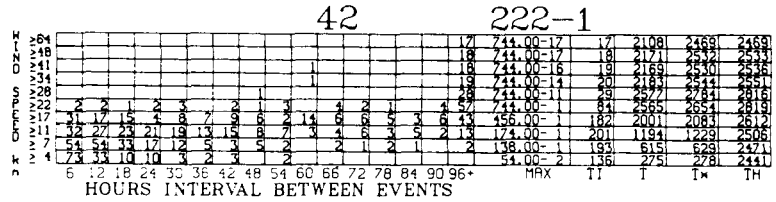

February

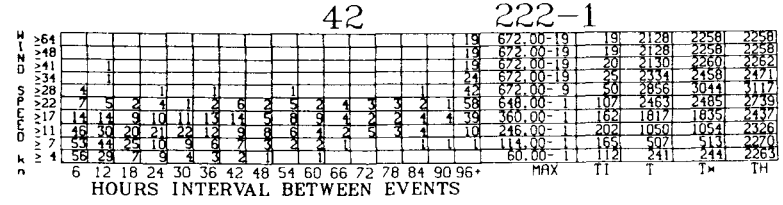

April

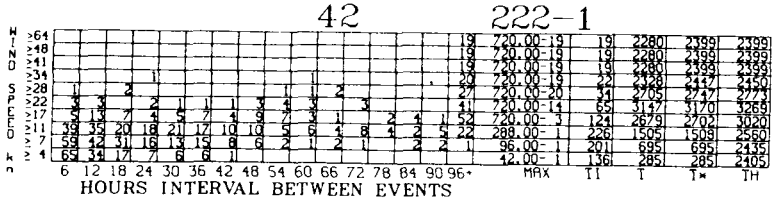

July

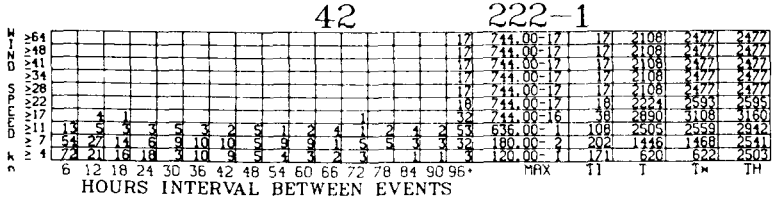

August

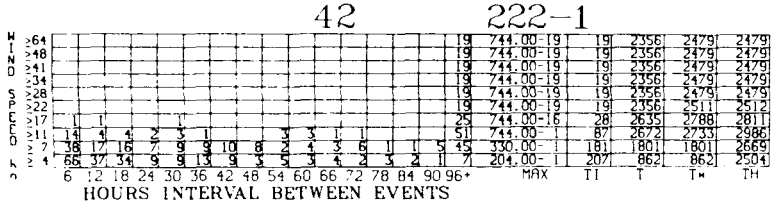

October

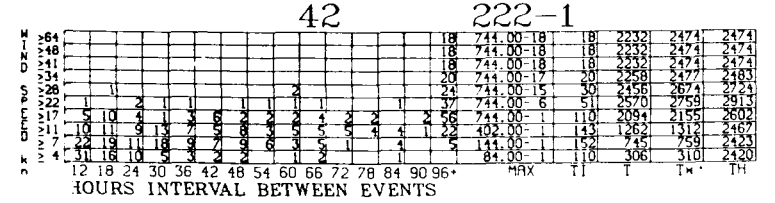

Table 14.13 Wind speed intervals, Atlantic grid point 49, location 24.2 N. latitude, 72.8 W. longitude.

January

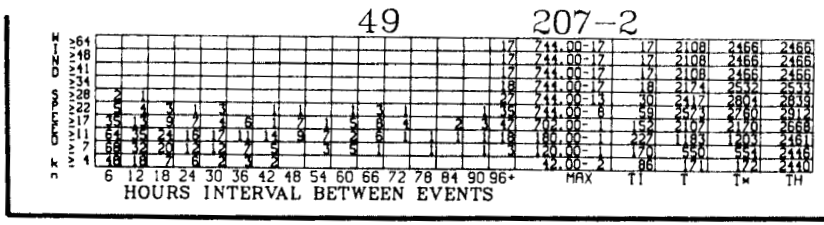

February

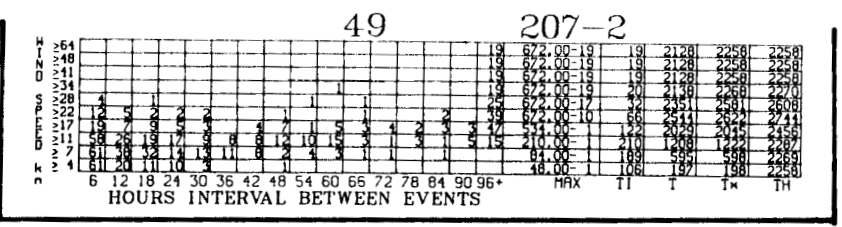

April

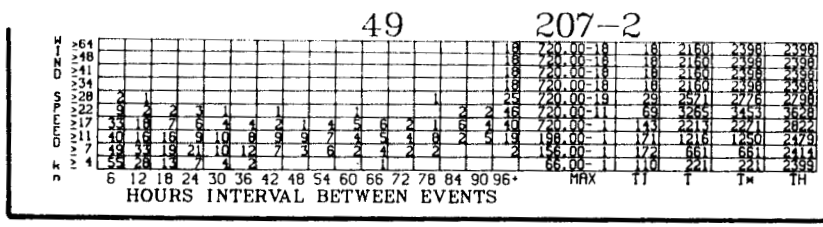

July

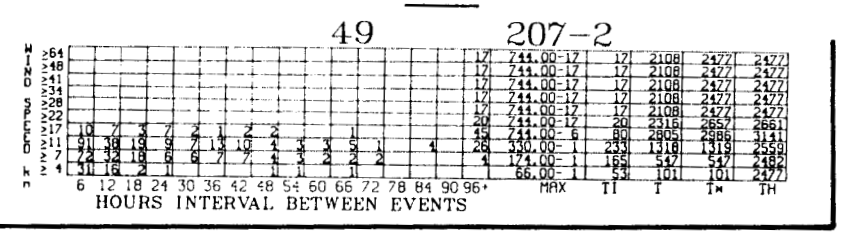

August

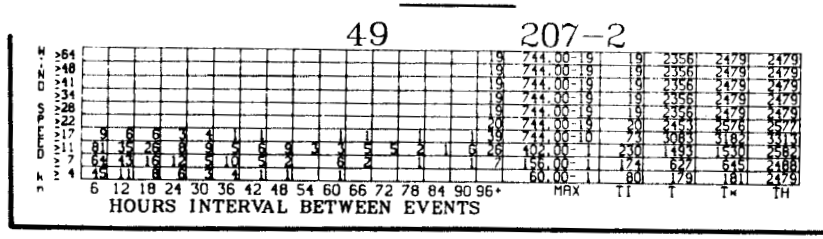

October

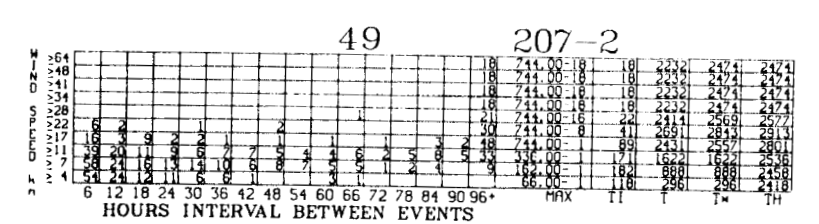

Table 14.14 Wave height duration, Atlantic grid point 42, location 30.4 N. latitude, 77.9 W. longitude.

January

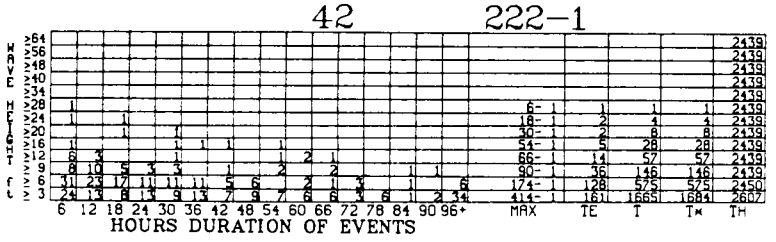

February

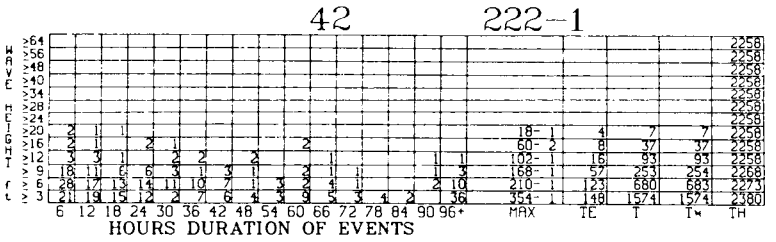

April

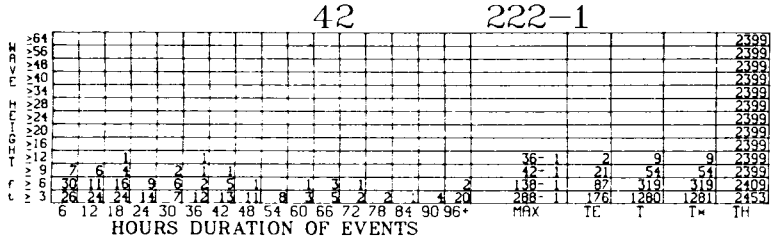

July

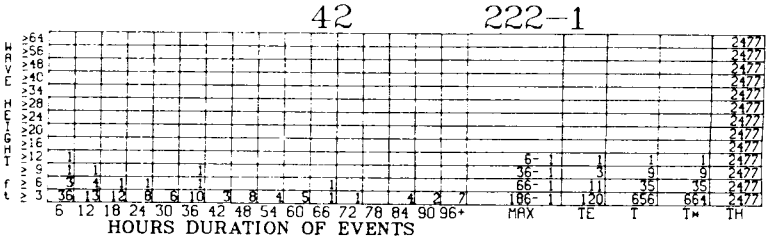

August

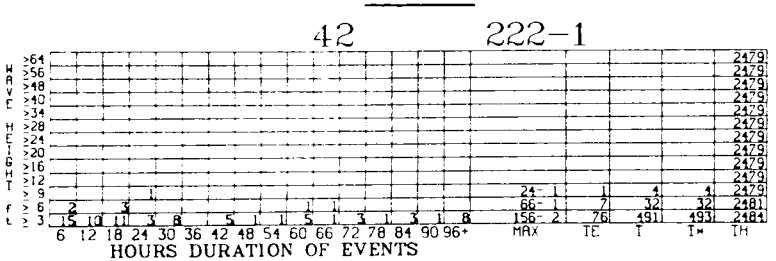

October

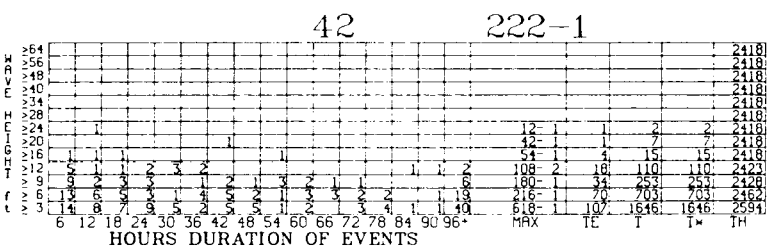

Table 14.15 Wave height duration, Atlantic grid point 49, location 24.2 N. latitude, 72.8 W. longitude.

January

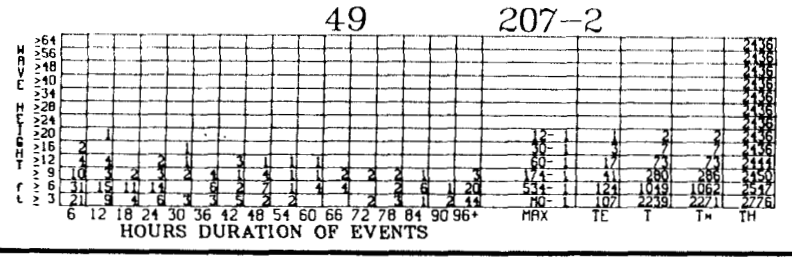

February

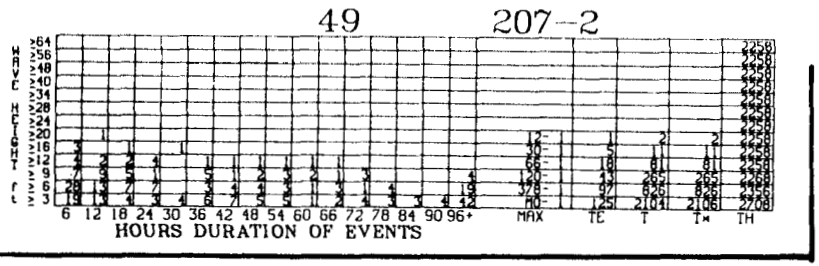

April

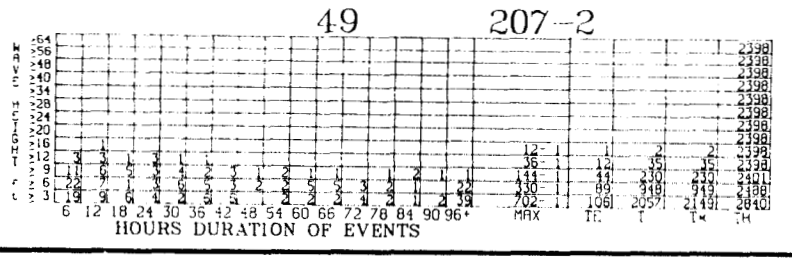

July

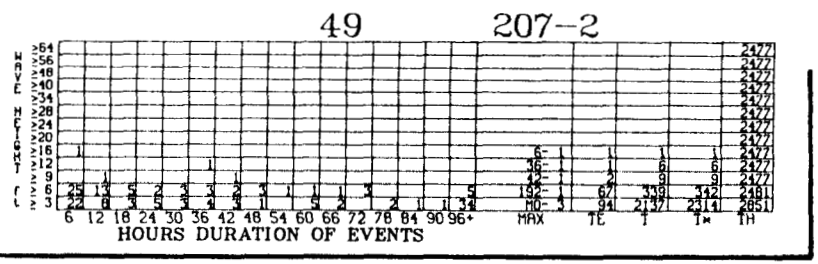

August

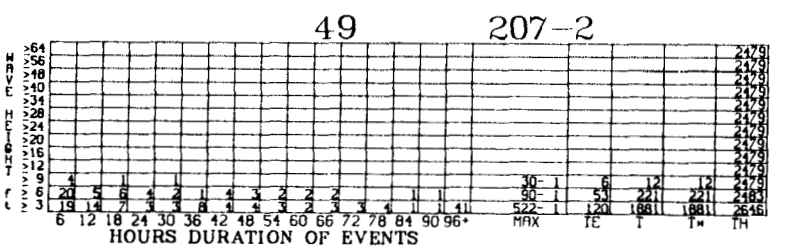

October

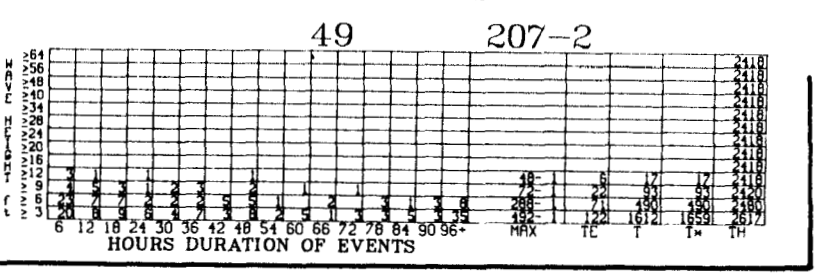

Table 14.16 Wave height intervals, Atlantic grid point 42, location 30.4 N. latitude, 77.9 W. longitude.

January

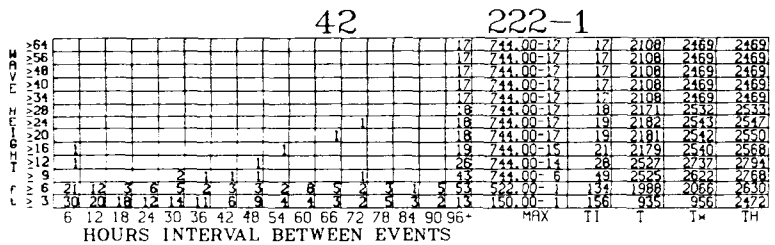

February

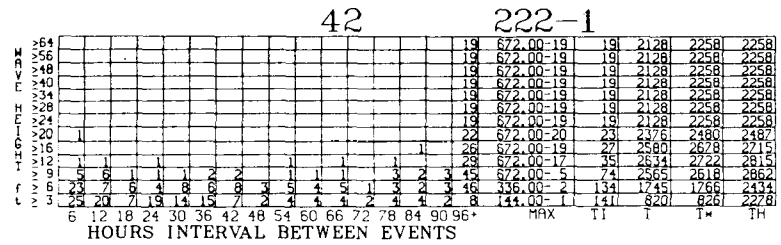

April

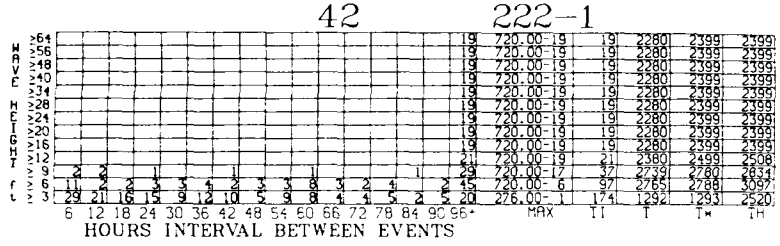

July

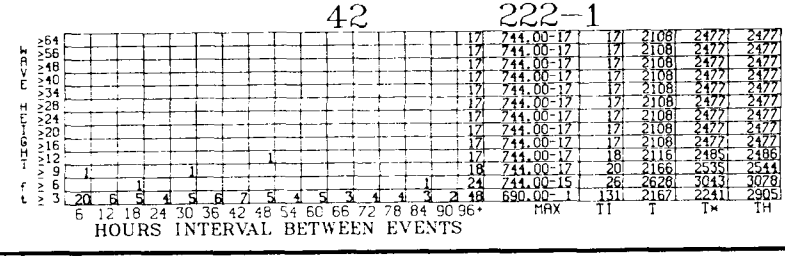

August

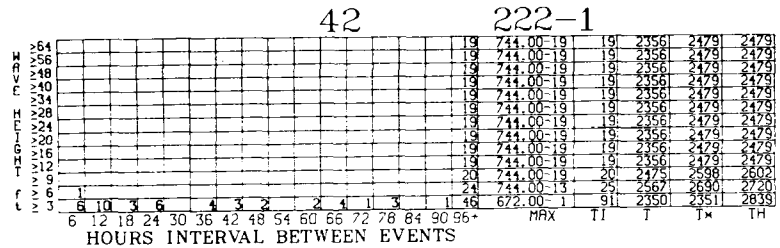

October

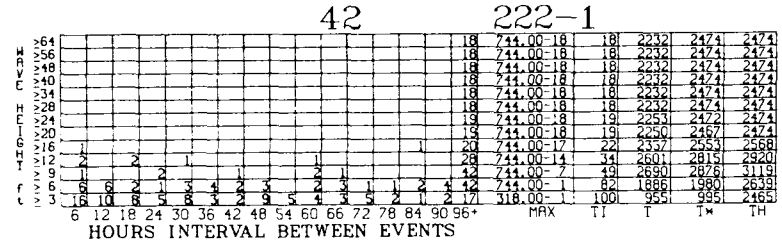

Table 14.17 Wave height intervals, Atlantic grid point 49, location 24.1 N. latitude, 72.8 W. longitude.

January

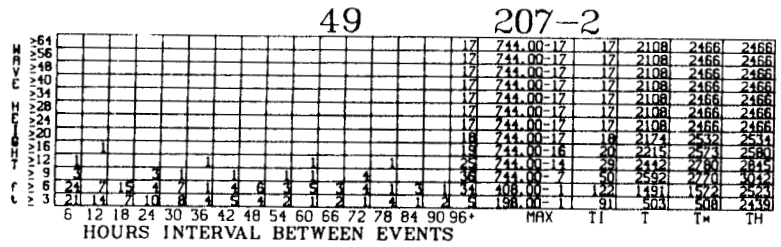

February

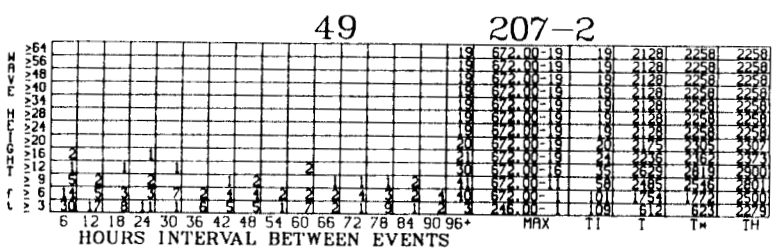

April

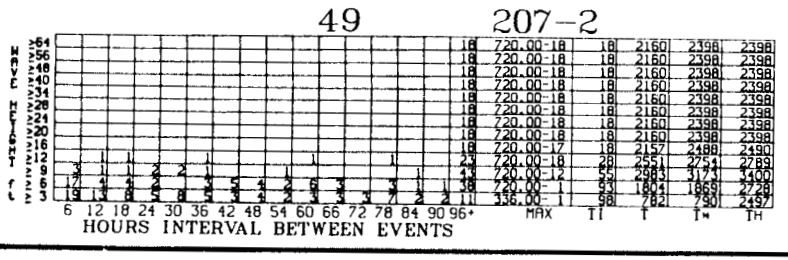

July

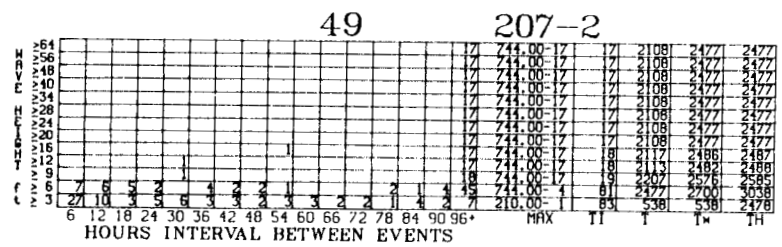

August

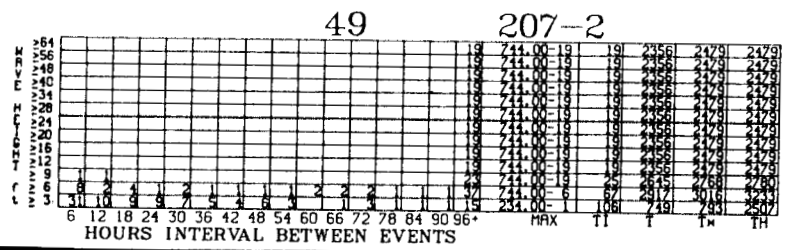

October

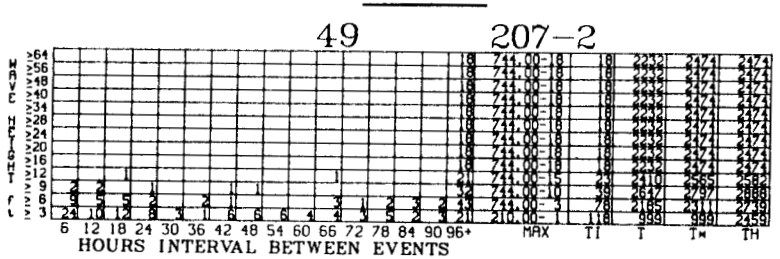

Table 14.18 Wind speed durations, Pacific grid point 37.

Winter

37 — 32.9 N. Latitude, 119.4 W. Longitude

WIND SPEED kn	6	12	18	24	30	36	42	48	54	60	66	72	78	84	90	96+	MAX	TE	T	T*	TH
≥64																					4333
≥48																					4333
≥41																					4333
≥34	2																6–2	2	2	2	4333
≥28	19	9	2	3													24–3	33	55	56	4333
≥22	48	16	11	11	7	1	2	2		2							60–2	100	248	248	4335
≥17	88	43	30	22	11	13	8	4	2	6	1		1	4		2	114–1	235	768	768	4355
≥11	92	51	45	23	27	32	21	9	14	14	12	4	3	7	6	22	306–1	382	2154	2158	4391
≥ 7	90	32	31	12	16	11	13	9	11	12	4	7	6	9	5	74	582–1	342	3350	3395	4458
≥ 4	55	24	16	5	6	8	12	4	9	5	5	5	7		3	76	1218–1	241	3968	4192	4700

HOURS DURATION OF EVENTS

Spring

37 — 32.9 N. Latitude, 119.4 W. Longitude

WIND SPEED kn	6	12	18	24	30	36	42	48	54	60	66	72	78	84	90	96+	MAX	TE	T	T*	TH
≥64																					4241
≥48																					4241
≥41																					4241
≥34			1														18–1	1	3	3	4241
≥28	32	17	3		1												30–1	53	80	80	4241
≥22	103	59	24	5	4	13	10		3	2	2						66–2	225	550	552	4243
≥17	121	70	32	9	19	22	12	5	6	3	9	4	3	7	3	14	228–1	339	1504	1548	4272
≥11	114	44	23	8	10	13	9	5	1	9	12	4	1	8	7	65	552–1	333	3126	3349	4418
≥ 7	27	14	10		2	3	6	1	5	3	3	1	1	2	4	57	1668–1	139	3794	4374	4693
≥ 4	19	4	4		1	2		1	4	1	3				1	42	SEA–1	82	3957	5035	5185

HOURS DURATION OF EVENTS

Summer

37 — 32.9 N. Latitude, 119.4 W. Longitude

WIND SPEED kn	6	12	18	24	30	36	42	48	54	60	66	72	78	84	90	96+	MAX	TE	T	T*	TH
≥64																					4100
≥48																					4100
≥41																					4100
≥34																					4100
≥28	10																6–10	10	10	10	4100
≥22	48	19	1	1			2	1			1						66–1	73	126	126	4100
≥17	144	73	26	5		1	6	1	1	7	4	1		1		2	114–2	272	631	631	4100
≥11	150	100	71	7	10	8	19	5	5	15	8	2	6	3	7	41	324–2	457	2479	2555	4124
≥ 7	40	24	15	4	3	8	5	4	2	2	4		1	3	4	69	1002–1	188	3526	3797	4209
≥ 4	20	11	4	3	2	2	2	2	1	1	2				4	52	1620–1	106	3389	4043	4246

HOURS DURATION OF EVENTS

Fall

37 — 32.9 N. Latitude, 119.4 W. Longitude

WIND SPEED kn	6	12	18	24	30	36	42	48	54	60	66	72	78	84	90	96+	MAX	TE	T	T*	TH
≥64																					4543
≥48																					4543
≥41																					4543
≥34																					4543
≥28	6	2	2														18–2	10	16	16	4543
≥22	30	20	9	4	4	2	2										42–2	71	159	159	4543
≥17	61	37	22	18	10	8	9	3	3	1		1					72–1	173	507	507	4548
≥11	124	58	39	16	19	22	14	10	12	7	8	12	8	5	7	14	180–1	375	1798	1804	4582
≥ 7	117	44	47	12	20	14	23	9	12	8	12	5	8	7	9	68	378–1	415	3344	3422	4742
≥ 4	61	37	27	15	10	8	8	5	10	3	6	6	2	3	4	84	600–1	289	3839	4139	4815

HOURS DURATION OF EVENTS

Table 14.19 Wind speed durations, Pacific grid point 47.

Winter

47 — 25.0 N. Latitude, 119.4 W. Longitude

WIND SPEED (kn)	6	12	18	24	30	36	42	48	54	60	66	72	78	84	90	96+	MAX	TE	T	T*	TH
≥64																					4333
≥48																					4333
≥41																					4333
≥34	1																6–1	1	1	1	4333
≥28	4																6-4	4	4	4	4333
≥22	13	5	3	1		1	1										42–1	24	49	49	4333
≥17	75	24	23	13	4	6	3	2	1				1			1	126–1	153	380	388	4335
≥11	143	47	38	17	20	12	10	15	13	11	8	7	6	2	4	22	312–1	375	1894	1927	4378
≥ 7	86	36	29	19	13	12	8	7	10	8	9	4	4	2	5	74	558–1	326	3197	3288	4478
≥ 4	42	14	20	9	9	3	10	4	7	2	3	4	4	2	3	79	1608–1	215	4396	4575	5036

HOURS DURATION OF EVENTS

Spring

47 — 25.0 N. Latitude, 119.4 W. Longitude

WIND SPEED (kn)	6	12	18	24	30	36	42	48	54	60	66	72	78	84	90	96+	MAX	TE	T	T*	TH
≥64																					4241
≥48																					4241
≥41																					4241
≥34																					4241
≥28				1													24–1	1	4	4	4243
≥22	15	1	2		1												30–1	19	28	29	4244
≥17	72	26	18	6	8	4	3	2	3		1						66–1	143	341	345	4248
≥11	160	60	35	21	17	9	15	7	6	13	9	6	3	5	5	23	336–1	394	1841	1909	4258
≥ 7	68	36	16	9	10	11	12	12	8	9	6	4	6	8	4	74	642–1	293	3250	3446	4336
≥ 4	21	8	10	2	2	2	4	3	2	1	3	3	1	1	1	61	1350–1	125	3832	4492	4744

HOURS DURATION OF EVENTS

Summer

47 — 25.0 N. Latitude, 119.4 W. Longitude

WIND SPEED (kn)	6	12	18	24	30	36	42	48	54	60	66	72	78	84	90	96+	MAX	TE	T	T*	TH
≥64																					4100
≥48																					4100
≥41																					4100
≥34																					4100
≥28	1	2															12–2	3	5	5	4100
≥22	9	2	3		1	1	1										42–1	17	40	41	4100
≥17	29	15	3	6	3	2	3	1			1						66–1	63	159	161	4100
≥11	155	62	31	22	17	17	13	11	5	9	4	2	3	1	3	9	126–2	>54	1286	1314	4124
≥ 7	117	42	32	14	16	7	13	13	4	11	9	8	6	4	4	59	450–1	359	2875	2990	4203
≥ 4	40	9	16	4	6	5	9	1	3	2	2	2	2	4	3	69	1296–1	177	3870	4163	4476

HOURS DURATION OF EVENTS

Fall

47 — 25.0 N. Latitude, 119.4 W. Longitude

WIND SPEED (kn)	6	12	18	24	30	36	42	48	54	60	66	72	78	84	90	96+	MAX	TE	T	T*	TH
≥64																					4545
≥48																					4545
≥41																					4545
≥34	1																6–1	1	1	1	4545
≥28	1																6-1	1	1	1	4545
≥22	7	2	1		2												30–2	12	24	24	4548
≥17	77	26	12	7	8	3	2	1					1				78–1	137	286	293	4552
≥11	172	51	32	29	28	18	13	20	14	10	13	2	6	3	4	19	216–1	434	1941	1993	4599
≥ 7	72	34	20	13	8	7	11	13	6	13	6	1	8	4	9	72	582–1	297	3395	3661	4746
≥ 4	22	11	10	9	7	1	3	6	4	3	6	4	5	2	5	68	1074–1	166	3812	4492	4890

HOURS DURATION OF EVENTS

Table 14.20 Wind speed intervals, Pacific grid point 37.

Winter 37 32.9 N. Latitude, 119.4 W. Longitude

WIND SPEED		6	12	18	24	30	36	42	48	54	60	66	72	78	84	90	96+	MAX	TE	T	T*	TH
W	≥64																8	SEA–8	8	2944	4389	4389
I	≥48																8	SEA–8	8	2944	4389	4389
N	≥41																8	SEA–8	8	2944	4389	4389
D	≥34		1														8	SEA–7	9	2676	4451	4453
	≥28	2	1	3	2	1			2					1	1	2	25	SEA–3	40	3867	4944	4999
S	≥22	13	6	3	2	3	1	3	2	2	1	4	2	2	2	2	57	1296–1	105	3827	4361	4607
P	≥17	41	17	16	11	11	9	7	8	8	9	15	4	2	4	4	70	672–1	236	3325	3679	4425
E	≥11	120	52	33	19	16	21	20	16	14	9	7	7	8	3	4	28	228–1	377	2126	2237	4337
E	≥ 7	131	67	38	21	26	18	6	7	6	2	1	4	2	2		3	102–2	334	1036	1063	4333
D	≥ 4	116	58	22	12	14	4	4	1	1	1							60–1	233	495	508	4333
k		6	12	18	24	30	36	42	48	54	60	66	72	78	84	90	96+	MAX	TE	T	T*	TH
n		HOURS INTERVAL BETWEEN EVENTS																				

Spring 37 32.9 N. Latitude, 119.4 W. Longitude

WIND SPEED		6	12	18	24	30	36	42	48	54	60	66	72	78	84	90	96+	MAX	TE	T	T*	TH
W	≥64																6	SEA–6	6	2208	4265	4265
I	≥48																6	SEA–6	6	2208	4265	4265
N	≥41																6	SEA–6	6	2208	4265	4265
D	≥34																7	SEA–7	7	2576	4330	4333
	≥28	3	3	6		1	4	1			1					2	37	SEA–5	58	4194	5290	5370
S	≥22	48	40	22	1	2	4	7		2	7	9	2	3	1	9	67	SEA–1	224	3882	4689	5239
P	≥17	70	67	44	3	5	11	28	8	5	13	12	6	5	13	6	48	462–1	344	2775	2800	4317
E	≥11	144	54	58	7	11	14	10	5	6	5	5	1	4	1	2	6	132–1	333	1083	1087	4259
E	≥ 7	71	20	21	1	9	8	2	1			1			1			84–1	135	318	319	4241
D	≥ 4	45	11	10	3	4	1	2										42–2	76	149	150	4241
k		6	12	18	24	30	36	42	48	54	60	66	72	78	84	90	96+	MAX	TE	T	T*	TH
n		HOURS INTERVAL BETWEEN EVENTS																				

Summer 37 32.9 N. Latitude, 119.4 W. Longitude

WIND SPEED		6	12	18	24	30	36	42	48	54	60	66	72	78	84	90	96+	MAX	TE	T	T*	TH
W	≥64																6	SEA–6	6	2208	4224	4224
I	≥48																6	SEA–6	6	2208	4224	4224
N	≥41																6	SEA–6	6	2208	4224	4224
D	≥34																6	SEA–6	6	2208	4224	4224
	≥28	2		2													11	SEA–7	15	2811	4657	4667
S	≥22	8	7	15	1	1	3	2		1	2	1	2	1		1	30	SEA–1	75	2635	4111	4237
P	≥17	47	53	46	3	2	11	17	2	2	6	13		4	5	2	54	1602–1	267	3142	3844	4475
E	≥11	166	112	91	3	7	8	23	4	6	4	15	1	2	3	4	11	144–1	460	1566	1609	4140
E	≥ 7	98	51	16	2	5	4	4		1	1	2	1		1		1	114–1	187	419	424	4112
D	≥ 4	54	29	10	2	1	1	2	1	1							1	108–1	102	210	211	4108
k		6	12	18	24	30	36	42	48	54	60	66	72	78	84	90	96+	MAX	TE	T	T*	TH
n		HOURS INTERVAL BETWEEN EVENTS																				

Fall 37 32.9 N. Latitude, 119.4 W. Longitude

WIND SPEED		6	12	18	24	30	36	42	48	54	60	66	72	78	84	90	96+	MAX	TE	T	T*	TH
W	≥64																5	SEA–5	5	1840	4564	4564
I	≥48																5	SEA–5	5	1840	4564	4564
N	≥41																5	SEA–5	5	1840	4564	4564
D	≥34																5	SEA–5	5	1840	4564	4564
	≥28	1															14	SEA–2	15	2840	5230	5246
S	≥22	7	4	3	2		1	1	3		1	3		1	1	2	43	1650–1	72	3058	4714	4873
P	≥17	24	19	11	5	6	5	6	5	7	4	2	3	2	5	3	61	1134–1	168	3279	4251	4753
E	≥11	86	54	31	21	16	15	21	20	10	18	9	4	4	3	7	44	300–1	363	2604	2808	4573
E	≥ 7	175	77	54	23	24	10	12	12	2	7	3	2	3		1	7	120–1	412	1267	1325	4548
D	≥ 4	143	61	35	18	10	8	3	5	3	1	1					1	102–1	289	666	680	4547
k		6	12	18	24	30	36	42	48	54	60	66	72	78	84	90	96+	MAX	TE	T	T*	TH
n		HOURS INTERVAL BETWEEN EVENTS																				

Table 14.21 Wind speed intervals, Pacific grid point 47.

Winter

47 — 25.0 N. Latitude, 119.4 W. Longitude

WIND kn	6	12	18	24	30	36	42	48	54	60	66	72	78	84	90	96+	MAX	TE	T	T*	TH
≥64																8	SEA–8	8	2944	4389	4389
≥48																8	SEA–8	8	2944	4389	4389
≥41																8	SEA–8	8	2944	4389	4389
≥34																8	SEA–8	8	2944	4389	4390
≥28	1															10	SEA–8	11	3189	4634	4638
≥22					1											28	SEA–3	29	3868	5280	5329
≥17	36	7	6	4	7	4	8	3	3	5	3			3	2	65	2034–1	156	4039	4550	4936
≥11	117	47	39	18	19	17	10	7	15	7	11	7	6	6	3	44	390–1	373	2419	2471	4353
≥ 7	121	41	46	27	13	16	16	12	7	6	3		1	1	2	8	156–1	320	1181	1199	4342
≥ 4	110	47	22	8	5	5	2	2	2	2	2	1					72–1	208	459	463	4335

HOURS INTERVAL BETWEEN EVENTS

Spring

47 — 25.0 N. Latitude, 119.4 W. Longitude

WIND kn	6	12	18	24	30	36	42	48	54	60	66	72	78	84	90	96+	MAX	TE	T	T*	TH
≥64																6	SEA–6	6	2208	4265	4265
≥48																6	SEA–6	6	2208	4265	4265
≥41																6	SEA–6	6	2208	4265	4265
≥34																6	SEA–6	6	2208	4265	4265
≥28																6	SEA–6	6	2208	4263	4265
≥22																23	SEA–4	23	3526	5042	5068
≥17	29	15	9	8	2	1	2	2	1	3	5	1	2		1	68	2052–1	149	4348	4575	4913
≥11	132	58	35	20	21	16	15	8	10	7	11	4	10	2	7	40	354–1	396	2447	2463	4355
≥ 7	135	58	35	9	15	6	11	2	6	1	4	2	2	2	2	4	150–1	294	898	901	4252
≥ 4	67	25	15	4	4	3	2		1			1					72–1	122	251	252	4241

HOURS INTERVAL BETWEEN EVENTS

Summer

47 — 25.0 N. Latitude, 119.4 W. Longitude

WIND kn	6	12	18	24	30	36	42	48	54	60	66	72	78	84	90	96+	MAX	TE	T	T*	TH
≥64																6	SEA–6	6	2208	4224	4224
≥48																6	SEA–6	6	2208	4224	4224
≥41																6	SEA–6	6	2208	4224	4224
≥34																6	SEA–6	6	2208	4224	4224
≥28																8	SEA–6	8	2610	4483	4488
≥22	3		1					1								15	SEA–3	20	2634	4349	4390
≥17	7	1	2	2		2	2	2	1		2	2				44	1266–1	67	3161	4291	4452
≥11	118	50	39	12	9	10	11	6	4	9	9	10	8	4	13	53	366–1	365	2742	2859	4149
≥ 7	151	62	39	15	24	11	11	4	12	9	3	4	4	1	1	4	156–1	355	1198	1227	4114
≥ 4	106	35	14	9	6	3	1										42–1	174	309	313	4100

HOURS INTERVAL BETWEEN EVENTS

Fall

47 — 25.0 N. Latitude, 119.4 W. Longitude

WIND kn	6	12	18	24	30	36	42	48	54	60	66	72	78	84	90	96+	MAX	TE	T	T*	TH
≥64																5	SEA–5	5	1840	4566	4566
≥48																5	SEA–5	5	1840	4566	4566
≥41																5	SEA–5	5	1840	4566	4566
≥34	1															5	SEA–5	6	1841	4565	4566
≥28	1															5	SEA–5	6	1841	4565	4566
≥22	1															13	SEA–3	14	2655	5133	5154
≥17	25	9	3	7	4	1	3	2	1	1	4	2	4	1	1	69	972–1	137	3035	4436	4722
≥11	157	36	49	25	24	15	17	12	7	11	9	5	6	4	9	42	318–1	428	2496	2617	4556
≥ 7	125	51	23	18	21	12	9	7	5	5	2	4	1	6		7	126–2	296	1062	1085	4545
≥ 4	85	27	24	7	3	5	4	3	1	2		1		1			84–1	164	392	398	4545

HOURS INTERVAL BETWEEN EVENTS

Table 14.22 Wave height durations, Pacific grid point 37.

Winter

37 — 32.9 N. Latitude, 119.4 W. Longitude

WAVE HEIGHT t	6	12	18	24	30	36	42	48	54	60	66	72	78	84	90	96+	MAX	TE	T	T*	TH	f
≥64																					4333	
≥56																					4333	
≥48																					4333	
≥40																					4333	
≥34																					4333	
≥28																					4333	
≥24																					4333	
≥20	1																6–1	1	1	1	4333	
≥16	6		1	1													24–1	8	13	13	4333	
≥12	14	4	4	4	2	3	2			1						1	108–1	35	120	120	4333	
≥ 9	34	7	9	13	6	5	3	4	1	3	2	1				2	150–1	90	354	354	4335	
≥ 6	49	23	18	7	9	12	10	8	8	8	4	2	2	7	1	11	258–1	179	1042	1045	4358	
≥ 3	55	29	19	14	18	14	16	7	9	5	8	9	4	3	8	47	460–1	265	2518	2569	4386	

HOURS DURATION OF EVENTS

Spring

37 — 32.9 N. Latitude, 119.4 W. Longitude

WAVE HEIGHT t	6	12	18	24	30	36	42	48	54	60	66	72	78	84	90	96+	MAX	TE	T	T*	TH	f
≥64																					4241	
≥56																					4241	
≥48																					4241	
≥40																					4241	
≥34																					4241	
≥28																					4241	
≥24																					4241	
≥20	1																6–1	1	1	1	4241	
≥16	2			1													24–1	3	6	6	4241	
≥12	29	6	6	1	1												30–1	43	66	68	4241	
≥ 9	75	23	15	4	15	8	6	2	2	1	1						66–1	152	402	402	4241	
≥ 6	86	52	31	12	11	12	20	2	7	5	6	5	3	6	5	13	228–1	276	1360	1413	4261	
≥ 3	56	27	23	6	4	9	8	3	2	5	5	2	5	7	6	63	1290–1	231	3127	3443	4495	

HOURS DURATION OF EVENTS

Summer

37 — 32.9 N. Latitude, 119.4 W. Longitude

WAVE HEIGHT t	6	12	18	24	30	36	42	48	54	60	66	72	78	84	90	96+	MAX	TE	T	T*	TH	f
≥64																					4100	
≥56																					4100	
≥48																					4100	
≥40																					4100	
≥34																					4100	
≥28																					4100	
≥24																					4100	
≥20																					4100	
≥16																					4100	
≥12	2	2															12–2	4	6	6	4100	
≥ 9	24	7	1	2		1		1									48–1	36	63	63	4100	
≥ 6	74	32	16	3		5	4	1	1	1	8	1		1	1	1	102–1	149	429	429	4100	
≥ 3	116	70	57	7	12	8	12	4	5	13	13	1	3	5	6	36	426–1	368	2241	2299	4124	

HOURS DURATION OF EVENTS

Fall

37 — 32.9 N. Latitude, 119.4 W. Longitude

WAVE HEIGHT t	6	12	18	24	30	36	42	48	54	60	66	72	78	84	90	96+	MAX	TE	T	T*	TH	f
≥64																					4543	
≥56																					4543	
≥48																					4543	
≥40																					4543	
≥34																					4543	
≥28																					4543	
≥24																					4543	
≥20																					4543	
≥16	1																6–1	1	1	1	4543	
≥12	4	3	3	2		1	1										42–1	14	40	40	4543	
≥ 9	25	10	12	5	3	3	2	2				1				1	138–1	64	199	199	4543	
≥ 6	41	23	16	11	14	12	12	7	2	2	3	1	1	4	1	4	174–1	154	709	709	4551	
≥ 3	52	44	23	15	11	6	17	7	10	12	4	8	4	5	8	38	342–1	264	2106	2157	4611	

HOURS DURATION OF EVENTS

Table 14.23 Wave height durations, Pacific grid point 47.

Winter 47 25.0 N. Latitude, 119.4 W. Longitude

WAVE HEIGHT	6	12	18	24	30	36	42	48	54	60	66	72	78	84	90	96+	MAX	TE	T	T*	TH
≥64																					4333
≥56																					4333
≥48																					4333
≥40																					4333
≥34																					4333
≥28																					4333
≥24																					4333
≥20																					4333
≥16		1								1							12–1	1	2	2	4333
≥12	3		2	1	3	1				1							60–1	11	44	47	4333
≥ 9	16	3	5	11	5	3	3	1	2	2			2			1	144–1	54	241	247	4340
≥ 6	32	16	9	8	11	10	4	9	4	4	7	4			5	16	240–1	139	1012	1051	4347
≥ 3	38	22	12	8	11	6	5	9	8	7	5	3	5	4	4	61	1776–1	208	3306	3386	4858

HOURS DURATION OF EVENTS

Spring 47 25.0 N. Latitude, 119.4 W. Longitude

WAVE HEIGHT	6	12	18	24	30	36	42	48	54	60	66	72	78	84	90	96+	MAX	TE	T	T*	TH
≥64																					4241
≥56																					4241
≥48																					4241
≥40																					4241
≥34																					4241
≥28																					4241
≥24																					4241
≥20																					4241
≥16			1	1													24–1	2	7	7	4244
≥12	2	2	2	1	1	1				1							60–1	10	37	37	4245
≥ 9	12	7	3	3	4	6	2	3	3	3	3	4					72–4	53	279	298	4249
≥ 6	37	11	6	12	12	5	3	10	6	9	6	5	2	5	2	39	486–1	170	1734	1861	4268
≥ 3	15	2	3	3	2	1	3		1	2	1	3		2		42	1698–1	80	2965	4391	4838

HOURS DURATION OF EVENTS

Summer 47 25.0 N. Latitude, 119.4 W. Longitude

WAVE HEIGHT	6	12	18	24	30	36	42	48	54	60	66	72	78	84	90	96+	MAX	TE	T	T*	TH
≥64																					4100
≥56																					4100
≥48																					4100
≥40																					4100
≥34																					4100
≥28																					4100
≥24																					4100
≥20	1		1														18–1	2	4	4	4100
≥16		1	1		1												30–1	3	10	10	4100
≥12	2		1	1			1	1									48–1	6	24	24	4100
≥ 9	5		2	1	1	3	1				1	1					72–1	15	68	68	4100
≥ 6	32	7	11	7	4	6	4	8	3	3	4	4	1	1	1	14	216–1	110	758	785	4105
≥ 3	27	6	5	7	3	5	3	3	4	1		3	4	2	2	52	1098–1	127	2961	7705	4225

HOURS DURATION OF EVENTS

Fall 47 25.0 N. Latitude, 119.4 W. Longitude

WAVE HEIGHT	6	12	18	24	30	36	42	48	54	60	66	72	78	84	90	96+	MAX	TE	T	T*	TH
≥64																					4545
≥56																					4545
≥48																					4545
≥40																					4545
≥34																					4545
≥28																					4545
≥24																					4545
≥20																					4545
≥16	1																6–1	1	1	1	4545
≥12	2	2	2		3		2		1								54–1	12	50	50	4548
≥ 9	8	4	2		4	1	5		1	2	3	2		1	1		90–1	34	198	198	4554
≥ 6	33	23	10	9	6	7	7	6	3	1	6	1	3	2	2	14	174–2	133	810	825	4583
≥ 3	59	20	13	14	4	8	10	10	2	10	5	2	3	3	3	64	840–1	230	2907	3103	4829

HOURS DURATION OF EVENTS

Table 14.24 Wave height intervals, Pacific grid point 37.

Winter — 37 — 32.9 N. Latitude, 119.4 W. Longitude

		6	12	18	24	30	36	42	48	54	60	66	72	78	84	90	96+	MAX	TE	T	T*	TH
W	≥64																8	SEA–8	8	2944	4389	4389
A	≥56																8	SEA–8	8	2944	4389	4389
V	≥48																8	SEA–8	8	2944	4389	4389
E	≥40																8	SEA–8	8	2944	4389	4389
	≥34																8	SEA–8	8	2944	4389	4389
H	≥28																8	SEA–8	8	2944	4389	4389
E	≥24																8	SEA–8	8	2944	4389	4389
I	≥20																9	SEA–8	9	3152	4366	4369
G	≥16	1	1												1		12	SEA–7	15	3424	4066	4879
H	≥12	1	2	3					2		1					3	29	SEA–3	41	3562	4718	4838
T	≥ 9	13	4	1		3	2	3	6	1	2	2	1	3	2	2	51	1254–1	96	3724	4340	4692
	≥ 6	23	18	11	7	9	5	8	4	4	6	8	4	6	3	4	60	918–1	180	3193	3441	4461
f	≥ 3	65	30	26	21	18	8	11	8	9	9	6	8	4	4	5	26	222–2	258	1729	1821	4337
t		6	12	18	24	30	36	42	48	54	60	66	72	78	84	90	96+	MAX	TE	T	T*	TH

HOURS INTERVAL BETWEEN EVENTS

Spring — 37 — 32.9 N. Latitude, 119.4 W. Longitude

		6	12	18	24	30	36	42	48	54	60	66	72	78	84	90	96+	MAX	TE	T	T*	TH
W	≥64																6	SEA–6	6	2208	4265	4265
A	≥56																6	SEA–6	6	2208	4265	4265
V	≥48																6	SEA–6	6	2208	4265	4265
E	≥40																6	SEA–6	6	2208	4265	4265
	≥34																6	SEA–6	6	2208	4265	4265
H	≥28																6	SEA–6	6	2208	4265	4265
E	≥24																6	SEA–6	6	2208	4265	4265
I	≥20																7	SEA–6	7	2486	4264	4265
G	≥16																9	SEA–7	9	2853	4320	4334
H	≥12	4	2	5	2		1	1					1			1	29	SEA–5	46	40??	5516	5504
T	≥ 9	24	18	18	2	2	1	6	1	2	2	8	1	2		5	61	SEA–3	153	4148	4760	5162
	≥ 6	71	37	28	4	4	7	12	7	9	11	8	5	6	10	6	55	1074–1	280	3019	3065	4458
f	≥ 2	75	44	22	12	11	13	8	6	5	10	8	3	2	2	2	8	234–1	231	1053	1056	4245
t		6	12	18	24	30	36	42	48	54	60	66	72	78	84	90	96+	MAX	TE	T	T*	TH

HOURS INTERVAL BETWEEN EVENTS

Summer — 37 — 32.9 N. Latitude, 119.4 W. Longitude

		6	12	18	24	30	36	42	48	54	60	66	72	78	84	90	96+	MAX	TE	T	T*	TH
W	≥64																6	SEA–6	6	2208	4224	4224
A	≥56																6	SEA–6	6	2208	4224	4224
V	≥48																6	SEA–6	6	2208	4224	4224
E	≥40																6	SEA–6	6	2208	4224	4224
	≥34																6	SEA–6	6	2208	4224	4224
H	≥28																6	SEA–6	6	2208	4224	4224
E	≥24																6	SEA–6	6	2208	4224	4224
I	≥20																6	SEA–6	6	2208	4224	4224
G	≥16																6	SEA–6	6	2208	4224	4224
H	≥12			1		1											8	SEA–6	10	2534	4471	4477
T	≥ 9	10	3	1	1		1	1					2		1		19	SEA–2	39	2802	4383	4446
	≥ 6	33	19	12	5	4	6	4	4	2	1	2		4	1	3	48	1500–1	148	2829	3899	4328
f	≥ 3	137	75	38	12	16	10	16	2	2	9	8	3	3	3	6	26	306–1	366	1820	1919	4194
t		6	12	18	24	30	36	42	48	54	60	66	72	78	84	90	96+	MAX	TE	T	T*	TH

HOURS INTERVAL BETWEEN EVENTS

Fall — 37 — 32.9 N. Latitude, 119.4 W. Longitude

		6	12	18	24	30	36	42	48	54	60	66	72	78	84	90	96+	MAX	TE	T	T*	TH
W	≥64																5	SEA–5	5	1840	4564	4564
A	≥56																5	SEA–5	5	1840	4564	4564
V	≥48																5	SEA–5	5	1840	4564	4564
E	≥40																5	SEA–5	5	1840	4564	4564
	≥34																5	SEA–5	5	1840	4564	4564
H	≥28																5	SEA–5	5	1840	4564	4564
E	≥24																5	SEA–5	5	1840	4564	4564
I	≥20																5	SEA–5	5	1840	4564	4564
G	≥16																6	SEA–5	6	2076	4800	4801
H	≥12			1											1		17	SEA–2	19	3168	5503	5543
T	≥ 9	5	2	2		1		1	1	1	1	2	2			1	46	1326–1	65	3069	4754	4953
	≥ 6	14	10	9	7	2	9	6	5	10	1	4	3	2	2	2	65	1050–1	151	3139	4091	4792
f	≥ 3	66	22	22	14	14	15	12	9	8	6	6	2	4	3	1	53	468–1	258	2166	2502	4591
t		6	12	18	24	30	36	42	48	54	60	66	72	78	84	90	96+	MAX	TE	T	T*	TH

HOURS INTERVAL BETWEEN EVENTS

Table 14.25 Wave height intervals, Pacific grid point 47.

Winter 47 25.0 N. Latitude, 119.4 W. Longitude

W	≥64															8	SEA–8	8	2944	4389	4389
A	≥56															8	SEA–8	8	2944	4389	4389
V	≥48															8	SEA–8	8	2944	4389	4389
E	≥40															8	SEA–8	8	2944	4389	4389
	≥34															8	SEA–8	8	2944	4389	4389
H	≥28															8	SEA–8	8	2944	4389	4389
E	≥24															8	SEA–8	8	2944	4389	4389
I	≥20															8	SEA–8	8	2944	4389	4389
G	≥16															8	SEA–8	8	2944	4389	4391
H	≥12	1	2		1											13	SEA–5	17	3028	4597	4644
T	≥ 9	3	1	2		2		3	1		1		1			1	43	SEA–2	58	4423	4088	5128
	≥ 6	23	6	9	6	3	4	5	5	1	2	3	3	1	2	3	64	798–1	140	3223	3461	4498
f	≥ 3	43	28	20	10	12	12	8	7	3	10	5	4	5	6	5	18	348–1	196	1378	1474	4335
t		6	12	18	24	30	36	42	48	54	60	66	72	78	84	90	96+	MAX	TE	T	T*	TH

HOURS INTERVAL BETWEEN EVENTS

Spring 47 25.0 N. Latitude, 119.4 W. Longitude

W	≥64															6	SEA–6	6	2208	4265	4265
A	≥56															6	SEA–6	6	2208	4265	4265
V	≥48															6	SEA–6	6	2208	4265	4265
E	≥40															6	SEA–6	6	2208	4265	4265
	≥34															6	SEA–6	6	2208	4265	4265
H	≥28															6	SEA–6	6	2208	4265	4265
E	≥24															6	SEA–6	6	2208	4265	4265
I	≥20															6	SEA–6	6	2208	4265	4265
G	≥16															7	SEA–7	7	2576	4335	4339
H	≥12															13	SEA–5	13	2821	4562	4595
T	≥ 9	2	3	1		2	1		2	1		2	1			2	40	SEA–2	57	3600	4241	4531
	≥ 6	20	9	19	14	8	5	7	6	6	6	5	3	6	5	6	49	666–1	174	2429	2519	4353
f	≥ 3	22	12	6	6	6	5	10	2	2	1	1	3	1		1	5	180–1	83	452	452	4246
t		6	12	18	24	30	36	42	48	54	60	66	72	78	84	90	96+	MAX	TE	T	T*	TH

HOURS INTERVAL BETWEEN EVENTS

Summer 47 25.0 N. Latitude, 119.4 W. Longitude

W	≥64															6	SEA–6	6	2208	4224	4224
A	≥56															6	SEA–6	6	2208	4224	4224
V	≥48															6	SEA–6	6	2208	4224	4224
E	≥40															6	SEA–6	6	2208	4224	4224
	≥34															6	SEA–6	6	2208	4224	4224
H	≥28															6	SEA–6	6	2208	4224	4224
E	≥24															6	SEA–6	6	2208	4224	4224
I	≥20															7	SEA–6	7	2469	4484	4488
G	≥16															7	SEA–6	7	2468	4479	4489
H	≥12	1														8	SEA–4	9	2323	4463	4487
T	≥ 9								1	1							16	SEA–4	18	2685	4450	4518
	≥ 6	14	7	5	3	1	3	5	5	3	2	1	3	2	3	5	51	954–1	113	3005	3439	4219
f	≥ 3	32	19	19	10	6	3	2	4	3	5	5	4	5	1	1	8	204–2	127	725	759	4139
t		6	12	18	24	30	36	42	48	54	60	66	72	78	84	90	96+	MAX	TE	T	T*	TH

HOURS INTERVAL BETWEEN EVENTS

Fall 47 25.0 N. Latitude, 119.4 W. Longitude

W	≥64															5	SEA–5	5	1840	4566	4566
A	≥56															5	SEA–5	5	1840	4566	4566
V	≥48															5	SEA–5	5	1840	4566	4566
E	≥40															5	SEA–5	5	1840	4566	4566
	≥34															5	SEA–5	5	1840	4566	4566
H	≥28															5	SEA–5	5	1840	4566	4566
E	≥24															5	SEA–5	5	1840	4566	4566
I	≥20															5	SEA–5	5	1840	4566	4566
G	≥16															6	SEA–5	6	1866	4565	4566
H	≥12	2						1								12	SEA–3	15	2128	4809	4856
T	≥ 9	2				1		2	2	1	1			2	1		24	2046–1	36	2891	4850	5039
	≥ 6	16	4	6	9	5	2	5	6		4	2	1	4	3	1	58	960–1	126	3248	3983	4770
f	≥ 3	56	22	19	15	19	16	10	10	10	7	3	4	4	4	2	24	240–1	225	1601	1726	4545
t		6	12	18	24	30	36	42	48	54	60	66	72	78	84	90	96+	MAX	TE	T	T*	TH

HOURS INTERVAL BETWEEN EVENTS

REFERENCES

14.1 "Space Shuttle Flight and Ground System Specification." vol. X, appendix 10.10, revision B, JSC 07700, NASA/Johnson Space Flight Center, April 27, 1978.

14.2 "Natural Environment for the Space Shuttle Solid Rocket Booster." MSFC SE-019-043-2H, Marshall Space Flight Center, Huntsville, Alabama, May 20, 1975.

14.3 "U.S. Navy Hindcast Spectral Ocean Wave Model Climatic Atlas: North Atlantic Ocean." NAVAIR 50-1C-538, Naval Oceanography Command Detachment, Asheville, NC, October 1983.

14.4 "U.S. Navy Hindcast Spectral Ocean Wave Model Climatic Atlas: North Pacific Ocean." NAVAIR 50-1C-539, Naval Oceanography Command Detachment, Asheville, NC, March 1985.

14.5 "U.S. Navy Climatic Study of the Caribbean Sea and Gulf of Mexico, Vol. 3." Naval Oceanography Command Detachment, Asheville, NC, July 1986.

14.6 Climatology of California Coastal Waters, Fleet Weather Central NAS, Alameda, CA, July 1972.

14.7 "Summary of Synoptic Meteorological Observations." North American Coast Marine Areas, vol. 4, vol. 7, and vol. 8, Nos. AD707701, AD709055, and AD710771, respectively, U.S. Naval Weather Service Command, Washington, DC, May 1970.

14.8 "International Meteorological Codes, 1972." Hydrographic Office Publication No. 118, Naval Weather Service Environmental Detachment, Federal Building, Asheville, NC (reproduced and distributed to Naval Weather Command Units by direction of the Commander, U.S. Naval Weather Service Command), March 1972.

14.9 "Environmental Conditions Within Specified Geographical Regions." U.S. Department of Commerce, National Oceanic and Atmospheric Administration, Environmental Data Service, United States Department of Commerce Publication, National Data Buoy Center, April 1973.

14.10 Churgin, J., and Halminski, S.J.: "Temperature, Salinity, Oxygen, and Phosphate in the Waters Off United States." Key to Oceanographic Records, Documentation No. 2, vol. 2, "Gulf of Mexico," National Oceanographic Data Center, March 1974.

14.11 "Marine Climatological Summaries." Vol. 1 through 9, U.S. Department of Commerce, NOAA, EDS, National Climatic Center, Asheville, NC, June 1976.

SECTION XV. CONVERSION UNITS

15.1 Physical Constants and Conversion Factors

This section lists the preferred metric units, alternative units, and conversion factors for a number of commonly used quantities in the aerospace industry. The selection presented, while not intended to be restrictive, will prove helpful in presenting values of quantities in an identical manner in similar contexts within the industry.

The preferred metric units, alternative units, and conversion factors are presented and grouped according to the categories listed below. For convenience, tables 15-1 through 15-6 list the SI base units, supplementary units, derived units, acceptable non-SI units, standard prefixes, and definition for selected physical constants and non-SI units.

1. Space and Time
2. Mass
3. Force
4. Mechanics
5. Flow
6. Thermodynamics
7. Electricity and Magnetism
8. Light
9. Acoustics
10. SI Base and Supplementary Units
11. SI-Derived Units
12. Non-SI Units Accepted for Use With SI
13. Prefixes for SI Units
14. SI Definitions for Selected Physical Constants and Non-SI Units.

When the preferred unit appears without a prefix, multiples of that unit per table 15-5 may be used as necessary at the user's discretion. When a prefix appears with the unit, it is the preferred prefix. When the prefix is left to the user's discretion, however, units shall be consistent within any given document.

The conversion factors given are exact, unless the last digit is underlined. The level of error is 0.1 percent or less. Sources of the values given were obtained from references 15.1 through 15.4.

Table 15-1. Preferred metric units.

	Quantity	Preferred Metric Unit	Alternative Units	Conversion Factors
1.	Space & Time			
1.1	Time	s (second)	min (minute) h (hour) d (day)	
1.2	Plane angle	rad (radian)	° (degree) ' (minute) " (second)	
1.3	Solid Angle	sr (steradian)		
1.4	Length	mm (millimeter)		1 in = 2.54 cm = 25.4 mm 1 ft = 0.3048 m = 304.8 mm 1 yd = 0.9144 m = 914.4 mm
1.4.1	Distance	km (kilometer)	nautical mile	1 statute mile = 1.609 344 km 1 nautical mile (US) = 1.852 km
1.4.2	Distance	m (meter)		1 in = 2.54 cm = 25.4 mm 1 ft = 0.3048 m = 304.8 mm 1 yd = 0.9144 m = 914.4 mm
1.4.3	Visibility	km (kilometer)		1 statute mile = 1.609 344 km
1.4.4	Altitude	m (meter)		1 ft = 0.3048 m
1.4.5	Vibration amplitude	mm (millimeter)		1 in = 25.4 mm
1.4.6	Porosity; surface texture; thickness of surface coating	µm (micrometer)		1 microinch = 0.0254 µm
1.5	Area	m^2 (square meter)		1 in^2 = 645.16 mm^2 = 6.4516 cm^2 1 ft^2 = 0.092 903 04 m^2 1 acre = 0.4047 hectare 1 sq. mile = 2.590 km^2
1.6	Volume	m^3 (cubic meter)		1 in^3 = 16 387.064 mm^3 1 ft^3 = 0.028 316 847 m^3 1 yd^3 = 0.764 554 86 m^3 1 gal (dry) = 0.004 405 m^3
1.6.1	Fluid tank; water heating tank; high pressure oxygen	L (liter)	m^3 (cubic meter)	1 ft^3 = 28.317 L 1 gal (liquid) = 3.785 412 L 1 fl oz = 29.573 53 cm^3
2.	Mass			
2.1	Mass	kg (kilogram)		1 oz (avoir) = 28.349 52 g 1 lb (avoir) = 0.453 592 37 kg 1 long ton (2,240 lb) = 1016.047 kg 1 short ton (2,000 lb) = 907.184 7 kg 1 long ton = 1.016 047 metric ton 1 short ton = 0.907 185 metric ton

Table 15-1. Preferred metric units (continued)

	Quantity	Preferred Metric Unit	Alternative Units	Conversion Factors
2.	Mass (Continued)			
2.1.1	Gross mass; payload	kg (kilogram)	t (tonne)	
2.1.2	Hoisting provision	kg (kilogram)	t (tonne)	
2.1.3	Cargo capacity	kg (kilogram)	t (tonne)	
2.1.4	Fuel capacity (gravimetric)	kg (kilogram)	t (tonne)	
2.2	Linear density	kg/m (kilogram per meter)		1 lb/ft = 1.488 16 kg/m 1 lb/yd = 0.496 055 kg/m
2.3	Density, concentration	kg/m^3 (kilogram per cubic meter)	g/L (grams per liter)	1 lb/in^3 = 27 679.9 kg/m^3 1 lb/ft^3 = 16.018 46 kg/m^3 1 short ton/yd^3 = 1186.5526 kg/m^3 1 lb/gal = 119.8264 kg/m^3 1 oz/gal = 8.489 152 kg/m^3
2.3.1	Air density	kg/m^3 (kilogram per cubic meter)		1 $slug/ft^3$ = 515.379 kg/m^3
2.3.2	Cargo density	kg/m^3 (kilogram per cubic meter)	t/m^3 (tonne per cubic meter)	
2.3.3	Gas density	kg/m^3 (kilogram per cubic meter)		
2.3.4	Liquid density	kg/m^3 (kilogram per cubic meter)	g/L (gram per liter)	
2.4	Ambient humidity	mg/g (milligram per gram)		
2.5	Balance moment	kg m (kilogram meter)	g mm (gram millimeter)	
2.6	Moment of inertia	kg m^2 (kilogram square meter)		1 lb in^2 = 2.9264×10^{-4} kg m^2 1 lb ft^2 = 0.031 140 kg m^2
2.7	Momentum	kg m/s (kilogram meter per second)		1 lb ft/s= 0.138 255 kg m/s
2.8	Moment of momentum	kg m^2/s (kilogram square meter per second)		1 lb ft^2/s = 0.042 140 kg m^2/s
2.9	Floor loading	kg/m^2 (kilogram per square meter)	t/m^2 (tonne per square meter)	
2.10	Wing loading	kg/m^2 (kilogram per square meter)	t/m^2 (tonne per square meter)	

Table 15-1. Preferred metric units (continued)

	Quantity	Preferred Metric Unit	Alternative Units	Conversion Factors
3.	Force			
3.1	Force	N (newton)		1 lbf = 4.448 222 N
3.1.1	Handle operating load	N (newton)		
3.1.2	Jet and rocket engine thrust	kN (kilonewton)		
3.1.3	Rocket engine total impulse	N s (newton second)		
3.1.4	Rocket engine specific impulse	N s/kg (newton second per kilogram)		
3.2	Vacuum	Pa (pascal)		
3.3	Pressure	kPa (kilopascal)		1 psi = 6.894 757 kPa 1 in H_2O (39.2 °F) = 0.249 08 kPa 1 in H_2O (60 °F) = 0.248 84 kPa 1 in Hg (32 °F) = 3.386 39 kPa 1 in Hg (60 °F) = 3.376 85 kPa
3.3.1	Air pressure (general)	kPa (kilopascal)		1 atmos (std) = 101.325 kPa
3.3.2	Air pressure (meteorological)	kPa (kilopascal)		1 torr = 133.322 Pa = 0.133 32 kPa
3.3.3	Hydraulic pressure	kPa (kilopascal)		1 psi = 6.894 757 kPa
3.4	Stress	mPa (megapascal)		1 ksi = 6.894 757 mPa
3.4.1	Elastic limit; proportional limit; endurance limit	mPa (megapascal)		
3.4.2	Modulus of elasticity; Young's modulus; modulus of rigidity	mPa (megapascal)		10^6 psi = 6894.747 mPa
3.5	Fracture toughness	mPa · $m^{1/2}$ (megapascal meter$^{1/2}$)		1 ksi $in^{1/2}$ = 1.098 843 mPa · $m^{1/2}$
3.6	Strain energy per unit volume	J/m^3 (joule per cubic meter)		
3.7	Torque; moment of force	N m (newton-meter)		1 in lbf = 0.112 984 8 N m
3.8	Bending moment	N m (newton-meter)		1 in lbf = 1.355 818 N m
3.9	Bending moment per unit length; torque per unit length	N m/m (newton-meter per meter)		1 lbf ft/in = 53.378 66 N m/m 1 lbf in/in = 4.428 222 N m/m
3.10	Stiffness	N/m (newton per meter)		1 lbf/in = 175.127 N/m

Table 15-1. Preferred metric units (continued)

	Quantity	Preferred Metric Unit	Alternative Units	Conversion Factors
3.	Force (continued)			
3.11	Surface tension	mN/m (millinewton per meter)		
4.	Mechanics			
4.1	Section modulus	cm^3 (cubic centimeter)		1 in^3 = 16.387 064 cm^3
4.2	Second moment of area	cm^4		1 in^4 = 41.623 1 cm^4
4.3	Frequency	Hz (hertz)		
4.4	Rotational frequency	r/s (revolutions per second)	r/min (revolutions per minute)	
4.4.1	Rotational speed	r/min (revolutions per minute)		
4.5	Angular velocity	rad/s (radian per second)		
4.5.1	Rate of trim	°/s (degree per second)		
4.6	Angular acceleration	rad/s^2 (radian per $second^2$)		
4.7	Velocity	m/s (meter per second)	km/h (kilometer per hour)	1 ft/s = 0.304 8 m/s 1 mile/hour = 1.609 344 km/h
4.7.1	Air speed	km/h (kilometer per hour)		1 knot (US) = 1.8532 km/h
4.7.2	Land speed	km/h (kilometer per hour)		1 mile/hour = 1.609 344 km/h
4.7.3	Wind speed	km/h (kilometer per hour)	ms^{-1} (meter per second)	1 mile/hour = 1.609 344 km/h
4.7.4	Vertical speed	m/s (meter per second)		1 ft/s = 0.3048 m/s 1 ft/min = 0.005 08 m/s
4.8	Linear acceleration	m/s^2 (meter per $second^2$)		
4.9	Energy; work	J (joule)		1 ft lb/f = 1.355 818 J 1 hp H = 2.6845 mJ 1 kw H = 3.6 mJ
4.9.1	Kinetic energy absorbed by brakes	mJ (megajoule)		
4.10	Impact	J/m^2 (joule per square meter)		

Table 15-1. Preferred metric units (continued)

	Quantity	Preferred Metric Unit	Alternative Units	Conversion Factors
4.	Mechanics (continued)			
4.11	Power	W (watt)		
4.11.1	Shaft power; equivalent shaft power	kW (kilowatt)		
5.	Flow			
5.1	Mass flow	kg/s (kilogram per second)		1 lb/h = 0.000 125 998 kg/s 1 lb/min = 0.007 56 kg/s 1 lb/s = 0.453 592 kg/s
5.2	Gas flow	kg/s (kilogram per second)		
5.2.1	Ventilation air	g/s (gram per second)		
5.2.2	Gas leakage	m^3/min (cubic meter per minute)		
5.2.3	Engine airflow	kg/s (kilogram per second)		
5.3	Liquid flow (gravimetric)	g/s (gram per second)		1 lb/min = 7.560 g/s
5.3.1	Fuel flow	g/s (gram per second)	kg/h (kilogram per hour)	1 lb/hour = 0.453 6 kg/h 1 lb/s = 453.6 g/s
5.3.2	Fuel tank filling rate (gravimetric)	kg/min (kilogram per minute)		1 lb/min = 0.453 6 kg/min
5.3.3	Fuel consumption	kg/h (kilogram per hour)		1 lb/hour = 0.453 6 kg/h
5.3.4	Oil flow	L/min (liter per minute)		
5.4	Liquid flow (volumetric)	cm^3/s (cubic centimeter per second)	L/s (liter per second)	1 in^3/min = 0.273 cm^3/s 1 U.S. gal/min = 0.063 08 L/s
5.4.1	Pump capacity; fuel tank filling rate (volumetric)	L/min (liter per minute)		1 U.S. gal/min = 3.785 L/min
5.4.2	Oil leakage	cm^3/min (cubic centimeter per minute)		1 in^3/min = 16.39 cm^3/min
5.5	Viscosity (dynamic)	mPa s (millipascal second)		1 lb/ft s = 1.488 164 Pa s 1 lbf s/ft^2 = 47.880 26 Pa s
5.6	Viscosity (kinematic)	mm^2/s (square millimeter per second)		1 ft^2/s = 92 903 mm^2/s

Table 15-1. Preferred metric units (continued)

	Quantity	Preferred Metric Unit	Alternative Units	Conversion Factors
6.	Thermodynamics			
6.1	Temperature	K (kelvin)	°C (° Celsius)	°C = (°F – 32)/1.8 K = °C + 273.15
6.1.1	Standard day temperature; ambient temperature	°C (° Celsius)		
6.2	Coefficient of linear expansion	K^{-1} ($kelvin^{-1}$)	$°C^{-1}$ ($° Celsius^{-1}$)	
6.3	Quantity of heat	J (joule)		1 Btu (60 °F) = 1.05468 kJ
6.4	Heat flow per unit area	J/m^2 (joule per square meter)		
6.5	Heat flow rate	kW (kilowatt)		1 Btu/h = 0.293 071 W
6.5.1	Heat rate	mJ/kW h) (megajoule per kilowatt hour)		1 Btu/(hp h) = 1.415 kJ/(kW h)
6.6	Density of heat flow rate	W/m^2 (watt per square meter)		1 Btu/(h ft^2) = 3.154 59 W/m^2
6.7	Thermal conductivity	W/(m K) (watt per meter kelvin)		1 Btu–in/ft^2·h·°F = 0.144 23 W/(m K)
6.8	Thermal conductance	W/(m^2 K) (watt per square meter kelvin)		1 Btu/(ft^2·h·°F) = 5.678 26 W/(m^2 K)
6.9	Coefficient of heat transfer	W/(m^2 K) (watt per square meter kelvin)		
6.10	Thermal diffusivity	mm^2/s (square millimeter per second)		
6.11	Thermal resistivity	m K/W (meter kelvin per watt)		
6.12	Thermal resistance	m^2 K/W (square meter kelvin per watt)		
6.13	Heat capacity	kJ/K (kilojoule per kelvin)		
6.14	Specific heat capacity	kJ/(kg K) (kilojoule per kilogram kelvin)		1 Btu/(lb °F) = 4.1868 kJ/(kg K)
6.14.1	Specific heat	kJ/(kg K) (kilojoule per kilogram kelvin)		

Table 15-1. Preferred metric units (continued)

	Quantity	Preferred Metric Unit	Alternative Units	Conversion Factors
6.	Thermodynamics (continued)			
6.15	Entropy	kJ/K (kilojoule per kelvin)		1 Btu/°R = 1.8991 kJ/K
6.16	Specific entropy	kJ/(kg K) (kilojoule per kilogram kelvin)		1 Btu/(lb °R) = 4.1868 kJ/(kg K)
6.17	Gas constant	J/(kg K) (joule per kilogram kelvin)		1 ft lb/(lb °F) = 5.382 J/(kg K)
6.17.1	Molar gas constant	J/(mol K) (joule per mole kelvin)		R_o = 8.3143 J/(mol K)
6.18	Specific energy	J/kg (joule per kilogram)		
6.18.1	Heating value; enthalpy	mJ/kg (megajoule per kilogram)		1 Btu/lb = 2326 J/kg
6.19	Specific latent heat	J/kg (joule per kilogram)		
7.	Electricity and Magnetism			
7.1	Electric current	A (ampere)		
7.2	Current density	A/m^2 (ampere per square meter)		1 A/in^2 = 1.550 kA/m^2
7.3	Dielectric strength	V/mm (volt per millimeter)		
7.4	Electric potential	V (volt)		
7.5	Electric field strength	V/m (volt per meter)		
7.6	Power	W (watt)		1 hp (550 ft lbf /s) = 0.7457 kW 1 hp (metric) = 0.7355 kW 1 hp (electric) = 0.746 kW
7.7	Power (apparent)	VA (volt ampere)		
7.8	Electric resistance; impedance; modulus of impedance; reactance	Ω (ohm)		
7.9	Resistivity	Ωm (ohm meter)		
7.10	Conductance; admittance; modulus of admittance; susceptance	S (siemens)		
7.11	Conductivity	S/m (siemens per meter)		

Table 15-1. Preferred metric units (continued)

	Quantity	Preferred Metric Unit	Alternative Units	Conversion Factors
7.	Electricity and Magnetism (continued)			
7.12	Quantity of electricity	C (coulomb)		1 Ah = 3,600.0 C
7.13	Electric capacitance	F (farad)		
7.14	Permittivity	F/mm (farad per millimeter)		
7.15	Self inductance; mutual inductance	H (henry)		
7.16	Permeance	H (henry)		
7.17	Reluctance	H^{-1} ($henry^{-1}$)		
7.18	Permeability	H/m (henry per meter)		
7.19	Magnetic flux	Wb (weber)		1 maxwell = 0.01 μWb
7.20	Magnetic flux density	T (tesla)		1 gauss = 0.1 MT
7.21	Magnetic field strength	A/m (ampere per meter)		1 oersted = 1,000/4π A/M
7.22	Electromagnetic moment; magnetic moment	A m^2 (ampere square meter)		
7.23	Electric dipole moment	(coulomb meter)		
8.	Light			
8.1	Luminous intensity	cd (candela)		
8.2	Luminous Flux	lm (lumen)		
8.3	Luminous exitance	lm/m^2 (lumen per square meter)		
8.4	Illuminance	lx (lux)		
8.4.1	Cabin illumination	lx (lux)		1 ft candle = 10.764 lx
8.5	Luminance	cd/m^2 (candela per square meter)		1 foot lambert = 3.426 26 cd/m^2 1 lambert = 3183.1 cd/m^2
9.	Acoustics			
9.1	Noise level; sound level	dB (decibel)		
9.2	Period; periodic time	s (second)		
9.3	Frequency	Hz (hertz)		
9.4	Wavelength	m (meter)		
9.5	Mass density	kg/m^3 (kilogram per cubic meter)		

Table 15-1. Preferred metric units (continued)

	Quantity	Preferred Metric Unit	Alternative Units	Conversion Factors
9.	Acoustics (continued)			
9.6	Static pressure, instantaneous sound pressure	Pa (pascal)		
9.7	Instantaneous sound particle velocity	m/s (meter per second)		
9.8	Instantaneous volume velocity	m^3/s (cubic meter per second)		
9.9	Velocity of sound	m/s (meter per second)		
9.10	Sound energy flux; sound power	W (watt)		
9.11	Sound intensity	W/m^2 (watt per square meter)		
9.12	Specific acoustic impedance	Pa s/m (pascal second per meter)		
9.13	Acoustic impedance	Pa s/m^3 (pascal second per cubic meter)		
9.14	Mechanical impedance	N s/m (newton second per meter)		

Table 15-2 SI base and supplementary units

Quantity	Name	Symbol
Base Units:		
Length	meter	m
Mass	kilogram	kg
Time	second	s
Electric current	ampere	A
Thermodynamic temperature	kelvin	K
Amount of substance	mole	mol
Luminous intensity	candela	cd
Supplementary Units:		
Plane angle	radian	rad
Solid angle	steradian	sr

Table 15-3 SI derived units.

Quantity	Name	Symbol	Derivation
Frequency	hertz	Hz	$1\ Hz = 1\ s^{-1}$
Force	newton	N	$1\ N = 1\ kg\ m/s^2$
Pressure; stress	pascal	Pa	$1\ Pa = 1\ n/m^2$
Energy; work; quantity of heat	joule	J	1 J = 1 N m
Power	watt	W	1 W = 1 J/s
Electric charge; quantity of electricity	coulomb	C	1 C = 1 A s
Electric potential; electromotive force	volt	V	1 V = 1 W/A
Electric capacitance	farad	F	1 F = 1 A s/V
Electric resistance	ohm	Ω	1 Ω = 1 V/A
Electric conductance	siemens	S	1 S = 1 A/V
Magnetic flux	weber	Wb	1 Wb = 1 V s
Magnetic flux density; magnetic induction	tesla	t	$1\ t = 1\ V\ s/m^2$
Inductance	henry	h	1 h = 1 V s/A
Luminous flux	lumen	lm	1 lm = 1 cd sr
Illuminance	lux	lx	$1\ lx = 1\ lm/m^2$

Table 15-4 Non-SI units accepted for use with SI.

Quantity	Name	Symbol	Definition
Time	minute	min	1 min = 60 s
	hour	h	1 h = 60 min = 3,600 s
	day	d	1 d = 24 h = 86,400 s
	week	wk	1 wk = 7 d
	month	mo	1 mo
	year	yr	1 yr = 365.26 days
Plane angle	degree	°	1° = (π/180) rad
	minute	'	1' = (1/60)°
	second	"	1" = (1/60)'
Volume	liter	L	1 L = 1 dm^3 = 10^{-3} m^3
Area	hectare	ha	1 ha = 1 hm^2 = 10^4 m^2
Pressure	bar	Bar	1 Bar = 10^5 Pa
Energy	kilowatt-hour	kWh	1 kWh = 3.6 mJ
Temperature	degree Celsius	°C	
Mass	metric ton	t	1 t = 10^3 kg

Table 15-5 Prefixes for SI units.

Factor by Which the Unit is Multiplied	Prefix		Factor by Which the Unit is Multiplied	Prefix	
	Name	Symbol		Name	Symbol
10^{18}	exa	E	10^{-1}	deci*	d
10^{15}	peta	P	10^{-2}	centi	c
10^{12}	tera	T	10^{-3}	milli	m
10^{9}	giga	G	10^{-6}	micro	μ
10^{6}	mega	M	10^{-9}	nano	n
10^{3}	kilo	k	10^{-12}	pico	p
10^{2}	hecto*	h	10^{-15}	femto	f
10^{1}	deka*	da	10^{-18}	atto	a

* To be avoided where possible

Table 15-6 SI definitions for selected physical constants and non-Si units.

Unit	SI Equivalent
Angstrom unit (Å)	10^{-10} meter
Micron (μ)	10^{-6} meter
Light year	9.460 55 × 10^{12} kilometer
Speed of light	299,792.4580±0.0012 kilometer per second
Speed of sound (sea level US76)	340.294 meter per second
Gravitational constant (G_N)	9.806 65 newton-meter/kilogram-$second^2$
Centistoke	10^{-6} square meter/second

REFERENCES

15.1 Mechtly, E.A.: "The International System of Units: Physical Constants and Conversion Factors." NASA SP-7012. Second Revision, National Aeronautics and Space Administration, Washington, DC, 1973.

15.2 List, R.J.: "Smithsonian Meteorological Tables—Sixth Revised Edition." Smithsonian Miscellaneous Collections, vol. 114 (whole volume), Smithsonian Institution Press, Washington, DC, Fifth Reprint, 1984.

15.3 "Units of Weight and Measure (United States Customary and Metric) Definitions and Tables of Equivalents." United States Department of Commerce, National Bureau of Standards, Miscellaneous Publication 233, 1960.

15.4 "NBS Guidelines for Use of the Metric System." U.S. Department of Commerce, National Bureau of Standards, LC 1056, November 1974.

INDEX

REPORT DOCUMENTATION PAGE

Form Approved
OMB No 0704-0188

1. AGENCY USE ONLY (Leave blank)	2. REPORT DATE	3. REPORT TYPE AND DATES COVERED
	August 1993	Technical Memorandum

4. TITLE AND SUBTITLE
Terrestrial Environment (Climatic) Criteria Guidelines for Use in Aerospace Vehicle Development, 1993 Revision

5. FUNDING NUMBERS

6. AUTHOR(S)
D.L. Johnson, Editor

7. PERFORMING ORGANIZATION NAME(S) AND ADDRESS(ES)
George C. Marshall Space Flight Center
Marshall Space Flight Center, Alabama 35812

8. PERFORMING ORGANIZATION REPORT NUMBER
M-723

9. SPONSORING / MONITORING AGENCY NAME(S) AND ADDRESS(ES)
National Aeronautics and Space Administration
Washington, DC 20546

10. SPONSORING / MONITORING AGENCY REPORT NUMBER
NASA TM-4511

11. SUPPLEMENTARY NOTES This document was prepared based on the engineering problems which have developed or are anticipated for future programs by design and operational personnel of the NASA field centers. Various staff members of the Earth Science and Applications Division, Space Science Laboratory, MSFC/NASA and their supporting contracted personnel contributed to the contents of this document.

12a. DISTRIBUTION / AVAILABILITY STATEMENT
Unclassified — Unlimited
Subject Category 15

12b. DISTRIBUTION CODE

13. ABSTRACT *(Maximum 200 words)*

This document provides guidelines on terrestrial environment data specifically applicable in the development of design requirements/specifications for NASA aerospace vehicles and associated equipment development. The primary geographic areas encompassed are the John F. Kennedy Space Center, FL; Vandenberg AFB, CA; Edwards AFB, CA; Michoud Assembly Facility, New Orleans, LA; John C. Stennis Space Center, MS; Lyndon B. Johnson Space Center, Houston, TX; and the White Sands Missile Range, NM. In addition, a section has been included to provide information on the general distribution of natural environmental extremes in the conterminous United States that may be needed to specify design criteria in the transportation of space vehicle subsystems and components. A summary of climatic extremes for worldwide operational needs is also included. Although not considered as a specific vehicle design criterion, a section on atmospheric attenuation has been added since sensors on certain Earth orbital experiment missions are influenced by the Earth's atmosphere. This document presents the latest available information on probable climatic extremes and supersedes information presented in TM X-64589, TM X-64757, TM X-78118, and TM-82473. Information is included on atmospheric chemistry, seismic criteria, and on a mathematical model to predict atmospheric dispersion of aerospace engine exhaust cloud rise and growth. There is also a section on atmospheric cloud phenomena. The information in this report is recommended for use in the development of aerospace vehicle and associated equipment design and operational criteria, unless otherwise stated in contract work specifications. The environmental data in this report are primarily limited to information below 90 km.

14. SUBJECT TERMS
Environment Criteria, Terrestrial Environment, Surface Extremes, Wind, Temperature, Humidity, Precipitation, Density, Pressure, Atmospheric Electricity, Cloud Cover, Control Systems, Geology, Sea State, Severe Storms, Constituents, Radiation

15. NUMBER OF PAGES
472

16. PRICE CODE
A20

17. SECURITY CLASSIFICATION OF REPORT	18. SECURITY CLASSIFICATION OF THIS PAGE	19. SECURITY CLASSIFICATION OF ABSTRACT	20. LIMITATION OF ABSTRACT
Unclassified	Unclassified	Unclassified	Unlimited